Kenneth Freeman
Bruce Elmegreen
David Block
Matthew Woolway *Editors*

Lessons from the Local Group

A Conference in honour of David Block and Bruce Elmegreen

Springer

Lessons from the Local Group

Kenneth Freeman • Bruce Elmegreen
David Block • Matthew Woolway
Editors

Lessons from the Local Group

A Conference in honour of David Block and Bruce Elmegreen

Springer

Editors
Kenneth Freeman
Australian National University
Canberra
Australia

David Block
University of the Witwatersrand
Johannesburg
South Africa

Bruce Elmegreen
IBM T.J. Watson Research Center
Yorktown Heights, New York
United States

Matthew Woolway
University of the Witwatersrand
Johannesburg
South Africa

Cover Photo: Set within 120 hectares of land with luxuriant and rare vegetation in the Seychelles Archipelago, the Constance Ephelia Hotel was selected as the venue for the Block-Elmegreen Conference held in May 2014. Seen in our cover photograph are one of the restaurants frequented by delegates - the Corossol Restaurant. The restaurant is surrounded by pools of tranquil waters; lamps blaze forth before dinner, and their reflections in the surrounding waters are breathtaking. The color blue is everywhere: from the azure blue skies above, to the waters below. Above the Corossol Restaurant is placed a schematic of a spiral galaxy. From macrocosm to microcosm. Never before has an astronomy group of this size met in the Seychelles. The cover montage was especially designed for the Conference, by the IT-Department at the Constance Ephelia Hotel.

ISBN 978-3-319-10613-7 ISBN 978-3-319-10614-4 (eBook)
DOI 10.1007/978-3-319-10614-4
Springer Cham Heidelberg New York Dordrecht London

Library of Congress Control Number: 2014953222

Printed on acid-free paper

Springer is part of Springer Science+Business Media (www.springer.com)

Preface

The Block-Elmegreen conference (May 2014) celebrates the careers of David Block and Bruce Elmegreen. This year 2014 marks the 60th birthday year of David and the one millionth (base 2) birthday of Bruce. The island of Mahe in the Seychelles archipelago was selected for the meeting. About 50 astronomers from around the planet, many of whom are close collaborators and friends of David and Bruce, attended the conference and presented papers.

The venue for the conference was the Constance Ephelia Hotel. Its facilities are truly unsurpassed, from the conference venue itself to the exquisitely furnished suites and the five restaurants, each with a different theme, from Mediterranean to Chinese. The Gala Dinner was held on the beach at Port Launay. It is a pleasure to thank the entire staff at Constance Ephelia, especially Matthias, Harry and Lindy. We were privileged to have Dr. N. Shah, Chief Executive of Nature Seychelles, to speak to us one evening on conservation in the Seychelles.

The weather prospects for the week of the Conference did not look promising. Predicted was much rain—unusual for the month of May. The weather turned out to be perfect. It rained very hard in the midnight hours, but the mornings were truly beautiful. As Frank Shu once emphasized: "Make all the measurements you can, still no one can predict the weather seven days from now."

David's after-dinner talk on Hubble-Reynolds was attended by astronomers and their partners and appears first in this volume, as did the evening talk in the proceedings of the 2010 Namibia conference. David's talk generated much interest and much discussion during the week! The volume then presents the scientific papers in the same order as they were given at the conference. About 80 % of delegates provided written versions of their talks. A complete list of participants appears toward the end of this volume.

Our thanks go to the Munro family (David, Lil, Sophie, Grace and Tom) for their friendship and encouragement, and to NAMPAK for their corporate sponsorship. We are grateful to Marie-Lou Simaan at Mars Travel in Johannesburg for facilitating the Constance Ephelia Hotel arrangements.

It is a pleasure to acknowledge the support of the University of the Witwatersrand, Johannesburg throughout the organisation of the conference. We are grateful to the Vice-Chancellor Professor A. Habib, the Deputy Vice-Chancellor for Research Professor Z. Vilakazi and the Dean of the Faculty of Science Professor H. Marques for

their support and for their warm hospitality while we were editing the proceedings in Johannesburg. Our special thanks go to Professor Ebrahim Momoniat, Head of the School of Computational and Applied Mathematics at the University of the Witwatersrand, Johannesburg for his encouragement and for granting David the time to focus properly on the logistics for our conference.

We trust that the photographs of conference delegates, and of the conference environs, will bring back happy memories. These photographs (chosen at random) have been placed by the publisher just before the reference lists; they are not linked to the actual author(s) themselves.

Finally I would like to thank the Scientific Organizing Committee, the Local Organizing Committee, the chair persons and all delegates for making this conference so very memorable. Never before has an astronomy group of this size met in the Seychelles archipelago to celebrate the careers of two leading international researchers, David and Bruce!

Johannesburg, South Africa Ken Freeman, Chair, SOC

Editor Ken Freeman (centre) visited South Africa in June-July 2014, where he was hosted by Professor Adam Habib (right), Vice-Chancellor of the University of the Witwatersrand, Johannesburg. At left is David Block. Photo: Fidos Kleovoulou.

We have selected a woodcut initial above (the letter M), to denote the first letter in Milky Way, one of the most massive galaxies in The Local Group.

Geoffrey Chaucer in *The House of Fame*, c. 1380, penned these words:

> See yonder, lo, the Galaxyë
> Which men clepeth the Milky Wey,
> For hit is whyt.

A more modern rendition might be:

> Lift up your eyes; lo, see yonder the Galaxy,
> Which men call the Milky Way,
> Because it is white.

The exquisite foliated and floriated woodcut initials are almost 500 years old, and come from a volume printed by the legendary Jean Petit, in 1527.

Book Note

"Lessons from the Local Group"
The Block-Elmegreen Conference
May 18–May 24, 2014
Seychelles

1 Scientific Organizing Committee

Chair:
Ken Freeman (Australia)
Members:
Martin Asplund (Australia)
David Block (South Africa; Co-chair)
Francoise Combes (France)
Debra Elmegreen (USA)
Bruce Elmegreen (USA; Co-chair)
Giovanni Fazio (USA)
Yasuo Fukui (Japan)
Rob Kennicutt (UK)
John Kormendy (USA)
Martin Rees (UK)
Joe Silk (France)
Robert Smith (Canada)
Piet van der Kruit (Netherlands)

2 Local Organizing Committee (LOC)

Chair:
Ken Freeman (Australia)

Members:

David Block (South Africa)
Ebrahim Momoniat (South Africa)
Liz Block (South Africa)
Trevor Gould (South Africa)

LOC Secretariat:

Precious Shabalala

"MY evening came among the alien trees and spoke in a language which my morning stars did not know" (Nobel Laureate Rabindranath Tagore). Sunset at Port Launay, Seychelles. Photograph: Carme Gallart.

Contents

A Walk with Dr Allan Sandage—Changing the History of Galaxy Morphology, Forever

David L. Block and Ken C. Freeman

Abstract It was in 1926 that the most widely used galaxy classification scheme, known as the Hubble classification, was published in the Astrophysical Journal. The author was the American astronomer E. P. Hubble. Several years ago, Dr Allan Sandage took one of us (David) on a walk from his office, to the library at the Carnegie Observatories in Pasadena. What Dr Sandage showed David, left him speechless.

1 Editorial Note

The oral version was presented at the Seychelles Conference, as a lecture after dinner. It was open to astronomers and their partners. The Editors have decided to retain the same (non-technical) level for the printed version of the lecture. We remain deeply grateful to Springer for permission to publish large excerpts from our book "Shrouds of the Night" by Block and Freeman (2008).

2 The Years 1920 and 1926

It was in 1926 that the most widely used galaxy classification scheme, known as the Hubble classification, was published in the Astrophysical Journal. The author was the American astronomer E. P. Hubble. Several years ago, Dr Allan Sandage took one of us (David) on a walk from his office to the library at the Carnegie Observatories in Pasadena. What Dr Sandage held in his hands, left one speechless. It exposed Hubble's strategy, masterfully executed by him over a grand numbers of

D. L. Block (✉)
School of Computational and Applied Mathematics, University of the Witwatersrand, Johannesburg, South Africa
e-mail: david.block@wits.ac.za

K. C. Freeman
Research School of Astronomy & Astrophysics, Mount Stromlo Observatory, The Australian National University, Canberra, Australia
e-mail: kcf@mso.anu.edu.au

K. Freeman et al. (eds.), *Lessons from the Local Group,*
DOI 10.1007/978-3-319-10614-4_1

years. Hubble calmly failed to acknowledge the sources of his data and/or of his ideas.

In 1920, Hubble published his PhD thesis entitled "Photographic Investigations of Faint Nebulae"—in it, he never developed a classification of his own, but rather made use of a classification by Max Wolf. Plate III of his thesis is entitled: 'Wolf's Classes of Nebulae.'

In the very same year (1920) in which Hubble published his PhD thesis, an unknown "starry messenger" in Britain had devised a morphological scheme of his own . . . But did Hubble ever write a letter to that astronomer, asking him to actually develop a galaxy scheme, prior to 1926? The letterhead in Figs. 1 and 2 is the Randolph Hotel, Oxford, written during one of Hubble's visits to England. We read in Hubble's hand:

"Classification of Spirals. All suggestions on this difficult subject, coming from one of your expertise are extremely welcomed . . . Could you not throw your ideas into the form of a precise classification so we could actually apply it to a large number of nebulae representing the various sizes and degrees of brightness with which we will be dealing? These are only passing thoughts which I offer. The great thing is that the discussion is started. This will eventually lead to something acceptable to us all. Sincerely, Edwin Hubble." (italics, ours)

Everyone knows that, in 1926, Hubble recognized three principal form families, and placed galaxies into one of three principal classes: there were elliptical galaxies, spiral galaxies and those with a rather chaotic optical appearance, known as irregular galaxies. Spiral galaxies themselves were separated into two separate families, the normal spirals and those with a central elongated feature, the barred spirals.

Sir John Herschel, working at the Cape of Good Hope (1834–1838), identified spiral structure in the Large Magellanic Cloud as well as a central bar. Sir John used rich imagery—an axis of light—to describe *the bar* which he *visually* discerned in that object.

We are most grateful to astronomer David Malin for drawing our attention to the following quote by Sir John Herschel:

"To the naked eye the greater nubecula (the Large Magellanic Cloud) exhibits the appearance of an *axis of light* (very ill-defined indeed, and by no means strongly distinguished from the general mass) which seems to open out at its extremities into somewhat oval sweeps" (italics, ours).

The recognition of a bar in photographs of spiral galaxies belongs to Heber D. Curtis. Curtis had recognized a class of spirals called the phi-type spirals, but Hubble later suggested that the Greek letter theta better represented this form. The Curtis phi-class was fully recognized in Hubble's final classification system, but Hubble used the terminology of barred spirals instead. Full credit must be given to the great observer Heber Curtis, for being the first astronomer to recognize bars in spiral galaxies. Normal and barred spirals were grouped into three principal morphological classes, of types a, b and c. Hubble used the prefix S for normal spirals and SB for barred spirals. From the multitudes of shapes and forms of galaxies presented on photographic plates, it became relatively simple to speak of three classes for normal spirals (Sa, Sb and Sc) and three types of barred spiral galaxies (SBa, SBb, SBc).

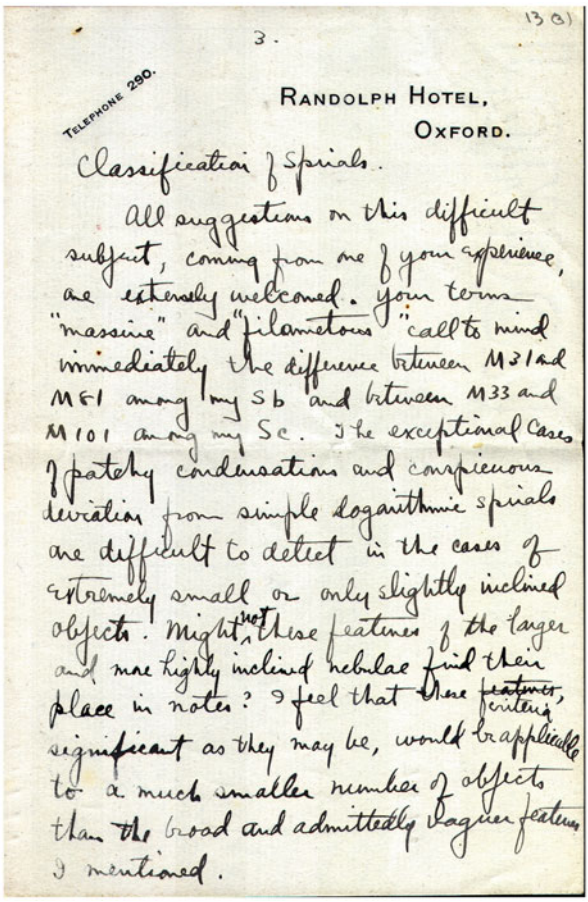
3.

1301

TELEPHONE 290.

RANDOLPH HOTEL,
OXFORD.

Classification of Spirals.

All suggestions on this difficult subject, coming from one of your experience, are extremely welcomed. Your terms "massive" and "filamentous" call to mind immediately the difference between M31 and M81 among my Sb and between M33 and M101 among my Sc. The exceptional cases of patchy condensation and conspicuous deviation from simple logarithmic spirals are difficult to detect in the cases of extremely small or only slightly inclined objects. Might not these features of the larger and more highly inclined nebulae find their place in notes? I feel that these features, criteria, significant as they may be, would be applicable to a much smaller number of objects than the broad and admittedly vaguer features I mentioned.

Fig. 1 The first page of a handwritten letter by Edwin Hubble to master morphologist Mr John Henry Reynolds in Britain. (From the archives of the Royal Astronomical Society of London)

The classification criteria for the Hubble system are threefold: firstly, the size of the central bulge compared to the flattened disk; secondly, the degree of openness or tightness of the spiral arms, and finally, the degree to which the eye can discern newly-born stars contained in clouds of ionized hydrogen gas. In general, Sa galaxies have large bulges, tightly wound spiral arms which are relatively smooth. In contrast, the bulges of Sc galaxies are invariably much smaller or even minute, as to appear point-like as a star ("semi-stellar"); Sc galaxies spawn wide open spiral arm patterns, knotted with newly born stars flooding their environs with energetic ultraviolet photons of light. Galaxies of type a were spoken of by Hubble as "early-type"; those of type c, "late-type".

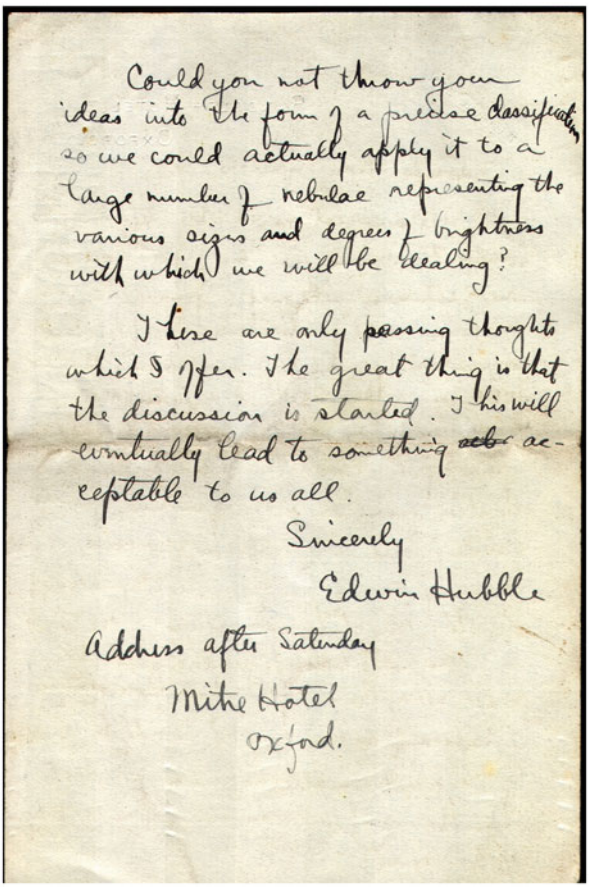
Could you not throw your ideas into the form of a precise classification so we could actually apply it to a large number of nebulae representing the various signs and degrees of brightness with which we will be dealing?

These are only passing thoughts which I offer. The great thing is that the discussion is started. This will eventually lead to something ~~ac~~ acceptable to us all.

Sincerely
Edwin Hubble

Address after Saturday
Mitre Hotel
Oxford.

Fig. 2 The second page of a handwritten letter by Edwin Hubble to Mr John Henry Reynolds. The first sentence at top reads: " Could you not throw your ideas into the form of a precise classification so we could actually apply it to a large number of nebulae . . .?" (From the archives of the Royal Astronomical Society of London)

3 On the Detective Trail

We followed some intriguing historical leads, by traveling to the United States and to the United Kingdom, and our findings below are based on our detailed readings of archival material at the Lowell Observatory in Arizona and the Royal Astronomical Society's archives at Burlington House in London.

The history of the International Astronomical Union's Commission on Nebulae and Star Clusters (Commission Number 28) spanning the period 1922–1925 is particularly rich and archival material is on file both in Arizona and London. Slipher, then acting director at Lowell Observatory, was the president of the Commission during those years. Commission members were the first to have an opportunity to study and react to Hubble's studies on the nebulae and their shapes. In the period 1922–1925, Commission 28 members included Slipher, Hubble, Curtis, W. H. Wright (Lick Observatory), S. I. Bailey (Harvard College Observatory), the venerable Irish astronomer J. L. E. Dreyer and France's G. Bigourdan, the Commission's

first president from 1919 to 1922. Also on the Commission was England's Mr J. H. Reynolds.

Herein lies a truly riveting story, in its own right.

The membership of the Commission clearly reads like a who's-who, containing the names of some truly great and pioneering astronomers. But Mr. Reynolds (1874–1949) was not an astronomer by profession, at all. Here was someone whose official occupation lay completely outside the scientific arena. He was the son of a subsequent Lord Mayor of Birmingham, whose company was a major producer and supplier of metal products in Birmingham. The company John Reynolds & Sons (Birmingham) Ltd was famous for its production of cut-nails (as opposed to hand-forged nails).

We conducted a fascinating telephone interview with Mr. Dennis Stamps, a retired director of John Reynolds & Sons, who together with his wife has a considerable knowledge of the Reynolds family history. Mr. Stamps recalls that the production of nails then was an enormously labour intensive process; cut nail factories employed operators and attendants for each machine, and the noise in those factories was deafening. The production of nails was a practice not restricted to only the lower classes. In fact, Thomas Jefferson (President of the United States in the period 1801-1809) was proud of his hand made nails. In a letter he once said: "In our private pursuits it is a great advantage that every honest employment is deemed honorable. I am myself a nail maker." From president downwards, nail making in those days was an very important facet of life. In fact, Jefferson was among the first to purchase the newly invented nail-cutting machine in 1796 and to produce nails for sale. In pre-1850 America, nails were exceedingly scarce; it is said that people would burn old buildings to sift through the ashes for nails. John Reynolds, born in 1874, clearly had a great financial enterprise at hand from his father's company in England which produced cut nails in enormous numbers. Cut nails dominated the marketplace from about 1820 until 1910, signaling the advent of the modern wire nail.

John Reynolds (Fig. 3) became a highly successful and wealthy industrialist. Reynolds purchased a 30-in mirror made by astronomer Andrew Ainslie Common for the sum of 80 £, and he was instrumental in the design of a 30-in reflector telescope which subsequently was transported to Helwan in Egypt. It was the first large telescope to study objects lying well into the southern skies. The 30-in Reynolds reflector at Helwan saw 'first light' in the year 1907, when the first photographs from that telescope were secured.

In the interim, John Reynolds decided to erect his own observatory at Harborne, by making a mirror of 28-in diameter with his own hands. No mean feat—a mammoth task indeed, for any amateur astronomer today! The telescope at his home "Low Wood" was obviously cumbersome to use, with Reynolds having to work from a heavy observing platform at the upper Newtonian focus of the tube. The 30-in Common mirror at the Helwan Observatory was eventually upgraded and replaced, and the Common mirror made its way back from Helwan to Birmingham. Reynolds decided to replace his 28-in mirror with the slightly larger mirror made by Andrew Common.

Reynolds was a man with a very generous spirit, and when light pollution in Birmingham became increasingly problematic, he decided to donate the instrument

Fig. 3 The starry messenger from Birmingham, the amateur astronomer Mr John Henry Reynolds, who rose to position of President of the Royal Astronomical Society of London. Mr Reynolds was approached by Edwin Hubble to throw his ideas into developing a galaxy classification system, which Reynolds published in 1920. Hubble studied that paper by Reynolds meticulously, and wrote annotations in the margin, including 'Sa, Sb and Sc' alongside the classification bins of Reynolds. Reynolds was without equal: undoubtedly one of the world's most profound thinkers regarding the classification of nebulae (galaxies). (From the archives of the Royal Astronomical Society of London)

to the Commonwealth Solar Observatory—later to become the Mount Stromlo and Siding Spring Observatories in Canberra, Australia. A steel dome of diameter 26-ft was constructed to house the telescope and until the 1950s, this telescope was one of the largest operational telescopes in the Southern Hemisphere.

Here follow some personal reflections by one of us (Ken) upon using the Reynolds telescope to secure photographs:

"The Reynolds telescope was refurbished in 1971 and emerged as a modern instrument. But when I arrived at Mount Stromlo in 1967, the telescope was still in its original state. The photographic camera at the Newtonian focus, situated at the top of the telescope tube, was just as it was in the 1950's when Gerard de Vaucouleurs made his pioneering observations of southern galaxies. I used the camera to take photographs of nearby galaxies in order to measure profiles of their brightness".

Determining the brightness of features on photographic plates is a rather messy and imprecise art. The efficiency with which the older emulsions on photographic glass plates stored photons was not high and we had to soak the plates of glass in nitrogen gas to increase their sensitivity. Even with the relatively fast f/4 focal ratio of the Newtonian focus, long exposure times were needed to acquire photographs with a good tonal range.

After the photographic plate was exposed and carefully developed by hand, the distribution of densities of light within the galaxy image could be measured using an instrument known as a microdensitometer, and it was at that point that the real analysis began.

It is fitting to remember that the man after whom the telescope is named "John Reynolds" had conducted his pioneering measurements of light profiles from photographic plates way back in 1913, using essentially the same telescope configuration at his "Low Wood" observatory, before that telescope was donated to Mt. Stromlo.

Acquiring a good photograph was an adventure. Those were eyeball days. Some words of clarification. In today's modern era, astronomers track stars as the earth rotates, by means of autoguiders. An autoguider can keep a telescope locked on to a bright star for hours.

Not so easy, guiding the telescope by eye.

To access the camera at the top end of the Reynolds telescope, the observer was perched on a rickety 2-m wooden stepladder which the observer had to drag around the dome as the telescope tracked across the sky. The camera itself comprised a microscope and photographic plate-holder mounted on a structure that could be moved in two directions.

The observer first pointed the telescope at a desired galaxy and then moved the microscope around to find a guide star (in other words, a star which the telescope would remain fixed on, as the earth rotates). Then the exposure would begin.

The telescope mechanism was far from perfect and constant adjustment was essential. For two or three hours, the observer would keep an eye glued to the microscope and both hands on the adjustment screws that moved the plate holder. If the guide star drifted as the telescope tracked across the sky, the observer moved the plate holder to keep the star central in the microscope. Each hour, the observer had to close the shutter, climb down from the ladder and manually rewind the main gear drive. The goal of every observation was to produce a guided photograph of the galaxy with perfectly round stellar images.

Each exposure was a battle between the observer and the old worn-out telescope gears, with the observer visually guiding the plateholder through the microscope, as the telescope tracked erratically across the sky.

Although the photographic process was notoriously unpredictable, an amazing amount of semi-quantitative astronomy was accomplished. There were some failures but everything mostly worked out well. We all had to develop photographic skills, because we had no other panoramic detectors until the early 1980s when the first of the digital charge coupled devices (CCDs) became available.

Data acquisition and analysis then became much easier and a new era of quantitative astronomy began. I was not sorry to see the end of photography in astronomy, although I know my co-author David deeply feels otherwise!"

John Hart, Head of the Opto-Mechanical Engineering Section at the Mount Stromlo Observatory, recalls that the Reynolds telescope "was very antiquated with decorative holes in a spherically shaped counterweight at the back of the mirror cell. We replaced many parts (during 1969 –1971) and re-machined the base and the centre section of the tube. Design and construction progressed in parallel. The existing mirror was fitted into a new mirror cell. I was a very new engineer at the time and was overawed by the responsibility of the job, which took a couple of years in total. I was in charge of the entire refurbishment. I was the only designer and had about six laboratory craftsmen in the workshop. Among the astronomers I met who used the

Reynolds telescope were Gerry Kron, Ben Gascoigne and Allan Sandage. Sandage only used the Reynolds telescope a couple of times but seemed very happy with it."

In his later years, Ben Gascoigne reminded us that he was allocated nine months of observing time on the 30-in Reynolds telescope in the early 1950s. He recalled his chilly experiences as follows:

"Time was when you worked alone, the telescope all to yourself, in the total dark, and in winter-time slowly freezing to death. But no matter how cold it had been, how difficult, or how successful for that matter, it always ended, dawn came along and you walked home, the sky all pink in the east, the birds tuning up for the day ahead, and just for a little while the world belonged to you. Nothing else I have known was quite like it, and only astronomers have experienced it."

The Reynolds telescope was used by some of the world's foremost galaxy experts of the era, including the late Gerard de Vaucouleurs. Between 1952 and 1955, de Vaucouleurs secured about 250 1-hour exposures of galaxies in the southern skies from Mt. Stromlo. The generosity of John Reynolds was indirectly crucial to the development of the galaxy classification criteria developed by Gerard de Vaucouleurs, as is clearly evident in *Memoirs of the Commonwealth Observatory* No. 13, published in July 1956.

The seeds of the de Vaucouleurs classification system were clearly born, in part, using the scores of galaxy photographs which Gerard de Vaucouleurs painstakingly secured in Canberra with the 30-inch Reynolds reflecting telescope.

4 Hubble and Reynolds: A Timeline

Reynolds was an individual with enormous vision, and Hubble recognized this. It would be no over-statement to say he was England's foremost observational expert on the morphology of the nebulae, but the letters between Hubble and Reynolds have (for decades) been in the archives.

Here is a timeline:

1920: Hubble publishes his PhD thesis.

1920: Hubble has not devised a classification scheme of his own.

1920: Mr John Reynolds publishes his classification.

Hubble's actual letter from Oxford (Figs. 1 and 2) is undated, but we know that Mr. Reynolds rose to the occasion in 1920. Six years prior to Hubble publishing his classification scheme in 1926, Reynolds devised seven bins or classes pertaining to the shapes of galaxies, which was published in volume 80 of the Monthly Notices of the Royal Astronomical Society.

Of these Reynolds classes, Sandage comments:

> Reynolds types I through VII are clearly identical with the Hubble spiral types Sa, Sb, early Sc, and later Sc. The correspondence is one-to-one.

Sandage recognizes that while Hubble has three spiral types a, b and c, the type c bin spans a wide range of shapes, which Reynolds had taken full cognizance of, by proposing his classes I to VII.

The question before us is therefore, was Hubble aware of the classification scheme devised by Mr. Reynolds in 1920, prior to publishing his seminal classification paper in 1926? The answer is a resounding—yes!

In the Reynolds archives housed at the Royal Astronomical Society, Burlington House, we found a copy of a memo from Hubble, dated July 1923, sent to Vesto Slipher as president of Commission 28. Slipher distributed the memo to members of the Commission. The front page of the memo contains the signature of J. H. Reynolds. In that unpublished memo, entitled "The Classification of Nebulae", Hubble writes to Slipher:

> The published suggestions of J. H. Reynolds are thoroughly sound . . . Reynolds introduced the term amorphous, emphasizing the unresolvable character of much of the nebulosity in non-galactic objects . . . Reynolds (ref. 17) has formulated seven classes of true spirals . . . the first five classes represent a series with increasing degree of condensation in the amorphous matrix of the outer arms.

Reference 17 in Hubble's 1923 memo is none other than the paper of Reynolds, contained in volume 80 of the Monthly Notices of the Royal Astronomical Society. It is abundantly clear that Hubble was fully aware of, and had very carefully studied, the classification scheme of Reynolds proposed in 1920. Although fully referenced in the 1923 memo to Slipher, Hubble moves on to publish his 1926 classification without *any reference* to the source of his classification bins—the classes of Mr J. H. Reynolds.

5 Partial Erasing Is Dangerous

Our conclusions are corroborated by a remarkable historical discovery made by Dr Allan Sandage in Pasadena:

> Remarkably, in the bound Volume 80 of the Monthly Notices that is in the Mount Wilson Observatory library in Pasadena, there are penciled notes in Hubble's handwriting in the margin of page 746 of the 1920 Reynolds paper placed beside the descriptions by Reynolds of his binning classes. Next to each of Reynolds class II, III and IV are the Sa, Sb and Sc notations penciled in by Hubble. Also in the margin is a penciled paragraph of notes. However, much of what is there has been erased, so that although one cannot read the notes, Hubble's Sa, Sb and Sc notations are there. (italics, ours).

While these penciled notes are undated, the 1923 memo by Hubble (a copy of which was sent to Reynolds and which was signed by Reynolds) lays to rest a historical uncertainty unanswered up to the present time— we can definitively say that Hubble had carefully read the Reynolds (1920) paper prior to writing his seminal 1926 work.

It remains a total mystery as to why Hubble makes no mention of the Reynolds classes in his preliminary classification discussion in 1922 or in his definitive 1926 paper; how amazing, in hindsight, to study the handwritten request of Hubble to Reynolds, to "throw your ideas into the form of a precise classification" . . .

The kernel of the system by which astronomers continue to optically classify galaxies today was conceived in the mind of one of Britain's most gifted amateur

astronomers—a man without any formal astronomical training—the great Mr. J. H. Reynolds of Birmingham.

To be immortalized in the minds of students of astronomy, Hubble needed a diagram to depict his classification classes, but in 1926 he did not have one.

6 Hubble Without a Tuning Fork

As explained by Allan Sandage:

"In the dry academic language of formal science, and with so few working extragalactic astronomers at the time (perhaps only 20 worldwide), without such a diagram there was the danger that the classification system, buried in the language of the Astrophysical Journal, might lay fallow. Why did the diagram become so overwhelmingly important? Despite the excellence of Hubble's 1926 word descriptions of the classification, the diagram is much easier to understand and to remember. It became the visual mnemonic. Indeed, we all learned to classify from it. Only later did we read the verbal descriptions in the 1926 fundamental paper. That was true in my generation. It is true now."

Hubble (1926) has no tuning fork diagram—from whence its origin? The British mathematical-physicist Sir James Jeans (1877–1946), one of the great popularisers of science of his time and a prolific author of popular books, such as "The Universe around Us" (1929), "The Mysterious Universe" (1930) and "The Growth of Physical Science" (1947), came to the rescue. To unravel the interplay between the works of Hubble and of Jeans, we purchased Jeans' books "Astronomy and Cosmogony" as well as "Science and Music." Jeans loved music, and he presented the first tuning fork diagram in 1929 (Fig. 4), seven 7 years before 'Realm of the Nebulae' appeared in print. In chapter XIII of "Astronomy and Cosmogony", Jeans argues that a Y-shaped diagram would be appropriate to graphically represent the classifications suggested by Hubble in 1926.

Hubble publishes the Jeans fork in "The Realm of the Nebulae" in 1936, without any reference to the top panel in Fig. 4.

Hubble very carefully "failed" to acknowledge two of his pivotal sources (Reynolds—Fig. 1—and the schematic by Jeans—Fig. 4) which now bear the name of the Hubble classification and the Hubble tuning fork. As agreed by Allan Sandage, the graphical representation of the Hubble tuning fork must be attributed to Sir James Jeans—a scientist who adored music, and who wrote a famous book "Science and Music", as noted above.

On April 22 1928, Curtis decided to bow-out. He wrote to Slipher:

"My own views as to any nebular classification are so at variance with those of many others who are now more actively engaged in actual work in this field that I think you had better simply 'count me out', and put it down, one member of the Committee dissenting, or something like that." A request to step out of the competition, from the very person who first recognized the bar phenomenon in his phi-type galaxy. In the mind of Hubble, he was the Emperor and custodian of morphological astronomy.

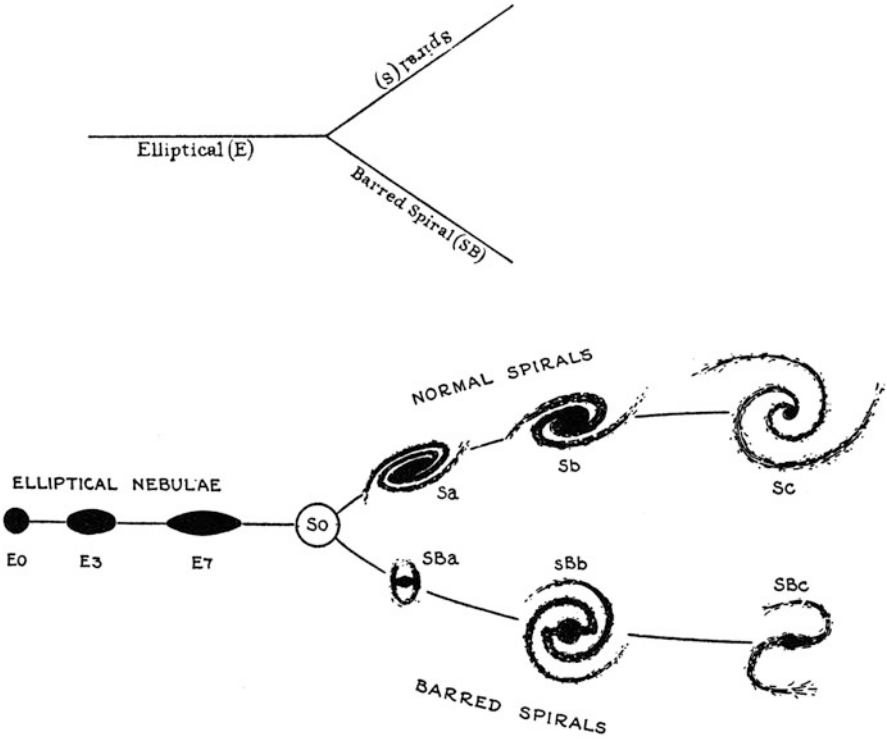

Fig. 4 At top is the tuning fork of Sir James Jeans (1929), rotated by ninety degrees. In 1936, Hubble used the Jeans fork in his book "Realm of the Nebulae"—as illustrated in the lower schematic. Hubble provides no reference to the upper Y-shaped diagram first drawn by Jeans in 1929.

Others, such as Knut Lundmark, presented similar (but not identical) classification schemes, but these were not published in the main-stream journals, and Hubble closely guarded his morphological terrain, *very* closely.

Sandage elaborates:

"[Hubble] guarded its priority in a revealing footnote in part I of his 1926 paper. There he comments on a classification system proposed at about the same time by Lundmark (1926, 1927). Some of Hubble's complaints, which he rarely made public, were unfounded, showing a sensitivity he generally kept hidden. Some of Hubble's accusations are addressed in a partially justifiably acerbic reply by Lundmark (1927), also in a footnote, in Lundmark's near great but largely neglected paper."

A portion of Lundmark's reply, contained in his 'Studies of Anagalactic Nebulae' presented to the Royal Society of Science of Uppsala on May 6, 1927, reads as follows:

"In his paper, E. P. Hubble makes an attack on me which is written in such a tone that I hesitate to give any answer at all . . . I was not then a member of the Commission

of Nebulae. I did not have any access whatsoever to the memorandum or to other writings of E. P. Hubble ... Hubble's statement that my classification except for nomenclature is practically identical with the one submitted by him is not correct. Hubble classifies his subgroups according to eccentricity [sic] or form of the spirals or degree of development while I use the degree of concentration towards the centre ... As to the three main groups, elliptical, spiral and magellanic nebulae it may be of interest to note that the two first are slightly older than Hubble and myself. The term elliptical nebulae thus is used by Alexander in 1852 and the term spiral by Rosse in 1845. The importance of the magellanic group has been pointed out by myself [Observatory, volume 47, page 277, 1924] earlier than by Hubble. As to Hubble's way of acknowledging his predecessors I have no reason to enter upon this question here."

Hubble was deeply inspired by the work of Reynolds. We have already discussed one of these at length: the Reynolds classification classes for spiral galaxies, published in 1920.

7 Hubble's Strategy Exposed by Lundmark

Let us stress the kernel of our detective trail, by highlighting one sentence above:

"As to Hubble's way of acknowledging his predecessors I have no reason to enter upon this question here."

The strategy repeats itself below ...

8 The Reynolds Luminosity Profile

A second story ...

In 1913, Mr. Reynolds pioneered the measurement of the profiles of light across the bulges of spiral galaxies, beginning his investigation with the Andromeda Spiral Galaxy.

Reynolds had secured photographs of the Andromeda Galaxy with his 28-inch reflector at 'Low Wood' in October 1912, and then measured the profile of light across its highly prominent bulge.

Using an instrument known as a photomicrometer, supplied by Toepfer of Potsdam, Reynolds found that the light brightness decayed from the centre, outward. Sandage calls this "the famous Reynolds profile" and notes that "Hubble (1930) later generalized [it] by making it scale free [dimensionless]." Today astronomers speak only of the Hubble luminosity profile—but why not the Reynolds (or, at least, the Reynolds-Hubble) luminosity profile? After all, it was Mr. John Reynolds who pioneered that work in 1913. In this regard, Allan Sandage was most emphatic to one of us (David), during a telephonic discussion: the *Hubble luminosity profile* should be called the *Reynolds' luminosity profile*.

Hubble to Reynolds:

"I find myself thinking along with you and *constantly following up suggestions which arise from your papers* . . . I brought along . . . a paper, ready for publication, on the distribution of luminosity in the images of non-galactic nebulae . . . This last follows up *your pioneer work on the Andromeda and other spirals* . . ." (Italics, ours). Constantly following up suggestions from the papers of Reynolds? No sense of precisely how fundamental Reynolds was to Hubble in "The Realm of the Nebulae", where the source of the luminosity profile (Reynolds 1913) is not referenced.

Mr. Reynolds was elected a Fellow of the Royal Astronomical Society of London in 1899 (at age 25), served as Treasurer in 1929–1935 and President during the period 1935–1937. Mr. Reynolds is one of the only persons ever to rise to the rank of President of the Royal Astronomical Society, whose official occupation was not an astronomer. Reynolds was among the last of the great amateur scientists. His technical skills in using photographic plates for quantitative intensity measurements were unsurpassed for the time and his vision has influenced generations.

In popular astronomical textbooks, we only read of the *Hubble* classification classes, the *Hubble* tuning fork and the *Hubble* luminosity profile for elliptical galaxies.

Behind the stage loomed the giant Mr. Reynolds, a man whose name is almost unknown to students of astronomy.

As fundamental as the Hertzsprung-Russell diagram is to stellar astronomy, so the "Hubble" tuning-fork has become a Rosetta stone in the classification of galaxies.

Astronomy textbooks will not change; the *Hubble classification scheme* and the *Hubble tuning fork* will continue to be taught to students worldwide; but may it be a source of much inspiration to younger readers that some of the grandest of ideas in the area of galaxy morphology did not spring forth from a professional astronomer trained at one of the world's prestigious Universities, but rather from the mind of Mr. John Henry Reynolds —a student of the heavens above—a gifted amateur who simply was passionate about the wonders to behold in the Night Sky, and who devoted a large sector of his energies and finances to spearheading new cosmic horizons.

Were Reynolds and Jeans the only astronomers to be sidelined (not referenced) by Hubble? No. Two immediate names spring to mind: Vesto Slipher and Georges Lemaître. Glaringly absent in Hubble (1929) are all references as to where Hubble sourced almost all of his radial velocity data: from V.M. Slipher of Lowell. For the 22 velocities in Hubble (1929), he gives references for only four of them (NGC 6822, 221, 224, 5457) which Hubble credits to his assistant Humason. What about the source for the majority of 18?

Slipher's name: buried in the sands of time, by Hubble (1929). The strategy of Hubble had succeeded in a scintillating fashion, yet again.

It of course was Lemaître who first determined the rate of expansion of the universe (e.g., Kragh and Smith 2003), two years prior to Hubble (1929); see Fig. 5. Could it perhaps be true, that Hubble never knew about Lemaître's paper (published in French) prior to "The Realm of the Nebulae" in 1936? We have in our possession a book "The Expanding Universe" (published in 1933) authored by Sir Arthur Eddington – and which is inscribed by Hubble himself (Fig. 6). The date of Hubble's handwritten inscription is February 1934.

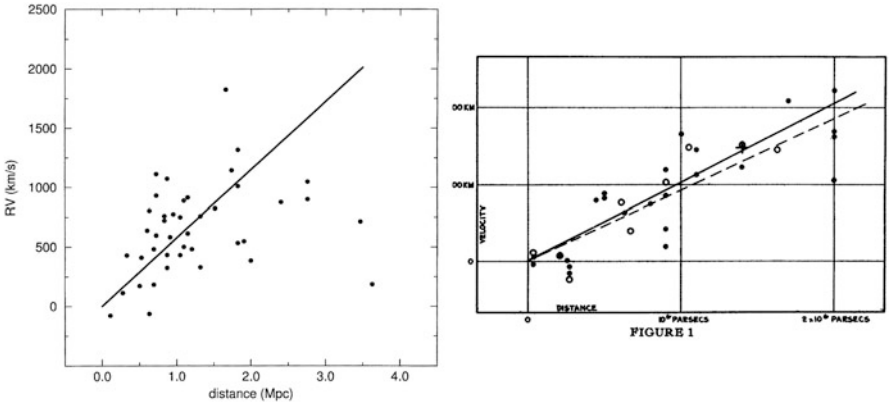

Fig. 5 *Left hand panel*: The data used by Lemaître (1927) to yield the first empirical value of the rate of expansion of the Universe in which v/r is predicted to be constant (see Eq. 24 in his paper. Lemaître derived values of 625 km/s/Mpc and 575 km/s/Mpc. The solid line at left has a slope of 575 km/s/Mpc and is reconstructed by H. Duerbeck. Right hand panel: The radial velocity—distance diagram published by Hubble, 2 years later, in 1929, with a "best slope" of 530 km/s/Mpc. (Left hand panel: courtesy H. Duerbeck).

In that book "The Expanding Universe", Eddington cites Lemaître six times, and Hubble twice. Eddington gives full credit to Georges Lemaître as the first one to fuse relativistic theory with astronomical observations:

"The deliberate investigation of non-static solutions was carried out by A. Friedmann in 1922. His solutions were rediscovered in 1927 by Abbé G. Lemaître, *who brilliantly developed the astronomical theory resulting therefrom . . .*" (italics, ours)

"During a visit to Cambridge, Albert Einstein stayed with Arthur Stanley Eddington and his sister Winifred. For Einstein it was an opportunity to be updated on cosmological matters. On Friday, 10 January 1930, Eddington had attended a lecture by Willem de Sitter, who, in a meeting of the Royal Astronomical Society, had talked about Hubble's observationally found linear relationship between the radial velocities of distant spiral nebulae and their distances (Hubble 1929). Neither de Sitter nor Eddington could provide a theoretical explanation, although both agreed that it had to be the consequence of some cosmological manifestation. The discussion of the two scientists was published in The Observatory (February 1930), whereupon George Lemaître sent them his publication of 1927. There he had shown that redshifts were the signature of an expanding universe, and that such redshifts depended linearly on the nebular distances (Lemaître 1927). Both, Eddington as well as de Sitter, immediately accepted Lemaître's theory of a dynamic universe; they published their opinion in March and May 1930." (Nussbaumer, in press).

Although Eddington (1933) well understood who discovered the expanding universe, credit (for whatever reason) now rests Hubble. As clearly emphasized in Hubble's book "Observational Approach to Cosmology" published in 1937, Hubble himself was in favour of a stationary universe: *"On the other hand, if the recession factor is dropped, if red-shifts are not principally velocity shifts, the picture is simple*

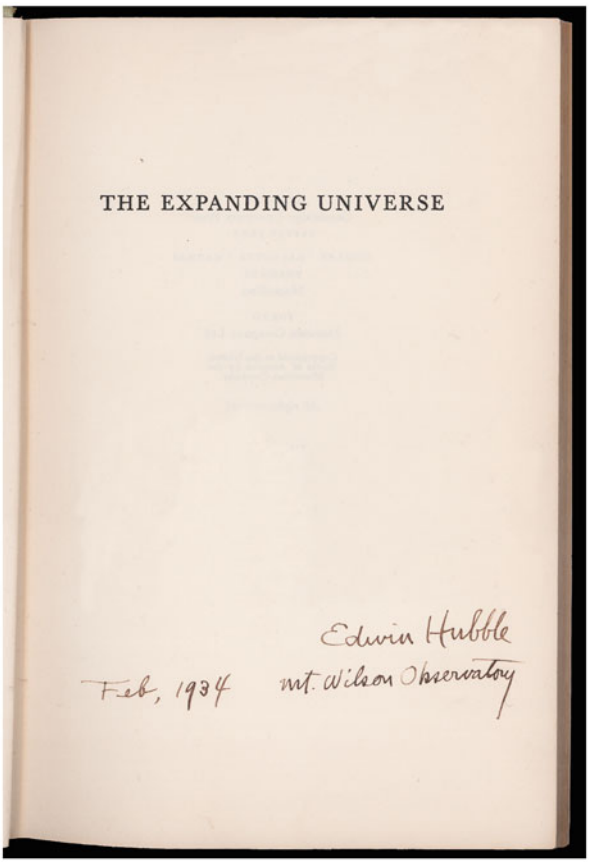

Fig. 6 A book signed by Edwin Hubble, dated 1934. The book, entitled "The Expanding Universe" was authored by Sir Arthur Eddington in 1933. Eddington (unlike Hubble) was very meticulous in his referencing: Eddington cites Lemaître six times, and Hubble twice. Already in 1923, Eddington included Slipher's redshifts in his "Mathematical Theory of Relativity"

and plausible" and *"Observations at the moment seem to favour one picture [the stationary universe], but they do not rule out the other [redshifts being velocity shifts]."* (Words in square brackets: ours). The point we do wish to highlight is this: Hubble was fiercely territorial about the (radial velocity, distance) graph. Fiercely territorial indeed: "*. . . I consider the velocity-distance relation, its formulation, testing and confirmation, as a Mount Wilson contribution and I am deeply concerned in its recognition as such.*" (A letter from Hubble to de Sitter, dated 21 August 1930). The territorial strategy spills over in the referencing style for the redshifts: Slipher is not referenced in Hubble (1929), at all.

In the index of "The Realm of the Nebulae" (1936) one alphabetically finds the names of many astronomers, from Baade, Walter to Reynolds, John to Zwicky, Fritz. Generally, as footnotes. But the focus are the achievements of Hubble. No mention of Reynolds (1920). The reader is blissfully unaware of the masterful eclipsing of the classification of Reynolds (1920), by Hubble. The game is on. The outcome: very serious. Hubble knows this. Hubble, as Emperor of the Nebulae, also knew precisely how to write glowing letters to some colleagues, whom he would intentionally

eclipse. We see this in "The Realm"—Hubble does makes mention of a short paper by Reynolds, published in *The Observatory*, in 1927, but what about the seeds for the Hubble classification scheme? *Would it not have been honorable for Hubble to inform the world that he (Hubble) had approached Reynolds to actually devise a classification scheme* (Figs. 1 and 2)*—one which now universally carries Hubble's name only?*

An accurate timeline is provided by van den Bergh (2011):

> 1927: Lemaître derives the expansion rate of the Universe and explains its expansion in terms of the general theory of relativity.
> 1929: Hubble repeats Lemaître's work with essentially the same data and obtains similar results.

A delightful read is a book "Discovering the Expanding Universe" co-authored by Nussbaumer and Bieri (2009); the foreword is by Allan Sandage (Fig. 7). Nussbaumer and Bieri emphasize, in no uncertain terms, that "Hubble himself was exceedingly partial in selecting his references. Even in his influential *The Realm of the Nebulae*, published in 1936, he avoided any reference to Lemaître (Hubble 1936). Was he afraid that a gem might fall from his crown if people became aware of Lemaître's pioneering fusion of observation and theory two years before Hubble delivered the confirmation?" Our conjecture, partly based on thoughts by a colleague of Hubble, is that Hubble returned from the IAU General Assembly held in Leiden in 1928, brimming with ideas. The time was ripe for confirming a more accurate (radial-velocity, distance) correlation.

ESO Director General Tim de Zeeuw writes: "The history of science contains examples where the credit did not go to the actual discoverer. This appears to be the case as well for the discovery of the expanding universe." For a detailed historical read, see Block (2012).

In future astronomy books, we would urge authors that a crucial entry should be under L—to honor Lemaître. He first developed the astronomical theory of an expanding universe in 1927, and is now (correctly) regarded as the scientist of one of the greatest discoveries of all time: the Expanding Universe.

The 30-inch Reynolds telescope at Mt. Stromlo was totally destroyed by the bush fires which devastated sections of Canberra in January 2003. But the legacy of Mr. John Henry Reynolds (1874–1949) lives on.

Why Hubble behaved in the manner he did, we will never know. A naked emperor he stands, for all to observe his strategy. How appropriate to cite "The Emperor's New Clothes" (Danish: Kejserens nye Klæder), a short story by Hans Christian Andersen in 1837. Two weavers promise the Emperor a new suit of clothes which are invisible to those unfit for their positions, stupid, or incompetent. When the Emperor parades before his subordinates in his new clothes, a child cries out, "But he isn't wearing anything at all!"

Tragically, Edwin Hubble was a man with a highly opaque mask. Few ever penetrated it.

Fig. 7 Dr Allan Sandage at the Athenaeum in Pasadena, beneath a magnificent painting by S. Seymour Thomas. Standing in the painting is Nobel laureate Robert A. Millikan, flanked by former MIT President Arthur A. Noyes (at *left*) and the astronomer George Ellery Hale (at *right*). Photographed with Allan Sandage is one of the co-authors of this paper (David).

9 Concluding Thoughts: A Poem by Bruce Elmegreen

Time Travel Cop
Bruce Elmegreen

There once was a famous cosmologist
who plotted up galaxies from a list,
his numbers from Slipher
led him to decipher
the code of the Cosmic Chronologist.

But y versus x was the easy part,
we wonder what gave him the early start?
We looked for his patron
and found with Lemaitre
a nearly identical Hubble chart!

He thought about bars all his younger days
but writing was page after empty page.
Then he saw that James Jeans
knew what it all means
and published Sir James' model side-a-ways.

When asked about curls in the galaxies,
he answered with empty apologies.
But Reynolds, he knew,

had ordered them true
(just not in the Realm of the Nebulae . . .).

So listen young ladies and gentlemen,
if stars are your passion and sentiment.
Don't cross David Block,
the time travel cop,
unless you acknowledge your precedent!

10 Postscript

Volume 80 of Monthly Notices of the Royal Astronomical Society, containing Hubble's penciled notes alongside the "highly neglected" 1920 paper by Reynolds is of exceptional historical value and no longer lies in the shelves of the Mount Wilson Observatory library in Pasadena; before he died, Allan Sandage had it removed, for safekeeping. Its value: priceless.

Acknowledgements It is a pleasure to thank our referee, Debbie Elmegreen, for her comments.

References

Block, D.L. 2012, Georges Lemaître and Stigler's Law of Eponomy. Published in "Georges Lemaître: Life, Science and Legacy", Cambridge University Press, 89.
Block, D.L. & Freeman, K.C. 2008, Shrouds of the Night (Springer, New York)
Hubble, E. 1926, Extra-galactic nebulae. ApJ, 64, 321.
Hubble, E. 1929, A relation between distance and radial velocity among extra-galactic nebulae. PNAS, 15, 168.

Kragh, H. & Smith, R.W. 2003, Who discovered the expanding universe? History of Science, 41, 141.
Lemaître, G. 1927, Un univers homogène de masse constante et de rayon croissant, rendant compte de la vitesse radiale des nébuleuses extra-galactiques. Annales de la Société scientifique de Bruxelles, Série A, 47, 49 translated into English in MNRAS, 91, 483.
Lundmark, K. 1927, Studies of Anagalactic Nebulae—First Paper, Nova Acta Regiae Societatis Scientiarum Upsaliensis, Volumen Extra Ordinem Editum, page 1.
Nussbaumer, H. & Bieri, L. 2009, Discovering the Expanding Universe. CUP.
Reynolds, J.H. 1913, The Light Curve of the Andromeda Nebula (N.G.C. 224), MNRAS, 74, 132.
Reynolds, J.H. 1920, Photometric measures of the nuclei of some typical spiral nebulae. MNRAS. 80, 746.
Van den Bergh, S. 2011, The Curious Case of Lemaitre's Equation No. 24. Journal of the Royal Astronomical Society of Canada (in press). Preprint: arXiv: 1106.1195v1.

Lessons From the Milky Way: The Kapteyn Universe

P. C. van der Kruit

Abstract Jacobus Cornelius Kapteyn (1851–1922) presented a model for the distribution of stars in space together with a dynamical interpretation in terms of an equilibrium between the gravitational field of the stars and their random motion and rotation. In the vertical direction Kapteyn's results are substantially correct. Usually the Kapteyn Universe is described as being flawed due to neglect of interstellar absorption. Kapteyn was led to adopt this on the basis of widely accepted evidence by Shapley on an absence of reddening of stars in globular clusters. But another, equally important misconception was Kapteyn's interpretation of the two Star Streams as manifestations of two groups of stars rotating around a center in opposite directions. This was supported by the observation of very different mixes in stellar types in the two streams. Had Kapteyn adopted the absorption as he himself had determined it he would not have been able to arrive at a consistent picture.

1 Introduction

In 1920 Jacobus C. Kapteyn, together with his student and successor Pieter van Rhijn, published his well-known model for the distribution of stars in space, (Kapteyn and van Rhijn 1920), and a year later presented a description of its 'mechanics', providing a consistent explanation of how the system could be in equilibrium by a precise balance between the gravitational force of the stars and their random motions and organized rotation, (Kapteyn 1922). Ten years later the vertical dynamics was proved substantially correct, but in the plane of the Milky Way the discoveries of differential rotation and interstellar extinction had shown the Kapteyn Universe to be completely wrong. Jan Hendrik Oort, who although completing his thesis after his death always considered himself a student of Kapteyn, played a major role in this with his discovery of Galactic rotation and the introduction of the 'Oort constants' in 1928, (Oort 1928) and extended Kapteyn's work in the vertical direction with the 'Oort limit' in 1932, (Oort 1932). Oort obtained his doctorate under van Rhijn

P. C. van der Kruit (✉)
Kapteyn Astronomical Institute, University of Groningen, P.O. Box 800,
9700 Groningen, AV, the Netherlands
e-mail: vdkruit@astro.rug.nl

K. Freeman et al. (eds.), *Lessons from the Local Group,*
DOI 10.1007/978-3-319-10614-4_2

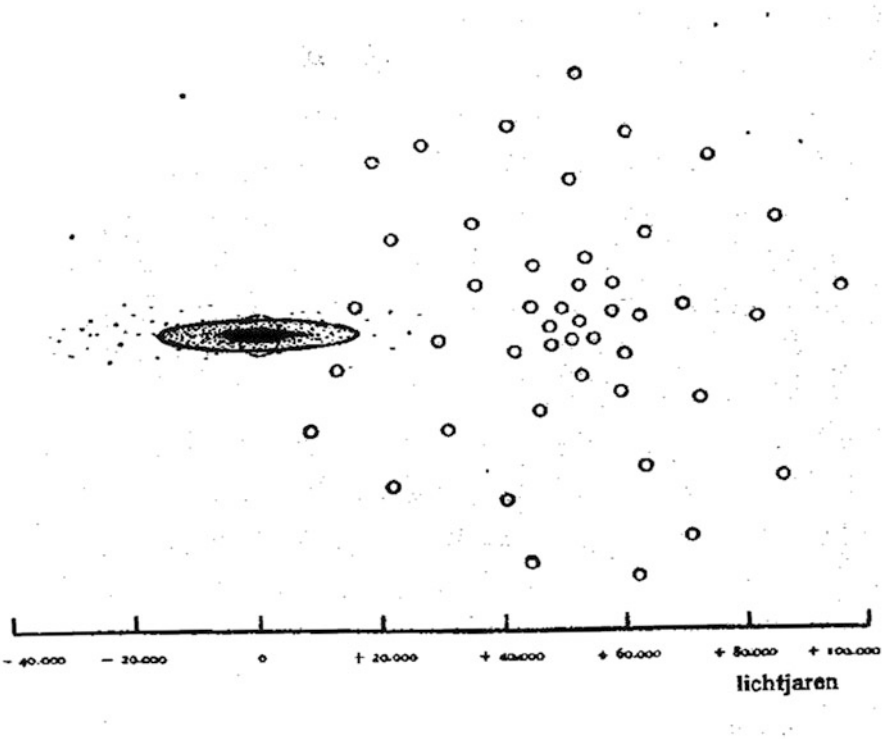

Fig. 1 Oort's illustration of the discrepancy of the Kapteyn Universe and Shapley's system of globular clusters. It appeared in de Sitter's book 'Kosmos'

in May 1926 on a study of stars of high velocity and accepted in November of that year a position as 'privaat-docent' in Leiden with a public lecture on *Non-light emitting matter in the Stellar System*. This was only 4 years after Kapteyn's demise and preceded his discovery of Galactic rotation by almost 2 years. In this lecture, of which I provided a translation in Appendix A of a Legacy volume on Kapteyn, (van der Kruit et al. 2000), he concluded that the 'least contrived' solution to the disparity between Shapley's system of globular clusters and the Kapteyn Universe (Fig. 1) was the assumption of an absorption of light in space. Why had this not been anticipated by Kapteyn? What would have happened had Kapteyn included an absorption correction in his modeling?

2 The Arrangement of Stars in Space

Kapteyn had from his earliest research efforts had an interest in the spatial distribution of stars. Distances were of prime importance to this problem. His inaugural lecture on the occasion of his appointment of professor in Groningen in 1878, had

the title *The parallaxes of the fixed stars*. And early on in his career he did some remarkably accurate measurements of trigonometric parallaxes of stars from differential timing measurements of meridian passages, using the Leiden meridian circle. He had not succeeded in securing funds for his own observatory in Groningen in spite of positive support from his university; Leiden and Utrecht opposed the founding of a third, competing observatory in the Netherlands. The stars in Kapteyn's sample were selected as probably nearby on the basis of large proper motion. It is amazing that he was able to measure parallaxes with this method, since for a distance of 10 pc the effect of the annual parallax on the meridian passage is—depending on declination—a few hundredths of a second of time.

Kapteyn devised a clever method to derive absolute declinations, free from systematic errors due to atmospheric refraction and telescope flexure. For this he only measured differences in zenith angles of two stars that crossed the meridian at about the same time at similar zenith angles on either side of the zenith, azimuths and times of passages through the prime vertical. In 1884, he found David Gill at the Cape Observatory interested in undertaking such a project. Being struck by the possibilities of photographic plates to register star images, Gill decided on the production of the *Cape Photographic Durchmusterung* and lured Kapteyn in offering his services to measure the plates. To do this Kapteyn invented his 'parallactic' method in which a small telescope at the focal distance from the plate could be used to directly read off celestial coordinates on its axes. This experience and his advisory role in the *Carte du Ciel*, caused Kapteyn to undertake extensive photographic work on parallaxes and proper motions, using plates taken for him by Anders Donner of Helsinborg.

He quickly realized that stars were too distant for direct parallax measurements on a grand scale and resolved to use the motion of the Sun with respect to nearby stars (which after all is about four radii of the Earth's orbit per year). To determine the arrangement of stars in space from star counts as a function of apparent magnitude and proper motion, he developed with the help of his mathematics brother Willem the necessary mathematical techniques, making three assumptions. (1) The 'luminosity curve', the distribution of absolute magnitudes, was the same everywhere, (2) there was no preferred direction among the motions of the stars in space, and (3) there was no absorption of starlight.

3 Star Streams

However, around 1902 Kapteyn came to the realization that stars did not move completely randomly, but that there were two preferred directions in space, corresponding to positions, 'vertices', about 100° apart on the sky. When these were corrected for the solar velocity, they were found to be roughly opposite and in the Milky Way (and in agreement with our current understanding, roughly in the direction of the Galactic center and anti-center). To Kapteyn this suggested the existence of two Star Streams. He first announced this in 1904 at a large astronomical congress during the Louisiana Purchase Exhibition in St. Louis, and at the meeting of the British Association in

Cape Town the next year. It was almost instantly accepted, undoubtedly helped by quick confirmation of the results by other astronomers, notably a young Arthur Stanley Eddington, who had just graduated from Cambridge. The two streams moved at a relative velocity, determined from radial velocities, of order 40 km/s.

Considering the evidence and data available, this discovery is one of great skill. And observationally it still stands. However, it did not take long before Karl Schwarzschild came up with what we now to be the correct explanation, namely that of an anisotropic velocity distribution, the directions of the Star Streams corresponding to the long axis of the velocity ellipsoid. Kapteyn was of course aware of this possible explanation, but all his life he believed in his own interpretation of two opposite streams. And he had good reasons for this. Throughout his studies the data available strongly suggested that the composition of the two streams was very different in terms of spectral types of the stars they contained. And Kapteyn was in good company; at the time he made his 'first attempt' to determine the distribution of stars in space, Eddington also favored Kapteyn's interpretation over Schwarzschild's.

4 Selected Areas

What was needed was large samples of stars with well-determined magnitudes and proper motions. This could in principle be turned into mean parallaxes as a function of apparent magnitude and proper motions. Together these could then be used to find the apex of the solar motion and the vertices of the streams. Radial velocities were necessary to find the magnitude of the Sun's velocity in space and spectra the types of stars involved for a determination of the mix of ages. Kapteyn interpreted the Main Sequence as an age sequence, blue stars being young. Trigonometric parallaxes were most welcome. Realizing that one needed to go to faint magnitudes, Kapteyn proposed an concerted effort by many observatories by restricting to small areas (size depending on star surface density on the sky), numbering 206 distributed regularly over the sky, for which of as many stars as possible as many parameters as possible would be observed. It is tribute to Kapteyn's diplomatic skills and international standing that he succeeded in bringing this international coordination about.

Edward Pickering at Harvard executed a Durchmusterung of Selected Areas across the whole sky. He agreed to this only after Kapteyn had extended the Plan to include next to the 'Systematic Plan' a 'Special Plan' proposed by Pickering that concentrated on areas in the Milky Way. Plates taken were sent to Groningen to provide positions and magnitudes. This work resulted in the Harvard-Groningen Durchmusterungs that provided positions and magnitudes down to $m = 16$ or so in all Selected Areas. This was published between 1918 and 1924, and was at least partly available for the Kapteyn and van Rhijn analysis. But that was not deep enough. Crucial to Kapteyn's program was the adoption by George Ellery Hale of the Plan as the prime observational program for his new 60-inch telescope at Mount Wilson. From 1908 onwards plates were taken for all northern Selected Areas (numbers 1 through 139), the result of which only appeared in print in 1930. Even preliminary work with these data could

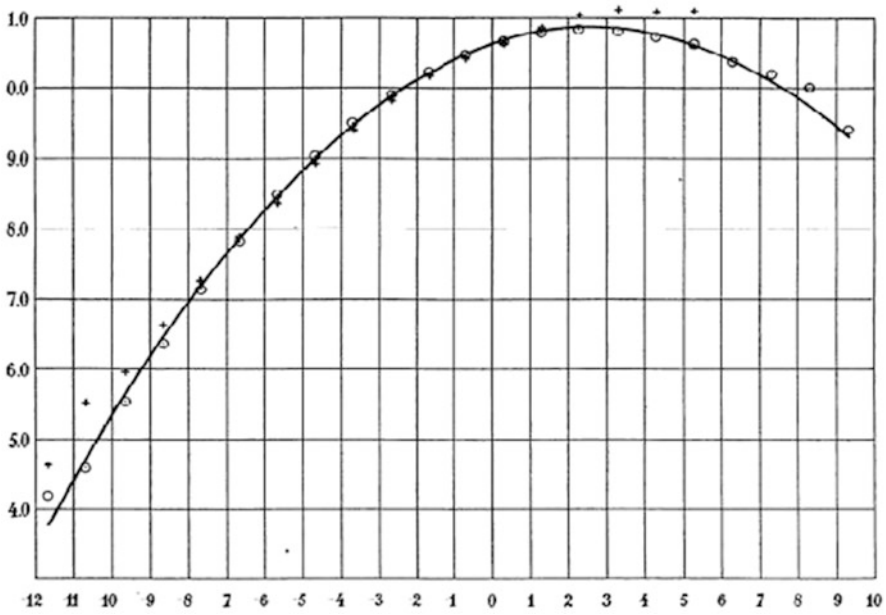

Fig. 2 The 'luminosity curve' derived by Kapteyn & van Rhijn in (Kapteyn J.C. & van Rhijn, P.J., 1920). Because Kapteyn had grudgingly accepted the term parsec, he felt obliged to redefine absolute magnitudes to a distance of 1 pc.

only be performed after Kapteyn's death. Most of the work was done by Frederick Seares or under his direction. Walter Adams used the 60-inch for spectroscopic work, in particular to determine radial velocities.

Hale's adoption of the Plan of Selected Areas for the 60-inch required in his view the personal involvement of Kapteyn and the latter was in 1908, when the telescope became operational, appointed as research associate of the Carnegie Institution. Kapteyn then started to make annual visits to Mount Wilson until World War I prevented him from returning after 1914. He, however, remained research associate until his death.

5 The Kapteyn Universe

The analysis in Kapteyn & van Rhijn (1920), (Kapteyn J.C. & van Rhijn, P.J., 1920), was preliminary. 'Now that, after so many years of preparation, our data seem at last to be sufficient for the purpose, we have been unable to restrain our curiosity and have resolved to carry through completely a small part of the work . . . '. From their data, and average parallaxes of stars as a function of magnitude and proper motion determined by van Rhijn (1920), they constructed a 'luminosity curve', see Fig. 2, which was assumed to be the same everywhere in space.

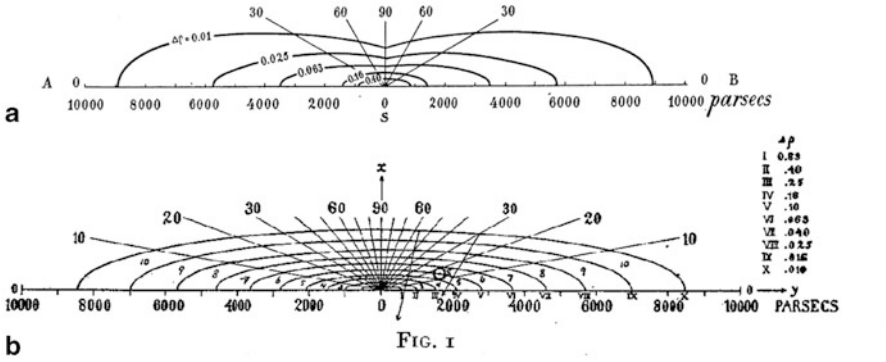

Fig. 3 On top the distributions of stars in space as determined by Kapteyn and van Rhijn 1920. The solution involves a dependence only with distance from the Sun at latitudes 0°, 30°, 60° and 90°. The bottom illustration is from Kapteyn (1922), where he fitted ellipsoids to the densities to facilitate computation of the gravitational potential. His interpretation of the Star Streams as two opposite rotations led him to adopt a position of the Sun 650 pc away from the center and on the basis of Hertzsprung study of the distribution of Cepheids on the sky at 38 pc from the plane. The Sun is at the circle designated 'S'

Using mathematical methods partly developed by Karl Schwarzschild, they solved the counts by transforming these into a density of stars as a function of distance. This process was done for four ranges of latitude, 0°, 30°, 60° and 90°. The (preliminary) solution only fitted to densities as a function of distance from the Sun, so effectively assumed that the Sun was at or close to the symmetry point of the system. The result found by Kapteyn and van Rhijn is in the top picture of Fig. 4.

With this result Kapteyn could do what he long had been preparing for and that was to study the 'mechanics'. He assumed that the system was in equilibrium. In his 1922 paper, (Kapteyn, J.C., 1922), he first assumed that the equi-density surfaces were ellipsoids (see Fig. 3, bottom). He did this so that he could calculate relatively straightforwardly the potential assuming that the star distribution and that of the density of gravitating matter was the same. He used a vertical mean velocity of stars of 10 km/sec (which corresponds to a velocity dispersion of 12 km/sec). In the vertical direction he then found that the system was in equilibrium if the mass of an average star was between 1.4 and 2.2 solar masses. The average measured mass of a binary was 1.6 in these units, so that if all stars were binaries there would be no need to invoke 'dark matter in the Universe'. At least, 'this mass cannot be excessive'. This is a first application of what we now call stellar or galactic dynamics. In modern terms, using the isothermal sheet description of van der Kruit & Searle (1981), Kapteyn's density distribution is fitted pretty well with $z_\circ = 650$ pc, rather close to the 700 pc or so we currently use. His velocity dispersion is a bit low compared to the modern 17 km/sec or so.

For the horizontal direction, equilibrium could only be achieved if there were some rotation. To Kapteyn it seemed natural that this was the phenomenon of his Star Streams; about half the stars rotating in one direction and the other in the opposite

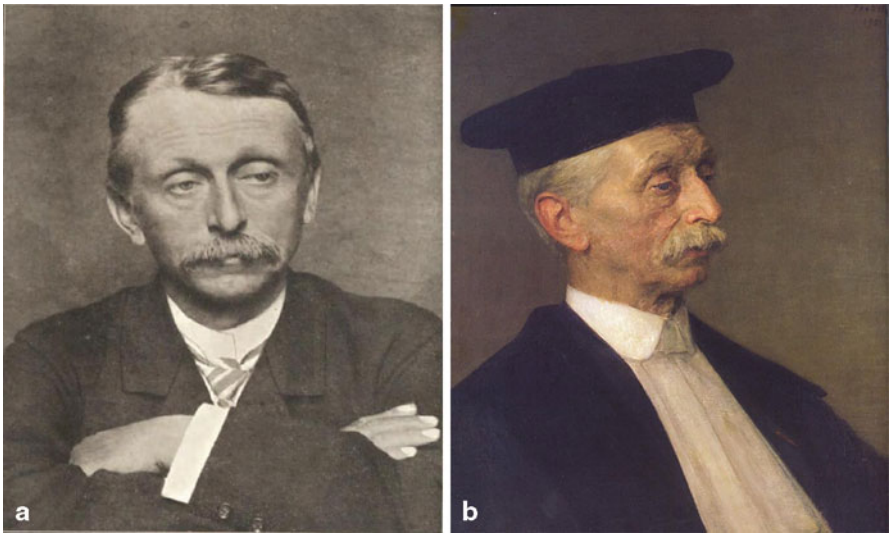

Fig. 4 Jacobus Cornelius Kapteyn (1851–1922) at age 40 and 70.

one. The direction towards the (rotation) center would be perpendicular to the streams and could then be in only two directions, one of which was Carina and indeed there the Milky Way is very bright. The relative velocity was 40 km/s, so it seemed natural to assume that the rotation velocity was 20 km/sec. Indeed, when he estimated what it had to be with the mass densities that he derived from the vertical equilibrium he found 18–20 km/sec! But for this to work, the Sun had to be away from the center. Kapteyn argued that this implied a distance up to 1.5 kpc, but for reasons having to do with details of the solutions in the density distributions he settled for 650 pc. For the vertical displacement he assumed 38 pc, based upon a study of the distribution of Cepheids by his son-in-law Ejnar Hertzsprung. The resulting position of the Sun has been indicated with the 'S' near the small circle in Fig. 3, bottom.

So we see, that the adoption of this model by Kapteyn had also a dynamical basis, partly correct (in the vertical direction), partly incorrect (due to his interpretation of the Star Streams). But it was ingenious and his introduction of a dynamical framework farsighted.

6 Kapteyn's Studies of Absorption

Kapteyn had always worried about absorption. Over his career he wrote four papers on this subject, one in the Astronomical Journal, three in the Astrophysical Journal. In 1903, Pickering (Pickering, E.C., 1903), had found that the star ratio (the ratio of numbers of stars between two consecutive magnitudes) deviated from the 'theoretical' value for a uniform distribution of stars in space. He suggested that there was

significant absorption, amounting in Kapteyn's notation to 0.18 magnitudes per unit distance. Since this unit is the distance corresponding to a parallax of 0″.1, this is an extremely large amount. Moreover, in 1904 George Comstock found that the mean proper motion of stars at a fixed magnitude depended on Galactic latitude (the smallest in the Milky Way), which also would indicate interstellar absorption, (Comstock G.C., 1904). In 1904, Kapteyn (Kapteyn, J.C., 1904), investigated these claims, showing how sensitively a small amount of extinction would change the inferred stellar distributions. He used the slope of the luminosity curve as a fiducial point to link to observed counts and concluded that some absorption indeed was likely. But he objected against the (extremely large) values of Comstock, since these would put the Sun in a very special place, namely near an extreme minimum in the star density.

In 1909 Kapteyn wrote two papers in the Astrophysical Journal on absorption, (Kapteyn, J.C., 1909a), (Kapteyn, J.C., 1909b). There was not much convincing evidence for absorption by gas (in stellar spectra), but he speculated that absorption by dust would result in a reddening of the starlight. He found values corresponding to 0.001 magnitude per parsec in the photographic band (and 0.0005 in the visual), which at present is a bit small but not far off the mark. In a paper in 1914, in which he returned to the issue by reviewing its status at the time, he reaffirmed this but concluded that from observational data it could not be proven that this was not be the result of a correlation of color with absolute magnitude, (Kapteyn, J.C., 1914).

The deciding piece of evidence, however, was Harlow Shapley's result in 1916, (Shapley, H., 1916), that the colors of the stars in the globular cluster M13 (at 10 kpc) should be 2.5 magnitudes redder than they were observed to be if Kapteyn's value for the absorption were adopted. Space was, according to Shapley, transparent. This must have convinced Kapteyn (and with him others) that absorption was only of secondary importance.

Shapley went on to map the distribution of globular clusters and found them to be scattered over a somewhat ellipsoidal volume with the center in the direction of Sagittarius, roughly perpendicular to Kapteyn's center, and at a distance of 20 kpc, see (Shapley, H., 1919 and Fig. 1 therein). Shapley's distance to the center was too large, as we now know, to some extent also as a result of absorption since many clusters are at a somewhat low latitude.

What did Kapteyn himself think of Shapley's result? In one of his last papers, written with van Rhijn in 1922, (Kapteyn, J.C. & van Rhijn, P.J., 1922), it was argued that Shapley's distances were too large because the local calibrating Cepheids of short periods had high proper motions and therefore had to be near and thus fainter than Shapley's variables in the globular clusters. The longer period variables were giving a different result and Kapteyn and van Rhijn argued that this result was inferior. It was supported by work of Kapteyn's student Schouten, who derived distances to globular clusters by adopting the same luminosity curve as locally. This of course ignored the fact that locally many stars are dwarfs, while all stars used in the clusters were giants.

7 What If Kapteyn Had Not Neglected Absorption?

I have been asked this question regularly. Obviously we do not know for sure. Kapteyn presented his model for the Sidereal System less than a year before his death. It was in accord with current knowledge and provided a consistent description. As a conclusion of this contribution I quote from the draft of my soon (later this year) to appear biography *Jacobus Cornelius Kapteyn: Born investigator of the Heavens*, (van der Kruit, P.C, 2014).

Finally, one might wonder what would have happened had Kapteyn adopted interstellar absorption. That would have been much in violation of Shapley's result and Kapteyn would for some reason or the other have had to assume it depended on latitude. He did find values for extinction in his earlier work that in hindsight are not unreasonable, but he derived that from relatively bright stars all over the sky. No latitude dependence was evident, and it seems unlikely that he would have detected any had he looked for it.

Had Kapteyn applied an absorption correction he would have found a significantly flatter vertical profile of star densities, which would have lowered the deduced average mass of a star, destroying the dynamical consistency that he found. Similarly, a much flatter radial density profile would have made the picture of the rotation as revealed by the star streams more problematic. If it would have had a central point of maximum density it would be further away than in the Kapteyn a universe and a rotation speed of 20 km/sec as revealed by the Star Streams would have to be linked to a rotation around a more distant center. As it was, Kapteyn's solution of such a rotation around a center a half to one kiloparsec away dynamically made sense, and it is not obvious that such a picture could be constructed with so small a rotation in an extended stellar system.

So there were at least *two* fundamental issues involved. Kapteyn's Universe was not only false because his assumption of transparent space turned out incorrect, but also his conviction that the star streams did not result from an anisotropy in the random stellar motions was essential for his arriving at a consistent picture. The Kapteyn Universe was built on both pillars and both eventually had to be replaced.

Kapteyn's picture of the Sidereal System was difficult to avoid. Lodewijk Woltjer in (van der Kruit, P.C. & van Berkel 2000) referred to it as 'Kapteyn's unfortunate Universe', on account of 'the unlucky moment at which Kapteyn presented his Universe and to the perhaps somewhat unphysical interpretation he gave to the two 'Star Streams', which had contributed so much to his fame'. It is more uncertain to speculate what would have happened had Kapteyn lived a decade or so longer and would have been around when Galactic differential rotation and interstellar absorption were established.

8 Lessons?

My chapter in (van der Kruit, P.C. & van Berkel 2000) started as follows: "Around 1990 the Kapteyn Astronomical Institute decided to start a preprint series and we chose to display on the covers a picture of Kapteyn. Some of us were told privately

and discretely by a few of our colleagues abroad (mostly in the U.S.) that is was inappropriate to use this picture. After all, Kapteyn had been proven wrong in almost all respects; his work on interstellar absorption was shown to seriously underestimate the effect, while his model of the distribution of stars in space and his description of the kinematics and dynamics in terms of circular motions in two star streams was also incorrect. A consensus among our staff eventually led to the replacement of that picture by a 'more current' one; I regret having not more strongly opposed that then." It was the picture at the right in Fig. 4, and I still do regret this.

Owen Gingerich, in the same volume, wrote: 'For American college students studying introductory astronomy, the chances are about even that they will encounter the name of Kapteyn. The distinguished astronomer of Groningen is mentioned in seven of ten recent textbooks that I examined, always associated with the Kapteyn Universe, and invariably as a foil for Shapley's larger and more modern conception of the Milky Way Galaxy. While the presentation in American textbooks places Kapteyn and Shapley as intellectual rivals and their systems as totally antithetical, the historical reality is much different.'

So, two lesson are: 'Don't take historical introductions in elementary textbooks too seriously. And be warned that your colleagues may very well have done that anyway'.

Acknowledgements I am very grateful to Ken Freeman for presenting the review when, due to family affairs, I had to cancel my participation to the conference at the last minute.

References

Comstock, G.C. (1904), A.J. 24, 43.
Kapteyn, J.C. (1904), A.J. 24, 115.
Kapteyn, J.C. (1909a), Ap.J. 29, 46.
Kapteyn, J.C. (1909b), Ap.J. 30, 284.
Kapteyn, J.C. (1914), Ap.J. 40, 187.
Kapteyn, J.C. (1922), Ap.J. 55, 302.
Kapteyn, J.C. & van Rhijn, P.J. (1920), Ap.J. 52, 23.
Kapteyn, J.C. & van Rhijn, P.J. (1922), B.A.N. 1, 37.
Oort, J.H. (1928), B.A.N. 4, 269.
Oort, J.H. (1932), B.A.N. 6, 249.
Pickering, E.C. (1903), ANn. HAR. 48, 149.
Shapley, H. (1916), Proc. Nat Acad. Sci. 2, 12.
Shapley, H. (1919), Ap.J. 49, 311.
van der Kruit, P.C (2014), *Jacobus Cornelius Kapteyn: Born investigator of the Heavens*, Springer, in preparation.
van der Kruit, P.C. & Searle, L. (1981), A.&A. 95, 105.
van der Kruit, P.C. & van Berkel, K. (2000), *The Legacy of J. C. Kapteyn. Studies on Kapteyn and the development of modern astronomy*, Springer, ISBN 0-7923-6393-0.
van Rhijn, P.J. (1920), Publ. Astron. Lab. Groningen, 30.

The Galactic Bulge

Ken C. Freeman

Abstract I will give a brief overview of galactic bulges and then discuss in more detail what is known about the bulge of our Galaxy. The Milky Way has a small boxy/peanut-shaped bulge which we believe formed via instabilities of the disk rather than through mergers. The bulge of the Milky Way therefore appears to be a dynamical product of the early Galactic disk, without significant contamination from mergers with other galaxies. The instabilities are believed to have occurred about 2 Gyr after the inner stellar disk was formed. The bulge therefore contains a relatively clean sample of the early disk as it was about 8 Gyr ago, trapped dynamically within the boxy bulge structure. The various components of the early disk (young thin disk, older thin disk, thick disk) are visible as substructure in the stellar metallicity distribution function and kinematics of the bulge stars.

1 Introduction

Galactic bulges are not an essential part of the formation process of disk galaxies, but when they do occur they can give some useful insights into the early evolution of their parent galaxies. The size of galactic bulges varies greatly from galaxy to galaxy, from vanishingly small to much more luminous than the disks of their parent galaxy (as in the Sombrero galaxy NGC 4594). Galaxies with relatively large circular velocities can have small bulges, as in the Milky Way. Such galaxies are not rare. Kormendy et al. (2010) found that giant galaxies with small bulges are common in the local neighborhood.

Large bulges are predominantly more or less round, while the smaller bulges often have a distinct boxy or peanut shape. The current belief is that large bulges are associated with merger events (e.g. Toomre 1977; Abadi et al. 2003). The smaller boxy bulges (like the bulge of the Milky Way) are believed to arise from instabilities of rotating stellar disks and are probably unrelated to merger events (e.g. Combes and Sanders 1981). The next section is on a large galaxy NGC 1316 which has had

K. C. Freeman (✉)
Research School of Astronomy & Astrophysics, Mount Stromlo Observatory,
The Australian National University, Canberra, Australia
e-mail: kcf@mso.anu.edu.au

K. Freeman et al. (eds.), *Lessons from the Local Group,*
DOI 10.1007/978-3-319-10614-4_3

Fig. 1 The late merger galaxy NGC 1316 in the Fornax cluster (Martin Pugh: APOD 2008)

a relatively recent major merger and appears now to be in the process of evolving towards a system like the Sombrero galaxy. Later sections focus on the bulges of later-type galaxies, including the Milky Way.

2 The Late-Merger System NGC 1316

NGC 1316 is a bright late-merger galaxy in the Fornax cluster which seems destined to evolve into a Sombrero-like disk galaxy with a large bulge. It is very bright ($M_B = -22.5$) with a Sersic index of about 6, appropriate to a large bulge or elliptical galaxy. Its light distribution still shows prominent structure in its outer regions (see Fig. 1), characteristic of a late-merger remnant. The color distribution of its globular clusters show that its youngest clusters have ages of about 3 Gyr (Goudfrooij et al. 2001), so this is the likely epoch of its last major merger-driven star formation event.

McNeil-Moylan et al. (2012) measured velocities of 796 planetary nebulae in NGC 1316, using counter-dispersed spectroscopy with the FORS2 spectrograph on the VLT. The optical light of late-type galaxies like NGC 1316 is dominated by low-mass giant stars. Planetary nebulae (PN) are the late stages of evolution of stars with masses less than about 8 $M_\odot$, so they are good tracers of the starlight. During the brief planetary nebula phase, about 15 % of the energy of the central star is converted into a single line of [OIII], which makes it possible to detect PN in the outer parts of galaxies at distances of many Mpc and measure their velocities (See the paper by Arnaboldi in this volume for more details about using PN as dynamical tracers in distant galaxies).

With such a large sample of tracer objects, it is possible to measure the rotational velocity and velocity dispersion of NGC 1316 out to a radius of about 50 kpc. The velocity dispersion σ drops from about 250 km s^{-1} at the center to about 130 km s^{-1} at 50 kpc, while the rotational velocity of the planetary nebulae is roughly constant at about 100 km s^{-1} from 10 kpc to 50 kpc (see Fig. 2). Much of the angular

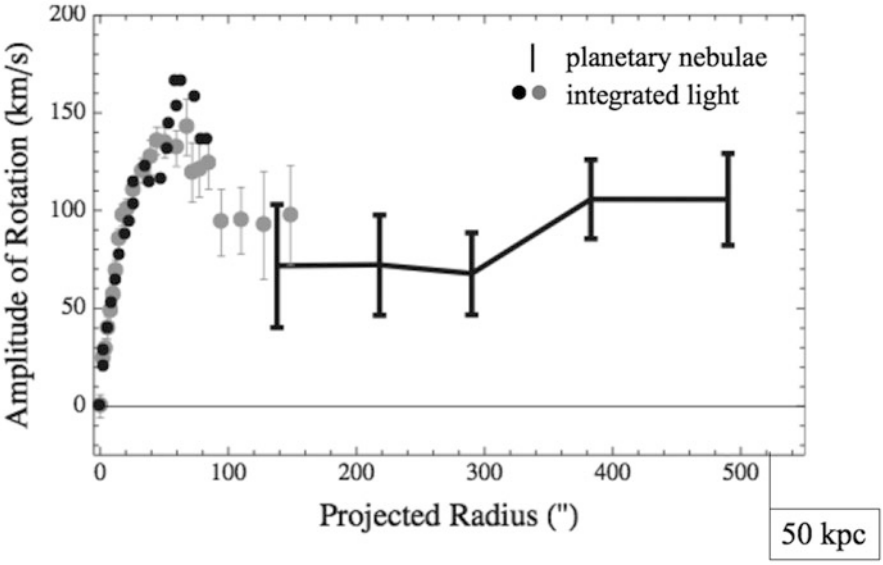

Fig. 2 The rotation curve of the starlight and the planetary nebulae in NGC 1316 (from McNeil-Moylan et al. 2012)

momentum of this merger remnant resides in its outer regions. McNeil-Moylan et al. (2012) successfully modelled the kinematics of the planetary nebulae with a Jeans model of constant anisotropy (β-parameter $= 0.5$) and a stellar mass-to-light ratio $M/L_B = 2.8$. In addition to the stellar component, a massive dark halo with a velocity dispersion of 289 km s^{-1} is needed to model the kinematics over the whole range of radius out to 50 kpc. This dark halo contributes about 80% of the total mass within 50 kpc. In summary, this post-merger galaxy appears to be approaching equilibrium: its dark halo is in place and the outer parts of its stellar component contain a substantial amount of ordered angular momentum. NGC 1316 is a relatively dusty system, so is likely to contain a significant amount of residual gas. Neutral hydrogen observations are difficult because NGC 1316 (Fornax A) is one of the brightest radio continuum sources in the sky (see Horellou et al. 2001 for a summary of its atomic and molecular gas content).

We can compare NGC 1316 with the more settled Sombrero galaxy which has a very large bulge and a rapidly rotating disk. Its bulge has a velocity dispersion of about 200 km s^{-1} (Kormendy and Illingworth 1982) and its stellar disk is rotating at about 300 km s^{-1} (Wagner et al. 1989). The rotation seen in HI is even larger: about 350 km s^{-1} (Bajaja et al. 1984). It seems likely that NGC 1316 will evolve into a system comparable to the Sombrero galaxy: from its velocity dispersion and integrated magnitude, its bulge may be even larger than the Sombrero's. The circular velocity of its dark halo as derived by McNeil-Moylan et al. indicates that the final disk of the evolved NGC 1316 will have a large circular velocity, rather similar to that of the Sombrero system.

3 The Bulges of Later-Type Galaxies

Later-type galaxies like the Milky Way mostly have small boxy bulges with near-exponential light distributions (e.g. Courteau et al. 1996). These small bulges are probably not merger products but were more likely generated by instabilities of the disk itself. The association of boxy bulges with the bar-forming and bar-buckling instabilities of disks goes back at least to the simulations by Combes and Sanders (1981) and the observations of Kuijken and Merrifield (1995) and Bureau and Freeman (1999). The observational association is based on long-slit spectra of edge-on disk galaxies with boxy bulges which show complex gas flows in their inner regions driven by the asymmetric rotating bar-like potential of the boxy bulge.

These flows are seen in all boxy bulge galaxies with gas in their inner regions: NGC 5746 is a particularly nice example (Bureau and Freeman 1999). The stellar kinematics of boxy bulges show a characteristic cylindrical rotation: the mean rotational velocity of the stars in the bulge depends mainly on the radius and only very weakly on the height above the plane. This was seen observationally by Kormendy and Illingworth (1982) and appears also in the simulations of boxy bulges that arise from disk instabilities.

4 The Galactic Bulge

Several recent surveys of stars in the Galactic bulge have studied its kinematics and chemical properties. Here I will discuss mainly the recent large ARGOS stellar survey of the bulge (Ness et al. 2012, 2013a, b; Freeman et al. 2013). The ARGOS survey acquired spectra of 28,000 candidate red giants towards the bulge and inner disk, with a spectral resolving power of about 11,000. This provides accurate radial velocities and the resolution is sufficient to measure abundances of Fe and most of the $\alpha-$elements.

The goal of the survey was to explore the idea that the Galactic bulge grew from the disk via bar-buckling instabilities. Rotating disks are often unstable to forming a flat bar structure at their centers. The bars grow naturally from instabilities of a disk that is dynamically relatively cold. The flat bar is in turn often unstable to vertical buckling which generates the boxy appearance of the bar seen edge-on. In the bar-buckling scenario, the bulge *structure* is younger than its oldest stars, which were originally part of the disk. In the N-body simulations, it typically takes about 2 Gyr for the bar to form in the disk and then to buckle vertically to generate the peanut-shaped bulge. So the stars of the bar/bulge may be chemically similar to stars of the adjacent thin and thick disk that are about 8 Gyr old.

The 28 fields of the ARGOS survey are shown in Fig. 3. They cover the southern bulge at latitudes $b = -5°, -7.5°$ and $-10°$, plus three relatively transparent northern bulge fields and some fields extending out into the adjacent thin and thick disk. The lines of sight through these fields pass through most of the Galactic components. The thin disk, the thick disk, the bulge itself, the stellar halo and the young spiral

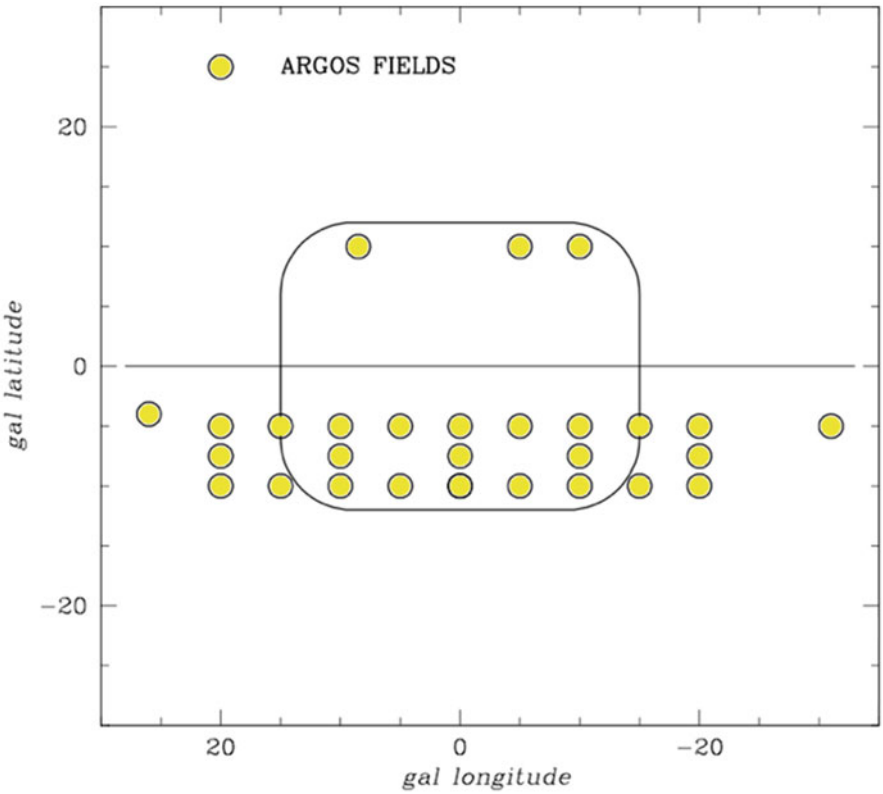

Fig. 3 The location of the ARGOS survey fields in galactic latitude and longitude. The filled circles show the 28 fields, each of about 1000 stars, and the rounded rectangle indicates the outline of the outer bulge

arm populations will all be represented along the line of sight. Because the bulge is at the center of the Galaxy, we expect to see the denser central regions of all of these Galactic components.

In order to study the stars of the bar/bulge, we need to reduce contamination by stars that lie in front of and behind the bulge, so photometric or spectroscopic parallaxes are needed. Ideally we would use stars for which relatively accurate distances can be derived. At a distance of about 8 kpc, large samples of spectra are possible only for the red giant stars. The Galactic bar/bulge is currently believed to lie at an angle of about 25° to the sun-center line and extends about 3 kpc from the center towards and away from us. The ARGOS stars were therefore selected from the 2MASS point source catalog, to have colors and magnitudes appropriate to giants within the bar region. Because metal-poor stars in the bulge region are interesting, as members of the inner stellar halo and also as potential first stars (eg Tumlinson 2010), the color criteria were chosen carefully so that metal-poor stars were not excluded by the selection process. Not all of these stars will turn out to be within the bar/bulge. Distances

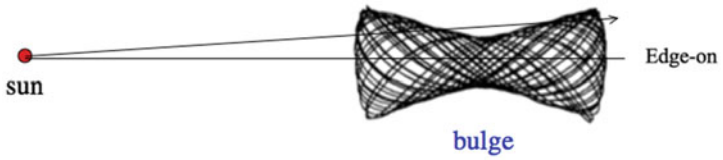

Fig. 4 Lines of sight from the sun through a peanut-shaped bulge seen close to end on. The peanut-shaped object shown here is an example of the kind of stellar orbits (seen edge-on) which support the peanut-shaped bulge. The upper line of sight passes through the two humps of the peanut, so the number of stars per unit length shows two peaks as it passes through the two humps

for the brighter red giants are difficult to measure accurately, but the clump giants have a narrow range of absolute magnitude around a mean $M_K = -1.61$ (Alves 2000) with a dispersion of only about 0.22 about the mean. For the ARGOS stars, we estimated isochrone distances from our temperatures and spectroscopic gravities and metallicities, and then selected stars that lie within a Galactocentric radius $R_G = 3.5$ kpc to be bulge stars.

The errors in the stellar parameters are estimated from observations of independently measured stars in the field, open and globular clusters and the bulge itself. The mean errors in the radial velocity, effective temperature, [Fe/H], [α/Fe] and log g are 0.9 km s^{-1}, 100K, 0.09, 0.10 and 0.30 respectively. Of our 28,000 stars, about 2500 are foreground dwarfs and 11,500 are giants outside the inner 3.5 kpc which we are taking as our bulge region. We see that only half of the stars towards the bulge with giant-like colors are actually giants within the bulge region. Foreground and background contamination is very significant in any such sample.

We were interested to know which stars contribute to the boxy peanut structure of the bulge. Nataf et al. (2010) and MacWilliam and Zoccali (2010) had discovered the bimodal luminosity function of clump giants along particular lines of sight through the bulge. The bimodality is interpreted as arising from the distribution of stars along the line of sight as it passes through the two humps of the peanut (see Fig. 4). The same bimodality is seen in the ARGOS sample, but only for the stars that are more metal-rich than [Fe/H] $= -0.5$. The more metal-poor stars are not part of the peanut structure. In the next section, we will discuss the likely reason.

5 The Metallicity Distribution of Bulge Stars

The metallicity distribution function (MDF) of the large sample of ARGOS bulge stars is broad, extending over the range [Fe/H] $= -1.0$ to $+0.5$ with a sparse tail of stars down to [Fe/H] < -2. The sample is large enough for structure in the MDF to be visible. All of the ARGOS fields show the same component structure as seen in Fig. 5. The Bayesian information criterion gives the optimal number of components for the MDF to be between 4 and 5. The main body of bulge stars with [Fe/H] between -1.0 and $+0.5$ has 3 distinct metallicity components denoted A, B and C

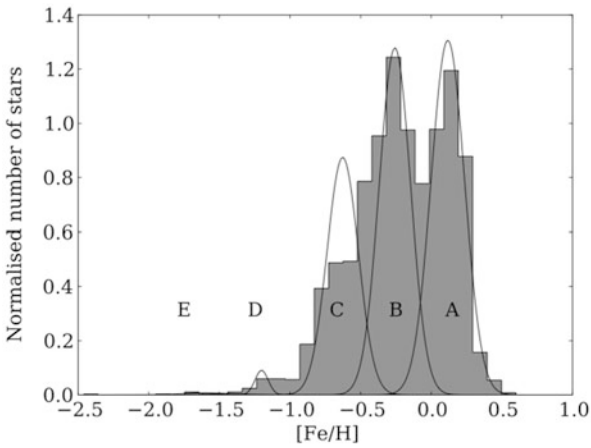

Fig. 5 The metallicity distribution of stars at $b = -5°$ in the bulge shows three major components denoted A, B and C, plus two weak metal poor components D and E. The relative weights of components A–C change with galactic latitude. The most metal rich component A is strong at lower latitudes but decreases in importance at higher latitudes (from Ness et al. 2013a)

as seen in Fig. 5, and their relative weights change with position in the bulge. The metal-richest component A is strongest near the Galactic plane, and the more metal-poor component C is stronger at higher latitudes. This changing weight generates an apparent vertical metallicity gradient in the bulge. Only components A and B are involved in the peanut structure of the bulge.

The MDF for stars in the inner disk field at $l = -31°, b = -5°$ show all of the same metallicity components that are seen within the bulge, with weights similar to those in the bulge at $b = -5°$. In the inner disk, these components are probably present in their undisturbed form, as disk stars, while in the bulge the stars of these components have been trapped dynamically into the bulge via the bar-forming and bar-buckling instability. Component A is weakly $\alpha-$enhanced (Fig. 6) and is strongly involved in the peanut bulge structure. We tentatively interpret component A as the colder more metal-rich part of the early thin disk. Component B is $\alpha-$enhanced

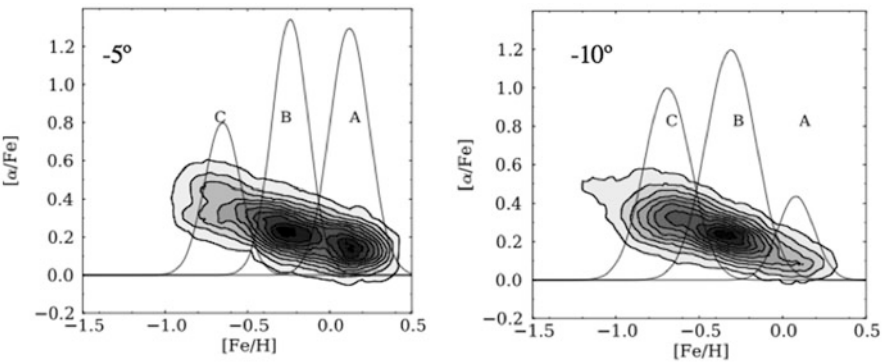

Fig. 6 The [α/Fe] - [Fe/H]) distribution of the bulge stars at $b = -5°$ and $-10°$ (from Ness et al. 2013a)

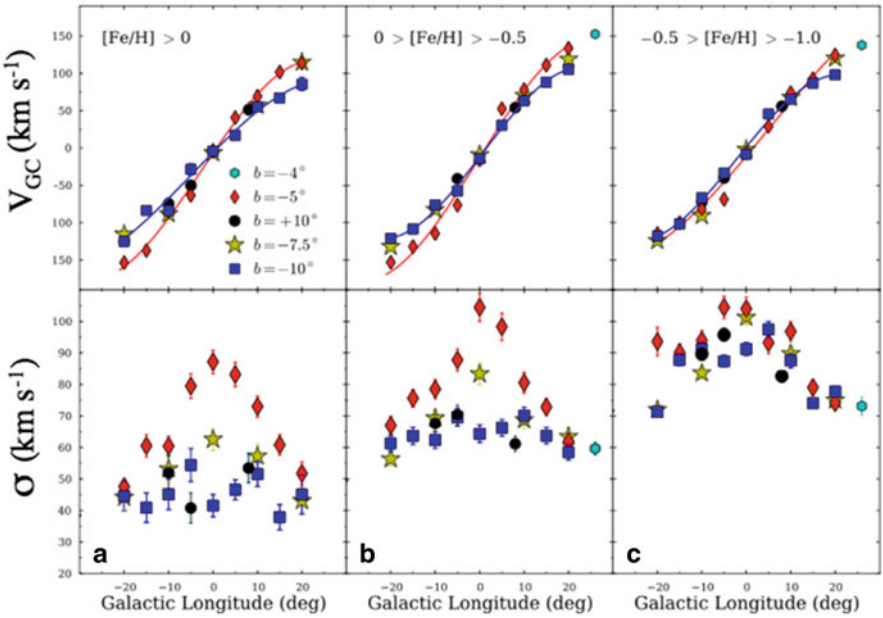

Fig. 7 The upper panels show the Galactocentric cylindrical rotation of the three major components of the Galactic bulge, corrected for the standard solar motion and an LSR circular velocity of 220 km s^{-1}. The different galactic latitude samples are shown by different symbols. The lower panels show their line of sight velocity dispersions. The shape of the velocity dispersion distributions is similar for components A and B, but the velocity dispersion of the metal-rich component A is clearly smaller (from Ness et al. 2013b)

and is the main component of the peanut bulge structure. Component C is more metal-poor and more $\alpha-$enhanced but not part of the bulge's peanut structure. Its stars have a similar range of [Fe/H] and [α/Fe] to the thick disk stars near the sun, so component C may be the stars of the early inner thick disk, now locked in the bulge, that were dynamically too hot to become significantly involved in the vertical redistribution of stars that lead to the peanut structure.

6 Kinematics of the Bulge Components

The mean rotation of the stars in the Galactic bulge ($-10^\circ < l < 10^\circ$) is close to cylindrical, as expected for a boxy bulge and found earlier by Kunder et al. (2012) from the BRAVA survey of cooler bulge giants (see Fig. 7). At larger $|l|$, extending out into the surrounding disk, the mean stellar rotation continues to increase up to more than 150 km s^{-1} in the disk at $|l| = 20^\circ$.

Component B rotates more rapidly than component A over the region of the bulge and is dynamically hotter (Ness et al. 2013b). As they are both moving in the same

potential gradient, this suggests that component A is more radially concentrated than component B. We have already seen from Fig. 5 that component A is the most vertically concentrated of the three major bulge components.

The two metal poor components D and E have very different kinematics. Their rotation is much smaller and the velocity dispersion higher, consistent with being part of the inner metal-poor halo of the Galaxy.

7 Interpretation of the Bulge Components

In the instability scenario for formation of the Galactic bulge, the disk evolved chemically and dynamically for about 2 Gyr before becoming unstable and buckling into the peanut structure. We can regard components A–E as relics of the early Galactic disk and halo which were trapped into the bulge by the action of the instability.

The instability process generates a mapping of the stars of the early disk into the boxy/peanut structure. In this way, the bulge preserves a dynamical imprint of the chemical distribution of the disk at the time that the buckling occurred. The bulge gives a chemical snapshot of the MDF of the early disk captured in the bar.

The mapping of disk into bulge depends on the location and motions of the stars at the time of the instability. Kinematically colder stars can suffer strong radial and vertical migration, and can therefore be strongly involved in the peanut structure (components A and B). Di Matteo et al. (2014) studied the N-body mapping of the early disk into the boxy bulge during the epoch of bar formation and buckling (see also Martinez-Valpuesta and Gerhard 2013). In their model, the bar begins to grow after about 0.8 Gyr, the vertical instability starts at 2 Gyr and the system is close to equilibrium by 4 Gyr. During the period of bar formation, the asymmetric gravitational field is changing rapidly, the Jacobi integrals of the stars are not conserved and substantial radial migration of disk stars occurs. This may be the event that brought the metal-rich stars from the inner Galaxy into the solar neighborhood (see e.g. Haywood 2008).

The instability maps stars from the entire disk into the bulge. Stars from the inner (outer) disk are preferentially mapped into the inner (outer) regions of the bulge. The boxy structure is defined by stars that initially have orbital radii $> 0.7 r_{bar}$ and lie near the vertical inner Lindblad resonance. Stars from the inner region are seen to migrate far out into the disk, and stars from larger radii migrate in to the bar. The N-body models suggest that components A and B originate in the early disk, with the stars of the compact metal-rich component A coming from nearer the center than the stars of the more extended and rapidly rotating component B. Component C, which is not involved in the peanut structure, is believed to come from the (hotter) old thick disk.


-KEN FREEMAN-

Acknowledgements I am grateful to Lia Athanassoula, Ortwin Gerhard, John Kormendy, Inma Martinez-Valpuesta and Melissa Ness for many discussions about bulges. My best wishes to David Block and Bruce Elmegreen on this notable occasion.

References

Abadi, M.G., Navarro, J.F., Steinmetz, M., Eke, V.R. 2003. ApJ, 597, 21
Alves, D. 2000. ApJ, 539, 732.
Bajaja, E., van der Burg, G. et al. 1984. A&A, 141, 309.
Bureau, M. & Freeman, K. 1999. AJ, 118, 126.
Combes, F. & Sanders, R. 1981. A&A, 96, 164.
Courteau, S., de Jong, R. et al. 1996. ApJ, 457, L73.
Di Matteo, P., Haywood, M. et al. 2014. astro-ph/1404.0304.
Freeman, K., Ness, M. et al. 2013. MNRAS, 428, 3660.
Goudfrooij, P., Alonso, M., et al. 2001. MNRAS, 328, 237.
Haywood, M. 2008. MNRAS, 388, 1175.
Horellou, C., Black, J. et al. 2001. A&A, 376, 837
Kormendy, J. & Illingworth, G. 1982. ApJ, 256, 460.
Kormendy, J., Drory, N. et al. 2010. ApJ, 723, 54.
Kunder, A., Koch, A. et al. 2012. AJ, 143, 57.
Kuijken, K. & Merrifield, M. 1995. ApJ, 433, L13.
Martinez-Valpuesta, I. & Gerhard, O. 2013. ApJ, 766, L3.
McNeil-Moylan, E., Freeman, K., et al. 2012. A&A, 539A, 11.
Mcwilliam, A. & Zoccali, M. 2010. ApJ, 724, 1491.
Nataf, D., Udalski, A. et al. 2010. ApJ, 721, L28.
Ness, M.K., Freeman, K.C. et al. 2012. ApJ, 756, 22.
Ness, M.K., Freeman, K.C. et al. 2013a. MNRAS, 430, 836
Ness, M.K., Freeman, K.C. et al. 2013b. MNRAS, 432, 2092.
Toomre, A. 1977. in "Evolution of Galaxies and Stellar Populations", ed. B. Tinsley & R. Larson (New Haven: Yale University Observatory), 401.
Tumlinson, J. 2010. ApJ, 708, 1398.
Wagner, S., Bender, R. et al. 1989. A&A, 215, 243.

The Galactic Bar

Ortwin Gerhard and Christopher Wegg

Abstract The Milky Way's bar dominates the orbits of stars and the flow of cold gas in the inner Galaxy, and is therefore of major importance for Milky Way dynamical studies in the Gaia era. Here we discuss the pronounced peanut shape of the Galactic bulge that has resulted from recent star count analysis, in particular from the VVV survey. We also discuss the question whether the Milky Way has an inner disky pseudo-bulge, and show preliminary evidence for a continuous transition in vertical scale-height from the peanut bulge-bar to the planar long bar.

1 Introduction

The Gaia satellite will soon provide us with exquisite data for the motions of stars in our Galaxy. The Milky Way's stellar bar has a strong influence on the orbits of stars inside the solar circle, and dominates the gas flow in the inner Galaxy. To understand the structure and dynamics of the Galactic bar better is therefore of prime importance in the Gaia era.

Renewed interest in the Galactic bar and bulge has also been triggered recently by unprecedented new near-infrared (NIR) photometric and spectroscopic surveys of the inner Galaxy. In this contribution, we summarize recent work on the structural properties of the Galactic bar and bulge based on such survey data.

About two thirds of all large disk galaxies are barred (Eskridge et al. 2000), including our Milky Way. Historically, several perceptive papers already suggested in the 1970s that the non-circular motions seen in HI observations towards the inner Galaxy could naturally be interpreted in terms of elliptical gas streamlines (Shane 1972; Peters 1975). But it was not until the 1990s that the barred nature of the Milky Way bulge was considered established. This revised view of our Galaxy was based on new data and ideas at that time: the NIR photometry by the COBE satellite (Weiland

O. Gerhard (✉) · C. Wegg
Max Planck Institute for extraterrestrial Physics, Giessenbachstr.
PO Box 1312, 85741, Garching, Germany
e-mail: gerhard@mpe.mpg.de

C. Wegg
e-mail: wegg@mpe.mpg.de

K. Freeman et al. (eds.), *Lessons from the Local Group,*
DOI 10.1007/978-3-319-10614-4_4

et al. 1994; Binney et al. 1997), enabling a global view of the bulge through the dust layer; new analysis of the inner Milky Way gas flows traced in longitude-velocity diagrams (Englmaier and Gerhard 1999; Fux 1999), in the context of triaxiality and bars in external galaxies; asymmetries in bulge star counts (Stanek et al. 1994; Lopez-Corredoira et al. 1997), and the newly measured optical depth for microlensing towards bulge fields (Paczynski et al. 1994; Bissantz et al. 1997). These data, as well as the kinematics of bulge stars available at the time (Zhao et al. 1994; Fux 1997), could all be consistently explained in terms of a barred bulge model with its major axis in the first quadrant. 2MASS NIR star counts (López-Corredoira et al. 2005; Skrutskie et al. 2006), the cylindrical rotation in the bulge (Kunder et al. 2012; Ness et al. 2013; Shen et al. 2010), and other data have since confirmed and refined our understanding of the Galactic bar.

In external disk galaxies seen at low inclination, bars are easy to see but their vertical structure is not well-constrained. However, we now know from gas- and stellar-kinematic data that box or peanut-shaped (b/p) bulges in edge-on systems are related to bars (Merrifield and Kuijken 1999; Chung and Bureau 2004). Photometric data (Lütticke et al. 2000; Bureau et al. 2006) are consistent with predictions from N-body models that bars in galaxies generally consist of an inner three-dimensional (3D) part, the b/p bulge, and a more extended 2D part of the bar (Athanassoula 2005). In these simulations, a bar first grows from an unstable disk and then becomes unstable to a buckling instability which leads to an inner boxy bulge (Combes et al. 1990; Raha et al. 1991; Athanassoula and Misiriotis 2002). The bar can then grow further through angular momentum loss to the dark matter halo, and eventually go through a second buckling instability which leads to the formation of a strongly peanut-shaped bulge (Martinez-Valpuesta et al. 2006). Similar secular evolution has been observed also in cosmologically more realistic simulations of disk galaxies, such as dissipative collapse models (Samland and Gerhard 2003; Ness et al. 2014), or hierarchical disk galaxy models in which strong feedback and the absence of significant mergers ensure a relatively quiescent star formation history (Martig et al. 2012; Guedes et al. 2013).

2 Bulge Distances from K-band Magnitudes of Red Clump Giants

Red clump giants are immensely useful for star count studies of the Galaxy. They are He core burning stars with a narrow range of luminosities and colours, hence can be employed to map out the distant-dependent structure of the Galactic bulge. Using the α-enhanced BASTI isochrones for various metallicities at age 10 Gyr from Pietrinferni et al. (2004), a metallicity-averaged luminosity function of bulge red clump (RC) stars has Gaussian $\sigma(K) = 0.18$ mag, $\sigma(J-K) = 0.05$, and $M_{K,RC} = -1.72$ in the K_S-band (Wegg and Gerhard 2013a). The K_S-band magnitude is slightly brighter than the value from solar-neighbourhood RC stars (Alves 2000). In the

colour-magnitude diagram, RC stars are spread because of variations in distance, reddening, age, and metallicity. The variations in absolute K_S-magnitude with age and metallicity are $\Delta_{\rm age} M_{K,RC} \sim 0.03$/Gyr at age 10 Gyr and $\Delta_Z M_{K,RC} \sim -0.28$/dex (Salaris and Girardi 2002). From the same study, for old stellar populations the number of RC stars per unit initial mass varies by $\sim 10\%$ for metallicities $\gtrsim 0.02$ solar. Therefore the distribution of RC stars is a good tracer of the stellar mass distribution in the bulge. Distances to individual RC giants in the upper bulge can be estimated with $\sigma_D \sim 10\%$. At low latitudes, residual dust extinction broadens the clump magnitude distribution, leading to $\sigma_D \sim 15\%$ at $|b| = 1$ deg (Gerhard and Martinez-Valpuesta 2012).

3 The Galactic Box/Peanut Bulge

The COBE data firmly established the boxy shape and the presence of longitudinal asymmetries in the Galactic bulge, which appears brighter and vertically more extended on the $l > 0$ side, but symmetric in latitude b (Weiland et al. 1994). These asymmetries are a signature of a triaxial bulge whose major axis is tilted in the Galactic plane relative to the line-of-sight (LOS) from the Sun to the Galactic centre (Blitz and Spergel 1991). From these asymmetries, parametric and non-parametric bulge luminosity models were reconstructed (Dwek et al. 1995; Bissantz and Gerhard 2002) and then used to study the influence of the Galactic bar on the gas dynamics and microlensing observations. However, uncertainties remained due to the lack of distance information in the COBE data and to the uncertainties in the extinction maps.

Red clump star counts in several fields across the bulge first illustrated the different distances to the near and far sides of the triaxial bulge (Stanek et al. 1994, 1997). With the 2MASS all sky data a first star count reconstruction of the bulge shape became possible, even if somewhat affected by the limit in the survey depth (López-Corredoira et al. 2005). More recent analysis of OGLE-III and 2MASS RC counts in upper bulge fields near the minor axis showed the presence of two density peaks along the LOS (Nataf et al. 2010; McWilliam and Zoccali 2010). These results were interpreted as an X-shape in the bulge density distribution such as seen in N-body models of peanut bulges. Abundances and velocities derived from spectra of large numbers of bulge stars showed that only the more metal-rich stellar populations participate in this 'split red clump' (Ness et al. 2012).

The recent VVV survey is $\sim 3-4$ mag deeper than 2MASS and RC stars are visible all through the bulge even quite close to the Galactic plane. These data have brought a quantum leap for constraining the bulge density distribution. First results at $b = \pm 1$ deg showed clearly the in-plane tilt of the barred bulge, and also a structural change in the central $|l| < 4$ deg (Gonzalez et al. 2011), indicating a less elongated distribution of stars in this region (Gerhard and Martinez-Valpuesta 2012). In our recent work (Wegg and Gerhard 2013a), we used the VVV DR1 data (Saito et al. 2012) for some 300 sightlines across $|l| < 10$ deg and -10 deg $< b < 5$ deg, to measure

the 3D density distribution of the Galactic bulge. For all these LOS, we constructed extinction- and completeness-corrected K_S-band magnitude distributions, and deconvolved these with the K-band luminosity function of RC giants and red giant branch bump (RGBB) stars. The extinction model was determined from the RC stars themselves, with a method very similar to Gonzalez et al. (2011). Completeness effects were corrected based on artificial stars inserted in the VVV images. For the deconvolution we used a Lucy-Richardson scheme including a 'background component' of stars not in the RC+RGBB. This is a good approximation because the magnitudes of these stars vary over a wide range. The deconvolved LOS density distributions clearly show the split red clump at latitudes $|b| \geq 4$ deg.

For constructing the entire 3D bulge density distribution, we then assumed that the bulge is eightfold triaxially symmetric. This assumption can be checked at the end: the rms deviations between the mirror-symmetric points in the final model are indeed small. Finding the best eightfold symmetric distribution determines the tilt angle of the bar-bulge to the LOS to be (27 ± 2) deg, where the dominant error is systematic, arising from the details of the deconvolution process. Our final density map covers the inner $(2.2 \times 1.4 \times 1.1)$ kpc of the bulge/bar. It is illustrated in Figs. 1 and 2. The density is typically accurate to $\sim 10\%$ except at $y > 1$ kpc along the intermediate axis of the bar. In the projected density maps shown in Fig. 1, the region $|b| < 1$ deg was extrapolated from $b \geq 1$ deg with a simple sech^2-model (Portail et al., in preparation), because at these low latitudes the extinction and completeness corrections are too large for a reliable density deconvolution.

Figure 1 shows a highly elongated bar, with projected axis ratios $\approx (1 : 2.1)$ for isophotes reaching major axis radii ~ 2 kpc. Above about 400 pc above the Galactic plane, a prominent X-structure is visible which explains the earlier measurements of the split red clump. This X-structure is characteristic for a class of b/p bulges (Bureau et al. 2006). In fact, the b/p bulge of the Milky Way is very strong, about as strong as in the proto-typical b/p bulge in NGC 128 (Wegg and Gerhard 2013b). Beyond about 1 kpc along the major axis, the iso-surface density contours in the edge-on projection bend down and outwards to the Galactic plane.

4 Does the Milky Way Have a Disky Pseudo-bulge?

Along the principal bar axes the density falls of approximately exponentially, as shown in Fig. 2. Exponential scale-lengths are (0.70:0.44:0.18) kpc, corresponding to axis ratios (10:6.3:2.6). The flattening of the major axis profile beyond ~ 1 kpc signifies the transition to the longer, planar bar.

Particularly noteworthy is the very short vertical scale height in the centre, perhaps indicative of a central disk-like, high-density pseudo-bulge structure as is seen in many early and late type b/p bulge galaxies (Bureau et al. 2006), including the edge-on Milky Way analogue NGC 4565 (Kormendy and Barentine 2010).

Additional support for this interpretation comes from the change-of-slope at $|l| \simeq 4$ deg seen in the VVV RC star count maxima longitude profiles for $b = \pm 1$ deg

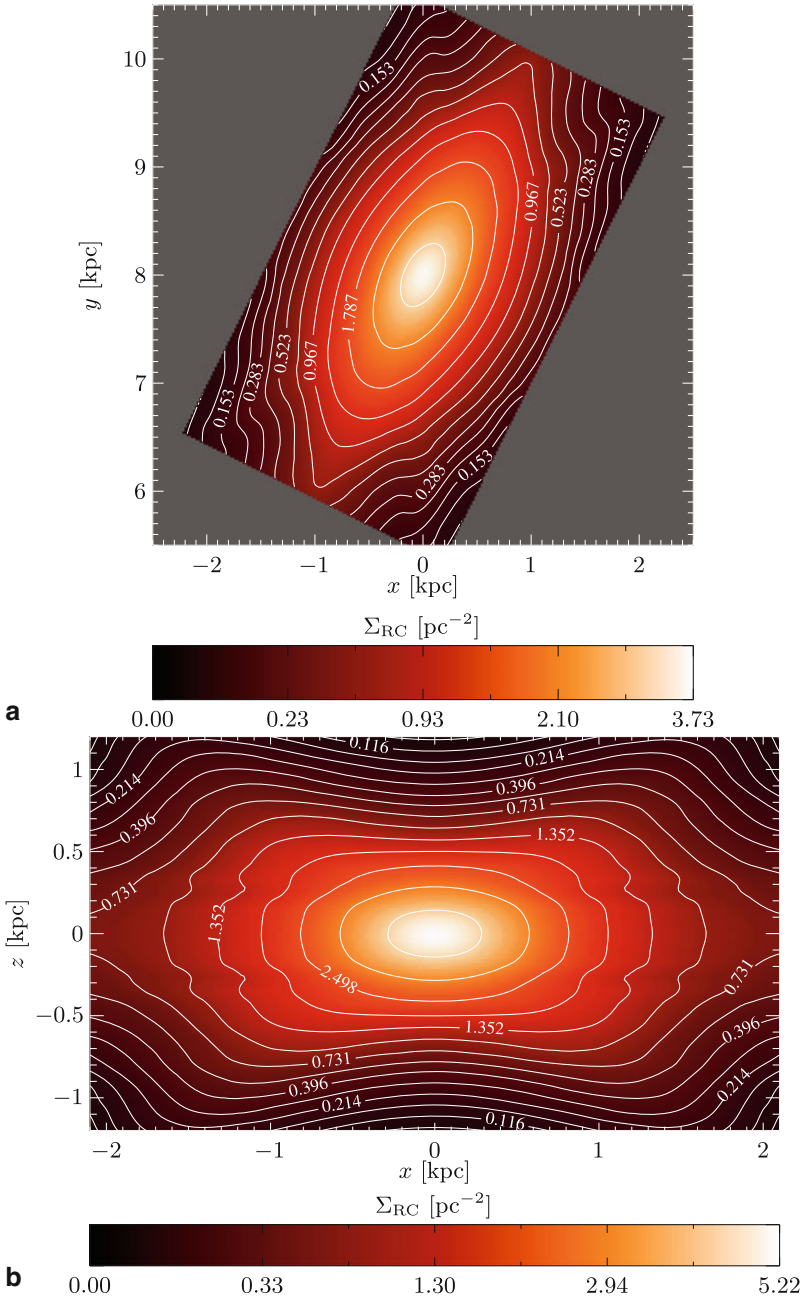

Fig. 1 **a)** *top*: The Galactic bulge as viewed from the north Galactic pole. **b)** *bottom*: The bulge 3D density projected along the intermediate axis. Numbers give the surface density of RC stars in pc^{-2}, contours are spaced by 1/3 mag. The 3D density map extends to 1.15 kpc along the minor axis and to 1.4 kpc along the intermediate axis, and the projections are within these limits

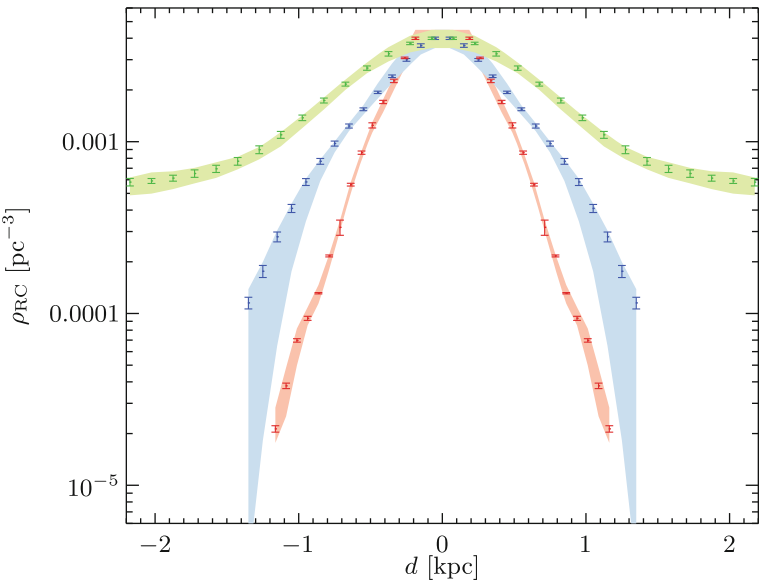

Fig. 2 Density of RC stars along the major axis (*green*), intermediate (*blue*), and minor axis (*red*) for the bulge. The major and intermediate axis profiles are offset from the Galactic plane by 187.5 pc. The error bars are the rms deviations between the eightfold symmetric points of the final bulge density distribution. The shaded regions show estimated systematic errors based on varying the details of the deconvolution procedure. From Wegg and Gerhard (2013a)

(Gonzalez et al. 2011; Wegg and Gerhard 2013a). The simplest interpretation of this result is the presence of a rounder, more nearly axisymmetric central part of the bar, as illustrated by Gerhard and Martinez-Valpuesta (2012) with an N-body model with this property (see Fig. 3). In fact, if the central parts of the Milky Way bar were completely axisymmetric, the inner slope of the longitude profile would be nearly zero. This model also predicted that the transition to the rounder inner parts was confined to a few degrees from the Galactic plane. This was later confirmed with VVV data by Gonzalez et al. (2012). However, more work is required particularly at low latitudes to confirm a disky pseudo-bulge in the Milky Way.

5 The Long Bar

Hammersley et al. (2000) first drew attention to an overdensity of stars in the Milky Way disk plane reaching outwards from the bulge region to $l \simeq 28$ deg. This structure was confirmed in several subsequent NIR star count investigations, e.g. with UKIDSS (Cabrera-Lavers et al. 2008). Due to its longitude extent and the narrow extent along the LOS it was termed the 'long bar'. In Spitzer Glimpse mid-infrared star counts (Benjamin et al. 2005), which are even less affected by dust, a corresponding long

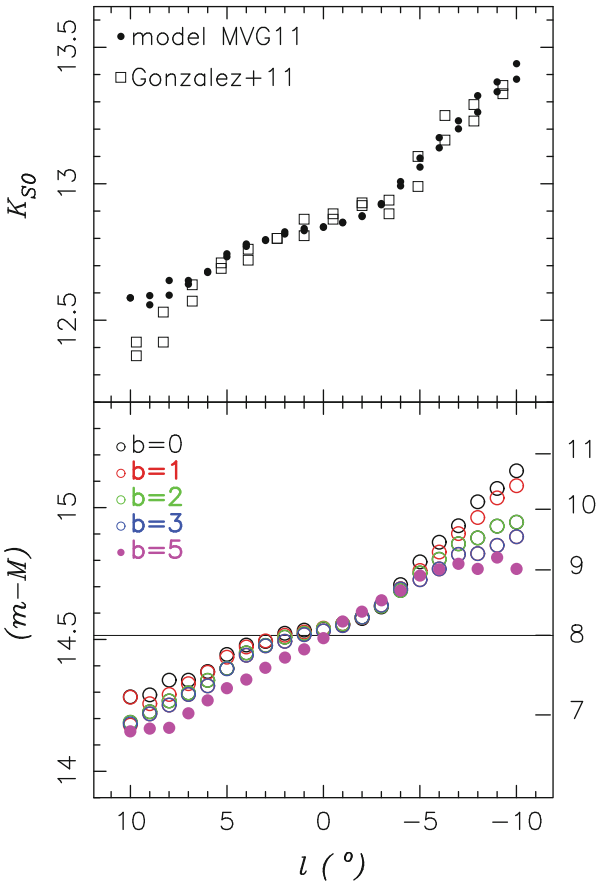

Fig. 3 Maxima of RC magnitude distributions in the strips $b = \pm 1$ deg across longitude. In the top panel for VVV K-band counts from Gonzalez et al. (2011, *open squares*) and for an N-body model from Martinez-Valpuesta and Gerhard (2011, *dots*). The model reproduces the data well because its central parts near the symmetry plane are more axisymmetric than the main bar. In the bottom panel for slices through the model with different latitude as seen from the Sun. The change of slope seen in the simulated RC magnitude distributions for $|b| < 2$ deg is absent at $|b| = 5$ deg. (From Gerhard and Martinez-Valpuesta 2012)

bar was inferred from a similar overdensity of sources observed on the $l > 0$ side. The long bar has a vertical scale-length of less than 100 pc, so is clearly a disk feature. Curiously, the orientation of the long bar inferred by all these investigations was at $\sim 45°$ with respect to the LOS to the Galactic centre.

Such a misalignment of the long bar with the b/p bulge is difficult to understand dynamically. Two independent, misaligned barred structures with sizes differing by only a factor of ~ 2 would be expected to align quickly, due to the mutual gravitational interaction. Note that secondary nuclear bars are generally ~ 8 times smaller than the primary bars in their host galaxies (Erwin 2011). Thus Martinez-Valpuesta and Gerhard (2011); Romero-Gómez et al. (2011) both argued that the long bar would more likely be the 2D part of the Milky Way bar continuing outwards from the 3D barred bulge, such as generally seen in secularly evolved N-body models. Martinez-Valpuesta and Gerhard (2011) predicted star counts from an N-body model with a bar and inner boxy bulge formed in a buckling instability. They argued that approximate agreement with the star count data could be achieved if the ends of the planar part of

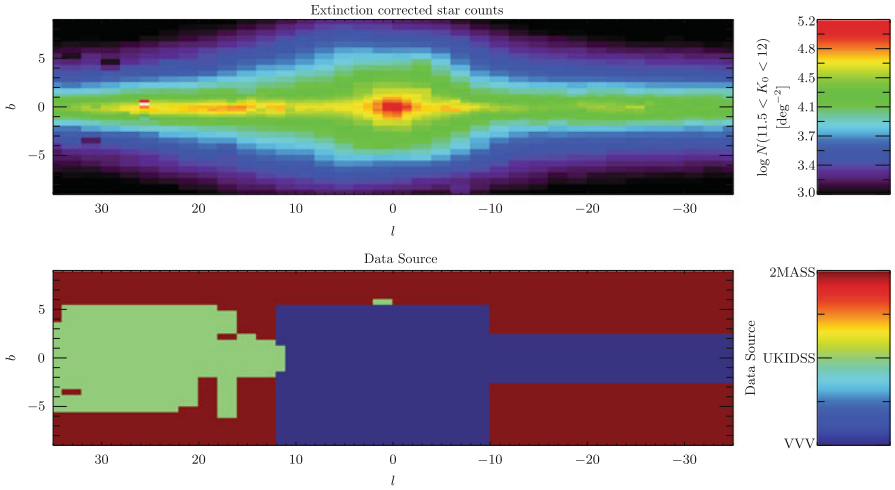

Fig. 4 The Galactic bulge and bar as seen from the Sun in K-band star counts combined from the cross-matched 2MASS, UKIDSS, and VVV surveys as shown in the lower panel. The magnitude range shown ($11.5 < M_K < 12$) is chosen such that the VVV data in the Galactic plane are not yet saturated and at the same time the 2MASS data are still complete in the region where they are used. This projection shows the continuous transition in the vertical scale-height from the inner 3D b/p bulge to the outer 2D bar

the bar have developed leading ends through interaction with the adjacent spiral arm heads. They found that such a configuration was present in their model for $\sim 40\,\%$ of the time in an evolutionary sequence from leading to straight to trailing, and also that some barred galaxies have bars with leading ends.

However, the star count maxima signifying the long bar (Cabrera-Lavers et al. 2008) show some discontinuities near $l = 10\,\mathrm{deg}$ and $l = 20\,\mathrm{deg}$, and the LOS distance dispersion of these RC stars shows a large scatter when plotted versus longitude. Therefore, in order to understand the Milky Way's planar bar better, we are currently reanalyzing the combined 2MASS, UKIDSS, and VVV surveys of the inner Galaxy (Wegg et al., in preparation). All data were extinction corrected and brought to a common photometric system. Figure 4 shows the total star counts across the Galactic bulge and inner disk in a magnitude interval common to all surveys. From this map it is apparent that the vertical scale-height of the star counts decreases continuously from the maximum in the X-region of the b/p bulge into the planar bar and disk. This is confirmed more quantitatively by measuring the vertical gradients of the RC stars on the $l > 0$ side. There is no indication for two separate components in these plots. Investigation into the LOS distribution of RC stars versus longitude in the combined data is on-going. This will give us a better understanding of the long bar and the transition region between the bar and the adjacent disk in the Milky Way.

References

Alves D. R., 2000, ApJ, 539, 732
Athanassoula E., 2005, MNRAS, 358, 1477
Athanassoula E., Misiriotis A., 2002, MNRAS, 330, 35
Benjamin R. A., Churchwell E., Babler B. L., Indebetouw R., et al. 2005, ApJL, 630, L149
Binney J., Gerhard O., Spergel D., 1997, MNRAS, 288, 365
Bissantz N., Englmaier P., Binney J., Gerhard O., 1997, MNRAS, 289, 651
Bissantz N., Gerhard O., 2002, MNRAS, 330, 591
Blitz L., Spergel D. N., 1991, ApJ, 379, 631
Bureau M., Aronica G., Athanassoula E., Dettmar R.-J., Bosma A., Freeman K. C., 2006, MNRAS, 370, 753
Cabrera-Lavers A., González-Fernández C., Garzón F., Hammersley P. L., López-Corredoira M., 2008, A&A, 491, 781
Chung A., Bureau M., 2004, AJ, 127, 3192
Combes F., Debbasch F., Friedli D., Pfenniger D., 1990, A&A, 233, 82
Dwek E., Arendt R. G., Hauser M. G., Kelsall T., et al. 1995, ApJ, 445, 716
Englmaier P., Gerhard O., 1999, MNRAS, 304, 512
Erwin P., 2011, Memorie della Societa Astronomica Italiana Supplementi, 18, 145
Eskridge P. B., Frogel J. A., Pogge R. W., Quillen A. C., Davies R. L., DePoy D. L., Houdashelt M. L., Kuchinski L. E., Ramírez S. V., Sellgren K., Terndrup D. M., Tiede G. P., 2000, AJ, 119, 536
Fux R., 1997, A&A, 327, 983
Fux R., 1999, A&A, 345, 787
Gerhard O., Martinez-Valpuesta I., 2012, ApJL, 744, L8
Gonzalez O. A., Rejkuba M., Minniti D., Zoccali M., Valenti E., Saito R. K., 2011, A&A, 534, L14
Gonzalez O. A., Rejkuba M., Zoccali M., Valenti E., Minniti D., Schultheis M., Tobar R., Chen B., 2012, A&A, 543, A13
Guedes J., Mayer L., Carollo M., Madau P., 2013, ApJ, 772, 36
Hammersley P. L., Garzón F., Mahoney T. J., López-Corredoira M., Torres M. A. P., 2000, MNRAS, 317, L45
Kormendy J., Barentine J. C., 2010, ApJL, 715, L176
Kunder A., Koch A., Rich R. M., de Propris R., Howard C. D., Stubbs S. A., et al. 2012, AJ, 143, 57
López-Corredoira M., Cabrera-Lavers A., Gerhard O. E., 2005, A&A, 439, 107
Lopez-Corredoira M., Garzon F., Hammersley P., Mahoney T., Calbet X., 1997, MNRAS, 292, L15
Lütticke R., Dettmar R.-J., Pohlen M., 2000, A&A, 362, 435
Martig M., Bournaud F., Croton D. J., Dekel A., Teyssier R., 2012, ApJ, 756, 26
Martinez-Valpuesta I., Gerhard O., 2011, ApJL, 734, L20+
Martinez-Valpuesta I., Shlosman I., Heller C., 2006, ApJ, 637, 214
McWilliam A., Zoccali M., 2010, ApJ, 724, 1491
Merrifield M. R., Kuijken K., 1999, A&A, 345, L47
Nataf D. M., Udalski A., Gould A., Fouqué P., Stanek K. Z., 2010, ApJL, 721, L28
Ness M., Debattista V. P., Bensby T., Feltzing S., Roškar R., Cole D. R., Johnson J. A., Freeman K., 2014, ApJL, 787, L19
Ness M., Freeman K., Athanassoula E., Wylie-de-Boer E., Bland-Hawthorn J., Asplund M., et al. 2013, MNRAS, 432, 2092
Ness M., Freeman K., Athanassoula E., Wylie-De-Boer E., Bland-Hawthorn J., Lewis G. F., et al. 2012, ApJ, 756, 22
Paczynski B., Stanek K. Z., Udalski A., Szymanski M., Kaluzny J., Kubiak M., Mateo M., Krzeminski W., 1994, ApJL, 435, L113
Peters III W. L., 1975, ApJ, 195, 617
Pietrinferni A., Cassisi S., Salaris M., Castelli F., 2004, ApJ, 612, 168

Raha N., Sellwood J. A., James R. A., Kahn F. D., 1991, Nature, 352, 411
Romero-Gómez M., Athanassoula E., Antoja T., Figueras F., 2011, MNRAS, 418, 1176
Saito R. K., Hempel M., Minniti D., Lucas P. W., et al. 2012, A&A, 537, A107
Salaris M., Girardi L., 2002, MNRAS, 337, 332
Samland M., Gerhard O. E., 2003, A&A, 399, 961
Shane W. W., 1972, A&A, 16, 118
Shen J., Rich R. M., Kormendy J., Howard C. D., De Propris R., Kunder A., 2010, ApJL, 720, L72
Skrutskie M. F., Cutri R. M., Stiening R., Weinberg M. D., et al. 2006, AJ, 131, 1163
Stanek K. Z., Mateo M., Udalski A., Szymanski M., Kaluzny J., Kubiak M., 1994, ApJL, 429, L73
Stanek K. Z., Udalski A., Szymanski M., Kaluzny J., Kubiak M., Mateo M., Krzeminski W., 1997, ApJ, 477, 163
Wegg C., Gerhard O., 2013a, MNRAS, 435, 1874
Wegg C., Gerhard O., 2013b, The Messenger, 154, 54
Weiland J. L., Arendt R. G., Berriman G. B., Dwek E., Freudenreich H. T., Hauser M. G., et al., 1994, ApJL, 425, L81
Zhao H., Spergel D. N., Rich R. M., 1994, AJ, 108, 2154

The Challenge of Galactic Cartography: Lessons from the Milky Way

Robert A Benjamin

Abstract In the early nineteenth century, as maps of the coastline of Africa were becoming increasingly accurate, cartographers were faced with the quandary of how or whether to include "historical" knowledge, based on traveler accounts, in their maps. I describe how we are now facing a similar problem in Galactic cartography as we try to reconcile older views of the Galactic disk based on the photometric distances to stars and kinematic distance to neutral and molecular gas with the current and upcoming high resolution radio and infrared surveys, and multiple parallax surveys. I then provide updates on two current issues of Galactic cartography: the "stellar break" of the Milky Way and the rapid increase in the amount of data that may be used to assess models of Galactic spiral structure.

1 The First Lesson: A Mapping Analogy

One of the best aspects of working on Galactic structure is that there is a present and objective reality that we seek to determine: the Milky Way **must** look like something as seen from the outside.[1] We just have to obtain the right data and be clever enough in its interpretation to reach robust and verifiable conclusions about this structure.

Conversely, one of the worst aspects of working on Galactic structure is that our ability to determine distances has not been up to the task of unambiguously discerning the non-axisymmetric (spiral) structure of the Galactic disk. Bart Bok, one of the pioneers of the early days of Galactic structure, and co-author with Priscilla Bok on five editions of textbooks on the Milky Way from 1941 to 1981, famously gave up working on spiral structure (allegedly at Priscilla's urging) in favor of easier problems (Bok 1983).

[1] Another notable aspect, particularly at this meeting, is that you can go outside on a dark, clear night and just look at it arching overhead.

R. A. Benjamin (✉)
Dept of Physics, University of Wisconsin-Whitewater, Whitewater, USA
e-mail: benjamir@uww.edu

K. Freeman et al. (eds.), *Lessons from the Local Group,*
DOI 10.1007/978-3-319-10614-4_5

Why has this been so hard? There are two principal distances methods that have been used in Galactic structure: photometric and kinematic. Unfortunately, the uncertainties in both methods are significant enough that mapping structure to a precision of a few hundred parsecs has been challenging.

The uncertainty in photometric distance depends on the photometric uncertainties (usually negligible), the uncertainty in extinction (sometimes important), and our ability to know the absolute magnitude. This last term is usually the sticking point; the conversion of spectral type to absolute magnitude has a significant scatter. Russeil (2003) estimates $\Delta M = 0.3-0.7$ for OB stars, corresponding to 14–32 % uncertainties (Russeil 2003). Moreover, since the uncertainty is fractional, distance resolution degrades with increasing distance; one reaches an uncertainty of $\Delta d = 200$ pc (a typical spiral arm width) at 0.6–1.4 kpc, and uncertainty of $\Delta d = 1$ kpc (a typical spiral arm spacing) at 3.1–7.1 kpc.

Kinematic distances have their own special problems (Burton 1992). There is the need to specify the velocity vector of the Sun, including circular motion, peculiar motion, and possibly bulk motion of the LSR (Bovy et al. 2012). Specifying the velocity field of the Galaxy usually involves adopting a distance to Galactic center, R_0, and choosing a rotation curve, $v_c(R)$ (a maddeningly non-standardized step). Most authors choose not to try to correct for the known non-circular motions near spiral arms (Humphreys 1976), the outer Galaxy (Levine et al. 2006), or too close to the regions affected by the bar (Fux 1999). These motions can mimic density structure if the tracer, like HI, fills much of the survey volume (Burton 1971). There is also the velocity projection problem: close to $l = 0°$ and 180° gas at all distances is compressed into a small velocity interval. This also produces a longitude-dependent term in distance uncertainties, assuming an intrinsic "scatter" in velocity. And finally, for gas inside the solar circle, there is the kinematic distance ambiguity: one value of velocity maps to two distances.

Despite these challenges, as a community we have soldiered on, amassing more and more data on our Milky Way and attempting to address the issues of its structure when we can. My opinion on the current state of affairs is that although current maps are rather unreliable, the evidence for non-axisymmetric structure in the Galactic disk is undeniable. The distribution of OB stars first evinced by Morgan, Sharpless and Osterbrock (Morgan et al. 1952) has persisted through the years and is (arguably) now confirmed by recent maser parallax work (Reid et al. 2014). Similarly, patterns seen in longitude-velocity space, first seen in the 21-cm surveys of neutral hydrogen by van de Hulst (van de Hulst et al. 1954) are now detected in multiple tracers (HI, CO, HII regions, etc). Most of the controversies of the decades past (and present) arise out of the *interpretation* of the patterns in data space, particularly regarding how and whether they can be converted into patterns in physical space.

While Galactic astronomy awaits the parallaxes of a billion stars that will be obtained by the Gaia mission, in several ways we have *already* entered an era of high precision cartography of the Galactic disk. Infrared surveys of the Galactic disk from 1.2 to 500 μm are now available, some with ∼arcsecond resolution (Churchwelland Benjamin 2013). Samples of red-clump giants, which can be photometrically identified in these surveys, appear to have a narrow luminosity function and can be used

Fig. 1 (*Left panel*) *Abissinorum sive Pretiosi Joannis imperiū* (Abyssinia or the Empire of Prestor John) by Gerhard Mercator (1512–1594), published ca. 1620. Key things to note in this map are the presence of several Great Lakes in the interior of Africa, a longitude system that pre-dates the currently used system, an east-west width of ∼40° at the equator and the lack of Mahe Island. (*Right panel*) *A New Map of Africa from the Latest Authorities* by John Cary (1754–1835), published in 1805. The coastline, east-west width of the continent, and location of Mahe Island are near modern precisions. Much of the interior is labeled as "Unknown Parts", but a few remnants of historical claims remain. The "Mountains of the Moon", the alleged source of the Nile River, derives from Ptolemy's *Geographia* (second century AD), and was based on travelers' reports. Current "maps" of the Galaxy, like Robert Hurt's *Artist's Conception of the Milky Way (2008)* (Churchwell et al. 2009), are probably more analogous to the map on the left. Current and future higher precision data raise the question of how to merge older and modern attempts to determine Galactic structure. (Maps are from the electronic archives of the Melville J. Herskovits Library of African Studies at Northwestern University)

to map the Galactic bar(s) and disk(s). Sub-millimeter and molecular line surveys have also dramatically increased in sensitivity and angular resolution. Finally, the VLBA BeSSeL and VERA projects have so far provided parallaxes to 105 masers in star formation region; most of these regions will be inaccessible with Gaia due to high extinction in the Galactic mid-plane.

An analogy to the present state of Galactic cartography can be found in the history of the cartography of Africa. The left map in Fig. 1 shows a map by Gerhard Mercator, published in approximately 1620. This marvelous map was based partially on historical records and traveller accounts recorded by Ptolemy. It contains features that turned out to have some basis in reality, but were very approximately drawn. Compare this to the map from 1805. While the coastline had reached nearly modern precision, mapping the interior of the continent presented a quandary: how should one merge the modern (highly reliable) techniques used to map the coastline with the older (less reliable) techniques for mapping the interior.[2] The map on the right of

[2] This analogy was first suggested by Craig Murphy of Wellesley College in the context of challenges in economics (MacFarquhar 2010), but it applies equally well to this case.

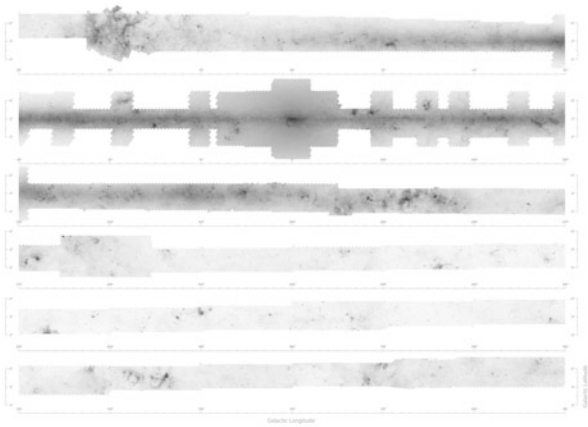

Fig. 2 Full mid-infrared mosaic of the Spitzer Space Telescope GLIMPSE coverage of the Galactic plane. A zoomable (*color*) version may be found at www.spitzer.caltech.edu/glimpse360

this figure, *Map of Africa from the latest authorities* shows one choice: much of the interior has been replace by the label "Unknown Parts", but some historical features like the "Mountains of the Moon", the alleged source of the Nile, remain. Merging the knowledge of Galactic structure from the past six decades with the modern data is a similar challenge, and the experience of the past leads to the first lesson we can take from the Milky Way (or more specifically, Earth).

Lesson 1: As the quality of our data gets better, our maps may look worse.

For those who believe Galactic structure to be a mostly solved issue, prepare for it to become unsolved over the next decade (and hopefully replaced with something more durable). But since no one technique will allow us to map all sections and all components of the Galaxy, significant uncertainties and debate can be expected.

2 The Second Lesson: Rediscoveries in the Galactic Disk

Figure 2 shows an edge-on view of the Milky Way obtained in mid-infrared wavelengths obtained by the *Spitzer Space Telescope*/GLIMPSE survey (Benjamin et al. 2003) (Churchwell et al. 2009). This survey covered a contiguous 360 degrees of longitude along the Galactic plane using the 3.6 and 4.5μm bands of IRAC, with limiting magnitudes ranging from 14 (inner Galaxy) to 16 (outer Galaxy). About half of the plane was also covered in 5.8 and 8.0 μm. Over four thousand hours of observing time over the last ten years were devoted to surveying ∼1200 square degrees of the plane, yielding a point source archive of 229 million sources. For comparison, the 2MASS all-sky survey contains 471 million sources (Skrutskie et al. 2006). Although this strip covers only 3 % of the total sky, it contains 64 % of the stars in the

Table 1 Other claims for a stellar/interstellar break in the Galactic Disk

Reference	Tracer	Break Radius (kpc)	Sky coverage
Robin et al. (1992)	Dwarf star/star counts	14	Four fields
Ruphy et al. (1996)	Red giants/star counts	15	$l = 217, 239°$
Freudenreich (1998)	IR light/param. model	12	All sky
Heyer et al. (1998)	CO	13.5	$l = 102 - 142°$
Reylé et al. (2009)	2MASS star count model	14	All sky
Sale et al. (2010)	A stars/star counts	13.0 ± 0.5	$l = 160 - 200°$
Minniti et al. (2011)	Red clump giants	13.9 ± 0.5	11 fields
Nidever et al. (2012)	Red giants [a]	12–15	$0 < l < 65°, 255 < l < 360°$

[a] Although this work did not claim that the maximum distance for red giants was due to a stellar break, we list this a possible detection of the break on the far side of the Galactic disk

Galactic bar/disk (Freudenreich 1998) and ∼90 % of the star formation. These data have been used in 650 refereed publications to date, nearly 12 % of the total number of publications using *Spitzer* data. Here we will focus on the stellar component, as traced by red giants and red-clump giants. There are several things we would like to know about the Galactic (thin) stellar disk.

First and foremost, what is the scale-length of this disk? The spread in published values in the literature, from two to four kiloparsecs, is much larger than the uncertainties for most of these measurements (Churchwell and Benjamin 2013). So who is correct? I will believe that this problem will be solved when an investigation shows not only how to derive the "correct" answer, but also how to reproduce the "incorrect" answers of the previous investigations. But several complicating factors will need to be addressed, including the possibility of multiple disks, changing vertical scale-heights, stellar breaks, the influence of the bar, non-axisymmetric structure, and populations effects. The model imposed may also have a lot to do with the spread in answers. For example, if there were ever a place to find evidence that stellar disks are not exactly exponential, it would be the Milky Way. Although sorting this out will prove to be complicated, this is a key parameter for Galactic structure.

In contrast to the scale-length, investigations of the location of the stellar "break" (Table 1) of the Galaxy show a surprising degree of concordance, particularly given the diversity of methods. I regard it as the *second* most obvious feature in the GLIMPSE point source catalog of the Galactic plane. (The *most* obvious feature was the enhancement of red-clump giants in the inner Galaxy at an apparent magnitude that changed with Galactic longitude (Benjamin et al. 2005). This was an independent rediscovery/confirmation of the "Long Bar" (Hammersley et al. 2000).) In the "raw" histograms of source counts (no extinction corrections, no color-selection) in the outer Galaxy there is a "flattening" in the histograms (Fig. 3). This flattening can be identified in histograms from $l = 80° - 250°$, a continuous $\sim 170°$ arc of the sky! It is visible in both *Spitzer*/IRAC and 2MASS H and K bands, as well as WISE W1 and W2 bands. We have fit the magnitude where the flattening occurs in

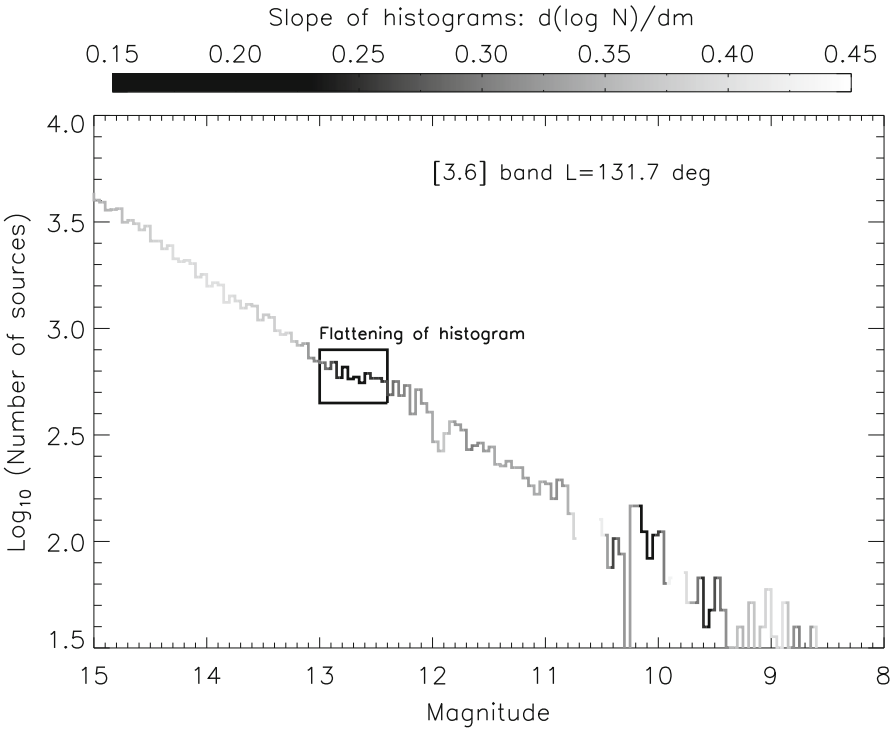

Fig. 3 Apparent magnitude histogram of [3.6] *Spitzer*/GLIMPSE sources extracted from the box $l = 131.7 \pm 0.1$ degrees and $b = 1.0 \pm 1.3$ degrees. A flattening in the histogram is evident at m[3.6]=12.6. The grayscale indicates the slope of the histogram, boxcar-smoothed over a magnitude range of 0.5 mag

the different bands (Fig. 4), finding a color difference of $(H - K) = 0.24 \pm 0.15$ and $(K - [3.6]) = 0.22 \pm 0.10$. The feature becomes much sharper after applying the RJCE extinction correction (Majewski et al. 2011), which relies on a standard $(H - [4.5])_0$ color for all sources. When this extinction correction is applied (on a star-by-star basis), we find that the "color" of the histogram flattening is nearly zero, $(H - K)_{corr} = 0.06 \pm 0.04$ and $(K - [3.6])_{corr} = 0.04 \pm 0.05$. Moreover, we are able to recover the histogram flattening in the J band for many more directions, with a color of $(J - K)_{corr} = 0.50 \pm 0.12$. This is the expected $(J - K)$ color of red-clump giants, empirically demonstrating that the histogram flattening is due to a change in the space density gradient of red clump giants along the line of sight. Models under development confirm that a drop in space density that is faster than the normal exponential decline is needed to produce this feature in the observed histograms.

Ours is not the first piece of evidence for a "stellar break". Some of the works listed in Table 1 measured a break in a limited number of directions; these results were subject to the criticism that the density drop was due to the line of sight exiting a warped stellar disk. (Moreover, in a single direction, a break in volume density

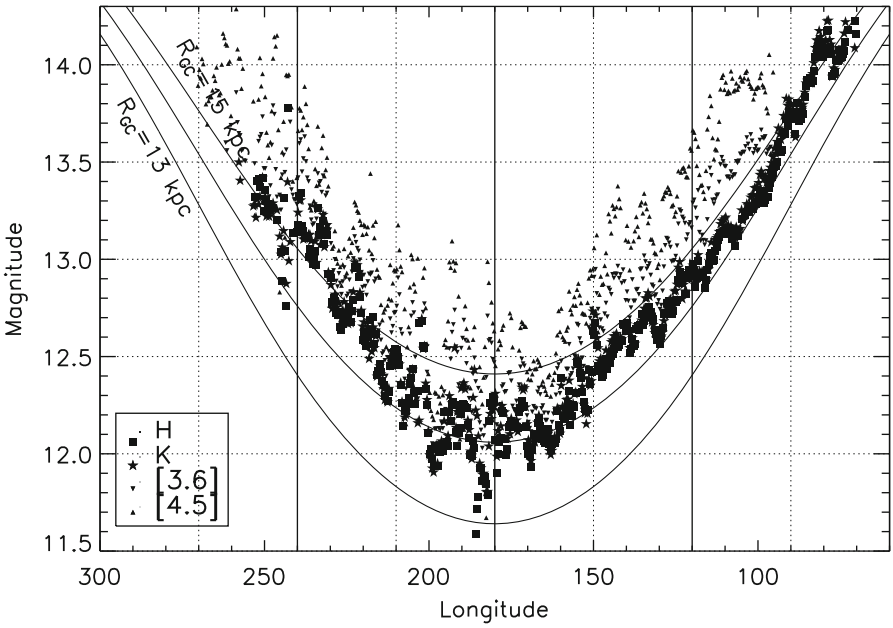

Fig. 4 Magnitudes marking the location of flattening in the "raw" 2MASS and *Spitzer*/GLIMPSE histograms in four bands. Note that the shorter wavelength bands are systematically at fainter magnitudes due to extinction. The curves show the inferred distance assuming a red-clump magnitude of $M = -1.72$ for all four bands. Correction for extinction shifts all bands to a band-independent distance, ranging from a Galactocentric radius of 13.5–15 kpc

does not immediately imply that the projected surface density has a break; there could be a concomitant increase in scale-height at the break radius.) Other works used star-count maps to constrain the parameters of a model for a warped stellar disk; these works were subject to the criticism that the adopted model was poorly posed. For example, most of these models assumed an outer scalelength of zero, e.g. a truncation; others assumed a symmetric warp. This assumption of a "truncation" has led to some confusion in the literature, since both red giants (Momany et al. 2006) and molecular clouds (Digel et al. 1994) are detected beyond the break radius. A pessimist might claim that we have discovered nothing new here since the break was "known", leading to our second lesson.

Lesson 2: Re-establishing the existence of a structure is good (confirmation is under-appreciated); mapping it is even better!

What's new here is the ability to map the break continuously along the entire Galactic plane. Surprisingly, this break is detected not just in red-clump stars (which must

be older than ~ 0.5 Gyr) but also in A stars and in molecular gas, tracers of recent and current star formation. It does not appear that the concomitant behavior of these different tracers is generally appreciated, but since the three-dimensional distribution of all of the gaseous and stellar components can be approximately determined, this region of the Galaxy provides a perfect environment in studying the factors that regulate star formation. Finally, I should note that since the flattening can be detected in 2MASS data (which covers the entire sky), one can map this feature as a function of both Galactic longitude *and* latitude.

3 The Third Lesson: Surprises in Spiral Structure

I haven't left a lot of room here to cover the rapidly evolving views of spiral structure in the Milky Way. (I will have more to say about this in the future.) In the last decade, three new structures in the Galactic disk have been identified: the Distant Arm (McClure-Griffithset al. 2004), the Far Three-Kiloparsec Arm (Dame and Thaddeus 2008), and the Outer Scutum-Centaurus Arm. All three discoveries were made using longitude-velocity diagrams; the most recent two discoveries hints that the Milky Way might be rather symmetric. The fact that these structure were lying undiscovered in archival data for years suggests that there are discoveries yet to be made in this area, and is a reminder of probably one of the most oft-repeated lessons of astronomy:

Lesson 3: Absence of evidence is not evidence of absence; the census of stars, molecular gas, and star formation in the Galaxy is far from complete.

Recent radio, sub-millimeter, and infrared surveys of the Galactic plane have now unleashed a flood of new data and new avenues for investigation. When complemented with the recent maser parallaxes, we have an opportunity to see how the "old" views of Galactic structure hold up when confronted with this new data. Here are some of what I consider some key new directions.

- *BeSSeL and VERA parallaxes are allowing for masers to be accurately mapped and all other distance methods to be better calibrated.* Fig. 1 of Reid et al. (2014) is one of the most encouraging figures of Galactic astronomy; masers that have been grouped by their position on the longitude-velocity plot do indeed trace out structures in space! Although the few hundred masers source that will be mapped out will provide the outlines of Galactic structure, I suspect an equally important result of this work will be the use of the star formation to test and calibrate some of the other distance methods to be better calibrated. Figure 1 of Reid et al. (2014).
- *Most of the HII regions and star forming regions of the Milky Way have been discovered in the past few years.* Several large projects have dramatically increased the number of star formation regions known in the Galaxy, including surveys of masers (Green et al. 2011), 8 μm bubbles (Simpson et al. 2012), mid-infrared

MSX sources (Urquhart et al. 2014), and the mid-infrared/radio based WISE HII region catalog (Anderson et al. 2014). An impressively large number of these now have kinematic distance in which the kinematic distance ambiguity has been resolved. Detailed comparison of this star formation and the neutral and molecular gas of the galaxy is bound to yield useful insights on star formation.

- *High angular resolution FIR, sub-mm, and molecular line surveys, are showing large-scale filaments, some of which are associated with spiral structure and some of which (apparently) are not.* More and more investigations are now focusing on " Massive Molecular Filaments" (Jackson et al. 2010); (Ragan et al. 2014), seen both in emission and absorption. While some of these extended structures seem related to previously identified spiral structure (Goodman et al. 2013), it is not yet clear if the rest of these structures are related to large-scale flows in the Galaxy.
- *Investigations vertical structure of spiral arms.* One of the chief advantages of studying Galactic structure from inside the Milky Way is that we can resolve the vertical dimension of what are otherwise very thin disks. The scale-height of diffuse ionized gas has been measured in the Perseus Arm (Haffneret al. 1999) and more recently the Scutum-Centaurus arm (Hill et al. 2014). Further investigations of the vertical structure of the neutral, molecular, and stellar components of of selected spiral arms could be extremely interesting.

As illustrated at this meeting, we are making significant strides in all areas of the Local Group, but in many respects our knowledge of the disk of our own Galaxy has lagged behind. With the radio surveys of the past, the infrared surveys of the present, and the parallaxes of the future, it is a time to hope once again that the venerable field of Galactic structure may see some major advances.

Acknowledgements It is my pleasure to thank David Block, both for his efforts in organizing this most excellent conference and for his work on the morphologies of galaxies in the optical and infrared, which has influenced my thinking about the Milky Way. I am also grateful for the interactions I have had over the past few years with Bruce Elmegreen, whose insights into star formation and spiral structure have also guided my research. (Bruce also made sure that I had the opportunity in 2008 to talk with Adriaan Blaauw about the early days of mapping Galactic spiral structure, a small kindness for which I will always be grateful.) Happy birthdays to both of our honorees! I also acknowledge the NASA Astrophysical Theory grant NNX10AI70G and the Jet Propulsion Lab RSA 1440126 (for the Spitzer Deep GLIMPSE program) for their financial support.

References

Anderson, L.D., Bania, T.M., Balser, D.S. et al. 2014, ApJS **212**, 1
Benjamin, R.A., Churchwell, E., et al. 2003, PASP **115**, 953
Benjamin, R.A., Churchwell, E., et al. 2005, ApJ **630**, L149
Bok, B.J. 1983, ApJ **273**, 411
Bovy, J. et al. 2012, ApJ **759**, 131
Burton, W.B. 1971, A&A **10**, 76
Burton, W.B. 1992, in *The galactic interstellar medium* Springer-Verlag
Churchwell, E., Benjamin, R.A. 2013, in *Planets, Stars, and Stellar Systems (vol 5)*, 447

Churchwell, E., Babler, B.L., Meade, M.R., Whitney, B.A. et al. 2009, PASP **121**, 213
Dame, T.M., Thaddeus, P. 2008, ApJ **683**, L143
Digel, S., de Geus, E. & Thaddeus, P. 1994, ApJ **422**, 92
Foster, J.B., Stead, J.J., Benjamin, R.A. et al. 2012, ApJ **751**, 157
Freudenreich, H.T. 1998, ApJ **492**, 495
Fux, R. 1999, A&A **345**, 787
Goodman, A.A. et al. 2013, BAAS **221**, 234.01
Green, J.A., Caswell, J.L., McClure-Griffiths, N.M. et al. 2011, ApJ **733**, 27
Haffner, L.M., Reynolds, R.J., Tufte, S.L. 1999, ApJ **523**, 223
Hill, A.S., Benjamin, R.A., Haffner, L.M., Gostisha, M.C. et al. 2014, ApJ, **787**, 106
Hammersley, P.L., Garzón, F., Mahoney, T.J. et al. 2000, MNRAS **317**, L45
Heyer, M.H., Brunt, C., Snell, R.L. et al. 1998, ApJS **115**, 241
Humphreys, R.M. 1976, ApJ **206**, 114
Jackson, J.M., Finn, S.C., Chambers, E.T. et al. 2010, ApJ **719**, L185
Levine, E.S., Blitz, L., Heiles, C. 2006, ApJ **643**, 881
MacFarquhar, L. 2010, *The New Yorker*, 1 March issue, 38
Majewski, S.R., Zasowski, G., Nidever, D.L. 2011, ApJ **739**, 25
McClure-Griffiths, N.M., Dickey, J.M., Gaensler, B.M., Green, A.J. 2004, ApJ **607**, L127
Minniti, D., Saito, R.K., Alonso-García, J., Lucas, P.W., Hempel, M. 2011, ApJ **733**, L43
Momany, Y., Zaggia, S., Gilmore, G. et al. 2006, A&A **451**, 515
Morgan, W.W., Sharpless, S., Osterbrock, D. 1952, AJ **57**, 3
Nidever, D.L., Zasowski, G., Majewski, S.R. 2012, ApJ Supplement **201**, 35
Ragan, S.E., Henning, T., Tackenberg, J., Beuther, H. et al. 2014, arXiV 1403.1450
Reid, M.J., Menten, K.M., Brunthaler, A., Zheng, X.W. et al. 2014, ApJ **783**, 130
Reylé, C., Marshall, D.J., Robin, A.C., Schultheis, M. 2009, A&A **495**, 819
Robin, A.C., Creze, M., Mohan, V. 1992, ApJ **400**, L25
Ruphy, S., Robin, A.C., Epchtein, N., Copet, E.et al. 1996, A&A **313**, L21
Russeil, D. 2003, A&A **397**, 133
Sale, S.E., Drew, J.E., Knigge, C., Zijlstra, A.A. et al. 2010, MNRAS **402**, 713
Simpson, R.J., Povich, M.S., Kendrew, S., Lintott, C.J. et al. 2012, MNRAS **424**, 2442
Skrutskie, M.F., Cutri, R.M., Stiening, R., Weinberg, M.D. et al. 2006, **131**, 1163
Urquhart, J.S., Figura, C.C., Moore, T.J.T., Hoare, M.G. et al. 2014, MNRAS **437**, 1791
van de Hulst, H.C., Muller, C.A., Oort, J.H. 1954, BAN **12**, 117

Gould's Belt

Jan Palouš and Soňa Ehlerová

Abstract The local velocity patterns of star forming regions, young OB stars, nearby OB associations, atomic and molecular gas are confronted with models of an expanding region. We test free expansion from a point or from a ring, expanding 2D shell, and expanding 3D belt with abrupt or gradual energy injection snow-plowing the ambient medium with or without the drag forces including fragmentation and porosity of the medium. There is no agreement on the expansion time, which varies from 30 to 100 Myr. The inclination of the Gould belt is not explained by the above models of expansion. An oblique impact of a high velocity cloud may explain it, but the observed velocity pattern is difficult to reproduce. The Gould's belt may be one of the many structures resulting from shell-shell collisions in the galactic plane. The origin of the Gould's belt may be connected to instabilities in the curling gas flows downstream from the Galaxy spiral arms, forming ISM clouds and star formation complexes.

1 Introduction

Gould's belt is a flat system of young OB stars inclined $\sim 20°$ to the plane of the Milky Way, with the line of nodes pointing approximately in the direction of galactic rotation. In the direction to the galactic center, it extends up to ~ 250 pc from the Sun inclining towards positive z. In the opposite direction to the Galaxy anticenter, it reaches up to ~ 500 pc from the Sun inclining towards negative z. Nearby Scorpius-Centaurus, Perseus and Orion OB associations together with other associations in Vela, Scutum and Vulpecula form an elliptical belt-like structure with center in the second galactic quadrant at a distance ~ 100 pc from the Sun. Motions of young stars in the Gould's belt deviate from galactic differential rotation. It is a challenge to explain their space distribution and kinematics using a plausible model.

Besides stars, also HI gas feature A was discovered by Lindblad (1967). Later, it was designated as Lindblad's ring, which has a similar space distribution as OB stars.

J. Palouš (✉) · S. Ehlerová
Astronomical Institute, Academy of Sciences of the Czech Republic,
Boční II, 141 00 Prague 4, Prague, Czech Republic
e-mail: palous@ig.cas.cz

K. Freeman et al. (eds.), *Lessons from the Local Group,*
DOI 10.1007/978-3-319-10614-4_6

Its kinematics was analysed by Lindblad et al. (1973) and explained as an expanding HI shell. Also nearby CO and H_2 clouds showing a local hole may be parts of the Gould's belt (Dame et al. 1987; Taylor et al. 1987; see also Perrot and Grenier 2003). A comprehensive overview of the Gould's belt is given by Pöppel (1997): space distribution and kinematics of local young OB stars, HI, H_2 dark clouds and star forming regions are interpreted with two basic models: as a result of an explosive event connected to winds and SN in a young OB association, or as a consequence of a collision of a high velocity cloud (HVC) with the galactic plane.

Here we discuss the kinematics of local young OB stars, HI and local star forming regions, and we try to include it into the large-scale picture of galaxy flows compressing the ISM clouds and triggering star formation down-stream after passage through a galaxy spiral arm.

2 OB Stars

Radial velocities V_r, Hipparcos proper motions μ_l, μ_b and distances r derived using the Strömgren photometry may be used in condition equations describing the linearized approximation of the local velocity field:

$$\begin{aligned} V_r = {} & U_\odot \cos l \cos b - V_\odot \sin l \cos b - W_\odot \sin b \\ & + r \cos^2 b \, (K + A \sin 2l + C \cos 2l) \\ & + r \, (H \sin^2 b + D \cos l \sin 2b + G \sin l \sin 2b) \end{aligned} \tag{1}$$

$$\begin{aligned} 4.74 \, r \, \mu_l \cos b = {} & -U_\odot \sin l - V_\odot \cos l \\ & + r \cos b \, (B + A \cos 2l - C \sin 2l) \\ & + r \sin b \cos b \, [(E - D) \sin l \\ & + (G - F) \cos l] \end{aligned} \tag{2}$$

$$\begin{aligned} 4.74 \, r \, \mu_b = {} & -U_\odot \cos l \sin b + V_\odot \sin l \sin b - W_\odot \cos b \\ & - r \sin b \cos b \, [(K - H) + A \sin 2l + C \cos 2l] \\ & + 2r \sin^2 b \, [(E - D) \cos l + (F - G) \sin l] \end{aligned} \tag{3}$$

l, b are the galactic longitude and latitude and

$$A = -\frac{1}{2} \left(\frac{\partial U}{\partial Y} + \frac{\partial V}{\partial X} \right) \tag{4}$$

$$B = \frac{1}{2} \left(\frac{\partial U}{\partial Y} - \frac{\partial V}{\partial X} \right) \tag{5}$$

$$C = \frac{1}{2} \left(\frac{\partial U}{\partial X} - \frac{\partial V}{\partial Y} \right) \tag{6}$$

$$K = \frac{1}{2} \left(\frac{\partial U}{\partial X} + \frac{\partial V}{\partial Y} \right) \tag{7}$$

$$H = \frac{\partial W}{\partial X} \tag{8}$$

$$D = \frac{1}{2}\frac{\partial W}{\partial Y} \tag{9}$$

$$G = \frac{1}{2}\frac{\partial W}{\partial Z} \tag{10}$$

$$E = \frac{1}{2}\left(\frac{\partial U}{\partial Z} - \frac{\partial W}{\partial X}\right) \tag{11}$$

$$F = -\frac{1}{2}\left(\frac{\partial V}{\partial Z} - \frac{\partial W}{\partial Y}\right). \tag{12}$$

are the parameters describing the local velocity field. X, Y, and Z are the coordinates centered on the Sun pointing away from the galactic center, in the direction of the galactic rotation and perpendicularly to the galactic plane, and U, V, W are the components of the space velocity vectors along X, Y, and Z.

(U, V) components of the space velocity vectors of the OB stars within 1 kpc from the Sun and younger than 30 Myr are plotted in Fig. 1. We see that the differential galactic rotation of young stars around the distant center is locally perturbed by wave-like motion following more complex galactic orbits. Outside the Gould's belt, the condition Eqs. (1), (2) and (3) for young OB stars give $A = 12.8$ km s^{-1} kpc^{-1}, $B = -12.5$ km s^{-1} kpc^{-1}, and C, K, H, D, G, E and F close to zero, which may be interpreted as a consequence of rotation following a flat rotation curve with a circular angular velocity at the Sun of ~25 km s^{-1} kpc^{-1}, and no significant deviations from circularity when the Gould's belt region is excluded.

However, the solution of Eqs. (1), (2), and (3) for Gould's belt stars identified due to their position in the local flat inclined system, as it was proposed by Westin (1985); Palouš (1985); Comeron (1994) and Lindblad et al. (1997), presents significant kinematical deviation from galactic differential rotation. It shows that the Gould's belt moves away from the galactic center at about ~ 5 km s^{-1}. Large negative B and large positive K result from additional rotation around a local center combined with expansion from it. The values of H and D are also significantly different from 0 showing a gradient in W motions of ~ 7 km s^{-1} kpc^{-1}. The average W motion is proportional to the distance from the rotation axis pointing in the direction ~ 340° (Comeron 1999). This shows that W motions of the Gould's belt stars are coherent, however, the kinematic axis of W motions is displaced from the line of nodes between Gould's belt and the galactic plane.

3 Expansions

Expansion from a small region was examined since Blaauw (1952), who described the evolution of an expanding group in the galactic plane. Later, the model of an expanding group was applied to local O and B type stars by Lesh (1968, 1972a, b), who derived the plane parallel velocity gradients. Lindblad et al. (1973) used the free expansion model to reproduce the HI ring around the Sun: they concluded that the initial expansion velocity was 3.6 km/s and the expansion age was close to 60 Myr.

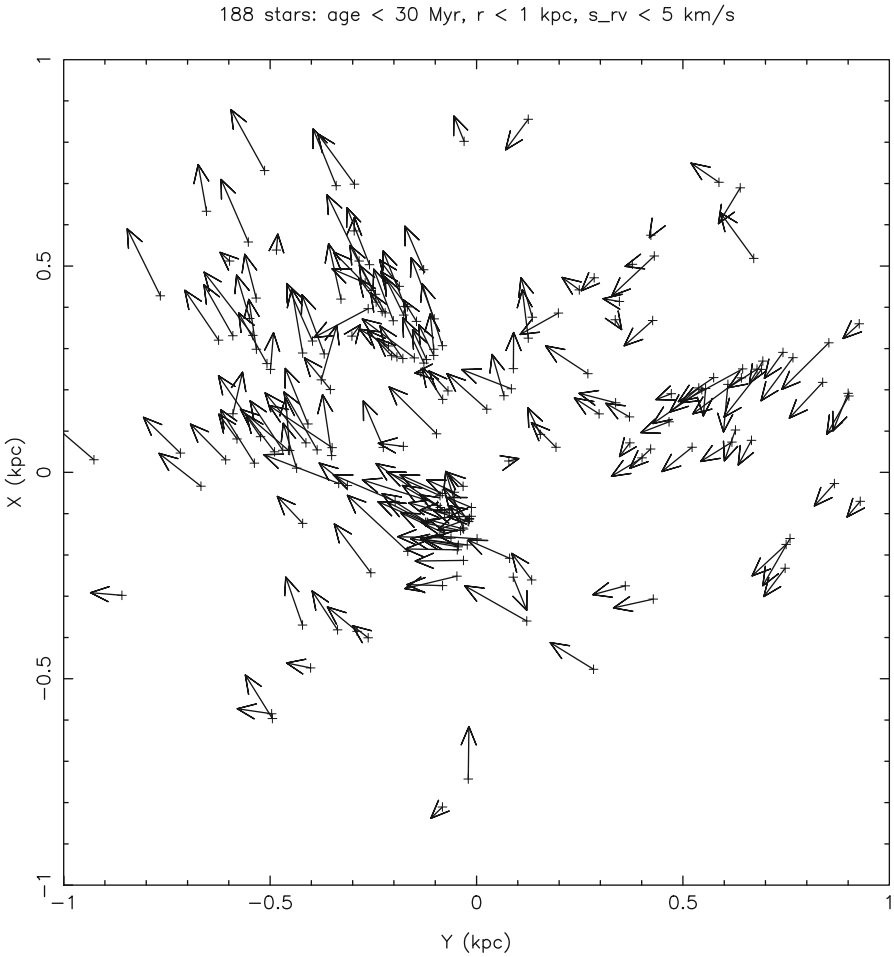

Fig. 1 Positions and space velocity vectors of young OB stars within 1 kpc from the Sun

The velocity field of free expansion from a small region (Lindblad 1980) shows a positive K similar to the observed value. However, B is time independent and equal to 0, which is far from the large negative value derived from the velocity field of Gould's belt stars. Later, the free expansion model was modified with initial rotation (Palouš 1998a, b), and expansion was decelerated in a model of an expanding supershell by Olano (1982). A model with 3D snow-plough in the differentially rotating galaxy was proposed by Ehlerová et al. (1997); Moreno (1999) used the snow-plough in 2D and compared its plane parallel shape to the distribution of OB associations in the Gould's belt. A supershell forming dense belt expanding in 3D was examined by Perrot and Grenier (2003), who tested gradual energy injection, pure snow-plough, pure drag without accretion, fragmentation of the shell with increasing porosity and

triggering star formation in pre-existing clouds. However, a common property of all these models of expansion is the small value of the constant B, which does not correspond to observations. The inclination of the Gould's belt and its size, which is much larger compared to the thickness of the galactic disk, remains also unexplained. In models by Perrot and Grenier (2003) an expanding inclined belt forms out of a gaseous disk, which has a pre-existing tilt relative to the galactic disk.

4 Impacts

Some of the shells and supershells observed in HI and CO in the Milky Way and nearby galaxies including M31 may have been formed by an impact of a high velocity cloud (HVC) into the Galaxy ISM. Tenorio-Tagle (1980) argues that the kinetic energy of a HVC corresponds to the energy requirements for formation of a supershell in a galactic disk. They show (Tenorio-Tagle et al. 1986) that the sizes of structures created by an HVC impact have radii of a few hundreds of parsecs and expanding velocities of 10 km/s or more. Gould's belt may have been formed by such HVC versus galactic disk collision, similar to some of the HI holes observed in nearby galaxies.

An impact of a HVC with a velocity component parallel to the galactic plane was studied by Comeron and Torra (1992). They show that such collision creates a shock-wave with some inclination to the Galaxy symmetry plane. An oblique impact of a HVC may explain the Gould's belt. Later, Comeron & Torra (1994) used an oblique impact to derive the observed gradients of the W velocity component. However, a full 3D hydrodynamic treatment of the supersonic impact of a HVC into the ISM of a galaxy including radiative transfer and all cooling and heating processes is still to be done.

5 Galactic Orbits

With positions and space velocity vectors, we may compute the galactic orbits of nearby young stars and explore how the shape of the current local system changes going to the past. If the Gould's belt has a common origin, its imprint should be recorded in orbits. Computing the orbits backwards in time may discover the shape of the original region where it was born.

The volume taken by members of Scorpius-Centaurus associaton gets smaller when we go to the past (Palouš 1998a, b). The smallest volume occupied by members of present OB associations in Lower Centaurus-Crux, Upper Centaurus-Lupus and Upper Scorpius is reached 10–12 Myr ago. At that time, the progenitors of current OB stars including Scorpius-Centaurus and Orion associations form a sheet-like region about 500 pc long and less than 100 pc wide with the main axis pointing in the direction l = 20–200°.

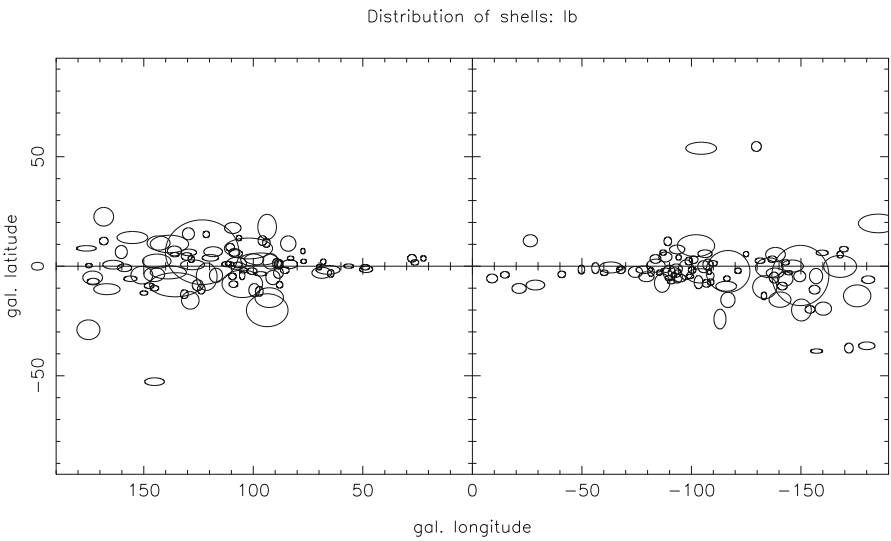

Fig. 2 HI shells in the Milky Way: the inner Galaxy and local shells are excluded

The local ISM was explored by Frisch (1981); Frisch and York (1983) and Heiles (1989), who describe the Local Bubble, which interacts with Loop I Bubble and Loop IV Bubble above the plane. A supersonic collision of two expanding supershells may create a sheet-like region composed of matter collected in both colliding shells. Formation of molecular clouds and subsequent star formation may have been triggered due to the shell-shell collision. Later, the young OB stars have expanded to the present configuration of the Gould's belt. The ISM sheet could be tilted relative to the galactic plane, which is a natural outcome of collisions between off plane asymmetrical supershells. 3D hydrodynamical simulations of shell - shell supersonic collisions, mass accumulation in a sheet-like region, formation of dense molecular clouds, and triggering of star formation is to be performed in future to explore this possibility that the Gould's belt may have been formed this way.

6 Are There Other Gould's Belts

Ehlerová and Palouš (2005, 2013) analyzed Leiden/Argentina/Bonn HI survey and discovered a few hundreds of shells (see Fig. 2). Their sizes range up to 1 kpc with a power-law distribution corresponding to the luminosity function of OB associations. Figure 3 shows the (l-b) distribution of HI in the region of the supershell GSH243.5-02.5+43.3 discovered by Heiles (1979) and its neighbouring shell GSH226.5-09.5+31.9 together with overlaid CO emission. In Fig. 4 we present the (l-v) diagram of the shell GSH226.5-09.5+031.9. Using the algorithm DENDROFIND

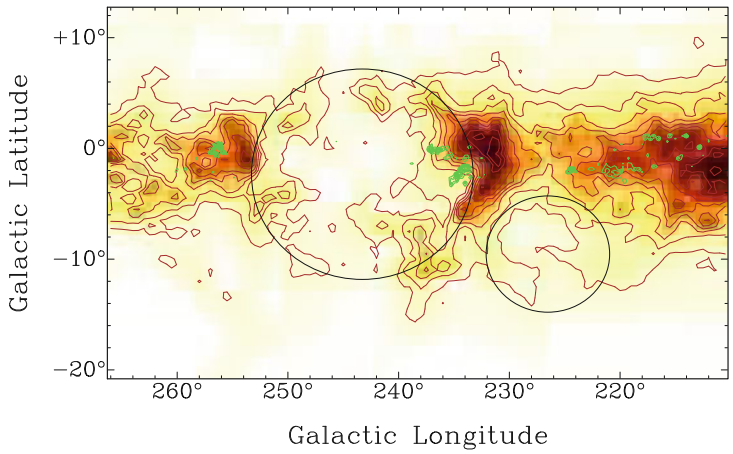

Fig. 3 HI emission in the region of GSH243.5-02.5+43.3 (*big circle*) and GSH226.5-09.5+31.9 (*small circle*) integrated in the radial velocity interval 30–50 km s^{-1} with overlaid CO contours

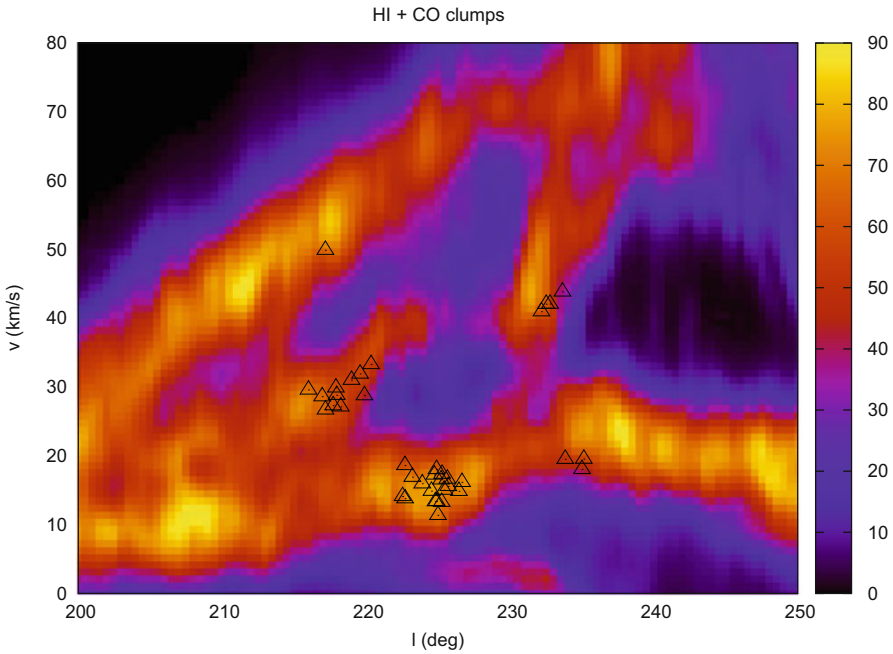

Fig. 4 GSH226.5-09.5+31.9: lv diagram. HI emission in the background with triangles showing the CO clumps

(Wunsch et al. 2012), we have identified HI clumps in shell walls complemented with CO clumps seen in the CO survey by Dame et al. (2001). In Fig. 5 we display the HI and CO clumps in walls of the supershell GSH226.5-09.5+31.9 as they would be

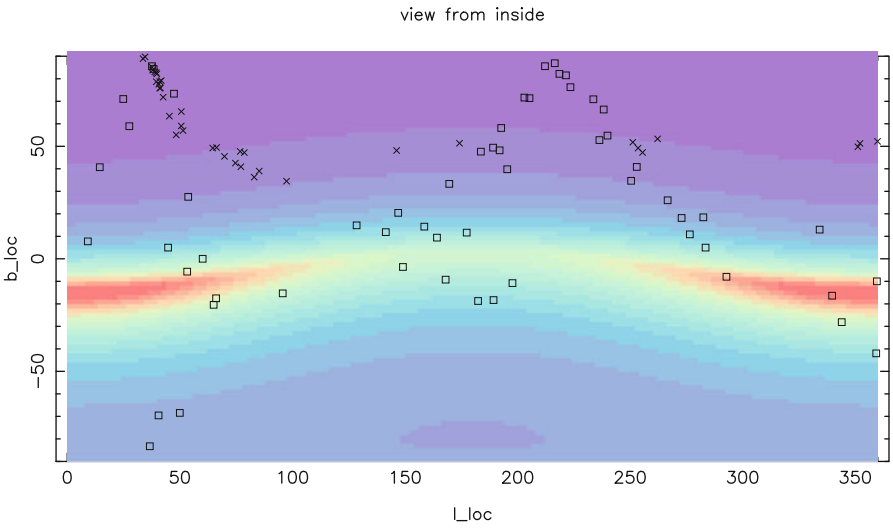

Fig. 5 GSH226.5-09.5+31.9: a view from inside. Crosses show the CO and squares HI clumps

seen if the observer resided in its center: they are distributed in a ring inclined relative to the galaxy symmetry plane resembling with its size, the plane-like distribution and of the tilt HI and CO clouds of the Gould's belt.

The existence of many HI holes in the HI distribution in the Milky Way, some of them expanding with velocities ranging between 10–30 km s^{-1}, and the correlation of their walls with CO distribution, show that in our Galaxy there may be many Gould's belts. The view from the current position of the Sun, which arrived into the local volume of the local HI hole surrounded by local molecular clouds and local young OB stars and associations, shows us the structure called Gould's belt. However, there may be many similar structures along the plane of the Milky Way.

7 Origins

The formation of molecular clouds in curling gas flows downstream spiral arms was shown in simulations by Dobbs et al. (2012). There we may see voids surrounded by clouds similar to Gould's belt. Star formation occurs in hierarchical patterns (Elmegreen 2011): star forming regions are grouped into complexes of 1 kpc size. This results from turbulent nature of the galaxy ISM, star formation following the dense filaments and knots formed in turbulent cascades. Gould's belt is a star formation complex which is a part of the turbulent cascade downstream from galaxy spiral arms.

Acknowledgement This study has been supported by Czech Science Foudation grant 209/12/1795 and by the project RVO: 67985815. This research made use of NASA's Astrophysics Data System. The authors would like to thank Anthony Whitworth for the help with the manuscript.

References

Blaauw, A., 1952, *Bull. Astron. Inst. Netherlands*, 11, 414
Comeron, F., Torra, J., & Gomez, A., 1994, *Astron. & Astrophys.*, 286, 789
Comeron, F., 1999, *Astron. & Astrophys.*, 351, 506
Dame, T. M., et al., 1987, *ApJ*, 322, 706
Dame, T., Hartmann, D., & Thaddeus, P., 2001, *ApJ*, 547, 792
Dobbs, C. L., Pringle, J. E., & Burkert, A., 2012, *MNRAS*, 425, 2157
Ehlerová, S., Palouš, J., Theis, Ch., & Hensler, G., 1997, *Astron. & Astrophys.*, 328, 121
Ehlerová, S., & Palouš, J., 2005, *Astron. & Astrophys.*, 437, 101
Ehlerová, S., & Palouš, J., 2013, *Astron & Astrophys.*, 550, A23
Elmegreen, B. G., 2011, in *Star Formation in the Local Universe*, C. Charbonnel and Montmerle, T. (eds), EAS Publication Series
Frisch, P. C., 1981, *Nat.*, 293, 377
Frisch, P. C., and York, D. G., 1983, in *Galaxy and the Solar System*, R. Smoluchowski, J. N. Bahcall and M. Mathews (eds), Univ of Arizona Press, Tucson, p. 83
Heiles, C., 1989, *ApJ*, 336, 808
Lesh, J. R., 1968, *ApJS*, 17, 371
Lesh, J. R., 1972a, *A&AS*, 5, 129
Lesh, J. R., 1972b, *IAU Colloq.*, 17
Lindblad, P. O., 1967, *BAN* 19, 34
Lindblad, P. O., 1980, *Mitt. Astron. Gess.*, 48, 51
Lindblad, P.O., Grape, K., Sandqvist, Aa., & Schober, J. 1973, *A&A*, 24, 309
Lindblad, P. O., Palouš, J., Lodén, K., & Lindegren, L., 1997, *Hipparcos Venice'97*, ESA, p. 507
Moreno, E., Alfaro, E. J., & Franco, J., 1999, *ApJ*, 522, 276
Olano, C. A., 1982, Astronomy and Astrophysics, vol. 112, p. 195

Palouš, J., 1985, *Bull. Astron. Inst. Czech*, 36, 261
Palouš, J., 1998a, in N. Capitaine and J. Vodrák (eds), *Journeé systemes de reference spatiotemporel 1997*, Praha, p.157
Palouš, J., 1998b, in W. J. Duschl and Ch. Einsel (eds), *Dynamics of Galaxies and Galctic Nuclei*, ITA Proceedings Series, Vol. 2, p. 157
Pöppel, W., 1997, *Fundamentals of Cosmic Physics* 18, 1
Taylor, D. K., Dickman, R. L., & Scoville, N. Z., 1987, *ApJ*, 315, 104
Tenorio-Tagle, G., 1980, *Astron. Astrophys.*, 88, 61
Tenorio-Tagle, G., Bodenheimer, P., Rozyczka, M., & Franco, J., 1986, *Astron. Astrophys*, 170, 107
Westin, T. N. G., 1985, *A&A Suppl.*, 60, 99
Wunsch, R., Jáchym, P., Sidorin, V., Ehlerová, S., Palouš, J., Dale, J., Dawson, J. R., & Fukui, Y., 2012, *Astron. & Astrophys.*, 539, A116

Interstellar Filaments and Their Role in Star Formation as Revealed by *Herschel*

Philippe André

Abstract Recent studies of the nearest star-forming clouds of the Galaxy at submillimeter wavelengths with the *Herschel* Space Observatory have provided us with unprecedented images of the initial conditions and early phases of the star formation process. The *Herschel* images reveal an intricate network of filamentary structure in every interstellar cloud. These filaments all exhibit remarkably similar widths - about a tenth of a parsec—but only the densest ones contain prestellar cores, the seeds of future stars. The *Herschel* results favor a scenario in which interstellar filaments and prestellar cores represent two key steps in the star formation process: first turbulence stirs up the gas, giving rise to a universal web-like structure in the interstellar medium, then gravity takes over and controls the further fragmentation of filaments into prestellar cores and ultimately protostars. This scenario provides new insight into the inefficiency of star formation, the origin of stellar masses, and the global rate of star formation as a function of the mass of dense molecular gas in galaxies. Despite an apparent complexity, global star formation may be governed by relatively simple universal laws from filament to galactic scales.

1 Introduction

Star formation is one of the most complex processes in astrophysics, involving a subtle interplay between gravity, turbulence, magnetic fields, feedback mechanisms, heating and cooling effects etc. Yet, despite this apparent complexity, the net products of the star formation process on global scales are relatively simple and robust. In particular, the distribution of stellar masses at birth or stellar initial mass function (IMF) is known to be quasi-universal (e.g. Kroupa 2002; Chabrier 2003; Elmegreen et al. 2008). Likewise, the star formation rate on both GMC and galaxy-wide scales is related to the mass of (dense molecular) gas available by rather well defined "star formation laws" (e.g. Kennicutt 1998; Gao and Solomon 2004; Lada et al. 2010). On the basis of recent results obtained with the *Herschel* Space Observatory on nearby

P. André (✉)
Laboratoire d'Astrophysique (AIM) de Paris-Saclay, CEA Saclay,
Gif-sur-Yvette, 91191 Paris, France
e-mail: pandre@cea.fr

K. Freeman et al. (eds.), *Lessons from the Local Group,*
DOI 10.1007/978-3-319-10614-4_7

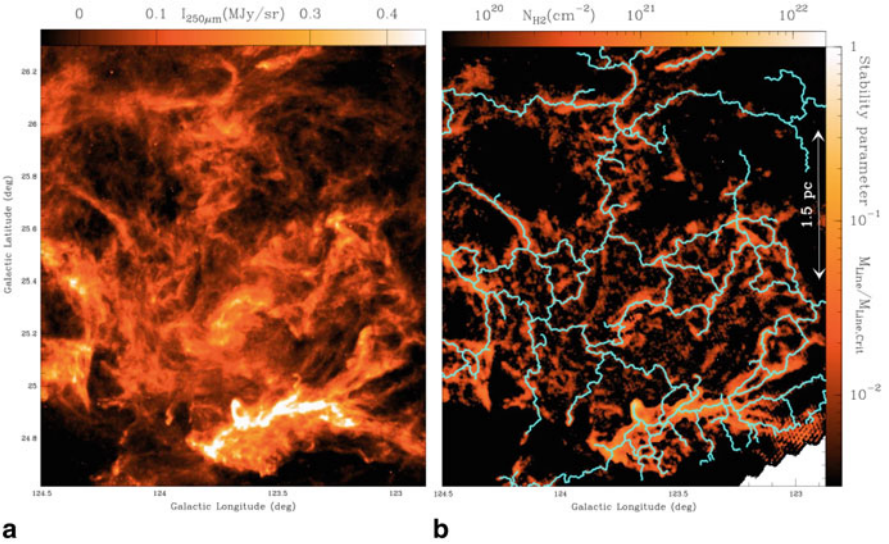

Fig. 1 **a** *Herschel*/SPIRE 250 μm dust continuum map of a portion of the Polaris flare translucent cloud (e.g., Miville-Deschênes et al. 2010; Ward-Thompson et al. 2010). **b** Corresponding column density map derived from *Herschel* data (e.g., André et al. 2010). The contrast of the filaments has been enhanced using a curvelet transform (cf. Starck et al. 2003). The skeleton of the filament network identified with the DisPerSE algorithm (Sousbie 2011) is shown in light blue. A similar pattern is found with other algorithms such as *getfilaments* (Men'shchikov 2013). Given the typical width ~ 0.1 pc of the filaments (Arzoumanian et al. 2011 – see Fig. 4 below), this column density map is equivalent to a *map of the mass per unit length along the filaments* (*see color scale on the right*)

interstellar clouds as part of the Gould Belt (André et al. 2010), HOBYS (Motte et al. 2010), and Hi-GAL (Molinari et al. 2010) surveys, the thesis advocated here is that it may be possible to explain, at least partly, the IMF and the global rate of star formation in terms of the quasi-universal filamentary structure of the cold interstellar medium out of which stars form.

2 Universality of Filamentary Structures in the Cold ISM

The high quality and dynamic range of the *Herschel* submillimeter dust continuum images are such that they provide key information on both dense cores on small (< 0.1 pc) scales *and* the structure of the parent clouds on large (> 1 pc) scales. In particular, one of the most spectacular early findings made with *Herschel* is the ubiquitous presence of long ($>$ pc scale) filamentary structures in the cold interstellar medium (ISM) and the apparently tight connection between the filaments and the formation process of dense cores (e.g. André et al. 2010; Men'shchikov et al. 2010; Molinari et al. 2010). While interstellar clouds were already known to exhibit large-scale filamentary structures long before *Herschel* (e.g. Schneider

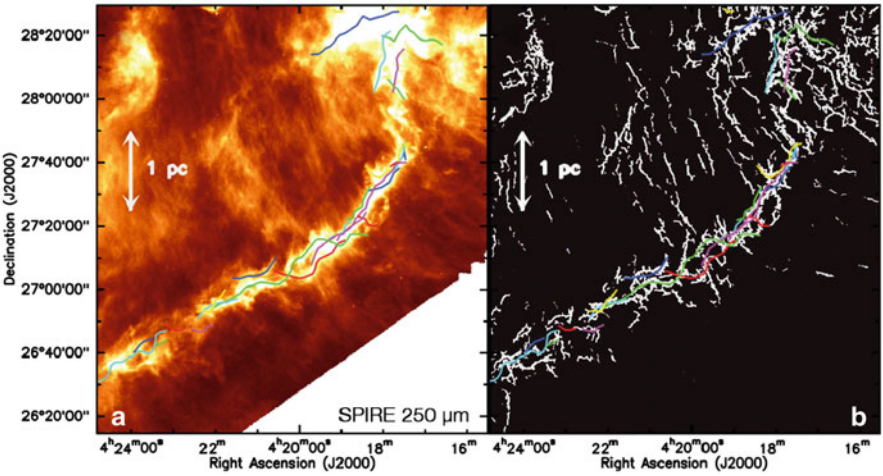

Fig. 2 **a** *Herschel*/SPIRE 250 μm dust continuum image of the B211/B213/L1495 region in Taurus (Palmeirim et al. 2013). The colored curves display the velocity-coherent "fibers" identified within the B213/B211 filament by Hacar et al. (2013) using $C^{18}O$(1–0) observations. **b** Fine structure of the *Herschel*/SPIRE 250 μm dust continuum emission from the B211/B213 filament obtained by applying the multi-scale algorithm *getfilaments* (Men'shchikov 2013) to the 250 μm image shown in panel (a). Note the faint striations perpendicular to the main filament and the excellent correspondence between the small-scale structure of the dust continuum filament and the bundle of velocity-coherent fibers traced by Hacar et al. (2013) in $C^{18}O$ (same colored curves as in (a))

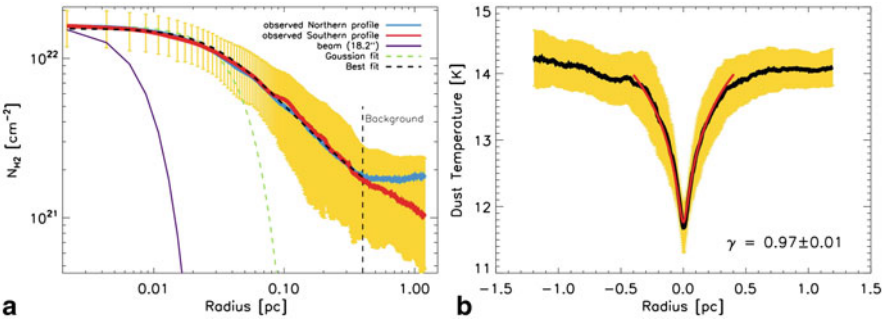

Fig. 3 **a** Mean radial column density profile observed perpendicular to the B213/B211 filament in Taurus (Palmeirim et al. 2013), for both the Northern (*blue curve*) and the Southern part (*red curve*) of the filament. The yellow area shows the ($\pm 1\Sigma$) dispersion of the distribution of radial profiles along the filament. The inner solid purple curve shows the effective 18" HPBW resolution (0.012 pc at 140 pc) of the *Herschel* column density map used to construct the profile. The dashed black curve shows the best-fit Plummer model (convolved with the 18" beam), which has a central diameter $2 \times R_{\rm flat} = 0.07 \pm 0.01$ pc and matches the data very well for $r \leq 0.4$ pc, **b** Mean dust temperature profile measured perpendicular to the B213/B211 filament in Taurus. The solid red curve shows the best polytropic model temperature profile obtained by assuming $T_{\rm gas} = T_{\rm dust}$ and that the filament has a density profile given by the Plummer model shown in the left panel and obeys a polytropic equation of state, $P \propto \rho^{\gamma}$ [and thus $T(r) \propto \rho(r)^{(\gamma-1)}$]. This best fit corresponds to a polytropic index $\gamma = 0.97 \pm 0.01$ (see Palmeirim et al. 2013 for further details)

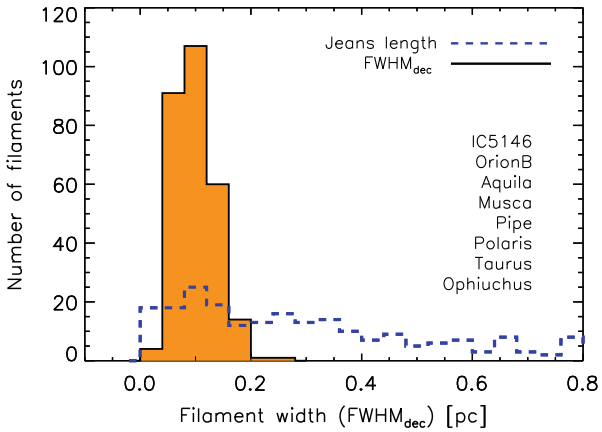

Fig. 4 Histogram of deconvolved FWHM widths for a sample of 278 filaments in 8 nearby regions of the Gould Belt, all observed with *Herschel* (at resolutions ranging from ~ 0.01 pc to ~ 0.04 pc) and analyzed in the same way (Arzoumanian et al., in prep.—see Arzoumanian et al. 2011 for initial results on a subsample of 90 filaments in 3 clouds). The distribution of filament widths is narrow with a median value of 0.09 pc and a standard deviation of 0.04 pc (equal to the bin size). In contrast, the distribution of Jeans lengths corresponding to the central column densities of the filaments (*blue dashed histogram*) is much broader

and Elmegreen 1979; Hartmann 2002; Hatchell et al. 2005; Myers 2009), *Herschel* now demonstrates that these filaments are truly ubiquitous in the giant molecular clouds (GMCs) of our Galaxy (Molinari et al. 2010) and provides an unprecedented large-scale view of the role of filaments in the formation of prestellar cores (see § 3).

Remarkably, filaments are omnipresent even in diffuse, non-star-forming complexes such as the Polaris translucent cloud (cf. Fig. 1—Miville-Deschênes et al. 2010; Ward-Thompson et al. 2010). Moreover, in any given cloud complex, the *Herschel* images reveal a whole network of filaments (see Figs. 1, 2, and 5a), making it possible to characterize their properties in a statistical manner. Detailed analysis of the radial column density profiles derived from *Herschel* data shows that the filaments are characterized by a very narrow distribution of central widths with a typical FWHM value of ~ 0.1 pc (Arzoumanian et al. 2011). A plausible interpretation of this characteristic width of interstellar filaments is that it corresponds to the sonic scale below which interstellar turbulence becomes subsonic in diffuse, non-star-forming gas (cf. Padoan et al. 2001; Federrath et al. 2010).

3 The Key Role of Filaments in the Core Formation Process

The observed correspondence between the filaments and the spatial distribution of compact cores is also remarkable (see Fig. 5), suggesting that *dense cores form primarily along filaments*. More precisely, the prestellar cores identified with *Herschel*

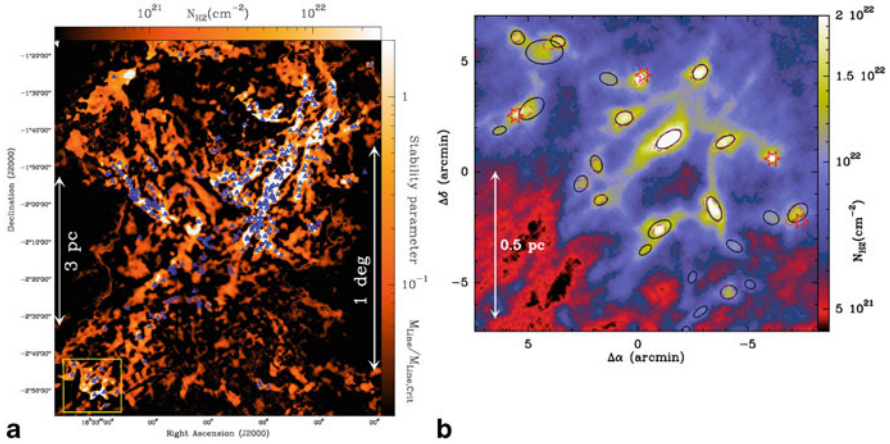

Fig. 5 **a** Column density map of a subfield of the Aquila star-forming region derived from *Herschel* data (André et al. 2010). The contrast of the filaments has been enhanced using a curvelet transform (cf. Starck et al. 2003). Given the typical width ~ 0.1 pc of the filaments (Arzoumanian et al. 2011 – see Fig. 4), this map is equivalent to a *map of the mass per unit length along the filaments*. The areas where the filaments have a mass per unit length larger than half the critical value $2\,c_s^2/G$ (cf. Inutsuka and Miyama 1997) and are thus likely gravitationally unstable are highlighted in white. The bound prestellar cores identified by Könyves et al. (2010) are shown as *small blue triangles*. **b** Close-up column density map of the area shown as a *yellow box* on the *left*. The *black ellipses* mark the major and minor FWHM sizes of the prestellar cores found with the source extraction algorithm *getsources* (Men'shchikov et al. 2012); four protostellar cores are also shown by *red stars*. The *dashed purple ellipses* mark the FHWM sizes of the sources independently identified with the *csar* algorithm (Kirk et al. 2013). The effective resolution of the image is $\sim$ 18" or ~ 0.02 pc at $d \sim 260$ pc

are preferentially found within the *densest filaments* with masses per unit length exceeding $\sim 16\,M_\odot$/pc and column densities exceeding $\sim 7 \times 10^{21}$ cm^{-2}. (André et al. 2010 and Fig. 5a).

3.1 A Column Density Threshold For Prestellar Core Formation

In the Aquila region, for instance, the distribution of background cloud column densities for the prestellar cores (Fig. 6a) shows a steep rise above $N_{\rm H_2}^{\rm back} \sim 5 \times 10^{21}$ cm^{-2} and is such that ~ 90 % of the candidate bound cores are found above a background column density $N_{\rm H_2}^{\rm back} \sim 7 \times 10^{21}$ cm^{-2}, corresponding to a background visual extinction $A_V^{\rm back} \sim 7$ (André et al. 2014; Könyves et al. in prep.). The *Herschel* observations of the Aquila Rift complex therefore strongly support the existence of a column density or visual extinction threshold for the formation of prestellar cores at $A_V^{\rm back} \sim 5$–10, which had been suggested based on earlier ground-based studies of, e.g., Taurus and Ophiuchus (cf. Onishi et al. 1998; Johnstone et al. 2004; Goldsmith

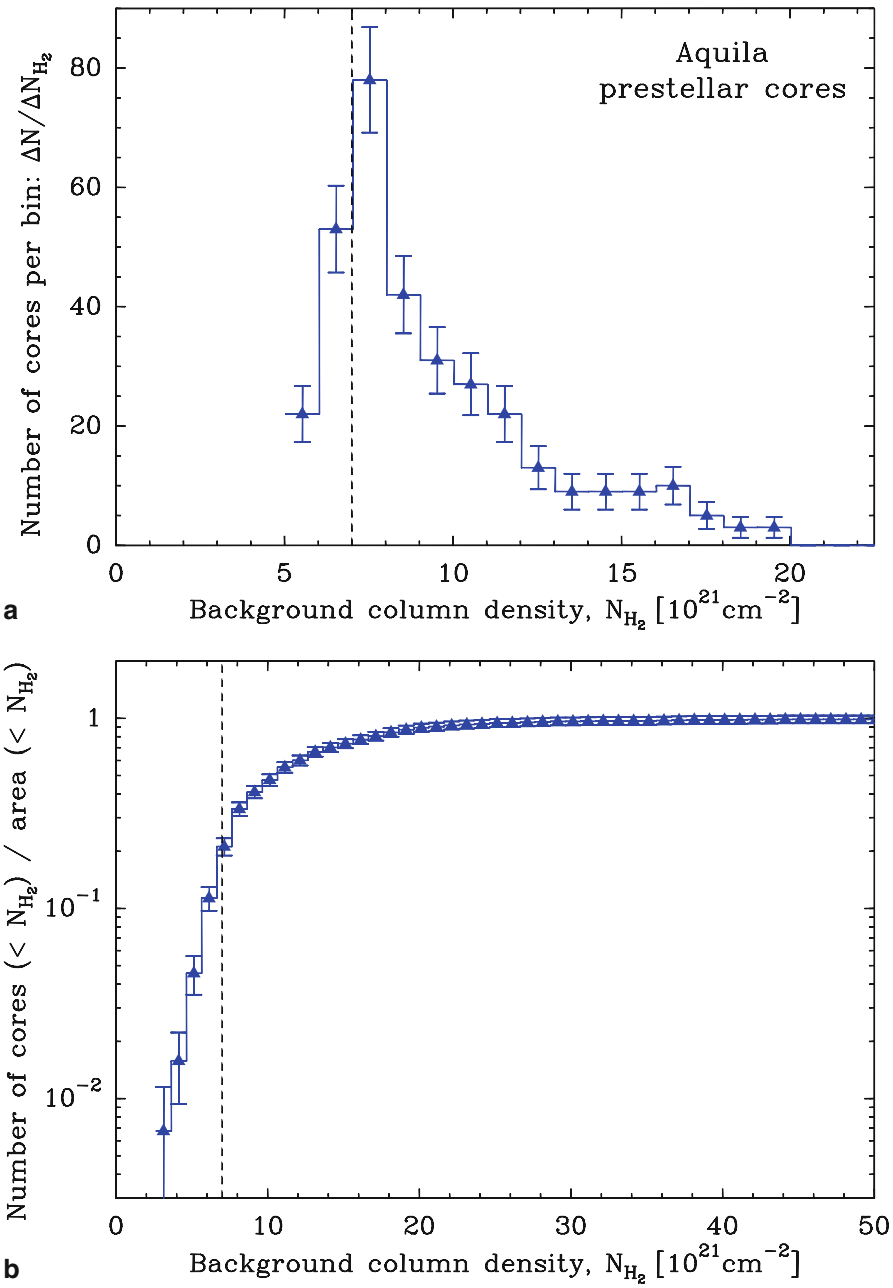

Fig. 6 **a** Distribution of background column densities for the candidate prestellar cores identified with *Herschel* in the Aquila Rift complex (cf. Könyves et al. 2010 and in prep.). The *vertical dashed line* marks the column density or extinction threshold at $N_{\rm H_2}^{\rm back} \sim 7 \times 10^{21}$ cm^{-2} or $A_V^{\rm back} \sim 7$ (also corresponding to $\Sigma_{\rm gas}^{\rm back} \sim 150\ M_\odot$ pc^{-2}). **b** Normalized probability of finding a *Herschel* prestellar core below a given background column density in Aquila as a function of background column

et al. 2008). In the Polaris flare, our results are also consistent with such an extinction threshold since the observed background column densities are all below $A_V^{\rm back} \sim 8$ and there are no examples of bound prestellar cores in this cloud.

We stress that two effects make this column density threshold very significant. First, the typical distribution of mass in star-forming clouds is such that there is much more low-density gas than high-density gas (in Aquila, for instance, $\sim$ 85 % of the cloud mass is below $A_V = 7$ and only $\sim$ 15 % of the mass lies at higher column densities). Second, the completeness of our *Herschel* census for prestellar cores increases in lower column density areas, due to a lower level of "cirrus noise" fluctuations (cf. Gautier et al. 1992). As a consequence, if prestellar cores were randomly distributed throughout the cloud independently of the local background (column) density, we would be much more likely to observe cores in lower column density areas. This is clearly not the case. Figure 6b shows the estimated probability of finding a *Herschel* prestellar core as a function of background column density, obtained by normalizing the number of *Herschel* prestellar cores identified below a given background column density by the total surface area imaged with *Herschel* below the same cloud column density in Aquila. It can be seen that this probability function resembles a smooth step function centered around $A_V^{\rm back} \sim 7$.

3.2 *Interpretation of the Star Formation Threshold*

The *Herschel* results provide an *explanation* of the core/star formation threshold in terms of the filamentary structure of molecular clouds. Given the characteristic width $\sim$ 0.1 pc measured for the filaments (Arzoumanian et al. 2011 – cf. Figs. 3a & 4), the threshold at $A_V^{\rm back} \sim 8$ or $\Sigma_{\rm gas}^{\rm back} \sim 150\ M_\odot\,{\rm pc}^{-2}$ corresponds to within a factor of $<< 2$ to the critical mass per unit length $M_{\rm line,crit} = 2\,c_s^2/G \sim 16\,M_\odot$/pc required for the hydrostatic equilibrium of isothermal filaments (cf. Ostriker 1964), where $c_s \sim 0.2$ km/s is the isothermal sound speed for a typical gas temperature $T \sim 10$ K. Thus, the core formation threshold approximately corresponds to the *threshold above which interstellar filaments are gravitationally unstable* to both radial contraction and fragmentation along their lengths (cf. Inutsuka and Miyama 1992, 1997). Prestellar cores are only observed above this threshold because they form out of a filamentary background and only the supercritical, gravitationally unstable filaments with $M_{\rm line} > M_{\rm line,crit}$ are able to fragment into bound cores (cf. André et al. 2010 and Fig. 5a).

←

Fig. 6 (continued) density (cf. from Könyves et al. in prep.). Note that this probability increases by more than one order of magnitude between $N_{\rm H_2}^{\rm back} \sim 4 \times 10^{21}$ cm^{-2} and $N_{\rm H_2}^{\rm back} \sim 10^{22}$ cm^{-2}. The *vertical dashed line* marks the same column density "threshold" at $A_V^{\rm back} \sim 7$ as in the left panel

4 Toward a Universal Scenario for Core and Star Formation on GMC Scales in Galaxies?

The *Herschel* results summarized in § 2 and § 3 provide key insight into the core formation process. They emphasize the role of filaments and support a scenario according to which the formation of prestellar cores occurs in two main steps. First, the dissipation of kinetic energy in large-scale magneto-hydrodynamic (MHD) turbulent flows generates a whole network of ~ 0.1 pc-wide filaments in the cold ISM; second, the densest filaments fragment into prestellar cores by gravitational instability above the critical mass per unit length $M_{\rm line,crit} = 2\,c_s^2/G \sim 16\,M_\odot$/pc.

That the formation of filaments in the diffuse ISM represents the first step toward core/star formation is suggested by the filaments *already* being omnipresent in a gravitationally unbound, non-star-forming cloud such as Polaris (cf. Fig. 1, Men'shchikov et al. 2010; and Miville-Deschênes et al. 2010). This indicates that some interstellar filaments are not produced by large-scale gravity and that their formation must precede star formation. It is also consistent with the view that the filamentary structure results primarily from the dissipation of large-scale interstellar turbulence (cf. Padoan et al. 2001; Hily-Blant and Falgarone 2007). In this view, interstellar filaments correspond to dense, post-shock stagnation gas associated with compressed regions between interacting supersonic flows. One merit of this picture is that it accounts for the characteristic ~ 0.1 pc inner width of the filaments as measured with *Herschel*: the typical thickness of shock-compressed structures resulting from supersonic turbulence in the ISM is expected to be roughly the sonic scale of the turbulence or about ~ 0.1 pc in diffuse interstellar gas (cf. Larson 1981). An alternative possibility, advocated by Hennebelle (2013), is that the filament width ~ 0.1 pc corresponds to the dissipation length of MHD waves due to ion-neutral friction in the primarily neutral gas of molecular clouds.

The second step appears to be the gravitational fragmentation of the densest filaments with supercritical masses per unit length ($M_{\rm line} > M_{\rm line,crit}$) into self-gravitating prestellar cores (André et al. 2010 – cf. § 3). Indeed, in active star-forming regions such as the Aquila complex, most of the prestellar cores identified with *Herschel* are concentrated within supercritical filaments (cf. Fig. 5a). In contrast, in non-star-forming clouds such as Polaris, all of the filaments have subcritical masses per unit length and only unbound starless cores are observed but no prestellar cores nor protostars (cf. Fig. 1b).

Interestingly, the peak of the prestellar core mass function (CMF) at $\sim 0.6\,M_\odot$ as observed in the Aquila complex (André et al. 2010; Könyves et al. 2010) corresponds to the Jeans or Bonnor-Ebert mass $M_{\rm BE} \sim 0.6\,M_\odot \times (T/10\,{\rm K})^2 \times \left(\Sigma/150\,M_\odot\,{\rm pc}^{-2}\right)^{-1}$ within marginally critical filaments with $M_{\rm line} \approx M_{\rm line,crit} \sim 16\,M_\odot$/pc and surface densities $\Sigma \approx \Sigma_{\rm gas}^{\rm crit} \sim 150\,M_\odot\,{\rm pc}^{-2}$. Likewise, the median spacing ~ 0.09 pc observed between the prestellar cores of Aquila roughly matches the thermal Jeans length within marginally critical filaments.

All of this is consistent with the idea that the gravitational fragmentation of filaments is the dominant physical mechanism generating prestellar cores in molecular

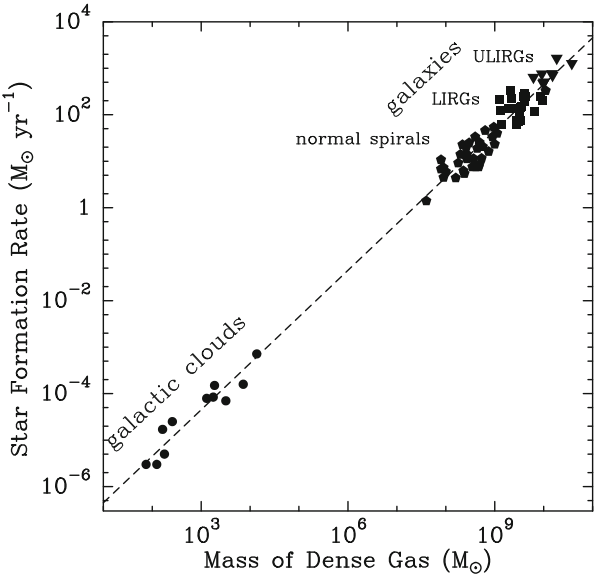

Fig. 7 Relation between star formation rate (SFR) and mass of dense gas ($M_{\rm dense}$) for local molecular clouds (Lada et al. 2010) and external galaxies (Gao and Solomon 2004). $M_{\rm dense}$ is the mass of dense gas above the star formation threshold ($n_{H_2} \sim 2 \times 10^4$ cm^{-3} – see text). The *dashed line* going through the data points represents the linear relation $SFR = 4.5 \times 10^{-8}\, M_\odot\,{\rm year}^{-1} \times (M_{\rm dense}/M_\odot)$ inferred from the *Herschel* results on prestellar cores in the Aquila cloud complex (see text and Könyves et al. in prep). (Adapted from Lada et al. 2012)

clouds. Furthermore, a typical prestellar core mass of $\sim 0.6\,M_\odot$ translates into a characteristic star or stellar system mass of $\sim 0.2\,M_\odot$, assuming a typical efficiency $\epsilon_{\rm core} \sim 30$ % (cf. Alves et al. 2007; André et al. 2010). Therefore, our *Herschel* findings strongly support Larson (1985)'s interpretation of the peak of the IMF in terms of the typical Jeans mass in star-forming clouds. Naively, one would expect gravitational fragmentation to result in a narrow prestellar CMF sharply peaked at the median thermal Jeans mass. However, a broad CMF resembling the log-normal shape of the IMF can be produced if turbulence has generated a field of initial density fluctuations within the filaments in the first place (cf. Inutsuka 2001). Overall, our results suggest that the gravitational fragmentation of supercritical filaments produces the prestellar CMF which, in turn, accounts for the log-normal "base" (cf. Bastian et al. 2010) of the IMF. It remains to be seen, however, whether the bottom end of the IMF and the Salpeter power-law slope at the high-mass end can also be explained by filament fragmentation. In particular, we note that the pre-brown dwarf core Oph B-11 recently identified by André et al. (2012) in the Ophiuchus protocluster is *not* associated with a filament and has most likely formed in a different manner through, e.g., turbulent fragmentation (e.g. Padoan and Nordlund 2004; Hennebelle and Chabrier 2008) (Fig. 7).

The realization that prestellar core formation occurs primarily along gravitationally unstable filaments of roughly constant width $W_{\rm fil} \sim 0.1$ pc also has potential implications for our understanding of star formation on galaxy-wide scales. Remarkably, the critical line mass of a filament, $M_{\rm line,crit} = 2\,c_s^2/G$, depends only on gas temperature (i.e., $T \sim 10$ K for the bulk of molecular clouds, away from the immediate vicinity of massive stars) and is modified by only a factor of order unity for filaments with realistic levels of magnetization (cf. Fiege

and Pudritz 2000). This may set a quasi-universal threshold for star formation in the cold ISM of galaxies at $M_{\rm line,crit} \sim 16\,M_\odot$/pc in terms of filament mass per unit length, or $M_{\rm line,crit}/W_{\rm fil} \sim 160\,M_\odot\,{\rm pc}^{-2}$ in terms of gas surface density, or $M_{\rm line,crit}/W_{\rm fil}^2 \sim 1600\,M_\odot\,{\rm pc}^{-3}$ in terms of gas volume density (i.e., a number density $n_{\rm H2} \sim 2 \times 10^4\,{\rm cm}^{-3}$). Indeed, recent near-/mid-infrared studies of the star formation rate as a function of gas surface density in both Galactic and extrgalactic cloud complexes (e.g. Heiderman et al. 2010; Lada et al. 2010, 2012) show that the star formation rate tends to be linearly proportional to the mass of dense gas above a surface density threshold $\Sigma_{\rm gas}^{\rm th} \sim 130\,M_\odot\,{\rm pc}^{-2}$ and drops to negligible values below $\Sigma_{\rm gas}^{\rm th}$ (see Gao and Solomon 2004 for external galaxies). Note that this is the *same* threshold as found with *Herschel* for the formation of prestellar cores (André et al. 2014—cf. § 3.1). Moreover, the relation between the star formation rate SFR and the mass of dense gas $M_{\rm dense}$ above the threshold is estimated to be $SFR = 4.6 \times 10^{-8}\,M_\odot\,{\rm year}^{-1} \times (M_{\rm dense}/M_\odot)$ by Lada et al. (2010), which is close to the relation $SFR = 2 \times 10^{-8}\,M_\odot\,{\rm year}^{-1} \times (M_{\rm dense}/M_\odot)$ found by Gao and Solomon (2004). Both of these values are very similar to the star formation rate per unit solar mass of dense gas of $0.15 \times 0.3/10^6 \sim 4.5 \times 10^{-8}\,M_\odot\,{\rm year}^{-1}$ that we may derive based on *Herschel* in the Aquila complex by considering that only ~ 15 % of the cloud mass above the column density threshold is in the form of prestellar cores (Könyves et al. in prep.), that the local star formation efficiency at the level of an individual core is $\epsilon_{\rm core} \sim 30$ % (cf. Alves et al. 2007; André et al. 2010), and that the typical lifetime of the Aquila cores is $\sim 10^6$ year (Könyves et al. in prep.). Despite relatively large uncertainties, the agreement with the extragalactic value of Gao and Solomon (2004) is surprisingly good, suggesting that there may well be a quasi-universal star formation law converting the dense molecular gas of self-gravitating filaments into stars above the threshold (Lada et al. 2012; André et al. 2014) and that the star formation scenario sketched above may well apply to the ISM of most galaxies.

References

Alves, J. F., Lombardi, M., & Lada, C. J. 2007, A&A, 462, L17
André, Ph., Men'shchikov, A., Bontemps, S. et al. 2010, A&A, 518, L102
André, Ph., Ward-Thompson, D., Greaves, J. 2012, Science, 337, 69
André, Ph., Di Francesco, J., Ward-Thompson, D., Inutsuka, S., Pudritz, R., & Pineda, J. 2014, in Protostars and Planets VI, Eds. H. Beuther et al., in press (astro-ph/1312.6232)
Arzoumanian, D., André, Ph., Didelon, P. et al. 2011, A&A, 529, L6
Bastian, N., Covey, K.R., & Meyer, M.R. 2010, ARA&A, 48, 339
Chabrier, G. 2003, PASP, 115, 763
Elmegreen, B.G., Klessen, R.S., & Wilson, C.D. 2008, ApJ, 681, 365
Federrath, C., Roman-Duval, J., Klessen, R.S. et al. 2010, A&A, 512, A81
Fiege, J.D., & Pudritz, R.E. 2000, MNRAS, 311, 85
Gao, Y., & Solomon, P. 2004, ApJ, 606, 271
Gautier, T.N., Boulanger, F., Pérault, M., Puget, J.L. 1992, AJ, 103, 1313
Goldsmith, P.F., Heyer, M., Narayanan, G. et al. 2008, ApJ, 680, 428

Hacar, A., Tafalla, M., Kauffmann, J., & Kovacs, A. 2013, A&A, 554, A55
Hartmann, L. 2002, ApJ, 578, 914
Hatchell, J., Richer, J. S., Fuller, G. A. et al. 2005, A&A, 440, 151
Heiderman, A., Evans, N.J., Allen, L.E. et al. 2010, ApJ, 723, 1019
Hennebelle, P. 2013, A&A, 556, A153
Hennebelle, P., & Chabrier, G. 2008, ApJ, 684, 395
Hily-Blant, P., & Falgarone, E. 2007, A&A, 469, 173
Inutsuka, S.-I. 2001, ApJ, 559, L149
Inutsuka, S-I, & Miyama, S.M. 1992, ApJ, 388, 392
Inutsuka, S-I, & Miyama, S.M. 1997, ApJ, 480, 681
Johnstone, D., Di Francesco, J., & Kirk, H. 2004, ApJ, 611, L45
Kennicutt, R. 1998, ApJ, 498, 541
Kirk, J.M., Ward-Thompson, D., Palmeirim, P. et al. 2013, MNRAS, 432, 1424
Könyves, V., André, Ph., Men'shchikov, A. et al. 2010, A&A, 518, L106
Kroupa, P. 2002, Science, 295, 82
Lada, C.J., Lombardi, M, & Alves, J. 2010, ApJ, 724, 687
Lada, C.J., Forbrich, J., Lombardi, M, & Alves, J. F. 2012, ApJ, 745, 190
Larson, R.B. 1981, MNRAS, 194, 809
Larson, R.B. 1985, MNRAS, 214, 379
Men'shchikov, A. 2013, A&A, 560, A63
Men'shchikov, A., André, Ph., Didelon, P. et al. 2010, A&A, 518, L103
Men'shchikov, A., André, Ph., Didelon, P., Motte, F. et al. 2012, A&A, 542, A81
Miville-Deschênes, M.-A., Martin, P.G., Abergel, A. et al. 2010, A&A, 518, L104
Molinari, S., Swinyard, B., Bally, J. et al. 2010, A&A, 518, L100
Motte, F., Zavagno, A., Bontemps, S. et al. 2010, A&A, 518, L77
Myers, P.C. 2009, ApJ, 700, 1609
Onishi, T., Mizuno, A., Kawamura, A. et al. 1998, ApJ, 502, 296
Ostriker, J. 1964, ApJ, 140, 1056
Padoan, P. & Nordlund, A. 2004, ApJ, 617, 559
Padoan, P., Juvela, M., Goodman, A.A., & Nordlund, A. 2001, *ApJ*, 553, 227
Palmeirim, P., André, Ph., Kirk, J. et al. 2013, A&A, 550, A38
Schneider, S. & Elmegreen, B.G. 1979, ApJS, 41, 87
Sousbie, T., 2011, MNRAS, 414, 350
Starck, J. L., Donoho, D. L., Candès, E. J. 2003, A&A, 398, 785
Ward-Thompson, D., Kirk, J.M., André, P. et al. 2010, A&A, 518, L92

Dust in the Local Group

Aigen Li, Shu Wang, Jian Gao and B. W. Jiang

Abstract How dust absorbs and scatters starlight as a function of wavelength (known as the interstellar extinction curve) is crucial for correcting for the effects of dust extinction in inferring the true luminosity and colors of reddened astrophysical objects. Together with the extinction spectral features, the extinction curve contains important information about the dust size distribution and composition. This review summarizes our current knowledge of the dust extinction of the Milky Way, three Local Group galaxies (i.e., the Small and Large Magellanic Clouds, and M 31), and galaxies beyond the Local Group.

1 Introduction

Interstellar dust is an important constituent of the Milky Way (MW) and external galaxies although it makes up only about 0.1 % of the visible matter of a typical galaxy. Understanding dust and its role in the universe are very important. Virtually all observations of astrophysical objects and their physical processes are affected by the presence of dust either within the system being studied or along its line of sight. Dust absorbs and scatters starlight efficiently in the ultraviolet (UV), optical and near infrared (IR) wavelength range. It is the dominant opacity source for continuum photons with wavelengths longward of the ionization edge of hydrogen. In order to infer the intrinsic properties (e.g., luminosity, color, spectral energy distribution) of an astrophysical object, it is crucial to correct for the effects of dust extinction—the sum of absorption and scattering. Correcting for dust extinction is also essential for inferring the stellar content of a galaxy, or the history of star formation in the universe. The uncertainty in the correction for dust extinction currently dominates

A. Li (✉)
Department of Physics and Astronomy, University of Missouri, Columbia, MO 65211, USA
e-mail: lia@missouri.edu

S. Wang · J. Gao · B. W. Jiang
Department of Astronomy, Beijing Normal University, 100875 Beijing, People's Republic of China

K. Freeman et al. (eds.), *Lessons from the Local Group,*
DOI 10.1007/978-3-319-10614-4_8

the uncertainty in the inferred star formation rate in high-z galaxies (see Madau and Dickinson 2014).

Dust absorbs and scatters starlight differently at different wavelengths, often with shorter-wavelength (blue) light more heavily obscured than longer-wavelength (red) light. Therefore, dust controls the appearance of a galaxy by dimming and reddening the starlight in the UV and optical (e.g., see Block and Wainscoat 1991; Block et al. 1994; Block 1996). Dust re-radiates the absorbed UV/optical stellar photons at longer wavelengths. Nearly half of the bolometric luminosity of the local universe is reprocessed by dust into the mid- and far-IR (Dwek et al. 1998).

Dust is an important agent of the galactic evolution. Dust plays an important role in interstellar chemistry by providing surfaces for the formation of the most abundant molecule (i.e., H_2) and by reducing the stellar UV radiation which otherwise would photodissociate molecules. The far-IR radiation of dust removes the gravitational energy of collapsing clouds, allowing star formation to occur. Dust dominates the heating of interstellar gas through photoelectrons (Weingartner and Draine 2001a).

In this review we will focus on dust extinction. The study of interstellar extinction has a long history (see Li 2005). As early as 1847, Wilhelm Struve already noticed that the apparent number of stars per unit volume of space declines in all directions receding from the Sun. He attributed this effect to interstellar absorption. From his analysis of star counts he deduced an visual extinction of $\sim$1 mag kpc^{-1}. In 1904, Jacobus Kapteyn estimated the interstellar absorption to be $\sim$1.6 mag kpc^{-1}, in order for the observed distribution of stars in space to be consistent with his assumption of a constant stellar density (see van der Kruit 2014). This value was amazingly close to the current estimates of $\sim$1.8 mag kpc^{-1} (see Li 2005).

How the interstellar extinction A_λ varies with wavelength λ—known as the "interstellar extinction law" or "interstellar extinction curve"—is one of the primary sources of information about the dust size distribution, and the extinction spectral features provide direct information on the dust composition (Draine 2003). The interstellar extinction curve is most commonly determined using the "pair method" which compares the spectrum of a reddened star with that of an unreddened star of the same spectral type (see Appendix 1 in Li and Mann 2012). This method, first used by Bless and Savage (1970), has since been used extensively to deduce the extinction curves for a large number of Galactic sightlines (see Valencic et al. 2004 and references therein). However, direct measurements of extragalactic UV extinction using individual reddened stellar sightlines are still limited to three Local Group galaxies: the Small Magellanic Cloud (SMC), the Large Magellanic Cloud, and M 31 (see Clayton 2004). In galaxies beyond the Local Group, individual stars can not be observed. Various approaches other than the "pair method" have been taken to determine the extinction curves.

In §2 we summarize our current knowledge of the UV, optical and IR extinction properties of the MW. The extinction curves of the SMC, LMC, M 31 are respectively discussed in §3, §4, and §5. We summarize in §6 the approaches to determining the extinction curve for dust in galaxies where individual stars cannot be resolved. We will not discuss the dust thermal IR/mm emission. The importance of the dust thermal emission of the MW (see Draine and Li 2001; Li and Draine 2001; Li 2004; Jones

et al. 2013), the SMC/LMC (Li and Draine 2002; Galliano et al. 2011; Gordon et al. 2011, 2014; Meixner et al. 2010, 2013), and other galaxies (e.g., see Draine and Li 2007; Draine et al. 2007) cannot be over-emphasized. A simultaneous investigation of the interstellar extinction, scattering, polarization and thermal emission would place powerful constraints on the nature of the dust (e.g., see Li and Greenberg 1997, 1998; Block et al. 1997; Block and Sauvage 2000; Hensley and Draine 2014).

2 The Milky Way

2.1 UV/Optical Extinction: Strong Dependence on Environments

The interstellar extinction curve is usually expressed as A_λ/A_V, where A_V is the extinction in the V band. This means of expressing the extinction curve is not unique; it has also been a common practice to use instead the ratios of two colors, $E(\lambda - V)/E(B - V)$, where $E(\lambda - V) \equiv A_\lambda - A_V$, and A_B is the extinction in the blue (B) band. The Galactic interstellar extinction curves have now been measured for a large number of sightlines over a wide wavelength range ($0.1\ \mu\text{m} < \lambda < 20\ \mu\text{m}$). As shown in Fig. 1, the extinction curves plotted against the inverse wavelength λ^{-1} rise almost linearly from the near-IR to the near-UV, with a broad absorption bump at about $\lambda^{-1} \approx 4.6\ \mu\text{m}^{-1}$ ($\lambda \approx 2175$ Å) and followed by a steep rise into the far-UV at $\lambda^{-1} \approx 10\ \mu\text{m}^{-1}$, the shortest wavelength at which the extinction has been measured. Note the extinction curve does not show any sign of a turnover in the far-UV rise.

The Galactic extinction curves are known to vary significantly among sightlines in the UV/optical at $\lambda < 0.7\ \mu$m, including strong and weak 2175 Å bumps, and steep and flat far-UV extinction (see Fig. 1). Cardelli et al. (1989) found that the variation in the UV/optical can be characterized as a one-parameter function (hereafter "CCM") of $R_V \equiv A_V/E(B-V)$, the optical total-to-selective extinction ratio. The value of R_V depends upon the environment along the line of sight. Low-density regions usually have a rather low value of R_V, having a strong 2175 Å bump and a steep far-UV rise at $\lambda^{-1} > 4\ \mu\text{m}^{-1}$. Lines of sight penetrating into dense clouds, such as the Ophiuchus or Taurus molecular clouds, usually have $4 < R_V < 6$, showing a weak 2175 Å bump, and a relatively flat far-UV rise. The "average" extinction law for the Galactic diffuse interstellar medium (ISM) is described by a CCM extinction curve with $R_V \approx 3.1$, which is commonly used to correct observations for dust extinction. Theoretically, R_V may become infinity in dense regions rich in very large, "gray" grains (i.e., the extinction caused by these grains does not vary much with wavelength), while the steep extinction produced completely by Rayleigh scattering would have $R_V \sim 0.72$ (Draine 2003). A wide range of R_V values have been reported for extragalactic lines of sight, ranging from $R_V \approx 0.7$ for a quasar intervening system at $z \approx 1.4$ (Wang et al. 2004) to $R_V \approx 7$ for gravitational lensing galaxies (Falco et al. 1999). However, the one-parameter CCM formula of R_V does not apply to sightlines beyond the MW (see Clayton 2004).

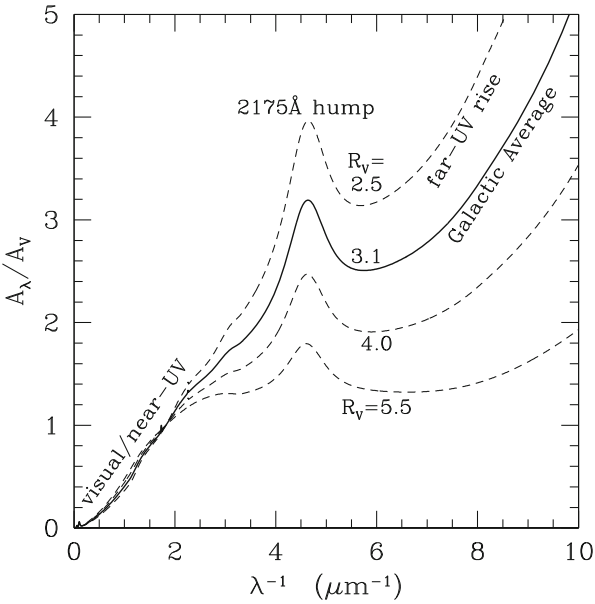

Fig. 1 Interstellar extinction curves of the Milky Way ($R_V = 2.5, 3.1, 4.0, 5.5$). There exist considerable regional variations in the Galactic optical UV extinction curves, as characterized by the total-to-selective extinction ratio R_V, indicating that dust grains on different sightlines have different size distributions

The exact nature of the carrier of the 2175 Å extinction bump remains unknown since its first discovery nearly half a century ago (Stecher 1965). Recently, a popular hypothesis is that it is due to the π–π^* transition of polycyclic aromatic hydrocarbon (PAH) molecules (Joblin et al. 1992; Li and Draine 2001; Cecchi-Pestellini et al. 2008; Malloci et al. 2008; Steglich et al. 2010; Mulas et al. 2013).

2.2 *Near-IR Extinction: A Universal Power Law?*

With the wealth of available data from space-borne telescopes (e.g., *ISO* and *Spitzer*) and ground-based surveys (e.g., *2MASS*) in the near- and mid-IR, in recent years we have seen an increase in interest in IR extinction. Understanding the effects of dust extinction in the IR wavelengths is important to properly interpret these observations.

As the UV/optical extinction varies substantially among various environments, one might expect the near-IR extinction at $0.9\ \mu\text{m} < \lambda < 3\ \mu\text{m}$ to vary correspondingly. However, for over two decades astronomers have believed that there is little, if any, near-IR extinction variation from one line of sight to another. The near-IR extinction law appears to be an approximately uniform power law of $A_\lambda \sim \lambda^{-\alpha}$ with $\alpha \approx 1.6$–1.8, independent of environment or R_V at $0.9\ \mu\text{m} < \lambda < 3\ \mu\text{m}$. Martin and Whittet (1990) found $\alpha \approx 1.8$ in the diffuse ISM as well as the outer regions of the ρ Oph and Tr 14/16 clouds. Using a large sample of obscured OB stars, He et al. (1995) found that the near-IR extinction can be well-fitted to a power law with $\alpha \approx 1.73 \pm 0.04$, even though R_V varies between 2.6 and 4.6. A "universal" power

law also well describes the near-IR polarization P_λ which, like the near-IR extinction, probes the large, submicron-sized grain population, $P_\lambda/P_{\rm max} \propto \lambda^{-1.8}$, where $P_{\rm max}$ is the peak polarization (Martin and Whittet 1990).

However, much steeper power-laws have also been derived for the near-IR extinction. Stead and Hoare (2009) determined $\alpha \approx 2.14^{+0.04}_{-0.05}$ for the slope of the near-IR extinction power law for eight regions of the MW between $l \sim 27^{\rm o}$ and $\sim 100^{\rm o}$. Nishiyama et al. (2009) explored the extinction law toward the Galactic center. They derived the index of the power law $\alpha \approx 1.99$. Fritz et al. (2011) found $\alpha \approx 2.11$ for the Galactic center extinction.

Based on a spectroscopic study of the 1–2.2 μm extinction law toward a set of nine ultracompact HII regions with $A_V > 15$ mag, Moore et al. (2005) found some evidence that the near-IR extinction curve may tend to flatten at higher extinction. They argued that flatter curves are most likely the result of increasing the upper limit of the grain-size distribution in regions of higher extinction. Naoi et al. (2006) determined the near-IR color excess ratio $E({\rm J}-{\rm H})/E({\rm H}-{\rm K_S})$, one of the simplest parameters for expressing the near-IR extinction law, for L1688, L1689, and L1712 in the ρ Oph cloud, and Cha I, Cha II, and Cha III in the Chamaeleon cloud. They found that $E({\rm J}-{\rm H})/E({\rm H}-{\rm K_S})$ changes with increasing optical depth, consistent with grain growth toward the inside of the dark clouds.

More recently, Wang and Jiang (2014) examined the apparent colors of 5,942 K-type giants whose intrinsic J, H, K_S colors are known from their effective stellar temperatures determined from the SDSS-III APOGEE survey. They derived a nearly constant near-IR color excess ratio of $E({\rm J}-{\rm H})/E({\rm H}-{\rm K_S}) \approx 0.64$ (which corresponds to $\alpha \approx 1.95$), independent of the amount of extinction in the color excess range of $0.3 < E({\rm J}-{\rm K_S}) < 4.0$.

A "universal" near-IR extinction law of a constant power-index α for regions with different physical conditions is difficult to understand. One would imagine that in denser regions the dust could be larger which would lead to a smaller α. However, this tendency is not observationally verified (see Fig. 7 of Wang et al. 2013).

2.3 Mid-IR Extinction: Universally Flat?

The mid-IR extinction at 3 μm $< \lambda <$ 8 μm (in between the power-law regime at $\sim$1–3 μm and the 9.7 μm silicate Si–O stretching absorption feature) is not well understood. The determination of the mid-IR extinction law has been more difficult because this wavelength range is best accessed from space. All dust models for the diffuse ISM predict an extinction curve steeply declines with λ at 1 μm $< \lambda <$ 7 μm (at $\lambda >$ 7 μm, the extinction increases because of the 9.7 μm silicate absorption band). As shown in Fig. 2, the Weingartner and Draine (2001b; WD01) silicate-graphite grain model predicts a power-law of $A_\lambda \propto \lambda^{-1.74}$ for the IR extinction at 1 μm $< \lambda <$ 7 μm, while the Mathis et al. (1977; MRN) model predicts a steeper power-law of $A_\lambda \propto \lambda^{-2.02}$. The model IR extinction curves reach their minimum at $\sim$7 μm where the extinction power-law intersects the blue-wing of the 9.7 μm silicate absorption band.

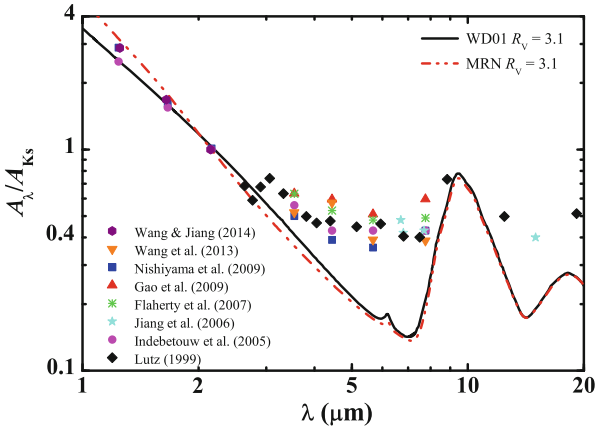

Fig. 2 Comparison of the IR extinction observed for various interstellar regions with that predicted from the MRN (*dot-dashed line*) and WD01 (*solid line*) silicate-graphite models for the diffuse ISM of which the UV/optical extinction is characterized by $R_V \approx 3.1$. The *little bump* at 6.2 μm arises from the C–C stretching absorption band of PAHs (see Li and Draine 2001)

Rieke and Lebofsky (1985) measured the IR extinction from 1 to 13 μm for the lines of sight toward o Sco, a normal A5 II star behind the edge of the ρ Oph cloud obscured by $A_V \approx 2.92$ mag, and toward a number of stars in the Galactic center. They derived a power-law of $A_\lambda \propto \lambda^{-1.62}$ for 1 μm $< \lambda <$ 7 μm for o Sco and the Galactic center sources. Draine (1989) compiled the IR extinction observed for a range of Galactic regions including diffuse clouds, molecular clouds, and HII regions. A power-law of $A_\lambda \propto \lambda^{-1.75}$ for 1 μm $< \lambda <$ 7 μm was obtained. Bertoldi et al. (1999) and Rosenthal et al. (2000) also derived a power-law extinction of $A_\lambda \propto \lambda^{-1.7}$ for 2 μm $< \lambda <$ 7 μm for the Orion molecular cloud (OMC) which displays an absorption band at 3.05 μm attributed to water ice.

However, numerous recent observations suggest that the mid-IR extinction at 3 μm $< \lambda <$ 8 μm appears to be almost *universally* flat or "gray" for both diffuse and dense environments, much flatter than that predicted from the MRN or WD01 silicate-graphite model for $R_V = 3.1$ (see Fig. 2).

Lutz et al. (1996) derived the extinction toward the Galactic center star Sgr A* between 2.5 μm and 9 μm from the H recombination lines. They found that the Galatic center extinction shows a flattening of A_λ in the wavelength region of 3 μm $< \lambda <$ 9 μm, clearly lacking the pronounced dip at $\sim$7 μm predicted from the $R_V = 3.1$ silicate-graphite model (see Fig. 2). This was later confirmed by Lutz (1999), Nishiyama et al. (2009), and Fritz et al. (2011).

Indebetouw et al. (2005) used the photometric data from the *2MASS* survey and the *Spitzer*/GLIMPSE Legacy program to determine the IR extinction. From the color excesses of background stars, they derived the $\sim$1.25–8 μm extinction laws for two very different lines of sight in the Galactic plane: the $l = 42^o$ sightline toward a relatively quiescent region, and the $l = 284^o$ sightline which crosses the

Carina Arm and contains RCW 49, a massive star-forming region. The extinction laws derived for these two distinct Galactic plane fields are remarkably similar: both show a flattening across the 3–8 μm wavelength range, consistent with that derived by Lutz et al. (1996) for the Galactic center.

Jiang et al. (2006) derived the extinction at 7 and 15 μm for more than 120 sightlines in the inner Galactic plane based on the ISOGAL survey data and the near-IR data from DENIS and 2MASS, using RGB tip stars or early AGB stars (which have only moderate mass loss) as the extinction tracers. They found the extinction well exceeding that predicted from the MRN or WD01 $R_V = 3.1$ models.

Flaherty et al. (2007) obtained the mid-IR extinction laws in the *Spitzer*/IRAC bands for five nearby star-forming regions. The derived extinction laws at $\sim$4–8 μm are flat, even flatter than that of Indebetouw et al. (2005).

Gao et al. (2009) used the *2MASS* and *Spitzer*/GLIPMSE data to derive the extinction in the four IRAC bands for 131 GLIPMSE fields along the Galactic plane within $|l| \leq 65^{\rm o}$ (Benjamin et al. 2003; Churchwell et al. 2006). Using red giants and red clump giants as the extinction tracers, they also found the mean extinction in the IRAC bands to be flat.

Wang et al. (2013) determined the mid-IR extinction in the four *Spitzer*/IRAC bands of five individual regions in Coalsack, a nearby starless dark cloud, spanning a wide variety of interstellar environments from diffuse and translucent to dense clouds. They found that all regions exhibit a flat mid-IR extinction.

All these observations appear to suggest an "universally" flat extinction law in the mid-IR, with little dependence on environments. Draine (2003) extended the WD01 model of $R_V = 5.5$ into the IR up to $\lambda < 30$ μm and found that the WD01 $R_V = 5.5$ model closely reproduces the flat mid-IR extinction observed toward the Galactic center (Lutz et al. 1996). Dwek (2004) hypothesized that the observed mid-IR extinction is largely due to metallic needles for which the opacity is high in the mid-IR. Wang et al. (2014) found that the mid-IR extinction as well as the UV/optical extinction could be closely reproduced by a mixture of submicron-sized amorphous silicate and graphite, and a population of micrometer-sized amorphous carbon which consumes $\sim$60 carbon atoms per million (ppm) hydrogen atoms (see Fig. 3).

2.4 IR Extinction as a Probe of the Galactic Structure

Whittet (1977) presented observational evidence for a small but appreciable variation in R_V with Galactic longitude. He suggested that the most likely explanation for this is a variation in the mean size of the dust in the local spiral arm. However, unfortunately only a few data points were used in that work and therefore no systematic variation of the extinction with Galactic longitude was reported. A major leap forward occurred recently thanks to the amazing success of the *Spitzer*/GLIMPSE Legacy programs (see Benjamin 2014).

Based on the IR extinction in the four IRAC bands derived for 131 GLIPMSE fields in the Galactic plane, Gao et al. (2009) demonstrated that the mid-IR extinction

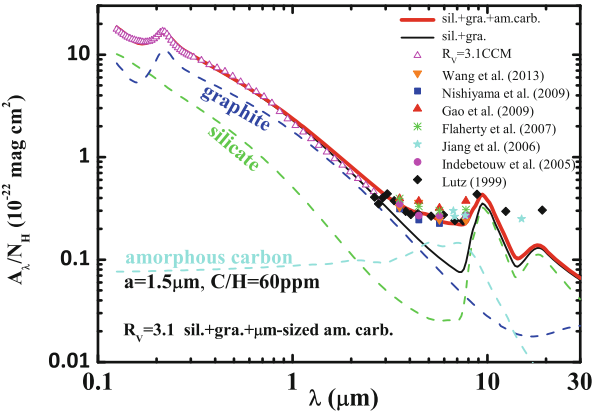

Fig. 3 Fitting the $R_V = 3.1$ UV/optical, near- and mid-IR extinction with a simple mixture (*dot-dashed line*) of amorphous silicate (*dotted line*) and graphite dust (*dashed line*), together with a population of large, μm-sized *amorphous carbon* of spherical radii $a \approx 1.5\ \mu m$ and $C/H \approx 60\ ppm$ (Wang et al. 2014). The *thick solid line* plots the model fit, while the *symbols* plot the observed extinction: the open pentagons plot the $R_V = 3.1$ UV/optical/near-IR extinction, and the other symbols plot the mid-IR extinction

appears to vary with Galactic longitude; more specifically, the locations of the spiral arms seem to coincide with the dips of the extinction ratios A_λ/A_{K_S} (see Fig. 4). In particular, the coincidence of the locations of the A_λ/A_{K_S} minimum and the spiral arms is outstanding at negative longitudes (e.g., the Crux-Scutum arm at $l = -50°$, the Norma arm at $-33°$, and the southern tangent of the 3 kpc ring around $-23°$). For the positive longitudes, the locations of the Scutum-Crux arm and the Sagittarius-Carina arm also coincide with the valleys of A_λ/A_{K_S}. For the broad dip around $l = 16°$, there is no clear tangent direction to any arms, but this direction points to the start of the Norma arm and the Scutum-Crux arm (see Fig. 2 of Vallée 2008), and probably one end of the Galactic bar.

Using data from *2MASS* and *Spitzer*/IRAC for G and K spectral type red clump giants, Zasowski et al. (2009) also found longitudinal variations of the 1.2–8 μm IR extinction over $\sim 150^o$ of contiguous Galactic mid-plane longitude; more specifically, they found strong, monotonic variations in the extinction law shape as a function of angle from the Galactic center, symmetric on either side of it: the IR extinction law becomes increasingly steep as the Galactocentric angle increases, with identical behavior between $l < 180^o$ and $l > 180^o$ (see Fig. 5).

3 SMC

As our nearest galactic neighbors, the Magellanic Clouds offer a unique opportunity to study the effects of different galactic environments on dust properties. As a metal-poor (with a metallicity only $\sim$1/10 of that in the MW; see Kurt and Dufour 1998)

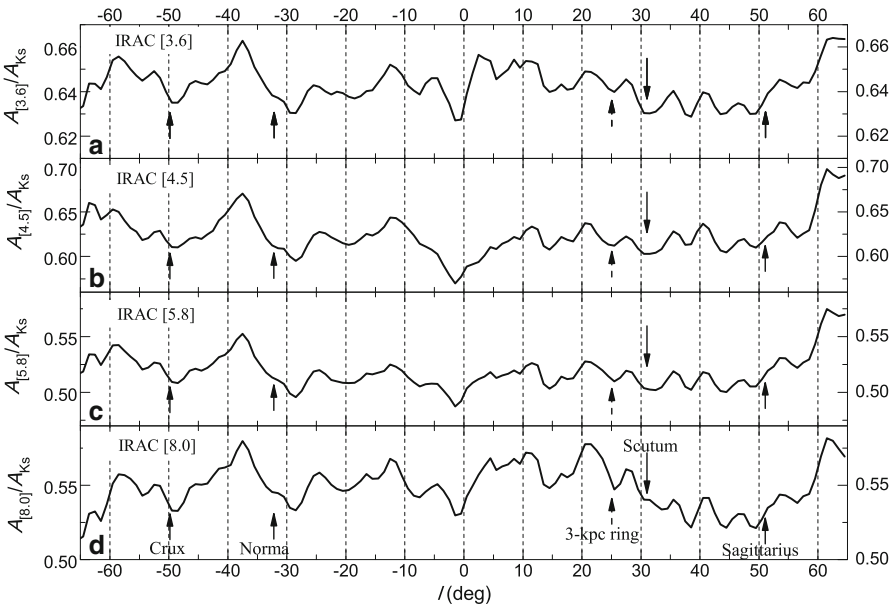

Fig. 4 Longitudinal distributions of A_λ/A_{K_S} in the four IRAC bands (*solid lines*; Gao et al. 2009). The dips of the extinction ratios A_λ/A_{K_S} appear to coincide with the locations of the spiral arms. The *solid vertical arrows* show the tangent directions of the spiral arms at $l = -50°, -33°, 31°$ and 51° (Vallée 2008). The *dashed arrow* shows the tangent direction of the 3 kpc ring at $l = 23°$ (Dame and Thaddeus 2008)

and gas-rich (with a dust-to-gas ratio over 10 times lower than in the MW; see Bouchet et al. 1985) irregular dwarf galaxy, the SMC is often considered as a local analog of primordial galaxies at high redshifts which must have formed at very low metallicity. Therefore, the dust in the SMC which differs substantially from that in the MW allows us to probe the primordial conditions in more distant galaxies. Indeed, the SMC-type extinction often provides better fits to the spectral energy distributions (SEDs) of many extragalactic systems than the "standard" MW-type extinction curve (e.g., see Richards et al. 2003 and Hopkins et al. 2004 for reddened quasars, and Vijh et al. 2003 for Lyman break galaxies). The 2175 Å feature seen in the MW-type extinction is absent in the attenuation curve inferred from radiative transfer modeling of starburst galaxies including stars, gas and dust (Calzetti et al. 1994; Gordon et al. 1997).

Due to its low metallicity, the dust quantity (relative to H) in the SMC is expected to be lower than that of the MW because there is less raw material (i.e., heavy elements) available for making the dust. The (relative) lack of the dust-making raw material could prevent the dust in the SMC from growing and hence the dust in the SMC may be smaller than the MW dust. Furthermore, the star-formation activity in the SMC could destroy the dust. Therefore, one would naturally expect the dust size distribution and extinction curve in the SMC to differ from that of the MW.

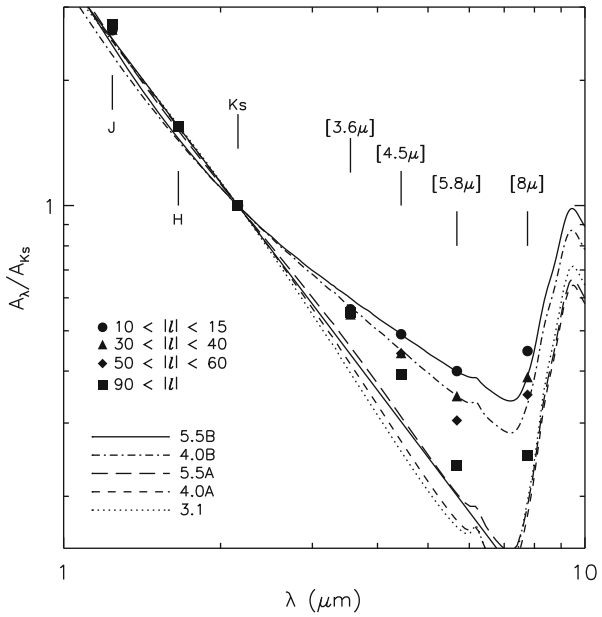

Fig. 5 Mean extinction curves for the indicated ranges of Galactic angle (*circles*: $10° < |l| < 15°$; *triangles*: $30° < |l| < 40°$; *diamonds*: $50° < |l| < 60°$; *squares*: $|l| > 90°$), compared to that of the WD01 model for $R_V = 3.1, 4.0, 5.5$. Also shown for comparison is an $A_\lambda \propto \lambda^{-\beta}$ power law, with $\beta = 1.66$ (*solid line*). It is apparent that the extinction curve becomes increasingly steep at larger Galactocentric angles (Zasowski et al. 2009)

There are significant regional variations in the UV/optical extinction properties of the SMC. As shown in Fig. 6, the extinction curve of the SMC Bar displays a nearly linear rise with λ^{-1} and no detectable 2175 Å extinction bump (Lequeux et al. 1982; Cartledge et al. 2005), presumably due to the destruction of the carriers of the 2175 Å hump by the intense UV radiation and shocks associated with star formation. In contrast, the extinction curve for the line of sight toward Sk 143 (AvZ 456) has a strong 2175 Å hump (Lequeux et al. 1982; Cartledge et al. 2005). This sightline passes through the SMC wing, a region with much weaker star formation (Gordon and Clayton 1998).

The overall IR emission spectrum of the SMC peaks at $\lambda \sim 100\,\mu$m with a local minimum at $\lambda \sim 12\,\mu$m which is commonly believed to be emitted by PAHs (see Li and Draine 2002). The PAH emission features have been detected locally in the SMC B1#1 quiescent molecular cloud (Reach et al. 2000), and in some star-forming regions (Contursi et al. 2000; Sanstrom et al. 2012). Based on the observed PAH emission and attributing the 2175 Å extinction bump to PAHs, Li and Draine (2002) predicted an extinction excess of $\Delta A_{2175} \approx 0.5$ mag at 2175 Å for sightlines through SMC B1#1. Maíz Apellániz and Rubio (2012) measured the UV extinction for four stars in the SMC B1#1 cloud from their HST/STIS slitless UV spectra. They found

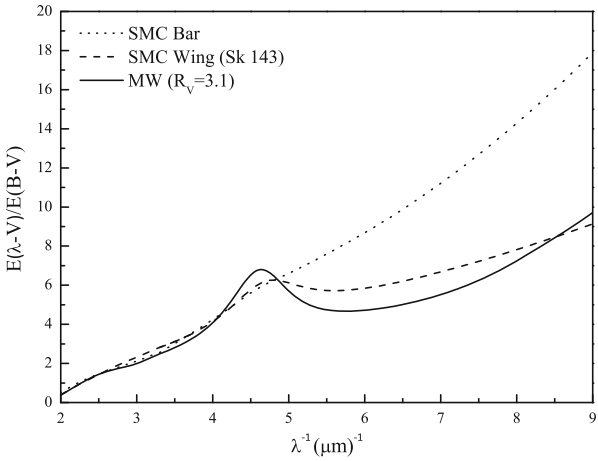

Fig. 6 Comparison of the SMC Bar (*dotted*) and MW $R_V = 3.1$ (*solid*) extinction curves. Also shown is the extinction curve for the sightline toward the SMC wing star Sk 143 (*dashed*)

that the 2175 Å bump is moderately strong in one star, weak in two stars, and absent in the fourth star.

4 LMC

Like the SMC, the LMC is also a low-metalicity irregular dwarf galaxy and a satellite of the MW. Since the metallicity of the LMC (which is only ∼1/4 of that of the MW; Russell and Dopita 1992) is similar to that of galaxies at red shifts $z \sim 1$ (see Dobashi et al. 2008), it offers opportunities to study the dust properties in distant low-metallicity extragalactic environments by studying the extinction properties of the LMC.

As illustrated in Fig. 7, the LMC extinction curve is intermediate between that of the MW and that of the SMC: compared to the Galactic extinction curve, the LMC extinction curve is characterized by a weaker 2175 Å hump and a stronger far-UV rise (Nandy 1981; Koornneef and Code 1981; Gordon et al. 2003). Strong regional variations in extinction properties have also been found in the LMC (Clayton and Martin 1985; Fitzpatrick 1985, 1986; Misselt et al. 1999; Gordon et al. 2003): the sightlines toward the stars inside or near the supergiant shell, LMC 2, which lies on the southeast side of the 30 Doradus star-forming region, have a weak 2175 Å hump (Misselt et al. 1999), while the extinction curves for the sightlines toward the stars which are > 500 pc away from the 30 Doradus region are closer to the Galactic extinction curve.

Based on the photometric data from the *Spitzer*/SAGE survey and with red giants as the extinction tracer, Gao et al. (2013) derived the mid-IR extinction for a number of regions of the LMC in the four IRAC bands. The average mid-IR extinction shows a flat curve, close to the MW $R_V = 5.5$ model extinction curve (see Fig. 8).

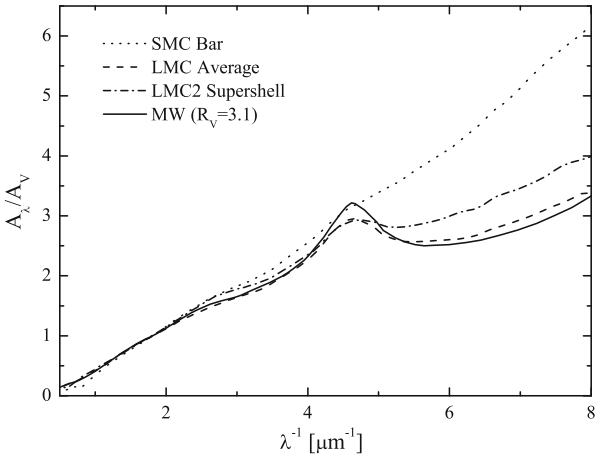

Fig. 7 Comparison of the "*LMC Average*" (*dashed*), *SMC* (*dotted*), and *MW* $R_V = 3.1$ (*solid*) extinction curves. Also shown is the LMC2 supershell extinction curve (*dot-dashed*). The "*LMC Average*" curve (also known as the "LMC" curve) is the mean extinction curve derived for the sightlines toward the stars outside of the 30 Dor star-forming region, while the LMC2 supershell curve (also known as the "LMC2" curve or the "LMC 30 Dor" curve) is for the dust inside the LMC2 supergiant shell which, lying on the southeast side of 30 Dor, was formed by the combined stellar winds and supernova explosions from the stellar association at its center

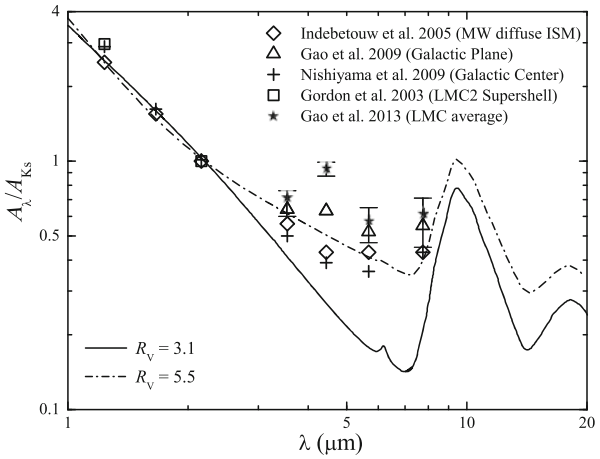

Fig. 8 IR extinction of the LMC compared with the WD01 model curves of $R_V = 3.1$ (*solid line*) and $R_V = 5.5$ (*dot-dashed line*). *Open squares*: the LMC near-IR extinction of Gordon et al. (2003). *Filled stars*: the mid-IR extinction at the four IRAC bands derived by Gao et al. (2013). *Open diamonds*: the near- and mid-IR extinction for the MW diffuse ISM of Indebetouw et al. (2005). *Open triangles*: the average extinction at the four IRAC bands derived from 131 GLIMPSE fields along the Galactic plane (Gao et al. 2009). *Pluses*: the near- and mid-IR extinction toward the Galactic center of Nishiyama et al. (2009)

In the 30 Dor star-forming region where large amounts of UV radiation and shocks are present, the dust is expected to be processed and its size distribution is expected to be modified. The difference between the UV extinction characteristic of the 30 Dor region and that outside the 30 Dor region could be understood in terms of dust erosion in the 30 Dor region which produces a dust size distribution skewed toward smaller grains, and leads to a steeper far-UV extinction and a weaker 2175 Å bump as the bump carriers could also be destroyed.

However, it is difficult to quantify the effects of star-formation activities on the dust size distribution and the corresponding UV extinction. Although the environment of the SMC Bar is likely to be less severe than for the 30 Dor region (which is a much larger star-forming region than any in the SMC), the UV extinction of the SMC Bar is more extreme than that of the LMC 30 Dor, with the former exhibiting a very steep far-UV rise and lacking the 2175 Å bump. The SMC has star formation occurring at only $\sim$1 % of the rate of a starburst galaxy. But starburst galaxies appear to be dominated by large, submicron- or micron-sized dust and are characterized by a flat or "gray" extinction curve (see Calzetti 2001).

Therefore, many factors including densities, metallicities, and star formation rates must be important in controlling the formation and destruction processes (such as shattering and coagulation) of dust (see Clayton 2004).

5 M 31

The Andromeda galaxy (M 31), at a distance of $\sim$780 kpc (McConnachie et al. 2005), is the only galaxy (other than the MW, and the SMC/LMC) of which individual stars can be resolved and adopted for extinction determination in terms of the "pair method". Unlike the Magellanic Clouds which are metal-poor, M 31 has a super-solar metallicity.

Bianchi et al. (1996) obtained the UV spectra in the $\sim$1150–3300 Å wavelength range of several bright OB stars in M 31, using the *Faint Object Spectrograph* (FOS) on board the *Hubble Space Telescope* (HST). The UV extinction was derived for three sightlines in M 31 and seems to show a MW-type extinction curve but with the 2175 Å feature possibly somewhat weaker than in the MW (see Fig. 9).

More recently, Dong et al. (2014) measured the extinction curve for the dust in the central $\sim 1'$ ($\sim$200 pc) region of M 31 at thirteen bands from the mid-UV to near-IR in the wavelength range of $\sim$1928 Å–1.5 μm. They examined five representative dusty clumps located in the circumnuclear region, utilizing data from the HST *Wide Field Camera 3* (WFC3) and *Advanced Camera for Surveys* (ACS) detectors as well as the *UV and Optical Telescope* (UVOT) on board *Swift*. They found that the extinction curves of these clumps, with $R_V \approx 2.4$–2.5, are steeper than the average Galactic one, indicating that the dust in M 31 is smaller than that in the MW. Dong et al. (2014) also found that one dusty clump (size $<$2 pc) exhibits a strong 2175 Å bump. They speculated that large, submicron-sized dust in M 31 may have been destroyed in the harsh environments of the bulges by supernova explosions or past activities of the central super-massive black hole, resulting in the observed steepened extinction curve.

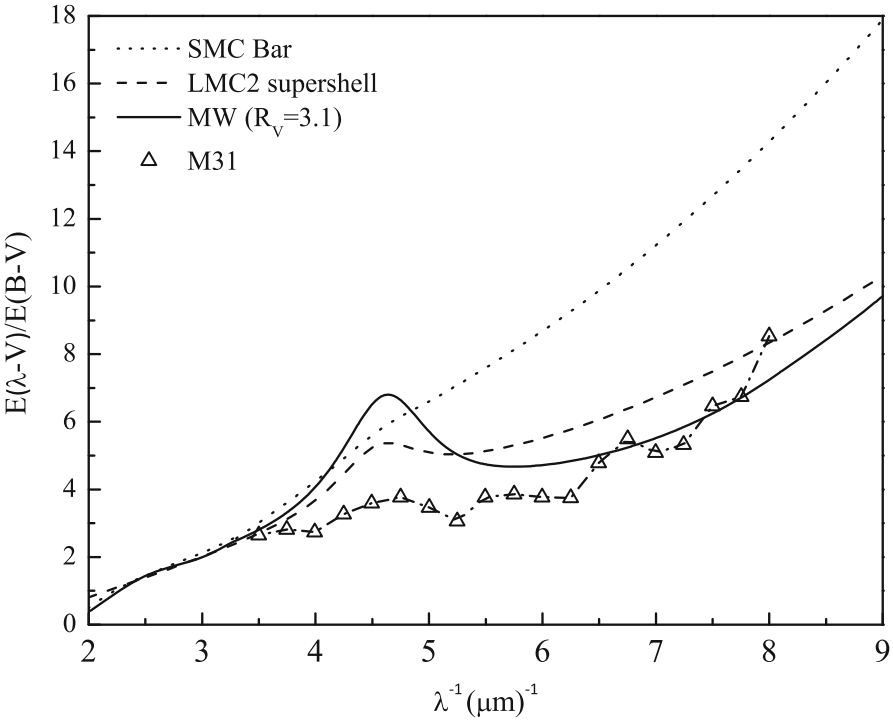

Fig. 9 Comparison of the M 31 (*dot-dashed line-connected triangles*), MW $R_V = 3.1$ (*solid*), SMC Bar (*dotted*), and LMC2 30 Dor "supershell' region (*dashed*) extinction curves. The M 31 extinction curve was obtained by Bianchi et al. (1996) with the "pair method" by comparing the HST/FOS spectra of reddened M 31 stars and that of unredded Galactic stars of the same spectral type. The M 31 extinction curve has an overall wavelength dependence similar to that of the average Galactic extinction curve but possibly has a weaker 2175 Å bump

6 Dust in Galaxies Beyond the Local Group

The CCM extinction relation is applicable to a wide range of interstellar dust environments in the MW, including lines of sight through diffuse dust and dark cloud dust, as well as dust associated with star formation. However, the CCM relation does not appear to apply beyond the MW even in other Local Group galaxies such as the Magellanic Clouds and M 31 (see Clayton 2004). Unfortunately, high signal-to-noise extinction curves are still available for only three galaxies, the MW, LMC, and SMC. Direct measurements of extragalactic UV extinction using individual reddened stellar sightlines are still limited to the LMC, SMC and a few sightlines in M 31 (see §5). As summarized by Draine (2003), there are several different approaches to determining the extinction curve for dust in galaxies where individual stars cannot be resolved.

White and Keel (1992) proposed that the dust extinction curve of an external galaxy can be determined directly if it lies in front of another galaxy. The ideal case consists of a face-on symmetric spiral galaxy half overlapping with a symmetric, background spiral or elliptical galaxy. The galaxies need to be symmetric so that their non-overlapping parts may be used to estimate the surface brightness of their overlapping parts. This method has been applied to a number of overlapping galaxy pairs (White and Keel 1992; White et al. 1996, 2000; Keel and White 2001a, 2001b).

Using this technique, Berlind et al. (1997) measured the extinction curves in the *BVRJHK* visual to near-IR wavelength range for the dust in the spiral arm and interarm regions of NGC 2207 which overlaps IC 2163. This pair consists of two symmetric, almost face-on interacting spiral galaxies which are partially overlapping. These galaxies have been observed and modeled in detail by Elmegreen et al. 1995a, b.

Berlind et al. (1997) found that the dust in NGC 2207 is mainly concentrated in its spiral arms, leaving its interarm regions mostly transparent. More interestingly, they found that the extinction curve in the spiral arm region of NGC 2207 is flat, resembling the MW extinction curve for $R_V \approx 5.0$, while the interarm dust appears to be even "grayer" (see Fig. 10). They proposed that an unresolved patchy dust distribution in NGC 2207 could be capable of producing the observed extinction curves; and the arm-interarm difference in the observed extinction could also be explained if the interarm region has a higher degree of dust patchiness (i.e., a larger density ratio between the high-density and low-density phases) than the arm region.

Finally, we note that there are some distant extragalactic point sources that can be used to construct extinction curves if their intrinsic SEDs are well characterized. These include QSOs and gamma-ray bursts (GRBs).

By comparing the composite spectra of unreddened and reddened quasars (Vanden Berk et al. 2001), one can derive the extinction curve for quasar sightlines. Richards et al. (2003) and Hopkins et al. (2004) found that the reddening toward thousands of SDSS quasars is dominated by SMC-type dust, but some studies argue for "gray" dust (see Li 2007).

Distant quasars have also been used as a background source to determine the dust extinction of damped Lyα absorption systems (e.g., see Wang et al. 2012) and intervening (e.g., Mg II) absorption systems (e.g., see Wang et al. 2004; Zhou et al. 2010; Jiang et al. 2010a, b, 2011).

Gravitationally-lensed quasars with multiple images can also be used to determine the extinction curves of distant galaxies (e.g., see Motta et al. 2002; but also see McGough et al. 2005).

GRBs, owing to their intense luminosity (emitting up to $\sim 10^{53}$ erg), allow their detection up to very high redshifts. Particularly, the featureless, power law-like spectral shapes of their afterglows, make GRBs an excellent probe of the dust extinction for the GRB host galaxies (e.g., see Li et al. 2008; Liang and Li 2009, 2010).

We note that the 2175 Å extinction bump has been detected in both nearby and distant galaxies (see Xiang et al. 2011 and references therein).

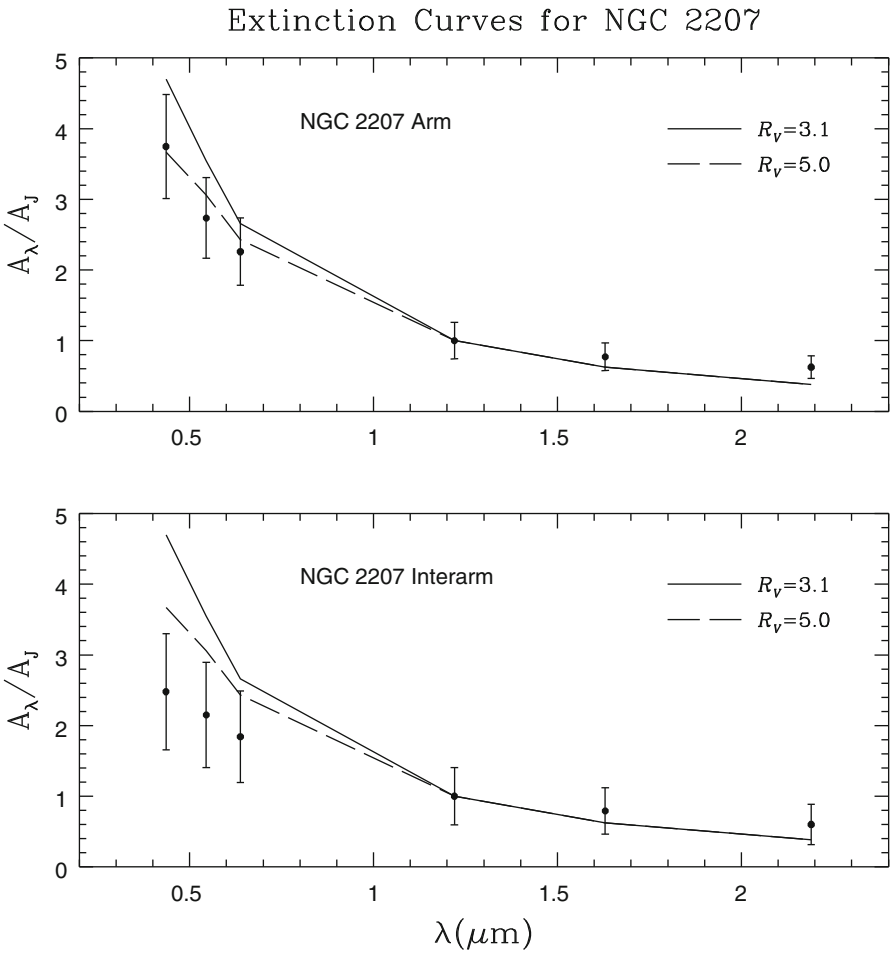

Fig. 10 Extinction curves in the $BVRJHK$ bands (normalized to the J-band extinction) for the dust in the spiral arm (*top*) and interarm (*bottom*) regions of NGC 2207, a spiral galaxy partially occulting the background spiral IC 2163 (Berlind et al. 1997). The *solid* and *dashed lines* plot the MW extinction curves for $R_V = 3.1$ and $R_V = 5.0$, respectively. Note that the extinction curves in both the spiral arm and interarm regions of NGC 2207 are flatter ("*grayer*") than the MW average of $R_V = 3.1$, while the interarm extinction curve is even "*grayer*" than that of the spiral arm

Acknowledgements We thank R.A. Benjamin, D.L. Block (DLB), G.C. Clayton, B.G. Elmegreen (BGE), B.T. Draine, G.G. Fazio, K.C. Freeman, M.L. Norman, M. Rubio, and A.N. Witt for helpful discussions. We are supported in part by NSFC 11373015 and 11173007, NSF AST-1109039, NASA NNX13AE63G, and the University of Missouri Research Board. It is a great pleasure to acknowledge the important role that DLB and BGE have played in pushing astrophysics to the new front. One of us (AL) would like to thank the SOC for inviting him to attend this fantastic, memorable conference in Seychelles.

References

Benjamin, R. A., et al. 2003, PASP, 115, 953
Benjamin, R.A. 2014, in Lessons from the Local Group – A Conference in Honour of David Block and Bruce Elmegreen, ed. K.C. Freeman, B.G. Elmegreen, D.L. Block, & M. Woolway (Springer: New York), in press
Berlind, A. A., Quillen, A. C., Pogge, R. W., & Sellgren, K. 1997, AJ, 114, 107
Bertoldi, F., Timmermann, R., Rosenthal, D., Dropatz, S., et al. 1999, A&A, 346, 267
Bianchi, L., Clayton, G. C., Bohlin, R. C., Hutchings, J. B., & Massey, P. 1996, ApJ, 471, 203
Bless, R. C., & Savage, B. D. 1970, in IAU Symp. 36, Ultraviolet Stellar Spectra and Related Ground-based Observations, ed. L. Houziaux & H. E. Butler (Dordecht: Reidel), 28
Block, D. L. 1996, in New Extragalactic Perspectives in the New South Africa, ed. D. L. Block & J. M. Greenberg (Dordrecht: Kluwer), 1
Block, D. L., & Sauvage, M. 2000, A&A, 353, 72
Block, D. L., & Wainscoat, R. J. 1991, Nature, 353, 48
Block, D. L., Bertin, G., Stockton, A., Grosbøl, P., Moorwood, A. F. M., & Peletier, R. F. 1994, A&A, 288, 365
Block, D. L., Elmegreen, B. G., Stockton, A., & Sauvage, M. 1997, ApJ, 486, L95
Bouchet, P., Lequeux, J., Maurice, E., et al. 1985, A&A, 149, 330
Calzetti, D. 2001, PASP, 113, 1449
Calzetti, D., Kinney, A. L., & Storchi-Bergmann, T. 1994, ApJ, 429, 582
Cardelli, J. A., Clayton, G. C., & Mathis, J. S. 1989, ApJ, 345, 245
Cartledge, S. I. B., Clayton, G. C., Gordon, K. D., et al. 2005, ApJ, 630, 355
Cecchi-Pestellini, C., Malloci, G., Mulas, G., et al. 2008, A&A, 486, L25
Churchwell, E, Povich, M. S., Allen, D., et al. 2006, ApJ, 649, 759
Clayton, G. C. 2004, in Astrophysics of Dust (ASP Conf. Ser. 309), ed. A.N. Witt, G.C. Clayton, & B.T. Draine (San Francisco, CA: ASP), 57
Clayton, G. C., & Martin, P. G. 1985, ApJ, 288, 558
Contursi, A., Lequeux, J., Cesarsky, D., et al. 2000, A&A, 362, 310
Dame, T. M., & Thaddeus, P. 2008, ApJ, 683, L143
Dobashi, K., Bernard, J. P. Hughes, A., et al. 2008, A&A, 484, 205
Dong, H., Li, Z., Wang, Q. D., et al. 2014, ApJ, 785, 136
Draine, B. T. 1989, in Infrared Spectroscopy in Astronomy, ed. B.H. Kaldeich (Paris: ESA Publications Division), 93
Draine, B. T. 2003, ARA&A, 41, 241
Draine, B.T., & Li, A. 2001, ApJ, 551, 807
Draine, B.T., & Li, A. 2007, ApJ, 657, 810
Draine, B. T., Dale, D. A., Bendo, G., et al. 2007, ApJ, 663, 866
Draine, B. T., Aniano, G., Krause, O., et al. 2014, ApJ, 780, 172
Dwek, E. 2004, ApJ, 611, L109
Dwek, E., Arendt, R. G., Hauser, M. G., et al. 1998, ApJ, 508, 106
Elmegreen, B.G., Sundin, M., Kaufman, M., Brinks, E., & Elmegreen, D.M. 1995a, ApJ, 453, 139
Elmegreen, D.M., Kaufman, M., Brinks, E., Elmegreen, B.G., & Sundin, M. 1995b, ApJ, 453, 100
Falco, E. E., Impey, C. D., Kochanek, C. S., et al. 1999, ApJ, 523, 617
Fitzpatrick, E.L. 1985, ApJ, 299, 219
Fitzpatrick, E.L. 1986, AJ, 92, 1068
Flaherty, K., Pipher, J., Megeath, S., et al. 2007, ApJ, 663, 1069
Fritz, T. K., Gillessen, S., et al. 2011, ApJ, 737, 73
Galliano, F., Hony, S., Bernard, J.-P., et al. 2011, A&A, 536, A88
Gao, J., Jiang, B. W., & Li, A. 2009, ApJ, 707, 89
Gao, J., Jiang, B. W., Li, A., & Xue, M.Y. 2013, ApJ, 776, 7
Gordon, K. D., & Clayton, G.C. 1998, ApJ, 500, 816
Gordon, K. D., Calzetti, D., & Witt, A. N. 1997, ApJ, 487, 625

Gordon, K. D., Clayton, G. C., Misselt, K. A., et al. 2003, ApJ, 594, 279
Gordon, K. D., Meixner, M., Meade, M. R., et al. 2011, AJ, 142, 102
Gordon, K. D., Roman-Duval, J., Bot, C., et al. 2014, ApJ, in press
He, L., Whittet, D. C. B., Kilkenny, D., & Spencer Jones, J. H. 1995, ApJS, 101, 335
Hensley, B., & Draine, B. T. 2014, AAS, 224, 220.15
Hopkins, P. F., Strauss, M. A., Hall, P. B., et al. 2004, AJ, 128, 1112
Indebetouw, R., et al. 2005, ApJ, 619, 931
Jiang, B. W., Gao, J., Omont, A., Schuller, F., & Simon, G. 2006, A&A, 446, 551
Jiang, P., Ge, J., Prochaska, J. X., et al. 2010a, ApJ, 720, 328
Jiang, P., Ge, J., Prochaska, J. X., et al. 2010b, ApJ, 724, 1325
Jiang, P., Ge, J., Zhou, H., Wang, J., & Wang, T. 2011, ApJ, 732, 110
Joblin, C., Leger, A., & Martin, P. 1992, ApJ, 393, L79
Jones, A. P., Fanciullo, L., Köhler, M., et al. 2013, A&A, 558, A62
Kapteyn, J.C. 1904, ApJ, 24, 115
Keel, W. C., & White, R. E., III. 2001a, AJ, 121, 1442
Keel, W. C., & White, R. E., III. 2001b, AJ, 122, 1369
Koornneef, J., & Code, A. D. 1981, ApJ, 247, 860
Kurt, C. M., & Dufour, R. J. 1998, RevMexAA Conf. Ser., 7, 202
Lequeux, J., et al. 1982, A&A, 113, L15
Li, A. 2004, in Penetrating Bars through Masks of Cosmic Dust, ed. D. L. Block, et al. (New York: Springer), 535
Li, A. 2005, J. Phys. Conf. Ser., 6, 229
Li, A. 2007, in The Central Engine of Active Galactic Nuclei (ASP Conf. Ser. 373), ed. L. C. Ho & J.-M. Wang (San Francisco, CA: ASP), 561
Li, A., & Draine, B.T. 2001, ApJ, 554, 778
Li, A., & Draine, B.T. 2002, ApJ, 576, 762
Li, A., & Draine, B.T. 2012, ApJ, 760, L35
Li, A., & Greenberg, J.M. 1997, A&A, 323, 566
Li, A., & Greenberg, J.M. 1998, A&A, 339, 591
Li, A., & Mann, I. 2012, in Astrophys. Space Sci. Library, Vol. 385, Nanodust in the Solar System, ed. I. Mann, N. Meyer-Vernet, & A. Czechowski (Springer: Berlin), 5
Li, A., Misselt, K. A., & Wang, Y. J. 2006, ApJ, 640, L151
Li, A., Liang, S. L., Kann, D. A., et al. 2008, ApJ, 685, 1046
Liang, S. L., & Li, A. 2009, ApJ, 690, 56
Liang, S. L., & Li, A. 2010, ApJ, 710, 648
Lutz, D., et al. 1996, ApJ, 315, L269
Lutz, D. 1999, in ESA-SP 427, The Universe as Seen by ISO, ed. P. Cox & M. F. Kessler (Noordwijk: ESA), 623
Madau, P., & Dickinson, M. 2014, ARA&A, in press (arXiv: 1403.0007)
Maíz Apellániz, J., & Rubio, M. 2012, A&A, 541, A54
Malloci, G., Mulas, G., Cecchi-Pestellini, C., & Joblin, C. 2008, A&A, 489, 1183
Martin, P. G., & Whittet, D. C. B. 1990, ApJ, 357, 113
Mathis, J. S., Rumpl, W., & Nordsieck, K. H. 1977, ApJ, 217, 425
McConnachie, A. W., Irwin, M. J., Ferguson, A. M. N., et al. 2005, MNRAS, 356, 979
McGough, C., Clayton, G. C., Gordon, K. D., & Wolff, M. J. 2005, ApJ, 624, 118
Meixner, M., Galliano, F., Hony, S., et al. 2010, A&A, 518, L71
Meixner, M., Panuzzo, P., Roman-Duval, J., et al. 2013, AJ, 146, 62
Misselt, K. A., Clayton, G. C., & Gordon, K. D. 1999, ApJ, 515, 128
Moore, T. J. T., Lumsden, S. L., Ridge, N. A., et al. 2005, MNRAS, 359, 589
Motta, V., et al. 2002, ApJ, 574, 719
Mulas, G., Zonca, A., Casu, S., & Cecchi-Pestellini, C. 2013, ApJS, 207, 7
Nandy, K. Morgan, D. H., Willis, A. J., et al. 1981, MNRAS, 196, 955
Naoi, T., Tamura, M., Nakajima, Y., et al. 2006, ApJ, 640, 373

Nishiyama, S., Tamura, M., Hatano, H., et al. 2009, ApJ, 696, 1407
Reach, W. T., Boulanger, F., Contursi, A., & Lequeux, J. 2000, A&A, 361, 895
Richards, G. T., Hall, P. B., Vanden Berk, D. E., et al. 2003, AJ, 126, 1131
Rieke, G. H., & Lebofsky, M. J. 1985, ApJ, 288, 618
Rosenthal, D., Bertoldi, F., & Drapatz, S. 2000, A&A, 356, 705
Russell, S. C., & Dopita, M. A. 1992, ApJ, 384, 508
Stead, J. J., & Hoare, M. G. 2009, MNRAS, 400, 731
Stecher, T. P. 1965, ApJ, 142, 1683
Steglich, M., Jäger, C., Rouillé, G., et al. 2010, ApJ, 712, l16
Struve, F.G.W. 1847, Etudes d'Astronomie Stellaire
Valencic, L. A., Clayton, G. C., & Gordon, K. D. 2004, ApJ, 616, 912
Vallée, J. P. 2008, ApJ, 681, 303
Vanden Berk, D. E., Richards, G. T., Bauer, A., et al. 2001, AJ, 122, 549
van der Kruit, P. C. 2014, in Lessons from the Local Group – A Conference in Honour of David Block and Bruce Elmegreen, ed. K.C. Freeman, B.G. Elmegreen, D.L. Block, & M. Woolway (Springer: New York), in press
Vijh, U. P., Witt, A. N., & Gordon, K. D. 2003, ApJ, 587, 533
Wang, S., & Jiang, B.W. 2014, ApJ, 788, L12
Wang, J., Hall, P. B., Ge, J., Li, A., & Schneider, D. P. 2004, ApJ, 609, 589
Wang, J.-G., Zhou, H.-Y., Ge, J., et al. 2012, ApJ, 760, 42
Wang, S., Gao, J., Jiang, B.W., Li, A., & Chen, Y. 2013, ApJ, 773, 30
Wang, S., Li, A., & Jiang, B.W. 2014, Planet. Space Sci., in press
Weingartner, J.C., & Draine, B.T. 2001a, ApJS, 134, 263
Weingartner, J.C., & Draine, B.T. 2001b, ApJ, 548, 296
Whittet, D. C. B. 1977, MNRAS, 180, 29
White, R. E., III, & Keel, W. C. 1992, Nature, 359, 129
White, R. E., III, Keel, W. C., & Conselice, C. J. 1996, in New Extragalactic Perspectives in the New South Africa, ed. D.L. Block & J.M. Greenberg (Dordrecht: Kluwer), 114
White, R. E., III, Keel, W. C., & Conselice, C. J. 2000, ApJ, 542, 761
Xiang, F. Y., Li, A., & Zhong, J. X. 2011, ApJ, 733, 91
Zasowski, G., Majewski, S. R., Indebetouw, R., et al. 2009, ApJ, 707, 510
Zhou, H., Ge, J., Lu, H., Wang, T., Yuan, W., Jiang, P., & Shan, H. 2010, ApJ, 708, 742

Milky Way Metallicities and Fossil Cosmology

Misha Haywood

Abstract Taking into account the structural characteristics of the Milky Way stellar populations leads us to reconsider our concepts of the chemical evolution of our Galaxy. In particular it is suggested that the solar vicinity provides an unrepresentative sampling of the disk MDF and that no G-dwarf problem generalizable to the whole disk can be inferred from the solar vicinity, nor constrains on the infall time scale. I suggest that the best place to look for an unbiased and representative disk MDF is the Galactic bulge, and show how the chemical properties of the disk and the bulge can be reconciled. A new way to measure the SFH of the Galaxy shows that the thick disk is massive, supporting the mass deduced from structural properties. A massive thick disk population implies that large amounts of gas were present at early times, in contradiction with the long infall time scales inferred by standard chemical evolution models. Finally, comparisons of the MW with the mass growth history of similar galaxies at high redshift suggest that the thick disk is not a contingent population, but may be generic to all galaxies of the class of the Milky Way.

1 Introduction

One of the first and best known example of fossil cosmology is the G-dwarf problem, or the discovery that the solar vicinity contains too few low metallicity dwarfs compared to the "closed-box" model. In other words, observations of the solar vicinity would suggest that the enrichment rate has been faster than the star formation rate. Infall models have been introduced in order to solve this problem, by limiting the dilution of rejected metals in a disk parsimoniously provisioned with gas. An inherent shortcoming of these models is the fact that density distributions (such as MDFs) are considered to result solely from chemical evolution, while, obviously, other processes are also at work in determining the large scale scale distribution of metallicities, and hence the MDF at the solar radius. Thanks to recent large scale spectroscopic surveys, we are now able to sample the disk MDF beyond the solar

M. Haywood (✉)
GEPI - Observatoire de Paris- UMR 8111, 5 Place Jules Janssen 92195 Meudon Cedex France
e-mail: Misha.Haywood@obspm.fr

K. Freeman et al. (eds.), *Lessons from the Local Group,*
DOI 10.1007/978-3-319-10614-4_9

vicinity, and to distances where the shape of the MDF is also an effect of density variations in stellar populations. The following pages show that the structural parameters of stellar populations, when taken into account, can change our views on chemical evolution constraints. Two examples are given in the following section, both due to the recent measurement of a short thick disk scale length. These show firstly, that the local vicinity MDF is a biased representation of the disk, and secondly, that the bulge MDF can be simply explained as the projection of the disk(s) MDF into the central regions through density laws, supporting the view that the thick disk is a massive population in the Milky Way. I develop thereafter (Sect. 3) arguments calling for a change of perspective in chemical evolution modelling, which is required in order to correctly account for these effects. I then present the star formation history of the MW reported by Snaith et al. (2014a), which provides independent confirmation that the thick disk is massive. The mass growth derived from the SFH, driven in the first Gyrs by the formation of the thick disk, shows good agreement with the evolution of galaxies of the same class at high redshifts, suggesting that thick disks are a generic feature in these objects (Lehnert et al. 2014), see Sect. 4.

2 Local vs General MDFs: Unifying the Inner Disk and Bulge MDFs

The study of Galactic chemical evolution is based on reproducing metallicity distributions and trends in chemical characteristics (e.g. [α/Fe] *vs* [Fe/H], [Fe/H] *vs* age). Models usually assume that variations in distributions involving number densities (such as the MDF) depend on chemical parameters only, and not on the stellar density parameters of the populations under study. These principles have been applied (e.g. Chiappini et al. 1997; Naab and Ostriker 2006) to modelling the disk of the Milky Way, as sampled in the solar vicinity, as well as its bulge (Matteucci and Broccato 1990; Tsujimoto and Bekki 2012; Grieco et al. 2012). The most recent elaboration of this kind of models is the introduction of radial migration to explain the presence of metal-rich or metal-poor dwarfs at the solar vicinity (Schönrich and Binney 2009). Apart from the fact that the effect of radial mixing at the solar radius is more than elusive (Haywood et al. 2013, 2014), these modifications are however second order because structural parameters of stellar populations, if not taken into account, have much more important implications.

In the solar vicinity, the MDF is (mainly) a mixture of thin and thick disk stars. The ratio of thick to thin disk in this mixture would remain constant with Galactic radius as defined in the solar vicinity if the scale lengths of the two populations were the same. Recent measurements (Cheng et al. 2012; Bensby et al. 2011; Bovy et al. 2012) based on spectroscopic selection of thick disk stars show that this population most probably has a short scale length ($\sim$ 2 kpc), smaller than the thin disk scale length (Bovy et al. 2012), 3.6 kpc. A shorter scale length makes the thick disk more massive than usually assumed, and most of its stars must therefore reside within the

solar circle. Hence, it is expected that the solar vicinity severely underestimates the number of intermediate metallicity objects.

This is supported by two independent recent results. The first comes from preliminary APOGEE data. Figure 14 of Anders et al. (2014) shows that, between 4 and 7 kpc from the Galactic center, the α-enhanced population with [Fe/H] < -0.2 dex represents about 35 % of the stars. This is what is expected for a thick disk population of 2 kpc scale length and 10 % local density, together with a thin disk of 3.6 kpc scale length.

The second comes from recent studies of the bulge. It has been proposed by Shen et al. (2010), on the basis of the BRAVA survey, that any classical bulge component, if it exist at all in the MW, must be limited to at most 10 % of the of the stellar mass. The ARGOS survey provided further support by decomposing the bulge in three main components, and showing that they can all be explained by the thick and thin disks. Di Matteo et al. (2014a) arrived at a similar conclusion using N-body simulations, and further demonstrated that component B identified by Ness et al. (2013a) is, in all probability, mostly made of stars of the young thick disk. If so, this means that the thick disk represents no less than 60 % of the stars at all latitudes studied by Argos. This is much higher than expected if the thick disk has a scale length similar to the thin disc, and not possible if the thick disk scale length is larger than that of the thin disk. This suggests that within the first few kpcs of the Galactic center the thick disk becomes the dominant population.

There are two consequences of this: The first is that the use of solar vicinity MDF provides only a very limited and biased view of the MDF of the disk. Hence, deriving a formation time scale for the whole disk from the solar vicinity alone would not be suitable. Models have been introduced with accretion time scales increasing with distance to the galactic center in order to generate gradients from radially varying MDFs. These models imply that the star formation history varies likewise, if some kind of Schmidt–Kennicutt law is assumed. If this is correct, it should, however be reflected in a significant dispersion in the age-[α/Fe] distribution because each SFH generates its own age-[α/Fe] relation. However, sampling of this distribution in the solar vicinity shows a remarkable small dispersion (Haywood et al. 2013), in spite of the fact that the thick disk stars in the solar vicinity have eccentricities which imply origins from a wide range of radii. In other words, the small dispersion of the age-[α/Fe] relation testifies a uniform SFH throughout the Galactic thick disk, in contradiction to the idea of a radially varying accretion time scale (in the inner disk, < 10kpc, see Haywood et al. (2013)), if the SFH is to reflect the accretion history.

The second consequence concerns the bulge chemical evolution. If the MW is a pure disk Galaxy, as is now advocated (Shen et al. 2010; Kunder et al. 2012; Ness et al. 2013a, b; Di Matteo et al. 2014a, b), its bulge should show a pure disk chemical evolution. Yet, all studies so far have modelled the bulge chemical evolution has an isolated system, not considering the possible contributions of the thin and thick disk to the bulge. While a detailed discussion is beyond the scope of the present contribution (see Haywood 2014, in prep.), it is known that several recent observations suggest correspondence between the disks and the bulge chemical characteristics. For example, detailed chemical abundances of microlensing events

by Bensby et al. (2013) have shown that chemical abundances in the bulge are similar, if not identical to those measured of solar vicinity stars. While some small systematic shifts exist for some elements (magnesium), it is reasonable to advocate for matches between inner disk and bulge chemical abundance patterns (compare, for instance, Fig. 27 of Bensby et al. and Fig. 26 of Bensby et al. 2014, for stars with $R_{mean} < 7$ kpc; the chemical tracks are indeed almost identical). Also, the age-metallicity distribution derived from Bensby et al. (2013) is compatible with the one found by Haywood et al. (2013)—even though the error bars on bulge stars are admittedly large.

The most discrepant characteristics between the two populations are their MDFs: the bulge MDF is much broader, with significantly more metal-poor and metal-rich stars. If the bulge *is* the disk, why are their MDFs so different? In Haywood (2014, in prep.) and as discussed hereafter, we suggest the answer is not one of chemical evolution but more likely a problem of accounting properly for structural parameters of stellar populations.

Reconstructing the Bulge MDF

The study by Bovy et al. (2012) shows that the disk components with the shorter scale lengths are the thick disk ($h_R < 2$ kpc) and the metal-rich thin disk, while the metal-poor thin disk has scale length larger than 4 kpc and the solar metallicity thin disk has scale length of the order of 3.6 kpc. Although they are minor components at the solar radius, the thick disk and metal-rich thin disk will dominate the counts at the Galactic center, because of their small scale lengths. On the contrary, the outer thin disk, with scale length greater than 4 kpc, will have minor contribution. This is already seen in Anders et al. results: the metal-weak thin disk (-0.8 dex$<$[Fe/H]<-0.2 dex) is absent in the inner regions surveyed by APOGEE. The abundance measurements from Bensby et al. (2013) further confirm that this component is also absent from the bulge. On the contrary, the thick disk and metal-rich disk are prominent in counts of Anders et al. (2014, their Fig. 14, lower-left plot): the thick disk represents the vast majority of the stars at [Fe/H]<-0.2 dex, and metal-rich ([Fe/H]>0.0 dex) stars have a strikingly large contribution.

Figure 1 from Haywood (2014, in prep.), shows the result of projecting local densities in the Galactic centers using these scale lengths. Due to the short scale length of the thick disk and metal-rich thin disk, these two components dominate the counts at all latitudes except $b = 0°$, where the solar component is still important. At latitudes of 5° and higher, the two components of the thick disk dominate the counts.

Figure 1 shows that simply taking into account the contribution of the thick and thin disks at the Galactic center suffices to reproduce the bulge MDF. It also tells us that, given that most of the mass of the disk(s) is concentrated within a few kpc of the Galactic center, it is to be expected that the "bulge" MDF provides in fact the most representative disk MDF, and the least biased. This is because the scale lengths of various populations are expected to have the least effect in the central regions.

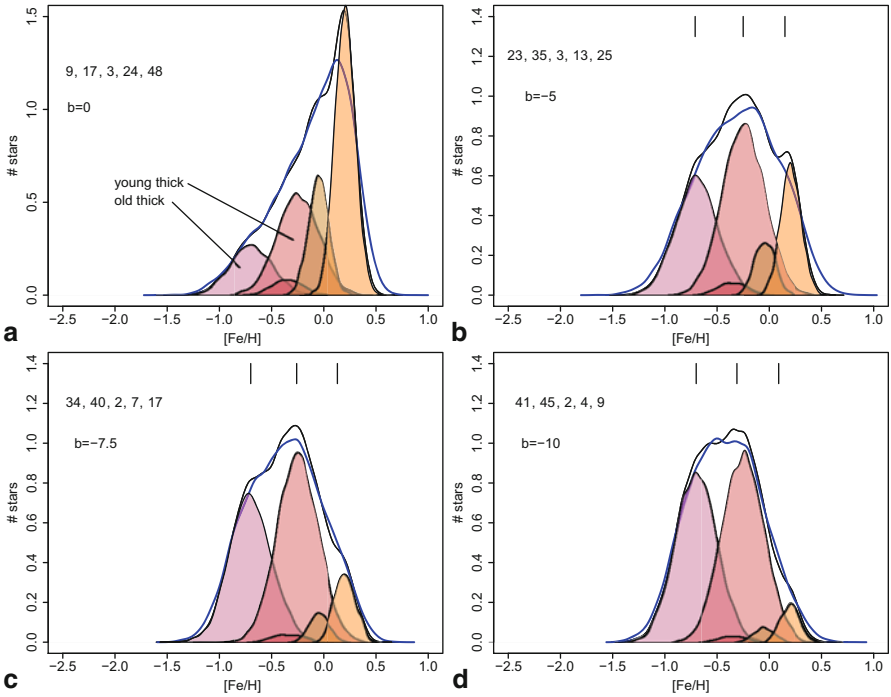

Fig. 1 Illustrative MDF of the bulge at different galactic latitudes, resulting from the combination of the five components of the disk projected at the Galactic center. The percentage of each component is given in the following order: old thick disk, young thick disk, metal-poor, solar and metal-rich thin disk. The two components of the thick disk are indicated in the first plot, the three other components are thin disk. The *black curve* is the sum of all components, the *blue curve* is the sum convolved with a 0.11 dex uncertainty. *Vertical ticks* in (*b*), (*c*) and (*d*) indicate the metallicity of the three main components found by Ness et al. (2013a). (Source: Haywood (2014, in prep.)

3 The Chemical Evolution of the Disk(s) System

Fitting the MDF to constrain the accretion time scale, is problematic, as I argued in the previous section. A strong constraint, independent of stellar densities, is provided by the age-[α/Fe] distribution. In Fig. 2 (Haywood et al. 2013), this distribution shows two distinct segments which correspond to the thick disk and thin disk phases. The rate at which [α/Fe] decreases as a function of age is a direct function of the SFR intensity through the creation of iron. Hence, this distribution provides a fundamental constraint on the star formation history of the disk(s). In order to retrieve this information, one must assume a model to link the SFH and corresponding chemical properties of the system at a given time.

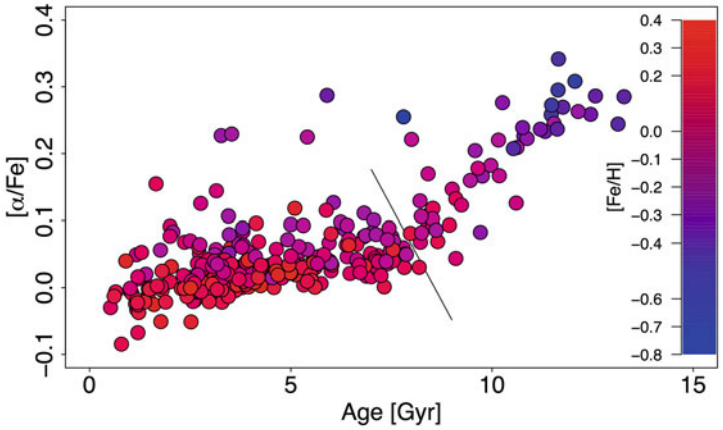

Fig. 2 The age-[α/Fe] distribution from Haywood et al. (2013), showing distinctly the thick and thin disk phases. The rate of variation of [α/Fe] is a function of the SFR intensity, allowing the derivation of the Star Formation History with unprecedented accuracy (Snaith et al. 2014a)

3.1 Modelling the Disk: the Return of an Old Case

A short scale length makes the thick disk massive. Hence, we expect to find a lot of intermediate metallicity stars in the inner Galaxy (and as mentioned in Sect. 2, preliminary APOGEE data seems to confirm this). Since the thick disk is old, it implies in turn that huge quantities of gas must have been available for consumption in the first Gyrs. While this is at variance with the standard credo of infall models (see e.g. Fraternali 2013), this is also in qualitative agreement with the high fractions of gas in disks at high redshifts, where the mass of gas to star ratio can easily reach more than 50 % (Carilli and Walter 2013). This suggests that instead of minimising the amount of gas in the disk, as is done with infall models, we should try to maximise it. Another clue as to what model to choose comes from the MDF discussion of Sect. 2: qualitatively, the MDF of the disk, as sampled by the MDF of the bulge, is strongly reminiscent of a closed-box distribution. The model that maximises the amount of gas is the closed-box model, and it is worth re-examining it in this new context.

Note that the "closed-box" is interesting because it approximates a system strongly dominated by gas at early times, and the fact that it is closed/open has no bearing in this case. Instead of being viewed as the unrealistic limiting case of chemical evolution models, we consider it as an approximation of the case where either most accretion in the inner disk have occurred early in the Galactic history, or where accretion has maintained a sufficiently high gas fraction in the disk at early times not to limit the SFR. In the following, I discuss the application of the closed-box model to the solar vicinity data, as developed in Snaith et al. (2014a).

3.2 The Star Formation History of the Milky Way

In standard chemical evolution models, the SFR reflects the accretion history through some kind of Schmidt-Kennicutt law. This is, however, an unnecessarily restrictive assumption, because the SFH can be determined by fitting models to observed chemical tracks in the age-[α/Fe] plane. In addition, there are some doubts that the accretion history can be directly reflected in the SFH (through the SK law) at high redshifts, because others processes in the ISM probably regulate the intensity of the SFR at these epochs, such as feedback (Hopkins et al. 2013).

In Snaith et al. (2014a), instead of deriving the SFH from an unknown accretion history, the SFH was derived by fitting the [E_i/Fe]-Age sequence iteratively for Silicon data. This method has the huge advantage that if stars have different origins in the disk, as is the case here, and follow a uniform chemical evolution—as testified by the low dispersion in the α-age plane—the measured SFH is non-local, and valid for the entire population[1]. Moreover, the method does not rely on stellar density, it uses only abundance variations as a function of age, thus it is not limited by number densities-related problems, such as the design of volume complete samples, scale height corrections, etc. Finally, it gives access to detailed variations of the SFH at ancient epochs, a domain that is likely to remain inaccessible with standard methods at least until the data from the ESA astrometric mission, Gaia is available. Counting stars as a function of age for ancient populations is indeed impractical for the time being, simply because there are not enough old stars with sufficiently accurate ages.

The result of the fitting is given in Fig. 3a, with the corresponding SFH in Fig. 4a, normalized in order to amount to 5×10^{10} $M_\odot$ total stellar mass in the disks. The star formation history obtained suggests that:

(1) the Galaxy underwent a phase of intense star formation between 9 and 13 Gyr ago, during the formation of the thick disk. At those epochs, the SFR peaked at 3–4 times the value characterizing the thin disk formation phase. This phase produced as much mass in stars as are produced in the following 8 Gyr, during the thin disk formation. In other words, the thick disk of the Galaxy is about as massive as the thin disk.
(2) the SFH shows a distinct dip at $\sim$ 8–9 Gyr. Analysis by Snaith et al. (2014b) indicates that this dip is robust, and implies that the end of the thick disk formation phase is marked by a decrease in the star formation rate.
(3) during the thin disk phase, the SFR remains moderate at $\sim 2M_\odot$/yr, in agreement with estimates of the present day SFR in the Galaxy.

Figure 3b shows the chemical evolution in the [Si/Fe]–[Fe/H] plane generated by the recovered SFH (the curve is obtained by averaging several individual [Si/Fe]–[Fe/H] tracks derived using the best fit SFH solutions obtained by fitting the Age-[Si/Fe] relation through bootstrapping the data). It is striking to see that, even if the model has

[1] While this is true for the thick disk, it may become less correct for younger stars that have orbits more confined to the solar circle.

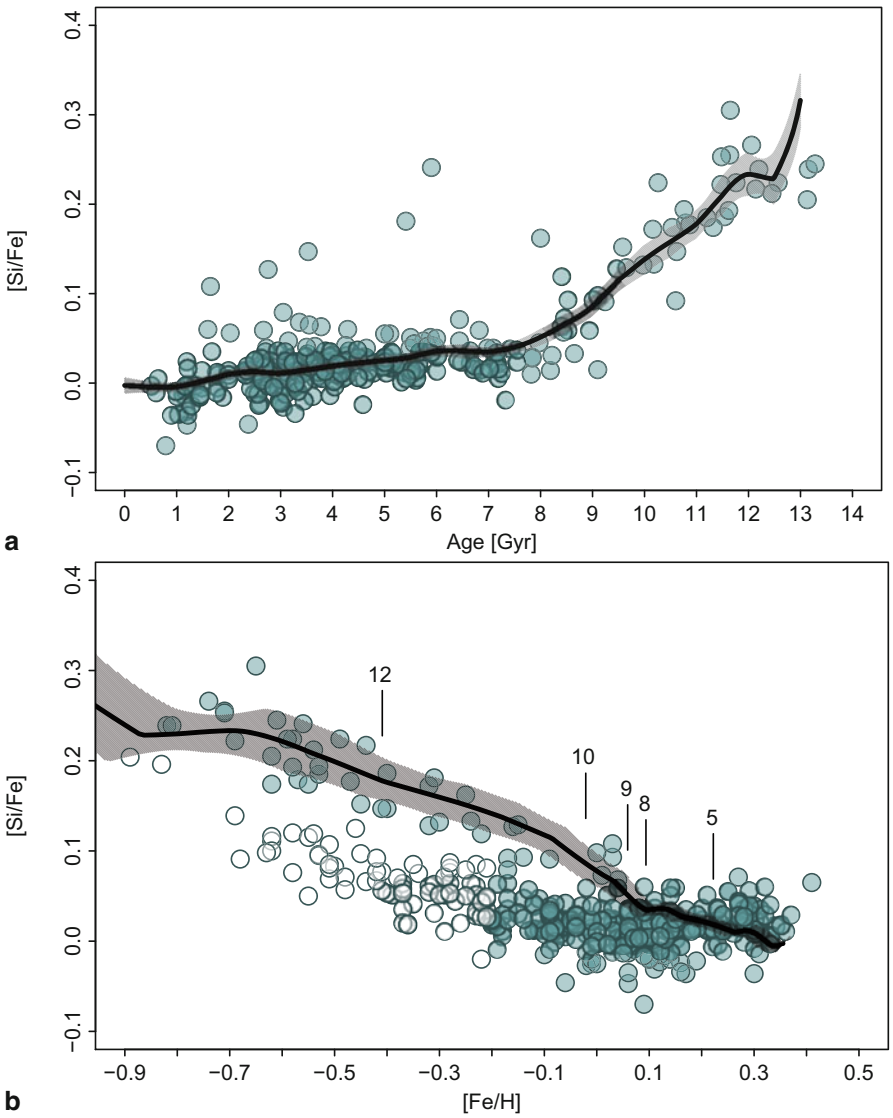

Fig. 3 **a** The age-[Si/Fe] distribution of stars from spectroscopic observations of F and G stars (Adibekyan et al. 2012) and ages from Haywood et al. (2013). The curve shows the result of the iterative fit made to derive the star formation history. **b** The chemical track in the [Si/Fe]–[Fe/H] plane obtained from the model, assuming our best fit SFH. This *not* a fit to the data

not been designed to fit the [Si/Fe]–[Fe/H] distribution, its chemical tracks describe very well the thick disk sequence (ages above 8 Gyr). In contrast, the thin disk is less well described, as expected: although the variation of [Si/Fe] *vs* [Fe/H] in the thick disk is de facto a temporal sequence, this is much less the case for thin disk stars,

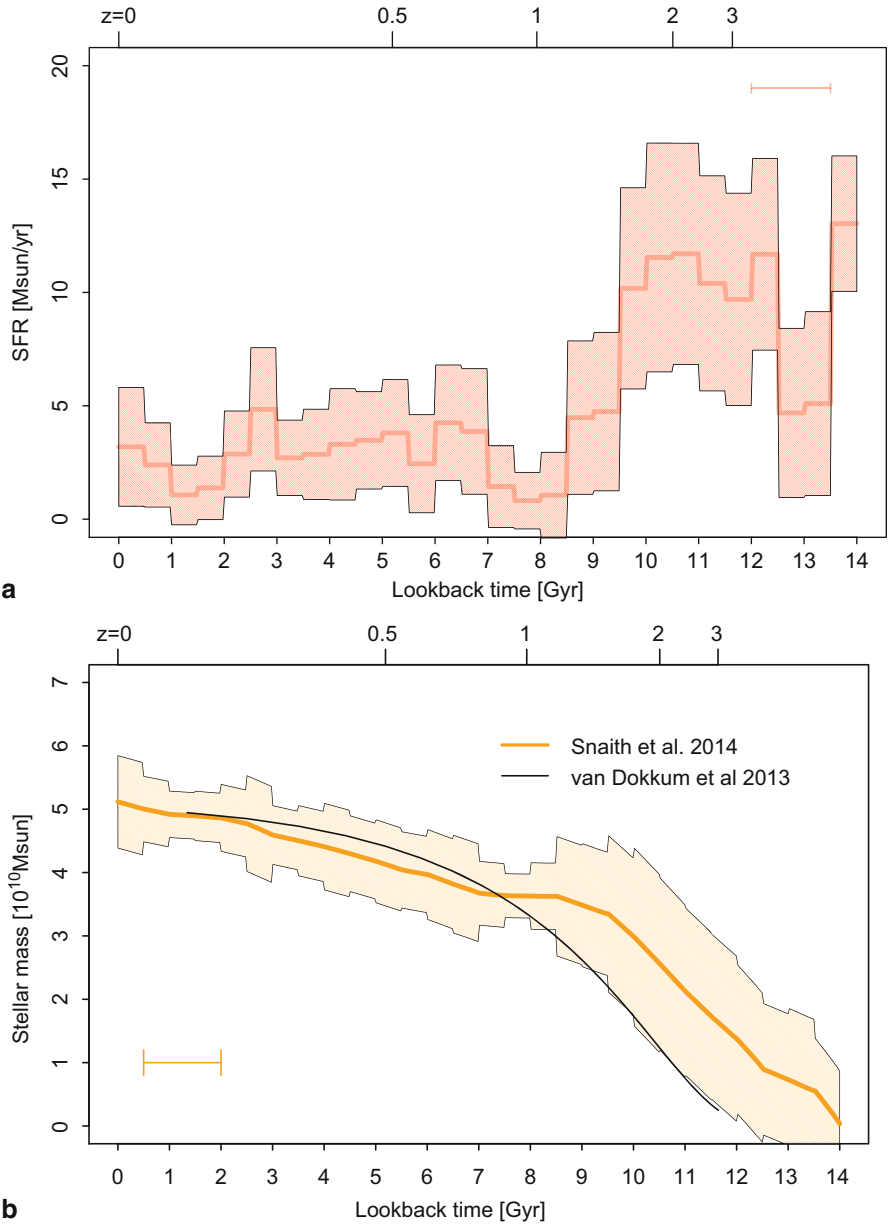

Fig. 4 **a** Star Formation History as derived from abundances in Snaith et al. (2014a), and **b** the corresponding mass growth of the Milky Way, normalized to obtain a total stellar mass of the MW disk of $5 \times 10^{10} M_{\odot}$. Also shown is the mass growth measured by van Dokkum et al. (2013) for Milky Way-like galaxies. Error bars are representative of uncertainties on age determination

where the variation of α elements with metallicity reflects the contamination of the solar vicinity by stars of the inner and outer disk of all ages, not an evolution.

4 The Milky Way and Its Progenitors

These results lead to a fundamental revision of the role played by the thick disk in the evolution of our Galaxy. With the recognition that our MW's stellar mass is dominated by its disks, the thick disk is arguably the dominant old stellar population of the MW, and its formation corresponds to the dominant epoch of star formation in the Galaxy.

The SFH of our Galaxy in Fig. 4 fits well with observational studies of distant galaxies. Figure 4 (panel *b*) illustrates the evolution of the cumulative stellar mass as a function of age compared to the one obtain by van Dokkum et al. (2013) for Milky Way-type progenitors at different redshifts. Given possible systematic effects in the age scale, and the uncertainty in the stellar mass of the MW (at least $\pm 20\,\%$), good qualitative agreement is obtained. This indicates that MW progenitors had assembled more than half of their stellar mass by $z = 1$ (van Dokkum et al. 2013, Muzzin et al. 2013). These direct observations, together with the properties of local disk galaxies, which do not show any presence of substantial old, classical spheroids (Kormendy et al. 2010; Fisher et al. 2010), suggest that the stellar mass formed at these early epochs was likely in thick disks. These results give strong hints that the formation of the thick stellar disk is a fundamental part of the evolution of the MW. Conversely, it is possible that the formation of thick disks in MW progenitors makes their mass growth similar with that of the Milky Way. Inasmuch as classical bulges are not responsible for half the mass growth of MW progenitors since $z = 2.5$, something that would be difficult to reconcile with the known characteristics of these objects, it is the formation of the thick disk which makes the MW have a mass growth similar to other galaxies of its class. It suggests that the formation of thick disks is a generic phase of the growth of disk galaxies of the mass of the MW. Note that these results are opposite to the analysis supporting long time scale infall (e.g. Fraternali 2013), and in particular from standard chemical evolution models (e.g. Naab and Ostriker 2006), where it is inferred that most of the stellar mass formed after $z = 1$.

5 Conclusions

I discussed the impact of the structural parameters of stellar populations on the MDF of the disk and bulge. The small scale length of the thick disk, recently found via spectroscopic surveys, implies that stars of intermediate metallicities are under-represented at the solar radius. Taking into account the scale lengths of disks populations, it is shown that the solar vicinity MDF, projected at the Galactic center, reproduces the main characteristics of the bulge MDF as observed in the Argos survey. I argue that the best place to find an unbiased disk MDF is the bulge. The chemical evolution of the bulge can thus be reconcile with that of the disks.

The derivation of the SFH of the MW from abundances using a new technique independent of stellar densities shows that the thick disk is a massive population (Snaith et al. 2014a), hereby confirming the estimate that can be made from the new small scale length (2 kpc) measured for this population. These results lead to a change of paradigm in the way we see the mass growth and the chemical evolution of the MW, since a massive old stellar population implies that huge amounts of gas must have been available at early times in order to sustain the measured SFR. This is in contrast with standard infall models, which minimize the amount of gas available and so the number of intermediate metallicity stars formed, in order to solve the G-dwarf problem.

These results seem to be echoing the recent finding that galaxies, selected by abundance matching techniques to be Milky Way-like galaxies at different redshifts, have acquired at least half their stellar mass already by $z = 1.0$. Such rapid evolution, corresponding to a phase of high star formation intensity, corresponds to the formation of the thick disk in our Galaxy, suggesting this population could well be a generic feature of all galaxies of this class (Lehnert et al. 2014).

Acknowledgements It is a pleasure to thank the organisers, Ken Freeman, David Block and Bruce Elmegreen for giving me the opportunity to present this work and for a very enjoyable conference. I'm very grateful to Paola Di Matteo for stimulating discussions and comments during the preparation of this talk and Owain Snaith for help with the manuscript.

References

Adibekyan, V. Z., Sousa, S. G., Santos, N. C., et al. 2012, A&A, 545, A32
Anders, F., Chiappini, C., Santiago, B. X., et al. 2014, A&A, 564, A115
Bensby, T., Alves-Brito, A., Oey, M. S., Young, D. & Melendez, J. 2011, ApJL, 735, 46
Bensby, T., Yee, J. C., Feltzing, S., et al. 2013, A&A, 549, A147
Bensby, T., Feltzing, S., & Oey, M. S. 2014, A&A, 562, A71
Bovy, J., Rix, H.-W., Hogg, D. W., et al. 2012, ApJ, 755, 115
Carilli, C. L., & Walter, F. 2013, ARA&A, 51, 105
Cheng, J. Y., Rockosi, C. M., Morrison, H. L., et al. 2012, ApJ, 752, 51
Chiappini, C., Matteucci, F., & Gratton, R. 1997, ApJ, 477, 765

Di Matteo, P., Haywood, M., Gomez, A., et al. 2014a, arXiv:1404.0304, accepted A&A
Di Matteo, P., Gomez, A., Haywood, M., et al. 2014b, submitted
Fisher, D. B., & Drory, N. 2010, ApJ, 716, 942
Fraternali, F. 2013, IAU Symposium 298, eds S. Feltzing, G. Zhao, N.A. Walton & P.A. Whitelock; arXiv:1310.2956
Grieco, V., Matteucci, F., Pipino, A., & Cescutti, G. 2012, A&A, 548, A60
Haywood, M., Di Matteo, P., Lehnert, M., Katz, D., & Gómez, A. 2013, A&A, 560, A109
Haywood, M. 2014, arXiv:1401.1864
Hopkins, P. F., Keres, D., Onorbe, J., et al. 2013, arXiv:1311.2073
Kormendy, J., Drory, N., Bender, R., & Cornell, M. E. 2010, ApJ, 723, 54
Kunder, A., Koch, A., Rich, R. M., et al. 2012, AJ, 143, 57
Lehnert, M. D., P. Di Matteo, M. Haywood, O. Snaith 2014, ApJL accepted
Matteucci, F., & Brocato, E. 1990, ApJ, 365, 539
Muzzin, A., Marchesini, D., Stefanon, M., et al. 2013, ApJ, 777, 18
Naab, T., & Ostriker, J. P. 2006, MNRAS, 366, 899
Ness, M., Freeman, K., Athanassoula, E., et al. 2013a, MNRAS, 430, 836
Ness, M., Freeman, K., Athanassoula, E., et al. 2013b, MNRAS, 432, 2092
Schönrich, R., & Binney, J. 2009, MNRAS, 396, 203
Shen, J., Rich, R. M., Kormendy, J., et al. 2010, ApJL, 720, L72
Snaith, O. N., Haywood, M., Di Matteo, P., et al. 2014a, ApJL, 781, L31
Snaith, O. N., Haywood, M., Di Matteo, P., et al. 2014b, A&A submitted
Tsujimoto, T., & Bekki, K. 2012, ApJ, 747, 125
van Dokkum, P. G., Leja, J., Nelson, E. J., et al. 2013, ApJl, 771, L35

The Local Group Through the Eyes of the *Spitzer Space Telescope*

G. G. Fazio

Abstract The *Spitzer Space Telescope*, one of NASA's Great Observatories, has made numerous and important contributions to our understanding of the properties of the Local Group of Galaxies. *Spitzer* offers many unique capabilities for the study of the composition and structure of these nearby galaxies. In this paper some of the highlights are presented of *Spitzer's* Legacy and Exploration Science Programs associated with observations of the Milky Way galaxy, the Large and Small Magellanic Clouds, the Andromeda galaxy (M31), and the Triangulum galaxy (M33). Also presented are many of the spectacular images of these galaxies that *Spitzer* has produced.

1 Introduction

The *Spitzer Space Telescope* (Fig. 1), launched in August 2003, is producing an exciting new view of the Universe at infrared wavelengths (Werner et al. 2004). *Spitzer* is the fourth and final space telescope in NASA's Great Observatory series. Its "cold mission" consisted of an 85-cm telescope and three cryogenically-cooled instruments providing imaging and spectroscopic capability from mid-infrared to far-infrared wavelengths: Infrared Array Camera (IRAC; Fazio et al. 2004); Multiband Imaging Photometer (MIPS; Rieke et al. 2004), and Infrared Spectrometer (IRS; Houck et al. 2004). Combining the intrinsic sensitivity achievable with a cryogenic telescope in space with the high sensitivity of modern, large-area infrared detector arrays, *Spitzer* has provided the astronomical community with huge gains in capability for exploring the infrared Universe. *Spitzer's* "cold mission" lasted more than five-and-a-half years, terminated by the depletion of its liquid helium coolant on 15 May 2009. However, two of its cameras at 3.6 and 4.5 μm wavelength in IRAC continue to operate during the new "warm mission" phase, which started on 28 July 2009. *Spitzer* is in a solar orbit, gradually drifting away from the Earth, and currently more that 1 AU from the Earth. It continues to provide the astronomical community

G. G. Fazio (✉)
Harvard Smithsonian Center for Astrophysics,
60 Garden St., Cambridge, MA 02138, USA
e-mail: gfazio@cfa.harvard.edu

K. Freeman et al. (eds.), *Lessons from the Local Group,*
DOI 10.1007/978-3-319-10614-4_10

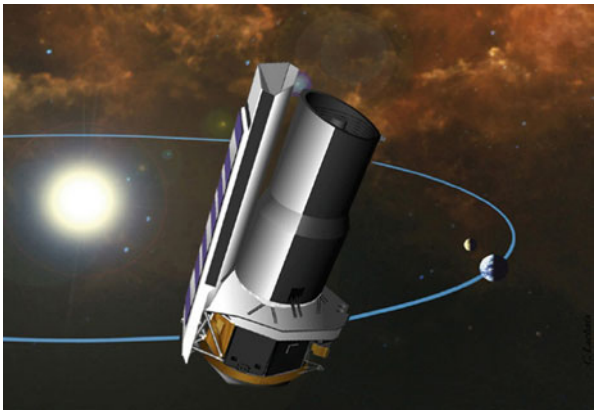

Fig. 1 The *Spitzer* Space Telescope in solar orbit, trailing the Earth (NASA/JPL-Caltech)

with a uniquely powerful mid-infrared imaging and sensitivity capability that will be unsurpassed until the launch of JWST. *Spitzer's* scientific results include the study of the formation and evolution of galaxies, observations of exoplanets and their atmospheres, the most accurate measurements of the Hubble constant, understanding energy sources in ultraluminous galaxies, the study of star formation and evolution, determining the structure and evolution of planetary disks around nearby stars, exploring the nature and distribution of brown dwarfs and brown dwarf "weather maps," and galaxy clusters. Additional information about the *Spitzer Space Telescope*, its focal plane instruments, its image gallery, and the data archive can be obtained at http://www.Spitzer.caltech.edu and http://ssc.Spitzer.caltech.edu.

In this paper we will discuss Spitzer's contribution to observations of the Local Group of galaxies, including the Milky Way, the Large and Small Magellanic Clouds, the Andromeda Nebula (M31), and M33. Since the number of publications on this topic is very large and the size of this paper is limited, we will present only a sample of the highlights.

2 *Spitzer's* Surveys of the Local Group

Spitzer's large surveys of the Local Group can be divided into two types: The Legacy Programs and the Exploration Science Programs. The *Spitzer* Legacy Programs enabled major science observing programs early in the *Spitzer* mission, with the goal of creating a substantial and coherent database of observations that could be used by subsequent *Spitzer* researchers. Legacy Programs are large and coherent science projects, of general and lasting importance to the astronomical community, in which the reduced data become available to the public immediately upon validation. The Exploration Science Programs are part of the *Spitzer* Warm Mission and focus on programs that require more than 500 h of *Spitzer* observing time, thus providing

the opportunity for large-scale programs that were not possible during the cryogenic mission.

The major Legacy Programs associated with the Local Group include:

(a) SWIRE: The *Spitzer* Wide-area Infrared Extragalactic Survey (Carol Lonsdale, PI)
(b) SINGS: The *Spitzer* Infrared Nearby Galaxies Survey—Physics of the Star-Forming ISM and Galaxy Evolution (Robert Kennicutt, Jr., PI)
(c) SAGE: *Spitzer* Survey of the Large Magellanic Cloud: Surveying the Agents of a Galaxy's Evolution (Margaret Meixner, PI)
(d) SAGE—Spectroscopy: The Life Cycle of Dust and Gas in the Large Magellanic Cloud (Alexander Tielens, PI)
(e) The Local Volume Legacy Survey (Janice C. Lee, PI)
(f) SAGE—SMC: Surveying the Agents of Galaxy Evolution in the Tidally-Disrupted, Low Metallicity Small Magellanic Cloud (Karl Gordon, PI)
(g) GLIMPSE: Galactic Legacy Infrared Mid-Plane Survey Extraordinaire (Ed Churchwell, PI)
(h) GLIMPSE II: Imaging the Central $+/-$ 10 Degres of the Galactic Plane with IRAC (Ed Churchwell, PI)
(i) GLIMPSE 3D: The Vertical Stellar and Interstellar Structure of the Inner Galaxy (Robert Benjamin, PI)
(j) MIPSGAL: A 24 and 70 μm Survey of the Inner Galactic Disk with MIPS (Sean Carey, PI)
(k) MIPSGAL II: Surveying the Innermost part of the Galactic Plane at 24 and 70 μm with MIPS (Sean Carey, PI)
(l) Cygnus-X: A *Spitzer* Legacy Survey of the Cygnus X Complex (Joseph Hora, PI)
(m) SMOG: *Spitzer* Mapping of the Outer Galaxy (Sean Carey, PI)

The major Exploration Science Programs associated primarily with the Local Group include:

(a) GLIMPSE 360: Completing the *Spitzer* Galactic Plane Survey (Barbara Whitney, PI)
(b) DEEPGLIMPSE: Deep GLIMPSE: Exploring the Far Side of the Galaxy (Barbara Whitney, PI).

3 *Spitzer's* Ability to Observe Galactic Composition and Structure

Spitzer offers many unique advantages in the study of the composition and structure of nearby galaxies. In addition to significantly higher sensitivity and higher angular resolution (1.4 arcsec FWHM at 3.6 μm) than previous infrared space missions, *Spitzer's* mid- and far-infrared cameras can penetrate dust obscuration to see the true structure of a galaxy. Figure 2 shows the spectrum of a star forming galaxy

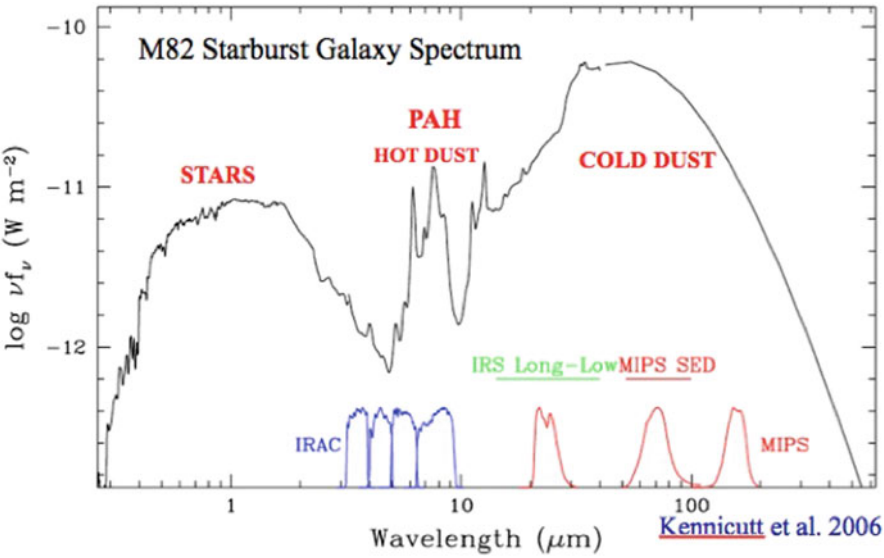

Fig. 2 A schematic spectral energy distribution of the starburst galaxy M82, extending from the near-ultraviolet to submillimeter wavelengths, with the infrared data smoothed to the low-resolution spectral mapping mode of *Spitzer*. The corresponding *Spitzer* imaging bandpasses of IRAC and MIPS are also shown (Kennicutt et al. 2003)

(e.g., M82) and the location of IRAC and MIPS filter bands. Note that IRAC's 3.6 and 4.5 μm bands sample stars, the 8.0 μm band samples the PAH bands and hot dust, and MIPS 24, 70 and 160 μm bands cold dust. As a result *Spitzer* can dissect a galaxy's composition and structure into its component parts. IRAC can map the stellar component of a galaxy and determine its stellar mass, as well as map the diffuse emission from polycyclic aromatic hydrocarbons (PAHs). MIIPS can locate the sites of massive star formation and map the diffuse emission of cold dust. The IRS offers both high- and low-resolution spectroscopy at mid-infrared wavelengths, detecting strong bands of dust, PAH, and ice, as well as atomic emission lines (Fig. 3). The atomic, fine structure lines of Ne, O, Si, and S, cover a range in ionization potentials and the ratios of these lines can be used to gauge the dominant ionizing source, whether it be hot stars or an active nucleus (Armus et al. 2004; Brandl et al. 2004).

4 Milky Way Galaxy

One of the most notable achievements of the *Spitzer Space Telescope* has been the new zoomable panorama of 360-degree mosaic of the galactic plane, which comes primarily from the GLIMPSE360 Project[1] (Churchwell et al. 2009). It consists of

[1] http://www.spitzer.caltech.edu/glimpse360/downloads.

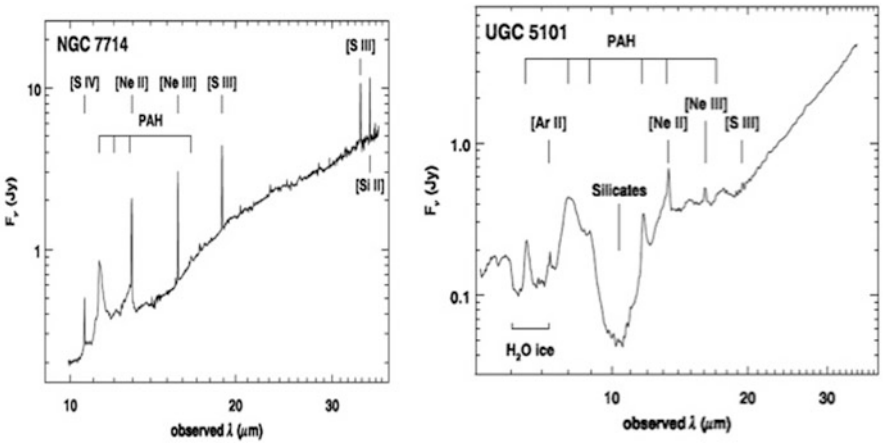

Fig. 3 Spectral energy distributions as measured by *Spitzer*/IRS of the starburst galaxies NGC 7714 at high resolution and UGC 5101 at low resolution (Houck et al. 2004)

multiple surveys with more than 2 million observations taken over 10 years (Fig. 4). This series of GLIMPSE surveys has produced a new view of our Galaxy, yielding insights into the physics of interstellar dust, star formation, and large-scale structure of the Milky Way as traced by stars. Objects observed at 3.6 to 24 μm include: HII regions/infrared bubbles, young stellar objects (YSOs), massive star-formation regions, infrared dark clouds (IRDCs), diffuse dust and PAH emission, and tens of millions of stars (Fig. 5). The GLIMPSE surveys have produced more than 500 publications in refereed journals. One of the largest mid-infrared bubbles lies on the periphery of the HII region M17. Povich et al. (2009) have proposed that M17 may have been triggered by the expansion of the bubble when it collided with the M17 SW molecular cloud. The distribution and morphologies of dust and PAHs in the interstellar medium, as well as the infrared extinction law were also determined.

GLIMPSE also determined the large-scale structure of our Galaxy, as traced by the distribution of red giant stars, including the radius and orientation of the central bar, and the stellar radial scale length. The Milky Way galaxy now appears as a barred, grand- design spiral (Fig. 6) with two arms (Scutum-Centaurus and Perseus) and at least two secondary arms (Sagittarius outer arm and the 3 kpc expanding arm).

Figure. 7 shows *Spitzer's* dazzling image of the center of the Milky Way galaxy. In visible light this region cannot be seen at all due to dust absorption. In this false-color image cool stars are blue while heated dust regions are shown in red. The bright white spot in the middle of the image is the center of the galaxy (S. Stolovy; Arendt et al. 2008)

Allen et al. (2004) and Megeath et al. (2004) demonstrated that the IRAC color-color diagram ([3.6]–[4.5] vs. [5.8]–[8.0]) is an extremely important tool for identifying young stars having infrared excess emission. Such a diagram can distinguish Class I (protostars), Class II (stars with disks) and Class III (photospheres)

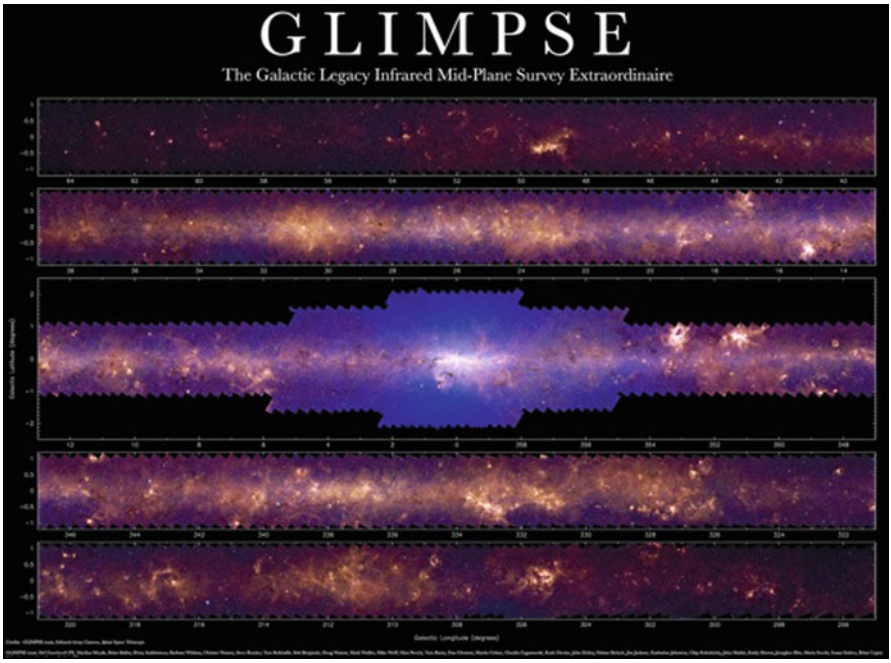

Fig. 4 A compilation of the *Spitzer*/GLIMPSE surveys: A New View of the Milky Way Galaxy at infrared wavelengths (Churchwell et al. 2009)

sources, a process that was difficult to near impossible to achieve with previous ground-based observations. They found that the distribution of measured IRAC colors of sources in four young clusters is very consistent with the distribution of model colors.

5 Large Magellanic Cloud

The primary *Spitzer* imaging survey of the Large Magellanic Cloud (LMC) is SAGE: Surveying the Agents of a Galaxy's Evolution (Meixner et al. 2006). SAGE is a uniform and unbiased imaging survey of the LMC ($\sim 7^\circ \times 7^\circ$) using both IRAC and MIPS instruments, with the agents being the interstellar medium and stars in the LMC (Figs. 8 and 9). It was carried out in 2005 in two epochs separated by 3 months. The primary *Spitzer* spectroscopic survey of the LMC is SAGE-Spec, which is a follow-up to the SAGE-LMC imaging survey (Kemper et al. 2010; Woods et al. 2011). The SAGE-Spec studies the life cycle of gas and dust in the LMC and provides information essential to the classification of the point sources observed in the imaging survey. Power spectra of the LMC emission at 24, 70, and 160 μm of the LMC were carried out by Block et al. (2010). Blum et al (2006) produced

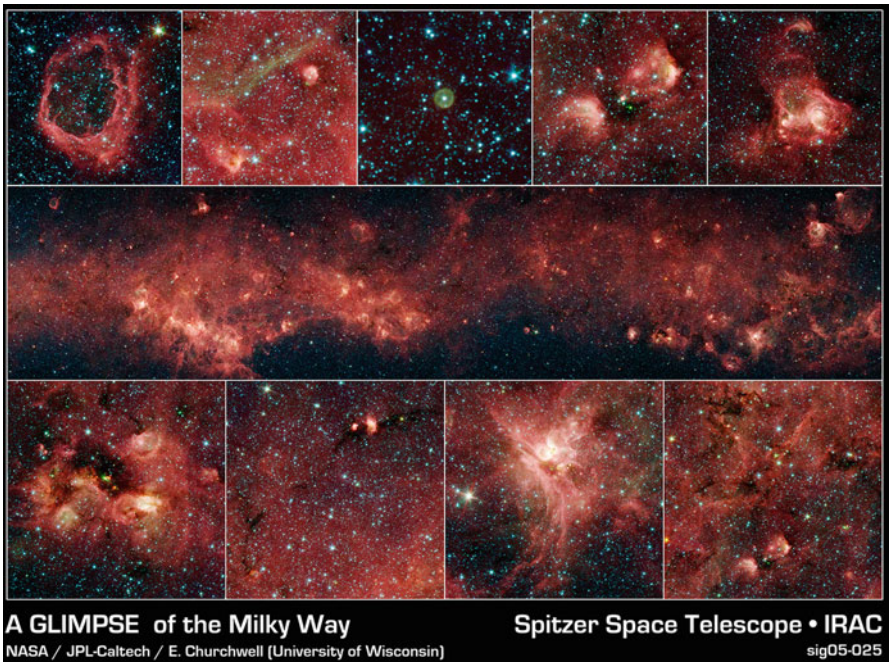

Fig. 5 A sample of images from the GLIMPSE survey of the plane of the Milky Way Galaxy. The center row image spans 9° of the plane. These images represent only 7.5 % of the total GLIMPSE survey (Churchwell et al. 2009; NASA/JPL-Caltech)

color-magnitude diagrams (CMDs) for stars in the *Spitzer* SAGE survey of the LMC at IRAC and MIPS 24 μm wavelengths (epoch 1 data). These data represent the deepest, widest mid-infrared CMDs of their kind ever produced in the LMC.

6 Small Magellanic Cloud

The *Spitzer* Legacy program SAGE-SMC (Surveying the Agents of Galaxy Evolution in the Tidally Stripped, Low Metallicity Small Magellanic Cloud; Gordon et al. 2011) had the specific goals of studying the amount and type of dust in the present SMC interstellar medium, the sources of dust in the winds of evolved stars, and how much dust is consumed in star formation. This program mapped the full SMC (30 deg^2) including the body, wing, and tail in seven bands from 3.6 to 160 μm using IRAC and MIPS on the *Spitzer Space Telescope* (Gordon et al. 2011; Fig. 10). As part of the SAGE- SMC program Boyer et al. (2011) investigated the infrared properties of cool, evolved stars in the SMC, including the red giant branch stars and the dust-producing red supergiant and asymptotic giant branch stars. This survey included full spatial coverage of the SMC bar, wing and tail regions from 3.6 to 160 μm.

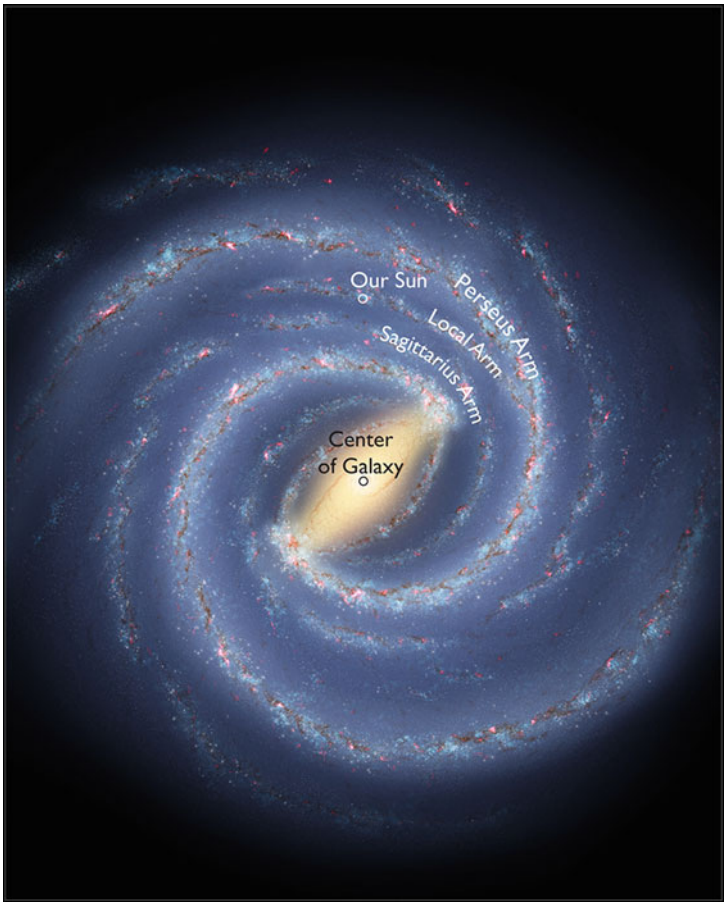

Fig. 6 A drawing of how the MW Galaxy is likely to appear when viewed face-on. Based on radio, infrared and visible wavelength data (Churchwell et al. 2009; R. Hurt; W. Benjamin)

Using the IRAC and MIPS (24 and 70 μm) catalogs and images from SAGE-SMC Sewilo et al. (2013) in combination with near-infrared (JHKs) and visible (UBVI) data, identified $\sim$ 1000 intermediate- to high-mass young stellar objects (YSOs) in the SMC, which was three times more than previously known.

7 M31 (Andromeda Galaxy)

Mapping the entire disk of M31 at mid-infrared wavelengths with *Spitzer* permits both local and global studies of the galaxy. IRAC's 3.6 and 4.5 μm observations trace the oldest stars in the disk and bulge, while the 8 μm observations trace the hot dust

Fig. 7 A Spitzer/IRAC image of the center of the MW Galaxy, with 3.6 μm wavelength in blue, 4.5 μm in *green*, 5.8 μm in orange; and 8.0 μm in *red*. The brightest spot in the middle of the image is the center of the galaxy (S. Stolovy)

in the spiral arms, without the extinction, Block et al. (2006). Barmby et al. (2006), using IRAC, mapped M31 over an area of 3.7° by 1.6°, which included the galaxies M33 and NGC 205 (Fig. 11). The IRAC images of M31 change dramatically over the wavelength bands. The 3.6 μm image of the bulge and disk is smooth, while the 8 μm image is dominated by the "10 kpc ring." Comparison of visual and 3.6 μm images over the inner 400 arcsec shows that there is no significant extinction at visual wavelengths in the bulge of M31. There is no evidence of an infrared-bright active galactic nucleus (AGN). The integrated 8 μm non-stellar luminosity implies a star formation rate of 0.4 $M_{\odot}$/yr. The 3.6 μm luminosity can be used to estimate the galaxy's stellar mass: 1.1×10^6 $M_{\odot}$.

Using *Spitzer's* MIPS instrument, Gordon et al. (2006) produced images of M31 at 24, 70 and 160 μm, revealing the morphology of the dust in the galaxy (Fig. 12). The structure consists of a composite of two logarithmic spiral arms and a circular 10-kpc ring of star formation, which is offset from the nucleus. The spiral arms are not continuous, but composed of spiral segments. The lack of well-defined spiral arms and the very circular star formation ring suggest that M31 has been distorted by interactions with its satellite galaxies (M32 and NGC 205).

Since the 10 kpc star formation ring's center is offset from the galaxy nucleus, the outer galaxy disk is warped, and the halo contains numerous loops and ripples, there exists some additional evidence, as noted also by Gordon et al. (2006), that M31

Fig. 8 Full Large Magellanic Cloud mosaics of the IRAC epoch 1 data of SAGE showing the location of the surveyed region on the sky. The IRAC data are shown in three colors, with 3.6 μm in *blue*, 4.5 μm in *green*, and IRAC-4.8 μm in *red* (Meixner et al. 2006)

has had a violent history. Using *Spitzer*/IRAC data, Block et al. (2006) discovered an inner dust ring spanning 1.3 × 1 kpc that is offset from the nucleus by ∼0.5 kpc. The two rings appear to be density waves propagating in the disk. Based on numerical simulations, the authors propose that the morphology can be explained by a companion galaxy, possibly M32, having an almost head-on collision though the center of the disk of M31 approximately 210 million years ago (see Fig. 13).

Recently, using both *Spitzer* and Herschel imaging of M31 combined with dust models, Draine et al. (2014) measured the dust properties of M31 and the distribution of dust in the galaxy. The authors constructed maps of the dust surface density, the gas-to-dust ratio, starlight heating intensity and the PAH abundance out to R = 25 kpc.

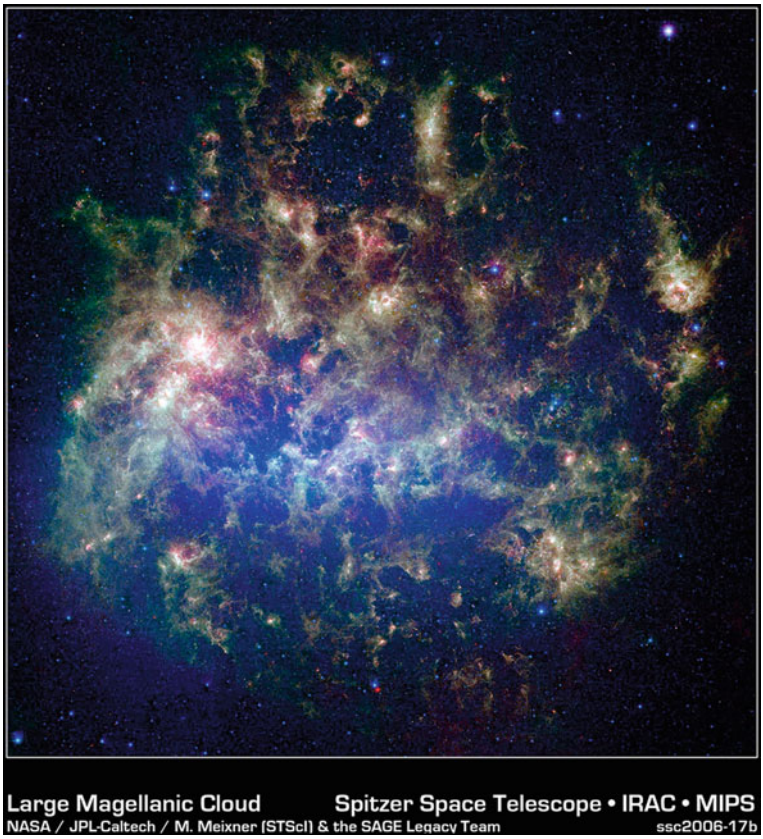

Fig. 9 Full Large Magellanic Cloud mosaics (epoch 1) of the SAGE data shown in three colors: IRAC 3.6 μm in *blue*, 4.8 μm in *green*, and MIPS 24 μm in *red* (Meixner et al. 2006)

8 M33 (Triangulum Galaxy)

There are more than 30 papers listed associated with *Spitzer* observations of M33, a Local Group spiral with slightly subsolar metallicity. *Spitzer* images (Figs. 14 and 15) of M33 (Hinz et al. 2004) show it to be surprising large—bigger than its visible-light appearance would suggest. With its ability to detect cold, dark dust, *Spitzer* can see emission from cooler material well beyond the visible range of M33's disk. Block et al. (2007) detected an enhanced number of intermediate age (0.6–2 Gyr) carbon stars in the outer arcs or spiral arms of M33 that may be an indicator of recent star formation, fueled by gas accretion from the HI-warp reservoir.

Of particular interest are two recent papers combining *Spitzer* and *Herschel* observations. Calapa et al. (2014) that combined *Spitzer* data with the observations of the *Herschel* M33 Extended Survey (HERM33es). The authors find that the 8 μm emission is better correlated with the 250 μm emission, which traces cold interstellar

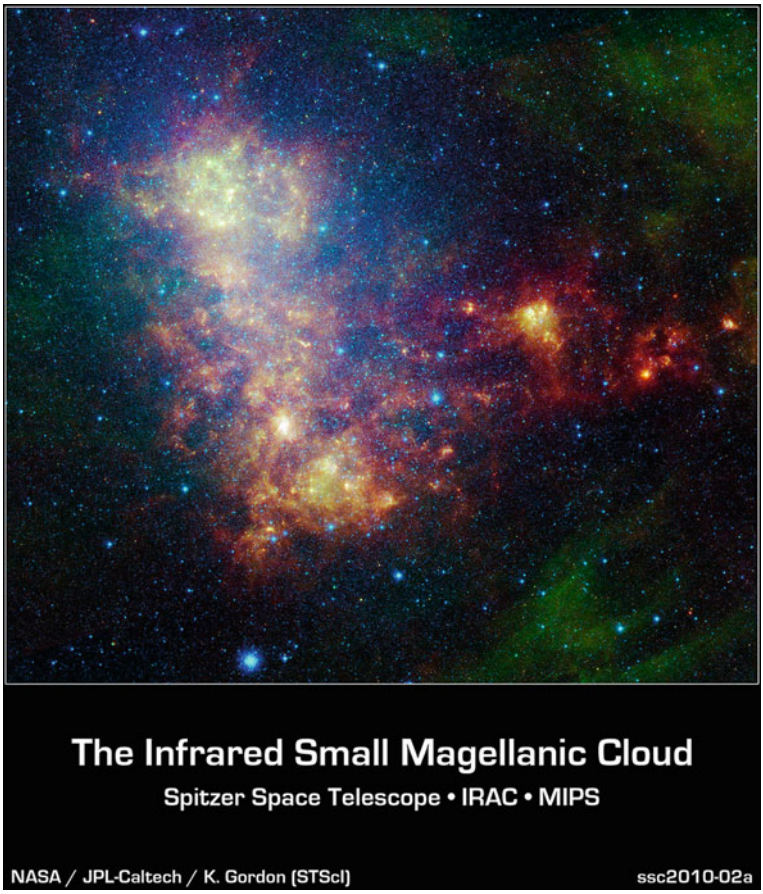

Fig. 10 A combination of IRAC and MIPS images of the SMC (*blue* is 3.6μm wavelength; *green* is 8.0 μm; and *red* is combination of 24-, 70- and 160μm; Gordon et al. 2011)

gas, than with the 24 μm emission. They also noted that the L(8)/L(250) luminosity ratio is tightly correlated with the IRAC 3.6 μm emission, which is a tracer of evolved stars and stellar mass, rather than with tracers of star formation rate. They also find that the fraction of 8 μm emission associated with the diffuse interstellar radiation ranges between $\sim$ 60 and 80 %.

Tabatabaei et al. (2014), also as part of the HERM33es program, studied the wavelength dependence of the dust emission as a function of position and environment across the disk of M33. M33 has a decreasing radial gradient in star formation and molecular-to-atomic gas ratio such that the regions bright in Hα or CO tend to trace the inner disk, which makes it difficult to distinguish between their effects on the dust.

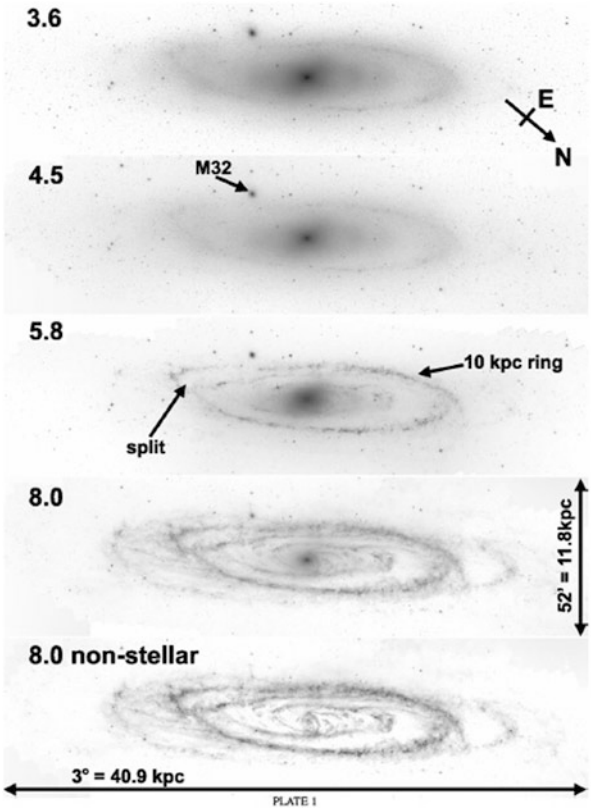

Fig. 11 IRAC images of M31 at 3.6, 4.5, 5.8, and 8.0 μm. The gray scales are approximately logarithmic with intensity (Barmby et al. 2006)

9 Other Galaxies in the Local Volume

Jackson et al. (2006) has published *Spitzer* 4.5 and 8.0 μm images of 15 Local Group and nearby dwarf galaxies. They find that the diffuse 8 μm emission of hot dust and PAHs is spatially correlated with regions of active star formation, and in particular, with the current star formation rate and the nebular metallicity of these galaxies. They propose that the lack of diffuse 8 μm emission in low-metallicity systems may be due to the destruction of dust grains by supernova shocks, assuming a long timescale to re-grow dust particles.

The *Spitzer* Local Volume Legacy Survey (Dale et al. 2009) observed near-,mid-, and far-infrared fluxes for 258 galaxies in local Universe out to 11 Mpc. The survey covered an unbiased, representative, and statistically robust sample of nearby star-forming galaxies, exploiting *Spitzer's* relatively high angular resolution. It was determined that these galaxies show a large spread in mid-infrared colors, likely due to the conspicuous deficiency of 8 μm PAH emission from low–metallicity, low-luminosity galaxies, and that the far-infrared emission tightly tracks the total infrared emission.

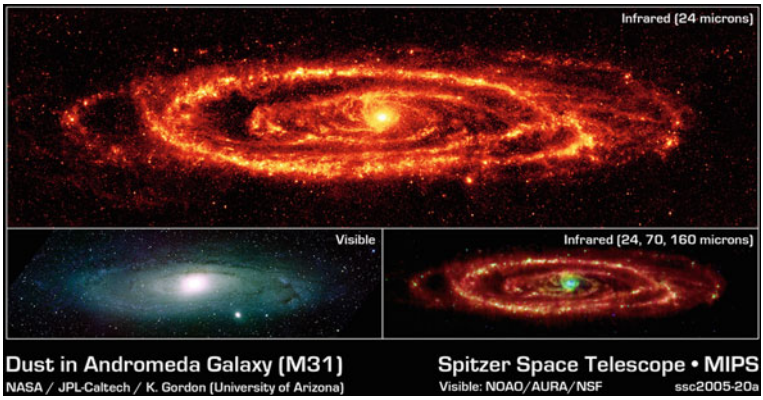

Fig. 12 *Spitzer's* 24-μm wavelength mosaic of M31 (*top panel*) is the sharpest image ever taken of the dust in another spiral galaxy. The lower left panel shows the visible light image of M31 for comparison. The multi-wavelength view of Andromeda (lower right panel) combines images taken at 24 μm (*blue*), 70 μm (*green*), and 160 μm (*red*). Using all three bands from MIPS allows astronomers to measure the temperature of the dust by its color (NASA/JPL-Caltech; NOAO, AURA, NSF; Gordon et al. 2011)

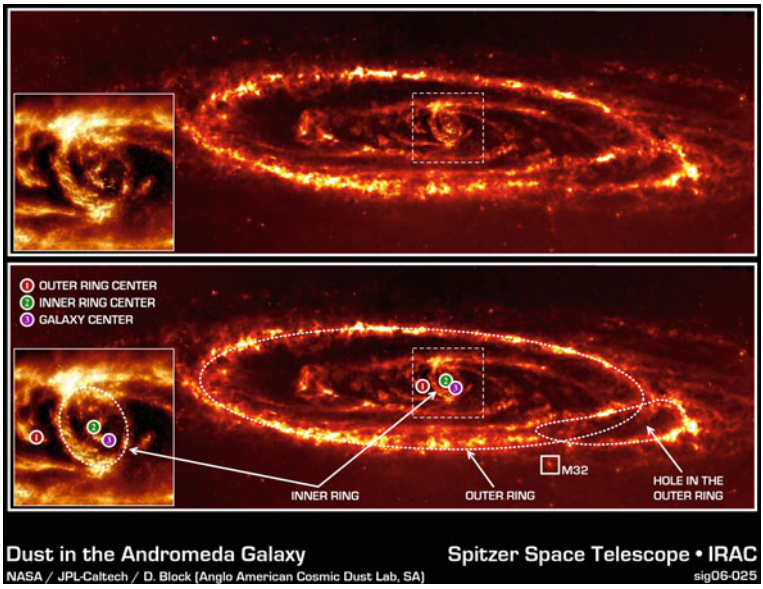

Fig. 13 M31 observed with IRAC at 8 μm wavelength, tracing the warm dust and PAH emission in the interstellar medium and showing the two rings (1×1.5 kpc inner ring offset by 0.5 kpc from the galaxy nucleus and the 10 kpc outer ring; Block et al. 2006)

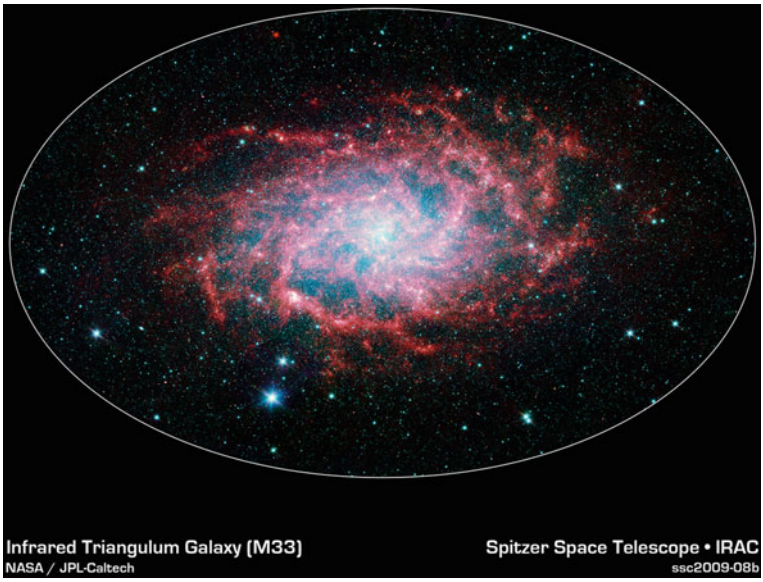

Fig. 14 A *Spitzer*/IRAC image of the center of the M 33 (Triangulum Galaxy), with 3.6 μm wavelength in *blue*, 4.5 μm in *green* and 8.0 μm in *red* (NASA/JPL-Caltech)

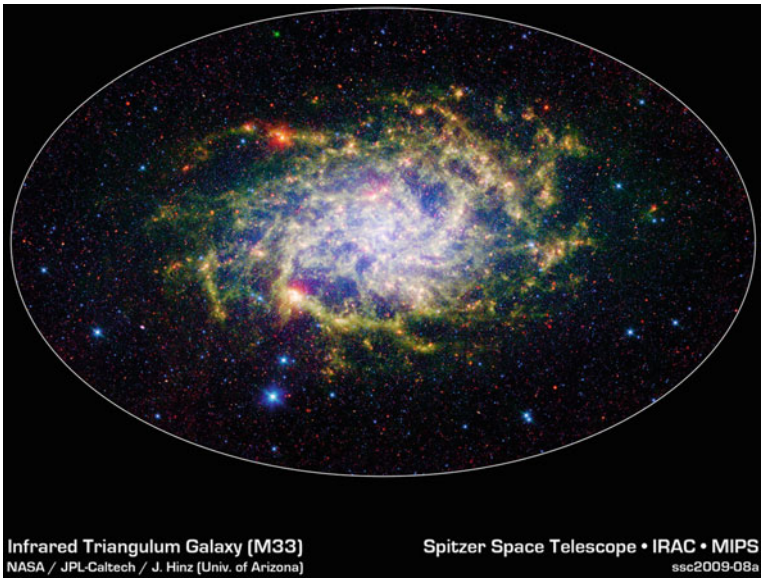

Fig. 15 A *Spitzer*/IRAC/MIPS image of M 33 (Triangulum Galaxy), with 3.6 and 4.5 μm wavelength in *blue*, 8.0 μm in *green*, and 24 μm in *red* (Hinz et al. 2004; NASA/JPL-Caltech)

Acknowledgements This work is based on observations made with the Spitzer Space Telescope, which is operated by the Jet Propulsion Laboratory, California Institute of Technology under a contract with NASA. Support for this work was provided by NASA through an award issued by JPL/Caltech.

References

Allen, L. E. et al. 2004, ApJ, 154, 363
Arendt, R. G., et al. 2008, 682, 384
Armus, L. et al. 2004, ApJS, 154, 178
Barmby, P. et al. 2006, ApJ, 650, L45
Block, D. L. et al. 2006, Nature, 443, 832
Block, D. L. et al. 2007, A&A, 471,467
Block, D. L. et al. 2010, ApJLetters, 718, L1
Blum, R. D. et al. 2006, AJ, 132, 2034
Boyer, Martha L. et al. 2011, ApJ, 142:103
Brandl, B. R. et al. 2004, ApJS, 154, 188
Calapa, Marie D. et al. 2014, ApJ, 784:130
Churchwell, E. et al. 2009, PASP, 121, 213
Dale, D. A. et al. 2009, ApJ, 703, 517
Draine, B. T. et al. 2014, ApJ, 780:172

Fazio, G. G. et al. 2004, ApJS, 154, 10
Gordon, K. D. et al., 2006, ApJ, 638, L87
Gordon, K. D. et al., 2011, ApJ, 142:102
Hinz, J. L. et al. 2004, ApJS, 154, 259
Houck, J. R. et al. 2004, ApJS, 154, 18
Jackson, D. C. et al. 2006, ApJ, 646, 192
Kemper, F. et al. 2010, PASP, 122, 683
Kennicutt, R. C. et al. 2003, PASP, 115, 928
Megeath, S. T. et al. 2004, ApJ, 154, 367
Meixner, Margaret et al. 2006, ApJ, 132, 2268
Povich, M. S. et al. 2009, ApJ, 696, 1278
Rieke, G. H. et al. 2004, ApJS, 154, 25
Sewilo, M. et al. 2013, ApJ, 778:15
Tabatabaei, F. S. et al. 2014, A&A, 561, A95
Werner, M. W. et al. 2004, ApJS, 154, 1
Woods, P.M. et al. 2011, MNRAS, 411, 1597

Models of the Stellar Initial Mass Function

Ralf S. Klessen and Simon C. O. Glover

Abstract In the past decade, we have witnessed a paradigm shift in star formation theory away from a quasi-static picture, where magnetic fields dominate the process, towards a much more dynamic and realistic approach. We now think that the process of stellar birth is controlled by the complex interplay between self-gravity and a number of opposing physical agents, the most important of which is the supersonic turbulence ubiquitously observed in the interstellar medium. On large scales it can support clouds against contraction, while on small scales it can provoke localized collapse. Turbulence establishes a complex network of interacting shocks, where dense cores form at the stagnation points of convergent flows. Some of these fluctuations become gravitationally unstable to form stars. Stellar birth is a highly intermittent process and any theory of star formation therefore must be statistical in nature. In this short contribution we review some of the current theoretical models of stellar birth. As mass is the most important parameter determining the evolution of individual stars, our focus lies on explaining the distribution of stellar masses of birth, the so-called initial mass function. Our text is a short excerpt of a lecture given at a Saas Fee winter school in 2013.

1 Observations of the Stellar IMF

Explaining the distribution of stellar masses at birth, the so-called initial mass function (IMF), is a key prerequisite to any theory of star formation. The IMF has three properties that appear to be relatively robust in diverse environments. These are the power law behavior, $dN/dM \propto M^{\alpha}$, with slope $\alpha \approx 2.3$ for masses M above about $1\mathrm{M}_{\odot}$, originally measured by Salpeter (1955), the lower mass limit for the power law and the broad plateau below it before the brown dwarf regime, and the maximum mass of stars at around $100\mathrm{M}_{\odot}$. Comprehensive reviews of cluster and field IMFs

R. S. Klessen (✉) · S. C. O. Glover
Zentrum für Astronomie, Institut für Theoretische Astrophysik, Universität Heidelberg, Albert-Ueberle-Straße 2, 69120 Heidelberg, Germany
e-mail: klessen@uni-heidelberg.de

S. C. O. Glover
e-mail: glover@uni-heidelberg.de

K. Freeman et al. (eds.), *Lessons from the Local Group,*
DOI 10.1007/978-3-319-10614-4_11

may be found in Scalo (1986), Kroupa (2002), Chabrier (2003), and Bastian et al. (2010).

There are two widely accepted functional parameterizations of the IMF. The first one is based on the continuous combination of multiple power-law segments. It is proposed by Kroupa (2001, 2002), and introducing the dimensionless mass $m = M/1\mathrm{M}_\odot$, it reads

$$f(m) = \begin{cases} Ak_0\, m^{-0.3} & \text{for } 0.01 < m < 0.08 \\ Ak_1\, m^{-1.3} & \text{for } 0.08 < m < 0.5 \\ Ak_2\, m^{-2.3} & \text{for } 0.5 < m < 1 \\ Ak_3\, m^{-2.3} & \text{for } 1 < m \end{cases} , \tag{1}$$

where A is a global normalization factor, and $k_0 = 1$, $k_1 = k_0 m_1^{-0.3+1.3}$, $k_2 = k_1 m_2^{-1.3+2.3}$, and $k_3 = k_2 m_3^{-2.3+2.3}$ are chosen to provide a continuous transition between the power-law segments at $m_1 = 0.08$, $m_2 = 0.5$ and $m_3 = 1$.

Another parameterization is based on Chabrier (2003). It combines a log-normal function with the Salpeter (1955) power-law,

$$f(m) = \begin{cases} Ak_1 m^{-1} \exp\left[-\frac{1}{2} \left(\frac{\log_{10} m - \log_{10} 0.079}{0.69} \right)^2 \right] & \text{for } m < 1 \\ Ak_2 m^{-2.3} & \text{for } m > 1 \end{cases} . \tag{2}$$

Again A is a global normalization factor, and $k_1 = 0.158$ and $k_2 = 0.0443$ provide a continuous connection at $m = 1$ (Chabrier 2005). Equation (1) is easier to integrate than (2), as this does not involve special functions. On the other hand it has several kinks. Both exhibit the Salpeter (1955) power law behavior with slope -2.35 for large masses. They differ by about a factor of 2 at low masses, however, within the observational errors, both functional forms are more or less equivalent.

We need to point out that the observational knowledge of the IMF is quite limited at the extreme ends of the stellar mass spectrum. Because massive stars are very rare and short lived, only very few are sufficiently near to study them in detail and with very high spatial resolution, for example to determine multiplicity (Zinnecker and Yorke 2007). We do not even know what is the upper mass limit for stability, both in terms of observations as well as theoretical models (Massey 2003; Vink et al. 2013). Low-mass stars and brown dwarfs, on the other hand, are faint, so they too are difficult to study in detail (Burrows et al. 2001). Such studies, however, are in great demand, because secondary indicators such as the fraction of binaries and higher-order multiples as function of mass, or the distribution disks around very young stars and possible signatures of accretion during their formation are probably better suited to distinguish between different star-formation models than just looking at the IMF.

2 IMF from Simple Statistical Theory

As a first approximation, the problem of the origin of the IMF can be approached from a purely statistical point of view without specifying up front which physical processes will become important. We consider the distribution of stellar masses as a consequence of a sequence of independent stochastic processes. Invoking the central limit theorem then naturally leads to a log-normal IMF. Our assumption it that the mass M of a star can be expressed as the product of N independent variables x_j. At this point it is not necessary to specify these variables, as long as they are statistically independent and their values are determined by stochastic processes. We introduce again the dimensionless mass variable $m = M/(1\,\mathrm{M}_\odot)$ and write,

$$m = \prod_{j=1}^{N} x_j. \tag{3}$$

The logarithm of the mass is then the sum of the random variables,

$$\ln m = \sum_{j=1}^{N} \ln x_j + \text{constant}, \tag{4}$$

where the constant term includes all quantities that are truly constant, e.g., the gravitational constant G or Boltzmann's constant k_B or others. The stellar mass is determined by a composite random variable which is the sum of N independent random variables $\ln x_j$. The central limit theorem shows that the distribution of the composite variable always approaches a normal distribution as the number N of variables approaches infinity. For the application of the theorem, a transformation into normalized variables is useful,

$$\xi_j = \ln x_j - \langle \ln x_j \rangle = \ln \left(\frac{x_j}{\langle x_j \rangle} \right), \tag{5}$$

where the brackets denote the logarithmic average. The normalized variables ξ_j have zero mean and their dispersions σ_j are given by

$$\sigma_j^2 = \int_{-\infty}^{\infty} \xi_j^2 f_j(\xi_j)\, d\xi_j. \tag{6}$$

The composite variable Ξ finally is defined by

$$\Xi \equiv \sum_{j=1}^{N} \xi_j = \sum_{j=1}^{N} \ln \left(\frac{x_j}{\bar{x}_j} \right). \tag{7}$$

It also has zero mean and, since the variables are assumed to be independent, its variance Σ is the sum of the dispersions of each variable,

$$\Sigma^2 = \sum_{j=1}^{N} \sigma_j^2. \tag{8}$$

For $N \rightarrow \infty$, the central limit theorem describes its distribution function as being Gaussian with

$$f(\Xi) = (2\pi\,\Sigma^2)^{-1/2} \exp\left(-\frac{1}{2}\frac{\Xi^2}{\Sigma^2}\right), \tag{9}$$

independent of the individual distribution functions f_j. Equation (4) then becomes

$$\ln\, m = \ln m_0 + \Xi, \tag{10}$$

with m_0 being a characteristic mass scale defined by

$$\ln\, m_0 \equiv \sum_{j=1}^{N} \left\langle \ln \bar{x}_j \right\rangle. \tag{11}$$

Combining (9) and (10), we can write the distribution f of stellar masses in the form

$$\ln f(\ln m) = A - \frac{1}{2\Sigma^2}\left[\ln\left(\frac{m}{m_0}\right)\right]^2, \tag{12}$$

where A is a constant. This is the log-normal form of the IMF first introduced by Miller and Scalo (1979). It fits very well the mass distribution of multiple stellar systems in the solar vicinity with masses less than few solar masses (e.g., Kroupa et al. 1990) and it is often used to describe the peak of the single star IMF.

3 IMF from Stochastically Varying Accretion Rates

To obtain the observed power-law behavior at the high-mass end of the IMF, we need to add complexity to the model and extend this simple statistical approach. As a highly illustrative example, we follow the discussion by Maschberger (2013a, 2013b) and consider the case where the stellar mass is determined by accretion in a stochastically fluctuating medium. If we disregard the fluctuating part for the time being, and if we assume that the accretion rate depends on the mass to some power of α, then the growth of an individual star can be described by the simple differential equation,

$$dm = m^{\alpha} A dt, \tag{13}$$

where the constant $A > 0$ and the exponent α account for all physical processes involved. For example, if the protostars move with constant velocity v through isothermal gas with temperature T and sound speed $c_{\rm s} = k_{\rm B}T/\mu$ with Boltzmann constant $k_{\rm B}$ and mean gas particle mass μ, we can apply the Bondi-Hoyle-Lyttleton accretion formula to obtain

$$A = \frac{2\pi G^2 \rho}{\left(v^2 + c_{\rm s}^2\right)^{3/2}},$$

$$\alpha = 2.$$

Note that this is an approximate formula. Replacing the factor 2π by 4π gives a better fit to the Hoyle–Lyttleton rate, when the object moves highly supersonically and we can neglect the contribution of the sound speed. Detailed numerical simulations can yield a more complex parameterization of A, depending on the physical parameters of the system (e.g., Krumholz et al. 2006; Ruffert and Arnett 1994). What remains, however, is the quadratic power-law dependence of the accretion rate on the mass.

Now assume that the star grows with statistically fluctuating mass accretion rate. This could be due to the stochastic nature of gas flows in turbulent media and/or due N-body dynamics in dense embedded clusters (e.g., Bonnell et al. 2001a; Bonnell et al. 2001b; Klessen 2001) or due to other processes that lead to stochastic protostellar mass growth. In this case Eq. (13) turns into a stochastic differential equation,

$$dm = m^{\alpha}(Adt + BdW), \tag{14}$$

where Adt describes the mean growth rate and BdW models the fluctuations around this mean. Depending on the statistical properties of BdW the sum $Adt + BdW$ could become negative, which would imply mass loss and could potentially lead to negative masses. In order to avoid that, it is often sensible to restrict the stochastic variable BdW to positive values or to very small amplitudes. For $\alpha \neq 1$ (as well as for $\alpha \neq 0$) we can then obtain the formal solution,

$$m(t) = \left[(1-\alpha) \left(\frac{m_0^{1-\alpha}}{1-\alpha} + At + BW(t) \right) \right]^{\frac{1}{1-\alpha}}, \tag{15}$$

where the integration constant m_0 is the initial mass and $W(t) = \int_0^t dW$ is the integral of the stochastic variable. For Gaussian fluctuations its distribution has zero mean and variance t, as is well known from the random walk problem. To get a mass spectrum, many realizations of the random variable need to be considered. For $B = 0$, Eq. (15) reduces to the solution of the deterministic growth problem, which for $\alpha > 1$ reaches infinite mass in the finite time

$$t_{\infty} = \frac{m_0^{1-\alpha}}{A(1-\alpha)}. \tag{16}$$

For $B \neq 0$, the time t_{∞} no longer takes on a single value, but instead depends on the stochastic path $W(t)$. In reality, this solution is not desired, because the mass of a cloud core is limited. In addition, once feedback from massive stars sets in, the local reservoir of gas available for star formation is reduced even further. Consequently, the solution (15) is only sensible for $t \ll t_{\infty}$.

If we know the statistical properties of the random process $W(t)$, we can calculate the mass spectrum for an ensemble of stars. For Gaussian fluctuations with zero mean and variance t, we obtain

$$f(m,t) = \frac{1}{(2\pi)^{1/2}} \frac{1}{m^{\alpha}} \frac{n_{\infty}(t)}{Bt^{1/2}} \exp\left[-\frac{1}{2B^2 t} \left(\frac{m^{1-\alpha} - m_0^{1-\alpha}}{1-\alpha} - At \right)^2 \right], \tag{17}$$

where $f(m,t)dm$ gives the fraction of stars in the mass range $[m, m+dm[$. The factor $n_\infty(t)$ corrects for the possible contributions of stars with masses approaching infinity for $\alpha > 1$. It needs to be introduced to ensure the normalization of $f(m,t)dm$ as probability distribution function at any time t (for further details, see Maschberger 2013b). For $\alpha < 1$ we set $n_\infty(t)$ to unity. For $\alpha \to 1$, i.e. for average exponential growth, we obtain the log-normal distribution function motivated above (see Eq. 12),

$$f(m,t) = \frac{1}{(2\pi)^{1/2}} \frac{1}{m} \frac{1}{Bt^{1/2}} \exp\left[-\frac{1}{2B^2 t} (\log m - \log m_0 - At)^2\right], \tag{18}$$

where the factor $1/m$ is due to the conversion from $\log m$ to m, as $d \log m = dm/m$. The log-normal distribution function peaks at the mass m_0. For all values $\alpha > 1$ the function $f(m,t)dm$ develops a power-law tail at large masses m with slope α, reaches a maximum slightly below m_0, and exhibits a sharp decline for small masses. The case $\alpha = 2.33$ is very similar to the observed stellar IMF.

4 IMF from Turbulence Statistics

ISM turbulence is intrinsically a scale-free process as long as one stays within the inertial range. So it is conceivable that it could play a key role in producing the power-law tail at the high-mass end of the stellar mass distribution. Most analytic models that attempt to do so involve the following four steps. First, they come up with a model that relates key parameters of the turbulent ISM to the probability distribution function (PDF) of gas density. Second, they relate the density PDF to the clump mass spectrum. Third, they identify a set of criteria by which some of these clumps go into gravitational collapse and begin to form stars. Typically, these involve some variant of the Jeans argument (Eq. 22) and give preference to the most massive and densest clumps in the cloud. Fourth, they involve a mapping procedure, which converts a certain fraction of the clump mass into the final stellar mass.

We would like to mention, that alternative statistical models have been proposed that are based on stochastic sampling in fractal media (Elmegreen 1996, 1997a, b, 1999, 2000a, 2002a).

Density Distribution Function Analytical theory as well as numerical simulations show that the distribution of the gas density in isothermal ($\gamma = 1$), non self-gravitating, and well sampled turbulent media follows a log-normal distribution,

$$\mathrm{PDF}(s) = \frac{1}{\sqrt{2\pi\sigma_s^2}} \exp\left(-\frac{(s-s_0)^2}{2\sigma_s^2}\right). \tag{19}$$

Here, we introduce the logarithmic density,

$$s = \ln(\rho/\rho_0), \tag{20}$$

and $\rho_0 = \langle\rho\rangle$ as well as $s_0 = \langle s\rangle$ denote the corresponding mean values. For a purely Gaussian distribution, the mean s_0 is related to the variance σ_s^2 of the logarithmic density s via the equation

$$s_0 = -\frac{1}{2}\sigma_s^2. \tag{21}$$

Deviations from the pure log-normal behavior occur when parts of the gas undergo gravitational collapse and form stars. The velocity field, and as a consequence, the density distribution are no longer solely governed by turbulence statistics but also influenced by varying degrees of self-gravity (e.g., Klessen 2000). Furthermore, Passot and Vázquez-Semadeni (1998) found deviations of the log-normal behavior in simulations of non-isothermal gas. Depending on the polytropic exponent γ in the equation of state, $P \propto \rho^\gamma$, the PDF develops a low-law at low density for $\gamma > 1$ and at high densities for $\gamma < 1$ (see, e.g., Li et al. 2003). The latter effect is very similar to gravitational collapse. In addition, the PDFs from hydrodynamic simulations typically change with time as the overall cloud evolution progresses (Ballesteros-Paredes et al. 2011). For example, Federrath and Klessen (2013) quantify how the slope of the high-density tail of the PDF in their numerical models flattens with increasing star-formation efficiency. Girichidis et al. (2014) demonstrate analytically that free-fall contraction of a single core or an ensemble of collapsing spheres forms a power- law tail similar to the observed PDFs.

Clump Mass Function The next step in this sequence is to relate the density PDF to the clump mass function (CMF). A first attempt to analytically derive the CMF from turbulence properties goes back to Elmegreen (1993) and has then been refined by Padoan et al. (1997) and Padoan and Nordlund (2002). They argue that high-density clumps are simply the shock-compressed regions that are the natural outcome of supersonic turbulence. They then invoke the shock jump conditions to calculate the achievable density contrast from the distribution of Mach numbers in the flow. Because they consider magnetized media, they base their considerations on the Alfvénic Mach number ($\mathcal{M}_\mathrm{A} = v_\mathrm{A}/C_\mathrm{s}$), but similar conclusions follow for purely hydrodynamic flows (Elmegreen 2002b). To get the number of cores at a given density and length scale they argue that the flow is self-similar and that this quantity is simply determined by the available volume compressed to the density under consideration. This method has a number of shortcomings and we refer the reader to Krumholz (2014) for a more detailed account.

Collapsing Cores Once the CMF is obtained, the next step towards the stellar mass function is to select the subset of clumps that is gravitationally unstable and begins to collapse in order to form stars. The most simple approach is to base the selection of bound clumps on a thermal Jeans argument. Jeans (1902) studied the stability of isothermal gas spheres, and found that the competition between thermal pressure gradients and potential gradients introduces a critical mass,

$$M_\mathrm{J} = \frac{\pi^{5/2}}{6}\frac{k_\mathrm{B}/m}{G}\rho^{-1/2}T^{3/2}, \tag{22}$$

with k_B and G being the Boltzmann and gravitational constants, and m being the mean particle mass. M_J is a function of density ρ and temperature T only. If the clump is more massive, it collapses. Otherwise, it expands. This approach can be expanded by including the effects of micro turbulence and by considering the presence of magnetic fields. For a more detailed account of the historic development of star formation criteria, see Mac Low and Klessen (2004). Probably the most intuitive approach to assess the stability of molecular cloud clumps is based on the virial theorem, which relates the time evolution of the tensor of inertia of an object to its volumetric energy densities and surface terms, and allows us to take all physical processes into account that influence the dynamical evolution of the system (e.g., Ballesteros-Paredes 2006).

The problem that arises from the turbulent compression (Padoan et al. 1997; Padoan and Nordlund 2002) or Press-Schechter approach is that it provides an estimate of the mass of a clump, but not of the density and of other physical properties that allow us to calculate the stability of the clump. To solve this problem, Padoan and Nordlund (2002) for example take a typical cloud temperature T and pick a random density ρ from the assumed density PDF (see above) for each clump M in the CMF. With these values they calculate the Jeans mass (22). If the clump is more massive ($M > M_J$), it is considered bound and forming stars, if not, it is disregarded. The probability for massive clumps to be unstable for randomly picked ρ and T values is very high, and the mass spectrum of bound clumps is similar to the CMF at high masses. However, for lower-mass clumps the chances to pick a combination of ρ and T such that its mass exceeds the Jeans mass gets smaller and smaller. As a consequence, the mass spectrum of bound clumps turns over towards smaller masses. The overall peak of the mass spectrum is most likely determined by the balance between heating and cooling processes in the star forming gas which set a characteristic range of values for M_J and its variants. The apparent universality of the IMF in the Milky Way and nearby galaxies may be caused by the insensitivity of the dust temperature on the intensity of the interstellar radiation field (Elmegreen et al. 2008).

Stellar IMF Once an ensemble of collapsing cloud clumps is selected, as outlined above, the stellar IMF is often determined by simply mapping the clump mass to the stellar mass with some given fixed efficiency. Typical values are around 30 %. As a result the IMF has the same functional form as the mass function of bound cores. However, this simple approach has its problems. If indeed each core only forms one star (or maybe a binary system), then it needs to have about one Jeans mass. Otherwise the core is likely to fragment. Because $M_J \propto \rho^{-1/2}$ for a given temperature T, high-mass clumps should be less dense then low mass ones. This immediately leads to a timescale problem (Clark et al. 2007). Because of $\tau_{ff} \propto \rho^{-1/2}$, the collapse time scales linearly with the clump mass. The time it takes to build up a star with $10M_\odot$ is sufficient to form ten stars with $1M_\odot$. As a consequence the resulting stellar IMF should be considerably steeper than the CMF. In addition, high-mass clumps are not observed to be less dense than low-mass ones. If anything, they tend to be denser, and they are typically highly Jeans-unstable (Ragan 2013).

A potential way out of this dilemma is to assume that high-mass clumps are hotter. High mass stars can indeed heat up their surroundings quite considerably, their luminosity scales L with stellar mass M as $L \propto M^{3.5}$. However, there are many low-mass star forming regions which show no signs of massive star formation (e.g., Taurus or ρ-Ophiuchi) and where the temperatures inferred for prestellar cores is uniformly low.

In general there is thus no good reason to believe in a one-to-one mapping between the core mass function and the stellar IMF. None of the current analytic models for the IMF includes processes such as stellar feedback in form of radiation or outflows, or fragmentation during core collapse and during the accretion disk phase, in a realistic and consistent way. Altogether, it is likely that the transition from core to stars follows a complicated and stochastic pathway that may change with varying environmental conditions.

5 Conclusion

Identifying the physical processes that govern the formation of stars and that determine the observed distribution of stellar masses remains a highly exciting and challenging task of modern astronomical and astrophysical research.

Acknowledgement This paper is an excerpt from a Saas-Fee lecture given in 2013 to be published by Springer. We thank Springer for permission to reproduce this excerpt in these proceedings.

References

Ballesteros-Paredes J., *MNRAS*, **372**, 443 (2006)
Ballesteros-Paredes, J., et al., *MNRAS*, **416**, 1436 (2011)
Bastian, N., Covery, K. R., & Meyer, M. R., *ARA&A*, **48**, 339 (2010)
Bonnell, I. A., Bate, M. R., Clarke, C. J., & Pringle, J. E., *MNRAS*, **323**, 785 (2001a)
Bonnell, I. A., Clarke, C. J., Bate, M. R., & Pringle, J. E., *MNRAS*, **324**, 573 (2001b)
Burrows, A., et al., *Rev. Mod. Phys.*, **73**, 719 (2001)
Chabrier, G., *PASP*, **115**, 763 (2003)
Chabrier G., *Astrophys. Space Sc. Lib.*, **327**, 41 (2005)
Clark, P. C., Klessen, R. S., & Bonnell, I. A., *MNRAS*, **379**, 57 (2007)
Elmegreen, B. G., *ApJ*, **411**, 170 (1993)
Elmegreen B. G., *ApJ*, **477**,196 (1997a)
Elmegreen B. G., *ApJ*, **486**, 944 (1997b)
Elmegreen B. G., *ApJ*, **515**, 323 (1999)
Elmegreen B. G., *MNRAS*, **311**, L5 (2000a)
Elmegreen B. G., *ApJ*, **564**, 773 (2002a)
Elmegreen, B. G., *ApJ*, **577**, 206 (2002b)
Elmegreen B. G., Falgarone E., A., *ApJ*, **471**, 816 (1996)
Elmegreen, B. G., Klessen, R. S., & Wilson, C. D., *ApJ*, **681**, 365 (2008)
Federrath, C., & Klessen, R. S., *ApJ*, **763**, 51 (2013)
Girichidis P., Konstandin L., Whitworth A. P., Klessen R. S., *ApJ*, **781**, 91 (2014)

Jeans J. H., *Phil. Trans. A.*, **199**, 1 (1902)
Klessen, R. S., *ApJ*, **535**, 869 (2000)
Klessen, R. S., *ApJ*, **550**, L77 (2001)
Kroupa P., *MNRAS*, **322**, 231 (2001)
Kroupa, P., *Science*, **295**, 82 (2002)
Kroupa, P., Tout, C. A., Gilmore, G., *MNRAS*, **244**, 73 (1990)
Krumholz, M. R., arXiv:1402.0867 (2014)
Krumholz, M. R., McKee, C. F., & Klein, R. I., *ApJ*, **638**, 369 (2006)
Li, Y., Klessen, R. S., & Mac Low, M.-M., *ApJ*, **592**, 975 (2003)
Mac Low, M., & Klessen, R. S., *Rev. Mod. Phys.*, **76**, 125 (2004)
Maschberger T., *MNRAS*, **429**, 1725 (2013a)
Maschberger, T., *MNRAS*, **436**, 1381 (2013b)
Massey, P., *ARA&A*, **41**, 15 (2003)
Miller, G. E., & Scalo, J., *ApJS*, **41**, 513 (1979)
Padoan, P., & Nordlund, Å., *ApJ*, **576**, 870 (2002)
Padoan, P., Nordlund, A., & Jones, B. J. T., *MNRAS*, **288**, 145 (1997)
Passot, T., & Vázquez-Semadeni, E., *PRE*, **58**, 4501 (1998)
Ragan S. E., Henning T., Beuther H., *A&A*, **559**, A79 (2013)
Ruffert, M., & Arnett, D., *ApJ*, **427**, 351 (1994)
Salpeter, E. E., *ApJ*, **121**, 161 (1955)
Scalo, J., *Fund. Cosm. Phys.*, **11**, 1 (1986)
Vink J. S., Heger A., Krumholz M. R., et al., arXiv:1302.2021 (2013)
Zinnecker, H., & Yorke, H. W., *ARA&A*, **45**, 481 (2007)

Cloud and Star Formation in Spiral Arms

Clare Dobbs and Alex Pettitt

Abstract We present the results from simulations of GMC formation in spiral galaxies. First we discuss cloud formation by cloud–cloud collisions, and gravitational instabilities, arguing that the former is prevalent at lower galactic surface densities and the latter at higher. Cloud masses are also limited by stellar feedback, which can be effective before clouds reach their maximum mass. We show other properties of clouds in simulations with different levels of feedback. With a moderate level of feedback, properties such as cloud rotations and virial parameters agree with observations. Without feedback, an unrealistic population of overly bound clouds develops. Spiral arms are not found to trigger star formation, they merely gather gas into more massive GMCs. We discuss in more detail interactions of clouds in the ISM, and argue that these are more complex than early ideas of cloud–cloud collisions. Finally we show ongoing work to determine whether the Milky Way is a flocculent or grand design spiral.

1 Introduction

Theoretically, there are three main mechanisms for the formation of Giant Molecular Clouds (GMCs) in galaxies; gravitational instabilities, cloud–cloud collisions and Parker instabilities. In the past decade or so, numerical simulations have explored these scenarios. Here I focus on cloud–cloud collisions and gravitational instabilities, the regimes where these mechanisms dominate, and the properties of clouds that are predicted. I will also argue that although historically cloud–cloud collisions have been proposed as an important mechanism, in the ISM, interactions of clouds and diffuse gas are more complex than this simple description.

C. Dobbs (✉) · A. Pettitt
School of Physics & Astronomy, University of Exeter, Exeter EX4 4QL, UK
e-mail: dobbs@astro.ex.ac.uk

A. Pettitt
e-mail: alex@astro.ex.ac.uk

K. Freeman et al. (eds.), *Lessons from the Local Group,*
DOI 10.1007/978-3-319-10614-4_12

2 Simulations of Cloud–Cloud Collisions, Gravitational Instabilities and Stellar Feedback in Grand Design Spirals

Cloud–cloud collisions were originally investigated in relatively simplistic calculations which follow a population of typically spherical clouds, employing a statistical description for the the formation of small clouds, the coalescence of clouds, and collapse of clouds above a given size (Field and Saslaw 1965; Scoville and Hersch 1979; Kwan and Valdes 1983, 1987; Tomisaka 1984, 1986). Most assume clouds completely coalesce, although Roberts and Stewart (1987) allow dissipative collisions, which results in clouds clustering together at points along the spiral arms. In various papers (Dobbs et al. 2006; Dobbs 2008; Dobbs et al. 2008) I demonstrated that GMCs can build up from smaller scale structure in hydrodynamic simulations. Instead of the Jeans length and mass, the sizes and masses of clouds formed in this way is dependent on the strength of the spiral shock. In particular the epicyclic radius which determines the amount of mass that can be gathered together into a single GMC. This mechanism is most evident in discs where the gas is not strongly gravitationally unstable, found to be when $\Sigma_{gas} \lesssim 10$ M$_\odot$pc^{-2}. At higher surface densities, gravitational instabilities start to dominate in the disc, although self gravity also increases collisions between clouds and GMCs. We show an example from a simulation with $\Sigma_{gas} = 8$ M$_\odot$pc^{-2}, where both cloud–cloud collisions and self gravity are significant, in Fig. 1 (from Dobbs and Pringle 2013).

One criticism of the cloud–cloud collision model for forming massive GMCs is the long timescale thought to be required (Blitz and Shu 1980), of order 100s Myr. However in a galaxy with spiral arms, the cloud number density is significantly increased in the spiral arms (Casoli and Combes 1982; Dobbs 2008). The time for the growth of a GMC can be estimated from the mean free path divided by the cloud–cloud velocity dispersion, giving

$$t = \frac{1}{\pi r_{cl}^2 n_{cl} \sigma} \tag{1}$$

where r_{cl} is an average cloud radius, n_{cl} is the cloud number density and σ is the cloud–cloud velocity dispersion. With values of $r_{cl} = 30$ pc, $\sigma = 4$ km/s and an average $n_{cl} = 9 \times 10^{-8}$ clouds per pc^3 (based on the numerical simulation of Dobbs and Pringle 2013), this gives a timescale of $\sim$900 Myr. However in the spiral arms, n_{cl} can be 20 or more times higher giving timescales of 10 or a few 10s Myr. Work by Fujimoto et al. (2014) also finds similar timescales.

A limitation of this previous work though is that in the absence of stellar feedback, the star formation rate is orders of magnitude too high (see Bonnell et al. 2013; van Loo et al. 2013; Dobbs et al. 2011; Kim et al. 2013), whilst stellar feedback may also disperse clouds (Elmegreen 1994). We included a simple treatment of stellar feedback by inserting kinetic and thermal energy according to a Sedov solution when star formation is assumed to occur. The amount of energy inserted is given by

$$E = \frac{\epsilon M(H_2) \times 10^{51} ergs}{160 M_\odot} \tag{2}$$

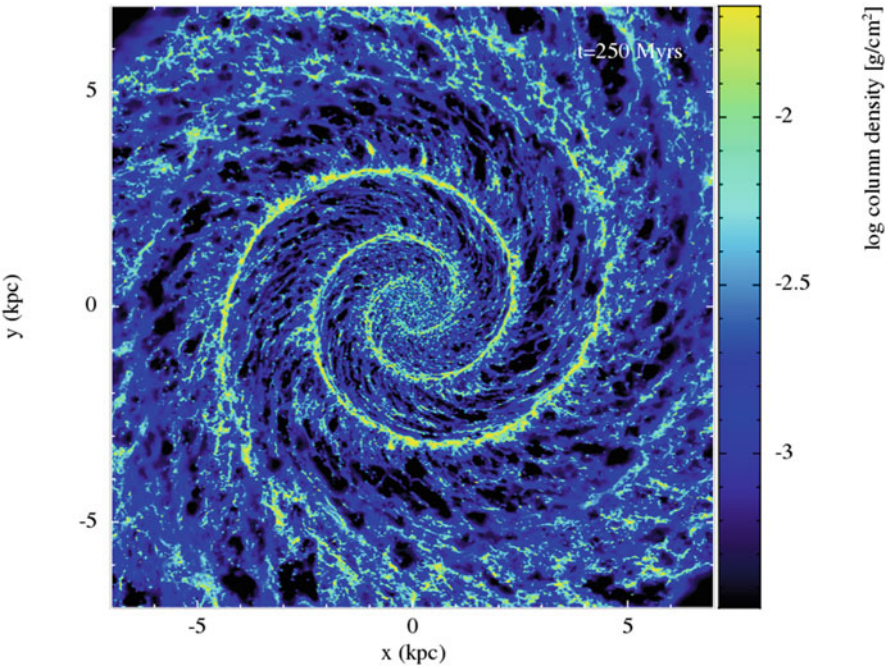

Fig. 1 Example simulation of a galaxy with an $m = 2$ imposed spiral potential. The simulation includes self gravity, cooling and heating of the ISM and stellar feedback (producing a multiphase ISM), but not magnetic fields. Dense regions shown by *yellow* in the colour table correspond to molecular clouds

where M(H_2) is the mass of molecular hydrogen within roughly a smoothing length, the 160 $M_\odot$ assumes that one massive star forms per 160 $M_\odot$ of gas, and the 10^{51} ergs is assumed to be the energy released from one massive star. ϵ is the star formation efficiency at the resolution of the simulation (few 10^4 $M_\odot$ for particle masses of 312.5 $M_\odot$), our fiducial value is 5 %. Energy is inserted instantaneously and is presumed to be associated with stellar winds and supernovae. In Dobbs et al. (2011), we indeed showed that the cloud mass spectra are shifted to lower masses depending on the level of stellar feedback. We also find that the star formation rate is in much better agreement with observations if stellar feedback is included (Dobbs et al. 2011). Generally the properties of clouds vary according to the level of feedback as described in the next section.

2.1 Properties of GMCs in Simulations

We considered some properties of GMCs in the absence of stellar feedback in Dobbs (2008). In particular we showed that in a low surface density case, where self gravity

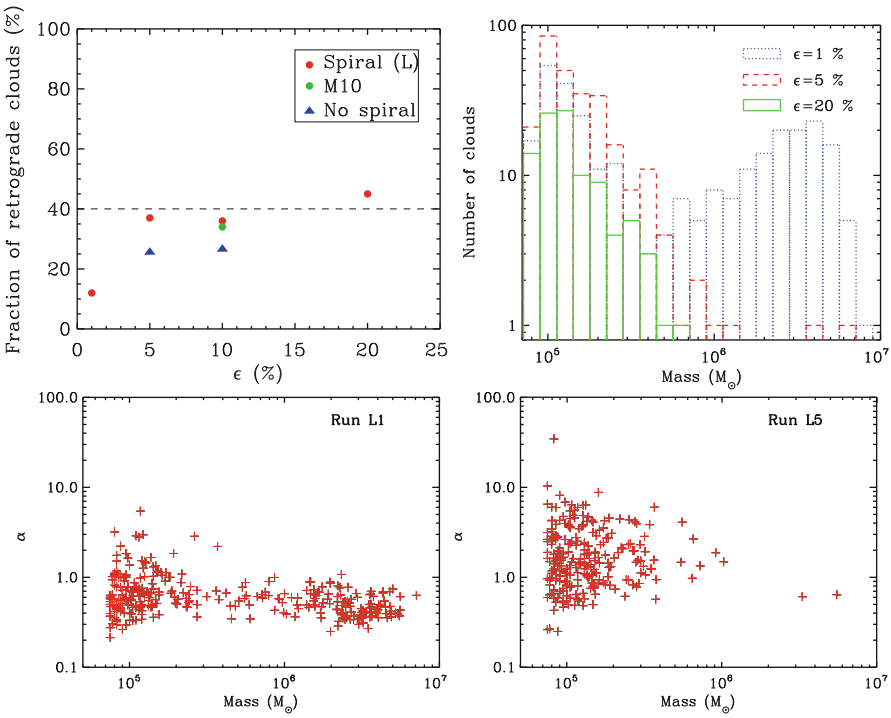

Fig. 2 Properties of clouds are shown from simulations in Dobbs et al. (2011). The *top left panel* shows the fraction of retrograde clouds versus the level of stellar feedback. The *top right panel* shows mass spectra for different levels of feedback. The *lower panels* show the virial parameter when $\epsilon = 0.01$ (*left*, minimal feedback) and 0.05 (*right*, moderate feedback)

has less effect, clouds exhibit retrograde as well as prograde rotation. Although we did not show the comparison for the high surface density case, there were comparatively more prograde clouds. We have since more extensively considered cloud properties in Dobbs et al. (2011), with stellar feedback. Here we showed a transition between gravitationally dominated clouds in simulations with minimal feedback ($\epsilon = 0.01$) compared to clouds in simulations where there is roughly a balance between stellar feedback, self gravity and the spiral shock (for our simulations $\epsilon = 0.05$). The surface density in these calculations was 8 $M_\odot$ pc^{-2}.

We show three cloud properties in Fig. 2; the cloud mass spectra, the cloud virial parameters, and the fraction of retrograde clouds, for simulations with varying levels of feedback. Figure 2 shows a noticeable difference between clouds with and without significant feedback. Without stellar feedback, the clouds eventually become unable to disperse by shear and generic turbulence alone, and become gravitationally dominated. Gas eventually either falls into massive GMCs or lies in the warm component but there is no interaction between the components, and minimal interactions between clouds. This results in a mass spectrum centred on $10^6 - 10^7$ $M_\odot$ clouds. By

contrast, with feedback, the mass spectra display a typical $\sim M^{-2}$ power law, clearly in much better agreement with observations, the level of feedback determining the maximum mass.

Figure 2 also shows cloud rotations for different levels of stellar feedback. For our standard spiral galaxy models (red points), the fraction of retrograde rotating clouds is low with minimal feedback, but roughly constant when $\epsilon \geq 0.05$. Again this is because in the minimal feedback case, the gas is confined in clouds which are not interacting with each other. Finally we show the virial parameters of the clouds in Fig. 2 in simulations with $\epsilon = 0.01$ and 0.05. The distribution of α is less than 1 when $\epsilon = 0.01$ indicating that the clouds are strongly gravitationally bound. With stellar feedback, the velocity dispersions of the gas are generally higher, meaning gas is less bound, and gas is also ejected from clouds before it can become too gravitationally bound.

2.2 The Nature of 'Cloud–Cloud Collisions'

The term 'cloud–cloud collisions' is commonly used to describe interactions of clouds in a galaxy, to form more massive GMCs or induce star formation (Tan 2000). However in reality the ISM is a continuum, rather than divided separately into cold clouds surrounded by a warm diffuse medium. According to simulations, a substantial fraction of gas is in an intermediate regime between cold and warm ISM (Gazol et al. 2001, Dobbs et al. 2011) whilst transitions of gas between cold, intermediate, warm, and molecular phases may be relatively frequent. Furthermore interactions between clouds may not be particularly violent, or induce much change in momentum. Interactions can take the form of grazing collisions, where there is little interaction or mass transfer between the clouds, or full mergers, where the two clouds collide and all the mass from both clouds end up in one resultant cloud.

We examined the formation and destruction of GMCs in more detail in Dobbs and Pringle (2013). The simulation in Dobbs & Pringle includes an $m = 2$ spiral component, self gravity, heating and cooling and stellar feedback. Thus there are a number of processes which contribute to the formation and dispersal of clouds. The particle mass of the simulation was 312.5 $M_\odot$, thus massive, 10^5 or 10^6 K GMCs are well resolved but clouds of $\lesssim$ few 10^4 K are not well resolved. Figure 3 shows the evolution of a cloud over a period of 40 Myr. The cloud was selected at a time of 250 Myr, as shown in the middle panel, and has a mass of 2×10^6 $M_\odot$. The earlier timeframes (earlier panels) show that the gas which goes into the cloud is a mixture of diffuse gas and smaller clouds. Some clouds seem to simply adjoin onto the massive GMC, then move away again as the GMC disperses, without really mixing with the gas in the GMC. Similarly the GMC then disperses into smaller clouds and diffuse gas. The GMC disperses through a combination of stellar feedback and shear (Dobbs and Pringle 2013). We also note that whilst the 2×10^6 $M_\odot$ cloud forms through the accumulation of other gas and clouds, and similarly disperses, some clouds evolve quite differently. Some clouds end their lives by being added on to the forming GMC.

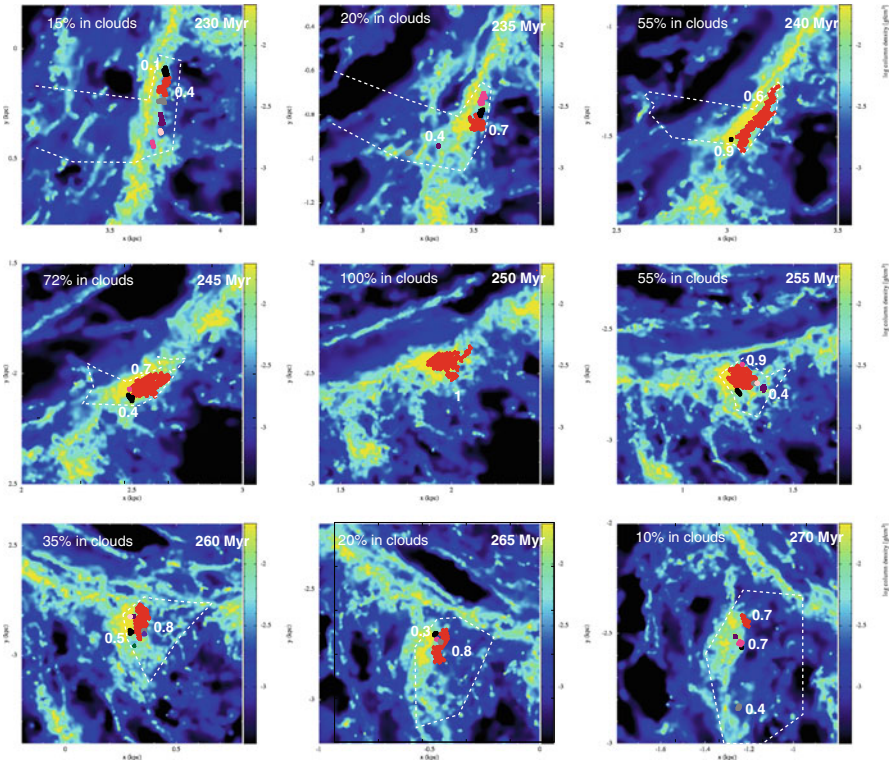

Fig. 3 The evolution of a 2×10^6 $M_\odot$ GMC (coloured *red*) is shown over a 40 Myr time period. Other clouds which coalesce with this GMC, or are the result of dispersal of the GMC, are shown in other *bold colours*. The locus of the gas which is situated in the chosen GMC at 250 Myr (*middle panel*) is indicated by the *white dashed lines* in the other panels. The total amount of gas in 'clouds' is indicated on the *top left* of each panel, whilst the rest of the gas is more diffuse

Conversely, some clouds are formed as a result of the GMC dispersing. Clouds tend to evolve and form stars on roughly a crossing time (Dobbs and Pringle 2013), as supposed by Elmegreen (2000).

In forthcoming work (Dobbs et al. in prep) we investigate whether collisions are full mergers, grazing collisions, and how much gas is transferred into a resultant cloud upon a collision. We find that a substantial fraction of cloud–cloud collisions are more like grazing collisions than mergers.

3 Star Formation in Grand Design and Flocculent Galaxies

So far we have considered galaxies with a fixed spiral potential. It is not clear how many galaxies exhibit grand design structure and how many flocculent, whilst some galaxies appear different in IR compared to optical tracers (Block and Wainscoat

1991; Block et al. 1994). We consider in our models an extreme case where we impose no spiral potential, and the gas is subject to a completely smooth stellar potential. This produces a very flocculent spiral structure. In this case, with no spiral arms to concentrate clouds together, there are fewer cloud–cloud interactions, clouds tend to be smaller (for the same level of stellar feedback) compared to the case with spiral arms, and form largely due to gravitational instabilities (Dobbs et al. 2011).

Previous observations have found that the star formation rate does not appear to significantly differ between flocculent and grand design galaxies (Elmegreen and Elmegreen 1986; Stark et al. 1987). We have investigated the amount of star formation by comparing galaxies with different strength spiral potentials (Dobbs and Pringle 2009) and with and without a spiral potential (Dobbs et al. 2011). Although they did not include star formation explicitly, Dobbs and Pringle (2009) estimate the star formation rate from the mass of bound regions (and their corresponding free fall times) in the simulations. They found that the velocity dispersion increases with higher strength shocks, so the amount of bound gas (and therefore star formation) is not found to increase significantly. Dobbs et al. (2011) found that although spiral shocks have a noticeable impact on the velocity dispersion, when present stellar feedback has the greatest impact on the velocity dispersion of gas in the disc, and generally the evolution of the ISM (fractions of gas in different ISM components, density PDFs). Consequently the stellar feedback has biggest effect on the star formation rate. If star formation is increased, more energy is injected into the ISM through stellar feedback, so that molecular clouds disperse and there is more hot gas. This in turn reduces star formation. Conversely if star formation is reduced, there is nothing to stop dense clouds gravitationally collapsing (in the absence of magnetic fields) and the star formation rate increases. In this sense, star formation is self regulating. Figure 4 shows the star formation rates for simulations with different star formation efficiencies. Although there is a factor of 4 difference between the maximum and minimum efficiency, the change in star formation rate is more like a factor of 2.

In Dobbs et al. (2011), we also compared star formation rates in galaxies with and without a spiral potential. Again the spiral arms did not seem to have a large effect on the star formation rate (see Fig. 4), only increasing the star formation rate by less than a factor of 2. Again, the star formation seems to be regulated by feedback, and resembles the scenario put forward (e.g. by Elmegreen et al. (1986) and Vogel et al. (1988)) that spiral arms merely gather clouds together in the spiral arms. However it is evident from Dobbs et al. (2011) that the spiral arms do have an effect, namely that in gathering smaller clouds they lead to a population of more massive clouds, absent in the simulations without spiral arms. These more massive GMCs ($> 10^6$ $M_\odot$) live longer and tend to produce a higher fraction of stars compared to their smaller mass counterparts. In Dobbs et al. (2011) this only led to a small difference in star formation rate because the number of such massive clouds was small, but potentially (e.g. with a stronger shock) the spiral arms could have more influence.

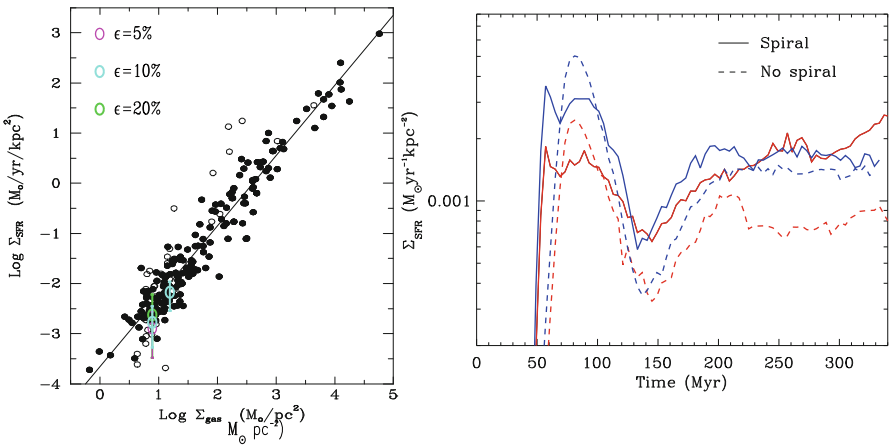

Fig. 4 The star formation rate is shown for simulations with different feedback efficiencies (*left*) and with and without a spiral potential (*right*). The *red* lines are for $\epsilon = 0.05$ and the *blue* $\epsilon = 0.1$. The *black dots* on the *left panel* are observations from Kennicutt (2008)

4 Is the Milky Way Flocculent or Grand Design?

We touched on the spiral structure of galaxies, and the differences (or lack of differences) for star formation in the previous section. In recent work we have been investigating whether our own Galaxy, the Milky Way, is likely to be flocculent or grand design. There is still debate about the number of arms in the Galaxy (see e.g. Vallée 2005) and whether the dynamics fit slowly or dynamically evolving spiral arms (Baba et al. 2010). We have recently been using the radiative code TORUS to generate synthetic HI and CO maps of simulated galaxies for comparison with observations (Acreman et al. 2010, 2012; Duarte-Cabral et al. in prep.). One application of this work has been to perform a large number of simulations (which do not include self gravity or stellar feedback and are therefore require relatively less computational time) and see which best fits ISM maps of galaxy. Pettitt et al. (2014) perform simulations specifically of spirals with fixed potentials, with a bar, 2 or 4 spiral arms and across a large parameter space of pitch angles and pattern speeds. They then carry out fitting between synthetic CO maps and the map of Dame et al. (2001). Whilst observations of ISM tracers can be used to interpret the structure of the Galaxy, using simulations has the significant advantage that there are no difficulties finding the distance to features in velocity space.

Figure 5 shows one of the more successful simulations from Pettitt et al. (2014) in reproducing the structure of the Galaxy in CO. Generally, we found that it was difficult to reproduce the full spiral structure (including the Local, Perseus and Outer arms) with only two spiral arms and a bar, and on the whole we needed four spiral arms. The main difficulty then for the simulations with fixed spiral potentials, is that it is difficult to reproduce the Carina arm correctly. Either the Carina arm appears at too low velocities compared to that observed (as in Fig. 5), or, if the Carina arm is

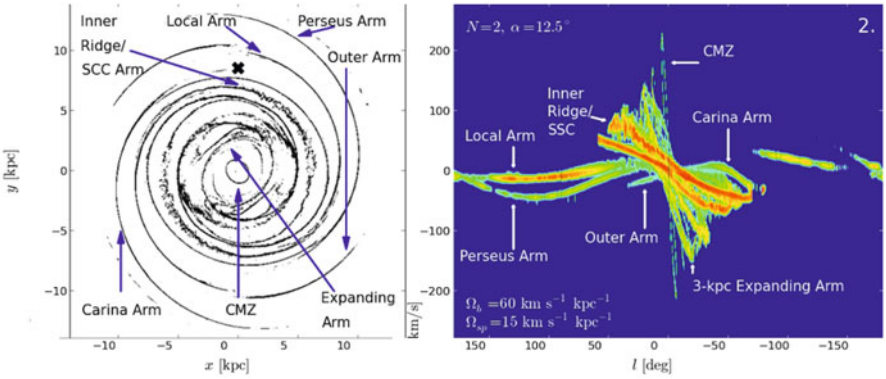

Fig. 5 Results are shown for a hydrodynamical model of a possible Milky Way, with a bar and 2 spiral arms with pitch angle 12.5°, and spiral arm pattern speed of 15 km/s/kpc. The map of CO emission for the model is shown on the *right*. The structure compared to actual observations (Dame et al. 2001) is in reasonable agreement, but the Carina arm is at the wrong velocities. We were unable to find a model which reproduced the full structure of the Milky Way with fixed potentials. From Pettitt et al. (2014)

in the correct position, the continuation of the arm in the vicinity of the Sun leads to far more emission at $v_{los} \sim 0$ km/s than observed. Thus Pettitt et al. (2014), conclude that either the Carina arm exhibits a substantial kink, or the Carina arm is not visible in CO locally, but the latter seems extremely unlikely. Consequently Pettitt et al. (2014) suggest that a transient spiral arm pattern generated by transient stellar instabilities may be better able to reproduce a more irregular spiral structure, or that a local interaction with another galaxy or satellite may have produced a large kink. Further work will examine simulations of transient spiral arms.

5 Conclusions

We present the results of hydrodynamic galaxy scale simulations with stellar feedback, self gravity, and ISM heating and cooling. GMCs appear to form by a combination of the coalescence, or agglomeration of smaller clouds, and gravitational instabilities. Some low level of feedback is required to prevent clouds from becoming very gravitationally dominated, and unable to disperse as they move away from the spiral arms. A low level of feedback similarly ensures that properties of GMCs are in good agreement with observations. Star formation appears to be regulated by the velocity dispersion of the ISM, which in turn is dependent on stellar feedback and/or the spiral shock. Spiral arms do not appear to influence the star formation rate significantly in our models, rather the spiral arms simply gather the gas into more massive GMCs.

We highlighted the evolution of one GMC in particular, and argued that GMC evolution is quite complex involving the accumulation of both smaller clouds, and more diffuse gas, whilst cloud–cloud interactions are often less disruptive than

inferred by the term ‘collision’, often taking the form of grazing, rather than head on collisions. Finally we discuss whether the Milky Way is a grand design or flocculent spiral. It is found that is difficult to reproduce the structure of the Milky Way with static potentials, suggesting a more complex model involving an interaction and/or a transient spiral pattern is required.

Acknowledgements CLD acknowledges funding from the European Research Council for the FP7 ERC starting grant project LOCALSTAR.

References

Acreman D. M., Douglas K. A., Dobbs C. L., Brunt C. M., 2010, MNRAS, 406, 1460
Acreman D. M., Dobbs C. L., Brunt C. M., Douglas K. A., 2012, MNRAS, 422, 241
Baba J., Saitoh T. R., Wada K., 2010, PASJ. , 62, 1413
Blitz L., Shu F. H., 1980, ApJ, 238, 148
Block D. L., Wainscoat R. J., 1991, Nature, 353, 48
Block D. L., Bertin G., Stockton A., Grosbol P., Moorwood A. F. M., Peletier R. F., 1994, A&A, 288, 365
Bonnell I., Dobbs C. L., Smith R. J., 2013, MNRAS, 431, 1062
Casoli F., Combes F., 1982, A&A, 110, 287
Dame T. M., Hartmann D., Thaddeus P., 2001, ApJ, 547, 792
Dobbs C. L., 2008, MNRAS, 391, 844
Dobbs C. L., Pringle J. E., 2009, MNRAS, 396, 1579
Dobbs C. L., Pringle J. E., 2013, MNRAS, 432, 653
Dobbs C. L., Bonnell I. A., Pringle J. E., 2006, MNRAS, 371, 1663
Dobbs C. L., Glover S. C. O., Clark P. C., Klessen R. S., 2008, MNRAS, 389, 1097
Dobbs C. L., Burkert A., Pringle J. E., 2011, MNRAS, 417, 1318
Elmegreen B. G., 1994, ASPC, 66, 61
Elmegreen B. G., 2000, ApJ, 530, 277
Elmegreen B. G., Elmegreen D. M., 1986, ApJ, 311, 554
Field G. B., Saslaw W. C., 1965, ApJ, 142, 568
Fujimoto Y., Tasker E. J., Wakayama M. & Habe A., 2014, MNRAS, 439, 936
Gazol A., Vázquez-Semadeni A., Sánchez-Salcedo F. J., Scalo J., 2001, ApJ, 557, 121
Kennicutt Jr. R. C., 2008, in J. H. Knapen, T. J. Mahoney, & A. Vazdekis ed., Pathways Through an Eclectic Universe Vol. 390 of Astronomical Society of the Pacific Conference Series, The Schmidt Law: Is it Universal and What Are its Implications?. pp 149+
Kim C-G., Ostriker E. C., Kim W-T., 2013, ApJ, 776, 1
Kwan J., Valdes F., 1983, ApJ, 271, 604
Kwan J., Valdes F., 1987, ApJ, 315, 92
Pettitt A. R., Dobbs C. L., Acreman, D. M., Price, D. J., 2014, arXiv, 1406, 4150
Roberts W. W., Stewart G. R., 1987, ApJ, 314, 10
Scoville N. Z., Hersch, K., 1979, ApJ, 229, 578
Stark A. A., Elmegreen B. G., Chance, D., 1987, ApJ, 322, 64
Tan J. C., 2000, ApJ, 536, 173
Tomisaka K., 1984, PASJ, 36, 457
Tomisaka K., 1986, PASJ, 38, 95
Vallée J. P., 2005, AJ, 130, 569
Van Loo S., Butler M. J., Tan J. C., 2013, ApJ, 764, 36
Vogel S. N., Kulkarni S. R., Scoville N. Z., 1988, Nature, 334, 402

Chemical Evolution of M31

Francesca Matteucci and Emanuele Spitoni

Abstract We review chemical evolution models developed for M31 as well as the abundance determinations available for this galaxy. Then we present a recent chemical evolution model for M31 including radial gas flows and galactic fountains along the disk, as well as a model for the bulge. Our models are predicting the evolution of the abundances of several chemical species such as H, He, C, N, O, Ne, Mg, Si, S, Ca and Fe. From comparison between model predictions and observations we can derive some constraints on the evolution of the disk and the bulge of M31. We reach the conclusions that Andromeda must have evolved faster than the Milky Way and inside-out, and that its bulge formed much faster than the disk on a timescale ≤ 0.5 Gyr. Finally, we present a study where we apply the model developed for the disk of M31 in order to study the probability of finding galactic habitable zones in this galaxy.

1 Introduction

The Andromeda galaxy is the spiral galaxy closest to the Milky Way (MW) and it is ~ 1.5 times more massive. In early studies, it was pointed out that the average metallicity of M31 stellar halo ($< [M/H] >\sim -0.5$ dex, e.g. Holland et al. (1996)) is much higher than the average metallicity in the MW halo ($< [Fe/H] >\sim -1.8$ dex, e.g. Ryan and Norris (1991)). However, this conclusion is not fair since the comparison was made between the global metal content, M or Z, which is dominated by α-elements, and Fe which evolves quite differently (see Matteucci 2012). In particular, M31 halo stars could show an overabundance of α-elements relative to Fe, as the Galactic halo stars. Therefore, if we assume $[\alpha/\mathrm{Fe}] = +0.3$ dex for the stars in the M31 halo, we obtain that the $< [M/H] >\sim -0.5$ dex transforms into ($< [Fe/H] >\sim -1.5$ dex, more similar to the metallicity of Galactic halo stars. In fact,

F. Matteucci (✉) · E. Spitoni
Department of Physics, Astronomy Section, Trieste University,
Via G.B. Tiepolo, 11, 34131 Trieste, Italy
e-mail: matteucci@oats.inaf.it

E. Spitoni
e-mail: spitoni@oats.inaf.it

K. Freeman et al. (eds.), *Lessons from the Local Group,*
DOI 10.1007/978-3-319-10614-4_13

Kalirai et al. (2006), by assuming $[\alpha/\mathrm{Fe}] = +0.3$ dex, derived a $< [Fe/H] > \sim -1.5$ dex for red giant branch stars in the outer halo of Andromeda. It should be reminded that the chemical abundances of M31 stars are generally measured by means of color-magnitude diagrams, which are interpreted through stellar tracks computed for a given stellar metallicity Z (M). We should therefore be careful not to confuse Z with Fe, as it is still done in several papers. More recently, Koch et al. (2008) measured the [Fe/H] in the halo of M31 by means of spectroscopy (CaII triplet) and also found stars in the outermost region with [Fe/H] < -2.0 dex, thus implying that there is indeed a metal poor halo also in M31. Sarajedini and Jablonka (2005) measured the metallicity distribution function (MDF) of stars in the bulge of M31 by means of the colour -magnitude diagram, and Worthey et al. (2005) also performed imaging of 11 fields in M31 with HST, and the chosen fields sample all galactocentric radii up to 50 kpc. The metallicity distributions thus obtained show a mild negative gradient that flattens outside 20 kpc along the M31 disk. An interesting fact is that stars in the outer regions of M31 are 10 times more metal rich than the MW halo stars and the globular clusters at the same galactocentric distance. This fact was interpreted as if the disk dominates over the halo at all radii out to 50 kpc. This can mean that many studies claiming to observe the halo of M31 were in reality observing the disk and this could be an additional fact, beyond the α elements versus Fe argument, to explain the apparent difference found between the average metallicity in the halo of M31 and that of the MW.

Chemical abundances in M31 have been measured also from HII regions, planetary nebulae and young massive stars. In particular, Zurita and Bresolin (2012), Sanders et al. (2012), Esteban et al. (2009) and Galarza et al. (1999) measured abundances in HII regions, while Przybilla et al. (2008), Trundle et al. (2002) and Venn et al. (2000) measured abundances in supergiants. On the other hand, Blair et al. (1982) and Dennefeld and Kunth (1981) derived abundances also from supernova remnants.

The star formation rate in M31 has been estimated by Braun et al. (2009), Boissier et al. (2007) and Williams (2003a, b).

Chemical evolution models for M31 have been developed by Diaz and Tosi (1984), Mollá et al. (1996), Renda et al. (2005), Ballero et al. (2007), Yin et al. (2009), Marcon-Uchida et al. (2010), Spitoni et al. (2013) and Robles-Valdez et al. (2013). In most of these papers it has been concluded that M31 must have evolved faster than the MW with a higher efficiency of star formation. This can be expressed as a down-sizing in star formation, in analogy to what happens in elliptical galaxies (see for example Matteucci 2012), since M31 is more massive than our Galaxy. Most of the models suggested also a star formation efficiency decreasing with increasing galactocentric distance in order to reproduce the O abundance gradient, except Spitoni et al. (2013) who included radial gas flows in their chemical model and did not find necessary to assume a variable star formation efficiency. It is well known, in fact, that radial gas flows have the effect of steepening the gradients (see Mott et al. 2013).

Here, we will review the main results of some of these papers and their conclusions and try to infer the history of formation and evolution of M31. Then we will present

a study aimed at exploiting a detailed chemical evolution model for M31 in order to find the galactic habitable zones (GHZ) in this galaxy (Spitoni et al. 2014).

2 Modelling Chemical Evolution of M31

As suggested by Renda et al. (2005), when compared to the MW, Andromeda seems to have been more active in forming stars in the past although its current star formation rate (SFR) appears lower, since on average it has been estimated to be $1 M_{\odot} yr^{-1}$ (Williams 2003a, b) against an average of 2–6 $M_{\odot} yr^{-1}$ for the solar neighbourhood (Boissier and Prantzos 1999), which also can represent an average value along the disk. This means that M31 evolved faster than the MW: in other words, it must have had a higher star formation efficiency and/or a shorter timescale for gas accretion relative to the MW.

The SFR, in most of the available models, is expressed by means of the Kennicutt law as:

$$SFR(r,t) = \nu \sigma_{gas}^{k} \quad \left(M_{\odot} Gyr^{-1} pc^{-2}\right) \tag{1}$$

where σ_{gas} is the surface gas density and ν is the SFR per unit mass of gas, namely the star formation efficiency, expressed in Gyr^{-1}. Kennicutt (1998) suggested an average $\nu = (0.25 \pm 0.07) Gyr^{-1}$ and $k = 1.4 \pm 0.15$ for a sample of star forming galaxies. Models of galactic chemical evolution adopting this formulation have adopted similar values for ν and k, always tuned to reproduce the observed properties of the studied galaxies.

Most chemical evolution models (Renda et al. 2005; Yin et al. 2009; Marcon-Uchida et al. 2010; Spitoni et al. 2013) assumed that the disk of Andromeda formed, like that of the MW, by accretion of cold gas with an infall law of the form:

$$I(r,t) = A(r) e^{-t/\tau(r)} \left(M_{\odot} Gyr^{-1} pc^{-2}\right), \tag{2}$$

where A(r) is a parameter obtained by imposing:

$$\sigma_{tot}(r, T_G) = \int_0^{T_G} A(r) e^{-t/\tau(r)} dt \tag{3}$$

where $\sigma_{tot}(r, T_G)$ is the present time surface mass density profile and $\tau(r)$ is the time scale for gas accretion, which can be a function of galactocentric distance. In MW models it has been suggested (Matteucci and François 1989; Boissier and Prantzos 1999) that the disk forms inside-out and therefore it has been assumed that $\tau(r)$ is an increasing function of the galactocentric distance. The present time surface mass density is an observed quantity and either in the MW or M31 it is well described by an exponential profile with a typical scale length. The initial mass function is generally assumed to be constant in space and time and its form is either that of Scalo (1986) or Kroupa et al. (1993).

Detailed chemical evolution models relax the instantaneous recycling approximation and consider the stellar lifetimes. In this way, stellar nucleosynthesis and therefore the contributions of supernovae (SNe) of different type can be taken into account precisely. With this kind of models one can predict the evolution in space and time of the abundances of several single chemical elements in the gas.

In summary, once an IMF has been fixed, the main free parameters are the timescale of gas accretion, the efficiency of star formation and the exponent of the surface gas density in the Kennicutt law. In the following, we will present some results of chemical evolution models obtained by varying these three main parameters in order to fit the observed features of M31.

2.1 Results About the Chemical Evolution of M31

First we show the results of Yin et al. (2009) who adopted an inside-out formation for the disk of M31, a Kroupa et al. (1993) IMF and a Kennicutt law for the SFR with $k = 1.5$ and $\nu_{M31} = 0.2 Gyr^{-1}$. They adopted similar assumptions for the MW model with the exception of the efficiency of star formation assumed to be $\nu_{MW} = 0.1 Gyr^{-1}$, and the masses of the two disks which are $7.0 \cdot 10^{10} M_{\odot}$ for Andromeda and $5.0 \cdot 10^{10} M_{\odot}$ for the Milky Way. In Fig. 1 we show the results of that paper which illustrate the differences between MW and M31. In particular, in this Figure are shown the predicted and observed behaviours of the gas, the stars, the SFR, the gas fraction and the O gradient ($\Delta(log(O/H) + 12)$) along the disks of M31 and the MW.

The model of Marcon-Uchida et al. (2010) assumed that the disk of M31 forms inside-out with the time scale for gas accretion varying as:

$$\tau(r) = 0.62r + 1.62(Gyr). \tag{4}$$

The efficiency of star formation was also assumed to vary with r as:

$$\nu(r) = 24/r - 1.5 \left(Gyr^{-1}\right) \tag{5}$$

until it reaches a minimum value of $0.5 Gyr^{-1}$, which is kept constant for the largest radii. A threshold gas density for star formation of $5 M_{\odot} pc^{-2}$ (Braun et al. 2009) was also adopted. The surface mass density profile for the disk was taken from Geehan et al. (2006) with a scale radius $R_D = 5.4$ kpc, while in the MW $R_D = 2.3 - 2.5$ kpc. Also this model predicts a faster evolution for Andromeda relative to the MW. In fact, although both disks are assumed to have formed inside-out, the time scales for gas accretion are shorter and the efficiencies of star formation are higher in Andromeda at the same galactocentric distance than what is generally assumed for the MW (e.g. Chiappini et al. 2001).

Spitoni et al. (2013) adopted a model similar to that of Marcon-Uchida et al. (2010) and included galactic fountains and radial gas flows with the aim of studying the effects of these processes on the O gradient in M31. By means of a ballistic

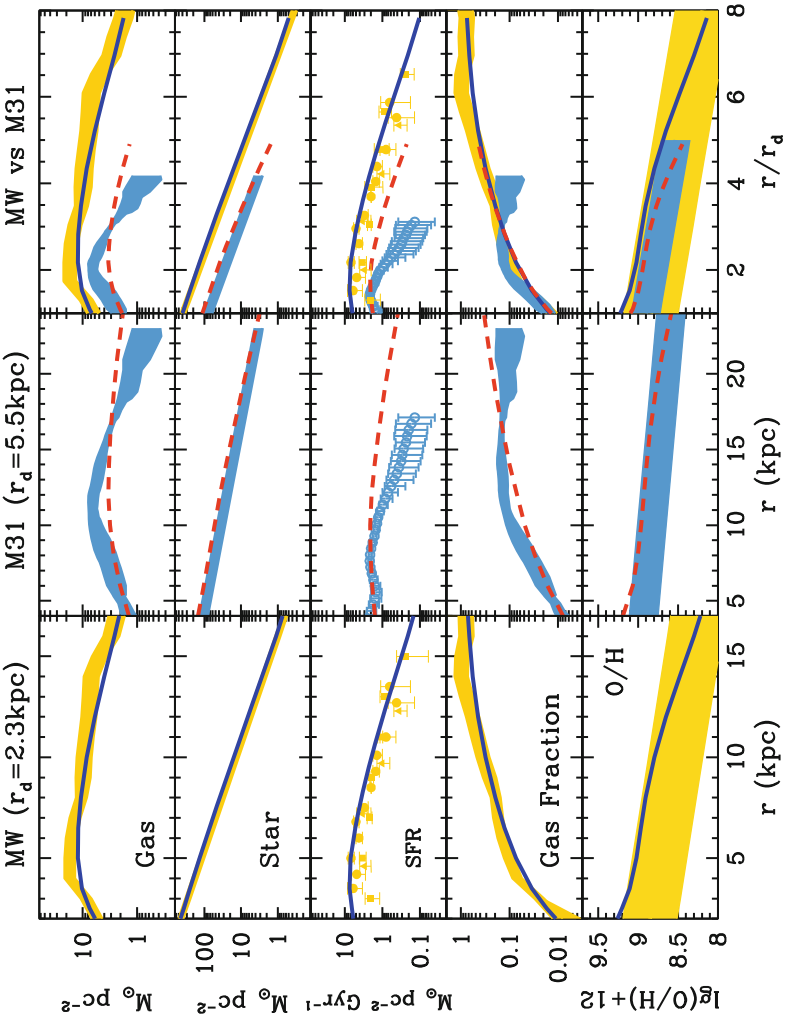

Fig. 1 MW versus M31: the observations are indicated by the *shaded areas* whereas the *continuous line* represents the model for the MW and the *dashed line* the model for M31. Figure 5 from Yin et al. (2009)

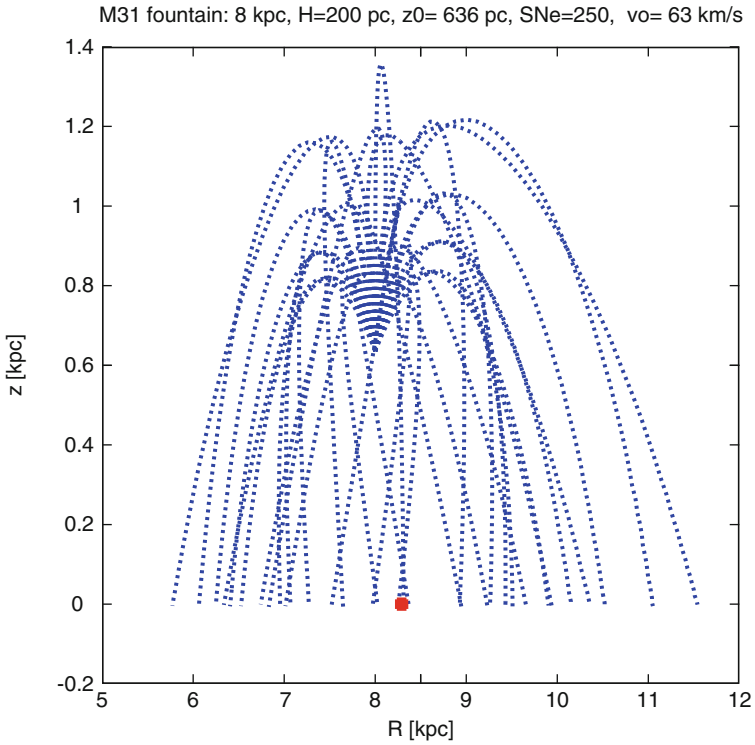

Fig. 2 Predicted galactic fountains in M31. The starting radius is 8 kpc and the height reached by the gas fountain is 636 pc. The *red filled circle* indicates the average falling radius coordinate. Figure from Spitoni et al. (2013)

method for the galactic fountains, they found that the landing coordinate of the gas expelled above the galactic disk from SNe is no more than 1 kpc from the starting point, thus not affecting the abundance gradients along the M31 disk (see Fig. 2). They also found that including radial gas flows allowed them to reproduce very well the observed abundance gradient of oxygen without the necessity of assuming an efficiency of star formation strongly decreasing with radius or a threshold in the gas density for star formation. The existence of such a star formation threshold has, in fact, been questioned by GALEX observations (see Boissier et al. 2007). In Fig. 3 we show the predicted O gradient for M31 compared with a large compilation of data including HII regions, young stars and SN remnants. The presence of radial gas flows derives from the assumption of the disk forming by infall of gas; in fact, the infalling gas has a lower angular momentum than that of the gas in the disk and the mixing of these two gases induces a net radial gas inflow. Chemical evolution models with radial gas flows have been discussed by several authors in the past, including Lacey and Fall (1985), Portinari and Chiosi (2000), Schönrich and Binney (2009), Spitoni and Matteucci (2011), but only Spitoni et al. (2013) applied the radial flow

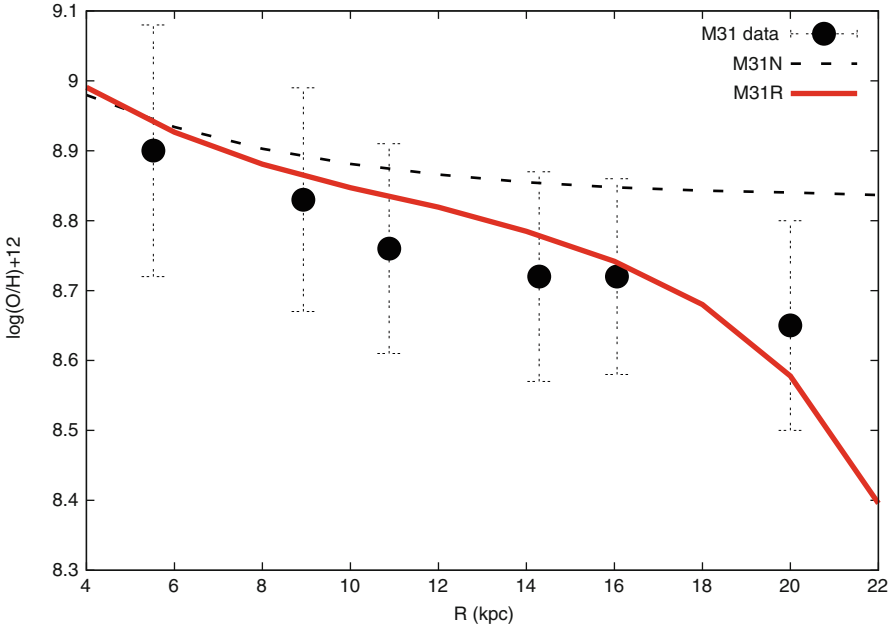

Fig. 3 Oxygen gradient in M31. The *dotted line* represents a model without radial gas flows, whereas the *dashed line* represents a model with gas flows (Spitoni et al. 2013). Data are from HII regions, young stars and SN remnants (Zurita and Bresolin 2012; Sanders et al. 2012; Venn et al. 2000; Esteban et al. 2009; Galarza et al. 1999; Przybilla et al. 2008; Trundle et al. 2002; Blair et al. 1982; Dennefeld and Kunth 1981).To better understand the trend in the data, we divided them into six bins as functions of the galactocentric distance. In each bin, we computed the mean value and the standard deviation for the oxygen abundance and the associated error

model to M31: in particular, they assumed a speed for the gas flow which is linearly increasing with decreasing galactocentric distance and it varies from 1.5 km/sec at 22 kpc down to 0.55 km/sec at 2 kpc.

3 The Chemical Evolution of M31 Bulge

The chemical evolution of the bulge of M31, a classical bulge more massive than the bulge of the Milky Way, has been computed by Sarajedini and Jablonka (2005), Worthey et al. (2005) and Ballero et al. (2007). The first two models were simple models of chemical evolution with instantaneous recycling approximation, whereas the model of Ballero et al. (2007) was taking into account fast gas accretion, stellar lifetimes, detailed nucleosynthesis and SN progenitors. These last authors concluded that the bulge of M31 must have evolved very quickly and on a timescale no longer than 0.5 Gyr, with an intense burst of star formation with star formation efficiency of $\sim 20 Gyr^{-1}$. This agrees with more recent studies (Saglia et al. 2010) which

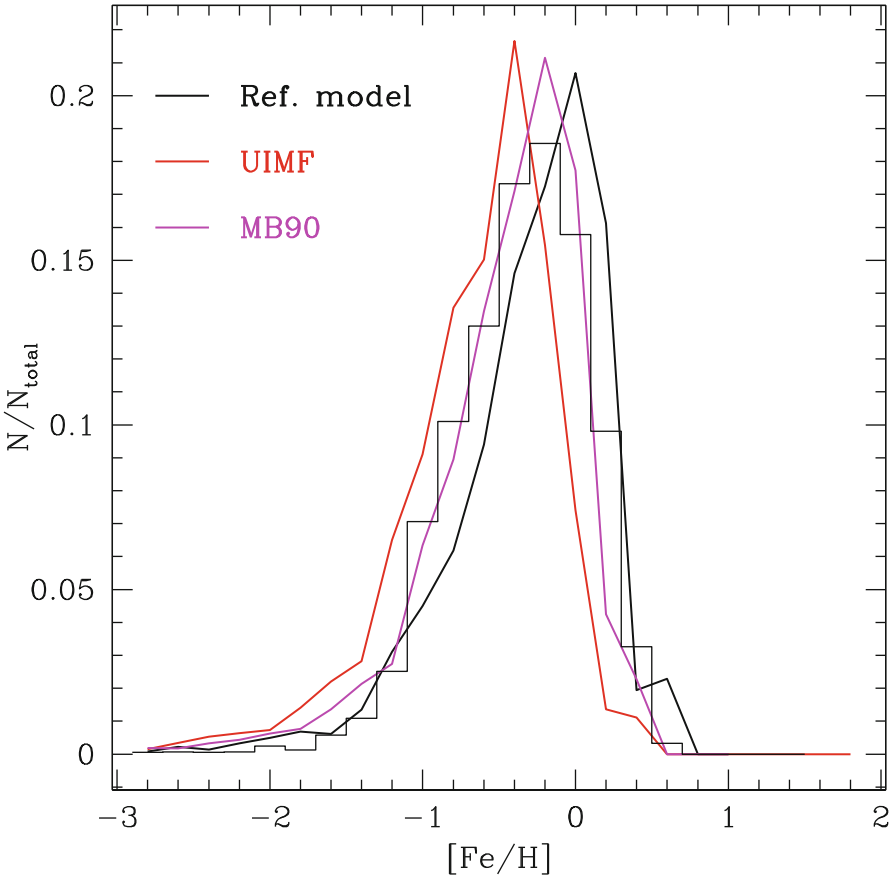

Fig. 4 MDF for the M31 bulge. The best fit for the M31 bulge is obtained with an IMF with x = 1.1, which is indicated by MB90. The model labelled *UIMF* represents the universal IMF of Kroupa (2001). Figure from Ballero et al. (2007)

concluded that with the exception of the region in the inner arcsecs, the stars in the bulge of M31 are uniformly old (≥ 12 Gyr) and with an overabundance of α-elements [α/Fe]$\sim +0.2$ dex and solar metallicity. Sarajedini and Jablonka (2005) derived the stellar metallicity distribution function (MDF) for M31, showing a peak at around the solar metal content (Z). In Fig. 4 we report the predicted and observed MDFs for the M31 bulge; the predictions are from Ballero et al. (2007), who claimed that a flatter IMF than Salpeter (1955) and universal IMF of Kroupa (2001) is necessary to fit the data. In this Figure, the MDF is a function of [Fe/H]: the authors transformed the data from [M/H] to [Fe/H], by assuming $[\alpha/Fe] = +0.3$ dex as suggested in Sarajedini and Jablonka (2005). All of these findings suggest that the bulge of M31 must have formed mainly by dissipational collapse during a strong burst of star formation.

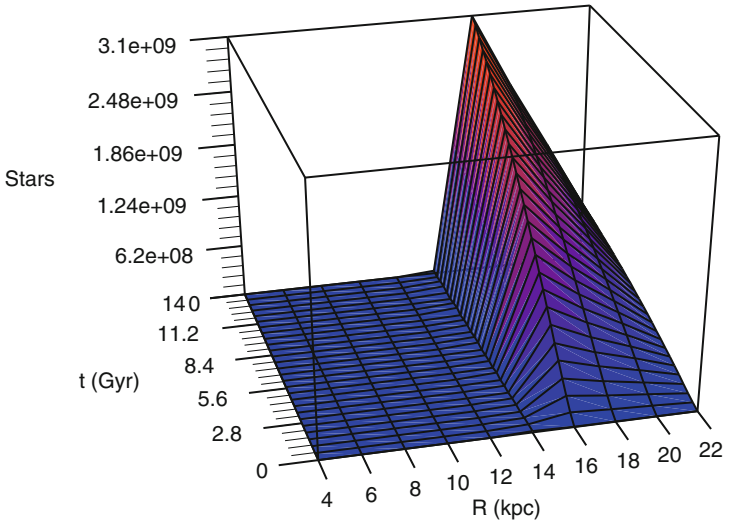

Fig. 5 A 3-D plot relative to the number of stars with habitable planets expected in M31. The chemical evolution model is that of Spitoni et al. (2013) with radial gas flows. Figure from Spitoni et al. (2014)

4 The GHZ in M31

Finally, we show some predictions concerning the Galactic Habitable Zone (GHZ) for the disk of M31 (Spitoni et al. 2014). We have assumed that the probability of forming Earth-like planets depends on the [Fe/H], the SFR and the SN rate of the studied region. In particular, we define the effective probability of finding stars with Earth-like planets that survived SN explosions as a function of the galactic radius as:

$$P_{GHZ} = \frac{\int_0^R SFR(r,t')P_E(r,t')P_{SN}(r,t')dt'}{\int_0^R SFR(r,t')dt'}, \tag{6}$$

where $P_E(r,t)$ is the probability for the creation of Earth like planets and not giant planets and is a function of the Fe abundance, $P_{SN}(r,t)$ is the probability that a SN occurs close to the Earth-like planets and SFR(r,t) is the star formation rate. The metallicity, the star formation rate and the SN rate are those predicted by the Spitoni et al. (2013) model for M31.

Therefore, the number of stars hosting Earth-like planets with possible life is given by the product of the probability of having such planets, P_{GHZ}, multiplied by the total number of stars formed at each radius. Figure 5 shows the predicted number of stars with habitable planets in Andromeda and the highest probability of finding them lies at 16 kpc from the center.

5 Conclusions

The Andromeda galaxy has an average metallicity higher than the MW but a shallower metal gradient along the disk at the present time, its bulge looks more evolved than the bulge of the MW, since it is mainly made of old stars exhibiting overabundances of α-elements relative to Fe. All of this indicates that M31 has suffered a more intense star formation and shorter timescales for the formation of all its components, than our Galaxy. On the other hand, M31 is more massive than the MW: this fact suggests that the baryonic galactic mass (stars plus gas) is linked to the star formation rate and that a down-sizing in star formation is present also in spiral galaxies. This process can be described by simply assuming that the efficiency of star formation is a function of the galactic baryonic mass. We also estimated which galactocentric region of the Andromeda disk has the highest probability of having stars hosting habitable planets and found that this region is centered at 16 kpc from the centre. Future detailed abundance determinations will greatly help in assessing all the above mentioned points.

Acknowledgements We acknowledge financial support from PRIN-MIUR2010-2011, project "Chemical and Dynamical Evolution of the Milky Way and Local Group Galaxies", prot. 2010LY5N2T.

References

Ballero, S., Kroupa, P. Matteucci, F. 2007, A&A, 467, 117
Blair, W. P., Kirshner, R. P., Chevalier, R. A. 1982, ApJ, 254, 50
Boissier S. & Prantzos, N., 1999, MNRAS, 307, 857
Boissier et al., 2007, ApJS, 173, 524
Braun, R., Thilker, D.A., Walterbos, R.A.M.,Corbelli, E., 2009, ApJ, 695, 937
Chiappini, C., Matteucci, F., Romano, D., 2001, ApJ, 554, 1044
Dennefeld, M., Kunth, D., 1981, AJ, 86, 989
Diaz, A.& Tosi, M., 1984, MNRAS, 208, 365
Esteban C., Bresolin F., Peimbert M., García-Rojas J., Peimbert A., Mesa-Delgado A., 2009, ApJ, 700,654
Galarza, V. C., Walterbos, R. A. M., Braun, R. 1999, AJ, 118, 2775
Geehan, J.J., Fardal, M.A., Babul, A., Guhathakurta, P., 2006, MNRAS, 366, 996
Holland, S., Fahlman, G.G., Richer, H.B., 1996, AJ, 1121035
Kalirai, J.S. et al., 2006, ApJ, 648,389
Kennicutt, R.C. Jr., 1998, ARA&A, 36, 189
Koch, A. et al. 2008, ApJ, 689, 958
Kroupa, P., 2001, MNRAS, 332, 231
Kroupa, P., Tout, C.A., Gilmore, G., 1993, MNRAS, 262, 545
Lacey, C.G.& Fall, M., 1985, ApJ, 290, 154
Marcon-Uchida, M., Matteucci, F., Costa, R., 2010, A&A, 520, 35

Matteucci. F., 2012, Chemical Evolution of Galaxies: Astronomy and Astrophysics Library. ISBN 978-3-642-22490-4. Springer-Verlag Berlin Heidelberg, 2012
Matteucci. F. & François, P., 1989, MNRAS, 239, 885
Mollá, M., Ferrini, F., Diaz, A., 1996, ApJ, 466, 668
Mott, A., Spitoni, E., Matteucci, F., 2013, MNRAS, 435, 2018
Portinari, L. & Chiosi, C., 2000, A&A, 355, 929
Przybilla N, Butler K., Kudritzky R., 2008, in "The Metal Rich Universe" Conference Proceedings, Cambridge University Press, Cambridge, U. K., 2008, p. 332
Renda, A., Kawata, D., Fenner, Y., Gibson, B.K., 2005, MNRAS, 356, 1071
Robles-Valdez, F., Carigi, L., Peimbert, M., 2013, arXiv:1310.1420
Ryan, S.G. & Norris, J.E., 1991, AJ, 101, 1865
Saglia, R.P. et al., 2010, A&A, 509, 61
Salpeter, E.E., 1955, ApJ, 121, 161
Sanders N., Caldwell N., McDowell J., Harding P., 2012, ApJ, 758, 133S
Sarajedini, A. & Jablonka, P., 2005, ApJ, 130, 1627
Scalo, J.M., 1986, FCPh, 11, 1
Schönrich, R., Binney, J., 2009, MNRAS, 396, 203
Spitoni, E. & Matteucci,F., 2011, A&A, 531, 72
Spitoni, E., Matteucci,F., Marcon-Uchida,M., 2013, A&A, 551, 123
Spitoni,E., Matteucci, F., Sozzetti, A., 2014, MNRAS, 440, 2588
Trundle C., Dufton P., Lennon D., Smartt S., Urbaneja M., 2002, A&A, 395, 519
Venn K., McCarthy J., Lennon D., Przybilla N., Kudritzki R., Lemke M., 2000, ApJ, 541, 610
Williams, B.F., 2003a, AJ, 126, 1312
Williams, B.F., 2003b, MNRAS, 340, 143
Worthey, G., España, A., MacArthur, L. A., & Courteau, S., 2005, ApJ, 631, 820
Yin, J., Hou, J. L., Prantzos, N., et al., 2009, A&A, 505, 497
Zurita A., Bresolin F., 2012, MNRAS, 427, 1463

The Outer Disk and Halo of Andromeda: The View with PAndAS

Geraint F. Lewis

Abstract The clues to galaxy formation and evolution should lie all about us in the form of dismembered remains of dwarf galaxies littering galaxy halos. The faintness and extent of this debris has, however, presented a significant observational challenge. The Pan-Andromeda Archeological Survey (PAndAS) has targeted the halos of our nearest cosmic companions, Andromeda and Triangulum, to provide a deep, panoramic view of galaxy evolution in action. Now that the data-taking is complete, this article summarizes the key scientific findings in terms of the outer disk and halo, including the detection of extensive substructure, globular clusters and a large population of dwarf galaxies. While broadly inline with our expectations of galaxy evolution in a ΛCDM universe, PAndAS has revealed an unexpected plane of co-rotating dwarf galaxies which challenges our cosmological expectations.

1 Introduction

The mantra that in hierarchical models of structure formation, galaxies grow over time through the accretion of smaller systems has opened many a paper. While this picture accurately describes the large-scale universe, focus has switched to the scale of individual galaxy halos where there appears to be tension in the predicted and observed population of dwarf galaxies (Klypin et al. 1999; Moore et al. 1999).

ΛCDM cosmologies predict that galaxy halos should be richly structured, with long timescale interactions in the outer regions resulting in a wealth of tidal streams, whereas the shorter interaction times in the inner regions result in total destruction and mixing into a smoother stellar halo (Bullock et al. 2005). While our own Milky Way is enveloped in this substructure, its extremely low surface brightness has made detection difficult, although large scale surveys, such as the Sloan Digital Sky Survey, that allow the identification and isolation of particular stellar populations have begun to reveal the complex structure within the Galaxy halo (Belokurov et al. 2006).

G. F. Lewis (✉)
Sydney Institute for Astronomy, School of Physics, The University of Sydney,
NSW 2006, Sydney Australia
e-mail: Geraint.lewis@sydney.edu.au

K. Freeman et al. (eds.), *Lessons from the Local Group,*
DOI 10.1007/978-3-319-10614-4_14

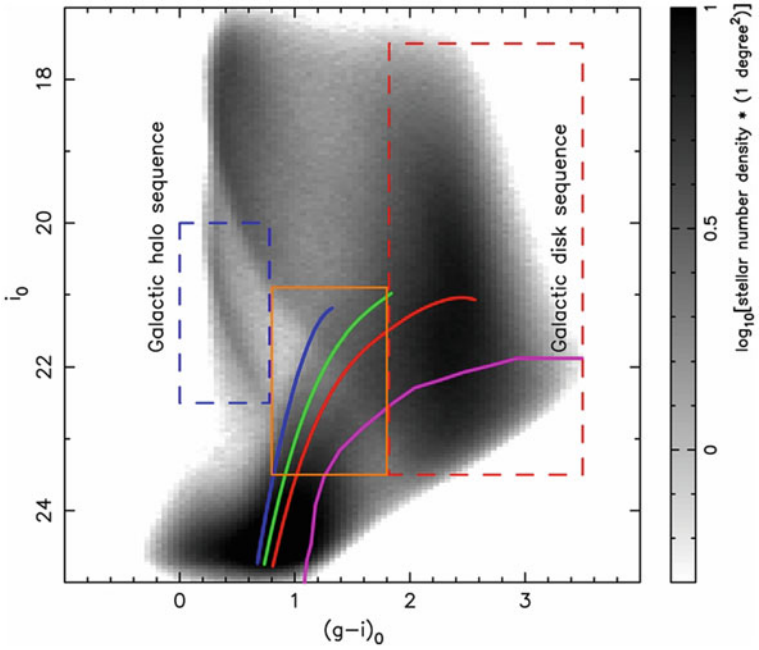

Fig. 1 The g & i colour-magnitude diagram for the PAndAS survey. The coloured lines represent red giant branch isochrones from metal-poor (*blue*) to metal-rich (*purple*) at the distance of Andromeda. The red and blue selection boxes identify contamination from the Galactic disk and halo, whereas the increasing density at i∼24 shows contamination from misidentified galaxies. Image originally appeared in Ibata et al. (2014b)

2 The Pan-Andromeda Archaeological Survey (PAndAS)

While the Sloan Digital Sky Survey has been highly successful, it has only probed the inner few 10 s of kpc of the Milky Way halo and only over a limited portion of the sky; the prospect of a deep, global view of the stellar populations within our Galactic halo is still some years off.

However, with the advent of wide-field cameras, we are now able to undertake panoramic surveys of our nearest cosmic companions, Andromeda and Triangulum. This was the goal of the Pan-Andromeda Archaeological Survey (PAndAS). Built upon earlier observations of the inner regions of Andromeda with the Isaac Newton Telescope, PAndAS was allocated large program status of the Canada-France-Hawaii Telescope (CFHT), using MegaCam to image ∼350 sq degrees down to several magnitudes below the tip of the Red Giant Branch (TRGB) at the ∼800 kpc distance of these two galaxies.

Figure 1 presents the colour-magnitude diagram of the PAndAS survey, identifying the location of the red giant branch for a range of metallicities, as well as prominent contamination from both Galactic and extra-galactic sources. Colour-cuts,

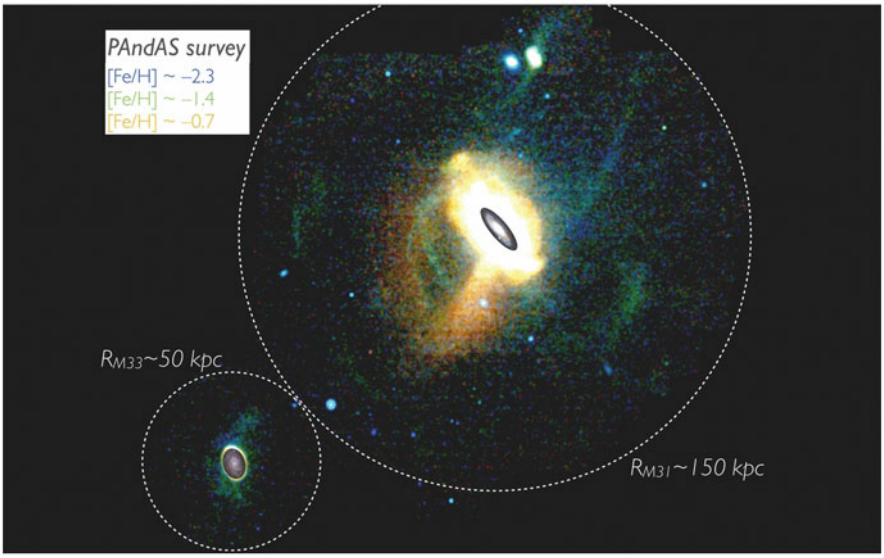

Fig. 2 The results of the PAndAS survey, mapping the halo of Andromeda out to a distance of 150 kpc, whereas Triangulum's halo is observed to a distance of 50 kpc. From Martin et al. (2013)

therefore, can be used to isolate stars in Andromeda and Triangulum, and a photometric metallicity assigned to each star based upon their proximity to the theoretical isochrones. Figure 2 presents a composite map of the locations of the stars identified as belonging to Andromeda and Triangulum, colour-coded by metallicity, with blue being more metal-poor, while red is metal-rich. Note the scale in this image, showing that we have mapped the halo of Andromeda out to a distance of 150 kpc, and Triangulum to 50 kpc, as well as the bridge between the two. Inset on both images are the traditional optical views of these two galaxies, representing the extent of their stellar disks.

2.1 A Wealth of Substructure

It is apparent from Fig. 2 that the halos of Andromeda and Triangulum possess significant substructure; a summary of the substructure is presented in Fig. 3. Beyond the traditional optical disk of Andromeda, the galaxy is sheathed in an extensive swathe of stars. This region is quite complex, possessing significant clumps and shells, indicative of aggressive accretion in this region.

Traveling outwards, it is apparent that there is significant substructure into the large-scale halo. The most prominent of these is the Giant Stellar Stream (GSS), a complex structure that possesses a metal-rich core enveloped in a more metal-poor distribution, stretching more than 100 kpc beyond Andromeda (Ibata et al. 2001;

2007; McConnachie et al. 2004), before falling back and threading itself again in the disk of Andromeda. The progenitor of the GSS must have been quite massive ($\sim 3 \times 10^9 M_\odot$; Fardal et al. 2013) although its orbit brings it perilously close to the heart of Andromeda and it is difficult to imagine it surviving multiple peri-galacticon passages.

While the GSS is the most prominent substructure, it is not the only one present in Andromedas halo. In the inner regions there are a series of other seemingly parallel streams, known imaginatively as A, B, C and D, which, while apparently collocated with the GSS, have significantly different metallicity, and hence, origin (Ibata et al. 2007).

In the northern part of the halo, Andromeda possesses a relatively thin stream (known as the NW stream), which is clearly associated with the demise of And XXVII, a small dwarf galaxy. Given the apparent coldness of this stream, it has been suggested that it structure may be an ideal probe for the presence of significant population of sub-galactic dark matter halos, although the low density of stars in this stream makes an accurate determination difficult (Carlberg et al. 2011).

Significant, seemingly distinct, substructure, namely the Eastern Cloud and South West Cloud, are also apparent at distances of ~115 and ~85 kpc respectively. While isolated, these shredded stellar systems provide vital clues to galaxy evolution, a point we will return to later.

Moreover, it is apparent that there are other tidal features within the PAndAS footprint, with Triangulum possessing significant stellar tidal debris that mimics the earlier discovered warp in the gas disk (Putman et al. 2009; McConnachie et al. 2009; Lewis et al. 2013), while there is further additional tidal substructure associated with the NGC 147/184 sub-group. Clearly, substructure is ubiquitous within the halo of Andromeda and these smaller members of the Local Group.

2.2 The Smooth Stellar Halo

One of the key goals of PAndAS was the identification of the smooth underlying stellar halo; this extensive component of the galaxy is a combination of a primordial stellar component and mixed stellar debris of disrupted systems. However, it is clear from Fig. 3 that the significant quantity of stellar debris makes the isolation of this halo component difficult, but in Ibata et al. (2014a) we were able to use the detailed map of substructure to effectively mask out regions of overlying debris, fitting only the remaining component; an example of the masks employed, as a function of metallicity, are presented in Fig. 4.

With the substructure masked out, fits of 3-dimensional oblate power-law distributions were made for the remaining stellar components; the best fits are apparent as colour shading in Fig. 3. In general, these fits favored near spherical stellar halo components at all metallicities, with a slope of $\gamma \sim -3$ from the inner 30 kpc out to ~300 kpc, with an inferred mass of $\sim 8 \times 10^9 M_\odot$.

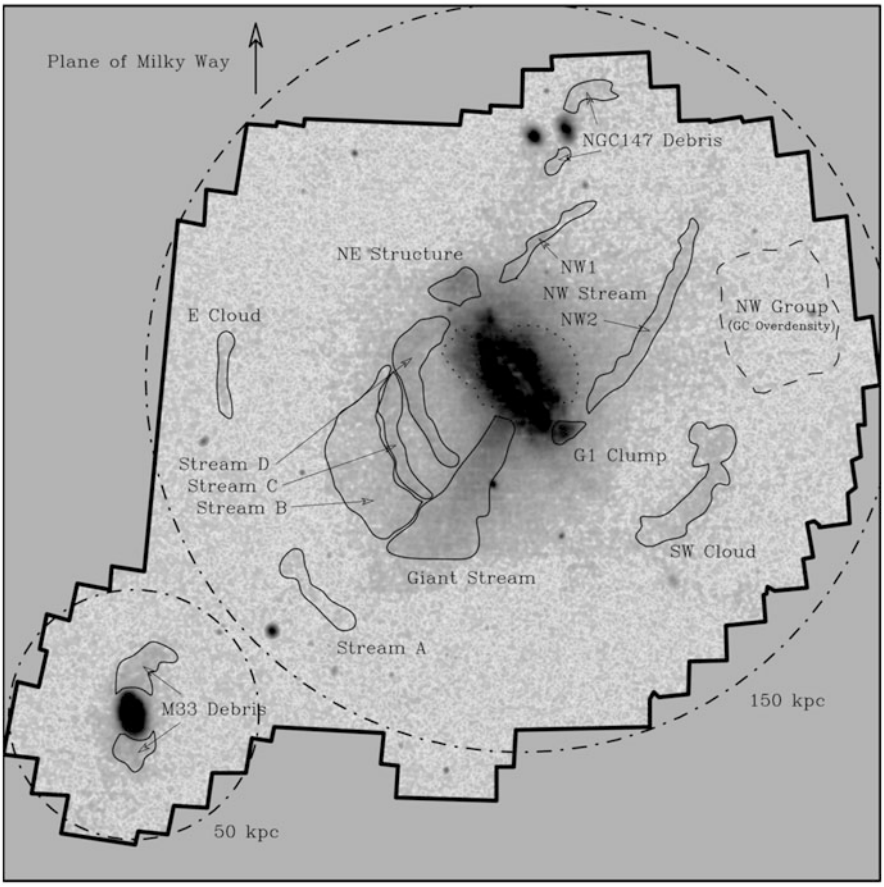

Fig. 3 A summary of the prominent substructure seen through the halo of Andromeda and Triangulum. The inner regions are dominated by stellar debris that wraps the optical disk, but the halo possesses substructure in the form of the Giant Stellar Stream, a series of other streams (labeled A to D), the NW stream region, and two clouds, one in the East and the other in the South West. Notice also the tidal debris associate with Triangulum and with NGC 147/185 subgroup. (From Lewis et al. 2013)

It is important to note, however, that while we have this global picture of the stellar halo, an examination of the fits reveal that there are difference in terms of the metallicity distribution, with metallicity steadily increasing towards the centre. This is remarkable fossil evidence for the process of accretion, demonstrating that the most massive systems must deposit the majority of their stars in the inner regions, possibly brought there by increased dynamical friction. As such, this presents a crucial test of computational models for the build up of the stellar halo.

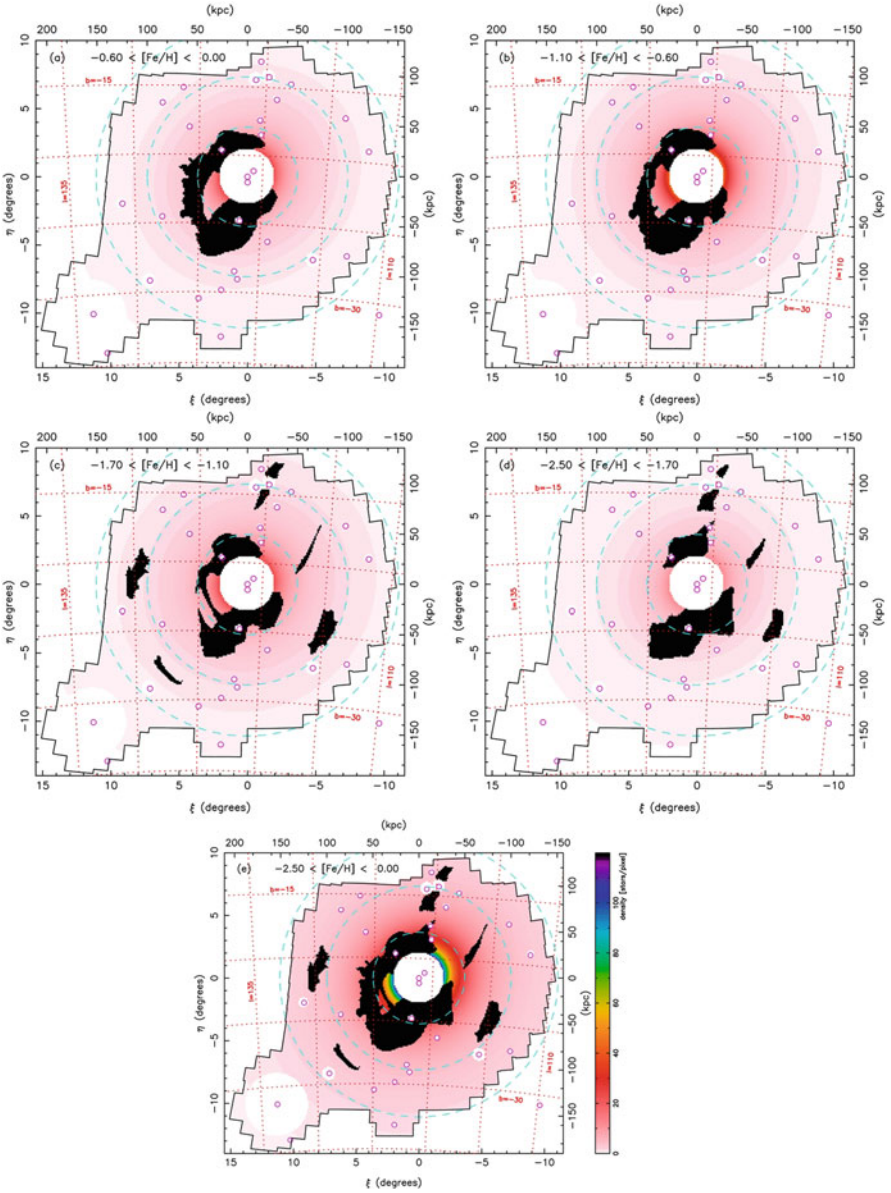

Fig. 4 Examples of the substructure masks employed in the halo fitting of Ibata et al. (2014b). From top to bottom, the masks are presented as a decreasing function of metallicity, illustrating how the Giant Stellar Stream dominates at high metallicity, whereas other components of substructure, such as the additional stream and clouds, become apparent at lower metallicities. The bottom panel presents the sum of the masks; note that the halo of Triangulum has been excised. The predominantly red underlying shading corresponds to the best-fit power-law model at each metallicity. These find the stellar halo to be almost spherical with an inferred stellar mass of $\sim 8 \times 10^9$ $M_\odot$

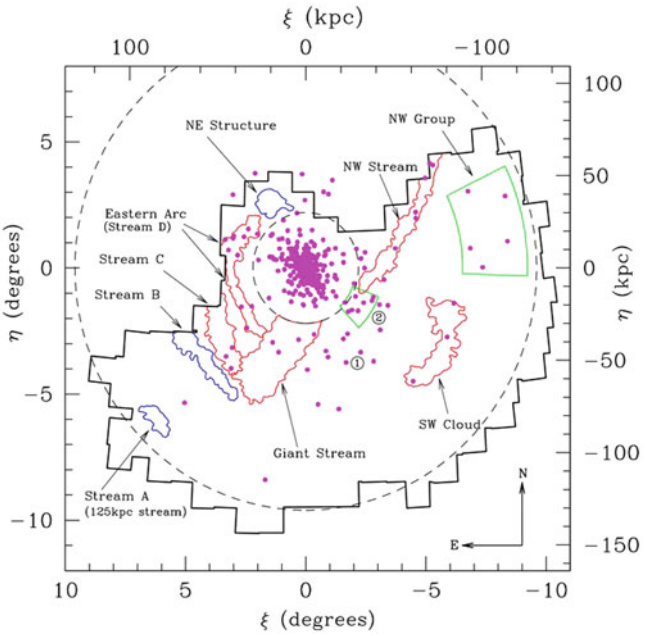

Fig. 5 From Mackey et al. (2010), this presents the location of the M31 globular clusters (*purple dots*) with prominent substructures; those that appear to be associated with globular clusters are *outlined in red*, whereas those that appear devoid of globular clusters appear are blue. There is less than a 1 % chance that the apparent alignment is by chance. The PAndAS footprint is smaller than in previous images as data-taking was not complete at the stage of the analysis

2.3 Substructure and Globular Clusters

The fact that the halo of Andromeda possesses substantially more globular clusters than our Milky Way has been known for a number of years, but what is the source of this discrepancy? One of the key findings of PAndAS has been the identification of globular clusters within the halo of Andromeda, some at the very outer reaches of the survey (e.g. Veljanoski et al. 2013).

With the identification of both globular clusters and substructure, it is natural to ask whether the two are correlated, both spatially and kinematically; if this is the case, then it would demonstrate that a faction of the globular clusters were accreted along with the systems that are now undergoing disruption.

Mackey et al. (2010) undertook such an analysis when only a fraction of the PAndAS data was obtained. Figure 5 presents the footprint of the reduced survey area, with purple dots denoting the locations of the globular clusters; note the clustering of globular clusters close to Andromeda, as well as more extensive distribution through the halo. Prominent substructure apparently associated with globular clusters is outlined in red, whereas those devoid of clusters appear in blue. The resulting spatial analysis revealed that there is less than a 1 % chance these apparent alignment

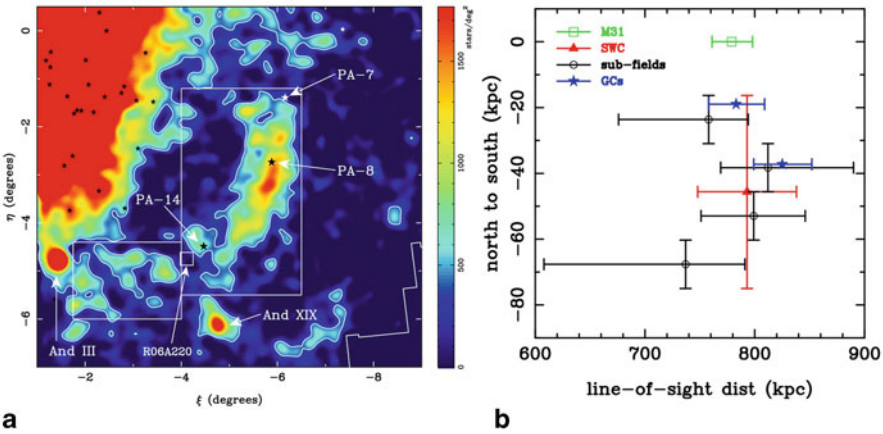

Fig. 6 The left-hand panel presents the stellar density map in the vicinity of the South West Cloud (*boxed*). The increasing stellar density towards Andromeda is apparent, as are two dwarf galaxies, And III and And XIX. Also noted are three associated globular clusters, PA-7, PA-8 and PA-14. The right-hand panel presents the distances to two of the globular clusters (*blue*), the South West Cloud (*red*) and three subfields of the Cloud (*black*). The fields are at the same distance, within errors

are by chance, providing significant evidence that a substantial portion of the halo globular cluster population in Andromeda was deposited there via accretion events.

The Case of the South West Cloud

While the positive on-sky spatial correlation of substructure and globular clusters is evidence for their common origin, more significant evidence would be the demonstration that they are truly associated in terms of being co-spatial and possessing similar kinematics. While identifying the spatial and kinematic properties of globular clusters is relatively straightforward, the inherent sparseness of the underlying substructure makes an equivalent measure more problematic

Bate et al. (2014) turned their attention to the South West Cloud to examine this in more detail. As well as being associated with three globular clusters, as relative brightness makes it a potential target for determining distance and kinematics. Using a new Bayesian-based technique to isolate the TRGB (Conn et al. 2011, 2012), the substructure distance was found to be ∼800 kpc, making it co-spatial with the three globular clusters (see Fig. 6). The analysis of Bate et al. (2014) found the South West Cloud to be at the same distance (within errors) as the two northern globular clusters, whose distances have been previously determined, showing that these structures are spatially coherent. With an average metallicity of [Fe/H]∼ −1.3, and a broad metallicity spread of ∼0.5, and inferred luminosity of Mv∼ −12.1, the progenitor of the South West Cloud must have been amongst the most massive satellites orbiting Andromeda, consistent with it currently being associated with globular clusters,

but also suggesting that a fractions of its population has been lost to the halo of Andromeda.

The kinematics of the globular clusters have been determined, showing a gradient from North to South of ∼70 km/s. A serendipitous spectroscopic field was obtained as part of the SPLASH survey at the Southern end of the South West Cloud (Gilbert et al. 2012; noted in Fig. 6) with a similar velocity as the nearby globular PA-14 (-373.5 ± 3.0 km/s and -363.5 ± 9.0 km/s respectively) demonstrating that they are also kinematically associated. A more recent analysis of a field close to PA-8, near the centre of the South West Cloud, also reveals a kinematic association, and indicating that globulars have been added to Andromeda's halo though accretion events.

3 The Dwarf Galaxy Population of Andromeda

An examination of Fig. 2 reveals that the halo of Andromeda possesses an extensive population of dwarf galaxies, now numbering ∼30; the majority of these have been identified in recent years with large-scale surveys such as PAndAS and SDSS. As with the presences of substructure, the dwarf population within galactic halos is an important probe of the of the underlying cosmological model, although there is existing tension between the expected and observed number of dwarf galaxies seen around the Milky Way and Andromeda (Klypin et al. 1999; Moore et al. 1999). How do the properties of the observed dwarf galaxies compare with expectations?

Figure 7 presents the cumulative two-dimensional distribution of dwarf galaxies within the PAndAS footprint. Theoretical expectations are that the dwarf galaxy population should be centrally concentrated, but clearly the dwarfs in PAndAS appear to be uniformly distributed.

3.1 Dwarf Galaxy Distances and Velocities

The initial study by Richardson et al. (2011) considered only the relative 2-dimensional positions of the dwarf galaxies throughout Andromeda's halo. There has, however, been considerable effort to obtain kinematics of the dwarf systems (e.g. Collins et al. 2014), while accurate distances have been established through robust TRGB measurements by Conn et al. (2011, 2012).

With these observations, we now have the first 3-dimensional view of the dwarf population. An analysis of the spatial distribution confirms what is seen in the 2-D case, lacking the central concentration expected from theoretical models. However, the most startling aspect of the 3-dimensional distribution is a pronounced asymmetry in the overall dwarf population, with the majority of the dwarfs located in the hemisphere towards the Milky Way (Fig. 8).

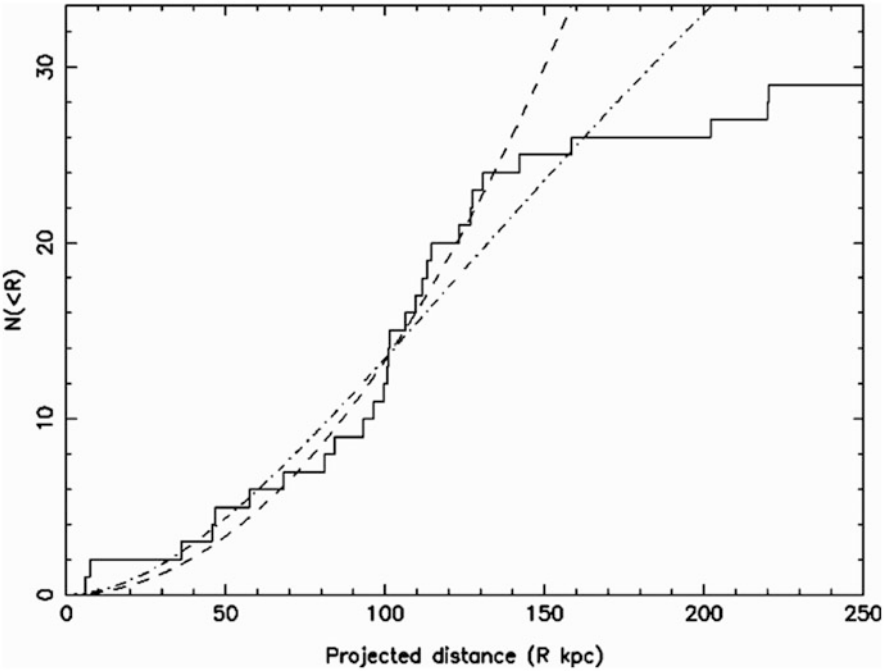

Fig. 7 The cumulative 2-dimensional density distribution of dwarf galaxies within the PAndAS footprint. Theoretical models predict the dwarf population should be centrally concentrated, but the result from PAndAS show an almost uniform density across the field. (From Richardson et al. 2011)

3.2 An Unexpected Plane of Dwarf Galaxies

As well as the radial and overall asymmetry properties of the dwarf galaxy population, the Andromeda dwarfs were also examined to identify any further substructure in the population; computational simulations of galaxy evolution suggest that lose dwarf alignments may occur, but there are no predictions for well-aligned sub-populations of dwarfs.

The focus in the work of Ibata et al. (2013) and Conn et al. (2013) was to identify statistically significant planes of subsets of dwarf galaxies. This, of course, presents a significant combinatorics problem, with an extremely large number of possible subsample from an over all population of $\sim$30, but the problem is tractable considering smaller and larger subsets of dwarfs. For a broad range of subpopulation numbers, the most significant plane possessed many of the same members. Further investigation revealed the presence of an extremely thin ($<$13 kpc rms) significant plane of roughly half the entire dwarf population of Andromeda; the members of this plane are denoted in red in Fig. 8, with the remaining dwarf galaxy population appearing in blue (Fig. 9).

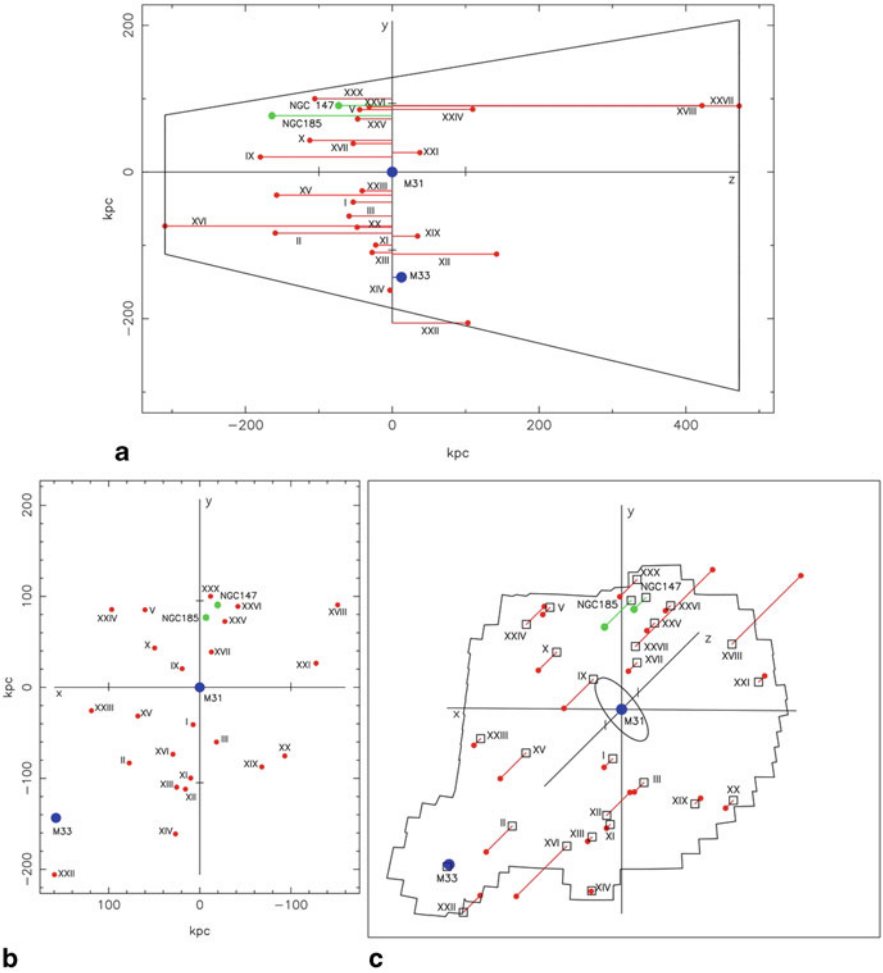

Fig. 8 The three-dimensional distribution of dwarf galaxies about Andromeda, as established by Conn et al. (2011, 2012). While the lower panels present the on sky distribution of dwarfs, the top panel shows their location relative to Andromeda. Clearly, there is a significant asymmetry in the distribution, with the majority of dwarfs located on the near-side of Andromeda, relative to the Milky Way

By eye, this plane of dwarf galaxies already possesses some surprising properties; as seen from us, this plane is almost directly edge-on, and, while significantly tilted with regards to Andromeda, it is aligned with the North-South axis of the Milky Way.

More surprising was the kinematics of the dwarfs in the plane, with all but two possessing apparently coherent rotation; the Northern galaxies in the plane are moving towards us, whereas those in the South are moving away, relative to Andromeda. Such a coherently rotating plane is significant at the 99.998 % level compared to a random chance alignment.

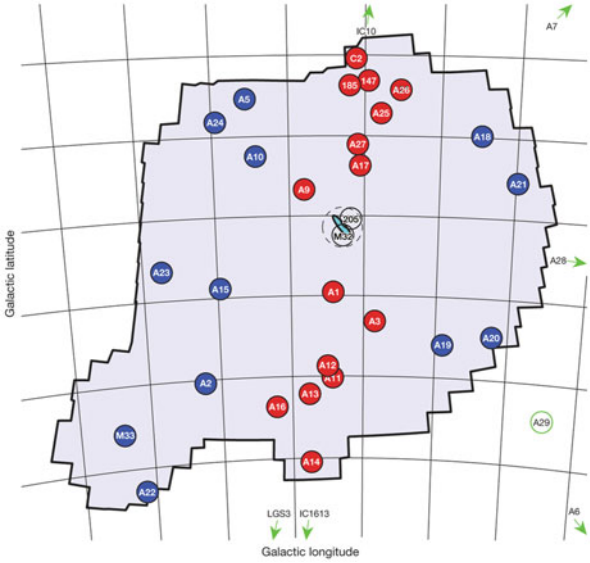

Fig. 9 The dwarf plane of Andromeda. The shaded area corresponds to the PAndAS footprint, with Andromeda itself appearing as a light blue ellipse. The circles represent the locations of the dwarf galaxies, with blue denoting those not associated with the plane. The red dwarfs are found to sit on a statistically significant plane, with a thickness of less than 13kpc. All but two galaxies in this plane move in a coherent fashion, with the Northern dwarfs moving towards us, while those in the South are moving away, relative to Andromeda. This figure originally appeared in Ibata et al. (2013)

4 Conclusions

PAndAS has given us an unparalleled deep panoramic survey of the halo of the Andromeda galaxy, providing a snapshot of galaxy formation and evolution in action. The broad picture that a large galaxy like Andromeda should have grown over time through the accretion of smaller systems is borne out by the almost ubiquitous presence of tidal debris enveloping the entire galaxy.

This picture is further bolstered through the identification of an extensive stellar halo underlying the substructure; this halo should be comprised of primordial populations of stars, formed in the earliest epoch of the life of Andromeda, as well as completely phase-mixed stars, the remnants of dwarf galaxies accreted long ago.

Additionally, the spatial and kinematic association between substructure and globular clusters is providing further evidence of accretion, demonstrating that the large globular population of Andromeda may be due to an aggressive accretion history. Currently we care comparing these observations to state-of-the-art simulations of galaxy formation to see if they truly support our underlying models.

But ΛCDM is not out of the water yet, as PAndAS has also revealed a population of dwarf galaxies that are seen to the edge of the survey. With new distance and kinematic measures, we have been able to show that the dwarf population is highly asymmetric

and not as centrally concentrated as theoretical expectations. But more problematic is the identification of a thin plane consisting of half of the entire dwarf population, co-rotating about Andromeda, something highly unexpected in our cosmological models. If such planes are ubiquitous, CDM has some serious explaining to do.

Acknowledgements GFL acknowledges that PAndAS has been a collaborative effort, and its success is due to the blood, sweat and tears of a smart and dedicated team. He gratefully thanks them all. He also thanks the organizers of the conference for inviting him to speak, and for organizing the conference in such a wonderful location.

References

Bate et al., Monthly Notices of the Royal Astronomical Society, (2014), 437, 3362
Belokurov et al., The Astrophysical Journal, (2006), 647, L111
Bullock et al., The Astrophysical Journal, (2005), 635, 931
Carlberg et al., The Astrophysical Journal, (2011), 731, 124
Collins, et al., The Astrophysical Journal, (2014), 783, 7
Conn et al., The Astrophysical Journal, (2011), 740, 69
Conn et al., The Astrophysical Journal, (2012), 758, 11
Conn et al., The Astrophysical Journal, (2013), 766, 120
Fardal et al., Monthly Notices of the Royal Astronomical Society, (2013), 434, 2779
Gilbert et al., The Astrophysical Journal, (2012), 760, 76
Ibata et al., Nature, (2001), 412, 419
Ibata et al., The Astrophysical Journal, (2007), 671, 1591
Ibata et al., Nature, (2013), 493, 62
Ibata et al., The Astrophysical Journal, (2014a), 784, L6
Ibata et al., The Astrophysical Journal, (2014b), 780, 128
Klypin et al., The Astrophysical Journal, (1999), 522, 82
Lewis et al., The Astrophysical Journal, (2013), 763, 4
Mackey et al., The Astrophysical Journal, (2010), 717, L11
Martin, et al., The Astrophysical Journal, (2013), 776, 80
McConnachie et al., Monthly Notices of the Royal Astronomical Society, (2004), 350, 243
McConnachie et al., Nature, (2009), 461, 66
Moore et al., The Astrophysical Journal, (1999), 524, L19
Putman et al., The Astrophysical Journal, (2009), 403, 1486
Richardson et al., The Astrophysical Journal, (2011), 732, 76
Veljanoski et al., The Astrophysical Journal (2013), 768, 33

Gas and Star Formation in M33: An Artistic Pathway

Edvige Corbelli

Abstract M33 is the closest blue, star forming, flocculent spiral galaxy for which it has been possible to combine an overwhelming quantity of multiwavelength high resolution data to shed light on its assembly and star formation across cosmic time. I will summarize some of the key ingredients related to the formation and evolution of this galaxy, such as its dark matter, the baryonic distribution and the metallicity gradients. M33 is a pure disk galaxy with a lower baryonic fraction than M31, of order 0.02, and a dark matter profile typical of structure growth in ΛCDM cosmology. Disk dynamics and the growth of perturbations can be visualized in a detailed 2-D map. The consequent star forming sites across the disk, analyzed using mid-infrared observations, points out young stellar clusters spanning 4 orders of magnitude in luminosity. This database has allowed to study IMF sampling at the high mass end and the concept of a cluster birthline. Stars and gas, present beyond 2-optical radii, point out to the occurrence of possible cosmic gas infall fueling star formation. Bruce Elmegreen's outstanding contribution to science becomes evident in the analysis of M33, here underlined also through an artistic pathway.

1 Prologue

In the last few years the interest towards the possibility that cosmic gas accretion regulates star formation in galaxies has grown, a drawback for closed box models in galaxy evolution. Science evolves as human relations do too. One gets to know new people at unpredictable moments. I had met Bruce 10 years ago at the IMF@50 meeting in Spineto. Being the organizer of that meeting I have not had the chance to really know Bruce until, as a result of a question to him a couple of years later, we worked together on M33 stellar clusters (Corbelli et al. 2009). When the referee report arrived, in the Fall of 2008, I was in the US, visiting Ed Salpeter during his last illness. Bruce kindly offered to meet me to work on the report, in a museum of my choice in Manhattan, on my way back home. Since I love modern art, I had no doubt: the only museum I would have loved to see again was the Museum of

E. Corbelli (✉)
INAF-Osservatorio di Arcetri, L. E. Fermi, 5 - 50125 Firenze, Italy
e-mail: edvige@arcetri.astro.it

K. Freeman et al. (eds.), *Lessons from the Local Group,*
DOI 10.1007/978-3-319-10614-4_15

Modern Art. At MOMA there was an astonishing unexpected surprise, a temporary exhibition on *van Gogh and the Colors of the Night*. This stimulated my curiosity in investigating deeply later on the relation between van Gogh, one of my favorite painters, and astronomy. My contribution to these proceedings starts with the attempt to relate the astronomical knowledge and imagination present in van Gogh paintings to recurrent themes in Bruce's papers, often used in the analysis of M33.

During a working period in a bookshop and his long visit to Paris, van Gogh become aware of the emergence of a new science, astrophysics. The expanding knowledge of what stars are made of, the view of a non static cosmos spread across Europe thanks to books of popular science such as those by C. Flammarion. Van Gogh is aware of the colors and spectral classification of stars, of the sun as a star with a hot corona, of the spiral structure of some of the nebulae, and of the attempt to understand the shape and extent of the Milky Way. That is what made him conclude that "putting little white dots on the blue-black is not enough to paint a starry sky". While in Provence he makes the transition from prospective skies to ones full of colors, movement and imagination. For example, in the celebrated painting Starry Night, one sees stars of different colors and sizes, stars with an interior and an atmosphere, and the endless flowing spiral which, because of its extent, is reminiscent of the Milky Way, but which might as well be the faint M33 nebula. At that time M33 was in fact the closest known nebulae to the Aries constellation. This constellation has been clearly painted by van Gogh because it was present in the sky that night, just before the dawn of June 19 1889. The Starry Night has real and conceptual elements, also linked to religion. Van Gogh clearly wants to go beyond the current knowledge of astrophysics because painters, as he used to write, should use the power of their imagination to go deeper, beyond what the eyes can see.

We know today of the importance of many conceptual elements present in van Gogh paintings and well understood one century later in astrophysics and underlined in Bruce's contributions to science. I will highlight here two of them: the understanding and measure of the stellar Initial Mass Function, from the solar neighborhood to primordial galaxies, and the relevance of spiral density waves and of turbulence in the gas-to-star conversion. Turbulence is what keeps galaxies alive slowing down the star formation efficiency, and turbulence is also what makes the landscape and people alive in the late artistic work of van Gogh. You can find it in day and night skies, in the backgrounds of portraits as well as in Bruce's papers. In many studies of M33 carried out with my collaborators I have often found Bruce's work very helpful and often M33 has confirmed his theoretical predictions. There is, however, an exception, and that concerns dark matter. Similarly, there is also one element in van Gogh paintings which seems uncorrelated to Bruce's work or interests: the moon. The gibbous or waxing moon is a recurrent element in van Gogh's work. A full moon is present in the artistic work *Landscape with Wheat Sheaves and Rising Moon* made in July 1889. Here, part of the moon has a reddish color. And what I have discovered by checking the lunar eclipse calendar around the time van Gogh was painting the rising moon with a red shadow, is that a lunar eclipse was visible in southern France at that time! This confirms van Gogh's love and interest for astronomy. Despite the fact I know very little about Bruce (and about his interests on moon science) I had

Fig. 1 *The Starry Night* painted by V. van Gogh in June 1889 with many astrophysical concepts emerging at the end of the XIX century: stars of different colors and sizes with a structure, the moon and Venus (*outlined in red*), the Aries constellation (*in green*), and a large flowing spiral nebula

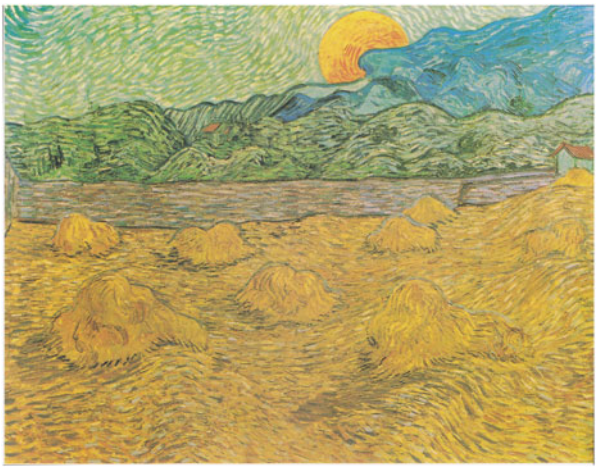

Fig. 2 *Landscape with Wheat Sheaves and Rising Moon* by V. van Gogh. The moon has a reddish color close to the mountain since the painter wants to emphasize the lunar eclipse which took place in southern France in July 1889

the chance to appreciate his care for people which makes him a great scientist to have around at any meeting (Fig. 1, 2).

2 Young Stellar Clusters and the IMF

Many years have past since the first description of M33 spiral arms appeared in a scientific journal, as "swarms of meteorites" in the sky. We know today that spiral arms host the brightest HII regions of M33 because here giant molecular clouds

grow by disk gravitational instabilities or collisions and coalescence. However it is become more and more evident that star formation in M33 is present throughout the whole disk in small units (Verley et al. 2009; Corbelli et al. 2011), and there is also evidence of occasional events in the extended warped gaseous disk (Sharma et al. 2011; Grossi et al. 2011). Thanks to Spitzer satellite 24 μm data it has been possible to select Young Stellar Cluster candidates spanning 4 orders of magnitude, in bolometric luminosity, down to 10^{37} erg s^{-1} as faint as embedded B2-type stars. YSC mid-infrared photometry needs to be complemented with UV data from the GALEX satellite to estimate luminosities because M33 has a low dust content (Verley et al. 2009; Grossi et al. 2010). Moreover, AGB stars contribute to the faint 24 μm source population in M33 and need to be identified. The YSC mass and size are correlated with a log-log slope of 2.09, similar to that measured for giant molecular clouds in M 33 and the Milky Way, which represent the protocluster environment. Faint clusters make up a non negligible fraction of the total star formation rate of M33 but their masses and ages have large uncertainties due to the lower probability of finding hot stars compared to brighter counterparts. When the IMF is not fully populated up to its high mass end, stochastic sampling of the IMF can take place and hot stars are born randomly in some clusters (e.g. Corbelli et al. 2009). Stochasticity allows for example a 5×10^{39} erg s^{-1} luminous cluster to be made by a single "outliers", a 100 $M_\odot$ star, or by a more massive ensemble of small mass stars distributed according to a fully populated IMF up to about 30 $M_\odot$. If instead clusters are populated according to a truncated IMF, whose maximum stellar mass depends on cluster mass (Weidner and Kroupa 2006), no high mass stars can ever be formed in intermediate mass clusters. Large cluster samples can indeed be used to analyze the IMF at its high mass end using two integrated observables: the cluster bolometric and Hα luminosity. To test IMF sampling in YSC Corbelli et al. (2009) have introduced the concept of cluster birthline. The cluster birthline is the place in the log L_{bol} – log $L_{bol}/L_{H\alpha}$ plane where newborn young stellar clusters lie. If the stellar cluster is massive enough that the IMF is fully populated up to its high mass end, the ratio between the bolometric and Hα luminosity is constant and it does not depend on the cluster mass. For stars less massive than 20 $M_\odot$ the Hα luminosity drops with stellar mass much more quickly than the bolometric luminosity does. This implies that when the newly born cluster is small and very massive stars are lacking the birthline turns up towards higher values of log $L_{bol}/L_{H\alpha}$ and its exact shape depends on whether the IMF is stochastically sampled or truncated according to the cluster mass. An important property of the cluster birthline is that aging moves the clusters above it. This is because the death of massive stars makes the cluster Hα luminosity fade away more rapidly than the bolometric luminosity does. For a given IMF the cluster birthline is a theoretical lower boundary for the $L_{bol}/L_{H\alpha}$ ratio. In fact possible leakage or dust absorption of ionizing photons in the HII region increases the value of the observed $L_{bol}/L_{H\alpha}$ ratio. In Fig. 3 we compare the observed values of $L_{bol}/L_{H\alpha}$ ratio for an infrared selected sample of stellar clusters in M33 with the cluster birthline relative to the maximum mass case and to the case of a universal stochastically sampled IMF. As discussed by Corbelli et al. (2009) a stochastically sampled universal IMF is in better agreement with the data. Since 2009 there has been other evidence in favor of a stochastically

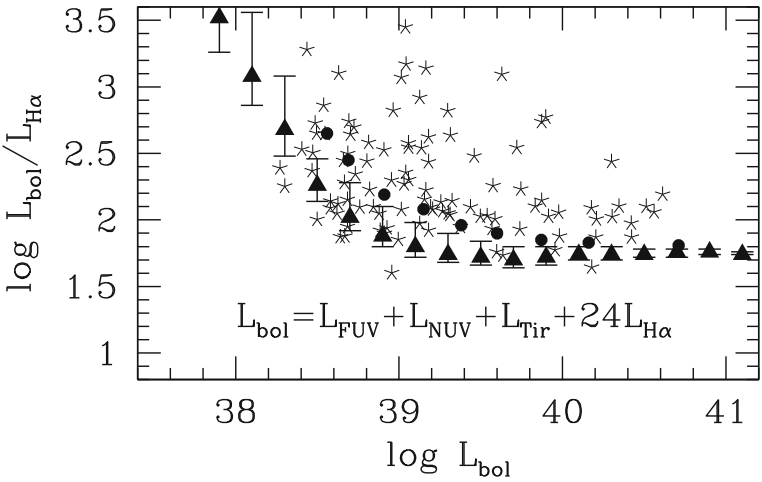

Fig. 3 The cluster birthline. Filled triangles show the resulting birthline for clusters with a stochastically sampled IMF while the filled dots are for clusters populated according to a truncated IMF with a maximum stellar mass. Clusters are born along the birthline and aging moves them upward. No clusters can be found below the birthline. Star symbols show the locations of a MIR selected sample of YSC in M33 in better agreement with a stochastic universal IMF

sampled IMF (e.g. Corbelli et al. 2011 for MIR sources embedded in CO clouds which lie along the birthline).

3 Disk Dynamics and Star Formation: From the Center to the Galaxy Outskirts

Moving up to larger scales one interesting issue is to look at the disk dynamics and instabilities which trigger star formation. M33 is a smaller, more quiescent and younger galaxy than M31; it is bulgeless and hosts a higher SFR per unit area and a more extended gaseous disk than the brighter Local Group spirals. Using extinction corrected UV and Hα maps we estimate a global SF rate in M 33 over the last 100 Myr to be 0.45 ± 0.10 $M_{\odot}$/yr (Verley et al. 2009). The SF rate declines radially with a scale length of about 2 kpc. The development of disk instabilities, with the consequent formation of new stars, has been widely studied by Bruce using a two component model (e.g. Elmegreen 1991, 1995, 2011; Hunter et al. 1998). Following Elmegreen's work and using azimuthal averages of the gas and stellar surface density (this last one from the dynamical analysis of the rotation curve) Corbelli (2003) has shown that Toomre and shear rate criteria are effective in explaining the drop in the SFR beyond 7 kpc, as indicated by the Hα surface brightness. But the proximity of M33 allows to go one step further. The number of surveys today available and the high resolution power for Local Group galaxies has stimulated the current effort of

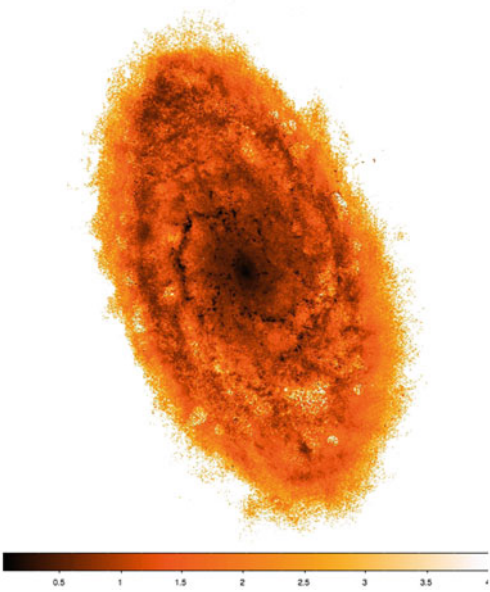

Fig. 4 A Q-map of the optical disk of M33. Darker regions are prone to instabilities and fragmentation. *Courtesy of C. Giovanardi*

one of my collaborator at Arcetri, C. Giovanardi, who has been looking at resonances and producing a full map of the instabilities in the M33 disk. This has been possible thanks to the stellar surface density map of the bright optical disk by synthesis models, to the new rotation curve, and to the dispersion map resulting from the 21-cm VLA database (Corbelli et al. 2014). A first analysis of the instability maps of M33 suggest that the shear rate criteria is more effective in the innermost regions and along the two bright spiral arms while in the rest of the optical disk unstable filaments according to the Toomre criterion with the use of the epicyclic frequency are in place. We show in Fig. 4 one example of the M33 disk instability map (Fig. 5, 6).

A weak small bar might be in the process of formation in the center but no clear evidence of a bulge has been found (Corbelli and Walterbos 2007). Further out several flocculent spiral arms form (Elmegreen 2003). Following the Tremaine and Weinberg (1984) method C. Giovanardi has determined the pattern speed to be about 17 km s^{-1} kpc^{-1} with no inner resonance, an outer resonance in the outer disk at about 12 kpc and corotation at 5.7 kpc. The stellar mass surface density map made via synthesis models using optical colors, highlights a steeper disk mass scalelength in the innermost kpc where the mass-to-light ratio is also higher. The mass-to-light ratio map is shown in Fig. 5 where local variations can be seen, such as the contrast between arm and interarm regions.

The outer disk of M33 is not a pure gaseous disk but host stars as well. There is not only evidence of an extended star-formation episode 2.5 $\sim$ Gyr ago but also of more recent ones: deep optical surveys have in fact revealed stars of about 200 Myr of age (Grossi et al. 2011) and MIR surveys have found evidence of possible star

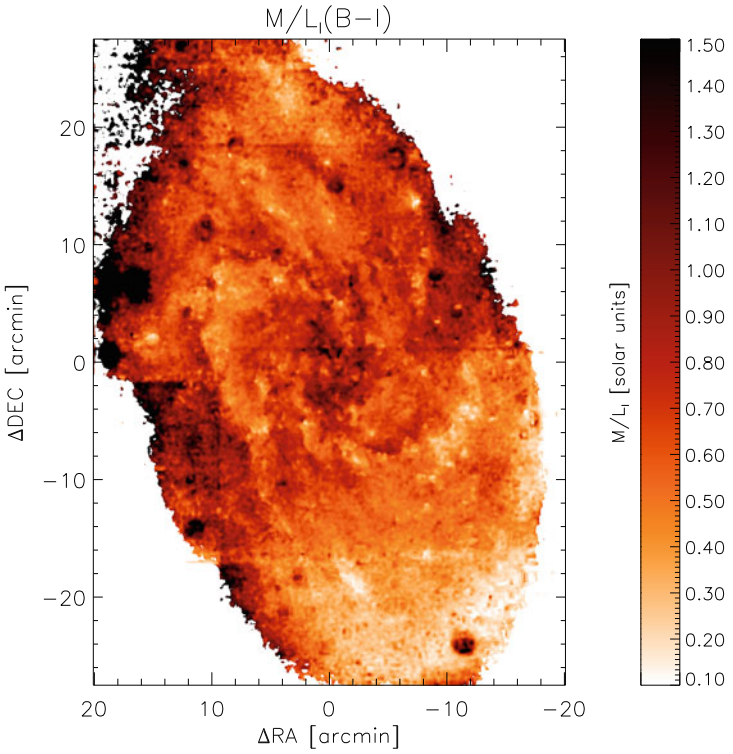

Fig. 5 The mass-to-light ratio map in the star forming disk of M33 from accurate stellar mass synthesis models of the light distribution observed by in several bands by Massey et al. (2006)

forming sites as young as 10 Myr (Sharma et al. 2011). It is likely that in the outer disk star formation is not persistent but major events occur in bursts triggered either by interactions or by gas accreting, as explained better in the next Section.

4 The Dark Halo and the Evolution of M33

The evolutionary history of M33 can be understood by selecting a chemical evolution model which reproduces the observed distribution of gas, star formation, metals etc. but also by pinning down the main characteristics of its dark matter halo. The halo is important not only because it provides a link to the cosmological model and to the galaxy formation process but also for understanding the past and future tidal interactions with other group members. It is still an open question whether galaxies like M33 will be refilled by accreting gas and keep on forming stars or else will be starving after a close encounter with a massive group member. The dynamical analysis of the rotation curve of M33, recently traced by Corbelli et al. (2014), has

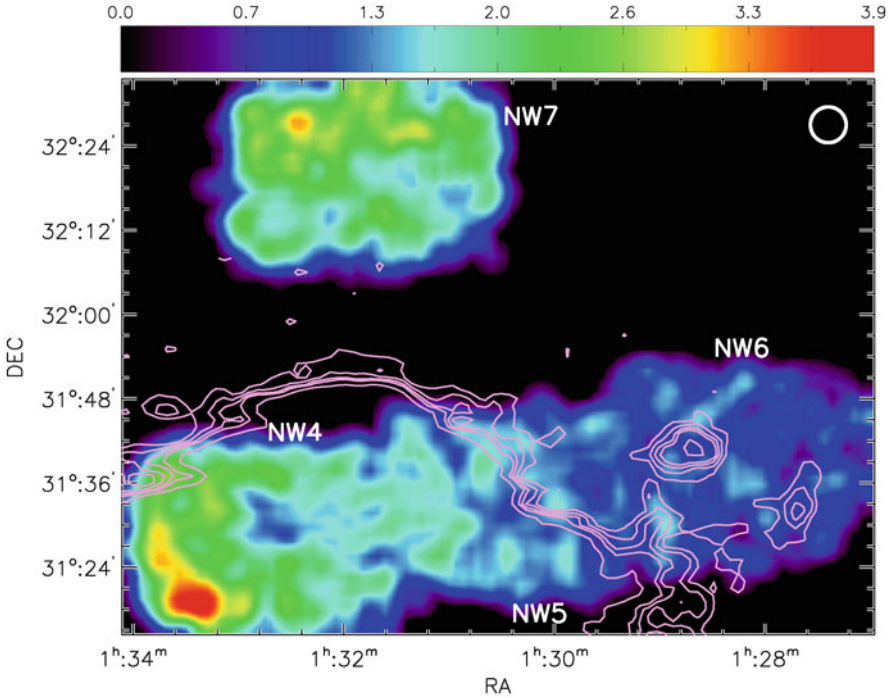

Fig. 6 The distribution of stars in the northern part of the outer disk. As discussed by Grossi et al. (2011) in the outer disk there is evidence of an intermediate age stellar population with a scalelength similar to that of the local atomic gas counterpart

shown unambiguously that a dark matter halo with a Navarro-Frenk-White (Navarro et al. 1997) density profile, mass and concentration as predicted by hierarchical clustering and structure formation in a ΛCDM cosmology (Maccio' et al. 2008), is in place. Dark matter is relevant at all radii in shaping the rotation curve and the most likely dark halo has a concentration C$\simeq$10 and a total mass of 4.3($\pm$ 1.0) 10^{11} $M_{\odot}$. This, given the stellar and gaseous mass maps, implies a baryonic fraction of order 0.02 and the evolutional history of this galaxy should account for loss of a large fraction of its original baryonic content. The low baryonic fraction of M33 is puzzling in the frame of the most recent picture that emerged from the proper motion measurements of M31 and M33 and of the satellite plane found around M31. These findings imply that M33 is now approaching M31 and has not been already disrupted by M31 tidal forces (van der Marel et al. 2012; Shaya and Tully 2013). Hence the low baryonic fraction should result from an internal removal mechanism such as outflows or from some mechanism that prevented the collapse of a large gas fraction into the disk. The recent estimate of the average galaxy baryonic content as a function of halo mass, as from the halo to stellar luminosity function matching technique, underline the fact that galaxies with the same halo mass as M33 do indeed have a similar low baryonic content (Moster et al. 2010, 2013). The halo mass we

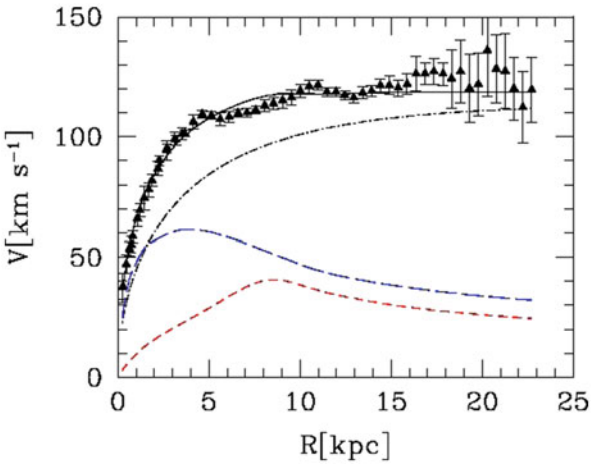

Fig. 7 The rotation curve of M33 from CO (FCRAO) and HI (VLA) data with the best fitting ΛCDM dark halo model (*dot-dashed line*), the stellar and gas (*long and short dashed lines respectively*) contributions to it. The stellar mass map with its error bars has been used to compute the stellar contribution to the rotation curve and the molecular gas surface density has been added to the atomic gas distribution (Corbelli et al. 2014)

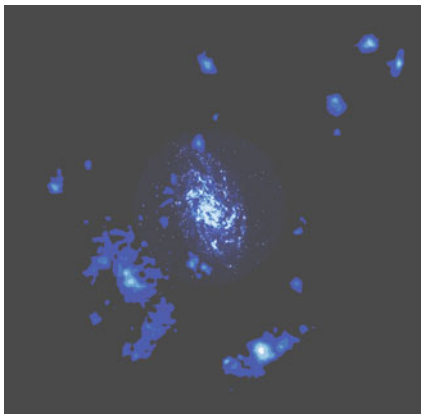

Fig. 8 The HI clouds in the circumgalactic medium of M33 observed with the Arecibo telescope by Grossi et al. (2008) overplotted on the GALEX image of the star forming disk of the galaxy

find for M33 is sufficiently high to prevent a softening of the dark matter cusp due to past outflows from the nuclear region of M33 (di Cintio et al. 2014).

For the halo mass of M33 it is still possible to have accretion from cosmic filaments at z = 0 to fuel star formation. Grossi et al. (2008) have found HI clouds associated with the circumgalactic medium of M33 which follow the rotational pattern of the galaxy. Given the low observed HI column densities, these clouds are likely to be highly ionized by the extragalactic ultraviolet radiation and the total gas mass associated with them is $> 5x10^7$ $M_\odot$. If the gas is steadily falling towards the M33 disc, (there are signs of non circular motion in the outer disk with amplitude of 10 km s^{-1}) it can provide the fuel needed to sustain the current star formation rate. The unlikely occurrence of a closer encounter between M33 and M31 in the past does not support their tidal origin, and the absence of stellar structures within the clouds (Grossi et al. 2011) supports their association with the neutral parts of cosmic filaments which cool and recombine after entering the potential well of M33.

The gas accreting into the outer disk has its angular momentum aligned with the cosmic filaments, tilted with respect to the inner disk which formed early on. The chemical evolution model of M33, which reproduces the metallicity gradient and its time evolution, the baryonic distribution and the star formation rate in this galaxy (Magrini et al. 2010) require a slow gas accretion rate through cosmic time (Fig. 7, 8).

References

Corbelli, E. 2003, MNRAS, 342, 199
Corbelli, E. and Walterbos, R. A. M. 2007, ApJ, 669, 315
Corbelli, E., Verley, S., Elmegreen B. G. and Giovanardi, C. 2009, A&A, 495, 479
Corbelli, E., Giovanardi, C., Palla, F., and Verley, S. 2011, A&A, 528, 116
Corbelli, E., Thilker, D., Giovanardi, C., Zibetti, S. and Salucci, P. 2014, A&A, submitted
Di Cintio, A., Brook, C. B., Macciò, A. V. Stinson, G. S., Knebe, A., Dutton, A. A., and Wadsley, J. 2014, MNRAS, 437, 415
Elmegreen, B. G. 1991, ApJ, 378, 139
Elmegreen, B. G. 1995, MNRAS,. 275, 944
Elmegreen, B. G. 2011, ApJ, 737, 10
Elmegreen, B. G., Leitner, S. N., Elmegreen, D. M. and Cuillandre, J.-C. 2003, ApJ, 593, 333
Grossi, M., Giovanardi, C., Corbelli, E., Giovanelli, R., Haynes, M. P., Martin, A. M., Saintonge, A. and Dowell, J. D. 2008, A&A, 487, 161
Grossi, M., Corbelli, E., Giovanardi, C. and Magrini, L. 2010, A&A, 521, 41
Grossi, M., Hwang, N., Corbelli, E., Giovanardi, C., Okamoto, S., and Arimoto, N. 2011, A&A, 533, 91
Hunter, D. A. and Elmegreen, B. G. and Baker, A. L., 1998, ApJ, 493, 595
Macciò, A. V. and Dutton, A. A. and van den Bosch, F. C. 2008, MNRAS, 391,1940
Magrini, L. and Stanghellini, L. and Corbelli, E. and Galli, D. and Villaver, E., 2010, A&A, 512, 63
Massey, P. and Olsen, K. A. G. and Hodge, P. W. and Strong, S. B. and Jacoby, G. H. and Schlingman, W. and Smith, R. C., 2006, AJ, 131, 2478
Moster, B. P., Somerville, R. S., Maulbetsch, C., van den Bosch, F. C., Macciò, A. V., Naab, T. and Oser, L. 2010, ApJ, 710, 903
Moster, B. P., Naab, T., and White, S. D. M. 2013, MNRAS, 428, 3121
Navarro, J. F., Frenk, C. S., and White, S. D. M. 1997, ApJ, 490, 493
Sharma, S., Corbelli, E., Giovanardi, C., Hunt, L. K. and Palla, F. 2011, A&A, 534, 96
Shaya, E. J. and Tully, R. B. 2013, MNRAS. 436, 2096
Tremaine, S. and Weinberg, M. D., 1984, ApJ, 28, 5
Verley, S., Corbelli, E., Giovanardi, C. and Hunt L. K. 2009, A&A 493, 453
Weidner, C. and Kroupa, P. 2006, MNRAS, 365, 1333
van der Marel, R. P., Besla, G., Cox, T. J., Sohn, S. T., and Anderson, J. 2012, ApJ, 753, 9

Depicting the Early Evolution of Globular Clusters Through the Lens of Multiple Stellar Populations

Corinne Charbonnel

Abstract A major paradigm shift has recently revolutionized the classical picture depicting globular star clusters (GC) as simple systems of coeval stars born out of homogeneous material. Indeed, detailed spectroscopic studies of GC long-lived low-mass stars performed with 8–10 m class telescopes, together with high-precision photometry of Galactic GCs obtained with HST, have brought compelling evidences on the presence of multiple stellar populations in individual GCs. These stellar subgroups can be recognized thanks to their different chemical properties (more precisely by abundance differences of light elements from carbon to aluminium) and in some cases by the appearance of multimodal sequences in the GC colour-magnitude diagrams. These findings have opened unexpected roads to do GC archeology. They provide in particular invaluable clues on the possible ways massive stars have shaped the intra-cluster medium evolution (ICM) and induced secondary star formation in the very early evolution of these fantastic objects. Here we first recall what are the main chemical properties of the long-lived low-mass stars observed today in GCs. Then we summarize the implications for the initial mass of the GCs, as well as for their contribution to field star populations and to cosmic reionisation. Finally we recall the detailed timeline proposed by Krause et al. (Astron Astrophys 546(L5) 2012, Astron Astrophys 552(A121) 2013) for the first 40 Myrs in the lifetime of a typical GC following the general ideas of our so-called "Fast Rotating Massive stars scenario" and taking into account the dynamics of interstellar bubbles produced by stellar winds and supernovae.

1 Chemical Properties of Multiple Stellar Populations in GCs

Today, globular star clusters (GC) contain only old low-mass stars, the chemical properties of which have been intensively scrutinized thanks to high-resolution spectroscopic instruments on 8–10 m telescopes. Significant star-to-star abundance

C. Charbonnel (✉)
Department of Astronomy, University of Geneva, CH 1290 Versoix Geneva, Switzerland
e-mail: Corinne.Charbonnel@unige.ch

CNRS UMR 5277 IRAP, University of Toulouse, 31400 Toulouse, France
Tel.: + 41-22-3792452

K. Freeman et al. (eds.), *Lessons from the Local Group,*
DOI 10.1007/978-3-319-10614-4_16

variations of light elements (from C to Al) are found in all Galactic GC. In particular, the systematic presence in each GC studied so far of the well-documented O-Na anti-correlation is now commonly used to differentiate between the so-called first- and second-generation GC stars (hereafter 1G and 2G; e.g. Prantzos and Charbonnel (2006); Carretta et al. (2009); Carretta (2013), see also D'Orazzi, this volume). Together with the Mg-Al anticorrelation, it is the signature of hydrogen-burning at high temperature of the order of ~ 75 MK.

These chemical features are observed both in main sequence and red giant GC stars that do not reach such high internal temperatures. Therefore, they must have been inherited by the low-mass stars at the time of their birth, and produced in massive, fast-evolving 1G GC stars (hereafter referred to as polluters), which ejecta (depleted in oxygen and enriched in sodium, aluminum, and helium) mixed to various degrees with original intracluster material and gave birth to 2G stars (e.g. Prantzos et al. 2007).

2 General Implications on the GC IMF, and on the GC Contribution to the Stellar Halo and to Cosmic Reionisation

Different scenarii of secondary star formation invoke different types of 1G polluters, namely fast rotating massive stars (25-120 $M_{\odot}$, hereafter FRMS; Maeder and Meynet (2006); Prantzos and Charbonnel (2006); Decressin et al. (2007a); Krause et al. (2013)) on one hand, and massive asymptotic giant branch stars (6-11 $M_{\odot}$, AGB; Ventura et al. (2001); Ventura et al. (2013); D'Ercole et al. (2010); Ventura and D'Antona (2011)) on the other hand. In some cases the possible contribution of massive binary stars is also considered (de Mink et al. (2009); Izzard et al. (2013)), as well as that of FRMS paired with AGB stars (Sills and Glebbeek 2010), and of FRMS paired with high-mass interactive binaries (Bastian et al. (2013); Cassisi and Salaris (2014)).

Whatever the actual polluting stars, an immediate consequence of the self-enrichment scenario is that, in order to reproduce the present proportion of 1G to 2G stars (being today typically 30–70 %) with acceptable values of the polluters IMF, the initial stellar masses of GCs must have been considerably larger than their present-day value (Prantzos and Charbonnel (2006); Decressin et al. (2007b); D'Ercole et al. (2008); Decressin et al. (2010a); Carretta et al. (2010); Schaerer and Charbonnel (2011)).

Schaerer and Charbonnel (2011) have explored in detail a dynamical scenario that allows for the loss of stars from the 1G and possibly 2G, and showed that:

(1) The initial stellar masses of GCs must have been $\sim$ 8–10 times larger than the current (observed) mass, when no 2G stars were lost from the GCs (see also Prantzos and Charbonnel (2006); Carretta et al. (2010).) If 2G halo stars originated from the present population of GCs, as suggested by observations finding stars characteristics of the 2G in the Milky Way halo (Carretta et al. (2010); Martell and Grebel (2010)), the initial cluster masses must have been $\approx$ 25 times larger than the current masses.

(2) The mass in low-mass stars ejected from GCs must be $\sim 2.5-3.2$ times their presently observed value if all 2G stars were retained by the GC, or $\sim$ 5–10 times the present day mass if 2G stars were lost. These numbers translate to a contribution of 5–8 or 10–20 % respectively of the ejected low-mass stars to the Galactic stellar halo mass.

(3) The observations of 2G stars in the Galactic halo can also be used to constrain the initial mass function of the GC population (GCIMF). In particular the often assumed power-law with a slope $\beta \approx -2$ is in contradiction with recent determinations of the fraction of 2G stars in the halo, whereas a log-normal GCIMF is compatible with these observations. This finding revived the question about a common mass function and about the physical processes leading to a distinction between GCs with multiple stellar populations and other clusters.

(4) Due to their high initial masses, the amount of Lyman continuum photons emitted by GCs during their youth must have been substantial, reinforcing the conclusion of Ricotti (2002) that GCs should have significantly contributed to reionise the IGM at high redshift (above ~ 6).

3 Timeline for the First 40 Myrs in the Lifetime of a Typical GC in the Framework of the FRMS Scenario

Here we summarize the results presented in Krause et al. (2012, 2013) who revisited the FRMS scenario that successfully explains the observed abundance patterns of present-day "typical" GCs like e.g. NGC 6752 (i.e., where no star-to-star [Fe/H] abundance variations is observed). This model has also been tested with N-body simulations (see Decressin et al. 2010b). The initial mass of such a GC must have been of the order of 9×10^6 $M_\odot$, with a half-mass radius of $\sim$ 3 pc, and a star formation efficiency of 30 %. Such a cluster must therefore have hosted $\sim$ 5700 1G massive stars (with masses above 25 $M_\odot$) under the assumption of a Salpeter IMF for 1G stars more massive than 0.8 $M_\odot$ (note that we assume a log-normal IMF for 1G and 2G stars of lower mass). Krause et al. (2013) take into account the dynamics of interstellar bubbles produced by stellar winds and supernovae as well as the interactions of FRMS with the ICM and follow the kinematics with a thin-shell model. The first 40 Myrs of the evolution of the GC (the initial time being set at the assumed coeval birth of 1G stars) can then be described with three distinct phases discussed below and depicted in Fig. 1.

3.1 Wind Bubble Phase and 2G Star Formation

During the very first Myrs after the formation of the 1G, the cluster is strongly impacted by the fast radiative winds of the numerous massive stars (1st and 2nd row in Fig. 1). Because their integrated energy is much smaller than the ICM's

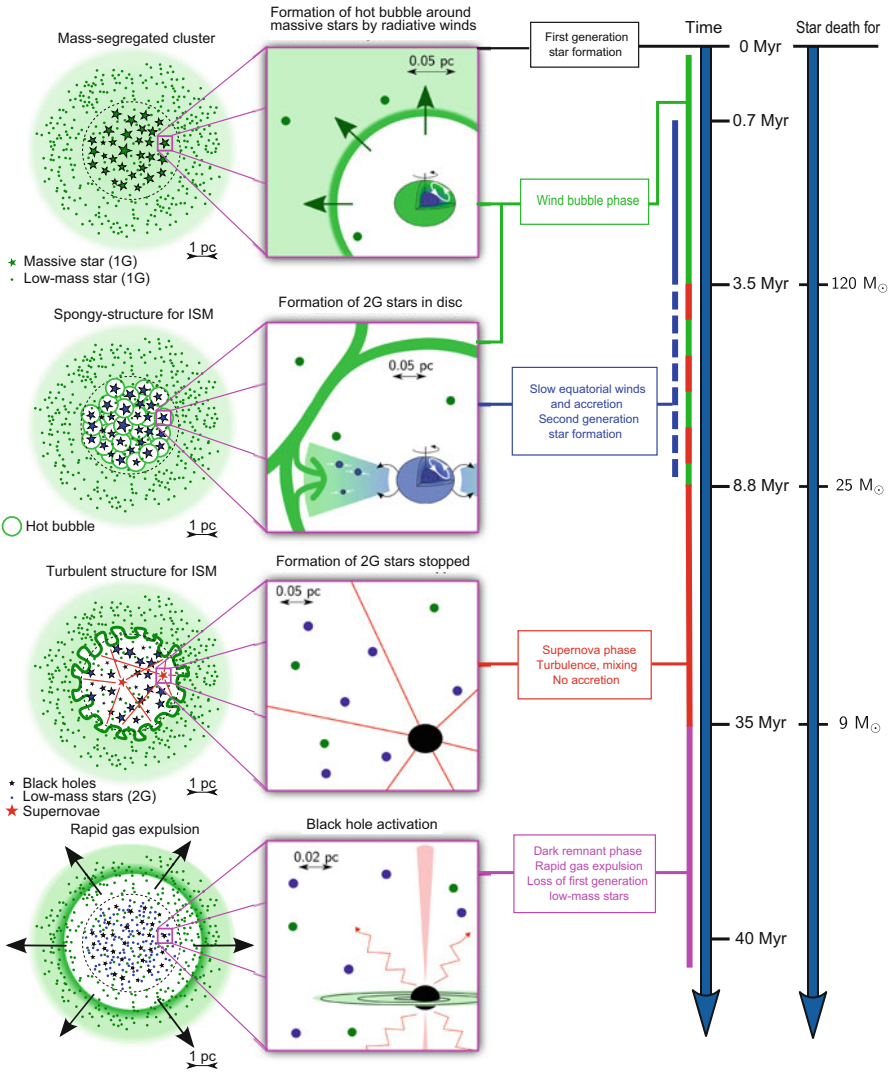

Fig. 1 Sketch of the first 40 Myrs of evolution of a two-generations GC according to the model proposed by Krause et al. (2013). The global timeline (*top to bottom*) and the associated time when the stellar life ends for selected stars are shown on the *right*. The *leftmost* column shows the global evolution of the whole GC. The second column from the *left* represents a zoom on to a FRMS. Four important stages are depicted. *First row from top:* First a mass segregated star cluster is formed with all the FRMS inside the half-mass radius (*dashed line*) and with the initial gas (*light pistachio green shade*) remaining after the star formation. Each massive star (the *blue* interior signifies the convective hydrogen burning core, the *bright forest green envelope* depicts the convective envelope, which has still the pristine composition at this stage) creates a hot bubble around it. The corresponding wind shell is shown in a *darker shade of green* than the uncompressed gas. *Second row:* All the hot bubbles connect and create a spongy-structure in the centre. At the same time, slow mechanical winds around the FRMS create a disk around them. The *outer* envelope of the FRMS is now *blue* to denote that it has been contaminated by hydrogen burning products. In

binding energy, those winds can not lift any noteworthy amount of gas out of the GC (Krause et al. 2012). However they are expected to create large hot bubbles around massive stars and to compress the ICM into thin filaments. Additionally in this environment "classical" star formation is inhibited by the high Lyman-Werner flux (see also Conroy and Spergel (2011)) during the wind bubble phase as well as the subsequent supernova phase described below.

However if massive stars have equatorial mass ejections that form decretion disks as originally proposed in the FRMS scenario (Decressin et al. (2007b); Krtička et al. (2011)) and as observed e.g. around Be-type stars (see e.g. Rivinius et al. (2001); Townsend et al. (2004); Haubois et al. (2012)), accretion of pristine gas may proceed in the shadow of the equatorial stellar ejecta (2d row in Fig. 1). Even if a substantial fraction of the power of the dominantly polewards-directed (because of rotation) fast wind would be channeled into the decretion disks, this would still be insufficient to unbind them from their parent stars. Similarly, close encounters with other stars at sufficiently small impact parameter are too unlikely to affect the disks significantly on an interesting timescale. 2G low-mass stars are then expected to form due to gravitational instability in the discs around 1G massive stars, those disks being fed both by the H-burning ashes ejected by the FRMS and by pristine gas.

The total amount of gas that is made available to form 2G stars through this non-classical mode and with abundance properties similar to those observed today is high. Indeed Decressin et al. (2007b) models predict that FRMS lose about half of their initial mass via equatorial ejections loaded with H-burning products during the main sequence and the luminous variable phase. As a consequence about ~ 1 Myr after the birth of the 1G, the total mass lost through this mechanism by all the FRMS is of the order of 10^4 $M_\odot$/Myr. On the other hand a similar amount of pristine gas is expected to be brought by the accretion flow, with mixing proportions depending on the FRMS orbit-averaged accretion rate. 2G stars will therefore form with the current light element abundances of the self-gravitating disk of their massive 1G parent star, in agreement with the detailed abundance calculations of Decressin et al. (2007b) that reproduce nicely the observed [O/Na] distribution in the typical GC NGC 6752.

The formation of 2G low-mass stars is expected to be complete after $\sim$ 9–10 Myrs (i.e., roughly the lifetime of a 25 $M_\odot$ star) after the formation of the 1G. Note however that the duration of the wind bubble phase is rather uncertain since it depends on the mass limit (and therefore on the lifetime) at which stars explode as SNe or turn silently into black holes, which value is not settled yet.

←

Fig. 1 (continued) the interaction between the ejected disc (*blue*) and the accreting interstellar medium (*ISM*, *green*), a 2G of chemically different stars is born (*blue filled circles*). *Third row:* SNe (*red stars* with *straight lines*) fail to eject the gas but create a highly turbulent convection zone. Further accretion on to the remaining FRMS discs is inhibited. The equatorial ejections also end around this time and the formation of the second generation stars is completed by about 10 Myrs on the global time axis. *Bottom row:* Later, rapid gas expulsion takes place and removes all the remaining gas together with the majority of the less tightly bound first generation stars out of the cluster potential well. Such rapid gas expulsion is likely to be due to the activation of black holes by accretion of matter. Figure and caption are taken from Krause et al. (2013)

3.2 Supernova Phase

Krause et al. (2012) showed that gas expulsion via supernovae explosions, which is generally invoked to drastically change the GC potential well and to induce substantial loss of 1G stars (Decressin et al. (2007a); Bekki et al. (2007); D'Ercole et al. (2008); Schaerer and Charbonnel (2011)) does not work for typical GCs. Indeed, while the energy released by SNe usually exceeds the binding energy, SNe-driven shells turn out to be destroyed by the Rayleigh-Taylor instability before they reach escape speed; therefore the shell fragments that contain the gas remain bound to the cluster.

Although the SNe-ejecta will likely be mixed with the cold phase of the ICM, they are not expected to appear in the composition of 2G stars. Indeed once the first very energetic SNe explode, the ICM becomes highly turbulent and, since the Bondi-accretion rate depends on v^3, where v is the relative velocity between the star and the local ICM, can not be accreted anymore onto FRMS decretion disks nor (yet) onto any dark remnants that are being continuously produced (i.e., stellar black holes from stars initially more massive than 25 $M_\odot$ stars and later neutron stars from initially less massive stars). The SNe phase is therefore expected to be sterile as far as star formation is concerned (3d row in Fig. 1).

3.3 Dark Remnant Accretion Phase

The FRMS and the AGB scenario strongly differ on many aspects of the early dynamical and chemical evolution of the young GCs. They both agree however on the fact that GCs must have been much more massive initially than today and call for substantial loss of 1G low-mass stars in order to explain todays observed proportions between 1 and 2G stars (Carretta et al. 2010; Schaerer and Charbonnel 2011). Within the framework of the AGB cooling flow scenario, this powerful event is expected to occur before the formation of 2G stars. At the opposite, 2G stars are expected to form much earlier in the FRMS scenario.

Krause et al. (2012) proposed that very fast gas expulsion, which is expected to unbind a large fraction of 1G low-mass stars sitting initially in the GC outskirts, may be powered by the sudden and concomitant activation of 1G dark-remnants (i.e., 1.5 $M_\odot$ neutron stars from stars with masses between 10 and 25 $M_\odot$, and stellar mass black holes with 3 $M_\odot$ from more massive stars; 4th row in Fig. 1). Accretion of interstellar gas onto these objects can set in only once turbulence has sufficiently decayed in the ICM after the type II SNe have ceased, i.e. about 35–40 Myrs (corresponding to the lifetime of a 9 $M_\odot$ star) after the coeval birth of 1G stars. Assuming coherent onset of accretion onto all the 1G stellar remnants and considering that they could contribute to gas energy at 20% of their Eddington luminosity, Krause et al. (2012) showed that a sufficient amount of energy is released in at most 0.06 Myrs (i.e., about half a crossing time), which is short enough to avoid

gas fall back due to Rayleigh–Taylor instability and to eject the ICM together with the outer weakly bound 1G low-mass stars.

After the major expulsion event described above, the cluster is expected to be devoid of pristine gas. However the dark remnants may be reactivated later, this time through the eventual accretion of slow-AGB winds. When this happens we expect again quick gas expulsion, which would inhibit any subsequent star formation from the AGB ejecta. This situation is alike the possible activation of super-massive black holes in nuclear star clusters and elliptical galaxies by AGB-winds (e.g. Davies et al. (2007); Schartmann et al. (2010); Gaibler et al. (2012)).

Importantly, Krause et al. (2012) find a limiting initial cloud mass of $\sim 10^7$ $M_\odot$ for the dark remnant scenario to work. Above that mass, the cold pristine gas may not be ejected, and subsequent star formation may proceed in the ICM that would then be enriched in SNe ejecta. This can explain the fact that the more massive (and atypical) GCs (Omega Cen, M22, M54, NGC 1851, NGC 3201; Carretta et al. (2010); Johnson and Pilachowski (2010); Marino et al. (2011); Simmerer et al. (2013)) do exhibit internal [Fe/H] spread, while less massive (typical) ones do not.

4 Conclusions and Perspectives

After the tremendous paradigm shift that has recently revolutionized our view of GCs, new observational and theoretical advances make the present a particularly exciting time for the study of the origin, formation, and evolution of these objects in the Milky Way as well as in external galaxies.

On the theoretical front one of the fundamental issues concerns the physics of the interstellar medium and its interactions with stars. Also, the formation of 2G stars in massive disks fed by both equatorial ejections of parent FRMS and accretion of pristine gas has to be studied in details. Cutting-edge strategies have to be established in order to tackle the open issues from an innovative point of view. In particular, relevant multi-dimensional MHD simulations would greatly help in clarifying details of chemical and dynamical feedback of 1G massive stars and of secondary star formation. Work is in progress in that direction.

Celebrating fifty years of spiral density waves at the Lin-Shu Symposium held at the Tsinghua University in Beijing, China. From left to right are Bruce Elmegreen, Frank Shu, David Block and Debbie Elmegreen. The bust depicts C.C. Lin. Photo: Matthew Woolway.

Acknowledgement I acknowledge support from the Swiss National Science Foundation (FNS), from the ESF EUROCORES Programme "Origin of the Elements and Nuclear History of the Universe", and from ISSI (Berne, ISSI Team 271 "Massive Star Clusters across the Hubble time"). I warmly thank all my collaborators on the GC project, mainly N. Prantzos, M. Krause, G. Meynet, T. Decressin, and D. Schaerer with whom the FRMS scenario was developed.

References

Bastian N., Lamers H. J. G. L. M., de Mink S. E., Longmore S. N., Goodwin S. P., Gieles M., 2013, MNRAS, 436, 2398

Bekki K., Campbell S. W., Lattanzio J. C., Norris J. E., 2007, MNRAS, 377, 335

Carretta E., 2013, A&A, 557, A128

Carretta E., Bragaglia A., Gratton R. G., Lucatello S., Catanzaro G., Leone F., Bellazzini M., Claudi R., D'Orazi V., Momany Y., Ortolani S., Pancino E., Piotto G., Recio-Blanco A., Sabbi E., 2009, A&A, 505, 117

Carretta E., Bragaglia A., Gratton R. G., Recio-Blanco A., Lucatello S., D'Orazi V., Cassisi S., 2010, A&A, 516, A55

Cassisi S., Salaris M., 2014, A&A, 563, A10
Conroy C., Spergel D. N., 2011, ApJ, 726, 36
Davies R. I., Müller Sánchez F., Genzel R., Tacconi L. J., Hicks E. K. S., Friedrich S., Sternberg A., 2007, ApJ, 671, 1388
de Mink S. E., Pols O. R., Langer N., Izzard R. G., 2009, A&A, 507, L1
Decressin T., Charbonnel C., Meynet G., 2007a, A&A, 475, 859
Decressin T., Meynet G., Charbonnel C., Prantzos N., Ekström S., 2007b, A&A, 464, 1029
Decressin T., Meynet G., Charbonnel C., 2010a, in Charbonnel C., Tosi M., Primas F., Chiappini C., eds, IAU Symposium Vol. 268 of IAU Symposium, Helium-rich stars in globular clusters: constraints for self-enrichment by massive stars. pp 135–140
Decressin T., Baumgardt H., Charbonnel C., Kroupa P., 2010b, A&A, 516, A73
D'Ercole A., Vesperini E., D'Antona F., McMillan S. L. W., Recchi S., 2008, MNRAS, 391, 825
D'Ercole A., D'Antona F., Ventura P., Vesperini E., McMillan S. L. W., 2010, MNRAS, 407, 854
Gaibler V., Khochfar S., Krause M., Silk J., 2012, MNRAS, 425, 438
Haubois X., Carciofi A. C., Rivinius T., Okazaki A. T., Bjorkman J. E., 2012, ApJ, 756, 156
Izzard R. G., de Mink S. E., Pols O. R., Langer N., Sana H., de Koter A., 2013, Mem. Soc. Astron. Italiana, 84, 171
Johnson C. I., Pilachowski C. A., 2010, ApJ, 722, 1373
Krause M., Charbonnel C., Decressin T., Meynet G., Prantzos N., Diehl R., 2012, A&A, 546, L5
Krause M., Charbonnel C., Decressin T., Meynet G., Prantzos N., 2013, A&A, 552, A121
Krtička J., Owocki S. P., Meynet G., 2011, A&A, 527, A84
Maeder A., Meynet G., 2006, A&A, 448, L37
Marino A. F., Sneden C., Kraft R. P., Wallerstein G., Norris J. E., da Costa G., Milone A. P., Ivans I. I., Gonzalez G., Fulbright J. P., Hilker M., Piotto G., Zoccali M., Stetson P. B., 2011, A&A, 532, A8
Martell S. L., Grebel E. K., 2010, A&A, 519, A14
Prantzos N., Charbonnel C., 2006, A&A, 458, 135
Prantzos N., Charbonnel C., Iliadis C., 2007, A&A, 470, 179
Ricotti M., 2002, MNRAS, 336, L33
Rivinius T., Baade D., Štefl S., Maintz M., 2001, A&A, 379, 257
Schaerer D., Charbonnel C., 2011, MNRAS, 413, 2297
Schartmann M., Burkert A., Krause M., Camenzind M., Meisenheimer K., Davies R. I., 2010, MNRAS, 403, 1801
Sills A., Glebbeek E., 2010, MNRAS, 407, 277
Simmerer J., Ivans I. I., Filler D., Francois P., Charbonnel C., Monier R., James G., 2013, ApJL, 764, L7
Townsend R. H. D., Owocki S. P., Howarth I. D., 2004, MNRAS, 350, 189
Ventura P., D'Antona F., 2011, MNRAS, 410, 2760
Ventura P., D'Antona F., Mazzitelli I., Gratton R., 2001, ApJL, 550, L65
Ventura P., Di Criscienzo M., Carini R., D'Antona F., 2013, MNRAS, 431, 3642

Globular Clusters and Two Phase Galaxy Formation: The Milky Way and Beyond

Jean P. Brodie and Aaron J. Romanowsky

Abstract The SLUGGS (SAGES Legacy Unifying Globular clusters and GalaxieS) survey uses Subaru Suprime-Cam and Keck DEIMOS to obtain 2-D kinematic and metallicity maps for 25 nearby early type galaxies out to, typically, 2-3 R_e for galaxy starlight, and 8-10 R_e for globular clusters. While other surveys have much larger galaxy samples, the SLUGGS "claim to fame" is its unprecedentedly wide field coverage coupled with exquisite velocity resolution ($\sim$12 km s^{-1}). We find strong evidence for 2-phase, or inside out, galaxy formation; major mergers do not appear to have played a dominant role in forming the majority of galaxy bulges. As a spin-off from the main survey we are discovering a significant number of novel objects. These can be loosely classified as UCDs (ultra compact dwarfs), although they occupy areas of size–luminosity–density parameter space hitherto unexplored. Many appear to be the remnant nuclei of stripped galaxies, and may thus be important for "cosmic accounting". Observations are nearing completion and already nearly 40 papers have been published using data from the survey (see http://sluggs.ucolick.org for a list of publications and collaborators).

1 Introduction

The two-phase paradigm of galaxy formation has become popular as a result of observations of significant size evolution of galaxies over the last $\sim$ 10 billion years (e.g., Daddi et al. (2005); van Dokkum et al. (2009)), coupled with theoretical predictions (e.g., Oser et al. (2010); Porter et al. (2014)). The notion that galaxies form as nuggets at z$\sim$2 (the *in-situ* component) and then grow by the continuous accretion of smaller satellite galaxies until the present can best be tested with wide-field observations, since >90 % of the total mass and angular momentum reside beyond one effective radius (R_e), as illustrated in Fig. 1. Globular clusters (GCs) are predominantly old (>10 Gyr) and are bright enough to be observable out to

J. P. Brodie (✉) · A. J. Romanowsky
University of California Observatories, 1156 High Street, Santa Cruz, CA 95064, USA
e-mail: brodie@ucolick.org

A. J. Romanowsky
Department of Physics and Astronomy, San José State University, San Jose, CA 95192, USA

K. Freeman et al. (eds.), *Lessons from the Local Group,*
DOI 10.1007/978-3-319-10614-4_17

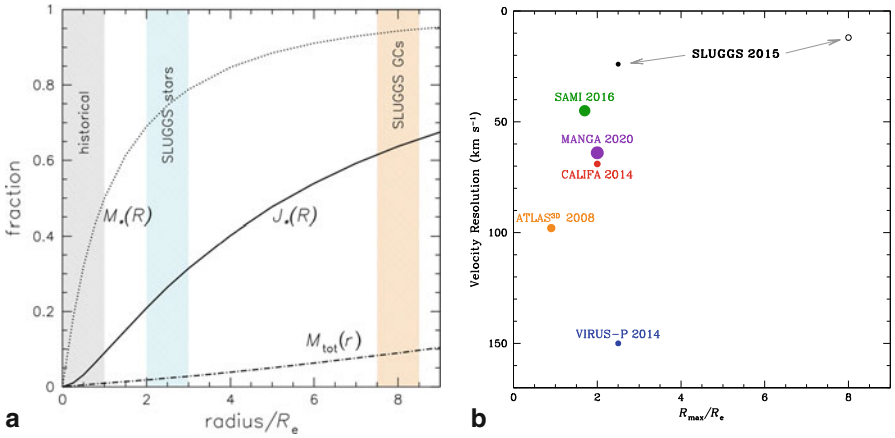

Fig. 1 Left panel: Cumulative fraction of physical quantities versus radius in an ordinary elliptical galaxy. The galaxy is approximated as a very simple $R^{1/4}$ projected density profile with a rotation velocity that is constant with radius. The projected stellar mass and angular momentum profiles are thus shown as $M_*(R)$ and $J_*(R)$. The total mass profile including dark matter, $M_{\rm tot}(r)$ is derived from cosmologically-based models. The shaded area at left reaches out to one effective radius, the typical extent of detailed galaxy kinematics studies to date, which therefore miss ~ 50 % of M_*, ~ 90 % of J_*, and ~ 99 % of $M_{\rm tot}$. The other shaded areas show the radii reached by the SLUGGS survey (see description in the Introduction) - capturing much larger fractions of these important parameters. Right panel: SLUGGS survey figure of merit from Brodie et al. (2014). Instrumental velocity resolution (σ) is plotted (with superior resolution at the top) vs. maximum galactocentric radial extent for a typical survey galaxy, in units of effective radii. The symbols show the different 2-D chemodynamical surveys with their data completion dates indicated in the legend. Symbols are scaled by the log of the number of early-type galaxies surveyed. The open circle represents the globular cluster aspect of the SLUGGS survey. SLUGGS is complementary to previous, or currently underway, 2-D spectroscopic surveys; it covers a more limited number of galaxies but offers better radial coverage and higher velocity resolution.

large galactocentric radii, with GC spectroscopy feasible for galaxies as distant as $\sim$50 Mpc. As such they are bright fossils that are "along for the ride" during all the mergers and acquisitions that build the galaxies we see today.

In addition to being bright, old and associated with galaxies of all morphological types, the GC systems of most bright galaxies are bimodal in color, reflecting bimodality in their metallicity distributions, as illustrated in the left panel of Fig. 2 from Brodie et al. (2012). The red (metal rich, MR) and blue (metal poor, MP) GC subpopulations in galaxies also display distinct kinematics (Pota et al. (2013) – two examples are shown in the right panel of Fig. 2), and are thought to trace the build up of galaxy bulges and halos, respectively (see Brodie & Strader (2006), and references therein). The presumption is that the blue GCs are slightly older than the red ones, but our ability to measure age in extragalactic GCs is limited to about $\pm 1 - 2$ Gyr. Since the difference between a redshifts of formation of 8 and 3 is only $\sim$1 Gyr, this is an important limitation on our ability to verify GC origins. Recently, however, Hansen et al. (2013) used White Dwarf (WD) cooling sequences to show

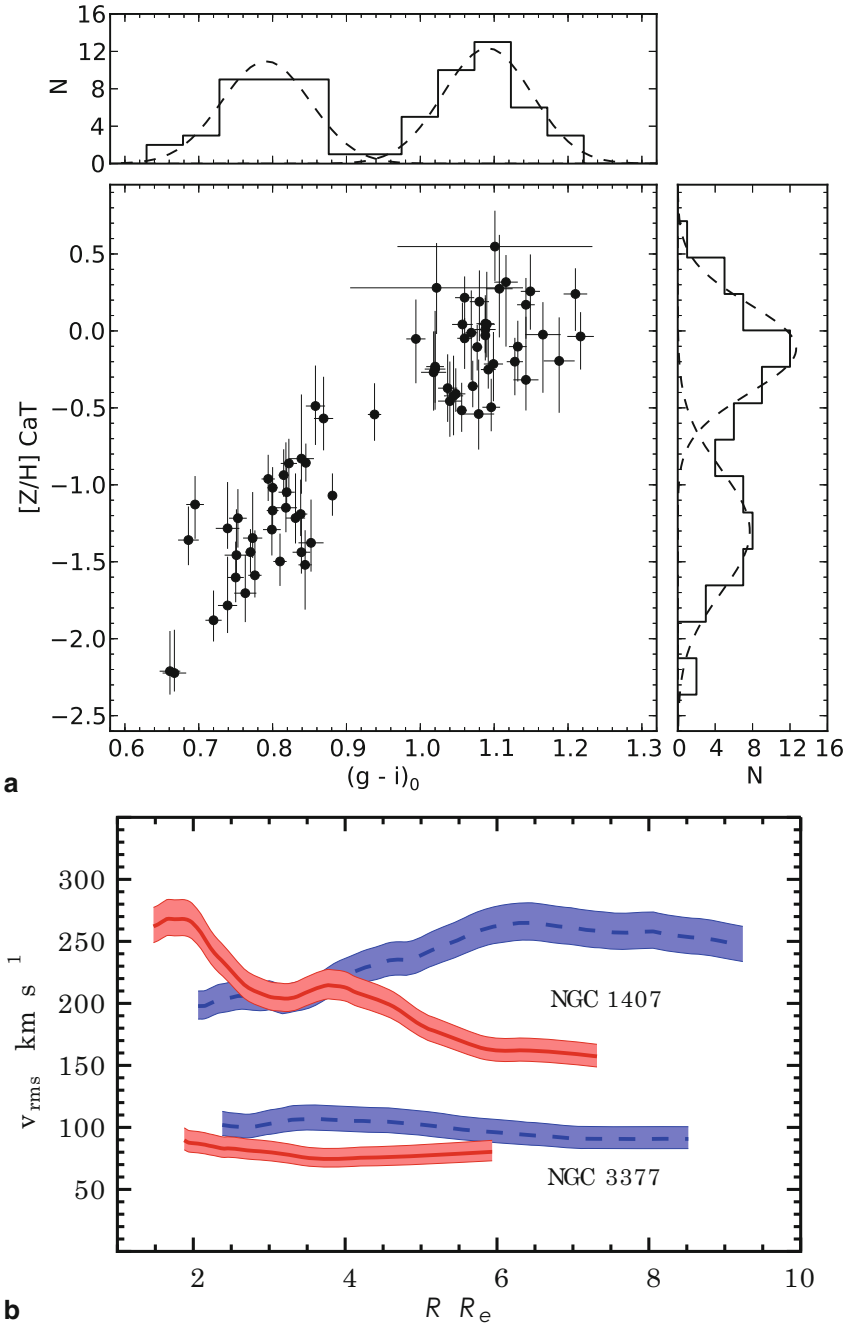

Fig. 2 Figures from Brodie et al. (2014). Left panel: CaT index measurements vs. $(g-i)_0$ Brodie et al. (2012). The solid and dotted histograms are the spectroscopic (71 GCs) and the entire, background-decontaminated, photometric (253 candidates) samples, respectively. The overall color

that red GCs are indeed $\sim 1-2$ Gyr younger than blue GCs. WD-derived ages are accurate to ~ 0.5 Gyr, but the sample is still extremely small, and these results are not necessarily generalizable to entire GC systems beyond the Local Group.

Globular clusters (GCs) have a distinguished history as indicators of the assembly histories of galaxies for the Milky Way and beyond (Searle & Zinn (1978); Brodie & Huchra (1991); Abadi et al. (2006); Brodie & Strader (2006); Forbes & Bridges (2010)). Searle & Zinn (1978) used the combination of GC positions, velocities, and mentalities *jointly* to to establish the 2-phase, inside out, formation of the Milky Way. Before the existence of GC subpopulations was discovered, Brodie & Huchra (1991) showed that the mean metallicity of a GC system is dependent on parent galaxy luminosity, with a relationship that mimics the galaxy mass-galaxy metallicity relation. We now know that MR GCs trace the build up of galaxy bulges, the MP GCs reveal the presence and properties of MP stellar halos, and the properties of both subpopulations depend on host galaxy mass (Larsen et al. (2001); Brodie & Strader (2006); Peng et al. (2006)).

As discussed by several presenters at this conference (see, for example, contributions by Lewis, Mackey, Majewski and Grillmair), the substructure visible in the stellar light distributions of the Milky Way (MW) and M31 is a "smoking gun". It directly reveals the minor mergers and accretions of smaller satellite galaxies that assemble the outskirts of galaxies under the two-phase paradigm. Accompanying GCs are often found embedded in the stellar light substructures, suggesting that they may be key to unraveling the details of halo build up beyond the Local Group, where galaxy starlight is too faint for detailed analysis. Indeed, the presence of a MP halo in M31 was apparent from the MP GC population long before it was detected in starlight.

As a first step to using GCs to understand galaxy formation beyond the Local Group, it is instructive to ask what can be learned from a comparison of the MW and M31 GC systems. M31 has about 400 GCs, in contrast to the MW's $\sim$150. M31's GC are roughly evenly split between MP and MR, while in the MW there are twice as many MP GCs as MR ones. Nonetheless, the number of MR GCs per unit bulge light is very similar. Given our assertion that MR GCs trace the build up of galaxy bulges, this similarity suggests that MR GCs formed with similar efficiencies with respect to stars in both M31 and the MW. Perhaps surprisingly, and in contrast to the bimodal MW system, the M31 GC metallicity distribution is not bimodal, although there

Fig. 2 (continued) distribution is well represented by the spectroscopic sample. Over plotted on the histograms are the best-fit Gaussians from a standard mixture-modeling analysis. Bimodality is preferred over unimodality at the >99.9 % and 99.8 % levels for the color and CaT index distributions, respectively. Right panel: GC system rms velocities vs. galactocentric radius, normalized by the galaxy effective radius, for NGC 1407 (top curves) and NGC 3377 (bottom curves) from Brodie et al. (2014). Dashed blue and solid red curves correspond to the blue and red GC subpopulations separately. Uncertainties are indicated by shaded regions. The radii have been circularized to account for galaxy ellipticity. The blue and red GCs show kinematical differences that reflect distinct spatial and orbital properties.

are hints of metallcity peaks at [Fe/H]= −1.4, −0.7, −0.2 (Caldwell et al., 2011). This suggests that M31 had a more complex history of minor mergers and accretions than the MW.

Further afield, while many insightful imaging studies of GCs have been carried out using the *Hubble Space Telescope* (*HST*, which generally covers only the central regions of galaxies; e.g., Larsen et al. (2001); Kundu & Whitmore (2001); Peng et al. (2006); Strader et al. (2006); Mieske et al. (2010)), and from the ground (which affords a much wider field of view; e.g., Forte et al. (2007); Hargis & Rhode (2012)), there has so far not been a homogeneous *spectroscopic* survey of GC systems for a large sample of ETGs covering the full range of environments.

1.1 The SLUGGS Survey

To address this deficit, we launched the SAGES Legacy Unifying Globulars and GalaxieS (SLUGGS) survey (Brodie et al., 2014). The survey uses a combination of imaging from Subaru/Suprime-Cam and spectroscopy from Keck/DEIMOS to obtain the *spatial*, *kinematical*, and *chemical* properties of both *diffuse stellar light* and *GCs*, in two dimensions and over wide areas, around 25 nearby early type galaxies (ETGs) spanning a broad range of galaxy properties and environments.

All of the spectroscopic aspects of the survey exploit the strong Ca II triplet absorption line feature in the near-infrared (~ 8500 Å), where DEIMOS has both a high efficiency and a high spectral resolution for separating the galaxy and GC lines from the forest of near-infrared sky lines. In addition, the Stellar Kinematics from Multiple Slits (SKiMS) technique that we pioneered allows us to map out the kinematics and metallicities of diffuse starlight in 2-D to large radii (e.g., Norris et al. 2008; Proctor et al. 2008, 2009).

The main advantages of the SLUGGS survey, in comparison to existing and planned surveys of ETGs, are the superior velocity precision (median 12 km s^{-1}) on a very stable, high-throughput instrument, and the large radial coverage (typically $\sim$2–3 R_e for stars, extending to $\sim$8–10 R_e when GCs are included Fig 3).

2 Rotation Maps

Simulations of major mergers (e.g., Hoffman et al. (2010); Bournaud et al. (2005)), generally predict that angular momentum will be pushed outwards as a result of the merger, leading to a rise in the velocity profile of the resultant galaxy with increasing galactocentric radius. We have produced 2-dimensional (2-D) rotational velocity maps for the SLUGGS galaxies (Arnold et al., 2014). We have analyzed our 2-D kinematics maps and made detailed comparisons with 2-D maps derived from cosmological simulations (Romanowsky et al., in preparation). Results, in particular the decline of rotation at large radius, suggest that major mergers are

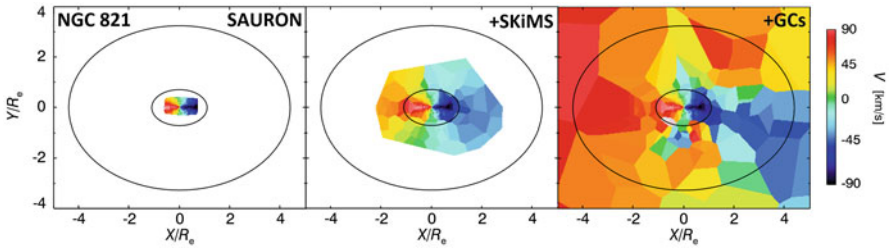

Fig. 3 Stellar mean line-of-sight velocity field of the elliptical galaxy NGC 821, where the color scale indicates the velocity amplitude. Ellipses mark schematic isophotes at 1 R_e and 4 R_e. The left panel shows an ATLAS^{3D}/SAURON pointing of the central region (Emsellem et al. (2004); Cappellari et al. (2011)), the middle panel incorporates the intermediate-radius regions reconstructed from SLUGGS/DEIMOS data using the SKiMS technique along with major- and minor-axis long-slit data from the literature, and the right panel folds in GC velocities to large radii. Note that the SLUGGS methods have sparser spatial sampling than a true integral-field unit, requiring some smoothing in creating these maps (described in Romanowsky et al., in preparation). The central regions do not reveal the kinematic twist that is apparent in the wide field map.

minor contributors to the star formation that built the galaxies we see today. The data are strikingly consistent with simulations of "Wild Disks" that form at $z \sim 2$ from cold gas flows along filaments of the cosmic web (e.g., Ceverino et al. (2010)) combined with ongoing satellite accretion to the present day.

3 Metallicity Maps

Evidence for 2-phase galaxy formation can also be found in radial metallicity gradients and, with hindsight, the clues were present over a decade ago in MW GC data. Harris (2001) showed that [Fe/H] declines as a function of radius for both subpopulations out to about 10 kpc, beyond which there are no more MR GCs in the MW. At ~10 kpc, there is a break in the MP GC metallicity distribution, which is flat beyond this radius. The simulations of Font et al. (2011) for MW mass disk galaxies suggest that such flattening at large radius is due to accretion and predict that higher *in situ* mass fractions lead to higher mean metallicities and more prominent metallicity gradients. We find similar "broken" metallicity profiles for both MR and MP GCs in some of our SLUGGS galaxies (e.g., NGC 1407, Forbes et al. (2011) and NGC 3115, Arnold et al. (2011)), although a well-studied and inherently populous GC system is needed to detect these trends at large radius. Further simulations are required to establish where the break should occur for galaxies with different masses, morphologies and ratios of *in situ* to accreted stars/GCs. Stellar metallicity gradients for SLUGGS galaxies (Pastorello et al., 2014) depend on galaxy mass, with lower mass galaxies generally having steeper gradients, as illustrated in the left panel of Fig. 4 from Brodie et al. (2014). Again, it is unclear whether this trend is consistent

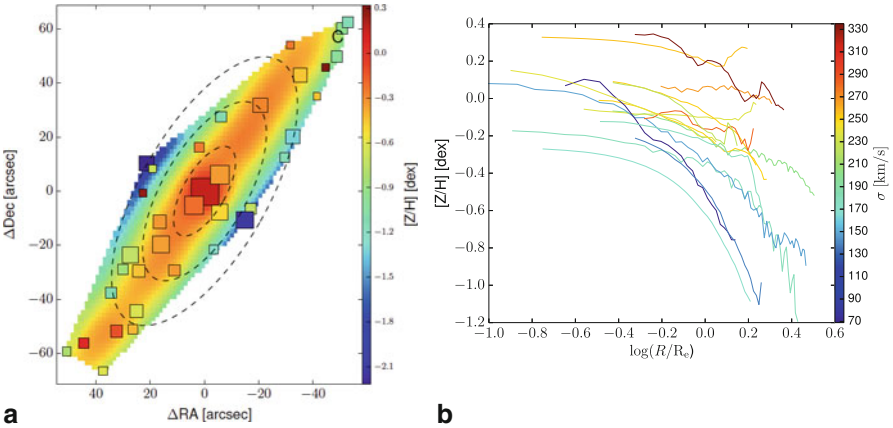

Fig. 4 Left panel: NGC 4111 stellar metallicity map from Pastorello et al. (2014). The square symbols show the SKiMS metallicity values, color coded according to their metallicity (see scale bar at right) and with the size inversely proportional to the associated uncertainty. The pixel values are obtained via kriging interpolation of the SKiMS points and are color coded according to the same metallicity scale. From the center to the outskirts, the dashed lines present the galaxy isophotes with circularized radius $R = 1, 2, 3\ R_e$. The coordinates on the axes are relative to the center of the galaxy. An extended metal-rich disk is apparent from this map (note that the slight tilt of the disk is an artifact of the incomplete spatial sampling). A strong negative metallicity gradient emerges along the minor axis. Right panel: Radial metallicity profiles for the galaxies in the Pastorello et al. (2014) SLUGGS sample. The plot shows metallicity versus galactocentric radius scaled by R_e and color coded according to the galaxy central velocity dispersion.

with theoretical expectations. Maps produced using the SKIMS technique, an example of which is shown in the right panel of Fig. 4 from Brodie et al. (2014), can be directly compared with maps derived from cosmological simulations in which *in situ* and accreted particles can be individually tagged, a technique which is explored to great effect in Romanowsky et al., in preparation.

4 Novelties: Markers of tidal interactions and accretion

Although designed to target GCs and field stars, the SLUGGS survey has produced some important serendipitous results. New types of stellar systems have been discovered that have turned out to be markers of tidal interactions and minor mergers, both past and ongoing. Figure 5 shows two such objects, highlighting a continuum of dense stellar systems, or Ultra Compact Dwarfs (UCDs), spanning a wide range of densities and ages. All our newly-discovered objects are likely to be the remnant nuclei of tidally stripped galaxies, lending support for the idea that many, if not most, UCDs are galaxies rather than giant GCs. The object on the left in Fig. 5, M60-UCD1, set a density record for stellar systems and is likely to have a central

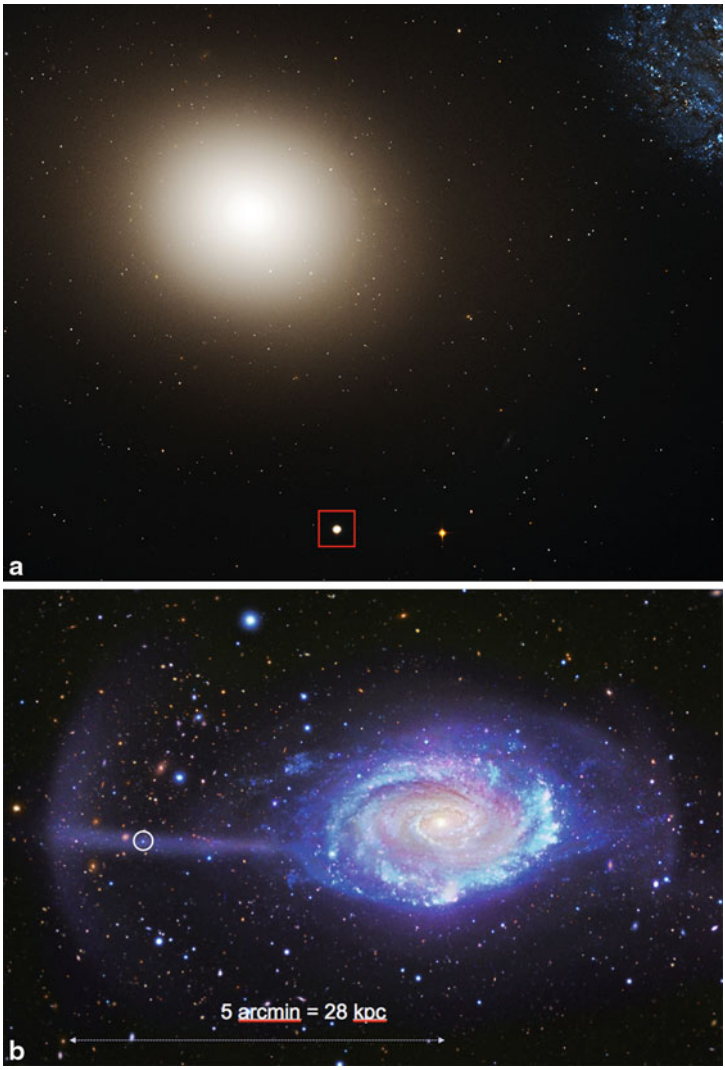

Fig. 5 Top panel: Optical image of M60-UCD1 from Chandra press release 092413. This was the densest known galaxy in 2013 and likely the victim of tidal stripping (Strader et al., 2013). Bottom panel: The UCD in the vicinity of the Umbrella Galaxy, NGC 4651, is indicated within the white circle. It is embedded in a stellar stream that resembles the Sagittarius stream in the MW. Based on modeling of its orbit, the UCD is likely to be the nucleus of the galaxy that is being stripped.

black hole (Strader et al., 2013). Its location in the size-luminosity plane for all stellar systems with spectroscopically confirmed distances and accurately measured sizes ("The Everything Plot") is shown in Fig. 6. The object illustrated on the right in Fig. 5, a UCD in NGC 4651, is embedded in a Sagittarius stream analog (Foster et al. 2014)

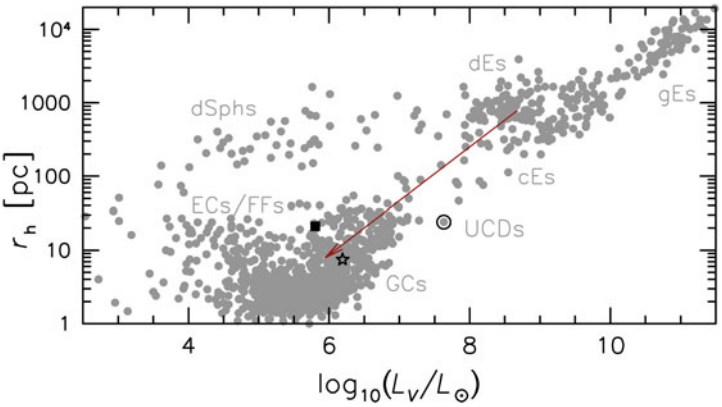

Fig. 6 The "Everything Plot" updated from the version in Brodie et al. (2011) to include newly discovered massive compact stellar systems that are filling in previous gaps in the size luminosity plane. The figure contains only distance-confirmed objects. The star symbol and filled square represent ω Cen and NGC 2419, respectively. The encircled object is M60-UCD1. The inferred stripping trajectory is shown by the arrow. Although new objects are filling the space between UCDs and compact elliptical galaxies, no stellar system has yet been found that lies to the right of the sloping constant-density boundary at the right hand edge of the data points.

and is likely to be the nucleus of the galaxy being stripped. It can be thought of as an Omega-Cen analog in the process of forming. Now that we know UCDs exist in regions of size–luminosity-density parameter space that were formerly thought to be empty (e.g., Brodie et al. 2011; Forbes et al. 2013; Norris et al. (2014)), we are "widening the net" in our data search criteria. New UCD-like objects are now being discovered increasingly frequently. Although we do not know how to assign them to early dark matter (DM) halos, if they indeed originate in galaxies, their numbers suggest that they could be an important factor in addressing the missing satellite problem.

Finally, galaxies have been discovered that appear to host over-massive black holes and it has been suggested that these are local "red nuggets", objects that formed at $z \sim 2$ but somehow avoided the ongoing accretions that built the majority of present day galaxies (e.g., NGC 1277, van den Bosch et al. (2012)). Blom et al. (2014) have shown that, at least sometimes, an apparently primordial red nugget is just a stripped galaxy remnant. These authors showed that the "red nugget" NGC 4342 is being stripped by NGC 4365 and the process is being marked by a stream of GCs and stars that share its velocity and stellar populations characteristics. NGC 4342, and NGC 1277, are thought to have DM halos, which raises the question of how stars and GCs can be stripped from galaxies while keeping their DM halos at least partially intact. Nonetheless, if reasonable amounts of stripping are assumed, these outliers from the BH-galaxy mass scaling relations, can likely be reconciled with the standard correlations.

5 Concluding Remarks

The SLUGGS survey (Brodie et al., 2014) is producing a wealth of chemodynamical information for 25 nearby early-type galaxies covering a broad range of masses and environments. 2–D kinematic and metallicity maps are being generated out to large effective radii (typically 2–3 R_e for galaxy starlight, and 8–10 R_e for GCs) with a velocity precision of $\sim$12 km s^{-1}. Details of the survey, including collaborators and publications may be found at http://sluggs.ucolick.org. Among the results are spectroscopic confirmation that metallicity bimodality is common among GC systems (Brodie et al. (2012); Usher et al. (2012)), and that the metallicity subpopulations are kinematically distinct (Pota et al., 2013). Based on age estimates from WD cooling sequence measurements (Hansen et al., 2013), MR GCs, predominantly tracing galaxy bulges, appear to be 1–2 Gyr younger than the MP ones, which trace the build up of MP halos. Based on GC specific frequencies and metallicity distributions, M31 appears to have had a more complex accretion history than the MW. Our 2–D wide-field imaging and spectroscopy suggest that disk instabilities and accretions, not major mergers, are responsible for the characteristics of the majority of early type galaxies. We find that stellar radial metallicity gradients depend on galaxy mass and are steeper in lower mass galaxies. Where the data extend out far enough, we find that inner metallicity gradients flatten at large radius; it appears that the break radius reveals the transition between the *in situ* and accreted components. New classes of UCDs, discovered during the SLUGGS survey, suggest that UCDs are often stripped galaxy nuclei. As such, they are easily observable tracers of minor mergers and may be important in solving the "missing satellite problem" that plagues Lambda CDM cosmology. Open questions, that would benefit from theoretical input, include: Where should the break occur in radial metallicity profiles for galaxies with different masses, morphologies and ratios of *in situ* to accreted stars? Is the dependence of metallicity gradient on galaxy mass consistent with theoretical expectations? What proportion of UCDs and local red nuggets are stripped galaxies? Can a significant fraction of stars be stripped without destroying a galaxy's DM halo?

Acknowledgements We thank all the members of the SAGES collaboration (http://sages.ucolick.org) for their contributions to the work reported here. This work was carried out under NSF grants AST-1211995 and AST-1109878.

References

Abadi M. G., Navarro J. F., Steinmetz M., 2006, MNRAS, 365, 747
Arnold J. A., Romanowsky A. J., Brodie J. P., Chomiuk L., Spitler L. R., Strader J., Benson A. J., Forbes D. A., 2011, ApJL, 736, L26
Arnold J. A., Romanowsky A. J., Brodie J. P., Forbes D. A., Strader J., Spitler L. R., Foster C., Kartha S. S., Pastorello N., Pota V., Usher C., Woodley K. A., 2014, ApJ, submitted
Blom C., Forbes D. A., Foster C., Romanowsky A. J., Brodie J. P., 2014, MNRAS, 439, 2420
Bournaud F., Jog C. J., Combes F., 2005, A&A, 437, 69
Brodie J. P., Huchra J. P., 1991, ApJ, 379, 157
Brodie J. P., Romanowsky A. J., Strader J., Forbes D. A., 2011, AJ, 142, 199
Brodie J. P., Romanowsky A. J., Strader J., Forbes D. A., Foster C., Jennings Z. G., Pastorello N., Pota V., Usher C., Blom C., et al., 2014, arXiv preprint arXiv:1405.2079
Brodie J. P., Strader J., 2006, ARA&A, 44, 193
Brodie J. P., Usher C., Conroy C., Strader J., Arnold J. A., Forbes D. A., Romanowsky A. J., 2012, ApJL, 759, L33
Caldwell N., Schiavon R., Morrison H., Rose J. A., Harding P., 2011, AJ, 141, 61
Cappellari M., Emsellem E., Krajnović D., McDermid R. M., Scott N., Verdoes Kleijn G., Young L. M., Alatalo K., Bacon R., Blitz L., et al., 2011, Monthly Notices of the Royal Astronomical Society, 413, 813
Ceverino D., Dekel A., Bournaud F., 2010, MNRAS, 404, 2151
Daddi E., Renzini A., Pirzkal N., Cimatti A., Malhotra S., Stiavelli M., Xu C., Pasquali A., Rhoads J. E., Brusa M., di Serego Alighieri S., Ferguson H. C., Koekemoer A. M., Moustakas L. A., Panagia N., Windhorst R. A., 2005, ApJ, 626, 680
Emsellem E., Cappellari M., Peletier R. F., McDermid R. M., Bacon R., Bureau M., Copin Y., Davies R. L., Krajnović D., Kuntschner H., Miller B. W., de Zeeuw P. T., 2004, MNRAS, 352, 721
Font A. S., McCarthy I. G., Crain R. A., Theuns T., Schaye J., Wiersma R. P. C., Dalla Vecchia C., 2011, MNRAS, 416, 2802
Forbes D. A., Bridges T., 2010, MNRAS, 404, 1203
Forbes D. A., Pota V., Usher C., Strader J., Romanowsky A. J., Brodie J. P., Arnold J. A., Spitler L. R., 2013, MNRAS, 435, L6
Forbes D. A., Spitler L. R., Strader J., Romanowsky A. J., Brodie J. P., Foster C., 2011, MNRAS, 413, 2943
Forte J. C., Faifer F., Geisler D., 2007, MNRAS, 382, 1947
Foster, C., Lux, H., Romanowsky, A. J. et al. 2014, MNRAS, 442, 3544
Hansen B. M. S., Kalirai J. S., Anderson J., Dotter A., Richer H. B., Rich R. M., Shara M. M., Fahlman G. G., Hurley J. R., King I. R., Reitzel D., Stetson P. B., 2013, Nature, 500, 51
Hargis J. R., Rhode K. L., 2012, AJ, 144, 164
Harris W. E., 2001, in Labhardt L., Binggeli B., eds, Saas-Fee Advanced Course 28: Star Clusters Globular cluster systems. p. 223
Hoffman L., Cox T. J., Dutta S., Hernquist L., 2010, ApJ, 723, 818
Kundu A., Whitmore B. C., 2001, AJ, 121, 2950
Larsen S. S., Brodie J. P., Huchra J. P., Forbes D. A., Grillmair C. J., 2001, AJ, 121, 2974
Mieske S., Jordán A., Côté P., Peng E. W., Ferrarese L., Blakeslee J. P., Mei S., Baumgardt H., Tonry J. L., Infante L., West M. J., 2010, ApJ, 710, 1672

Norris M. A., Kannappan S. J., Forbes D. A., Romanowsky A. J., Brodie J. P., Faifer F. R., Huxor A., Maraston C., et al. 2014, MNRAS, submitted
Norris M. A., Sharples R. M., Bridges T., Gebhardt K., Forbes D. A., Proctor R., Raul Faifer F., Carlos Forte J., Beasley M. A., Zepf S. E., Hanes D. A., 2008, MNRAS, 385, 40
Oser L., Ostriker J. P., Naab T., Johansson P. H., Burkert A., 2010, ApJ, 725, 2312
Pastorello N., Forbes D. A., Foster C., Brodie J. P., Usher C., Romanowsky A. J., Strader J., Arnold J. A., 2014, MNRAS, in press
Peng E. W., Jordán A., Côté P., Blakeslee J. P., Ferrarese L., Mei S., West M. J., Merritt D., Milosavljević M., Tonry J. L., 2006, ApJ, 639, 95
Porter L. A., Somerville R. S., Primack J. R., Johansson P. H., 2014, MNRAS, submitted, arXiv:1407.0594
Pota V., Forbes D. A., Romanowsky A. J., Brodie J. P., Spitler L. R., Strader J., Foster C., Arnold J. A., Benson A., Blom C., Hargis J. R., Rhode K. L., Usher C., 2013, MNRAS, 428, 389
Proctor R. N., Forbes D. A., Brodie J. P., Strader J., 2008, MNRAS, 385, 1709
Proctor R. N., Forbes D. A., Romanowsky A. J., Brodie J. P., Strader J., Spolaor M., Mendel J. T., Spitler L., 2009, MNRAS, 398, 91
Searle L., Zinn R., 1978, ApJ, 225, 357
Strader J., Brodie J. P., Spitler L., Beasley M. A., 2006, AJ, 132, 2333
Strader J., Seth A. C., Forbes D. A., Fabbiano G., Romanowsky A. J., Brodie J. P., Conroy C., Caldwell N., Pota V., Usher C., Arnold J. A., 2013, ApJL, 775, L6
Usher C., Forbes D. A., Brodie J. P., Foster C., Spitler L. R., Arnold J. A., Romanowsky A. J., Strader J., Pota V., 2012, MNRAS, 426, 1475
van den Bosch R. C. E., Gebhardt K., Gültekin K., van de Ven G., van der Wel A., Walsh J. L., 2012, Nature, 491, 729
van Dokkum P. G., Kriek M., Franx M., 2009, Nature, 460, 717

Globular Clusters in the Local Group

Dougal Mackey

Abstract Globular clusters are fossil relics from which we can obtain critical insights into the merger and accretion events that underlie hierarchical galaxy assembly. Those hosted by galaxies in the Local Group play a key role in this work, as they may be studied in great detail on a star-by-star basis along with the surrounding field populations. In this contribution I describe how new results from the PAndAS survey are revolutionising our view of the outer halo globular cluster system of Andromeda. A brief appendix provides an updated census of Local Group globular cluster systems taking into account numerous recent discoveries.

1 Introduction

As relatively simple objects which are integral to many fundamental astrophysical processes, globular clusters (GCs) are central to a wide variety of astronomy research over all scales—from star formation and stellar and binary evolution, through stellar exotica and variable stars, and the dynamics of self-gravitating systems, to galaxy formation and evolution, with implications for cosmology. In studies of this latter field, globular clusters are particularly invaluable. They represent highly visible signatures of the dominant processes driving galaxy development and provide important insight into the formative stages of a given host (Brodie and Strader 2006; West et al. 2004).

For example, the GC systems of large galaxies are believed to be comprised of two distinct sub-components. A "native" population of GCs is thought to form *in situ* during the major star-forming episodes that accompany the early stages of galaxy assembly; subsequent gas-rich merger events may lead to the formation of additional members (Zepf and Ashman 1993). This system is augmented by a second component that accumulates over cosmological time via the accretion and destruction of smaller satellites hosting their own GC retinues (Mackey et al. 2010b; Searle and Zinn 1978). Hence by studying the GC systems of large galaxies we can hope to

D. Mackey (✉)
Research School of Astronomy & Astrophysics, Australian National University, Mount Stromlo Observatory, Cotter Road, Weston Creek, ACT 2611, Australia
e-mail: dougal.mackey@anu.edu.au

K. Freeman et al. (eds.), *Lessons from the Local Group,*
DOI 10.1007/978-3-319-10614-4_18

obtain constraints on the frequency and relative significance of galaxy interaction, merger and accretion processes at all epochs, with important implications for models of hierarchical structure formation.

GCs thus fulfil a vital role in "galaxy archaeology"—the detailed study of nearby resolved galaxies with a view to inferring their evolutionary history from present-day structure and content. Galaxies in the Local Group are crucial to this problem as they offer the opportunity to correlate highly detailed information on GC systems with the properties of surrounding field populations, enhancing our understanding of exactly how these different "fossil tracers" relate to each other. Such work is of tremendous importance to studies of galaxy evolution in the more distant Universe where individual field stars can no longer be resolved and luminous GCs are amongst the few accessible tracers of ancient populations.

2 Lessons from the Milky Way

The GC system of our own Milky Way has been instrumental for our understanding of how GCs trace galaxy assembly processes. Full details may be found in the review by Brodie and Strader (2006). Here, I will focus on the accumulation of GCs in the Galactic halo via the assimilation of their small host galaxies. That some fraction of the Galactic GC system has an external origin was first recognized by Searle and Zinn in their seminal 1978 paper (Searle and Zinn 1978). These authors noted that halo GCs outside the solar circle exhibit no abundance gradient with Galactocentric radius, and further that their horizontal branch (HB) morphologies (taken as a proxy for age) show little correlation with abundance. They argued that this is evidence that, whilst the inner halo may have been formed in the initial collapse of the Galaxy, the outer halo GC system has been built up from merger remnants in slower, chaotic, formation. This work constituted some of the first observational evidence for the presently-favoured idea that large galaxies are assembled through the hierarchical merging and accretion of smaller systems.

Modern studies with vastly improved datasets still support this scenario—it is now known that the abundances, velocities, ages, HB morphologies and sizes of many remote Milky Way GCs are consistent with an external origin (Zinn 1993; Mackey and Gilmore 2004b; van den Bergh and Mackey 2004; Mackey and van den Bergh 2005; Marín-Franch et al. 2009; Dotter et al. 2011). In principle some properties of the now-defunct parent galaxies may be inferred from their subsumed GCs (Forbes and Bridges 2010). However this problem has so far proven intractable because our only *direct* and *unambiguous* observation of the GC accretion process is the disrupting Sagittarius dwarf, which is depositing at least five objects into the Milky Way halo (Ibata et al. 1994; Da Costa and Armandroff 1995; Bellazzini et al. 2003; Law and Majewski 2010). We know of just this one family of accreted GCs in the Milky Way halo; no other groups of associated GCs have been definitively identified. Thus the extent to which the observed properties of sub-groups within the

Milky Way GC system reflect the assembly history of the halo remains a key open question.

3 Lessons from the Outskirts of Andromeda

The remainder of the contribution I dedicate to new research on the outer halo globular cluster system of Andromeda (M31). M31 is of critical importance in providing a second and unique system beyond the Milky Way for testing hierarchical models, and in particular for addressing the problems sketched in the previous section; it is the nearest giant galaxy to our own, and the only other one in which GCs may be resolved into stars.

Our group has pioneered the resolved study of the M31 stellar halo via several wide-field imaging surveys (Ferguson et al. 2002; Ibata et al. 2007), most recently the *Pan-Andromeda Archaeological Survey* (PAndAS) which is dedicated to obtaining a contiguous deep panorama of M31 to a projected radius of $R_p \approx 150$ kpc (McConnachie et al. 2009). For full details of PAndAS and its main discoveries to date, I refer the reader to the contribution by G. Lewis in this volume. Several highlights are worth listing here in brief:

- A huge variety of stellar substructures in the M31 outer halo, in qualitative agreement with predictions from hierarchical formation models (McConnachie et al. 2009);
- A thin rotating plane of dwarf galaxies not easily explained in ΛCDM (Ibata et al. 2013);
- An extended smooth spherical stellar halo component with properties broadly in line with those predicted by hierarchical formation models (Ibata et al. 2014);
- The discovery of 16 dwarf galaxies and many candidates (Martin et al. 2006; McConnachie et al. 2008; Richardson et al. 2011; Martin et al. 2013);
- Foreground Milky Way halo streams arching across the survey footprint (Martin et al. 2014).

PAndAS has also been revolutionising our view of the M31 globular cluster system. Most previous investigations have targeted regions comparatively close to the centre of M31, typically within 20–25 kpc in projection. This is because the relative proximity of M31, while advantageous for detailed study, also poses a problem in that the full extent of its stellar halo subtends a substantial angle on the sky ($\gtrsim 20°$ in diameter) which is difficult to search uniformly for GCs, especially those with low luminosities and/or surface brightnesses. PAndAS almost completely obviates these issues: its imaging spans a very wide area, yet is sufficiently deep to allow the identification of even faint GCs.

We have used the PAndAS dataset to conduct the first detailed and uniform census of GCs across nearly the full extent of the M31 halo. In combination with discoveries from the precursor surveys (Huxor et al. 2008), we have identified nearly 100 new GCs in the outskirts of M31, including 80 with $R_p > 30$ kpc (Huxor et al. 2014). Of

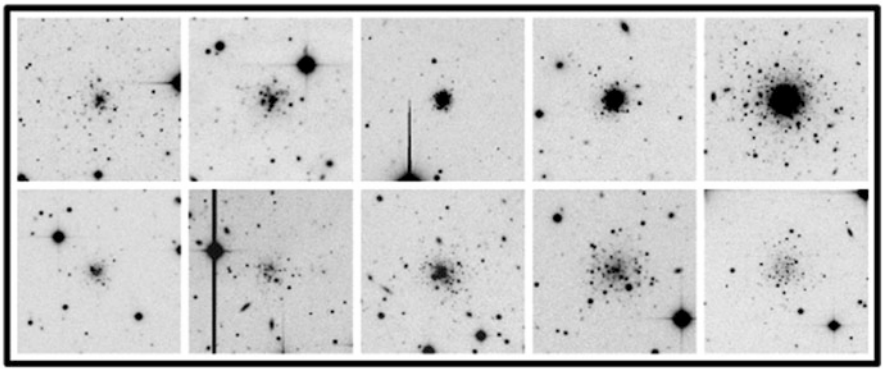

Fig. 1 CFHT MegaCam g-band thumbnail images of a representative sample of our new M31 halo GCs (Huxor et al. 2014). Each image is $1' \times 1'$ in size, with north to the top and east to the left

these, a substantial fraction lie at distances that were completely unexplored prior to our campaign: our catalogue contains 23 clusters beyond $R_p = 80$ kpc, of which 12 sit outside $R_p = 100$ kpc. For comparison, prior to our work only three globular clusters were known at $R_p > 30$ kpc.

The PAndAS footprint also covers the M31 satellite galaxies M33, NGC 147, and NGC 185. We have surveyed each of these systems for undiscovered remote GCs, turning up five objects in M33 (Huxor et al. 2009; Cockcroft et al. 2011), three in NGC 147, and one in NGC 185 (Veljanoski et al. 2013b).

Example g-band thumbnails of a representative sample of our new M31 globular clusters are shown in Fig. 1. These images clearly reveal the unambiguous classification of each catalogued object as a GC, highlighting the quality of the data. We used extensive artificial cluster tests to quantify the completeness of our GC survey as a function of cluster luminosity and structure (Huxor et al. 2014). The results suggest that our catalogue is complete down to a cluster luminosity of $M_V = -6.0$, and has a 50 % completeness limit at roughly $M_V \approx -4.1$. These values are only very mildly dependent on cluster size. In addition we find that an additional $\sim$ 3–5 GCs may lie undiscovered within the area covered by PAndAS imaging (i.e., within a radius $R_p \approx 150$ kpc), due to small gaps in the survey coverage. We cannot rule out that there may also be a population of very faint GCs with $M_V \gtrsim -4$ that we are unable to detect using PAndAS.

Combining our new catalogue with all previous discoveries, we now know of 91 M31 GCs lying outside $R_p = 25$ kpc, including 12 at projected distances larger than $R_p = 100$ kpc. Detailed study of a couple of exceptional objects (Mackey et al. 2010a, 2013b) suggests that the M31 GC system extends to radii larger than $\sim$ 200 kpc in three dimensions. These observations stand in stark contrast to the halo GC population in the Milky Way, in which there are only $\approx$ 13 objects known at Galactocentric radii larger than 30–35 kpc (corresponding to an average projected radius of $\sim$ 25 kpc for random viewing angles), including only one or two at a Galactocentric distance of $\approx$ 120 kpc (corresponding to an average projected distance

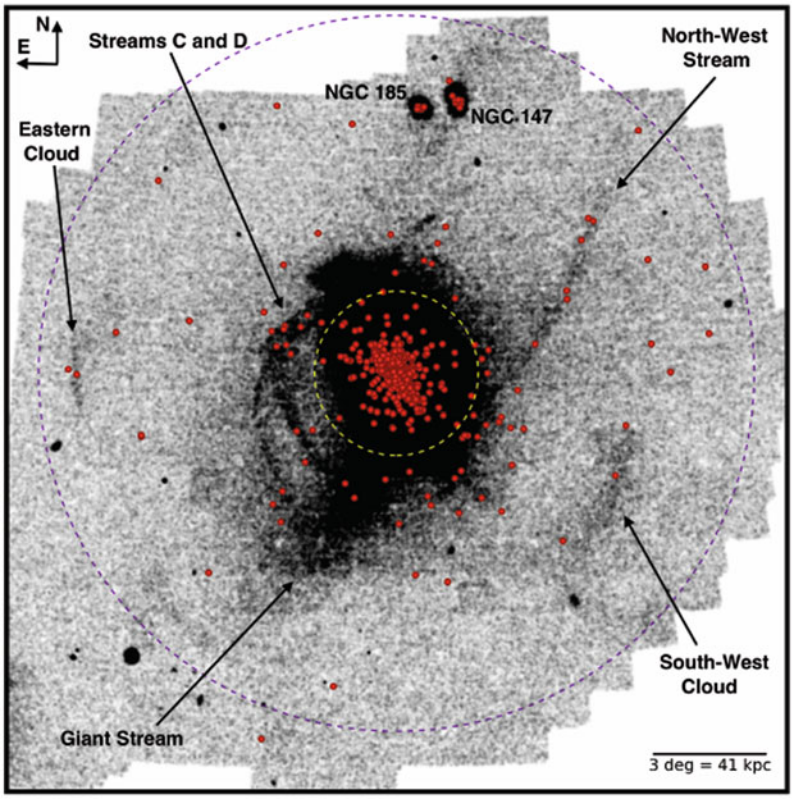

Fig. 2 PAndAS spatial density map for metal-poor ([Fe/H] $\lesssim -1.4$) M31 halo red giant stars. The main substructures are labelled; the two *dashed circles* mark projected radii of 30 and 130 kpc. Overplotted are all known M31 GCs (*red points*). Note that many GCs outside $R_p \sim 30$ kpc lie projected onto various streams and overdensities

of ~ 95 kpc for random viewing angles). While the disparity in the number of GCs in the Milky Way and M31 within $R_p \approx 25$ kpc is roughly 3:1 in favour of M31, our new catalogue reveals that outside this radius it is more like 7:1 in favour of M31 (Huxor et al. 2014).

It is also notable that, whereas all but a couple of the ≈ 13 very remote Milky Way GCs at Galactocentric radii larger than 30–35 kpc are rather faint objects with lumiosities $M_V \gtrsim -6$, the remote halo of M31 hosts many bright clusters. Around two-thirds of those sitting at $R_p > 25$ kpc have $M_V \lesssim -6$, and the sample extends to luminosities near $M_V \approx -9.5$. This difference between the two systems has previously been noted (Mackey et al. 2007; Huxor et al. 2011), but is much more explicit with our new dataset.

In Fig. 2 we plot the positions of all known M31 GCs on top of the PAndAS spatial density map of stars possessing colours and magnitudes consistent with being metal-poor red giants in M31. In the outer parts of the halo ($R_p \gtrsim 30$ kpc), where large,

coherent tidal debris streams are readily distinguished, there is a striking correlation between these features and the positions of a large fraction ($\sim$ 50–80 %) of the GCs. We have previously demonstrated that the probability of this system-wide alignment arising randomly is low—well below 1 % (Mackey et al. 2010b). This implies that the spatial coincidence between streams and GCs represents a genuine physical association, direct evidence that much of the outer M31 GC system has been assembled via the accretion of cluster-bearing satellites.

This argument is based on statistical grounds; to determine on an object-by-object basis which GCs are associated (or not) with a given substructure requires velocity information. A good starting point is to obtain velocity measurements for as many of the M31 outer halo GCs as possible—these extra data can then be folded into the statistics of the spatial association. Definitive answers require velocity measurements for the underlying field halo substructure(s) as well, which is a much more challenging prospect due to the extremely low surface brightnesses of these features.

With this in mind we embarked on a large spectroscopic campaign aimed at studying the kinematics of M31 outer halo GCs. The campaign involved eight separate observing runs conducted with three different facilities: the ISIS spectrograph mounted on the 4.2 m William Herschel Telescope (WHT), the RC spectrograph on the 4.0 m Mayall Telescope at the Kitt Peak National Observatory (KPNO), and the GMOS instrument installed on the 8.1 m Gemini-North telescope. Altogether we managed to acquire spectra for 71 clusters with $R_p > 30$ kpc, corresponding to 85.5 % of all known GCs in the M31 outer halo. There are 20 GCs in our kinematic sample beyond $R_p = 80$ kpc including 10 beyond 100 kpc. For full details of this investigation I refer the reader to Veljanoski et al. (2013a, 2014); here I simply summarise the main results.

In Fig. 3, taken from Veljanoski et al. (2014), we plot the positions of all GCs in our kinematic sample on top of the PAndAS spatial density map of metal-poor red giant stars in the M31 halo. The GC points are colour-coded according to their velocity in the M31-centric frame. Careful examination of this map reveals that objects projected onto a given substructure in the field halo tend to exhibit correlated velocities. It might naively be expected that coherent velocity patterns amongst GC groups would be quite unlikely to arise in the case where the GCs are randomly-selected members of a pressure-supported halo, but would be unsurprising in the case where they are associated with an underlying kinematically cold stellar debris feature.

We tested this hypothesis for a number of GC-stream associations using a simple Monte Carlo methodology, finding numerous instances exhibiting clear evidence for non-random behaviour indicative of a dynamical link between the GCs and the underlying overdensity (Veljanoski et al. 2014). Clusters on the North-West Stream and South-West Cloud reveal strong velocity gradients from one end of the substructure to the other, while those on the Eastern Cloud form a close group in phase space. GCs in the Stream C/D overlap area (highlighted in Fig. 2) and in "Association 2" (which is an overdense region of GCs near the base of the North-West Stream (Mackey et al. 2010b)) split into clear sub-groups by velocity. A striking feature of many of the ensembles we considered is the coldness of their kinematics—the GCs groups on the

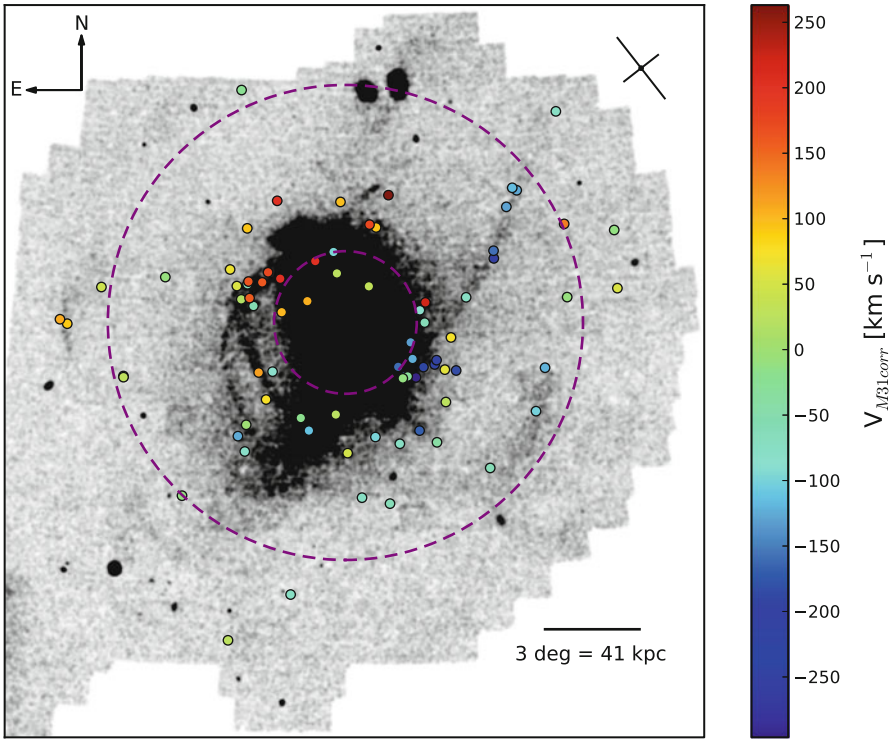

Fig. 3 PAndAS spatial density map for metal-poor ([Fe/H] $\lesssim -1.4$) M31 halo red giant stars, as per Fig. 2. GCs from our kinematic survey are overplotted as *coloured points*, where the colours correspond to the M31-centric radial velocities in units of km s^{-1}. The *purple dashed circles* correspond to $R_{\rm proj} = 30$ and 100 kpc. The *small schematic in the top right* shows the orientation of the major and minor axes of M31. (Source: Jovan Veljanoski ;Veljanoski et al. 2014)

NW Stream, SW Cloud, and Eastern Cloud, as well as the sub-groups in the Stream C/D overlap area and in Association 2, all exhibit velocity dispersions consistent with zero. Together these results strongly reinforce the notion outlined above that a substantial fraction of the outer halo GC population of M31 consists of objects accreted along with their now-defunct host galaxies.

To date there are only a couple of examples where GC velocities can be tied directly to measurements for an underlying stellar stream. The first unambiguous illustration is for the cluster HEC12 (also known as EC4 (Mackey et al. 2006b; Huxor et al. 2008)), which lies precisely on a narrow metal-poor sub-component to Stream C and shares a common velocity with this feature (Chapman et al. 2008; Collins et al. 2009). Recently we have made an effort to obtain information for additional fields in the vicinity of other probable GC-stream associations. One such case concerns the South-West Cloud, which has three probable GC members (Mackey et al. 2013a). We used Keck/DEIMOS to target a field near the central density peak of this substructure, in the vicinity of the cluster PA-8, as shown in the left panel of Fig. 4

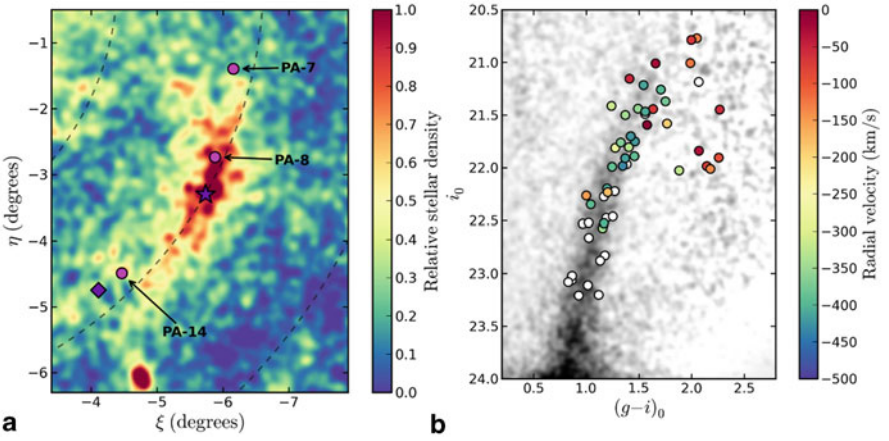

Fig. 4 *Left:* PAndAS map of the South-West Cloud, showing the surface density of red giant stars falling near the colour-magnitude sequence belonging to the substructure (see the *right-hand panel*). Contamination from foreground stars and background galaxies was subtracted using the model developed by Martin et al. (2013), and the colour-map scaled relative to the peak density in the central parts of the substructure. The three overlying GCs (*magenta circles*) are labelled. Our Keck field is indicated with a *star*; that from Gilbert et al. (2012) is marked with a *diamond*. The coordinates (ξ, η) represent a tangent plane centred on M31. Projected galactocentric distances of 60, 90, and 120 kpc are marked with *dashed lines*. *Right:* Heliocentric velocities for our target stars as a function of position on the CMD. The underlying density map shows all stars inside the main body of the South-West Cloud after subtraction of the contamination model from Martin et al. (2013). *White points* denote stars for which a good velocity solution could not be obtained. These plots originally appeared in Mackey et al. (2014)

(Mackey et al. 2014). An additional Keck field was previously observed by (Gilbert et al. 2012) at the southern end of the stream, near the cluster PA-14. The right panel of Fig. 4 shows the measured velocities for our target stars. There is a prominent kinematic signature for stars falling on or near the red giant branch of the South-West Cloud.

Using a maximum likelihood approach, we obtained a radial velocity of $v_r = -409.5 \pm 5.8$ km s^{-1} and an intrinsic velocity dispersion for the substructure of $\sigma_v = 13.7^{+6.7}_{-4.2}$ km s^{-1}. PA-8 is cospatial in three dimensions with the South-West Cloud (Mackey et al. 2013a; Bate et al. 2014) and has a velocity $v_r = -416 \pm 8$ km s^{-1} (Veljanoski et al. 2014), closely matching that measured from our Keck field. Moreover, Gilbert et al. (2012) serendipitously discovered a cold kinematic peak in their field with $v_r = -373.5 \pm 3.0$ km s^{-1}; the velocity of the nearby cluster PA-14 is $v_r = -363 \pm 9$ km s^{-1} (Veljanoski et al. 2014). Taken together, these provide compelling evidence that the globular clusters PA-8 and PA-14 are coherent in phase space with the stars that constitute the SWC, and hence that the GCs and the substructure share a common origin as previously argued statistically.

Returning now to our kinematic GC sample, we also considered the properties of the M31 outer halo GC system as a whole (Veljanoski et al. 2014). Close examination of Fig. 3 reveals the possibility of global rotation—those objects to the west of M31

appear to systematically possess negative velocities in the M31-centric frame, while those to the east typically have positive velocities. To assess this, we used a maximum likelihood approach to consider a simple family of rotating kinematic models. The rotation is assumed to have a constant amplitude A about an axis with position angle θ_0; the rotation component at any given position is then simply a sinusoidal function of the position angle relative to this axis—i.e., $v_{\rm rot} = A \sin(\theta - \theta_0)$. The velocity dispersion is assumed to have a Gaussian form and to vary as a function of projected radius in a power-law manner—i.e., $\sigma(R) = \sigma_0 (R/R_0)^{\gamma}$. Here R_0 is a scale radius set to be 30 kpc (which is roughly the inner limit of our sample, and the radius at which the M31 halo begins to dominate); the quantity σ_0 corresponds to the dispersion at this radius. Thus our models have four free parameters: A, θ_0, σ_0, and γ.

We obtained the following best-fit results: $A = 86 \pm 17$ km s^{-1}, $\theta_0 = 135° \pm 11°$, $\sigma_0 = 129^{+22}_{-24}$ km s^{-1}, and $\gamma = -0.45 \pm 0.22$. A rotating outer GC system is strongly favoured, with $A = 0$ excluded at a level of $\approx 5\sigma$. The axis of rotation closely corresponds to the M31 optical minor axis, which lies at $\sim 135°$ east of north. In the left panel of Fig. 5 we plot GC velocity in the M31-centric frame as a function of projected radius along the major optical axis (where the amplitude of rotation should be at a maximum). The rotation signature is clearly visible; a corresponding plot with respect to the minor optical axis (not shown here) exhibits no clear pattern, as expected if this corresponds to the rotation axis. It is noticeable from Fig. 5 that the rotation of the outer halo GC system is in the same sense as for the inner halo GCs (and indeed the M31 disk), albeit with smaller amplitude. Most intriguingly, the rotation is not driven purely by clusters that sit on the main halo substructures nor by those not clearly associated with any underlying halo feature—both groups apparently share in the pattern equally.

There is also substantial evidence for decreasing velocity dispersion with increasing projected radius—the power-law index γ is non-negative at a level of $\approx 2\sigma$. In the right panel of Fig. 5 we plot GC velocity in the M31-centric frame, now corrected for the global rotation, as a function of R_p. Our best-fitting halo dispersion profile is marked with a solid line. It is a good match to the velocity dispersion profile determined by Chapman et al. (2006) for metal-poor red giants in the M31 halo, at least over the range up to which stellar velocities are available (we extrapolate the model of Chapman et al. (2006) beyond $R_p \approx 70$ kpc).

In light of the clear association between many groups of M31 halo GCs and underlying field substructures, our finding that the GC population as a whole possesses a substantial degree of coherent rotation out to very large radii is quite puzzling. It is difficult to reconcile this property with the chaotic accretion of parent dwarf galaxies into the halo as implied by our kinematic observations and hierarchical galaxy formation models. One way that this phenomenon might arise is if a large fraction of the halo GC subsystem was brought into the potential well of M31 via one or two relatively large host galaxies. However, in this scenario it is, naively, difficult to explain the observed presence of distinct dynamically cold subgroups of GCs as well as the typically narrow stellar debris streams in the halo.

Another possibility is that the outer halo GC system of M31 is indeed the product of the assimilation of multiple dwarf galaxies, but that these were accreted into the

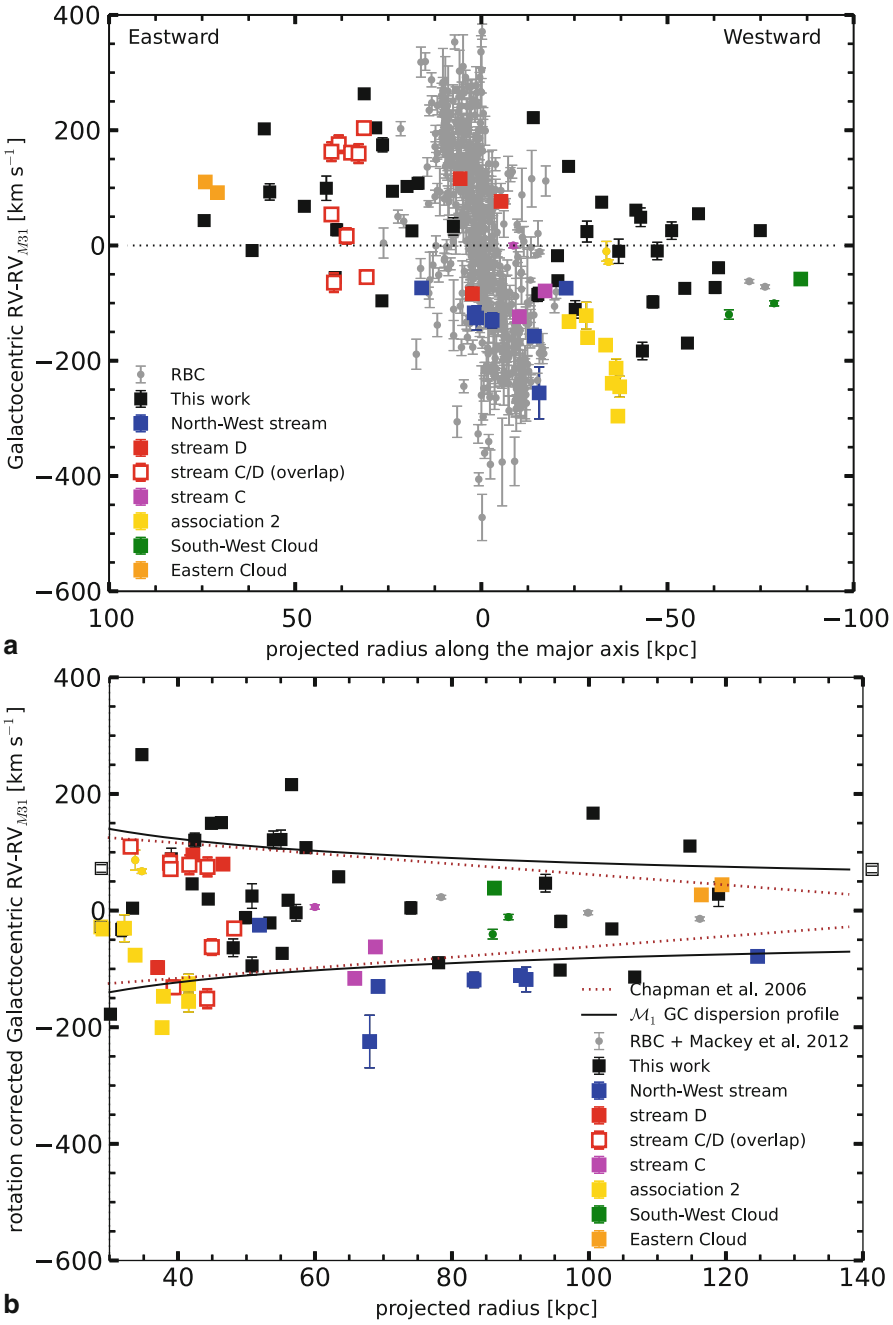

Fig. 5 *Upper:* Galactocentric radial velocities for our kinematic GC sample, corrected for the systemic motion of M31, versus projected distance along the major optical axis of M31. *Different colours* mark GCs that lie on specific stellar debris features as noted in Fig. 2 and the text. The rotation of the outer halo GC system is clearly evident, and is in the same sense as for GCs in

M31 potential well from a preferred direction on the sky. This scenario might well be related to the recent discovery that many dwarf galaxies, both in the Milky Way and M31, appear to lie in thin rotating planar configurations such that their angular momenta are correlated (Ibata et al. 2013; Pawlowski et al. 2012). We speculate that the parent galaxies of the accreted outer halo GC population may once have shared a similar, but now disrupted, configuration. In this context it is relevant that almost all of the dwarf galaxies thought to be members of the planes presently observed in both M31 and the Milky Way are insufficiently massive to host GCs. Hence the outer halo GC population in M31 might still have been assembled from only a few larger host systems, even if their accretion was related to a previous planar structure.

Appendix—A Census of Local Group Globular Cluster Systems

I conclude this contribution by providing a brief census of Local Group globular cluster systems. Although there are $\approx$ 70–80 known galaxies in the Local Group, depending on where the boundary is drawn (McConnachie 2012), only the few most luminous of these host GCs. While the existence of most of these systems has been known for nearly a century, the recent advent of deep wide-field survey imaging has resulted in many new discoveries in the past several years.

Milky Way There are 157 Galactic GCs listed in the most recent version of the McMaster catalogue (Harris 1996). These extend from the centre of the bulge out to a Galactocentric radius of at least 120 kpc. The vast majority are $\sim$ 11–13 Gyr in age (Marín-Franch et al. 2009; Dotter et al. 2010), although there is a handful of objects that are much younger, down to $\sim$ 7–8 Gyr old. New GCs are still typically uncovered once every few years, the most recent example being the controversial Crater system (Laevens et al. 2014; Belokurov et al. 2014).

Large Magellanic Cloud The LMC has long been recognised as a unique laboratory for star cluster research as it hosts a large number of massive clusters spanning the full age range 10^6–10^{10} years. However, the presence of an "age-gap" between $\sim$ 4–9 Gyr means that there is a well-defined group of 16 objects possessing ages commensurate with the range seen in the Galactic GC system (Mackey and Gilmore 2004a). The youngest GC in this group is the unusual object ESO121-SC03 (Mackey et al. 2006a).

←

Fig. 5 (continued) the inner parts of M31 but with a smaller amplitude. Notice that the rotation is observed even for the most distant GCs in our sample. *Lower:* Galactocentric radial velocities for our kinematic GC sample, corrected for the measured rotation and the systemic motion of M31, versus projected radius from the M31 centre. Again, the different *coloured symbols* mark groups of GCs projected onto various stellar streams. The *solid line* corresponds to our most-likely velocity dispersion profile for the outer halo GCs, while the *dotted line* describes the velocity dispersion of kinematically selected metal-poor giant stars as measured by Chapman et al. (2006). Note that in the latter case, the fit beyond 70 kpc is a linear extrapolation. (Source: Jovan Veljanoski ; Veljanoski et al. 2014)

Small Magellanic Cloud The SMC, by contrast, has numerous clusters with ages that would place them within the LMC age-gap (Glatt et al. 2008b), but perhaps only one, NGC 121, that could be considered as old as typical Galactic GCs (Glatt et al. 2008a).

Sagittarius Dwarf There are four well-studied GCs associated with the main body of this disrupting dwarf galaxy: M54, Arp 2, Terzan 7, and Terzan 8 (Ibata et al. 1994; Da Costa and Armandroff 1995). These exhibit a wide spread in age, $\sim$ 8–13 Gyr. A fifth cluster, Palomar 12, has already been stripped and sits embedded in the Sagittarius stream well away from the main body (Martínez-Delgado et al. 2002). A variety of other GCs in the Milky Way halo have been hypothesised to be former Sagittarius members (Bellazzini et al. 2003; Law and Majewski 2010).

Fornax Dwarf This dwarf spheroidal satellite of the Milky Way contains five GCs. Three of these were first discovered by Shapley (1939), and the remaining two by (Hodge 1961). Fornax is recognised as possessing a large number of GCs for its overall luminosity—i.e., its *specific frequency* is abnormally high.

NGC 6822 This star-forming Magellanic-type dwarf irregular galaxy has long been known to possess a population of young massive clusters; however it was thought that only one object, Hubble VII, is as old as typical Galactic GCs (Hubble 1925; Cohen and Blakeslee 1998). Very recently, however, deep wide-field imaging of the regions surrounding NGC 6822 has revealed another seven remote GCs extending out to $\sim$ 10 kpc from the galactic centre (Hwang et al. 2011; Huxor et al. 2013). Curiously, these exhibit an apparently linear configuration on the sky consistent with the major axis of the NGC 6822 stellar spheroid.

Andromeda (M31) M31 has by far the most extensive GC system in the Local Group with of order $\sim$ 500 confirmed members (Galleti et al. 2004). Recent work by our group, described in Sect. 3, has uncovered around 100 GCs in the outer halo of M31, extending to radii $\sim$ 140 kpc in projection (Huxor et al. 2008, 2014).

Triangulum (M33) M33 is the least massive spiral in the Local Group and possesses a wide variety of clusters projected against its disk (Sarajedini and Mancone 2007). Some of these appear to exhibit halo-like kinematics (Chandar et al. 2002). Recently, wide-field imaging of the region around M33 has uncovered five *bona fide* remote GCs spanning projected galactocentric radii $\sim$ 8–30 kpc and exhibiting properties very similar to typical Galactic GCs (Stonkutė et al. 2008; Huxor et al. 2009).

NGC 147 This dwarf elliptical companion to M31 has four central GCs first catalogued by (Baade 1944; Hodge 1976; Ford et al. 1977). Recent wide-field imaging around the outskirts of this galaxy has uncovered another six members (Sharina and Davoust 2009; Veljanoski et al. 2013b). Note that the nomenclature of the central GCs in NGC 147 is confused in the literature; a summary untangling these issues is provided by (Veljanoski et al. 2013b).

NGC 185 This galaxy is another dwarf elliptical companion to M31, and contains eight GCs. Seven of these were first catalogued many years ago (Baade 1944; Hodge

1974; Ford et al. 1977), while one relatively remote object was discovered only recently (Veljanoski et al. 2013b).

NGC 205 A third dwarf elliptical companion to M31, but residing at a much more central location than NGC 147 or 185, this galaxy possesses at least eight GCs, first catalogued by Hubble (Hubble 1932). Because of the proximity of this system to the inner halo of M31, which has many GCs, identification of NGC 205 members is not straightforward.

WLM This remote galaxy at the outskirts of the Local Group contains one *bona fide* ancient GC (Humason et al. 1956; Ables and Ables 1977); it is the lowest luminosity GC host in the Local Group.

Acknowledgements ADM is grateful for support by an Australian Research Fellowship (Grant DP1093431) from the Australian Research Council (ARC), and for contributions to this work by various members of the PAndAS collaboration—Avon Huxor, Annette Ferguson, Jovan Veljanoski, Geraint Lewis, Rodrigo Ibata, Nicolas Martin, Pat Côté, Alan McConnachie, Mike Irwin, Nial Tanvir, Nick Bate, Michelle Collins, Scott Chapman, and Jorge Peñarrubia.

References

Ables, H. D., Ables, P. G. 1977, ApJS, 34, 245
Baade, W. 1944, ApJ, 100, 147
Bate, N. F., et al. 2014, MNRAS, 437, 3362
Bellazzini, M., Ferraro, F. R., Ibata, R. A. 2003, AJ, 125, 188
Belokurov, V., Irwin, M. J., Koposov, S. E., Evans, N. W., Gonzalez-Solares, E., Metcalfe, N., Shanks, T. 2014, MNRAS, 441, 2124
Brodie, J. P., Strader, J. 2006, ARA&A, 44, 193
Chandar, R., Bianchi, L., Ford, H. C., Sarajedini, A. 2002, ApJ, 564, 712
Chapman, S. C., Ibata, R. A., Lewis, G. F., Ferguson, A. M. N., Irwin, M. J., McConnachie, A. W., Tanvir, N. R. 2006, ApJ, 653, 255
Chapman, S. C., et al. 2008, MNRAS, 390, 1437
Cockcroft, R., et al. 2011, ApJ, 730, 112

Cohen, J. G., Blakeslee, J. P. 1998, AJ, 115, 2356
Collins, M. L. M., et al. 2009, MNRAS, 396, 1619
Da Costa, G. S., Armandroff, T. E. 1995, AJ, 109, 2533
Dotter, A., et al. 2010, ApJ, 708, 698
Dotter, A., Sarajedini, A., Anderson, J. 2011, ApJ, 738, 74
Ferguson, A. M. N., Irwin, M. J., Ibata, R. A., Lewis, G. F., Tanvir, N. R. 2002, AJ, 124, 1452
Forbes, D. A., Bridges, T. 2010, MNRAS, 404, 1203
Ford, H. C., Jacoby, G., Jenner, D. C. 1977, ApJ, 213, 18
Galleti, S., Federici, L., Bellazzini, M., Fusi Pecci, F., Macrina, S. 2004, A&A, 416, 917
Gilbert, K. M., et al. 2012, ApJ, 760, 76
Glatt, K., et al. 2008a, AJ, 135, 1106
Glatt, K., et al. 2008b, AJ, 136, 1703
Harris, W. E. 1996, AJ, 112, 1487
Hodge, P. W. 1961, AJ, 66, 83
Hodge, P. W. 1974, PASP, 86, 289
Hodge, P. W. 1976, AJ, 81, 25
Hubble, E. P. 1925, ApJ, 62, 409
Hubble, E. P., 1932, ApJ, 76, 44
Humason, M. L., Mayall, N. U., Sandage, A. R. 1956, AJ, 61, 97
Huxor, A. P., Tanvir, N. R., Ferguson, A. M. N., Irwin, M. J., Ibata, R. A., Bridges, T., Lewis, G. F. 2008, MNRAS, 385, 1989
Huxor, A. P., Ferguson, A. M. N., Barker, M. K., Tanvir, N. R., Irwin, M. J., Chapman, S. C., Ibata, R. A., Lewis, G. F. 2009, ApJ, 698, L77
Huxor, A. P., et al. 2011, MNRAS, 414, 770
Huxor, A. P., Ferguson, A. M. N., Veljanoski, J., Mackey, A. D., Tanvir, N. R. 2013, MNRAS, 429, 1039
Huxor, A. P., et al. 2014, MNRAS, in press (arXiv:1404.5807)
Hwang, N., Lee, M. G., Lee, J. C., Park, W.-K., Park, H. S., Kim S. C., Park J.-H. 2011, ApJ, 738, 58
Ibata, R. A., Gilmore, G. F., Irwin, M. J. 1994, Nature, 370, 194
Ibata, R. A., Martin, N. F., Irwin, M. J., Chapman, S. C., Ferguson, A. M. N., Lewis, G. F., McConnachie, A. W., 2007, ApJ, 671, 1591
Ibata, R. A., et al. 2013, Nature, 493, 62
Ibata, R. A., et al. 2014, ApJ, 780, 128
Laevens, B. P. M., et al. 2014, ApJ, 786, L3
Law, D. R., Majewski, D. R. 2010, ApJ, 718, 1128
Mackey, A. D., Gilmore, G. F. 2004a, MNRAS, 352, 153
Mackey, A. D., Gilmore, G. F. 2004b, MNRAS, 355, 504
Mackey, A. D., van den Bergh, S. 2005, MNRAS, 360, 631
Mackey, A. D., Payne, M. J., Gilmore, G. F. 2006a, MNRAS, 369, 921
Mackey, A. D., et al. 2006b, ApJ, 653, L105
Mackey, A. D., et al. 2007, ApJ, 655, L85
Mackey, A. D., et al. 2010a, MNRAS, 401, 533
Mackey, A. D., et al. 2010b, ApJ, 717, L11
Mackey, A. D., et al. 2013a, MNRAS, 429, 281
Mackey, A. D., et al. 2013b, ApJ, 770, L17
Mackey, A. D., et al. 2014, MNRAS, submitted
Marín-Franch, A., et al. 2009, ApJ, 694, 1498
Martin, N. F., Ibata, R. A., Irwin, M. J., Chapman, S. C., Lewis, G. F., Ferguson, A. M. N., Tanvir, N. R., McConnachie, A. W. 2006, MNRAS, 371, 1983
Martin, N. F., Ibata, R. A., McConnachie, A. W., Mackey, A. D., Ferguson, A. M. N., Irwin, M. J., Lewis, G. F., Fardal, M. A. 2013, ApJ, 776, 80
Martin, N. F., et al. 2014, ApJ, 787, 19

Martínez-Delgado, D., Zinn, R., Carrera, R., Gallart, C. 2002, ApJ, 573, L19
McConnachie, A. W. 2012, AJ, 144, 4
McConnachie, A. W., et al. 2008, ApJ, 688, 1009
McConnachie, A. W., et al. 2009, Nature, 461, 66
Pawlowski, M. S., Pflamm-Altenburg, J., Kroupa, P. 2012, MNRAS, 423, 1109
Richardson, J. C., et al. 2011, ApJ, 732, 76
Sarajedini, A., Mancone, C. L. 2007, AJ, 134, 447
Searle, L., Zinn, R. 1978, ApJ, 225, 357
Shapley, H. 1939, PNAS, 25, 565
Sharina, M., Davoust, E. 2009, A&A, 497, 65
Stonkutė, R., et al. 2008, AJ, 135, 1482
van den Bergh, S., Mackey, A. D. 2004, MNRAS, 354, 713
Veljanoski, J., et al. 2013a, ApJ, 768, L33
Veljanoski, J., et al. 2013b, MNRAS, 435, 3654
Veljanoski, J., et al. 2014, MNRAS, in press (arXiv:1406.0186)
West, M. J., Côté, P., Marzke, R. O., Jordán, A. 2004, Nature, 427, 31
Zepf, S. E., Ashman, K. M. 1993, MNRAS, 264, 611
Zinn, R. 1993, in Smith, G. H., Brodie, J. P., eds, ASP Conf. Ser. 48, The Globular Cluster-Galaxy Connection. Astron. Soc. Pac., San Francisco, p. 38

Lessons from the Sagittarius dSph Tidal Stream

Steven R. Majewski, David R. Law, Sten Hasselquist and Guillermo Damke

Abstract As the most prominent and extensive halo substructure in the Milky Way, the Sagittarius (Sgr) tidal stream gives us an important tool for exploring a number of problems in galactic astronomy. Here we will focus on four distinct applications of the Sgr stream: (1) Because stellar orbits are a product of the gravitational potential, tidal streams offer a unique probe of the distribution of dark matter. The Sgr stream allows us to probe the shape of the Milky Way potential to ~ 50 kpc. (2) The particular orientation of the Sgr stream allows measurement of the Local Standard of Rest velocity in a way independent of the solar Galactocentric distance via the proper motions of stream stars. (3) Because tidal stream stars tend to be stripped from the outermost parts of the parent object, the chemical properties of stars along a tidal stream enable us not only to reconstruct the net enrichment history of the parent body, but the original *radial* distribution of chemical abundances. (4) By determining those stars and clusters that are in the stream now, we can assess what types of stars and clusters get contributed to large, MW-like galaxies through the accretion process. Although now well studied for nearly two decades, the Sgr stream is still offering us surprises.

1 Introduction

It is appropriate that this meeting, which is, in part, recognizing the scientific accomplishments of Bruce Elmegreen, should include discussion of the Sagittarius (Sgr) stream, given that one of the first attempts to create an N-body simulation of this system was by Edelsohn and Elmegreen (1997; "EE97"), just a few years after the discovery of the Sgr dSph core (Ibata et al. 1994). At the time of the EE97 paper only

S. R. Majewski (✉) · S. Hasselquist · G. Damke
Department of Astronomy, University of Virginia, Charlottesville, VA 22904, USA
e-mail: srm4n@virginia.edu

D. R. Law
Dunlap Institute for Astronomy and Astrophysics, University of Toronto,
Toronto, ON M5S 3H4, Canada

S. Hasselquist
Department of Astronomy, New Mexico State University, Las Cruces, NM 88003, USA

K. Freeman et al. (eds.), *Lessons from the Local Group,*
DOI 10.1007/978-3-319-10614-4_19

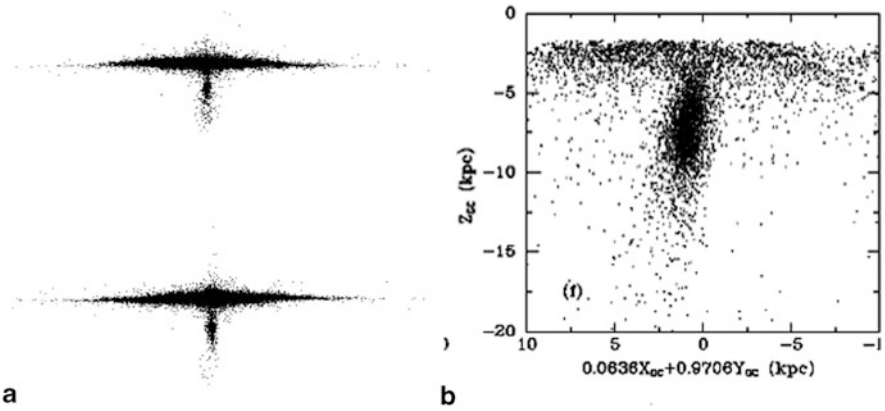

Fig. 1 The *left* figures show end stage configuration of the Sgr core (below the bulge of the Milky Way) from the early N-body simulation of the Sgr stream by Edelsohn and Elmegreen (1997). The *upper panel* is a simulation where the Sgr core is currently moving North (the correct direction), the *bottom panel* for the core moving South (the direction of motion of the core was not yet determined at the time). Note the remarkable similarity of the shape of the Sgr core (especially in the model for the correct motional direction of the core) in the simulation to the true shape of the core as traced by M giant stars (*right panel*) by Majewski et al. (2003)

rudimentary maps of the Sgr core were in hand (Ibata et al. 1997). Although Ibata et al. (1997) measured a rough proper motion for the satellite, the actual direction of motion was still in doubt; thus, EE97 modeled two general directions of motion, consistent with the directions along which the core was clearly elongated. The results of these early N-body simulations show a polar stream and a tidally disrupted dSph core having a remarkable resemblance to more recent, high quality maps of the Sgr core (Fig. 1). EE97 conclude from their work that the satellite is likely presently moving Northward and that its diffuse outer region is extended sufficiently to include the globular clusters M54, Arp 2, Ter 7 and Ter 8; both of these inferences are now known to be correct (see Siegel et al. 2011 for a 3-D, stereoscopic view of the Sgr core showing the relative orientation of these clusters within its diffuse stellar distribution).

In the subsequent, almost two decades since their discovery a considerable amount has been learned about the Sgr dSph and its tidal stream. Furthermore, as the most prominent and coherently long tidal tail system around the Milky Way (MW), with streams multiply wrapped around the Galaxy, the Sgr system uniquely lends itself to a number of scientific applications pointed at understanding Galactic structure, substructure, and dynamics, as well as the nature of hierarchical galaxy formation, at the finest levels of detail. In this short presentation, I select four areas where the Sgr stream is a useful tool for exploring these broader issues.

2 Shape of the Milky Way Dark Matter Halo

Using the Sgr stream to put constraints on the shape and strength of the MW's gravitational potential is an industry that extends back to the first, rudimentary assessments of its orientation and extent on the sky (e.g., Mateo et al. 1998; Majewski et al. 1999; Martínez-Delgado et al. 2001; Ibata et al. 2001) and the first N-body models of its interaction with the MW (Velazquez and White 1995; Johnston et al. 1995, EE97). Initial estimates from the apparently strong planarity of Sgr debris on the sky suggested that the Galactic dark halo is spherical in the Galactocentric distance range 16 kpc $< R_{GC} <$ 60 kpc (Ibata et al. 2001). Improved observational coverage and increasingly detailed modeling of the stream soon led, however, to conflicting conclusions regarding the shape of the Galactic halo depending on whether the velocities or positions of the stars in the stream were given more weight—a situation belying the fact that no axisymmetric model is capable of fitting the extant data. Specifically, while a model with an oblate to spherical dark halo can fit the positions of the Sgr stream (in particular, its leading arm) well (Johnston et al. 2005; Law et al. 2005; Fellhauer et al. 2006; Martínez-Delgado et al. 2007) it cannot at the same time produce the observed radial velocities of those stars, whereas a model with a prolate halo can match the leading arm velocities well, but not their positions (Helmi 2004; Law et al. 2005).

In hindsight, it is perhaps not too surprising that a solution to this quandary was offered by modeling the dark halo as having a *triaxial* configuration (Law et al. 2009; Law and Majewski 2010a—"LM10" hereafter), a gravitational potential that makes possible N-body simulations that can simultaneously match the positions and velocities of leading arm stars, as well as all other extant observations of the Sgr stream [except the observed bifurcation of the stream (Belokurov et al. 2006; Koposov et al. 2012), which continues to defy easy explanation (Penarrubia et al. 2010, 2011; Frinchaboy et al. 2012)]. Despite the success of this triaxial halo model, it is, however, a quite unsatisfying one because of the seemingly unlikely shape and orientation of the inferred dark matter distribution—i.e., strongly oblate (yielding a potential with $[c/a]_\phi = 0.72$ and $[b/a]_\phi = 0.99$), but with the minor axis within 7° of the Galactic X-axis (i.e., the Sun-Galactic Center axis). Such an unexpected orientation, being so strongly non-axisymmetric in the Galactic disk plane, is difficult to reconcile with stable disk star orbits and Cold Dark Matter models generally, which typically produce galaxies having aligned disk and halo minor axes (e.g., Debattista et al. 2008). Nevertheless, the LM10 model has remained amazingly resilient, as seen by its ability to successfully match even subsequently published data (e.g., Slater et al. 2013; Pila-Diez et al. 2014; see also Deg and Widrow 2013).

Note that LM10 never claimed that this model necessarily represented the true dark matter distribution, only that it was a numerical solution that produced N-body simulations that best match the observed data; these authors offered several potential alternative physical interpretations that may yield a similar numerical solution. One of many alternative explanations explored by LM10 focuses on the contributing gravitational influence of the Magellanic Clouds, which are orbiting in a plane whose axis is within 1° of that found for the minor axis of the triaxial halo. Although

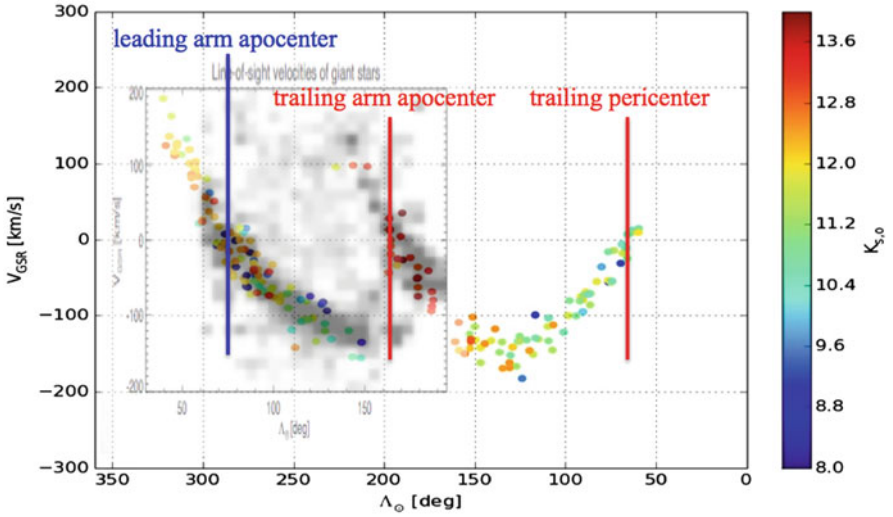

Fig. 2 The distribution of V_{GSR} as a function of Sgr stream orbital longitude for two samples of M giants along the Sgr stream plane. The *shaded inset* is a set of M giants selected from the SEGUE survey by Belokurov et al. (2014). The *points* are M giants selected from 2MASS by Majewski et al. (2004) and subsequent studies by this group, including data presented in Damke et al. (in prep.). The outer longitude scale is that defined by Majewski et al. (2003) and that on the *inset* is the inverted longitude system defined by Belokurov et al. (the two systems have been aligned in the figure). The *vertical lines* mark a pericenter and two apocenters of the stream

LM10 found that an LMC-mass in an LMC-orbital plane may perturb the Sgr orbit significantly, this issue is somewhat complicated by the issue of whether the LMC is on its first passage around the MW (see Besla, this proceedings). More recently, Vera-Ciro and Helmi (2013) have had success matching observations by adopting an even more complex Galactic potential than that of LM10—i.e., one that includes a variable shape with radius, from a "LCDM-normal", oblate potential flattened to the disk plane at small radius and only evolving into the "weird" LM10 shape at large radius. Moreover, the weird outer shape of the dark halo, the authors claim, can be accounted for by including perturbations from the LMC, thereby leading to an entirely "LCDM-palatable", composite gravitational potential.

Lest we be complacent in believing that we have, at last, arrived at a successful model that adequately explains the dynamics of the Sgr-MW merger and that successfully models the phase space distribution of Sgr debris, recent evidence reveals more unexpected complexity. Of course, the stream bifurcation remains a substantial thorn in the side of the modelers. But even seemingly more prosaic observational data are creating new mysteries! The previous debate about the dark halo shape focused on the dynamics of the Sgr leading arm, whereas, to date, almost all models could account for the dynamics of the Sgr trailing arm in the Southern Hemisphere. However, through further analyses of faint stars in both the SDSS and 2MASS databases, the trailing arm has been mapped to even greater lengths (Belokurov et al. 2014; Damke et al., in prep.). Figure 2 shows the radial velocities of M giant

stars independently identified by the SDSS and 2MASS, tracking the trailing arm into the Northern Hemisphere through and beyond its apogalacticon, and thereby clearly revealing its location (when the velocities are near 0 km s^{-1}). Unfortunately, the angular position of this trailing arm apocenter and its Galactocentric distance are dramatically different from those predicted by the LM10 and other models, and, based on our initial analysis, very difficult to accommodate with normal tweaking of the models. Belokurov et al. (2014) claim that the angular separation of apocenters on the sky imply that the dark matter density of the MW falls off faster than the isothermal haloes typically invoked (e.g., by LM10), but even this adjustment fails to account for the vastly different *distances* predicted for this section of the trailing arm. On the other hand, the derived distances for the confidently identified stream stars here are consistent with those previously measured for tentatively identified Sgr blue horizontal branch stars, as well as the globular cluster NGC 2419, a decade earlier by Newberg et al. (2003). The new problems that these observations create for our previously successful models shows us that the Sgr stream continues to surprise!

3 Constraining Fundamental Galactic Parameters

The Sgr stream is nearly polar, aligned closely to the Galactic X-Z plane. This particular orientation means that the proper motions of Sgr stream stars enable a measurement of the Local Standard of Rest (LSR) velocity, that, unlike most other methods, is independent of knowledge of the solar Galactocentric distance (Majewski et al. 2006): The V motion (equivalently, the $\mu_l \cos b$) of Sgr trailing arm stars is almost completely solar reflex, and the trailing arm nicely arcs across the Southern Galactic Hemisphere at distances tractable for measuring accurate proper motions.

As part of a proper motion program in the Kapteyn Selected Areas (SAs; see van der Kruit, this proceedings) led by SRM and D. Cassetti-Dinescu (e.g., Casetti-Dinescu et al. 2006) we have been matching recent photographic observations to original Mt. Wilson 60-inch plates taken from 1909–1912 (for J. Kapteyn) to derive $\sim$1–2 mas yr^{-1} per star proper motions in numerous SAs, and with a particular focus on SAs intersecting the Sgr trailing arm. An extensive spectroscopic program led by J. Carlin has enabled the identification of numerous Sgr stream stars in each of a half dozen SAs, allowing mean per field proper motions of the Sgr debris to 0.2–0.7 mas yr^{-1}. Using LM10-based models, but rerun with self-consistent gravitational potentials, the simulated Sgr debris yields a best match to the observations when the LSR velocity is Θ_{LSR} = 264$\pm$23 km s^{-1} (Carlin et al. 2012), a higher than traditional value consistent with other recent determinations of Θ_{LSR} or the solar rotation based on radio-interferometric proper motions of star forming regions in the outer disk (Reid et al. 2009) and Sgr A* (Reid and Brunthaler 2004) and the kinematics of disk stars from the SDSS APOGEE (Bovy et al. 2012) and SEGUE surveys (Schönrich 2012). Carlin et al. found that model fits that simultaneously reproduce known position, distance, and RV trends of the Sgr tidal streams, while significantly increasing Θ_{LSR}, can only be achieved by increasing the Galactic bulge and disk mass while leaving the dark matter halo fixed to LM10-like values.

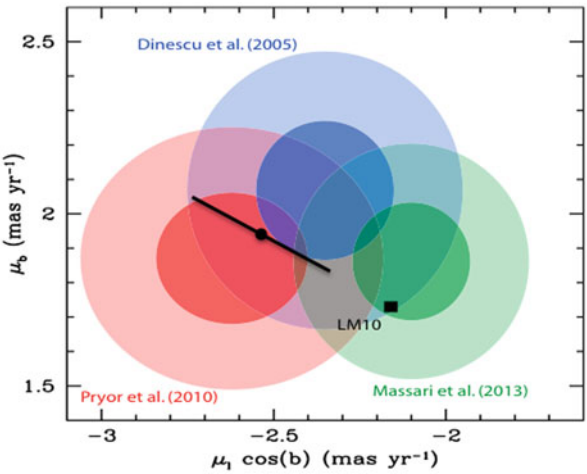

Fig. 3 Astrometric proper motions measurements (in Galactic coordinates) for the Sgr core (*large shaded circles* corresponding to 1σ and 2σ uncertainties) compared to that predicted by the standard LM10 model with $\Theta_{LSR} = 220$ km s^{-1} (*filled square*) and the LM10 model modified self-consistently by Carlin et al. (2012) for a $\Theta_{LSR} = 264 \pm 23$ km s^{-1} (*black filled circle with error bar*). The orientation of the *error bar* represents the allowed family of Sgr core proper motions modulated only by changes in Θ_{LSR}; the proper motion of the Sgr core is constrained to lie along this line because the orbital plane is fixed by the observed orientation of the Sgr tidal debris

Carlin et al. (2012) also noted that an apparent bonus of these self-consistent MW models is that they imply a proper motion for the Sgr core that is much more consistent with the mean of astrometric observations available at the time (Dinescu et al. 2005; Pryor et al. 2010) than that from an LM10 model with the traditional $\Theta_{LSR} = 220$ km s^{-1} (Fig. 3). Unfortunately, this satisfying self-consistency has been short-lived — now apparently foiled by a more recent Sgr core proper motion by Massari et al. (2013) that is more consistent with the original LM10 Θ_{LSR} (Fig. 3)!

4 Reconstructing the Original Sagittarius Galaxy and Sagittarius' Legacy to the Milky Way

4.1 Star Clusters

The census of stars and clusters observed to be in tidal streams gives extremely useful insights into the types of stars and clusters that get contributed to large, MW-like galaxies through the accretion process and on what timescales. The properties of globular clusters have long played a central role in ascertaining how the MW formed, with intense focus on the question of how those clusters formed *in situ* differ from those contributed through accretion (e.g., Searle and Zinn 1978). The prevailing lore

descended from Searle & Zinn is that clusters with properties conventionally interpreted as indicating that they are "younger"—e.g., clusters with horizontal branches too red for their metallicity (the second parameter effect) or with brighter main sequence turnoff magnitudes—would most likely be associated with accretion (e.g., Rodgers and Paltoglou 1984; Zinn 1993, 1996).

Thus, it is of great interest to determine what part of cluster parameter space is occupied by clusters we can see in the very process of being accreted. The latest comprehensive census of likely Sgr stream clusters is that by Law and Majewski (2010b, "LM10b"), which identified nine moderate (Ter 7, Pal 12, NGC 5053) to high (M 54, Arp 2, Ter 8, NGC 5634, Whiting 1, Berkeley 29) confidence candidates, based on matches to the present day configuration of Sgr debris as given by the LM10 model. This group of clusters closely follows the age-metallicity relation of stars in the Sgr core by Siegel et al. (2007), but, surprisingly, yields *few* candidate clusters with a second parameter effect. This is in contrast to the cluster populations currently bound to the Magellanic Clouds and Fornax dSphs (e.g., Buonanno et al. 1999), which will likely, someday, also be contributed to the MW halo. This contrast would seem to suggest that Sgr provides a striking contretemps to the traditional interpretation of the origins of "old" versus "young" clusters by suggesting that the strength of second parameter expression is less a division between accreted vs. in situ clusters and perhaps more simply a property exhibiting diversity among different cluster-contributing parent satellites.

However, this conclusion must now be revisited in light of the newly identified failure of the LM10 model to match the extreme ends of the Sgr trailing arm (§2, Fig. 2) and the fact that several of the LM10b Sgr cluster candidates are identified with older parts of that arm. The clear need to now include NGC 2419 among the Sgr candidates (§2) will not change the above interpretation regarding the diversity of cluster types that can be contributed to the halo, given that the extremely low metallicity and large age of this cluster matches the properties of other Sgr candidates, but it does raise interesting new questions given that now the two largest MW halo globulars (M54, NGC2419) can be associated with Sgr (excluding ω Cen as, itself, the residual core of an accreted dwarf galaxy–Lee et al. 1999; Majewski et al. 2000; Bekki and Freeman 2003). An exciting parallel development that promises even more vital insights into these questions is the ability to now study the properties of globular clusters in tidal streams in *other* spiral galaxies (Mackay, this proceedings).

4.2 Stars

Because the most loosely bound stars in a dwarf galaxy or star cluster tend to have the largest mean internal orbital radii, tidal stripping is generally the eating away of a satellite star system from the outside. When the orbit of that satellite in the parent potential lends itself to the formation of long, coherent tidal streamers—as in the case of Sgr—one can, to first order, read the variation in radial properties (e.g., the chemistry and ages of stars) of the original satellite as the variation of those properties along the tidal streamers. Of course, the situation is complicated by any

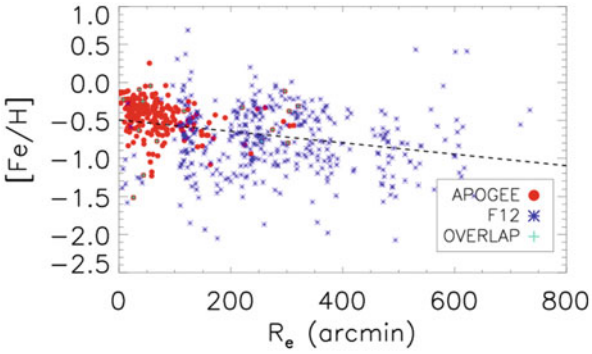

Fig. 4 Metallicities for Sgr stars as a function of elliptical radius in the dSph. *Star symbols* are abundances measured from infrared Ca triplet lines in $R \sim 15,000$ spectra from the Frinchaboy et al. (2012) sample. The *circles* show measurements of iron lines in $R \sim 22,500$ spectra from Data Release 10 (DR10) of the APOGEE project. *Stars* in both surveys are shown with *plus* signs and with the APOGEE [Fe/H]. The *dashed line* is a fit using a robust iterative outlier rejection method

star formation proceeding on timescales similar to the stripping timescale, as well as the fact that there is a "smearing out" of information by orbital phase overlap of stars stripped at different times, but, in fact, global metallicity variations along the Sgr stream have already clearly been identified (Bellazzini et al. 2006; Chou et al. 2007; Keller et al. 2010; Shi et al. 2012) and interpreted as indicating the likelihood of a strong metallicity gradient in the parent satellite (Chou et al. 2007). More recently, the existence of the predicted strong metallicity gradient in what remains of the Sgr core has been definitively mapped, using both medium and high resolution spectroscopy (Frinchaboy et al. 2012; Majewski et al. 2013; Hasselquist et al., in prep.), as collected in Fig. 4. A key lesson from these assessments of metallicity variations along the Sgr core and stream is that because of the time dependence of the specific populations contributed to the MW halo, the *current* content of a dSph is *not* representative of what it contributed to the halo. Thus, it may be dangerous to draw conclusions regarding the role or magnitude of accretion in galactic halos by comparing their stellar content to those in their currently bound satellites. The problem is exacerbated by the dominant contribution to stellar halos from satellites accreted early on, whereas current satellites have typically been accreted more recently (Font et al. 2006). In the same context, if one wants an accurate portrait of the star formation and chemical history of any particular satellite galaxy, one may have to *reconstruct it* by carefully accounting for the (likely different) stellar populations that have been previously stripped away (as attempted for Sgr in Chou et al. 2007, and warned about for the Carina dSph in Majewski et al. 2002).

Such differences between the Sgr core and tails are reinforced by exploration of their chemical abundance patterns in detail. Chou et al. (2010) show strong differences in s-process abundances (e.g., the heavy to light s-process element ratio [La/Y]) between Sgr tail and core stars. Only by putting together data from both the core and tails is the complete chemical history of Sgr revealed: As Chou et al.

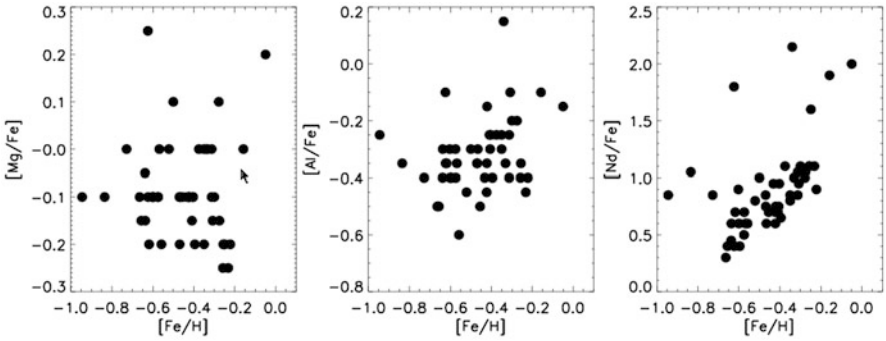

Fig. 5 Abundance trends for magnesium, aluminum and neodymium for Sgr stars as a function of iron abundance. The abundances were measured "by hand" (by SH) from APOGEE spectra (DR10) of stars in the Sgr core. The Nd values are preliminary, given that the transition probability for the Nd line in the APOGEE spectra is not yet firmly established; the handful of stars with the highest [Nd/Fe] may be on the asymptotic giant branch. For reference, the typical abundances for local MW stars by Bensby et al. (2005) are 0.0 to + 0.4 dex for both [Mg/Fe] and [Al/Fe]

show, the Ti, Y and La abundances across all metallicities reveals Sgr to have abundance patterns—and therefore an enrichment history—that closely resemble those of other dSphs and the Large Magellanic Cloud for these elements, only with different timescales for that enrichment, as reflected in *shifts* in the global abundance patterns with metallicity (Δ[Fe/H]). But these patterns are seen to be distinct from those seen in MW stars in the solar neighborhood—e.g., with Sgr showing a heavy s-process enhancement (La) and light s-process deficit (Y) with respect to MW field stars (see also McWilliam et al. 2013).

More recent analysis (Hasselquist et al., in prep.) of Sgr stars (for now, focused on the core) observed by the APOGEE project of SDSS-III (Majewski et al. 2010) also reveal Sgr to be deficient in Al and Mg with respect to Fe, and enhanced with respect to Nd (Fig. 5). The Al and Mg deficiencies, as well as deficiencies seen in other α-elements (McWilliam et al. 2013), could imply that Sgr's Initial Mass Function was deficient in the most massive Type II supernovae ("SNe"; McWilliam et al. 2013), or that the galaxy was not able to hold onto the yields from its Type II SNe. That Sgr is enhanced in heavy s-process elements like La and Nd (and that these increase with [Fe/H]) but not in the light s-process elements may be because of the dominance of leaky-box chemical enrichment of Sgr from low mass, metal-poor AGB stars that continues over multiple generations (McWilliam et al. 2013).

No matter their interpretation, these chemical patterns, which are so distinct from those seen in the local MW stars and include some features currently thought unique to Sgr, will be useful signatures for identifying Sgr stars now in the MW field through "chemical fingerprinting". Large-scale, high resolution spectroscopic surveys of the MW, such as GALAH and the dual hemisphere APOGEE-2 project, will be able to take advantage of these signatures to more completely map the current phase space distribution of Sgr stars throughout our Galaxy. No doubt, many more surprises are in store for us when this more complete mapping of the Sgr system is in hand.

References

Bekki, K., & Freeman, K. C. 2003, MNRAS, 346, L11
Bellazzini, M., Newberg, H. J., Correnti, M., Ferraro, F. R., & Monaco, L. 2006, A&A, 457, L21
Belokurov, V., Zucker, D. B., Evans, N. W., et al. 2006, ApJL, 642, L137
Belokurov, V., Koposov, S. E., Evans, N. W., et al. 2014, MNRAS, 437, 116
Bensby, T., Feltzing, S., Lundström, I., & Ilyin, I. 2005, A&A, 433, 185
Bovy, J., Allende Prieto, C., Beers, T. C., et al. 2012, ApJ, 759, 131
Buonanno, R., Corsi, C. E., Castellani, M., et al. 1999, AJ, 118, 1671
Carlin, J. L., Majewski, S. R., Casetti-Dinescu, D. I., et al. 2012, ApJ, 744, 25
Casetti-Dinescu, D. I., Majewski, S. R., Girard, T. M., et al. 2006, AJ, 132, 2082
Chou, M.-Y., Majewski, S. R., Cunha, K., et al. 2007, ApJ, 670, 346
Chou, M.-Y., Cunha, K., Majewski, S. R., et al. 2010, ApJ, 708, 1290
Debattista, V. P., Moore, B., Quinn, T., et al. 2008, ApJ, 681, 1076
Deg, N., & Widrow, L. 2013, MNRAS, 428, 912
Dinescu, D. I., Girard, T. M., van Altena, W. F., & López, C. 2005, ApJL, 618, L25
Edelsohn, D. J., & Elmegreen, B. G. 1997, MNRAS, 290, 7 (EE97)
Fellhauer, M., Belokurov, V., Evans, N. W., et al. 2006, ApJ, 651, 167
Font, A. S., Johnston, K. V., Bullock, J. S., & Robertson, B. E. 2006, ApJ, 638, 585
Frinchaboy, P. M., Majewski, S. R., Muñoz, R. R., et al. 2012, ApJ, 756, 74
Helmi, A. 2004, ApJL 610, L97
Ibata, R. A., Gilmore, G., & Irwin, M. J. 1994, Nature, 370, 194
Ibata, R. A., Wyse, R. F. G., Gilmore, G., Irwin, M. J., & Suntzeff, N. B. 1997, AJ, 113, 634
Ibata, R., Lewis, G. F., Irwin, M., Totten, E., & Quinn, T. 2001, ApJ, 551, 294
Johnston, K. V., Spergel, D. N., & Hernquist, L. 1995, ApJ, 451, 598
Johnston, K. V., Law, D. R., & Majewski, S. R. 2005, ApJ, 619, 800
Keller, S. C., Yong, D., & Da Costa, G. S. 2010, ApJ, 720, 940
Koposov, S. E., Belokurov, V., Evans, N. W., et al. 2012, ApJj, 750, 80
Law, D. R., & Majewski, S. R. 2010a, ApJ, 714, 229 (LM10)
Law, D. R., & Majewski, S. R. 2010b, ApJ, 718, 1128 (LM10b)
Law, D. R., Johnston, K. V., & Majewski, S. R. 2005, ApJ, 619, 807
Law, D. R., Majewski, S. R., & Johnston, K. V. 2009, ApJL, 703, L67
Lee, Y.-W., Joo, J.-M., Sohn, Y.-J., et al. 1999, Nature, 402, 55
Majewski, S. R., Siegel, M. H., Kunkel, W. E., et al. 1999, AJ, 118, 1709
Majewski, S. R., Patterson, R. J., Dinescu, D. I., et al. 2000, Liege International Astrophysical Colloquia, 35, 619
Majewski, S. R., Patterson, R. J., Palma, C., et al. 2002, Modes of Star Formation and the Origin of Field Populations, 285, 199
Majewski, S. R., Skrutskie, M. F., Weinberg, M. D., & Ostheimer, J. C. 2003, ApJ, 599, 1082
Majewski, S. R., Kunkel, W. E., Law, D. R., et al. 2004, AJ, 128, 245
Majewski, S. R., Law, D. R., Polak, A. A., & Patterson, R. J. 2006, ApJL, 637, L25
Majewski, S. R., Wilson, J. C., Hearty, F., Schiavon, R. R., & Skrutskie, M. F. 2010, IAU Symposium, 265, 480
Majewski, S. R., Hasselquist, S., Łokas, E. L., et al. 2013, ApJL, 777, L13
Martínez-Delgado, D., Aparicio, A., Gómez-Flechoso, M. Á., & Carrera, R. 2001, ApJL, 549, L199
Martínez-Delgado, D., Peñarrubia, J., Jurić, M., Alfaro, E. J., & Ivezić, Z. 2007, ApJ, 660, 1264
Massari, D., Bellini, A., Ferraro, F. R., et al. 2013, ApJ, 779, 81
Mateo, M., Olszewski, E. W., & Morrison, H. L. 1998, ApJL, 508, L55
McWilliam, A., Wallerstein, G., & Mottini, M. 2013, ApJ, 778, 149
Newberg, H. J., Yanny, B., Grebel, E. K., et al. 2003, ApJL, 596, L191
Peñarrubia, J., Belokurov, V., Evans, N. W., et al. 2010, MNRAS, 408, L26
Peñarrubia, J., Zucker, D. B., Irwin, M. J., et al. 2011, ApJL, 727, L2

Pila-Díez, B., Kuijken, K., de Jong, J. T. A., Hoekstra, H., & van der Burg, R. F. J. 2014, A&A, 564, A18
Pryor, C., Piatek, S., & Olszewski, E. W. 2010, AJ, 139, 839
Reid, M. J., & Brunthaler, A. 2004, ApJ, 616, 872
Reid, M. J., Menten, K. M., Zheng, X. W., et al. 2009, ApJ, 700, 137
Rodgers, A. W., & Paltoglou, G. 1984, ApJL, 283, L5
Schönrich, R. 2012, MNRAS, 427, 274
Searle, L., & Zinn, R. 1978, ApJ, 225, 357
Shi, W. B., Chen, Y. Q., Carrell, K., & Zhao, G. 2012, ApJ, 751, 130
Siegel, M. H., Dotter, A., Majewski, S. R., et al. 2007, ApJL, 667, L57
Siegel, M. H., Majewski, S. R., Law, D. R., et al. 2011, ApJ, 743, 20
Slater, C. T., Bell, E. F., Schlafly, E. F., et al. 2013, ApJ, 762, 6
Velazquez, H., & White, S. D. M. 1995, MNRAS, 275, L23
Vera-Ciro, C., & Helmi, A. 2013, ApJL, 773, L4
Zinn, R. 1993, The Globular Cluster-Galaxy Connection, 48, 38
Zinn, R. 1996, Formation of the Galactic Halo...Inside and Out, 92, 211

Dwarf Irregular Galaxies of the Local Group

Deidre A. Hunter

Abstract Local Group dwarf irregulars (dIrrs) cover an enormous range in star formation properties. Here I discuss these tiny galaxies as probes of star formation at the extremes of low gas densities and low metallicities. We have learned that (1) Star formation is inefficient in dIrrs and yet at very low $\Sigma_{\rm HI}$ (< 0.5 $M_\odot$ pc^{-2}) the star formation rate is higher than expected from a linear extrapolation from star formation at higher $\Sigma_{\rm HI}$. (2) Star formation correlates with existing stars and stellar feedback could be important. (3) Stellar disks go on for a long ways, often with very regular surface brightness profiles and reaching very low $\Sigma_{\rm HI}$. (4) Breaks in surface brightness profiles occur at about the same magnitude in both spirals and dwarfs, so something fundamental is taking place there. (5) Dwarf disks appear to grow from the "outside-in", contrary to spirals. (6) At low metallicity, star formation takes place in giant molecular clouds, but the photodissociation region is large.

1 Introduction

When I started graduate school, there were the "seven dwarfs" of the Local Group. Today of order 50 are known, and there are likely more to be found. Of these ~ 20 are dwarf irregulars (dIrrs), lumpy little galaxies with gas. These are the dwarfs that are forming, or could potentially form, stars, and they are the subject of this discussion.

The Local Group contains dIrrs that span a large range of properties. One extreme is exemplified by Leo T (Fig. 1), at a distance of 0.4 Mpc and a possible satellite of the Milky Way. It was discovered just recently (Irwin et al. 2007), and has an M_V of only -8, not much brighter than a large star cluster or even the kind of individual stars that my spouse (Phil Massey) works on. In fact it only has about 10^5 $M_\odot$ of stars and about 3 times that in HI (Ryan-Weber et al. 2008). The peak HI column density is a mere 7×10^{20} cm^{-2} and the gas is stable against gravitational instabilities. Nevertheless, the galaxy not only has old (>5 Gyr) stars, but young (200 Myr−1 Gyr) stars as well (de Jong et al. 2008). How could such a little puddle of gas form stars?

D. A. Hunter (✉)
Lowell Observatory, 1400 West Mars Hill Road, Flagstaff, AZ 86001, USA
e-mail: dah@lowell.edu

K. Freeman et al. (eds.), *Lessons from the Local Group,*
DOI 10.1007/978-3-319-10614-4_20

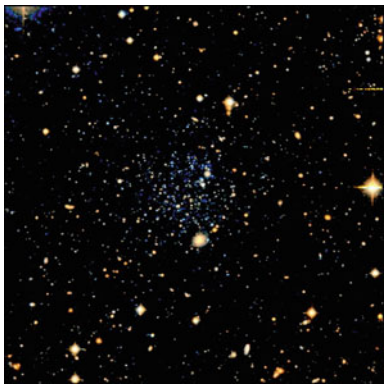

Fig. 1 Leo T from Irwin et al. (2007), by permission from M. J. Irwin

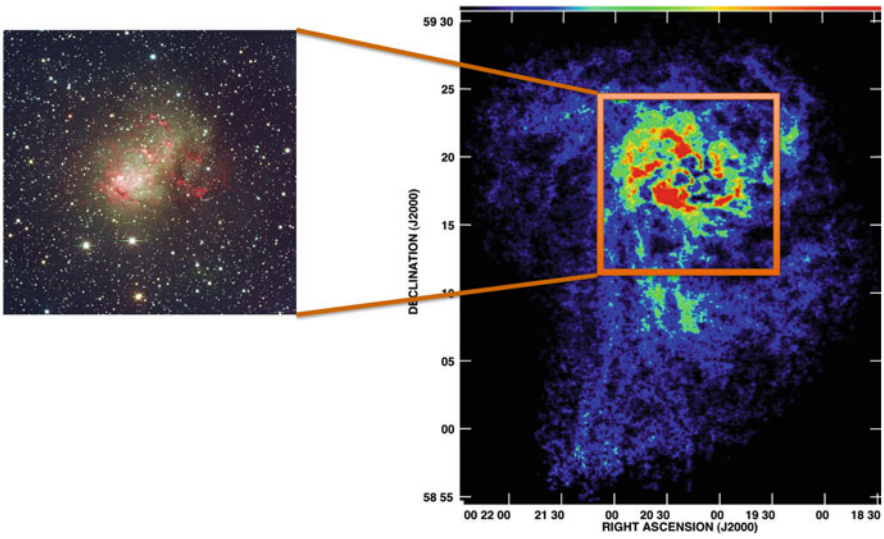

Fig. 2 IC10. An optical image is on the *left* and a false-color integrated HI from Hunter et al. (2012) is on the *right*

At the other extreme is IC 10 (Fig. 2), at 0.7 Mpc, a satellite of M31, and an M_V of -16. It is the only starburst galaxy in the Local Group. In fact, it hosts an extraordinary surface density of short-lived evolved massive WR stars (Massey and Holmes 2002), indicating a temporal coherence in the starburst across the galaxy. IC 10 contains $\sim 3 \times 10^7$ $M_\odot$ of HI gas with a peak column density of $\sim 10^{22}$ cm^{-2} (Wilcots and Miller 1998). The HI extends in a strange fan-like morphology to the south of the stellar disk, as well as to the east, and the kinematics are complex. Recently Nidever et al. (2013) discovered an HI filament stretching to a coherent gas blob and suggest that IC 10 may have merged with another dwarf.

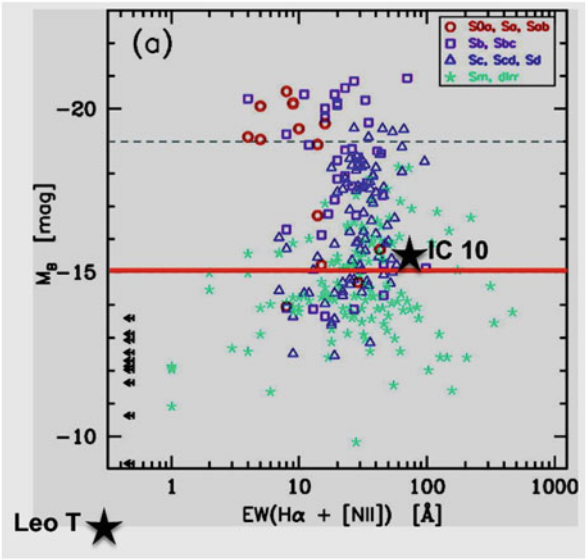

Fig. 3 Integrated Hα equivalent width, a measure of the ratio of new stars to old stars, plotted against M_B from Lee et al. (2007) by permission from J. Lee. IC 10 and Leo T are placed on this figure as *large stars*, using data from Kennicutt et al. (2008) for IC 10. Leo T actually has no current Hα emission, so it is placed at the *low end* of the logarithmic axis. The *horizontal line* at $M_B = -15$ marks the regime below which the EWs spread out to cover a larger range than above the line

Ricotti and Gnedin (2005) argue that Local Group dwarfs are defined by how they weathered the epoch of reionization in the early universe: "survivors" formed most of their stars after reionization, "true fossils" are those that became frozen in their pre-reionization state, and "polluted fossils" are those in between these two states. In their Fig. 5, IC 10 is a survivor. Ricotti (2009) argues that Leo T is a dark matter minihalo that accreted gas after reionization, producing the bimodal stellar population seen in that galaxy. This would make Leo T a "polluted fossil."

One thing we have learned about nearby dwarfs is that star formation rates become unstable in lower luminosity ($M_B > -15$) systems (Lee et al. 2007). Lee et al. plotted the integrated equivalent width of Hα, which is related to the ratio of new stars to old stars, against integrated galactic M_B. They find that giant spirals and brighter dwarfs occupy a narrow range of EWs, but lower luminosity systems cover a wide range. We show this plot in Fig. 3 with IC 10 and Leo T placed on it. IC 10 lies just above the line denoting the $M_B = -15$ transition and Leo T, a long ways below. Lee et al. suggest a change in star formation regulation at low luminosities so that systems swing from higher rates to lower rates, called "gasping" star formation by Marconi et al. (1995) and collaborators. There is a hint that lower luminosity dwarfs also become puffier in shape (Zhang et al. 2012; Johnson et al. 2014), and perhaps the shape goes hand in hand with a global regulation instability.

Here I would like to discuss Local Group dIrrs as probes of star formation at the extremes of low gas densities and low metallicities. Low gas densities are relevant to understanding star formation in outer stellar disks. In addition, dIrrs give us a glimpse into star formation processes under HI-dominated, very low metallicity conditions, such as expected in proto-galaxies at high z.

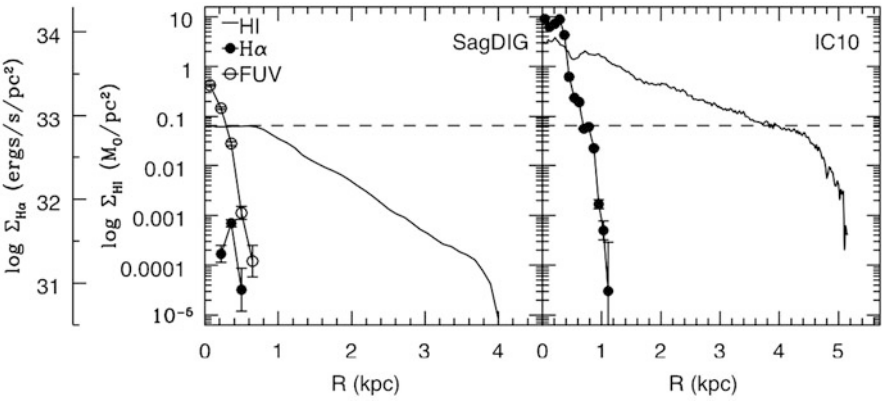

Fig. 4 HI surface density profiles from Hunter et al. (2012). The *horizontal dashed line* marks the highest surface densities in SagDIG, to allow comparison with IC 10. The radial profiles for Hα emission and FUV (which is not available for IC 10) are also shown; both are measures of recent star formation. We see that, at the surface densities where star formation is taking place in SagDIG, in IC 10 there is no star formation. This illustrates the problem in connecting HI and star formation.

2 Star Formation at Low Gas Densities

In the general picture of star formation, stars form from molecular clouds and molecular clouds form from atomic gas. Figure 4 illustrates the problem with understanding the connection between HI and star formation. Here I compare the HI surface density profile of IC 10 with that of SagDIG. SagDIG is a low star formation rate system and IC 10 is the starburst we discussed previously. The radial profiles of recent star formation tracers (Hα and FUV emission) are also shown. We see that at the radius in IC 10 ($\sim$ 4 kpc) where its $\Sigma_{\rm HI}$ drops to the value where all of the star formation is taking place in SagDIG ($\sim$ 0.1 $M_\odot$ pc^{-2}), there is no star formation. In IC 10 all of the star formation is taking place only at much higher $\Sigma_{\rm HI}$ ($\sim$ a few $M_\odot$ pc^{-2}). Why?

2.1 Empirical Star Formation Properties

With the lack of a true understanding of the large-scale drivers of star formation, people have turned to empirical laws relating the atomic gas to recent star formation. Bigiel et al. (2008, 2010) divided a sample of mostly spiral galaxies into sub-kpc cells and Ficut-Vicas et al. (2014) similarly divided a sample of 20 dwarfs into 400 pc cells. They plot the star formation rate per unit area versus the HI gas density $\Sigma_{\rm HI}$ in each cell. For the inner disks of spirals, there is a pretty good relationship: the higher the HI gas density, the higher the star formation rate, until most of the HI turns molecular above 10 $M_\odot$ pc^{-2}. For dwarf galaxies and the outer disks of

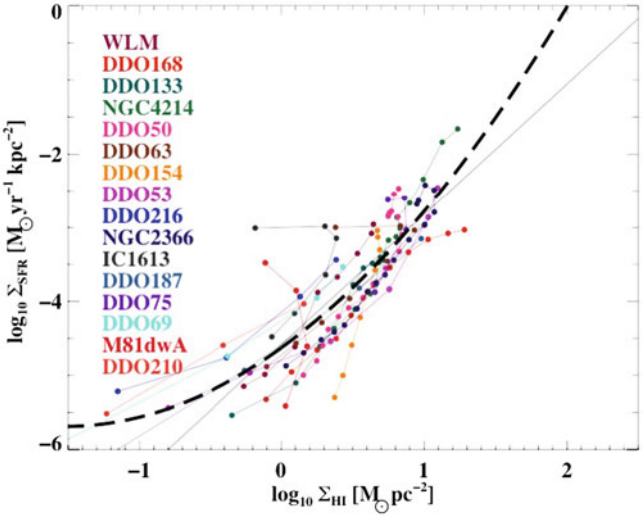

Fig. 5 Radial profiles of Σ_{SFR} versus Σ_{HI} for 20 dIrr galaxies examined in 400-pc cells (Ficut-Vicas et al. 2014, reproduced with permission of D. Ficut-Vicas.). The *straight gray line* is a linear fit to the profiles; the c*urved dashed black line* is a polynomial fit. The star formation rate is higher at low Σ_{HI} than predicted by the relationship at higher Σ_{HI}

spirals there is also a general relationship but with a much higher (up to a factor of 100) spread of star formation rates for a given gas density. In general, too, the star formation efficiency, defined as the star formation per unit gas mass, is much lower in dwarfs than in spirals (Leroy et al. 2008; Ficut-Vicas et al. 2014).

However, there is something very peculiar that happens at the low end of Σ_{HI} (< 0.5 $M_\odot$ pc^{-2}) in dwarfs. Ficut-Vicas et al. (2014) find that the actual star formation rate there is higher than predicted from a linear extrapolation from higher Σ_{HI} regions. This is shown in Fig. 5. What is driving star formation at very low gas densities?

Ficut-Vicas et al.'s (2014) study of dwarfs also shows that there is a strong correlation between star formation rate and the mass surface density of older stars. Are environmental conditions deterministic so that a given place in a galaxy always has the same star formation rate averaged over an appropriately long timescale? If so, then we don't know what the important environmental conditions are. Are stellar disk potentials important in determining star formation capability? But dIrrs are HI-dominated galaxies. Or is feedback from star formation crucial in dwarf galaxies that have nothing much else going for them to form star-forming gas clouds?

We know that star-induced star formation takes place. A beautiful example is Constellation III in the LMC (Dopita et al. 1985) where a star-forming event 15 Myr ago blew a hole in the HI 2 kpc across. The second generation of star formation is now taking place in the shell that surrounds the hole. But one of the consequences of this process is that sometimes the interstellar medium (ISM) of dwarfs ends up

looking like Swiss cheeese—full of holes. This is especially true of dwarfs where limited shear means holes last a long time. This raises the questions: What percentage of star formation is due to stellar feedback? And, what is the effect of porosity (the filling factor of the holes) on star formation?

In the LMC, Dawson et al. (2013) have looked at the overall percentage of secondary star formation caused by supergiant shells, of which the LMC has many. They find 4–11 % of the star formation today is due to stellar feedback. This is a lower limit since there are smaller shells that they did not include. In DDO 50, on the other hand, "most" of the star formation is associated with shells around holes (Stewart et al. 2000; Stewart and Walter 2000). Pohkrel et al. (2014) are currently in the process of addressing the two questions posed above for a large sample of dwarf galaxies spanning a wide range of properties.

There is another, less direct, potential connection between stars and star formation. This comes from the model of Ostriker et al. (2010). In this model ISM heating by stellar UV light plays a key role in regulating $\Sigma_{\rm SFR}$. It looks like there is a general correspondence between $\Sigma_{\rm SFR}$ and $\Sigma_{\rm stars}$ (compare, for example, their Fig. 4, panels c and d). However, in gas-dominated regions like dIrrs, $\Sigma_{\rm SFR} \propto \Sigma_{\rm gas} \times \sqrt{\rho_{\rm stars} + \rho_{DM}}$, so $\log \Sigma_{\rm SFR} \propto \log \Sigma_{\rm stars}$, as observed, isn't obvious.

2.2 *Outer Disks*

Dwarf outer disks are the realm of *very* low gas densities. Nevertheless, stellar disks can extend an extraordinarily long ways. Through star counts, Saha et al. (2010) have traced a disk of old stars in the LMC to 12 disk scale lengths, an equivalent μ_I of 34 mag arcsec^{-2}. The young stars were traced to 8 disk scale lengths. Furthermore, the surface density of stars is exponential in form all the way in spite of the LMC being a very irregular galaxy. In DDO 70 and DDO 75 Bellazzini et al. (2014) have traced star counts to an equivalent μ_V of 31 mag arcsec^{-2}, about 6 disk scale lengths. Ultra-deep V-band and *GALEX* FUV imaging of 5 dwarfs revealed stellar disks with young stars to μ_V of 30 mag arcsec^{-2}, traced into the realm of highly stable gas (Hunter et al. 2011).

The Ostriker et al. (2010) model, which built on Elmegreen and Parravano (1994), may provide a way to understand stellar disks that go on and on into highly subcritical gas densities. In their model star formation adjusts to provide the needed FUV heating to balance cooling and, thus, to match the thermal pressure to the mid plane pressure set by the vertical gravitational field. So, the star formation rate continues, although declining with decreasing efficiency, to large radii, and there is no sharp cutoff caused by a $\Sigma_{\rm HI}$ limit. On the other hand, a comparison of the $\Sigma_{\rm SFR}$ predicted by the model with FUV surface photometry in a sample of dIrrs shows some correspondence between model and observations, but is not generally good (Fig. 6)

Many of the dwarfs display broken stellar exponential profiles: an exponential surface density profile that changes slope in the outer disk with, usually, a downward

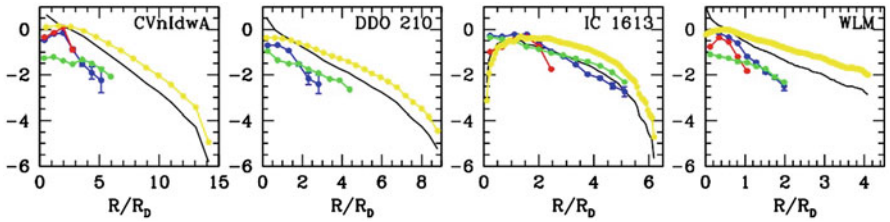

Fig. 6 Comparison of predicted SFR from the Ostriker et al. (2010) model for the gas dominated regime (*black line*) with observed SFR tracers (FUV in *blue*, Hα in *red*), as well as gas (*yellow*) and stars (*green*, Zhang et al. 2012). The y-axis is the logarithm of the quantity (or magnitude for FUV), and the zero point is adjusted to bring the profiles together but the intervals on the y-axis are the same. The radius is in units of disk scale length R_D. The model SFR follows the HI most closely and only in some cases follows the observed SFR tracers

bend. This break in the profiles implies a change in the cloud/star formation process at the break radius. Amazingly, however, this break occurs at about the same V-band surface brightness in spirals and in dwarfs (Herrmann et al. 2013). Clearly, something fundamental happens at the break in *both* spirals and dwarfs, but what?

Elmegreen and Hunter (2006) have proposed that the profile breaks represent a shift from gravitational instabilities driving cloud formation in the inner disk to turbulence compression in the outer disk. Turbulence adds nothing to star formation in the inner disk, but is, according to this model, crucial to the formation of clouds in the outer, stable gas disk. This model predicts the average break radius for dwarfs and that the break occurs closer to the center of the galaxy compared to spirals.

In some galaxies the outer disk surface brightness profiles are much more complex than a simple exponential with a break. In DDO 75, for example, the profile is flat to almost 1 kpc radius, then drops exponentially to 1.4 kpc. From there it drops less steeply to 2.6 kpc, brightens for a ways and then brightens some more to 4.4 kpc (Bellazzini et al. 2014). Bellazzini et al. suggest that DDO 75 has been disturbed. Ironically, DDO 75, being on the outer edge of the Local Group, had been thought to be one of the most pristine nearby dwarfs (Wilcots and Hunter 2002).

2.3 *Outside-In Disk Growth*

The current paradigm for spiral galaxies is that the stellar disks grow from the inside-out (see, for example, Muñoz-Mateos et al. 2007). However, for dwarfs disk growth appears to be from the outside-in. In a study of a 34 nearby dIrrs, Zhang et al. (2012) found that in systems with baryonic masses $< 10^8$ $M_\odot$ the star formation rate in the outer disk has been declining with time, while in the more massive dwarfs the radial ratios of star formation rates over different time scales is relatively flat. However, in the LMC, which is a massive dIrr, Meschin et al. (2013) also found outside-in disk growth from a study of star formation histories in 3 fields from 3.5 to 6 kpc radius.

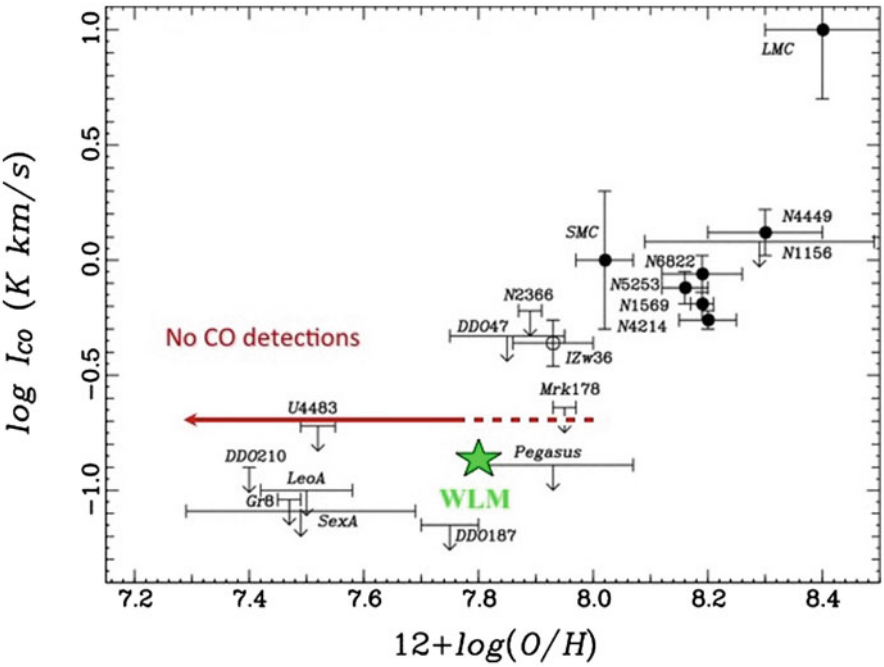

Fig. 7 Measurements of I_{CO} as a function of galaxy oxygen abundance at low metallicity. Measurements from Tacconi and Young (1987) and Taylor et al. (1998); plot courtesy of M. Rubio. Only the *solid black circles* and the *green star* marking WLM are detections. The measurement of CO in WLM extends the detections to 13 % of solar metallicity (Elmegreen et al. 2013)

In the inner regions stars formed 7 Gyr ago and 4 Gyr ago in equal amounts and star formation is continuing today. However, in the outer field, stars formed 7 Gyr ago, only 40 % more formed 4 Gyr ago, and star formation ceased about 1 Gyr ago. One possibilty is that gas is somehow being removed from outer disks of dwarfs making it increasingly difficult to form stars out there.

3 Star Formation at Low Metallicity

Atoms heavier than H and He and dust play an important role in cooling the gas so that it can make cold molecular clouds, where we typically find star formation. The oxygen abundances of dIrrs in the Local Group range down to roughly 1/50 solar.

One of the results of low metallicity is poor shielding of molecular clouds. As a consequence it is expected that the structure of the molecular cloud itself will change as the metallicity drops. In particular the CO core will shrink and the photodissociation region (PDR) will grow (Maloney and Black 1988; Bolatto et al. 1999; Röllig et al. 2006). In fact, it is possible that in galaxies with metallicities below a few

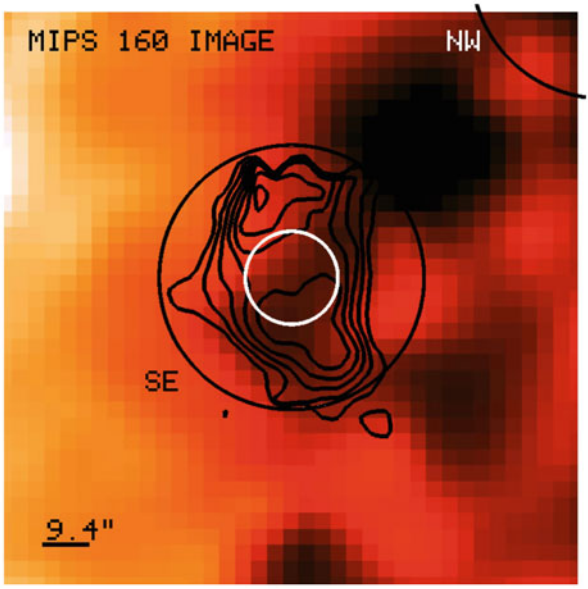

Fig. 8 *Spitzer* MIPS 160 μm image of a region where CO (3-2) was detected in WLM (Elmegreen et al. 2013). The *white circle* is the telescope beam size and pointing that produced the detection. The *black contours* are of [CII]λ158 μm, the primary fine-structure line of the PDR (Cigan et al. 2014). The *large black circle* is the field of view of pending ALMA CO (1-0) observations. These data reveal a PDR that is at least comparable in width to the diameter of the CO core at a metallicity 13 % of solar (Cigan et al. 2014)

percent of solar, star formation will proceed in the cold atomic gas rather than in molecular gas (Krumholz 2012).

The shrinking CO core with declining metallicity has meant that molecular gas has been hard to detect at metallicities below 20 % of solar. However, Elmegreen et al. (2013) used the APEX sub-mm telescope in Chile to observe CO (3-2) in WLM with a beam that is 87 pc at WLM. They detected two molecular clouds with H_2 masses of 1-2$\times 10^5$ $M_\odot$. Thus, at 13 % of solar metallicity, star formation is taking place in giant molecular clouds. Figure 7 shows the WLM detection in the context of other measurements as a function of oxygen abundance.

With the WLM CO detection we can now begin to test the model of shrinking CO core and growing PDR with decreasing metallicity. In Fig. 8, contours of a *Herschel* image of the [CII]λ158 μm fine-structure line of one region shows the PDR (Cigan et al. 2014). The white circle shows the CO detection. An ALMA CO (1$-$0) map that is currently pending will further resolve the CO core, but Cigan et al. can already show that the CO core is $<$ 86 pc diameter and the PDR is an annulus around the core with a thickness that is comparable to the core diameter. Additional CO observations with the ALMA sub-mm array of other dIrrs in the Local Group at even lower metallicity may finally allow us to construct a picture of molecular cloud structure as a function of metallicity.

Acknowledgements DAH would like to thank the organizers for putting this very interesting workshop together. She also appreciates funding by the Lowell Observatory Research Fund to attend and to prepare this talk.

References

Bigiel, F., et al., 2008, AJ, 136, 2846
Bigiel, F., et al., 2010, AJ, 140, 1194
Bellazzini, M., et al., 2014, A&A, 566, 44
Bolatto, A. D., et al., 1999, ApJ, 513, 275
Cigan, P., et al., 2014, in preparation
Dawson, J. R., et al., 2013, ApJ, 763, 56
de Jong, J. T. A., et al. 2008, ApJ, 680, 1112
Dopita, M. A., et al., 1985, ApJ, 297, 599
Elmegreen, B. G., & Hunter, D. A., 2006, ApJ, 636, 712
Elmegreen, B. G., & Parravano, A. 1994, ApJ, 435, L121
Elmegreen, B. G., et al., 2013, Nature, 495, 487
Ficut-Vicas, D., et al., 2014, in preparation
Herrmann, K. A., Hunter, D. A., & Elmegreen, B. G., 2013, AJ, 146, 104
Hunter, D. A., et al., 2011, AJ, 142, 121
Hunter, D. A., et al., 2012, AJ, 144, 134
Irwin, V., et al., 2007, ApJ, 656, L13
Johnson, M., et al., 2014, in preparation
Kennicutt, R. C., Jr., et al., 2008, ApJS, 178, 247
Krumholz, M. R., 2012, ApJ, 759, 9
Lee, J. C., et al., 2007, Ap, 671, L113
Leroy, A., et al., 2008, AJ, 136, 2782
Maloney, P., & Black, J. H., 1988, ApJ, 325, 389
Marconi, G., et al., 1995, AJ, 109, 173
Massey, P., & Holmes, S., 2002, ApJ, 580, 35
Muñoz-Mateos, J. C., et al., 2007, ApJ, 658, 1006
Nidever, D. L., et al., 2013, ApJ, 779, L15
Ostriker, E., et al., 2010, ApJ, 721, 975
Pohkrel, N. R., Simpson, C., et al. 2014, in preparation
Ricotti, M., 2009, MNRAS, 392, L45
Ricotti, M., & Gnedin, N. Y., 2005, ApJ, 629, 259
Röllig, M., et al., 2006, A&A, 451, 917
Ryan-Weber, E. V., et al., 2008, MNRAS, 384, 535
Saha, A., et al., 2010, AJ, 140, 1719
Stewart, S. G., & Walter, F., 2000, AJ, 120, 1794
Stewart, S. G., et al., 2000, ApJ, 529, 201
Tacconi, L, & Young, J. S., 1987, ApJ, 322, 681
Taylor, C. L., et al., 1998, AJ, 116, 2746
Wilcots, E. M., & Hunter, D. A., 2002, AJ, 123, 1476
Wilcots, E. M., & Miller, B. W., 1998, AJ, 116, 2363
Zhang, H.-X., et al., 2012, AJ, 143, 47

Morphological Transformations of Dwarf Galaxies in the Local Group

Giovanni Carraro

Abstract In the Local Group there are three main types of dwarf galaxies: Dwarf Irregulars, Dwarf Spheroidals, and Dwarf Ellipticals. Intermediate/transitional types are present as well. This contribution reviews the idea that the present day variety of dwarf galaxy morphologies in the Local Group might reveal the existence of a transformation chain of events, of which any particular dwarf galaxy represents a manifestation of a particular stage. In other words, all dwarf galaxies that now are part of the Local Group would have formed identically in the early universe, but then evolved differently because of morphological transformations induced by dynamical processes like galaxy tidal interaction, ram pressure stripping, photo-evaporation, and so forth. We start describing the population of dwarf galaxies and their spatial distribution in the LG. Then, we describe those phenomena that can alter the morphology of a dwarf galaxies, essentially by removing, partially or completely, their gas content. Lastly, we discuss morphological signatures in the Local Group Dwarf Galaxies that can be attributed to different dynamical phenomena. While it is difficult to identify a unique and continuous transformation sequence, we have now a reasonable understanding of the basic evolutionary paths that lead to the various dwarf galaxy types.

1 Introduction

The Local Group (LG) has a physical radius of ∼1.2 Mpc (van den Bergh 1999): this is defined as the radius of its zero-velocity surface, namely the surface which separates the LG from the field expanding with the Hubble flow. The LG is located at the outskirts of the large Virgo cluster. The actual LG is dominated by three spiral galaxies: M 31(NGC 224, the Andromeda galaxy), the Milky Way (MW), and M 33 (NGC 598, the Triangulum galaxy), in decreasing order of mass. There are no giant or intermediate-mass ellipticals in the LG. The remaining galaxies are dwarf galaxies (DG), and their number has been increasing over the years, since fainter and fainter

G. Carraro (✉)
European Southern Observatory, Alonso de Cordova 3107, 19001 Santiago de Chile, Chile
e-mail: gcarraro@eso.org

K. Freeman et al. (eds.), *Lessons from the Local Group,*
DOI 10.1007/978-3-319-10614-4_21

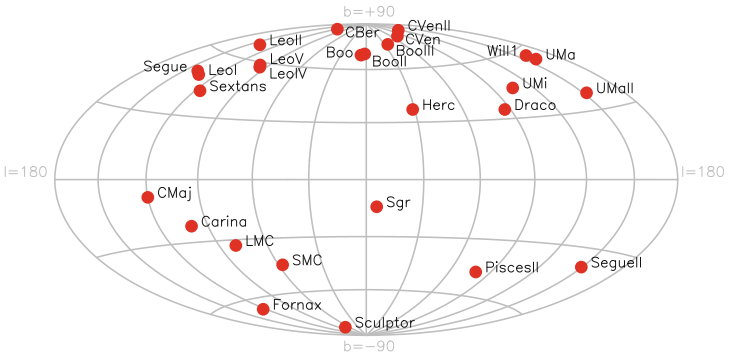

Fig. 1 Distribution of dwarf galaxies in the LG following McConnachie (2012): DGs associated with the MW (*red symbols*)

objects are being discovered (e.g. Crater, Belokurov et al. 2014) out of deep and wide area sky surveys (2MASS, SDSS, etc.). The exact number of DG in the LG is unknown. As of today, they would be $\sim$ 70 (McConnachie 2012).

The majority of these DGs groups are around M 31 and the MW. M 33, the smallest galaxy among the spirals, might have two possible companions (the Pisces and Andromeda XXII dwarfs). All the remaining galaxies are too distant from the three dominant spirals to be considered bound to them. NGC 3109 and Antlia may constitute a group themselves (the 14 + '12 group; McConnachie 2012), together with Sextans A and B, and, possibly, Leo P (Bernstein-Cooper et al. 2014). The membership of the NGC 3109 - and companions- to the LG is disputed, since this group shows a filamentary structure and seems to be in the verge to enter the LG (Bellazzini et al. 2013, 2014) for the first time.

In Figs. 1 and 2 we show the distribution of DG in the LG according to the recent compilation by McConnachie (2012). Figure 1 shows the DGs associated with the Milky Way, while Fig. 2 shows DGs associated with M 31 (blue symbols), and DGs that are believed not to be associated with the two major spirals (green symbols). A few DG discovered after 2012 (like Crater) are missing in this plot. Let me also mention that Segue 1 is still a controversial object (it might be globular cluster, Niederste-Ostholt et al. 2009), and, lastly, that Canis Major has been ruled out as a DG (Momany et al. 2006).

Many exhaustive reviews have been written on the LG structure (Grebel 1997; Mateo 1998; van den Bergh 2000), and I refer the reader to them for all additional details.

Instead, in this contribution I shall focus on the morphology of DGs, and to the variety of structures they exhibit. In many occasions this variety has been seen as an evolutionary chain (Moore et al. 1996; Kormendy and Bender 2012; Kormendy, this volume), in which more dynamical evolved galaxies contain less and less gas.

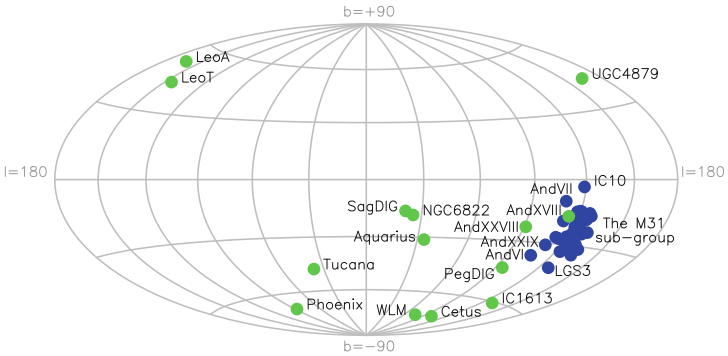

Fig. 2 Distribution of dwarf galaxies in the LG following McConnachie (2012): DGs associated with M 31 (*blue symbols*), and DGs considered not associated with these two major spirals

Table 1 Local Group dwarf galaxies basic physical parameters

Morphological type	μ_V	M_{HI}	M_{tot}
	$mag \times arcsec^{-2}$	$M_\odot$	$M_\odot$
Dwarf ellipticals	≤ 21	$\leq 10^8$	$\leq 10^9$
Dwarf spheroidals	≥ 22	$\leq 10^5$	$\sim 10^7$
Dwarf irregulars	≤ 23	$\leq 10^9$	$\leq 10^{10}$

2 Taxonomy of Dwarf Galaxies in the Local Group

Dwarf galaxies in the LG divide into three main morphological types: Spheroidals (**dSph**), Ellipticals (**dE**), and Irregulars (**dIrr**). Intermediate type are also known to exist in the LG.

Using Table 1 as a guideline, we can briefly describe their properties as follows:

- **Dwarf Irregulars**: These are atomic-gas (HI) dominated systems, and exhibit a variety of irregular shapes; SagDIG (Young and Lo 1997) and Sextans A (van Dyk et al. 1998) are two classical examples. This type of DGs is found in any environment: galaxy clusters, small galaxy groups, and in the general field. Several irregulars show a disk structure, but the disk does not seem to be ubiquitous. Zhang et al. (2012) demonstrated that most dIrrs start their life with a disk that then shrinks (outside-in scenario), so it is conceivable that all dIrrs form as low-mass spiral galaxies with extended gas discs. The evolution of star formation (SF) and disk structure is, however, different from large spirals, that are believed to assemble via an inside out scenario.
  Over their lifetime isolated dIrrs kept an almost constant SF (e.g. IC 1613, SagDIG), although some of them show signatures of a pristine significant peak of star formation (Skillman et al. 2014, Momany et al. 2005), in close similarity with Blue Compact Dwarfs. Whenever searched for, old stellar populations have been detected in irregular galaxies (see Leo I, Held et al. 2000). dIrr tend to be isolated systems.

- **Dwarf Ellipticals**: These DGs have a more regular shape, but are not depleted of gas. In the LG all the known dEs are located around M 31. The most known case is the one of NGC 205 (Monaco et al. 2009). They host a mixture of stellar populations, and show a complex star formation history (Carraro et al. 2001). They contain old, intermediate age and young stellar population. As for the dynamics, they are rotation supported. These galaxies tend to be concentrated closer to M31.
- **Dwarf Spheroidals**: These are dynamically evolved stellar systems, composed of intermediate age to old stellar populations. In most cases they are random motion supported, like Elliptical galaxies, although mild rotation has been detected in some of them. Being loose and dispersed systems, they are believed to be DM dominated. This is however based on the assumption that these systems are in virial equilibrium, which is not really completely proved (Lughausen et al. 2014). Typically, dSph are found close to M 31 or the MW. They are almost devoid of gas in their central parts, although gas has been detected in the surrounding of some of them (Sculptor and Phoenix, for example).

A few dwarfs such as Phoenix, Pegasus, Antlia, DDO 210, and LGS 3, are classified as transition objects (dIrr/dSph); possibly evolving from dIrr to dSph (Grebel et al. 2003). The idea of a single evolutionary endpoint is rather appealing: dE would be the remnants of dIrr that have lost their gas (by stripping in clusters or near large galaxies, i.e. an environmental effect), while dIrr/dSph would testify to an intermediate case of dwarfs that have maintained some of their gaseous content.

We believe there are no Ultra Compact Dwarf (**UCDs**) in the LG, although this depends on the precise definition of UDC in terms of mass and luminosity (Mieske et al. 2012). It might be that M 32 or Omega Cen are UCDs. There is some consensus that UCD are not precisely DGs, but simply the high-mass tail of the globular clusters mass function (Mieske et al. 2012). Lastly, the LG does not contain any Blue Compact or Starburst Blue Compact Dwarf (**BCD,SBCD**).

3 Spatial Distribution of Different Dwarf Galaxy Types in the Local Group

The first indication of a possible morphological evolution of DGs comes from their spatial distribution. Different morphological type are not randomly distributed across the LG volume, but shows a marked morphological segregation.

Gas poor DGs (dE and dSph) cluster close to MW and M31, while gas-rich DGs (dIrr) tend to be spread over a much larger volume (see Fig. 3). This is only on the average, since there are several exceptions.

dSph concentrates around M 31 and and the MW, while dEs are found in the surroundings of M31 only.

Cetus and Tucana are two examples of dSph not closely located to major spirals (see Fig. 3).

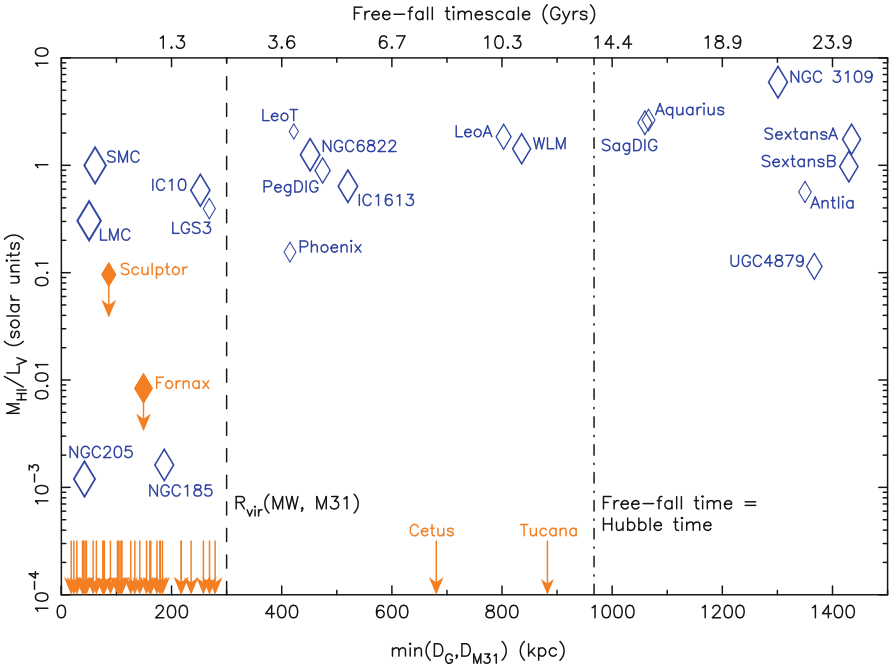

Fig. 3 Morphological segregation of DGs in the LG from McConnachie (2012)

4 Morphological Transformations

Structural modifications can occur in DGs as a result of a few dynamical (internal or environmental) processes:

4.1 Ram Pressure Stripping

Ram pressure stripping occurs when a DG is moving within a sufficiently dense multi-phase intra-cluster (ICM) medium. If the ICM ram pressure exceeds its gravitational force (Mori and Burkert 2000), a DG can loose partially or entirely its gas content. Lin and Faber (1983) firstly estimated that the ICM in the LG should have a density of the order of 10^{-6} cm^{-3} for ram pressure to be effective. Observational evidences are, however, scanty. The intra-group medium (IGM) in the LG seems to be multi-phase.

So far, observations allow us to identify two phases:

- Cold ($T \leq 10^4$ K) gas has been detected in HI (Richter 2012), and tends to be concentrated in the periphery (within 50 kpc) of the two major spirals (Andromeda and the Milky Way);
- Hot ($T \geq 10^4$ K) gas has been detected via O VI emission lines in the UV wavelength regime (Sembach et al. 2003), and in X-Ray, via O VIII emission lines (Gupta et al. 2012). This hot gas tends to occupy the outer regions of the LG.

No clear figures are available for the density of these two components in the LG. According to hydro-dynamical simulations (Nuza et al. 2014), the spatial distribution of these two components might be the result of the various processes which affects gas circulation, like inflows of extra-LG material and outflows from DGs internal or tidal evolution.

Nbody/gas-dynamical simulations (Mayer et al. 2006) confirm that ram-pressure can be the most efficient process to remove gas from a DG in a cluster of galaxies, but that this depends a lot on the evolutionary status of the DG and on the ICM.

4.2 Tidal Stirring

Most DGs are believed to be orbiting around one of the major spirals in the LG. NGC 3109 and Antlia seem to constitute a separate group (the 14 + 12 group, Bellazzini et al. 2013; Bernstein-Cooper et al. 2014). There are also a number of DGs that are too distant to be bound to either the MW or Andromeda. We refer to the tidal interaction exerted by a major galaxy on an orbiting DG, which can turn a disk-like dwarf into a spheroid (Moore et al. 1998 use the word *harassment* referring to this phenomenon in galaxy clusters). The result is typically tidal stirring of the DG which, in extreme cases, can also lead to tidal stripping and removal of the gas.

There is nowadays a lot of work in the field of dwarf galaxies orbits. This is a major requirement if one wants to understand their dynamical evolution and possible origin. The best known case is the LMC/SMC pair: accurate proper motions have been provided in many occasions, and modern orbits calculated with the aim to understand their complex three body problem. However, out of the very same figures different scenarios for the past orbital evolution, and the implied SFH and origin of the clouds have been discussed (Kallivayalil et al. 2013; Besla, this conference volume) and still rely on strong assumptions on the 3-D structure of the clouds and their possible binary nature. In any case the existence of the Magellanic bridge and stream clearly indicates that tidal interaction and induced SF is ongoing (Casetti-Dinescu et al. 2014; see also Fukui, this volume; Gallart, this volume).

The other obvious case is the one of the Sgr dSph (Ibata et al. 1994; Majewski, this volume), whose orbit is better constrained. The tidal arms are traced all over the Galactic halo (Majewski et al. 2004), and the Age-Metallicty relation (AMR, a consequence of the SFH) well defined.

As for the other MW dwarf galaxies, proper motions have been estimated for Fornax, Leo I, Sculptor, Draco, Carina, and Ursa Minor, and attempts have been done to reconstruct their orbits (Pasetto et al. 2003; Pasetto and Chiosi 2009) and spatial configuration (Pawlowski & Kroupa 2013; Kroupa, this volume). However, uncertainties associated to proper motion measurements are still too large to derive solid orbital solutions.

For M31 satellites, only two dwarf galaxies have measured proper motions (Watkins 2013), and for all the others proper motions expectations have been derived from dynamical considerations only.

4.3 Internal Stellar Evolution

One possibility for a DG to lose its gas content is via stellar evolution. As a consequence of a strong burst of star formation, SNae and stellar winds inject kinetic energy in the surrounding gas. If the gas acquires a velocity high enough to over-pass the galaxy potential well, it can escape the galaxy (blown-away) after having been displaced into the halo (blown-out) from the disk. This phenomenon has been analytically and numerically studied by Mac Low and Ferrara (1999) as a function of the DM halo mass. In order for this to happen, a strong collimated burst of star formation needs to occur, which is not seen in LG DGs (Recchi and Hensler 2013). It might be possible that BCD experiences such strong bursts of star formation, but there are no such DGs in the LG. Evidences of super bubbles which can be indicative of gas escaping from a DG have been found outside the LG (in I Zw 18 and NGC 1705).

4.4 Photo-evaporation

This can occur early during DG evolution in presence of strong UV radiation generated by the cosmic re-ionisation (Barkana and Loeb 1999). All galaxies formed before re-ionization having velocity dispersion lower than ~ 10 km s^{-1} can not survive, since they are turned into completely dark galaxies after the gas evaporation. When we analyse the Star Formation History in LG DGs, however, we do not find any indication of pristine abrupt interruption (quenching) of SF, which would be the case if gas is suddenly removed. This implies that re-ionisation did not have any impact in the SFH of DG, but that other processes conspired to shaped it (Grebel and Gallagher 2004; Hidalgo et al. 2011).

5 Examples in the Local Group

Having illustrated the physical processes that we believe are responsible for the gas removal from dwarf galaxies, we will now look more closely at the Local Group, and search for any signature of these phenomena among its population of dwarf galaxies. As we already mentioned, LG DG are divided in three main type: dSph, dE, and dIrr. They differ in the amount of gas and in their structural, dynamical, and stellar evolution properties. Intermediate types are also present, mainly transitional dSph/dIrr (Grebel 1999). These latter are of paramount importance since they help us to delineate a possible evolutionary path which transforms a dIrr into a dSph via one or more of the processes described above. Transitional dSph/dIrr have been suggested as the possible progenitor of classical dSph.

5.1 Pegasus: Ram Stripping Caught in the Act

Optical and HI observations as described in McConnachie et al. (2007) in the Pegasus isolated—but possibly associated with M3—dwarf have shown that stars and gas

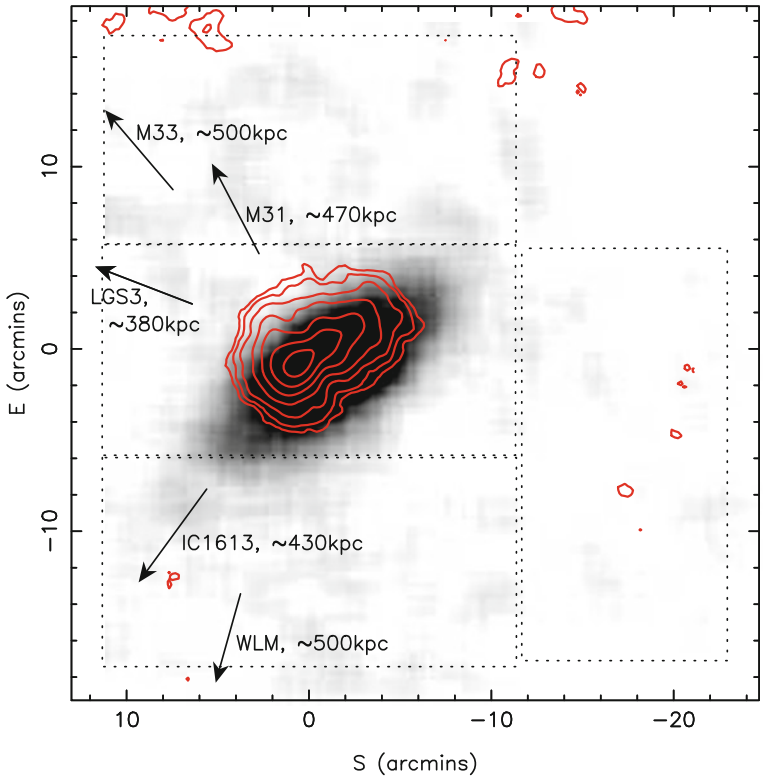

Fig. 4 The smooth disk-like star distribution in Pegasus, with over-imposed HI contours from McConnachie et al. (2007)

are distributed in a different way (see Fig. 4). While stars distribute in a disk-like structure, cold gas exhibits a cometary shape. This is interpreted as Pegasus is moving across the intra-group medium and its gas is undergoing ram pressure stripping. This would represent the best case of ram pressure stripping in the LG, and would suggest the existence of significant hot gas in it. We remind that such gas has been recently detected around the Milky Way and Andromeda (Lehner et al. 2014), but not in the most isolated regions of the LG. Therefore Pegasus would represent an intermediate dwarf, say a dIrr on the verge of turning—possibly—into a dE.

5.2 The 14 + 12 Group: Tidal Stirring at Work

Besides the prominent case of the Sgr dSph, there are numerous example of tidal interaction in the LG (e.g. the magellanic stream and bridge). Bellazzini et al. (2013, 2014) draw the attention of NGC 3109 and its companion, and nicely showed that

this group of 5 dwarfs (the 14 + 12 group: NGC 3109, Antlia, Sextans A, Sextans B, and Leo P) is moving along a filament. The observational evidences support the conclusion that this group has been tidally disturbed (*harassed*), or that has been accreted as a filamentary sub-structure (a tidal tail) produced by some major interaction event. Bernstein-Cooper (2014) HI observations, however, seem to rule out the membership of Leo P to this group. Leo P, instead, would represent the case for an isolated, gas rich, extremely metal deficient, dIrr.

5.3 Leo I: Harassment

The dSph galaxy Leo I possesses an extreme high radial velocity, and it seems to be unbound to both M 31 and the MW. This dwarf is almost tidally disrupted, possibly as a consequence of several peri-galactic passages in its motion around a massive galaxy (either MW or M 31). Unless its tangential motion has been severely underestimated, this galaxy is on the verge of leaving the LG, totally devoid of gas.

5.4 Andromeda XII: Untouched by the LG?

An interesting, opposite case, has been reported a few years ago. This dSph galaxy seems to be infalling at very high speed into the LG (Chapman et al. 2007). Chapman et al. (2007) argue that, because of the large velocity, this galaxy is entering the LG for the very first time, and therefore represents the best example of a late infall in the LG. Being depleted of gas, this dSph must have experience strong tidal interactions before joining the LG.

These examples, together with the Magellanic system and the Srg dSph, illustrate convincingly that DG in the LG are undergoing profound transformations. Detailed HI observations, in tandem with ultraviolet spectroscopy of the medium surrounding each DG (Lehner et al. 2014) can help us to understand better their individual dynamical status and measure the relative important of any of the most important dynamical processes that occur in the LG environment.

6 Conclusions

Due to their proximity, dwarf galaxies in the LG can be resolved into stars, and their SFH can be derived (Skillman et al. 2014). Irrespective of their morphological type, all DGs shows signature of old stellar populations, although in different amount (Weisz et al. 2014). This implies that DGs started to form stars at a sharply defined early epoch. The subsequent SFH was shaped by a variety of processes at work in the LG environment: ram pressure stripping, internal stellar evolution, harassment. SFH

have been derived for many DG in the LG so far, and indeed present a large variety of shapes. Beside modelling SFH, these processes also changed, dramatically in some cases, the DGs structure. We described these processes in details and show example of them in the actual LG. Overall, the LG turns out to be a vibrant environment, where several processes conspire to produce structural modifications in dwarf galaxies, and shape their SFH. As already emphasised in the past, gas removal is the trigger of any transformation, and this occurs differently from dwarf to dwarf, depending on their mass, orbit, and properties of the medium they are travelling in. A closer look at each individual DG will allow us in the future to understand better how they formed and evolved. Neutral and excited gas observations are crucial (e.g., ALFALFA, LITTLE THING) to map the gas structure and dynamics in and around DGs. Lastly, deep photometry is needed to extend the SFH derivation to the lowest-mass DG, because of their profound cosmological importance.

The birthday boys: Bruce Elmegreen and David Block photographed at *Siselwa*, Port Launay, the site of the Gala Dinner

Acknowledgements I warmly thank the organisers for inviting me to this great conference, and the ESO office for Science in Chile for the generous financial support. I also thank A. McConnachie and Y. Momany for fruitful discussions.

References

Barkana, R., Loeb, A.: The Photo-evaporation of Dwarf Galaxies during Reionisation, ApJ **523**, 54 (1999)

Bellazzini, M., Oosterloo, T., Fraternali, F., Beccari, G.: Dwarfs walking in a raw. The filamentary structure of the NGC 3109 association, A&A **559**, 11 (2013)

Bellazzini, M., Beccari, G., Fraternali, F., et al.: The extended structure of the dwarf irregular galaxies Sextans A and Sextans B. Signatures of tidal distortions in the outskirts of the Local Group, A&A **in press** (2014)

Belokurov, V., Irwin, M.J., Koposov, S.E., et al.: ATLAS lifts the Cup: discovery of a new Milky Way satellite in Crater, MNRAS **in press** (2014)

Bernstein-Cooper, E.Z., Cannon, J.M, Elson, E.C., et al.: ALFALFA discovery of the nearby gas-rich dwraf galaxy Leo P. V. Neutral gas dynamics and kinematics, AJ **in press** (2014)

Carraro, G., Chiosi, C. Girardi, L., Lia, C.: Dwarf elliptical galaxies: structure, star formation and color-magnitude diagrams, MNRAS **327**, 69 (2001)

Casetti-Dinescu, D., Moni Bidin, C., Girard, T.M., et al.: recent star formation in the leading arm of the Magellanic stream, ApJ **784**. L37 (2014)

Chapman, S.C., Penarrubia, J., Ibata, R., et al.: Strangers in the night: discovery of a dwarf spheroidal galaxy in its first Local Group infall, ApJ **662**, 79 (2007)

Grebel, E.: Star formation histories of local group dwarf galaxies, RvMA **10**, 29 (1997)

Grebel, E.K.: The stellar content of Local Group galaxies, IAUS 192, San Francisco: Astronomical Society of the Pacific, eds P. Whitelock and R. Cannon, 17 (1999)

Grebel, E., Gallagher, J.S.: The impact or deionisation on the stellar population of nearby dwarf galaxies, ApJ **610**, L89 (2004)

Grebel, E., Gallagher, J.S., Harbeck, D.: The progenitors of dwarf spheroidal galaxies, AJ **125**, 1926 (2003)

Gupta, A., Mathur, S., Krongold, Y.: A huge reservoir of ionised gas around the Milky Way: accounting for missing mass?, ApJ **756**, 8 (2012)

Held, E.V., Momany, Y., Saviane, I., Carraro, G.: The elusive old population of the dwarf spheroidal galaxy Leo I, ApJ **530**, L85 (2000)

Hidalgo, S.L., Aparicio, A., Skillman, E., et al.:The ACS LCID project.V. The star formation history of the dwarf galaxy LGS-3: clues to cosmic re-ionisation and feedback, ApJ **730**, 14 (2011)

Ibata, R.A., Gilmore, G., Irwin, M.J.: A dwarf satellite galaxy in Sagittarius, Nature **370**, 194 (1994)

Kallivayalil, N., van der Marel, R.P., Besla, G., et al: Third epoch Magellanic Cloud proper motion. HST/WFC3 data and orbit implications, ApJ **764**, 161 (2013)

Kormendy, J., Bender, R.,: A Revised Parallel-sequence Morphological Classification of Galaxies: Structure and Formation of S0 and Spheroidal Galaxies, ApJS **198**, 2 (2012)

Lehner, N. Hwok, J.C., Wakker, B.P.: Evidence for a massive, extended circumgalactic medium around the Andromeda galaxy, ApJ **in press** (2014)

Lin, D.N., Faber, S.M.: Some implications of non luminous matter in dwarf spheroidal galaxies, ApJ **266**, L21 (1983)

Lughausen, F., Famaey, B., Kroupa, P: A census of the expected properties of classical Milky Way dwarfs in Milgromian dynamics, MNRAS **in press** (2014)

Mac Low, M., Ferrara, A.: Starbust driven mass loss from dwarf galaxies: efficiency and metal ejection, ApJ **513**, 142 (1999)

Majewski, S.R., Kunkel, S.R., Law, D.R., et al.: A 2MASS view of the Sagittarius Dwarf Galaxy. Swope telescope spectroscopy of M giants in the dynamically cold Sgr tidal stream, AJ **128**, 245 (2004)
Mateo, M.:Dwarf Galaxies of the Local Group, ARA&A **36**, 435 (1998)
Mayer, L., Mastropietro, C., Wadsley, J., et al.: Simultaneous ram pressure and tidal stripping; how dwarf spheroidals lost their gas, MNRAS **369**, 1021 (2006)
McConnachie, A.W.: The observed properties of dwarf galaxies in and around the Local Group, AJ **144**, 4 (2012)
McConnachie, A.W, Venn, K.A, Irwin, M.J., et al.: Ram pressure stripping of an isolated local group dwarf galaxy: evidence for an intragroup media, ApJ **671**, L33 (2007)
Mieske, S., Hilker, M., Misgeld, I..: The specific frequency of ultra-compact dwarf galaxies, A&A **169**, 573 (2012)
Momany, Y., Held, E. V., Saviane, I., et al.: HST/ACS observations of the old and metal-poor Sagittarius dwarf irregular galaxy, A&A **439**, 111 (2005)
Momany, Y., Zaggia, S., Gilmore, G., et al.: Outer structure of the Galactic warp and flare: explaining the Canis Major over density, A&A **451**, 515 (2006)
Monaco, L., Saviane, I., Perina, S., et al.: The young stellar population at the center of NGC 205, A&A **509**, L2 (2009)
Moore, B., Katz, N., Lake, G., et al: Galaxy harassment and the evolution of cluster of galaxies, Nature **379**, 631 (1996)
Moore, B., Lake, G., Katz, N.: Morphological transformation from galaxy harassment, ApJ **495**, 139 (1998)
Mori, M., Burkert, A.: Gas stripping of dwarf galaxies in clusters of galaxies, ApJ **538**, 559 (2000)
Niederste-Ostholt, M., Belokurov, V., Evans, N.W., et al.: The origin of Segue 1, MNRAS **398**, 1771 (2009)
Nuza, S.E., Parisi, F., Scannapieco, C., et al.: The distribution of gas in the Local Group from constrained cosmological simulations: the case for Andromeda and the Milky Way galaxies, MNRAS, **in press** (2014)
Pasetto, S., Chiosi C.: Tidal effects on the spatial structure of the Local Group, A&A **499**, 385 (2009)
Pasetto, S., Chiosi, C., Carraro, G.: Morphological evolution of dwarf galaxies in the Local Group, A&A **405**, 931 (2003)
Pawlowski, M.S., Kroupa, P., Jerien, H. : Dwarf galaxy planes: the discovery of symmetric structures in the Local Group, MNRAS **435**, 1928 (2013)
Recchi, S., Hensler, G.: The fate of heavy elements in dwarf galaxies - the role of mass and geometry, A&A, **551**, 41 (2013)
Richter, P.: Absorption measurements of galaxy halos, EAS **56**, 225 (2012)
Sembach, K.R., Wakker, B.P., Savage, B.D., et al.: Highly ionised high-velocity gas in the vicinity of the Galaxy, ApJS **146**, 165 (2003)
Skillman, E.D., Hidalgo, S.L., Weisz, D.R., et al.: The ACS LCID project.X. The star formation history of IC1613: revisiting the over-cooling problem, ApJ **in press** (2014)
van den Bergh, S.: The Local Group of galaxies, A&ARv **9**, 273 (1999)
van den Bergh, S.: Updated information on the Local Group, PASP **112**, 529 (2000)
van Dyk, S.D., Puche, D., Wong, T.: The recent star formation in Sextans A, AJ **116**, 2341 (1998)
Watkins, L., Evans, N.W., van de Ven, G.: A census of orbital properties of M31 satellites, MNRAS **430**, 349 (2013)
Weisz, D.R., Dolphin, A.E., Skillman, E.D., et al.: The star formation history of local group dwarf galaxies. I. Hubble Space Telescope/ wide field planetary camera 2 observations, ApJ, **in press** (2014)
Young, L.M., Lo, K.Y.: The neutral interstellar medium in nearby dwarf galaxies. III. Sagittarius DIG, LGS 3, and Phoenix, ApJ **490**, 710 (1997)
Zhang, H.X., Hunter, D.A., Elmegreen, B.G., et al.: Outside-in shrinking of star-forming disk of dwarf irregular galaxies, ApJ **143**, 47 (2012)

The Star Formation History of the Magellanic Clouds: An Observer's Perspective

C. Gallart, M. Monelli, P. B. Stetson, L. Monteagudo-Narvión and R. Carrera

Abstract The nearby Magellanic Clouds are ideal laboratories for the study of galaxy formation and evolution. In particular, their field star formation history can be obtained in the greatest possible detail, from color-magnitude diagrams reaching the oldest main sequence turnoff. In this paper, we discuss the challenges involved in the determination of full, quantitative star formation histories for the Magellanic Clouds field stellar population, and our current knowledge of them. We show that both the LMC and the SMC have experienced an almost coincident enhancement of their central star formation activity in the second part of their lifetimes, and that both show an outside-in quenching of the recent star formation.

1 Introduction

At a distance of only $\simeq$ 50 Kpc, the Magellanic Clouds (MC) posses some characteristics that make them an ideal laboratory for the study of galaxy formation and evolution, and their closeness allows us to do so with the greatest possible detail. In particular, their field star formation history (SFH) can be obtained reliably for their whole lifetime, because it is possible to obtain color-magnitude diagrams (CMDs) that reach the oldest main sequence turnoff (oMSTO, at V=22.5 and V=23 for the

C. Gallart (✉) · M. Monelli · L. Monteagudo-Narvión · R. Carrera
Instituto de Astrofísica de Canarias, E-38200 La Laguna, Spain

Universidad de La Laguna, Dpto. Astrofísica, E-38206 La Laguna, Tenerife, Spain
e-mail: carme@iac.es

M. Monelli
e-mail: monelli@iac.es

L. Monteagudo-Narvión
e-mail: laram@iac.es

R. Carrera
e-mail: rcarrera@iac.es

P. B. Stetson
Dominion Astrophysical Observatory, Herzberg Institute of Astrophysics,
National Research Council, Victoria, BC, V9E 2E7, Canada
e-mail: Peter.Stetson@nrc-cnrc.gc.ca

K. Freeman et al. (eds.), *Lessons from the Local Group,*
DOI 10.1007/978-3-319-10614-4_22

LMC and SMC, respectively) with good photometric accuracy and precision. Indeed, observation of the whole main sequence is essential for a reliable and detailed determination of the full SFH (Gallart et al. 2005) through comparison of the distribution of stars in it to that predicted by the models, in this relatively well-known phase of stellar evolution. Additionally, their RGB stars are bright enough to be observed spectroscopically, including in high resolution, which gives the opportunity to derive metallicities and chemical abundances for a number of key elements, and thus to study their chemical enrichment history (CEH) in detail.

Once detailed and reliable SFH and/or CEH, including their spatial variations, are available, one can successfully address a number of important questions regarding galaxy evolution, and obtain satisfying answers. For example, how does star formation relate with gas content, and what characterizes global star formation patterns over time (e.g. inside-out *vs.* outside-in)? Can the global SFH of a galaxy be inferred from the properties of its clusters system? The MCs contain field stellar populations and stellar clusters of all ages, and therefore they provide a local test-bed of the use of star clusters as a proxy of the SFH of distant galaxies. The Large Magellanic Cloud (LMC) hosts the only resolved bar in the Local Group, and thus offers the possibility of studying the mixing effects of a bar in a stellar population, in addition to the formation and evolution of the bar itself. Finally, the MCs and the Milky Way form currently an interacting system which can provide important insight on the effects of interactions in galaxy evolution.

In this paper, we will discuss the challenges involved in the determination of a full, quantitative SFH for the MC field stellar populations, and our current knowledge of them, based on CMDs reaching the oMSTO complemented with spectroscopic studies. We will show that a coherent, fascinating picture of the LMC and SMC linked evolution is starting to emerge from the available data. Current photometric deep surveys, covering most of their bodies for the first time, hold the promise of reaching in the near future a complete, reliable view of their evolution.

2 The Vastness of the Magellanic Clouds: Strategies Toward a Representative Sample of Their Stellar Populations

The MCs are huge on the sky, and a complete coverage of their stellar populations is challenging. The spatial extent of the LMC has been traced by dwarfs below the oMSTO (Saha et al. 2010), and by spectroscopically confirmed RGB stars (Majewski et al. 2009). While the conclusions of these two works are somewhat at odds regarding the shape of the LMC luminosity profile at large radii (the first finds an exponential profile out to 12 inner-disk scale lengths, or $R_{gc} \simeq 14°$, while the second finds a flattened profile beyond $R_{gc} \simeq 9°$ and out to $R_{gc} \simeq 23°$, resembling that of a stellar halo), both agree that the LMC stellar populations extend out to at least $R_{gc} \geq 16°$. With similar techniques, Nidever et al. (2011) find that $R_{gc} \geq 11°$ for the SMC, with an exponential profile within $R_{gc} \simeq 7.5°$ and a shallower profile outward.

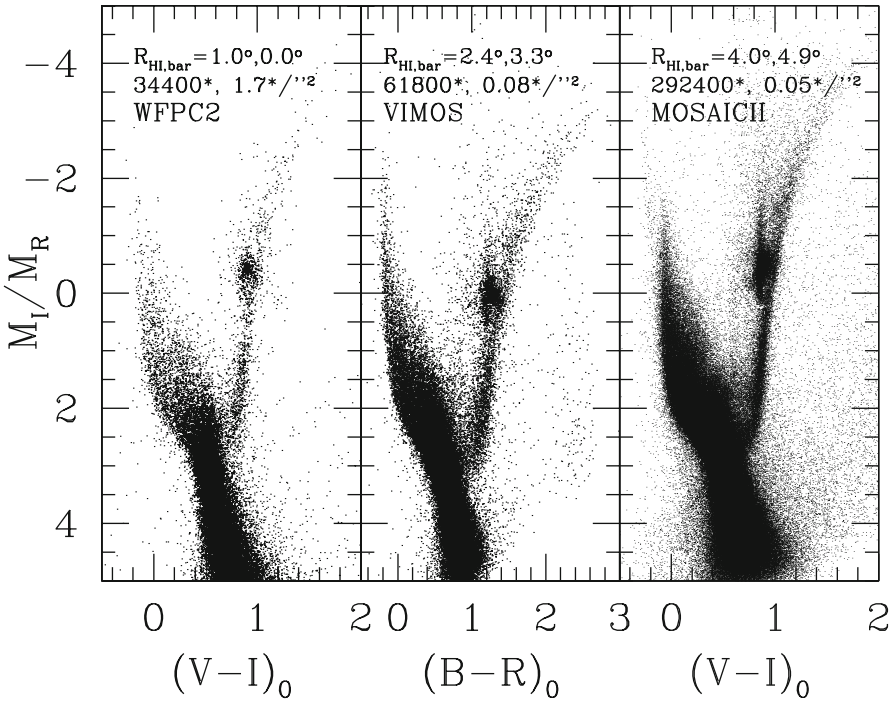

Fig. 1 Color-magnitude diagrams for three LMC fields located at different galactocentric distances. The distances from the dynamical center, as determined from HI observations, and from the center of the bar are labeled. Instruments delivering higher spatial resolutions have been used as distance to the center decreases, and thus stellar density (labeled) increases. Note that CMDs of similar depth are obtained with this strategy, for vastly different stellar surface densities

Imaging under good seeing conditions ($\simeq$ 1"−1.2"), with wide field ($\simeq 35' \times 35'$) cameras on ground based telescopes, such as the MOSAIC II on the CTIO 4 m Blanco telescope or the WFI on the 2.2 m ESO telescope, have demonstrated to be successful in providing photometry reaching the oMSTO with good precision and high completeness for most of the MCs bodies (e.g., Gallart et al. 2004; 2008; Saha et al. 2010; Nidever et al. 2011; Carrera et al. 2011; Meschin et al. 2014), except perhaps for the very crowded central regions. These kind of observations have the advantage over previous WFPC2 imaging (e.g., Holtzman et al. 1999; Smecker-Hane et al. 2002; Javiel et al. 2005) that a much larger area ($\geq \times 200$) is covered, and this leads to CMDs that are populated by a statistically significative number of stars. For the innermost regions of the LMC ($R_{gc} \lesssim 3°$), we have successfully reached the goal by using service mode observing with VIMOS on the VLT, and requiring excellent ($\leq$ 0.8") seeing conditions. For the extremely crowded LMC bar, however, HST observations remain the optimal solution, since they render very deep, well populated CMDs. Figure 1 displays example CMDs obtained using these complementary

approaches, showing that their combination leads to a very homogeneous database over all radii.

The recent commissioning of the Dark Energy Camera (DECam, Flaugher et al. 2012) on the CTIO 4 m telescope has oppened an unprecedented avenue. Its huge field of view (with a diameter of 2.2°) makes it possible to plan for a complete coverage, with CMDs reaching the oMSTO, of both MCs main bodies, and a good sampling of their periphery. The first will provide data for a definitive determination of their full SFHs, while the latter will allow us to search for relics of their formation and past interactions, and for a possible stellar counterpart of the gaseous structures of the Magellanic System. These are the main aims of the Survey of the MAgellanic Stellar History (SMASH, P.I. D. Nidever), which has obtained 40 nights to image 480 square degrees distributed over 2500 square degrees on the Magellanic system with DECam using $ugriz$ filters.

3 The Spatially Varying SFH of the Outer Disk of the LMC

We used MOSAIC II on the CTIO 4 m telescope and WFI on the ESO 2.2 m telescope, to obtain CMDs reaching the oMSTO in two dozen LMC fields spanning a range of R_{gc}=4°–11°, and a variety of position angles (PA), with most fields in the range PA≃0°–63° (Gallart et al. 2004; 2008; Meschin et al. 2014; Carrera et al. 2011). We also collected medium resolution spectra in the CaII triplet region using Hydra on the CTIO 4 m telescope and FLAMES on the VLT for some 900 stars in half of these fields (Carrera et al. 2008, 2011), and high resolution spectra with FLAMES on the VLT for some 300 stars in four of them (Carrera et al. 2014, in prep.). The location of the observed fields is indicated in Fig. 2.

Carrera et al. (2008, 2011) and have analyzed metallicity and velocity distributions, and age-metallicity relations, based on the Ca II triplet spectroscopy of RGB stars. The obtained metallicity distributions show a well-defined peak, with a tail toward low metallicities. The mean metallicity remains constant until $R_{gc} \simeq 6°$ ([Fe/H] $\simeq -0.5$ dex), while it is lower for the outermost fields. The age-metallicity relations are consistent with being the same at all galactocentric distances, possibly indicating a relatively well mixed interstellar medium at all ages. The lower mean metallicity in the outermost fields appears to be a consequence of the lower fraction of intermediate-age stars in them, which are more metal-rich than the older stars. The analysis of the high resolution spectroscopy that we have obtained in a fraction of these fields (Carrera et al. 2014, in prep.) will provide further, key details on the chemical evolution of the LMC over a range of galactocentric distances. The analysis of the radial velocities shows that the RGB stars follow a rotational cold disk kinematics. The velocity dispersion increases as metallicity decreases, indicating that the most metal-poor/oldest objects are distributed in a thicker disk than the most metal-rich/youngest ones. However, the velocities for the most metal-poor objects do not seem to be compatible with them being part of a hot halo.

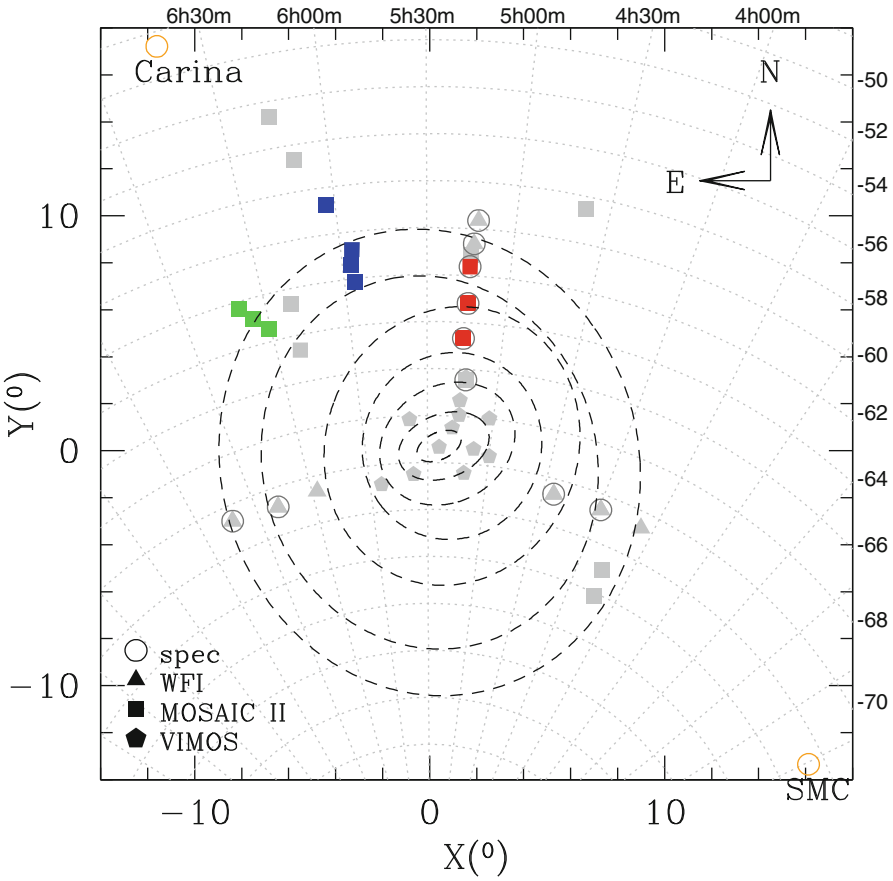

Fig. 2 Location of MOSAIC II, WFI, VIMOS and spectroscopic fields that constitute the database for the study presented in this paper. The ellipse fits to the LMC number density distribution provided by van der Marel (2001) are plotted as reference. Quantitative information is presented in this paper for the fields highlighted in color (same color code as in Fig. 5)

In Meschin et al. (2014) we have presented a determination of the full SFH of three of the MOSAIC II LMC fields, located at RA≃06:00 h and with DEC between − 62 and − 65 degrees. We nicknamed them LMC0, LMC1 and LMC2, in order of decreasing declination, which corresponds to decreasing distance to the center of the LMC. The reader is referred to Meschin et al. (2014) for details on the observations, data reduction, and determination of the SFHs. Figure 3 displays the star formation rate as a function of time, $\psi(t)$, for the three fields. It shows that the outer LMC disk has experienced two main epochs of star formation, separated by a period of lower star formation activity. The first epoch (which we will refer to as *old star forming epoch*, O_{SFE}) started at the earliest times considered, $\simeq$ 13 Gyr ago, and peaked around 10–8 Gyr ago. The period of low star forming activity extends from $\simeq$ 7 to $\simeq$

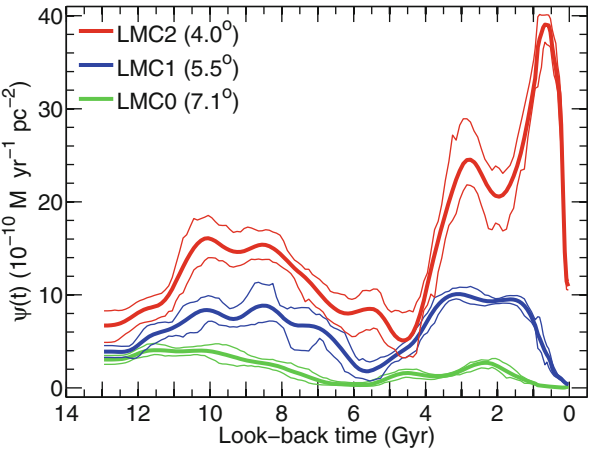

Fig. 3 Comparison of the star formation rate as a function of time for three LMC fields. The thin lines represent the uncertainties (see Meschin et al. 2014 for details)

4 Gyr ago, after which a second *young star forming epoch* (Y_{SFE} thereafter) occurs. The Y_{SFE} seems to be composed by at least two periods of enhanced star formation activity.

A very robust feature that can be observed in Fig. 3 is that the ratio between the amount of star formation in the Y_{SFE} and O_{SFE} (i.e. after and before the minimum $\psi(t)$) decreases with increasing galactocentric radius: Y_{SFE}/O_{SFE}= (1.1:0.8:0.4) for (LMC2:LMC1:LMC0). That is, the stellar population is older on average outwards. In the outermost field, LMC0, the star formation rate in the second half of the galaxy's life is lower than in the first half, both are similar in field LMC1, while in LMC2, it is substantially higher. In this innermost field, in addition, the two episodes in which the young star forming epoch can be split have a different star formation rate, the second, younger half being more intense than the first half.

Another robust feature visible in the SFH, and better quantified in terms of age through comparison of the CMDs with isochrones, is an outside-in quenching of the recent star formation activity. In the innermost field considered in this section, LMC2, the main sequence of the CMD is well populated up to magnitudes and colors corresponding to a young isochrone, thus we estimate that the star formation activity in this field has lasted till approximately the present time. The same type of comparison discloses that the star formation activity has lasted till $\simeq$ 0.8 and $\simeq$1.3 Gyr ago in fields LMC1 and LMC0 respectively. This corresponds to an inwards migration of the last epoch of star formation activity of $\simeq$ 2.7 Kpc/Gyr.

We have estimated, through comparison with isochrones (see Fig. 4 and its caption for details), the age of the last main star formation activity in a number of the CTIO fields, highlighted in colors in Fig. 2 (Monelli et al. 2014, in prep). The results are displayed in Fig. 5. We find a similar quenching rate for the fields out to $R_{gc} \simeq 9°$ and within a range of PA=0°–63° (that is, close to the major axis of the LMC). Beyond this radius, we find that the age of the last epoch with substantial star formation activity increases more abruptly, such that, at $R_{gc} \simeq 11°$ we estimate an age of around 7 Gyr.

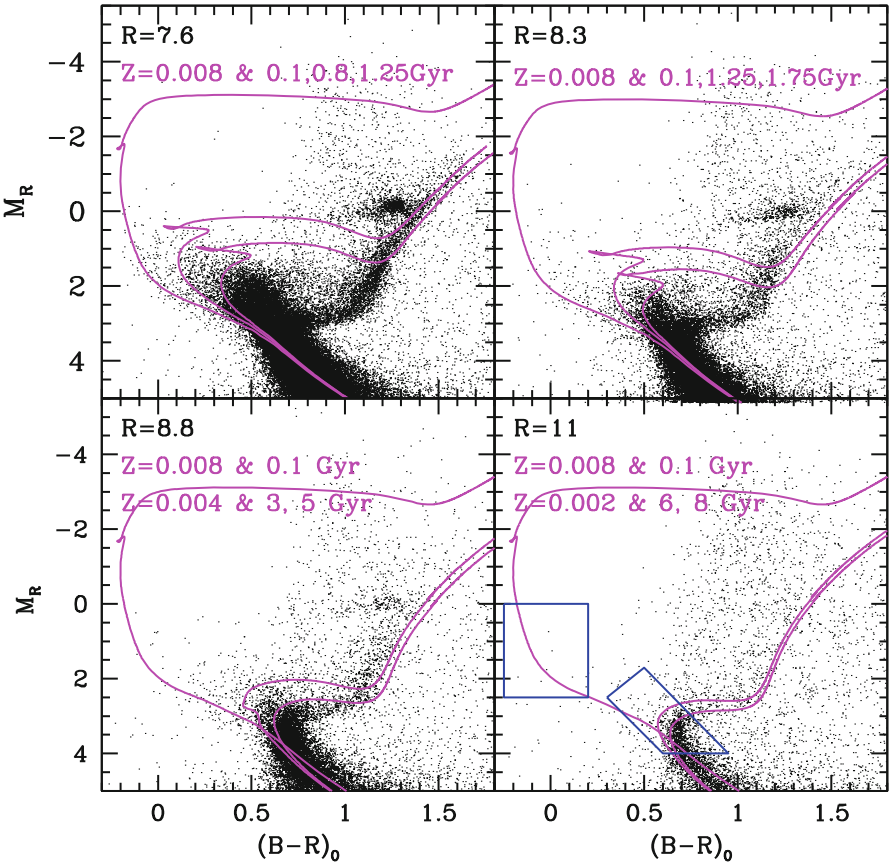

Fig. 4 CMDs for the four MOSAIC II fields located at PA$\simeq$ 35° and different galactocentric radius (labelled), and highlighted in blue in Fig. 2. Three isochrones have been plotted in each panel. A young, 0.1 Gyr isochrone is plotted in all panels to indicate the possible presence of stars of this age in all these fields, regardless of galactocentric distance. Two older isochrones, bracketing the turnoff corresponding to the last epoch of substantial star formation activity in each field, have also been displayed. An age metallicity relation consistent with that derived by Carrera et al. (2011) and Meschin et al. (2014) has been adopted. In the lower right panel, two boxes indicating the color and magnitude limits used to select young stars and stars of all ages have been overplotted (see Sect. 3)

In Fig. 4, a sprinkle of young stars, aged between 0.1 Gyr old and the age we have estimated for the end of the main star formation activity in each field, can be observed in all fields, regardless of position angle. No foreground Milky Way stars are expected at this position of the CMD. Also, background galaxies would be too bright or too close to appear as point sources at this magnitude level. We have calculated the ratio of the number of these 'young ubiquitous' stars, represented in a box that includes stars between 0.1 and 0.8 Gyr old, to the number of stars in a main sequence box that includes a representation of stars of all ages (see Fig. 4 for

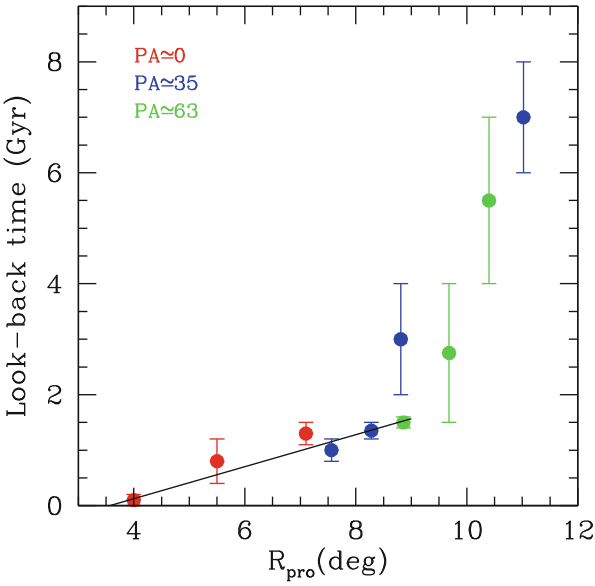

Fig. 5 Estimates of the age at which the last substantial star formation activity occurred in a number of fields in our database, obtained through comparison with isochrones. We have selected the fields highlighted in colors in Fig. 2, which have a limited range of position angles (PA=0°–63°). A least square linear fit to the points with $R_{pro} \leq 9^\circ$ is represented. Its slope indicates an inwards migration of the star formation activity of $\simeq$ 3.5°/Gyr or 3 Kpc/Gyr, which is in good agreement with the migration rate inferred by Meschin et al. (2014) for the three innermost fields only

the location of these boxes in the CMD). It turns out that this ratio is approximately constant. This provides additional support to the conclusion that these are genuine LMC stars. Assessing whether they are young stars possibly originated at smaller galactocentric radius and scattered to larger radius as a consequence of the effects of an interaction between the MCs, or blue straggler stars from the intermediate-age population, will need further investigation.

4 The SMC Star Formation History

SFHs for the SMC field, obtained from well populated CMDs reaching the oMSTO have been presented by Dolphin et al. (2001); Chiosi and Vallenari (2007); Noël et al. (2009); Chiosi et al. (2012); Cignoni et al. (2012, 2013). Figure 1 of Cignoni et al. (2012) summarizes the location of these fields, except for those of Chiosi et al. (2012), showing that a good range of galactocentric distances has been covered, albeit with relatively small fields. From these SFHs, an interesting picture of the SMC SFH and its variations with galactocentric distance can be obtained.

The fields close to the center of the SMC ($R_{gc} \lesssim 1$ Kpc) show an overall enhancement of the star formation rate around $\simeq$ 6 Gyr ago, with respect to their earlier SFH. In this second half of their history, time variations of the star formation rate are measured. The details of these variations (enhancement time, relative amounts), however, appear to vary from field to field (or among different studies using different methods of SFH derivation, or stellar evolution models). It is interesting that the second epoch of star formation activity in the LMC central part appears also to start at a

similar age, or somewhat later (by about 1 Gyr) than that in which an enhancement in the star formation activity is observed in the center of the SMC.

Also similar to what happens in the LMC, the SFH gets closer to constant over time, and therefore the stellar populations get older on average, for increasing galactocentric distances. A quenching of the recent star formation activity at large radius is also observed in the SMC, with ages of the last main event of star formation activity around 3 and 5 Gyr at $R_{gc} \simeq 3-5$ Kpc and 7 Kpc, respectively (Dolphin et al. 2001; Noël et al. 2007, Noël and Gallart 2007).

5 Summary and Conclusions

We have discussed the currently available SFHs for the LMC and the SMC, which have been obtained from well populated CMDs reaching the oMSTO with good completeness and photometric precision. These CMDs sample the MCs stellar populations from their central parts to large galactocentric radius, thus providing important insights on the spatially resolved evolution of both galaxies.

In the case of the LMC, the available SFHs for three fields with a range of galactocentric radius from 4° to 7° indicate a strong galactocentric stellar populations gradient in the sense that younger populations are more centrally concentrated. Two main epochs of star formation activity have been identified. The first, *old* star forming epoch, started at early times ($\simeq$ 13 Gyr ago) in all fields, and peaked around 10–8 Gyr ago. The second, *young* star forming epoch took place after a period of low activity occurred between 7 and 5–4 Gyr ago, and lasted till the present time, $\simeq$ 0.8 and 1.3 Gyr ago in fields at 4°, 5.5° and 7°, respectively. The relative importance of the two epochs varies smoothly, from almost the same amount of stars formed in the two epochs in the case of the innermost field, to only 40 % of the stars formed in the more recent epoch in the outermost field.

We have shown that the outside-in quenching of the recent star formation activity observed in these three fields, at a rate of $\simeq$2.7Kpc/Gyr, continues at a similar rate out to $R_{gc} \simeq 9°$. Beyond this radius, the age of the last epoch with substantial star formation activity increases more abruptly such that, at $R_{gc} \simeq 11°$, we estimate an age of around 7 Gyr. The variation of the age of most recent substantial star formation activity as a function of R_{gc} is correlated with the currently measured HI column density. Under the reasonable assumption that stellar migration is not a dominant factor in shaping the distribution of the LMC stellar populations, this gradient implies that a gradual displacement of the star formation activity towards smaller galactocentric radius occurred over the galaxy's lifetime.

Qualitatively similar patterns for the SFH and its galactocentric variations are observed in the case of the SMC. First, an overall enhancement of the star formation rate around $\simeq$ 6 Gyr ago, with respect to the earlier SFH, is observed at small galactocentric radius ($R_{gc} \lesssim 1°$). Second, a quenching of the recent star formation activity at large radius is also observed in the SMC.

As the orbital path of both MCs gets better constrained (e.g., Besla et al. 2012; Kallivayalil et al. 2013), we should be able to relate these particularities of their SFHs with their interaction history, if there is indeed a connection. In our current understanding of the MC system dynamics, is seems plausible that the almost simultaneous enhancement of the star formation rate, in approximately the second half of both the LMC and the SMC lifetime, may be related with them becoming gravitationally bound at that time, or approaching the Milky Way for the first time. The outside-in quenching of the recent star formation activity in the central parts could be due to ram pressure from the Milky Way halo acting on the LMC interstellar medium and resulting in a reshaped HI profile (Meschin et al. 2014; Nidever 2014). However, the fact that this process started very early on at large galactocentric radius may indicate that this is a generic process of low-mass disk galaxies, unrelated with environment (Zhang et al. 2012).

Acknowledgement We wish to thank a number of collaborators that have contributed to this project, or are taking part on ongoing work on the MCs not presented here: A. Aparicio, S. L. Hidalgo, I. Meschin, N. Noël and D. Nidever and rest of members of the SMASH collaboration.

References

Besla G., Kallivayalil N., Hernquist L., van der Marel R. P., Cox T. J., Kereš D., 2012, MNRAS, 421, 2109
Carrera R., Gallart C., Aparicio A., Hardy E., 2011, AJ, 142, 61
Carrera R., Gallart C., Hardy E., Aparicio A., Zinn R., 2008, AJ, 135, 836
Chiosi E., Vallenari A., 2007, A&A, 466, 165
Chiosi E., Baume G., Carraro G., Costa E., Vallenari A., 2012, MNRAS, 426, 1884
Cignoni M., Cole A. A., Tosi M., Gallagher J. S., Sabbi E., Anderson J., Grebel E. K., Nota A., 2012, ApJ, 754, 130
Cignoni M., Cole A. A., Tosi M., Gallagher J. S., Sabbi E., Anderson J., Grebel E. K., Nota A., 2013, ApJ, 775, 83
Dolphin A. E., Walker A. R., Hodge P. W., Mateo M., Olszewski E. W., Schommer R. A., Suntzeff N. B., 2001, ApJ, 562, 303
Flaugher B. L., Abbott T. M. C., Angstadt R., Annis J., et al., 2012, in Society of Photo-Optical Instrumentation Engineers (SPIE) Conference Series Vol. 8446 of Society of Photo-Optical Instrumentation Engineers (SPIE) Conference Series, Status of the Dark Energy Survey Camera (DECam) project
Gallart C., Stetson P. B., Hardy E., Pont F., Zinn R., 2004, ApJL, 614, L109
Gallart C., Zoccali M., Aparicio A., 2005, ARA&A, 43, 387
Gallart C., Stetson P. B., Meschin I. P., Pont F., Hardy E., 2008, ApJL, 682, L89
Holtzman J. A., Gallagher III J. S., Cole A. A., Mould J. R., Grillmair C. J., Ballester G. E., Burrows C. J., Clarke J. T., Crisp D., Evans R. W., Griffiths R. E., Hester J. J., Hoessel J. G., Scowen P. A., Stapelfeldt K. R., Trauger J. T., Watson A. M., 1999, AJ, 118, 2262
Javiel S. C., Santiago B. X., Kerber L. O., 2005, A&A, 431, 73
Kallivayalil N., van der Marel R. P., Besla G., Anderson J., Alcock C., 2013, ApJ, 764, 161
Majewski S. R., Nidever D. L., Muñoz R. R., Patterson R. J., Kunkel W. E., Carlin J. L., 2009, in Van Loon J. T., Oliveira J. M., eds, IAU Symposium Vol. 256 of IAU Symposium, Discovery of an extended, halo-like stellar population around the Large Magellanic Cloud. pp 51–56
Meschin I., Gallart C., Aparicio A., Hidalgo S. L., Monelli M., Stetson P. B., Carrera R., 2014, MNRAS, 438, 1067
Nidever D. L., 2014, in Seigar M. S., Treuthardt P., eds, Astronomical Society of the Pacific Conference Series Vol. 480 of Astronomical Society of the Pacific Conference Series, Disk Destruction and (Re)-Creation in the Magellanic Clouds. p. 27
Nidever D. L., Majewski S. R., Muñoz R. R., Beaton R. L., Patterson R. J., Kunkel W. E., 2011, ApJL, 733, L10
Noël N. E. D., Gallart C., 2007, ApJL, 665, L23
Noël N. E. D., Gallart C., Costa E., Méndez R. A., 2007, AJ, 133, 2037
Noël N. E. D., Aparicio A., Gallart C., Hidalgo S. L., Costa E., Méndez R. A., 2009, ApJ, 705, 1260
Saha A., Olszewski E. W., Brondel B., Olsen K., Knezek P., Harris J., Smith C., Subramaniam A., Claver J., Rest A., Seitzer P., Cook K. H., Minniti D., Suntzeff N. B., 2010, AJ, 140, 1719
Smecker-Hane T. A., Cole A. A., Gallagher III J. S., Stetson P. B., 2002, ApJ, 566, 239
van der Marel R. P., 2001, AJ, 122, 1827
Zhang H.-X., Hunter D. A., Elmegreen B. G., Gao Y., Schruba A., 2012, AJ, 143, 47

CO, HI and Star Formation in the Large Magellanic Cloud

Yasuo Fukui

Abstract The Large Magellanic Cloud is an ideal laboratory for studying cloud evolution and star cluster formation. We will review CO and HI observations and compare observational signatures of star formation with the molecular and atomic gas. High-mass star formation shows good spatial correspondence with CO, and the three types, Types I, II and III of GMCs, with different star formation activity represent an evolutionary sequence from the initial inactive phase to the subsequent highly active phase in star formation. The dense clumps within GMCs show a similar evolutionary trend on smaller scales. It is likely that star formation takes place rapidly in 1–10 Myr roughly close to the free-fall timescale at 10–100 pc. GMCs are enveloped by relatively dense HI having density of 100 cm^{-3}. The envelope is continuously accreting onto the GMCs to increase the GMC mass with an average mass accretion rate of $\sim$0.1 $M_\odot$ yr^{-1}. The HI filaments are formed by compression due to supergiant shells as seen in active cluster formation in 30 Dor, N159, N48, etc. Recent findings of the Galactic starburst regions suggest that the active high-mass star formation is often triggered by cloud-cloud collisions which cause efficient three dimensional compression of dense gas. The interface layer in such collisions creates higher turbulent speed and higher mass-accretion rate which facilitates rapid high-mass star formation in 10^5 yrs.

1 Introduction

Our scientific goal is to better understand evolution of galaxies. Because stars are formed in massive molecular clouds, formation and evolution of molecular clouds will provide key to elucidate formation of stars which build up galaxies. The Milky Way is not suited for such a study because of heavy contamination in the Galactic plane. On the other hand, the Large Magellanic Cloud (LMC) is an ideal object for such a study since it is located nearly face-on at a distance of 50 kpc. The LMC is also unique in studying high-mass star formation because young high-mass stars in populous clusters and in OB associations are extremely rich. In particular the

Y. Fukui (✉)
Department of Physics, Nagoya University, Chikusa-ku, Nagoya 464-8601, Aichi, Japan
e-mail: fukui@a.phys.nagoya-u.ac.jp

K. Freeman et al. (eds.), *Lessons from the Local Group,*
DOI 10.1007/978-3-319-10614-4_23

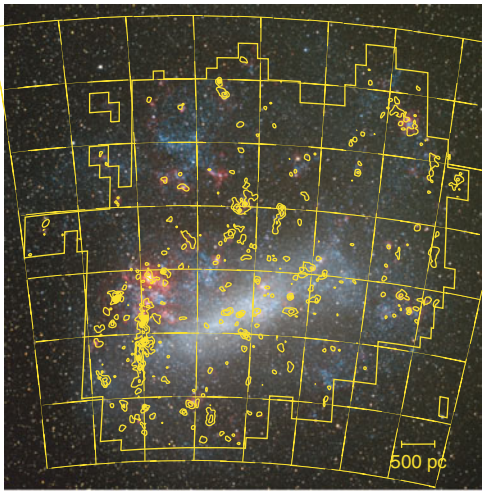

Fig. 1 Velocity-integrated intensity map of the ^{12}CO emission superposed on an optical image of the LMC. Contours are plotted every 2.4 K km s^{-1} from 1.2 K km s^{-1}

populous clusters are young massive clusters which are rare in the Milky Way and can provide a possible link to the globular clusters. The metalicity in the LMC is a factor of 2–4 lower than in the Milky Way and may provide a possible link to the early Universe along with the Small Magellanic Cloud (SMC) which has even lower metalicity.

In this paper, we highlight giant molecular clouds (GMCs) where most of the stars are formed. Molecular clumps in GMCs are possible precursors of clusters and the HI gas will act as mass reservoir to form GMCs. The interplay between turbulence and cloud gravity will regulate star formation and the resultant evolutionary timescale is a crucial parameter for understanding GMCs. Relevant review articles and references are found elsewhere (Fukui and Kawamura 2010; Blitz et al. 2007).

2 Molecular Clouds: Three Types

Molecular gas is distributed in a galaxy as GMCs having typical mass of 10^5–10^6 $M_\odot$, where most of the stars are believed to be formed. It is important to have a complete survey of a galaxy for spatially resolved GMCs in order to obtain a thorough understanding of the unbiased GMC properties. Although such a survey is hampered by its large extent, the LMC is the best candidate for a complete GMC survey among the nearest galaxies. The LMC was mapped at a low resolution of 8.8 arcmin in the 2.6 mm CO J = 1-0 transition (Cohen et al. 1988), whereas the GMCs were not spatially resolved by the beam. NANTEN, a 4-m mm telescope installed in Las Campanas Observatory, was used to survey GMCs in the CO J = 1-0 transition at 2.6 arcmin. The resolution corresponds to 40 pc at a distance of 50 kpc and allowed us to obtain the first spatially resolved complete sample of GMCs having typical sizes of 50–100 pc in a single galaxy (Fukui et al. 1999, 2008). In these surveys 270 GMCs were finally detected over the LMC (Fig. 1). These GMCs show a good

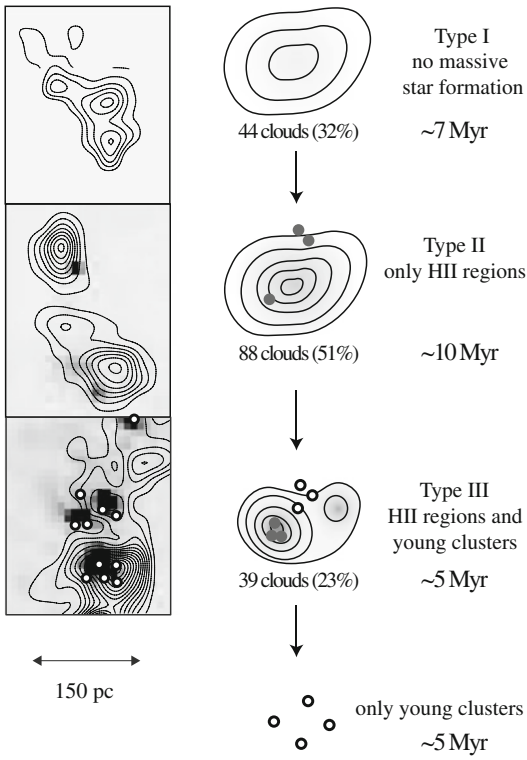

Fig. 2 Evolutionary sequence of GMCs (Kawamura et al. 2009). *Left panels* show examples of GMC Types I, II and III. Each panel presents Hα image with GMCs in *contours*, where *open circles* indicate the young clusters. The *middle panels* show illustration of the evolutionary stages. *Open* and *filled circles* represent young clusters and HII regions, respectively

spatial correspondence with the youngest star clusters having age less than 10 Myr, but they show much less correlation with more evolved clusters older than 10 Myr (Fukui et al. 1999; Kawamura et al. 2009). Fukui et al. (1999) found that GMCs are classified into three types according to the level of star formation activity: Type I shows no sign of star formation, Type II only a few small HII regions and Type III young rich clusters and well-developed HII regions. The cluster age is used to estimate the typical timescale of Type III GMCs to be 5 Myr as well as those of the Type I and Type II GMCs by assuming steady-state cluster formation in the galaxy (Kawamura et al. 2009). Figure 2 shows the evolutionary scheme of the three Types from inactive to fully active star formation. The Type III GMC will end up by rapid dissipation due to the stellar feedback. The estimated lifetime of a GMC is $\sim$ 20 Myr.

Recently, the small spiral galaxy M33 was fully surveyed in the CO J = 2-1 transition at 40 pc resolution with the IRAM 30 m telescope (Gratier et al. 2012) and the authors presented a classification scheme into the three GMC types similar to that in the LMC. This is the second galaxy which exhibits the evolutionary trend in spatially resolved GMCs. It is however to be noted that the CO J = 2-1 transition tends to be biased toward GMCs with higher star formation activity than in the J = 1-0 transition and the difference in the excitation conditions of the two transitions need to be considered in detailed comparison between the two galaxies.

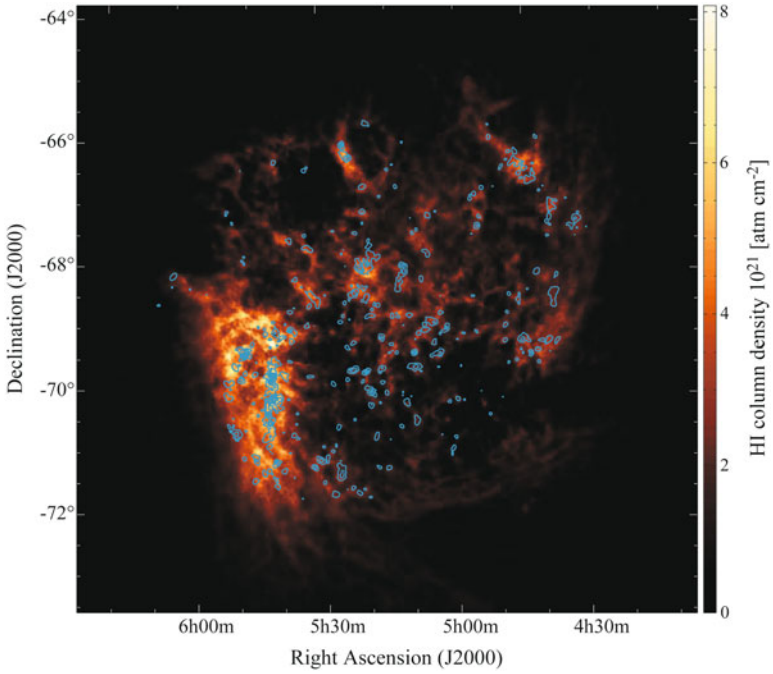

Fig. 3 HI integrated intensity distributions (Kim et al. 2003) with GMCs taken with NANTEN in contours (Fukui et al. 2009)

3 CO vs. HI: Formation of GMCs

It is a natural scenario that GMCs are formed of the less dense HI gas which has ten times more mass than GMCs (e.g., Blitz et al. 2007). The GMC distribution is indeed well correlated with the HI peaks in the LMC (Fig. 3). Fukui et al. (2009) made a first detailed analysis between the HI and CO in three dimensional space including the velocity with a 1.7 km s^{-1} bin. This study is distinguished from most of the previous studies on the Kennicut-Schmidt law of star formation rate which use velocity integrated intensity in correlating CO and HI at a $\sim$ 1 kpc scale (e.g., Bolatto et al. 2011). The results by Fukui et al. (2009) clearly indicate that GMCs are enveloped by HI "dresses" at 40 pc resolution, and it is shown that the HI dresses grow in mass from Type I to Type III, leading to a scenario that the surrounding HI gas accretes onto the GMCs by the cloud gravity to increase the GMC mass, i.e., mass of GMCs grows in 10 Myr. The mass accretion rate of the HI gas with a typical density of 100 cm^{-3} is estimated to be $\sim$ 0.1 M$_\odot$ yr^{-1}, where the HI optical depth effect is taken into account (Fukui et al. 2014b, c; see also Braun et al. 2009).

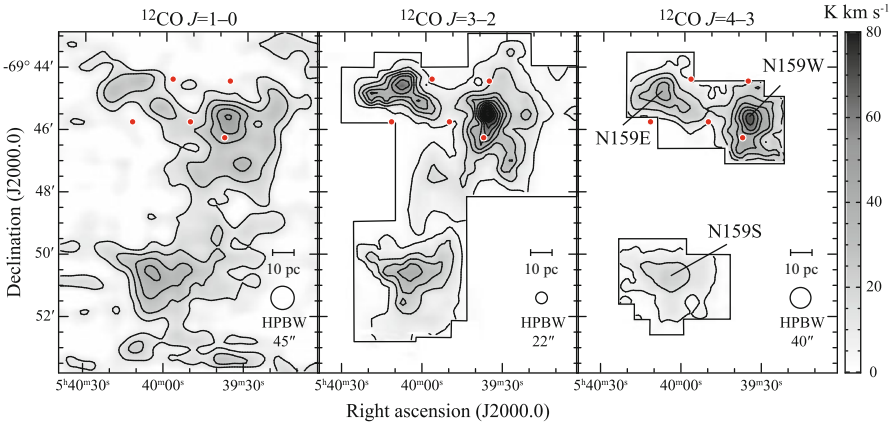

Fig. 4 Integrated intensity maps of the dense clumps in N159 in ^{12}CO $J = 1$-0 (*left*), ^{12}CO $J = 3$-2 (*middle*), and ^{12}CO $J = 4$-3 (*right*) (Mizuno et al. 2009). *Contours* are plotted at every 10 K km s^{-1} from the 3σ noise level (11, 5 and 5 K km s^{-1}, respectively). *Red circles* indicate positions of young clusters having ages less than 10 Myr (Minamidani et al. 2008)

4 Dense Clumps in GMCs

The actual cluster formation sites are dense clumps embedded in GMCs (Minamidani et al. 2008, see also references therein). Higher CO rotational transitions allow us to probe density and temperature of the clumps via LVG analyses of multiple line radiation transfer. Minamidani et al. (2008) and Mizuno et al. (2010) used NANTEN2, ASTE at Atacama and the Mopra 22 m telescope to observe CO J = 1-0, 3-2, 4-3 and 7-6 transitions, whose upper states lie from $\sim$ 5 K to $\sim$ 140 K above the ground state, in N159 and other star forming regions along the main CO ridge of the LMC (Fig. 4). Fujii et al. (2014) extended the survey with ASTE and Mopra to the N48 and N49 regions. The typical ranges of kinetic temperature, H_2 density and clump mass are 20–200 K, 10^3–10^5 cm^{-3} and 10^4–10^5 M$_\odot$, respectively, in these $\sim$30 clumps. Figure 5, $n(H_2)$-T_k plots, shows that there is a systematic trend that clumps with higher density have higher kinetic temperature. These authors interpret that high kinetic temperature is due to young stars formed in the clumps and the lack of high-density low-temperature clumps in Fig. 5 is consistent with the rapid formation of high-mass stars in the clumps. It has also been shown that Type I GMCs have no dense clumps and Type III GMCs are rich in high-mass clumps. The GMC evolution therefore accompanies rapid evolution of the internal clumps as well as the dynamical accretion of the outer HI envelopes.

As an attempt to model the evolutionary scheme of GMCs Goldbaum et al. (2011) made numerical simulations of the GMC evolution by incorporating effects of star formation and HI inflow. These authors showed that the three GMC Types are reasonably well reproduced by the model, whereas the scattering in the number of GMCs is not small for each Type. These simulations lend support for the evolutionary scenario in Fig. 2.

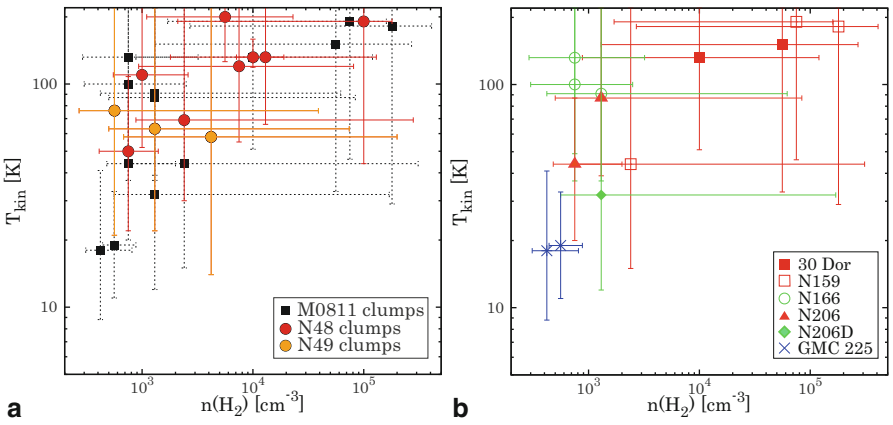

Fig. 5 **a** A plot of molecular hydrogen density and kinetic temperature of the clumps derived with the LVG analysis (Fujii et al. 2014). *Red* and *orange filled circles* indicate the clumps in the N48/N49 regions, and *black filled boxes* indicate those in the LMC molecular ridge regions (M0811 clumps). **b**Same as (a) but only for M0811 clumps. Each *mark* and *error bar* are lcolored according to the types of their parental GMCs; Type I in *blue*, Type II in *green*, and Type III in *red*

5 Triggered Formation of Super Star Clusters: Possible Role of Cloud-Cloud Collisions

In the LMC with no spiral arms, large-scale compression of the HI gas is mainly due to supershells driven by multiple SN explosions. Most of the super giant shells are indeed well delineated by HI filaments (see Fig. 3). Yamaguchi et al. (2001) first studied the spatial relationship between shells and high-mass young stars in the LMC and found weak correlation of the young stellar clusters with supergiant shells. Dawson et al. (2013) made a followed-up study and showed that 30–40 % of the GMCs are possibly associated by the super giant shells, suggesting that at least part of the cloud/star formation is triggered by shells. It is intriguing that the active star formation in the LMC, e.g., R136, N159, N48, are often found toward the regions of "interacting boundary" of two super giant shells.

Populous clusters like R136 are "mini-globulars" and called "super star clusters" which exhibit remarkably active high-mass star formation including ∼30 O stars in a small volume of 1 pc^3. It is yet difficult to see details of the natal molecular gas in the LMC at 50 kpc, whereas studies of similar nearby super star clusters in the Milky Way are able to offer some hint on populous cluster formation. It is particularly important that evidence for extremely rapid and coeval formation of super star clusters has been presented by a careful analysis of HST/VLT observations in the two super star clusters NGC3603 and Westerlund 1 (Kudryavtseva et al. 2012). The timescale of star formation there is estimated to be extremely short, in the order of 10^5 yrs or even less. This suggests that some highly supersonic gas motion is operating in collecting gas in a pc-scale volume and that the youngest stars are formed in less than 10^5 yr. The mass accretion rate is then estimated to be 10^{-3} $M_\odot$ yr^{-1} for a 100 $M_\odot$

star. NGC3603 is located at ∼2 kpc from us and shares similar properties to R136 including centrally condensed O stars whose mass range is 10–100 $M_{\odot}$. NGC3603 and Westerlund 1 in the Milky Way offer a unique lesson to infer formation of the populous clusters including R136.

In this context, it is important to note that cloud-cloud collisions are able to trigger formation of high-mass stars/clusters (e.g., for a review, Onishi 2013). Numerical simulations of supersonically colliding molecular clouds show that dense and massive cloud cores having large turbulent motion are formed in the compressed layer, where the compression is made three-dimensionally thanks to the curved magnetic field (Inoue and Fukui 2013; see also Habe and Ohta 1992). There are four cases of triggered formation of youngest super star clusters until now among nearly 20 super star clusters known to date in the Milky Way (Portegies Zwart et al. 2010). The first discovery of an unambiguous case of triggered formation of a super star cluster was made in Westerlund 2 in the Galactic disk (Furukawa et al. 2009; Ohama et al. 2010). These papers were followed up by another discovery of triggered formation due to a cloud-cloud collision in the super star cluster NGC3603 (Fukui et al. 2014a). The relative velocity between the two clouds in these collisions is highly supersonic,10–20 km s^{-1}, and the collision time scale is estimated to be 10^5 yr for a typical cloud thickness of 1 pc. This is consistent with the star formation timescale shorter than 10^5 yrs (Kudryavtseva et al. 2012). Triggering of a single O star between colliding lower mass clouds were also discovered in M20 (Torii et al. 2011) and RCW120 (Torii et al. 2014). Most recently, Fukui et al. (2014d) found evidence for spatially extensive triggering of mini-starburst toward the young HII regions NGC6357 and NGC6334 in $l = 350°$ to 354° (Fig. 6). The two clouds in the region have typical velocity separation of 10–20 km s^{-1} and shows broad CO features connecting the two colliding clouds over 100 pc in part of the spiral arm. The last case demonstrates that the cloud-cloud collisions are a common in the spiral arms in the Milky Way (Tasker and Tan 2009). It is natural to extend the scheme to the LMC where clouds are mainly driven by super giant shells and it is a promising scenario that cloud-cloud collisions are operating in forming populous clusters in the LMC. ALMA will be one of the instruments which are able to reveal details of cloud-cloud interactions in the LMC.

6 Summary

We presented recent observational results on the CO and HI in the LMC and discussed that the evolution of GMCs are rapid from the enveloping HI gas to dense clumps forming clusters. We summarize the present paper as follows;

1. The CO J = 1-0 survey of the LMC with NANTEN detected 270 GMCs at 40 pc resolution over the whole extent of the galaxy. This is the first spatially resolved sample of GMCs in a single galaxy.
2. The GMCs in the LMC are classified into three Types of different star formation activity, Types I, II and III. Type III shows tight correlation with youngest stellar clusters whose age is less than 10 Myr, allowing us to estimate the evolutionary

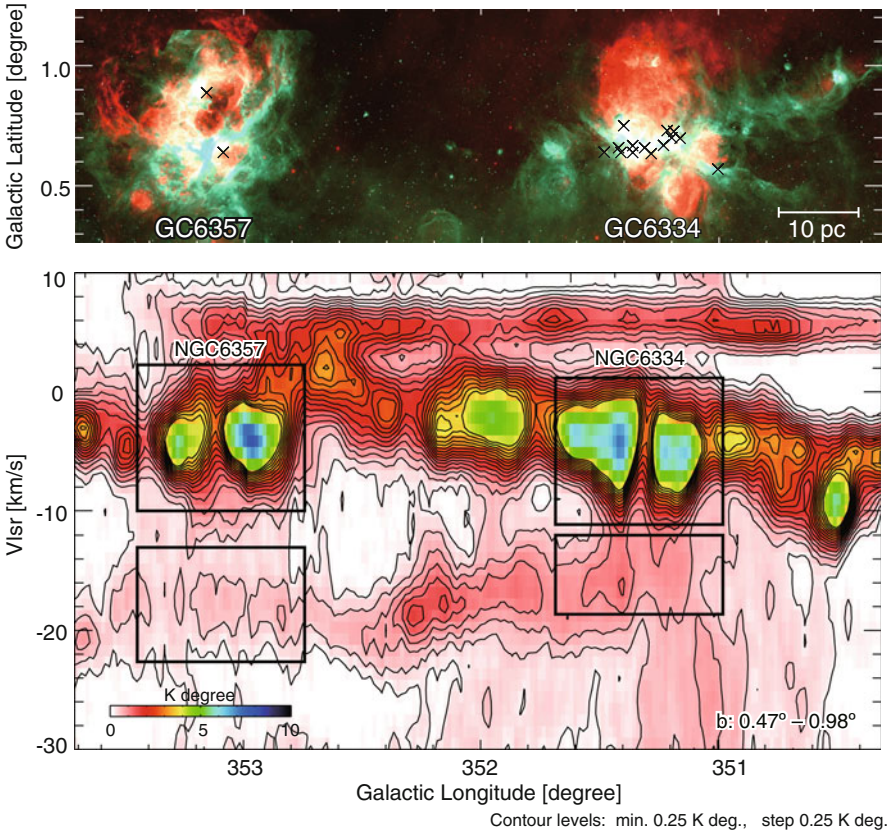

Fig. 6 **a** A composite image of NGC6357 and NGC6334, where *green* is the Spitzer 8 micron emission and *red* is H emission. *Crosses* indicate the cluster containing massive stars. **b** Longitude-velocity map of the 12 CO emission obtained with NANTEN2 toward the same region in (a). *Black boxes* show the colliding clouds in NGC6357 and NGC6334

timescales of each Type for a steady state along with the total GMC lifetime to be 20 Myr.

3. The GMCs are enveloped by HI having density of 100 cm^{-3}. A plausible scenario is that the HI envelopes are gravitationally accreting onto the GMCs to increase the molecular mass at a rate of 0.1 $M_{\odot}$ yr^{-1}.
4. Dense clumps in the GMCs evolve rapidly from cool/diffuse to warm/dense clumps according to analyses of multi-J CO observations at mm/sub-mm wavelengths.
5. The populous clusters are outstanding active high mass star formation in the LMC. Recent observations of Galactic super star clusters and starbursts strongly indicate cloud-cloud collisions play a role in triggering formation of these clusters. ALMA has a high potential to resolve such triggering by cloud-cloud collisions in forming populous clusters in the LMC.

Acknowledgements We thank the core members of the organizers for their invaluable role in realizing this memorable meeting.

References

Blitz, L., et al., 2007, in Protostars & Planets V, eds. B. Reipurth, D. Jewitt, & K. Keil, (U. Arizona: Tucson), p.81
Bolatto, A. D. et al. 2011, ApJ, 741, 12
Braun, R. et al. 2009, ApJ, 695, 937
Cohen, R. et al. 1988, ApJ, 331L, 95
Dawson, J. et al. 2013, ApJ, 763, 56
Fujii, K. et al. 2014, in preparation
Fukui,Y. and Kawamura, A., 2010, ARA&A, 48, 547
Fukui, Y. et al. 1999, PASJ, 51, 745
Fukui, Y. et al. 2008, ApJS, 178, 56
Fukui, Y. et al. 2009, ApJ, 705, 144
Fukui, Y. et al. 2014a, ApJ, 780, 36
Fukui, Y. et al. 2014b, arXiv1401.7398
Fukui, Y. et al. 2014c, arXiv1403.0999
Fukui, Y. et al. 2014d, in preparation
Furukawa, N. et al. 2009, ApJ, 696, 115
Goldbaum, N. J., et al. 2011, ApJ, 738, 101
Gratier, P. et al. 2012, A&A, 542A, 108
Habe, A. and Ohta, K. 1992, PASJ, 44, 203
Inoue and Fukui 2013, ApJ, 774, 31
Kawamura, A. et al. 2009, ApJS, 184, 1
Kim, S. et al. 2003, ApJS, 148, 473
Kudryavtseva, N. et al. 2012, ApJ, 750, 44
Minamidani, T. et al. 2008, ApJS, 175, 485
Mizuno, N. et al. 2009, The Magellanic System: Stars, Gas, and Galaxies, Proceedings of the International Astronomical Union, IAU Symposium, Volume 256, p. 203–214
Mizuno, Y. et al. 2010, PASJ, 62, 5
Ohama, A. et al. 2010, ApJ, 709, 975

Onishi, T. 2013, Proceedings of a Symposium held in Hakone, Japan 3–8 December 2012. ASP Conference Series, Vol. 476. San Francisco: Astronomical Society of the Pacific, 2013., p.85
Portegies Zwart, S. F., McMillan, S. L. W., Gieles, M. 2010, ARA&A, 48, 431
Tasker, E. J., Tan, J. C. 2009, ApJ, 700, 358
Torii, K. et al. 2011, ApJ, 738, 46
Torii, K. et al. 2014, in preparation
Yamaguchi, R. et al. 2001, PASJ, 53, 959

The Panchromatic Hubble Andromeda Treasury. Progression of Large-Scale Star Formation Across Space and Time in M 31

Dimitrios A. Gouliermis, Lori C. Beerman, Luciana Bianchi, Julianne J. Dalcanton, Andrew E. Dolphin, Morgan Fouesneau, Karl D. Gordon, Puragra Guhathakurta, Jason Kalirai, Dustin Lang, Anil Seth, Evan Skillman, Daniel R. Weisz and Benjamin F. Williams

Abstract We investigate the clustering of early-type stars younger than 300 Myr on galactic scales in M 31. Based on the stellar photometric catalogs of the Panchromatic Hubble Andromeda Treasury program that also provides stellar parameters derived

D. A. Gouliermis (✉)
Centre for Astronomy, Institute for Theoretical Astrophysics, University of Heidelberg, Albert- Ueberle-Str. 2, 69120 Heidelberg, Germany
e-mail: dgoulierm@googlemail.com

Max Planck Institute for Astronomy, Königstuhl 17, 69117 Heidelberg, Germany
e-mail: dgoulier@mpia.de

M. Fouesneau
Max Planck Institute for Astronomy, Königstuhl 17, 69117 Heidelberg, Germany

L. C. Beerman · J. J. Dalcanton · B. F. Williams
Department of Astronomy, University of Washington, Box 351580, Seattle, WA 98195, USA

L. Bianchi
Department of Physics and Astronomy, Johns Hopkins University, Baltimore, MD 21218, USA

A. E. Dolphin
Raytheon Company, 1151 East Hermans Road, Tucson, AZ 85756, USA

K. D. Gordon · J. Kalirai
Space Telescope Science Institute, 3700 San Martin Drive, Baltimore, MD 21218, USA

P. Guhathakurta
University of California Observatories/Lick Observatory, University of California, 1156 High Street, Santa Cruz, CA 95064, USA

D. Lang
Department of Astrophysical Sciences, Princeton University, Princeton, NJ 08544, USA

A. Seth
Department of Physics and Astronomy, University of Utah, Salt Lake City, UT 84112, USA

E. Skillman
Department of Astronomy, University of Minnesota, 116 Church Street SE, Minneapolis, MN 55455, USA

D. R. Weisz
Department of Astronomy, University of California at Santa Cruz, 1156 High Street, Santa Cruz, CA 95064, USA

K. Freeman et al. (eds.), *Lessons from the Local Group,*
DOI 10.1007/978-3-319-10614-4_24

from the individual energy distributions, our analysis focused on the young stars in three star-forming regions, located at galactocentric distances of about 5, 10, and 15 kpc, corresponding to the inner spiral arms, the ring structure, and the outer arm, respectively. We apply the two-point correlation function to our selected sample to investigate the clustering behavior of these stars across different time- and length-scales. We find that young stellar structure survives across the whole extent of M 31 for at least 300 Myr. Stellar distribution in all regions appears to be self-similar, with younger stars being systematically more strongly clustered than the older, which are more dispersed. The observed clustering is interpreted as being induced by turbulence, the driving source for which is probably gravitational instabilities driven by the spiral arms, which are stronger closer to the galactic centre.

1 Introduction

Stars are born in groups (Lada and Lada 2003) of various sizes and with various degrees of gravitational self-binding (Elmegreen et al. 2000). Observed length-scales of star formation range from few 100-pc, typical for loose stellar complexes, to few 10-pc, characteristic of unbound stellar aggregates and OB associations, and finally down to few pc, indicative of more compact young star clusters. All these types of stellar clusterings are not independent from each other and instead, they are structured into a hierarchical fashion (Elmegreen 2011), similar to that of the interstellar matter (ISM). Giant molecular clouds are indeed hierarchical structures (Elmegreen and Falgarone 1996; Stutzki et al. 1998), indicating that scale-free processes determine their global morphology, turbulence being considered the dominant (Elmegreen and Scalo 2004; Mac Low and Klessen 2004). It stands to reason that mechanisms regulating star formation (McKee and Ostriker 2007) consequently shape stellar structures, which then build up in a hierarchical fashion, due to the self-similar nature of turbulent cascade (e.g., Klessen and Burkert 2000). This structuring behavior is exemplified in Fig. 1 for the Galactic star-forming complex W3/4/5.

The formation of stars proceeds hierarchically also in time. The duration of star formation tends to increase with the size of the region as the crossing time for turbulent motions (Efremov and Elmegreen 1998). Small regions form stars quickly and large regions, which contain the small ones, form stars over a longer period. This relation between length- and time-scale underscores the perception that both, cloud and stellar structures, come from interstellar gas turbulence and suggests that star formation in a molecular cloud is finished within only few turbulent crossing times (e.g., Ballesteros-Paredes et al. 1999; Elmegreen 2000; Hartmann et al. 2001).

While this picture of clustered star formation explains the formation of young stellar assembles across different scales, the relation between ISM structure and stellar clustering is not well understood. In addition, apart from star formation, environmental conditions (local feedback, galactic dynamics, etc) influence the morphology of stellar clustering, and the observed variety of stellar systems in size, shape, and

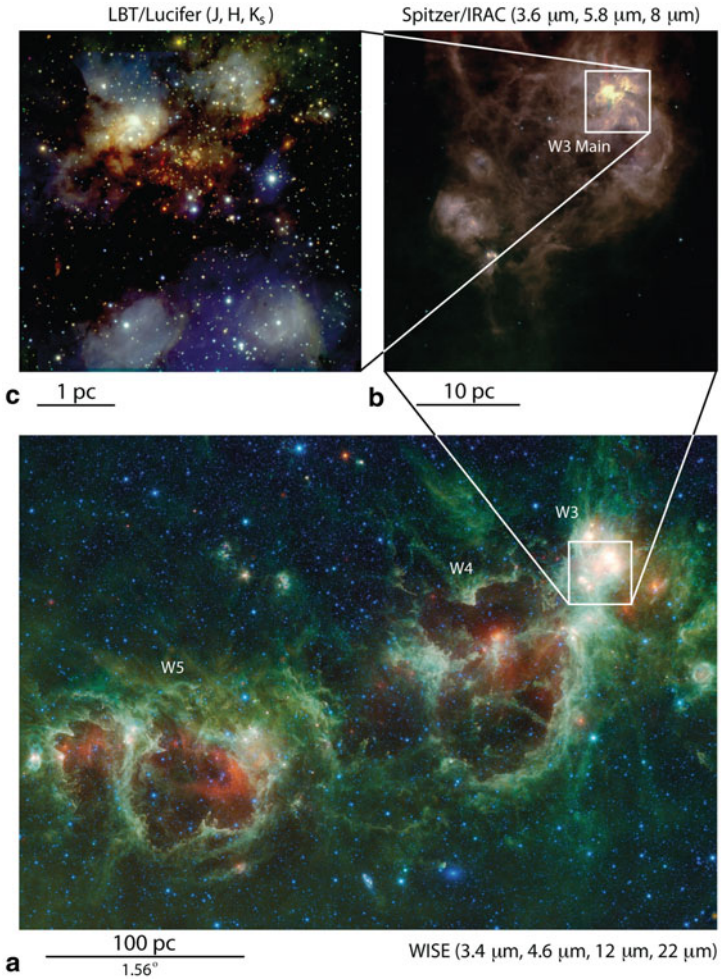

Fig. 1 Hierarchy in the ISM and stellar clustering in the general area of W3 complex. (**a**) On 100 pc-scale, the nebular structures W4 and W5 are shown in the mid-IR image from NASA/WISE, which covers the general region of the OB association Cas OB6. (**b**) On 10 pc-scale, the star-forming region W3, considered as part of W4, is shown from NASA/Spitzer images, with the active star-forming region W3 Main showing bright PAH emission at 8 μm. (**c**) Finally, on the 1 pc-scale high-resolution near-IR images from LUCI camera on the LBT reveal the embedded star-forming cluster of W3 Main (Bik et al. 2012, 2014). (WISE image credit: NASA/JPL-Caltech/WISE Team)

compactness. Dissentangling the relative importance of the heredity of star formation to the stellar clustering ("nature") in comparison to the environmental influence on its morphology and survival ("nurture") plays, thus, an important role to our understanding of clustered star formation.

We present our investigation of stellar structures formation over galactic scales from the census of bright blue stars, distributed over the typical length-scale of spiral arms. Our dataset is observed with the most complete stellar survey ever performed of M 31, obtained by the Panchromatic Hubble Space Telescope Andromeda Galaxy Treasury program[1]. We describe our analysis and present first results on the clustering behaviour of young stars up to ages of ∼300 Myr in this galaxy.

2 Observational Material

The Panchromatic Hubble Space Telescope Andromeda Treasury (PHAT) program (Dalcanton et al. 2012) provides deep coverage of 1/3 of M31 galaxy in six filters with HST. The survey spans the north east quadrant of the galaxy, continuously imaging from the nucleus to the last obvious regions of star formation visible with GALEX (e.g., Thilker et al. 2005). This part of M 31 is selected because of its lowest internal extinction, the highest intensity regions of unobscured star formation, and the least contamination from M 32. Imaging is performed blue-ward of 4000 Å, in filters F275W and F336W with the WFC3 camera, in the optical F475W and F814W filters with ACS/WFC, and in the near-IR, in the WFC3 filters F110W and F160W (Williams et al. 2014). This wide panchromatic coverage baseline allows us to confidently estimate stellar effective temperatures, masses, ages and reddenings through a self-consistent Bayesian Spectral Energy Distribution (SED) fitting technique (Gordon et al., in prep), and identify specific features on the color-magnitude diagrams (CMDs) for hot and cool stars for a wide range of extinctions. The homogeneity of the stellar photometric catalogs produced by PHAT over a wide spatial coverage provides the unique opportunity to address the clustering behavior of star formation at length-scales of few kpc, corresponding to spiral arms, down to the few pc scale, where individual star clusters reside (Johnson et al. 2012; Fouesneau et al. 2014; Simones et al. 2014).

Observations of the PHAT survey were performed in 3×6 mosaics of 18 parallel ACS and WFC3 pointings. Each mosaic builds a so-called 'brick', roughly corresponding to regions of 1.5×3 kpc at the distance of M 31. In total, 23 such bricks tile the complete survey area. The regions of interest in our study are covered by few such bricks, all including portions of the star-forming spiral arms and 10-kpc ring of Andromeda (Fig. 2). We name each area after the identification number of its first brick, e.g., areas 9, 15 and 21. Area 9 covers only one brick, while areas 15 and 21 cover somewhat more than two adjacent bricks. These (apart from a brick that covers part of the bulge) are the only areas for which preliminary stellar parameters are available through our SED fitting technique. We distinguish the bright hot stars with the best-fit values in each area, based on three selection criteria:

[1] http://www.astro.washington.edu/groups/phat/Home.html

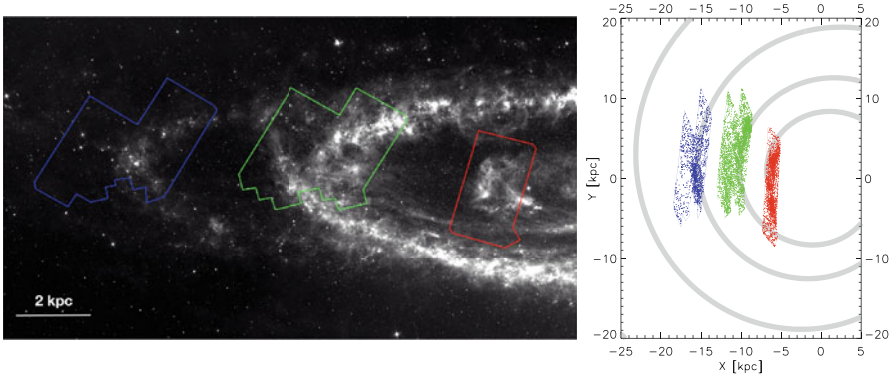

Fig. 2 Footprints of the selected regions on the Spitzer 8 μm image of M31 (*left panel*), and coverage of the selected regions in respect to the Andromeda disk corrected for the inclination of the galaxy, shown face-on (*right panel*), in respect to the spiral arms in accordance to Arp (1964). Area 9 (*red*) covers the northeastern turn-over of the inner spiral arm at ∼5 kpc from the centre, and area 15 (*green*) that of the second arm on the 10 kpc star-forming ring of Andromeda. Area 21 (*blue*) located at distance ∼15 kpc from the centre, includes various star-forming regions at the outskirts of M 31

1. Stars with $T_{\rm eff} \geq 10,000$ K, i.e., spectral type earlier than ∼ A0V.
2. Stars detected in at least three of the bluest filters, i.e., in F275W (NUV), F336W (U), and F475W (B).
3. Stars with equivalent U-band magnitude $m_{336} \leq 25.25$.

With these criteria, we ensure to select the brightest young stars with $L \gtrsim 80\,{\rm L}_{\odot}$, and also the most accurate determinations of physical parameters based on the preliminary assumed stellar models.

3 Evolution of Young Stellar Structure in M 31

3.1 The Two-Point Correlation Function

The spatial distribution of the early-type stars in the selected areas is characterized in terms of the two-point correlation function (TPCF). Originally introduced for measuring cosmological structure (e.g., Peebles 1980), the TPCF is a robust measurement of the degree of clustering in a sample of sources. Based on the original estimator by Peebles and Hauser (1974) the TPCF is estimated by counting the pairs of sources with different separations r. This function is defined as (see, e.g., Scheepmaker et al. 2009):

$$1 + \xi(r) = \frac{1}{\bar{n}N} \sum_{i=1}^{N} n_i(r), \tag{1}$$

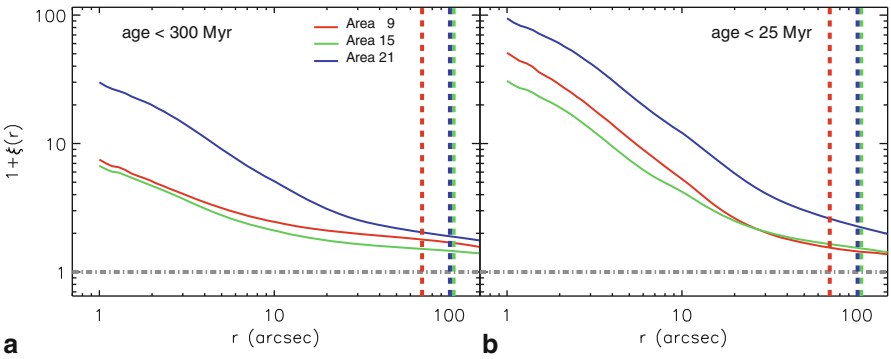

Fig. 3 The TPCF of the three areas of interest constructed for stars in two different age ranges, i.e., the complete samples with stellar ages up to ∼300 Myr and a subsample of stars with ages up to 25 Myr. All TPCFs behave as power-laws up to specific separations, beyond which the TPCF index evidently changes. *Vertical lines*, coloured accordingly, correspond to the limiting separations beyond which the effects of the limited field-of-view become dominant, and thus TPCF measurements are not trustful. (see, e.g., Gouliermis et al. 2014)

which measures the surface density enhancement $n_i(r)$ within radius r from star i with respect to the global average surface density $\bar{n}$ of the total sample of N stars. For a fractal distribution the TPCF yields a power-law dependency with radius of the form $1 + \xi(r) \propto r^{\eta}$. By definition, the total number of stars N_r within an aperture of radius r will be then increasing as $N_r \propto r^{\eta} \cdot r^2 = r^{\eta+2}$. The power-law index η is thus related to the (two-dimensional) fractal dimension, D_2, of the (projected) distribution as $D_2 = \eta + 2$ (Mandelbrot 1983).

This TPCF formalism allows for the direct interpretation of the absolute value of $1 + \xi(r)$, without any comparison with a reference random distribution (as, e.g., proposed by Gomez et al. 1993), because for a random (Poisson) stellar distribution the value of the TPCF is always $1 + \xi(r) = 1$, independent of r. For truly clustered distributions the value of the TPCF is a measurement of the clustering degree of the stars, and is always > 1; higher value at a given separation, stands for higher degree of clustering in the sample (for a complete description see Gouliermis et al. 2014, and references therein). The behaviour of the TPCF is illustrated by the examples given in Fig. 3, where the TPCFs of the three areas for the complete sample of stars with ages up to ∼300 Myr and stars with ages up to ∼25 Myr, are shown.

The log-log plots of Fig. 3 show that all TPCFs have broken power-law shape. We determine the index η of each part of the TPCF by applying a Levenberg–Marquard nonlinear least square minimization fit (Levenberg 1944; Marquardt 1963). The fitting function has the form:

$$\log\left(1 + \xi(r)\right) = \begin{cases} \alpha + \beta \cdot \log(r) & \text{for } \log(r) < \delta \\ \alpha + (\beta - \gamma) \cdot \delta + \gamma \cdot \log(r) & \text{for } \log(r) > \delta \end{cases} \quad (2)$$

where β and γ are the power-law slopes and δ is the logarithm of the position of the separation break along the abscissa, $S_{\rm break}$, where the TPCF index changes. Both slopes and the separation break are free parameters in our fit.

From the comparison of the TPCFs of Fig. 3 we derive two interesting results. First, the younger stars (age $\lesssim$25 Myr) show a more fractal, i.e., clumpy, clustering than stars in the whole sample (age $\lesssim$300 Myr). This is demonstrated by both the higher values of $1 + \xi$ at small separations and the steeper slopes of their TPCFs (the latter only for areas 9 and 15). Second, while the TPCF index of areas 9 and 15 changes significantly, becoming steeper for the younger sample, that of area 21 remains unchanged between the two samples. This indicates that older populations (up to ∼300 Myr) in areas 9 and 15 have higher filling factors (flatter TPCF slopes) than those in area 21. Considering that the latter is the most remote area, away from the centre of M 31, we can only assume that the more dispersed distribution of older stars in areas 9 and 15 is due to the dynamics of the galaxy. We investigate in more detail the evolution of the TPCF with stellar age in the following sections.

3.2 Evolution of the TPCF with Time

We construct the TPCF of the young stellar samples in the three areas of interest for stars of different ages. We divide each sample to several subsamples of stars, according to the best-fit ages assigned to each star with the SED-fitting. These ages are constrained by the stellar evolution models (Girardi et al. 2010) and atmosphere templates (Castelli and Kurucz 2004) preliminary used in our technique. Therefore, we select our subsamples of stars according to their effective temperatures, which are somewhat better-constrained by the SED fitting, and are clear indicators of the stellar evolutionary stage. In order for our analysis to be performed in samples of equivalent statistical significance (i.e., not being affected by different number statistics) we divided each stellar catalog into $T_{\rm eff}$-determined subsamples, containing the same number of stars, corresponding to ∼10 % of the total. We divided thus each stellar catalog into nine (in the case of area 9 into ten) subsamples that contain almost identical number of stars at different evolutionary stages. This number is ∼5000 in areas 9 and 21 and ∼10,000 in area 15. An example of the subsamples and the derived TPCF parameters for area 15 is shown in Table 1.

We determine the TPCF index η for both small and large separations, as well as the separation $S_{\rm break}$ where η changes, for each subsample by applying again a Levenberg–Marquard nonlinear least square minimization fit. The results are given in Fig. 4, where we show the relation of index η (and the derived D_2) to the average age of the corresponding stellar subsample for small ($r \leq S_{\rm break}$; top panel) and large ($r \geq S_{\rm break}$; middle panel) separations.

For small separations the plots of η (or D_2) versus stellar age show that there is a clear time evolution of the TPCF, with D_2 being smaller at younger ages, and becoming larger for older ages. In all areas D_2 starts with values $\lesssim 1$ at the smaller age bin of $\langle$age$\rangle \sim 9$ Myr, and increases almost monotonically to a value of ∼1.6 at

Table 1 Selected stellar subsamples and derived TPCF parameters for area 15

$\langle \log T_{\rm eff} \rangle$[a]	$\langle$age$\rangle$[b] (Myr)	age limits[c] (Myr)	$\bar{n}$[d] (10^{-4} pc^{-2})	D[e] (small separations)	D (large separations)	Separation break[f] (pc)
4.38	9 ± 7	0.2 – 29.0	2.7	0.955 ± 0.004	1.583 ± 0.012	83.37 ± 3.83
4.26	21 ± 15	1.0 – 52.7	3.3	1.485 ± 0.069	1.835 ± 0.016	51.40 ± 4.71
4.21	34 ± 24	0.9 – 75.4	3.5	1.626 ± 0.185	1.883 ± 0.020	43.70 ± 7.27
4.17	51 ± 30	1.0 – 84.1	3.3	1.646 ± 0.249	1.904 ± 0.028	46.37 ± 9.14
4.14	70 ± 37	3.8 – 109.0	2.7	1.624 ± 0.218	1.904 ± 0.026	47.61 ± 7.85
4.11	104 ± 40	7.7 – 151.0	2.2	1.729 ± 0.361	1.925 ± 0.024	39.79 ± 16.49
4.08	145 ± 44	10.2 – 188.0	2.6	1.668 ± 0.290	1.904 ± 0.021	36.28 ± 10.70
4.04	193 ± 51	11.0 – 242.0	2.5	1.628 ± 0.209	1.888 ± 0.020	37.58 ± 7.69
4.01	252 ± 63	13.1 – 318.0	2.6	1.601 ± 0.137	1.882 ± 0.022	50.90 ± 6.06

[a]Average logarithmic effective temperature of stars in the subsample
[b]Average age of stars in the subsample
[c]Age limits of stars in the subsample
[d]Mean stellar surface density
[e]Two-dimensional fractal dimension derived from the TPCF index η as $D = \eta + 2$
[f]Separation limit, where the TPCF shows a significant change in its slope η

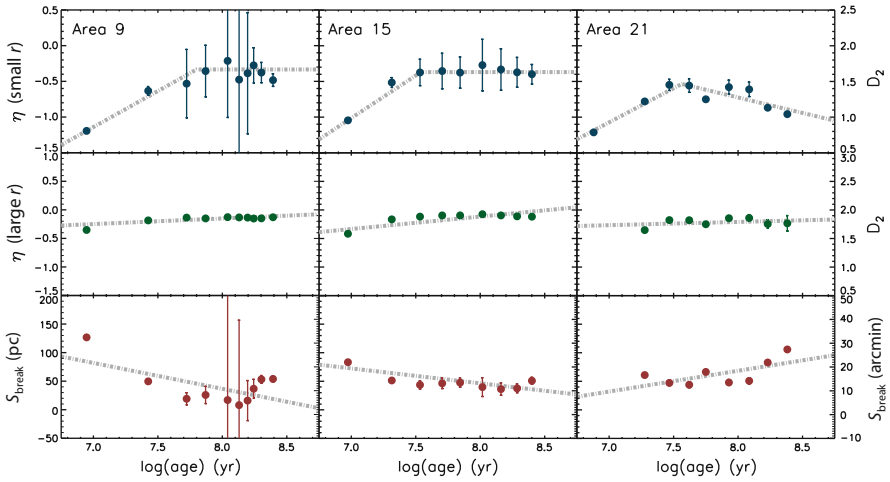

Fig. 4 Evolution of the TPCF as a function of stellar age for the three areas of interest. *Top panel*: Relation of the TPCF index η (or the equivalent fractal dimension D_2, given on the *right ordinate*) to average stellar age for small separations (smaller than the length $S_{\rm break}$ where the TPCF slope changes). *Middle panel*: The same relation for large separations, i.e., $r \geq S_{\rm break}$. *Bottom panel*: Relation of $S_{\rm break}$ to average stellar age for each subsample. The *grey dash-dotted lines* are linear fits to the data. The TPCF of stars in the youngest age range of area 21 is a single power-law, and therefore there is no measurement for D_2 at large separations and $S_{\rm break}$ for this age

$\langle$age$\rangle$ $\sim$75 Myr for area 9 and 35 Myr for area 15 (see also Table 1), and to $\sim$1.4 at $\langle$age$\rangle$ $\sim$45 Myr for area 21. It is worth noting that while for older stars in areas 9 and 15 the TPCF slope 'stabilizes' at almost constant value through the whole remaining age extent, in area 21 it drops again to the value of D_2 $\sim$1. For separations $r \geq S_{\rm break}$ (Fig. 4, middle panel) the TPCF shows no important evolution with stellar age, having a value of $D_2 \sim 1.85 \pm 0.02$ (area 9), $\sim 1.85 \pm 0.11$ (area 15), and $\sim 1.79 \pm 0.07$ (area 21). While this value for area 21 is somewhat smaller than those in areas 9 and 15, all values are high, close to the geometrical (projected) dimension, and thus consistent with almost uniform (non-clustered) stellar distributions. Interestingly, we observe from the bottom panels of Fig. 4, that the limit of the fractal regime, $S_{\rm break}$, seems to also evolve with stellar age.

4 Concluding Remarks and Summary

The value $D_2 \lesssim 1$ found for the youngest stars at separations $r \leq S_{\rm break}$ indicates that star formation is clumpy, forming well-clustered (highly fractal) stellar distributions. This clustering behavior becomes somewhat scattered (larger D_2) for older stars, stabilizing at D_2 $\sim$1.4–1.6, up to $\sim$300 Myr. This fractal dimension, however, is still characteristic of self-similarity, indicating that while stellar clustering does evolve with time, the original structure in M 31 persists over more than $\sim$300 Myr. This time-scale is in agreement with the lower limits placed for structure survival in dwarf galaxies (Bastian et al. 2011). Values of D_2 $\sim$1.5, measured in the distributions of size and luminosity of star-forming regions in the spiral galaxy NGC 628, and across the whole extend of star-forming galaxies of various types, are interpreted as indication of hierarchy induced by turbulence (Elmegreen et al. 2006; Elmegreen et al. 2014). Similarly, we conclude that the observed fractal dimensions in all three areas may be driven by turbulent processes on galactic scales.

The change of the TPCF index at $r \simeq S_{\rm break}$ and the stability of D_2 to an almost constant value for separations $r > S_{\rm break}$ suggests that possibly there is a maximum length-scale up to which stars sustain their clustering pattern, i.e., up to which their structures survive. Moreover, the apparent dependence of $S_{\rm break}$ to stellar age implies that this scale differs between stars at different evolutionary stages. Although the physical meaning of this break is not yet understood, its presence might be related to the scale of the galactic disk. For example, a break in the power spectra of ISM emission in the Large Magellanic Cloud is interpreted as due to the line-of-sight thickness of the galactic disk (Block et al. 2010). Indeed, in spiral galaxies stars tend to group up to scales comparable to the disk scale height, and larger structures become spiral-like (flocculent) because of their longer dynamical time-scales in comparison to the shear time (see, e.g., Elmegreen 2011).

Under these circumstances, with the use of the TPCF, we not only determine the time-scale for structure survival, but we may also specify the upper length-scale limit across the galactic disk where structure survives, before it 'dissolves' in it.

The observed difference in the behavior of the TPCF from one area to other, suggests a possible dependence of the clustering behavior of stars to the position of the areas across the disk of M 31, and thus the dynamical influence of the galaxy. Area 9 coincides with the first arm at distance ∼5 kpc, area 15 is located at the 10 kpc star-forming ring, and the more remote area 21 at a distance ∼15 kpc away from the galactic centre (see Fig. 2, right panel). Area 9, being closer to the centre, experiences stronger gravitational instabilities and possible disruption by the galactic potential. This is portrayed by the TPCF (at small separations) and $S_{\rm break}$ variabilities, which are seen in Fig. 4 only for area 9, and not for areas 15 and 21.

Considering the rotation of the galaxy (e.g., Sofue and Rubin 2001), based on their positions, all three areas have rotational velocities quite similar to each other varying between 236 km s^{-1} at ∼5 kpc, 260 km s^{-1} at ∼10 kpc, and 251 km s^{-1} at ∼15 kpc (see, e.g., Table 1 in Carignan et al. 2006). While all areas have similar velocities, being at different distances from the galactic centre, perform a complete orbit at different time-scales, the closest being fastest. As a consequence, the oldest stars in our samples, of ∼300 Myr, have performed thus far 10 % of an orbit in area 9, 6 % in area 15 and 4 % in area 21. This suggests that these stars have experienced different degrees of streaming motions driven by the spiral arms, which scatter stars as they shear by (e.g., Elmegreen and Struck 2013), with those in area 21 being less disrupted.

Based on the discussion above, the findings of this study can be summarized to the following points:

1. Stellar clustering occurs at length-scales that depend on both stellar age and position on the disk.
2. Star formation produces clumpy structures of young stars, on which galactic dynamics influence over time subsequent clustering processes or substructures.
3. Young stellar structures survive across the whole extent of M 31 for at least ∼300 Myr.
4. The distribution of young stars evolves as a function of stellar age, but remains fractal with $D_2 \sim 1.4$–1.6 up to this age limit.
5. The observed self-similarity in the stellar distribution is probably induced by large-scale turbulence.
6. Stars in the outer parts away from the galactic centre experience less disruption driven by the gravity of spiral arms.

Acknowledgement Based on observations made with the NASA/ESA Hubble Space Telescope, obtained from the data archive at the Space Telescope Science Institute (STScI). STScI is operated by the Association of Universities for Research in Astronomy, Inc. under NASA contract NAS 5-26555. D.A.G. acknowledges support by the German Research Foundation through grant GO 1659/3-1. I also acknowledge very useful discussions with Bruce Elmegreen, Ralf Klessen, Sacha Hony and Lukas Konstandin, which helped improve this manuscript. Finally, I would like to thank the organizers for a very interesting meeting in a wonderful location, and wish to our honourees and their beloved all the best for good health and happiness!

References

Arp, H. 1964, ApJ, 139, 1045
Ballesteros-Paredes, J., Hartmann, L., & Vázquez-Semadeni, E. 1999, ApJ, 527, 285
Bastian, N., Weisz, D. R., Skillman, E. D., et al. 2011, MNRAS, 412, 1539
Bik, A., Henning, T., Stolte, A., et al. 2012, ApJ 744, 87
Bik, A., Stolte, A., Gennaro, M., et al. 2014, A&A, 561, A12
Block, D. L., Puerari, I., Elmegreen, B. G., & Bournaud, F. 2010, ApJL, 718, L1
Carignan, C., Chemin, L., Huchtmeier, W. K., & Lockman, F. J. 2006, ApJL, 641, L109
Castelli, F., & Kurucz, R. L. 2004, A&A, 419, 725
Dalcanton, J. J., Williams, B. F., Lang, D., et al. 2012, ApJS, 200, 18
Efremov, Y. N., & Elmegreen, B. G. 1998, MNRAS, 299, 588
Elmegreen, B. G. 2000, ApJ, 530, 277
Elmegreen, B. G. 2011, EAS Publications Series, 51, 31
Elmegreen, B. G. & Falgarone, E. 1996, ApJ, 471, 816
Elmegreen, B. G., & Scalo, J. 2004, ARA&A,, 42, 211
Elmegreen, B. G., & Struck, C. 2013, ApJL, 775, L35
Elmegreen, B. G., Efremov, Y., Pudritz, R. E., et al. 2000, Protostars and Planets IV, 179
Elmegreen, B. G., Elmegreen, D. M., Chandar, R., et al. 2006, ApJ, 644, 879
Elmegreen, D. M., Elmegreen, B. G., Adamo, A., et al. 2014, ApJL, 787, L15
Fouesneau, M., Johnson, L. C., Weisz, D. R., et al. 2014, ApJ, 786, 117
Girardi, L., Williams, B. F., Gilbert, K. M., et al. 2010, ApJ, 724, 1030
Gomez, M., Hartmann, L., Kenyon, S. J., & Hewett, R. 1993, AJ, 105, 1927
Gouliermis, D. A., Hony, S., & Klessen, R. S. 2014, MNRAS, 439, 3775
Hartmann, L., Ballesteros-Paredes, J., & Bergin, E. A. 2001, ApJ, 562, 852
Johnson, L. C., Seth, A. C., Dalcanton, J. J., et al. 2012, ApJ, 752, 95
Klessen, R. S., & Burkert, A. 2000, ApJS, 128, 287
Lada, C. J., & Lada, E. A. 2003, ARA&A, 41, 57
Levenberg, K. 1944, Q. Appl. Math., 2, 164
Mac Low, M.-M., & Klessen, R. S. 2004, Reviews of Modern Physics, 76, 125
Mandelbrot, B. B. 1983, The fractal geometry of nature (Freeman, San Francisco)
Marquardt, D. 1963, SIAM J. Appl. Math., 11, 431
McKee, C. F., & Ostriker, E. C. 2007, ARA&A, 45, 565
Peebles, P. J. E. 1980, The Large-Scale Structure of the Universe. Princeton Univ. Press
Peebles, P. J. E., & Hauser, M. G. 1974, ApJSS, 28, 19
Scheepmaker, R. A., Lamers, H. J. G. L. M., Anders, P., & Larsen, S. S. 2009, A&A, 494, 81
Simones, J. E., Weisz, D. R., Skillman, E. D., et al. 2014, ApJ, 788, 12
Sofue, Y., & Rubin, V. 2001, ARA&A, 39, 137
Stutzki J., Bensch F., Heithausen A., Ossenkopf V., & Zielinsky M. 1998, A&A 336, 697
Thilker, D. A., Hoopes, C. G., Bianchi, L., et al. 2005, ApJL, 619, L67
Williams, B. F., Dalcanton, J. J., Lang, D., et al. 2014, ApJ, submitted

The Small Magellanic Cloud: Molecular Gas and Star Formation

Mónica Rubio

Abstract The Small Magellanic Cloud is the nearest galaxy in which we can study the gas, dust and star formation at low metallicities (1/10), resembling the early phases of galaxy formation in the Universe. The SMC has been studied in CO line emission but most of the molecular gas is likely to be in moderate extinction regions where CO is faint and photo dissociated. Dust emission is potentially a better molecular tracer because of its independence of photo-chemistry and density structures of the molecular clouds, allowing for a more complete census of the cold dense star forming gas distribution and its relationship to star formation. We present results of sub-mm observations which combined with Spitzer and Herschel confirm dust emission excess from the molecular gas and sets important constraint to use the dust emission at sub-millimeter as an alternative method to derive the amount of H_2 gas in which star formation takes place. We discuss these results and their impact on other low metallicity systems in the Local Group.

1 Introduction

Stars form in dense cold concentration of molecular gas H_2 that are traditionally traced by the emission of CO or other more complex molecules. But in dwarf irregular galaxies CO observations have yielded only upper limits even though tracers of recent star formation such as H_2 or far-ultraviolet (FUV) emission reveals young stars and star clusters. The supposition is that H_2 is present in star forming regions in these galaxies even when CO is undetected.

A correlation between gas surface density and star formation rate (SFR) surface density has long been known to hold on global scales (e.g. Schmidt 1959; Kennicutt 1998) but the pc-scale physics which drives this star formation (SF) "law" is unclear. At high spatial resolution the SF "law" breaks down (e.g. Schruba et al. 2010). The SF rate has been found to be correlated to the molecular gas surface density H_2 and not to the of HI surface density (Biegel et al. 2008). Thus, determining the H_2 molecular gas density and distribution is crucial to study star formation in galaxies.

M. Rubio (✉)
Departamento de Astronomía, Universidad de Chile, Chile
e-mail: mrubio@das.uchile.cl

K. Freeman et al. (eds.), *Lessons from the Local Group,*
DOI 10.1007/978-3-319-10614-4_25

The molecular gas H_2 does not emit at the temperature of the dense cold gas where star formation occurs. Thus, to determine and study the molecular gas and determine the amount and properties of the molecular regions, we need to use other molecular tracers. The CO molecule has become the preferred method as C and O are the two other most abundant elements after H and He. They combine to form CO which can be excited at low temperatures (5.5) emitting at 2.6 mm (115 GHz). Star formation rates and efficiencies are, hence, based on a reliable determination of the H_2 molecular gas content.

Irregular galaxies are very weak CO emitters (Tacconi and Young 1987). As the abundance of C and O decreases in the ISM of galaxies, it is more difficult to detect CO. For many years it was not possible to detect CO for galaxies which had metallicities lower than the SMC or Zw 36 (Taylor et al. 1998) and star formation was taking place.

Another methods to determine the molecular gas content in galaxies use the FIR dust emission and the mass estimates from virial determination, assuming that molecular clouds are gravitationally supported and follow a size line-width relationship.

2 Structure of Molecular Clouds

The structure of star-forming clouds at low metallicity is predicted to be different from that at high metallicity such as the Solar Neighborhood. As the metallicity drops, the cold and dense CO-emitting region of a cloud, where stars will form, shrink relative to the warm photo-dissociation region (PDR) around it. The molecular hydrogen area becomes much more extended than the CO region as well as the atomic hydrogen layer around the molecular cloud.

Low metallicity galaxies also have a smaller dust to gas ratios and therefore the less amount of dust allows UV photons to penetrate much deeper in the molecular regions photo dissociating the CO molecules while the H_2 molecules are able to selfshield. The low metallicity molecular clouds change their PDR structure due to a combination of their less C and O abundance which decreases the formation of CO. Also less dust implies a faster CO photo-dissociation as it impedes the protection from UV photons from nearby massive stars.

In these lower metallicity clouds the relationship between the intensity of the CO emission and the molecular hydrogen density $N(H_2)$ showed a different factor, larger than the one derived in the Galaxy. This relationship is known as the CO to H_2 conversion factor, X_{CO}, and is expected to vary with environment (Bolatto et al. 2013 and reference therein, Genzel et al. 2012). The H_2 to CO conversion factor was shown to increase at lower metallicity (Leroy et al. 2011).

3 The Small Magellanic Cloud (SMC)

The SMC is at 61 kpc distance (Hilditch et al. 2005) and has a metallicity of 12+ log [O/H]=8.0 ($\sim$ 0.5 Solar). Its Oxygen (O) and Carbon (C) abundance are 4 times (Dufour 1984) and 6 times (Dufour et al. 1982), respectively, smaller that Galactic and its dust to gas ratio is 10 times smaller than that of the MW. Thus, it is an ideal galaxy to study the effect of lower metallicity on the molecular gas and the molecular cloud structure and its relationship to star formation

To determine the molecular gas content in the SMC several methods have been used. The most important one has been to the CO emission of the galaxy. Lately, the SMC dust emission has been used.

3.1 SMC CO Emission and the Conversion Factor to Derive the N(H_2) Column Density

In our Galaxy, the conversion factor, X_{CO}, has been calibrated by several independent methods and established to be $X_{CO}=2 \times 10^{20}$ cm^{-2} (K kms^{-1})$^{-1}$ or α_{co}=4.2 Mo pc^{-2} (Leroy et al. 2011; Bolatto et al. 2013). This conversion factor is expected and debated to vary for different environments

In the SMC, this factor has been determined by different studies. The first study was done surveying CO(1-0) the entire galaxy (2 deg $\times$ 2 deg) with 9 arcmin resolution (160 pc at the SMC distance) by Rubio et al. (1991) who detected several molecular cloud complexes. These complexes followed a line width-size relationship similar to galactic molecular GMCs (Solomon et al. 1987) except that for a similar linewith the CO size of the cloud was a factor of 10 smaller. A molecular mass was determined applying virial theorem and an X_{CO} (SMC) factor of 20 times was derived. A new survey was done with the NANTEN telescope with a 2.6 arcsec resolution (45 pc at the SMC) and covered the NE and WS part of the SMC (Mizuno et al. 2001). From this survey a conversion factor of 2.5 $\times 10^{21}$ was estimated i.e. 10 times the galactic one. The CO clouds identified showed a very good positional correlation to star formation traces with ages less than 5–6 Myr, such as HII regions with embedded star cluster or high surface brightness compact HII regions. A total amount of molecular mass in the SMC was found to be 4.6×10^6 M, only 0.6 % of the neutral atomic gas (Stanimirovic et al. 1999).

The large spatial extent of the SMC in the sky plays against detailed studies as parsec resolution at millimeter wave have covered limited areas of the galaxy. The SEST CO program of the Magellanic Could at 40 arcsec resolution, 20 pc in CO(1-0), and 20 arcsec resolution in CO (2-1) (Rubio et al. 1993; Israel et al. 1993) covered mainly the SW Bar of the SMC and several other isolated regions (Rubio et al. 2000; Bolatto et al. 2003). Form these studies, Rubio et al. (1993) estimated a conversion factor value of 9×10^{20}, 4 times galactic at 10 pc, and introduced a size dependence

correlation with $X_{CO} \sim R^{0.7}$. suggesting that for smaller CO clouds the conversion factor approached the Galactic one.

3.2 Gravitationally Bound Clouds

Another method used to determine the amount of molecular gas molecular cloud is to assume that clouds are gravitationally bound and that a virial mass can be derived. To apply this method the SMC molecular clouds need to be resolved, meaning they have to be observed with ten parsec resolution.

In the Milky Way, the molecular clouds follow a size linewidth relationship which had a slope of 0.5 as expected from gravitationally bound clouds. In spiral galaxies the molecular clouds also follows this dependence, known as the Larson laws (Rosolowsky and Leroy 2006).

In the SMC it has been found that the CO molecular clouds follow a similar L_{CO} M_{vir} relationship as Galactic clouds (Solomon et al. 1987) but they are systematically less luminous that the galactic counterpart for the same virial mass suggesting that there could be additional molecular or atomic gas causing the large line-width which was "dark".

3.3 Emission From Dust and the Sub-Millimeter Excess

Sub millimeter, millimeter and FIR studies of the dust emission provide additional ways to measure the dark molecular gas, i.e, the molecular gas that does not emit in CO.

The HERITAGE project (Meixner et al. 2013) mapped the entire LMC, SMC and Magellanic Bridge at 160, 250 and 500 μm with HERSCHEL space telescope. Before, the SMC SPITZER MegaSAGE program (Bolatto et al. 2008; Gordon et al. 2010) imaged at 3.6, 4.5, 5.8, 8.0, 24, 70, 160 μm both Magellanic Clouds, a superb set of data in the Far-IR is available to perform these studies. Assuming a universal opacity of dust grains and knowing the gas to dust ratio we can derive the molecular hydrogen column density $N(H_2)$ from the sub-millimeter intensity

Combining the SMC Spitzer and Herchel 160 μm images with the neutral HI surface density gas, the molecular surface density of H_2 was determined (Leroy et al. 2007, 2009 and 2011).This method relies on the knowledge of the gas to dust ratio (GDR) in the SMC and the use of an adequate conversion factor to determine a molecular H2 mass. The derived $N(H_2)$ maps had a spatial extension larger by 30 % to 50 % than that of the CO emission and they concluded that the SMC was dominated by "dark" molecular gas (Bolatto et al. 2011). They obtained a total molecular mass of 3.2×10^7 for the SMC (10 % of the neutral HI mass) and surface density H_2 peaks of 180 Mo pc^{-2}.

Studies of the SMC dust emission in the sub millimeter range were possible only when bolometers were attached to southern telescopes such as SEST and APEX telescopes. The first millimeter dust continuum measurements in the SMC were made with the SIMBA bolometer at the SEST telescope. Rubio et al. 2004 found in the quiescent molecular cloud SMCB1#1, that the dust emission at 1.2 mm was much stronger than expected and that the gas mass derived from the dust emission was larger by a factor of 10 or more than the virial mass determined from the size and CO line width of SMCB1#1. Bot et al. 2007 studied the entire SMC SW region and found similar results for all the dust emission sources in which virial mass determination using the CO maps at 10 pc resolution could be done.

Sub-millimeter continuum observations at 870 μm were carried out and the SMC SWBar region was mapped with LABOCA Bolometer installed at APEX Telescope located at 5000 m altitude in the Chajnantor plateau in Chile (Bot et al. 2010). The sub-millimeter map showed several strong sources and diffuse weaker emission. The strongest sub millimeter sources were associated to CO clouds. We determine the gas mass for each source from the dust emission and using the dust to gas ratio for the SMC. We determined a molecular mass from virial assumption from CO data and the comparison of both molecular mass estimations showed that for all the SMC molecular clouds the molecular gas mass derived from the 870 μm dust emission was larger than the mass obtained from virial estimate. A comparison to galactic MW clouds masses using the same method was done and the result showed that the galactic molecular clouds showed an opposite behaviour, their virial masses were larger than the mass estimates form their dust emission, thus confirming the previous result of a 1.2 mm continuum emission excess for the SMC at these wavelength.

To determine and quantify the sub-millimeter excess, we started an ambitious program to map as many regions in the Magellanic Clouds with LABOCA based towards bright 160 μm emission regions (Verdugo 2012). In the SMC, five regions covering different environments were mapped as shown in Fig. 1. Fifteen new continuum sources were identified and for all them SED were constructed using their Far-IR plus the 870 μm emission. All the SMC sources showed the submillimeter excess with respect to what was expected from the dust emission law with β=2. (Verdugo 2012; Verdugo et al. 2014). To measure this excess, we fitted a modified blackbody using the Spitzer 100 μm and HERSCHEL 160, 250 and 500 μm emission (Fig. 2). The amount of 870 μm emission with respect to the SED fit was defined as the sub millimeter excess E(870)μm. The SMC sources show in average an sub millimeter excess of 1.7. The SED fit also determined the temperature, dust emissivity index β of the dust emission and the opacity for the sources. These show average dust temperature of 22 K (ranging 19 and 30 K) and opacities between 1.1 and 1.8. This excess does not shoew a correlate with temperature, opacity nor column density. The average excess for the SMC clouds is larger than the average excess of 1.4 found using the same method for LMC Clouds (Verdugo et al. 2014)

The submillimeter excess has also been observed in other dwarf galaxies (Galametz et al. 2011; O'Halloran et al. 2010; Madden et al. 2012). A 500 μm

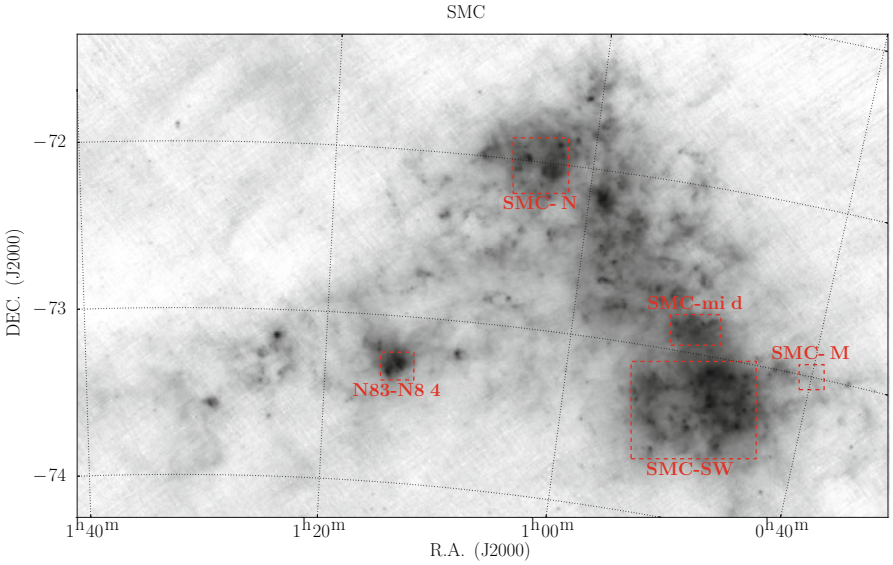

Fig. 1 The 160 μm Herchel image of the SMC. Red dotted boxes show the mapped regions at 870 μm

excess is also found in the SMC by Planck (Planck collaboration 2011). The origin of this excess is not known and new dust models are being proposed to explain it. These models explore a change of the dust emissivity at 500 μm longward (Gordon et al. 2014) or use different grain composition, silicates, spinning dust, etc.

This excess could be related to a cold dust component, (i.e 10 K) but it would require a large amount of cold dust and therefore increase the molecular mass in these regions as derived from the dust emission. This option does not seem to be consistent with observation as would imply an even large mass than the derived from virial estimates (Bot et al. 2010). The Planck collaboration concluded that the millimeter excess is unlikely to be caused by very cold dust emission and that it could be due to a combination of spinning dust emission and thermal dust emission by more amorphous dust grains than those present in our Galaxy.

4 Dark Molecular Gas

The structure of PDR regions changes dramatically as the metallicity decreases. Molecular clouds at low metallicity have a large envelope of molecular gas in the form of H2. PDR models exploring the conditions for the SMC were done by Lequeux et al. 1994 who showed that for SMC condition, 1/10 metallicity of Solar, a radiation field of 1000 and C and O abundaces of 1/4 and 1/6 respectively, CO is formed at column density of several times 10^{21} while H_2 forms at a column density of

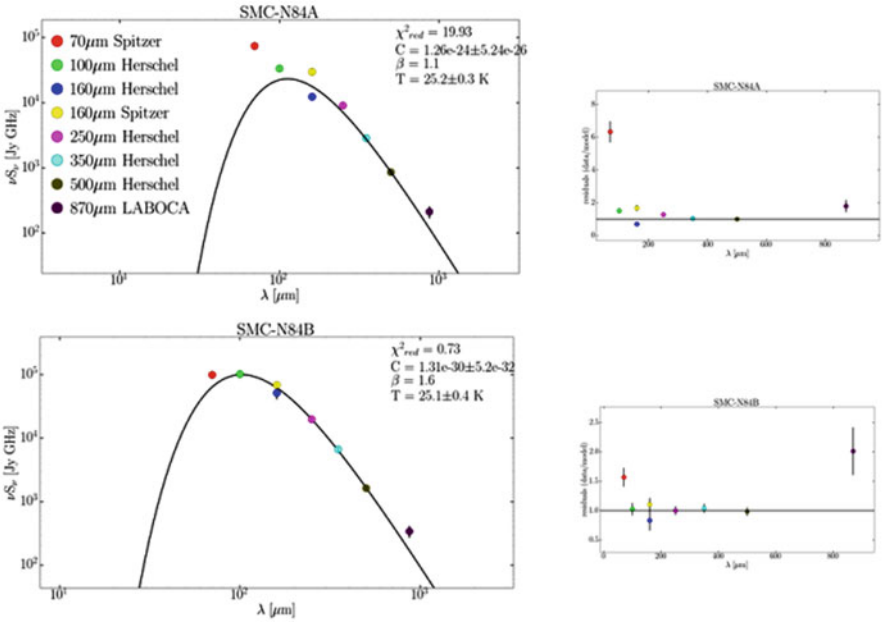

Fig. 2 Spectral Energy Distribution (SED) for N84 A and N84B SMC clouds. The sub-millimeter excess is E(870)μm is defined as the excess with respect to the modified black-body fit to the 100–500 μm points

10^{20}. Thus, there is a large envelope of gas which is dominated by H_2 and not CO. This envelope would also contain C and C+ which are products of the CO photo dissociation. Similar results are found by PDR models by Wolfire et al. 2011 which can quantify the size of the non-emitting CO gas.

Results of SMC Herchel spectrroscopy (PI. Bolatto) in 5 regions in the SMC show CII and OII emission spatially more extended than the mapped CO emission and thus could be tracing the dark molecular gas (Jameson, K. private comm.).

We initiated CO (2–1) deep observations toward the Herschel strips as high resolution CO1-0 observations covered limited areas of the SMC (Rubio et al. 1993, Rubio et al. 2000, Bolatto et al. 2003). Data was recently obtained in these regions (April 2014) and preliminary results show CO emission in all the regions where CII was detected In N83, we find that weak CO emission show a factor of 4 time higher CII emission compared to the typical CII/CO ratio of 1/1400 (2.4×10^{-4}) Galactic value (Crawford et al. 1985). Analysis of these data is underway(Rubio, Bolatto, Verdugo, in prep.).

5 Molecular Gas in Low Metallicity Systems

CO emission is weak in low metallicity systems and in local dwarf irregular galaxies has been very difficult to detect (Tacconi et al. 1998). No galaxy with metallicity lower than 8.0 had been detected in CO and these galaxies show high star formation rate. Thus, if stars formed in molecular gas then the gas must be mainly H_2 or CO emission may not detected because of beam dilution effects as the angular resolution of the observations is too large to detect tenfold parsec molecular sizes.

WLM is a dwarf galaxy only 960 kpc away and thus one of the nearest low metallicity systems after the SMC. Its metallicity is 7.8, only 13 % that of Solar. We detected CO emission and continuum 870 μm emission at two of five positions in this galaxy toward the most intense 160 μm region (Elmegreen et al. 2013). The molecular clouds are not resolved as the spatial resolution of our APEX observations is 80 pc at the WLM distance. The intensity of the CO emission is 10 times lower than the CO emission in SMC molecular clouds and have CO velocity width of 10 and 12 km/s. We estimated the CO-H_2 conversion factor and obtained a_{CO}=129 $M_\odot$ pc^{-2}. This value is the expected one for the metallicity dependence of the CO to H_2 conversion as determined by Leroy et al. 2011.

Thus, CO in low metallicity systems is a good tracer of high density molecular gas rather than a tracer of mass. ALMA observation will enable us to study molecular cloud properties in dwarfs at metallicities as low as 5 % of solar and study the molecular regikes.

Acknowledgments M.R. would like to express her gratitude to the organizers of the conference and for inviting her to give this summary talk. She would also like to thank Celia Verdugo for preparing the figures and A. Bolatto for many helpful discussion. M.R. wishes to acknowledge support from CONICYT through FONDECYT (Chile) grant N°1140839.

References

Bigiel, F.; Leroy, A.; Walter, F. et al. 2008, AJ 136, 248
Bolatto, A. Leroy, A. , Israel, Frank P., et al . 2003, ApJ 595, 167
Bolatto, A.D.; Leroy, A. K.; Rosolowsky, et al. 2008, ApJ 686, 948

Bolatto, A. , Leroy, A. Jameson, K. et al. 2011, ApJ 741, 12
Bolatto, Wolfire, M., Leroy, A. 2013, ARAA 51, 207
Bot, C., Boulanger, F., Rubio, M., & Rantakyro, F. 2007, A&A, 471, 103
Bot, C., Rubio, M. & Boulanger, F. et al. 2010, A&A 524, 52
Crawford, Genzel, Townes et al. 1985, ApJ 295, 755
Dufour, R. J. 1984 in Structure and Evolution of the Magellanic Clouds, IAU Symp. 108, p. 353.
Dufour, R. J., Shields, G. A., Talbot, R. J., Jr. 1982, ApJ 252, 461
Elmegreen, B. G., Rubio, M., Hunter, D. A., et al. 2013, Nature 495, 48
Galametz, M.; Madden, S. C.; Galliano, F. et al. 2011, A&A 532, 56
Genzel, R.; Tacconi, L. J.; Combes, F, 2012 ApJ 746, 69
Gordon, K. D., Galliano, F., Hony, S., et al. 2010, A&A 518L, 89
Gordon., K.D, Roman-Duval, J., Bot, C., et al. 2014. 2014arXiv1406.6066G
Hilditch, R.W., Howarth, I.D., & Harries, T.I., 2005, MNRAS 357, 304
Israel et al. 1993, A&A, 276, 25
Kennicut, R. 1998 ApJ 498, 541
Lequeux, J, et al, 1994, A&A 292, 371
Leroy, A., Bolatto, A., Stanimirovic, S., et al. 2007, ApJ 658,.1027L
Leroy, A., et al. 2008, AJ 136,2782
Leroy, A., Bolatto, A. , Bot, Caroline, et al, 2009, ApJ 702, 352
Leroy et al. 2011, ApJ, 737, 12
Madden, S. et al 2011 EAS 52, 95
Meixner, M., Panuzzo, P., Roman-Duval, J. et al. 2013, AJ 146, 62
Mizuno, N., Rubio, M., Mizuno, A., et al. 2001, Pub. Ast. Soc. Japan 53, 47.
O´Halloran, B., Galametz, M., Madden, S. et al., 2010, A&A 518, L58
Planck Collaboration: Ade, P. A. R., Aghanim, N., Arnaud, M et al. 2011 A&A 536, 17
Rosolowsky, E. & Leroy, A., 2006, Pub. Ast. Soc. Pacific 118, 590
Rubio, M. Garay, G., Montani, J. et al. 1991, ApJ, 368, 173
Rubio, M., Lequex, J, Boulanger, F. et al. 1993, A&A 271,
Rubio, M., Contursi, A., Lequeux, J., et al. 2000, A&A. 359, 1139
Rubio, M., Boulanger, F., Rantakyro, F. et al. 2004, A&A 425, L1
Schmidt, M. 1959, ApJ, 129, 243
Schruba, A. Leroy, A., Walter, F., et al. 2010, ApJ, 722, 1699
Schruba, A., Leroy, A., Walter, F., et al. 2011, AJ, 142, 37
Schruba,A.,Leroy, A.K.,Walter, F. et al. 2012 AJ 143, 138
Solomon, P.M., Rivolo, A. R., Barrett, J. et al. 1987, ApJ 319, 730
Stanimirovic, S., Staveley-Smith L., Dickey, J. M. et al. 1999, MNRAS 302, 417
Tacconi, L. & Young, J., 1987, ApJ 322, 681
Taylor, C, Kobulnicky,H.A. & Skillman, E., et al. 1998, AJ, 116, 2746
Verdugo, C. 2012, MSc Thesis, Universidad de Chile, Chile
Verdugo, C., Rubio, M., Bolatto, A, et al. 2014 A&A submitted
Wolfire, M., Hollenbach, D., & Mackee, C. F. 2010, ApJ 716, 1191
Wolfire, M.G., 2011, Ap&SS 336, 229
Wong, T. Hughes, A., Ott, J., et al. 2011, ApJS, 197, 16

The Orbits of the Magellanic Clouds

Gurtina Besla

Abstract This paper reviews our current understanding of the orbital history and mass of the Large and Small Magellanic Clouds. Specifically, I will argue that the Clouds are on their first infall about our Milky Way and that their total masses are necessarily ~ 10 times larger than traditionally estimated. This conclusion is based on the recently revised HST proper motions of the Clouds and arguments concerning the binary status of the LMC-SMC pair and their baryon fractions.

1 Introduction

Owing to their proximity to our Galaxy, the Magellanic Clouds (MCs) have been observed in wavebands spanning almost the entire electromagnetic spectrum, allowing us to study the interstellar medium (ISM) of two entire galaxies in unprecedented detail. Such observations have facilitated studies of how turbulence, stellar feedback and star formation are interrelated and how these internal processes affect galactic structure on small to large scales (e.g., Elmegreen et al. 2001; Block et al. 2010).

However, the MCs are also subject to environmental processes that can dramatically alter their internal structure. For example, the MCs are surrounded by a massive complex of HI gas in the form of a 150 ° long stream trailing behind them (the Magellanic Stream), a gaseous bridge connecting them (the Magellanic Bridge) and an HI complex that leads them (the Leading Arm) (Nidever et al. 2010). This material once resided within the MCs and was likely stripped out by some combination of external tides and/or hydrodynamic processes.

Recently, Fox et al. (2014) revealed that these HI structures harbor a significant amount of ionized gas, increasing the total gas mass budget *outside* the MCs from 4.87×10^8 $M_\odot$ to $\sim 2 \times 10^9$ $M_\odot$. This extended gas complex thus represents a non-negligible fraction of the MW's circumgalactic medium (CGM).

Identifying the formation mechanism of these structures depends sensitively on the amount of time the MCs have spent in close proximity to the MW. Constraining

G. Besla (✉)
Steward Observatory, University of Arizona, 933 North Cherry Avenue,
Tucson, AZ 85721, USA
e-mail: gbesla@email.arizona.edu

K. Freeman et al. (eds.), *Lessons from the Local Group,*
DOI 10.1007/978-3-319-10614-4_26

the dynamics of the MCs is thus critical to our understanding of the morphologies, star formation histories and ISM properties of these important galactic laboratories.

Our understanding of the orbital history of the MCs has evolved considerably over the past 10 years. The canonical view, wherein the MCs have completed multiple orbits about the MW over a Hubble time (Murai and Fujimoto 1980), has changed to one where they are recent interlopers, just completing their first passage about our Galaxy (Besla et al. 2007).

This dramatic change has been driven by two factors. Firstly, high precision proper motions measured using the Hubble Space Telescope (HST) have enabled accurate 3D velocities of both the Large and Small Magellanic Clouds (LMC and SMC). We now know the MCs are moving faster than previously believed, relative to not only the MW, but also to *each other* (Kallivayalil et al. 2006a, b, 2013).

Secondly, our understanding of the mass and structure of galactic dark matter halos has evolved. In the Λ Cold Dark Matter paradigm, low mass galaxies reside within massive dark matter halos, having much larger mass-to-light ratios than expected for galaxies like the MW. This means that the MCs are likely significantly more massive than traditionally modeled. Furthermore, the dark matter halos of massive galaxies are now understood to be poorly represented by isothermal sphere profiles at large distances. Instead, the dark matter density profile falls off more sharply, making it easier for satellites to travel to larger Galactocentric distances.

However, debate still ensues concerning the orbital history of the MCs. While the canonical picture, where the MCs have completed ~ 6 orbits about the MW with an orbital period of ~ 2 Gyr, has been largely dismissed, there are new proposed models where the MCs have completed one or two orbits about the MW within a Hubble time (Shattow and Loeb 2009; Zhang et al. 2012; Diaz and Bekki 2011; Diaz and Bekki 2012). The goal of this review is to explain why the controversy arises and why various lines of evidence support a first infall scenario.

2 Determining the Orbit of the MCs

Reconstructing the past orbital history of the MCs depends on 3 important factors. (1) An accurate measurement of the current 3D velocity vector and distance of the MCs with respect to the MW. (2) The mass of the MW and its evolution over time. (3) The masses of the MCs, which ultimately determines the importance of dynamical friction as the MCs orbit about of the MW and each other.

The 3D Velocity of the MCs Recently, Kallivayalil et al. (2013, hereafter K13) used HST to measure the proper motions of stars in the LMC with respect to background quasars, obtaining 3 epochs of data spanning a baseline of ~ 7 years and proper motion random errors of only 1–2 % per field. This astonishing accuracy is sufficient to explore the internal stellar dynamics of the LMC, allowing for the first constraints on the large-scale rotation of *any* galaxy based on full 3D velocity measurements (van der Marel and Kallivayalil 2014). This analysis has resulted in the most accurate measurement of the 3D Galactocentric velocity of the LMC and SMC to date. The

LMC is currently moving at 321 ± 23 km/s with respect to the MW. The SMC is moving at 217 ± 26 km/s with respect to the MW and 128 ± 32 km/s with respect to the LMC; the SMC cannot be on a circular orbit about the LMC. Errors on the velocity measurement are now limited by the errors on the distance measurement to the Clouds rather than the proper motions.

The Mass of the MW The mass of the MW is uncertain within a factor of ∼2. Values for the virial mass range from $M_{vir} = (0.75 - 2.25) \times 10^{12}$ $M_\odot$. Here, M_{vir} is defined as the mass enclosed within the radius where the dark matter density is Δ_{vir} =360 times the average matter density, $\Omega_m \rho_{crit}$.

HST proper motions over a six year baseline revealed that the Leo I satellite is moving with a Galactocentric velocity of 196.0 ± 19.4 km/s (Sohn et al. 2013). At 260 kpc away, this is faster than the local escape speed of ∼ 180 km/s for a M_{vir}=10^{12} $M_\odot$ MW model. Since unbound satellite orbits are statistically improbable within ΛCDM cosmology (Boylan-Kolchin et al. 2013), we do not explore MW models lower than 10^{12} $M_\odot$.

Few upper limits on M_{vir} exist apart from the timing argument, which limits the combined total mass of the MW and M31. Using the HST proper motions of M31 and other mass arguments in the literature, van der Marel et al. (2012) estimate the Local Group mass to be $3.17 \pm 0.57 \times 10^{12}$ $M_\odot$. It is thus unlikely that the MW individually contributes much more than 2×10^{12} $M_\odot$.

In the orbital analysis that follows, we explore 3 different mass models: 10^{12}, 1.5×10^{12} and 2×10^{12} $M_\odot$. Using WMAP7 cosmology, the corresponding virial radii are R_{vir} = 250, 300 and 330 kpc. The MW is modeled as a static, axisymmetric, three-component model consisting of dark matter halo, exponential disk, and spheroidal bulge. Model parameters are listed in Table 2 of K13.

Note that the MW mass is expected to have grown by roughly a factor of 2 over the past 6 Gyr (Fakhouri et al. 2010). K13 found that this mass evolution causes the orbital period of the LMC to increase substantially relative to static models. The orbital periods discussed in the following sections are thus underestimated.

The Mass of the LMC K13 found that the LMC's mass is the dominant uncertainty in its orbital history, since dynamical friction, which is proportional to the satellite mass squared, changes the LMC's orbit on timescales shorter than, e.g., the MW's mass evolution. The mass of the LMC also controls the orbit of the SMC, ultimately determining how long the two galaxies have interacted with each other as a binary pair (see § 5).

The LMC has a well defined rotation curve that peaks at Vc = 91.7 ± 18.8 km/s and remains flat out to at least 8.7 kpc (van der Marel and Kallivayalil 2014), consistent with the baryonic Tully-Fisher relation. This implies a minimum enclosed total mass of M (8.7 kpc) = 1.7 $\pm 10^{10}$ $M_\odot$; the LMC is dark matter dominated.

There is strong evidence that the stellar disk of the LMC extends to 15 kpc (Saha et al. 2010). If the rotation curve stays flat to at least this distance then the total mass enclosed is $M(15\ kpc) = GVc^2/r \sim 3 \times 10^{10}$ $M_\odot$. This minimum value is consistent with LMC masses adopted by earlier models (e.g., Gardiner and Noguchi 1996).

The total dynamical mass of the LMC can also be estimated using its baryon fraction. Currently, the LMC has a stellar mass of 2.7×10^9 $M_\odot$ and a gas mass of 5.0×10^8 $M_\odot$. The baryonic mass of the LMC is thus $M_{bar} = 3.2 \times 10^9$ $M_\odot$. Using the minimum total mass of $M_{tot} = 3 \times 10^{10}$ $M_\odot$, the baryon fraction of the LMC becomes $M_{bar}/M_{tot} = 11\,\%$. This is much higher than the baryon fraction of disks in galaxies like the MW, which is on the order of 3–5 %. In the shallower halo potentials of dwarf galaxies, stellar winds should be more efficient, making baryon fractions even lower, not higher.

This analysis is further complicated if material has been removed from the LMC. As mentioned earlier, Fox et al. (2014) have recently estimated the total gas mass (HI and ionized gas) outside the MCs at $2 \times 10^9 (d/55\text{kpc})^2$ $M_\odot$. If half of this material came from the LMC, as suggested by Nidever et al. (2008), its initial baryon fraction would be 14 %, approaching the cosmic value. Note that the bulk of the Magellanic Stream likely resides at distances of order 100 kpc, rather than 55 kpc, in which case the baryon fraction would increase to ∼20 %.

To get a baryon fraction matching observational expectations of $f_{bar} \sim 3$–5 %, the total mass of the LMC (at least at infall) needs to have been $20 - 6 \times 10^{10}$ $M_\odot$. This higher total mass is consistent with cosmological expectations from halo occupation models that relate a galaxy's observed stellar mass to its halo mass. Using relations from Moster et al. (2013), the mean halo mass for a galaxy with a stellar mass of 2.7×10^9 $M_\odot$ is 1.7×10^{11} $M_\odot$, implying a baryon fraction of $f_{bar} \sim 2$–4 % (see Table 1). Because there is large scatter in halo occupation models, we consider a maximal halo mass for the LMC of 2.5×10^{11} $M_\odot$ in the analysis that follows.

The Mass of the SMC The current dynamical mass of the SMC within 3 kpc is constrained between 2.7–5.1 $\times 10^9$ $M_\odot$, using the velocity dispersion of old stars (Harris and Zaritsky 2006). This is larger than the current gas mass of the SMC is 4.2×10^8 $M_\odot$ and stellar mass of 3.1×10^8 $M_\odot$; the SMC is dark matter dominated. In most orbital models, the total mass of the SMC is estimated at $M_{DM} = 1.4 - 3 \times 10^9$ $M_\odot$ (Besla et al. 2007; Kallivayalil et al. 2013; Diaz and Bekki 2011; Gardiner and Noguchi 1996). This yields f_{bar} ∼20–50 %, well above cosmological expectations.

This issue gets a lot worse when we account for the substantial amount of gas the SMC must have lost to form the Magellanic Stream, Bridge and Leading Arm. If we assume again that half the total gas mass outside the MCs comes from the SMC, then the initial baryon mass of the SMC must have been $M_{bar} = 1.73 \times 10^9$ $M_\odot$. Taking the traditional dark matter mass of 3×10^9 $M_\odot$ yields $f_{bar} \sim 60\,\%$. It would take a total mass order $M_{SMC} = 3 \times 10^{10}$ $M_\odot$ to obtain a baryon fraction of 5 %. This value is consistent with the choice of $M_{SMC} = 2 \times 10^{10}$ $M_\odot$ in B12 and B10 (see Table 1). Using cosmological halo occupation models the SMC dark matter mass is expected to be even higher. The mean expectation from relations in (Moster et al. 2013) is $M_{SMC} = 4.2 \times 10^{10}$ $M_\odot$.

Table 1 The total mass of the clouds

Baryonic mass ($10^9 M_\odot$)	Dark matter mass (10^{10} $M_\odot$)	Baryon fraction[a]	Motivation for dark matter mass
LMC			
3.2	3	0.11	Traditional models
	6	0.05	Minimum mass to get $f_{bar} < 5\,\%$
	17	0.02	B12, Mean ΛCDM[c]
	25	0.01	Maximal model
4.2–6.5[b]	3	0.14–0.22	
	6	0.07–0.11	
	17	0.03–0.04	
	25	0.02–0.03	
SMC			
7.3	0.3	0.24	Traditional models
	0.5	0.15	Max dynamical mass <3 kpc
	2	0.04	B12
	4.2	0.02	Mean ΛCDM[c]
17.3–40.3[b]	0.3	0.58–1.34	
	0.5	0.35–0.81	
	3	0.06–0.13	
	4.2	0.04–0.1	

[a]Gas mass/(Stellar Mass + Gas Mass)
[b]Including half the mass in the Magellanic Stream (total 2×10^9 M⊙) (Fox et al. 2014) at a distance of 55 kpc, or where half the stream is at 100 kpc (total 6.6×10^9 $M_\odot$). [c] Mean value from relations in Moster et al. (2013) for LMC/SMC stellar masses

3 Plausible Orbital Histories for the LMC

Following the methodology outlined in K13 and considerations for the mass of the MW and the mass and velocity of the LMC described in Sect. 3, the orbit of the LMC can be integrated backwards in time. For various combinations of MW and LMC mass, Monte-Carlo drawings from the LMC's 4σ velocity error distribution are used to explore plausible orbital histories. Figure 1 shows the resulting mean orbital solutions for each MW/LMC mass combination. The LMC is considered to be on its first infall if it has not experienced more than one pericentric approach within the past 10 Gyr. In all cases the LMC has made at least one pericentric passage, since it is just at pericenter now.

The illustrated dependence on LMC mass explains the discrepancy in the literature concerning different orbital solutions. Most studies have adopted low mass LMC models, which allows for orbital solutions with lower eccentricity. For example, (Zhang et al. 2012) explore a variety of MW models to constrain the orbital history

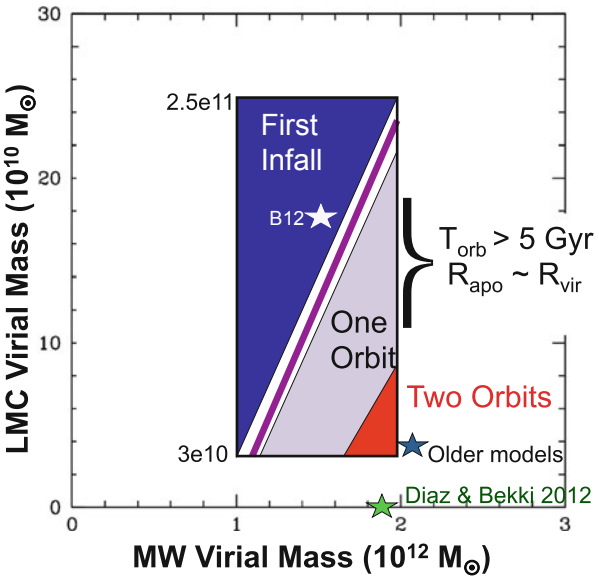

Fig. 1 Typical orbital histories for the LMC are indicated as a function of LMC and MW mass. Orbits are determined by searching the 4σ proper motion error space in Monte Carlo fashion and computing the mean number of pericentric passages completed within 10 Gyr. High mass LMC models experience greater dynamical friction and are consequently on more eccentric orbits, yielding first infall solutions (*dark blue regions*). Lower mass models allow for orbits where the LMC has made one pericentric passage (*light purple regions*); such solutions typically have orbital periods of order 5 Gyr. High MW mass and low LMC mass combinations are required for the LMC to have completed more than one orbit. The mass of the LMC needs to be larger than 3×10^{10} $M_\odot$ in order to account for LMC stars located at distances of ~ 15 kpc from the LMC center and greater than 6×10^{10} $M_\odot$ for the baryon fraction of the LMC to approach $\sim 5\,\%$. Most studies have not considered such high mass models, apart from B12

of the LMC, but they consider only one LMC mass model of 2×10^{10} $M_\odot$. Numerical models of the Magellanic System by (Diaz and Bekki 2012, 2011) consider a total mass of only 10^{10} $M_\odot$, which is discrepant with the dynamical mass determined from the LMC's rotation curve. Other recent orbital studies adopt LMC masses of 3×10^{10} $M_\odot$ (e.g., Růžička et al. 2010; Shattow and Loeb 2009). These low masses are at odds with mass estimates from arguments about the baryon fraction of the LMC, which require a minimum dark matter mass of at least 6×10^{10} $M_\odot$ (§ 3).

The numerical models presented in (Besla et al. 2010, 2012), hereafter B10 and B12) were designed to account for cosmological expectations, and thus adopt an LMC mass of 1.8×10^{12} $M_\odot$.

Note that while lower halo masses do allow for solutions where the LMC has completed one orbit about the MW, the mean orbital period is 5 Gyr. This timescale is much longer than the age of the Magellanic Stream. Furthermore, in this study, the MW mass is assumed to be static in time. If the mass evolution of the MW were included, the orbital period would be even longer.

4 The LMC-SMC Binary

At a distance of $\sim$50 kpc from the Galactic center, the LMC and SMC are our closest example of an interacting pair of dwarf galaxies. Evidence of their ongoing interaction is clearly illustrated by the existence of the Magellanic Bridge that connects the two galaxies. This structure likely formed during their last close approach $\sim 100 - 300$ Myr ago (B12, Gardiner and Noguchi 1996).

The tidal field of the MW makes it statistically improbable that the LMC could have randomly captured the SMC some 300 Myr ago while in orbit about the MW. It is more likely that the two galaxies were accreted as a binary; but the longevity of their binary status is unclear.

All models for the Magellanic Stream and Bridge invoke tidal interactions between the MCs to some degree. The MCs must therefore have interacted for at least the lifetime of the Stream. Based on the current high rate of ionization of the Stream (Weiner and Williams 1996) and large extended ionized component (Fox et al. 2014), it is unlikely that the Stream could have survived as a neutral HI structure for more than 1–2 Gyr (Bland-Hawthorn et al. 2007).

The star formation histories (SFHs) of the MCs also suggest a common evolutionary history. Weisz et al. (2013) illustrate that $\sim$ 4 Gyr ago, the SFHs of both the LMC and SMC appear to increase in concert. It is thus reasonable to assume the MCs have maintained a binary status for at least the past 4 Gyr.

Plausible Orbital Histories for the LMC-SMC Binary The orbital analysis presented in Fig. 1 is revisited, exploring the same LMC/MW mass range, but this time also searching the 4σ proper motion error space of the SMC in addition to that of the LMC. The goal is to identify the combinations of LMC and MW mass that allow for the relative velocity of the MCs to be lower than the local escape speed of the LMC for some time in the past (not necessarily including today). Figure 2 illustrates the resulting meanlongevity of the LMC-SMC binary as a function of LMC and MW mass.

The action of MW tides are detrimental to the longevity of the Magellanic binary. As the mass of the MW increases, its tidal field is stronger and thus long-lived binary configurations are rare. In particular, no long-lived solutions are found if the mass of the MW is greater than 2×10^{12} $M_{\odot}$. This places an interesting upper bound on the virial mass of the MW. If the MW is $> 2 \times 10^{12}$ $M_{\odot}$, the MCs could not have interacted for an appreciable amount of time in the past and their current proximity would be a random happenstance. Few upper bounds exist on the mass of the MW, making this a novel constraint.

The SMC has historically been modeled in a circular orbit about the LMC, with a relative velocity of order 60 km/s (Gardiner and Noguchi 1996). However, the new HST measurements reveal that the relative velocity between the Clouds is significantly larger. At a relative velocity of 128 ± 32 km/s (K13), the SMC is moving well above the escape speed of the LMC if its total mass is 3×10^{10} $M_{\odot}$ ($V_{esc} \sim 110$ km/s). This relative velocity measurement is a robust result that has been confirmed by other teams (Vieira et al. 2010; Piatek et al. 2008) and has not changed substantially from

the earlier HST results (Kallivayalil et al. 2006a, b). This high speed makes it very difficult to maintain a long-lived binary, unless the LMC is substantially more massive than traditionally modeled.

The preferred configuration for a long-lived LMC-SMC binary is a low/intermediate mass MW + a high mass LMC. This is exactly the opposite requirement for orbital solutions where the LMC makes at least one orbit about the MW. In fact, the colors in Fig. 2 correspond to the same as those in Fig. 1; all binary solutions that last longer than 4 Gyr are first infall solutions.

The high relative velocity between the Clouds implies that the SMC is on an eccentric orbit about the LMC. Such binary configurations are easily disrupted by MW tides, meaning that even one previous pericentric passage is sufficient to have destroyed the binary. This result is consistent with the fact that only 3.5 % of MW type galaxies host both an LMC and SMC stellar mass analog (Liu et al. 2011). Similarly, statistics from cosmological simulations find only 2.5 % MW type dark matter halos host both LMC and SMC mass analogs (Boylan-Kolchin et al. 2011). Our MW galaxy is thus an oddity in that it hosts two massive satellites in close proximity to each other. However, this rare configuration can be understood if the MCs have only recently passed pericentric approach for the first time; only now are MW tides operating to disrupt this configuration.

This study implies that all existing models in the literature that invoke the new HST proper motions in combination with low mass LMCs *do not allow for long-lived LMC-SMC binary solutions*. In particular, because of the high speeds, no binary LMC-SMC solutions can exist in a MOND framework (Zhao et al. 2013).

5 Further Support for a First Infall of a Binary LMC/SMC

The simplest argument in favor of a recent infall is the unusually high gas fractions of both the LMC and SMC, given their proximity to the MW. van den Bergh (2006) conducted a morphological comparison of the satellites of the MW and M31, finding that the L/SMC are the only two gas-rich dwarf Irregulars at close Galactocentric distance to their host. There are numerous environmental factors that work to quench star formation and morphologically change galaxies after they become satellite galaxies of massive hosts (see chapter by Carraro). It is thus remarkable that a satellite such as the SMC could have retained such a high gas content if it were accreted over 5 Gyr ago.

In this volume, Burkert discusses the gas consumption timescale for galaxies; upon accretion, satellites are cut off from their gas supply and thus their star formation rates should decline over time. However, Gallart (also in this volume) has illustrated that the star formation rates of the LMC have been *increasing*, with no signs of quenching over the past 4 Gyr until very recently.

Taken together these arguments strongly support a scenario where the Clouds are on their first infall to our system, having only been within the virial radius of the MW for the past 1–2 Gyr.

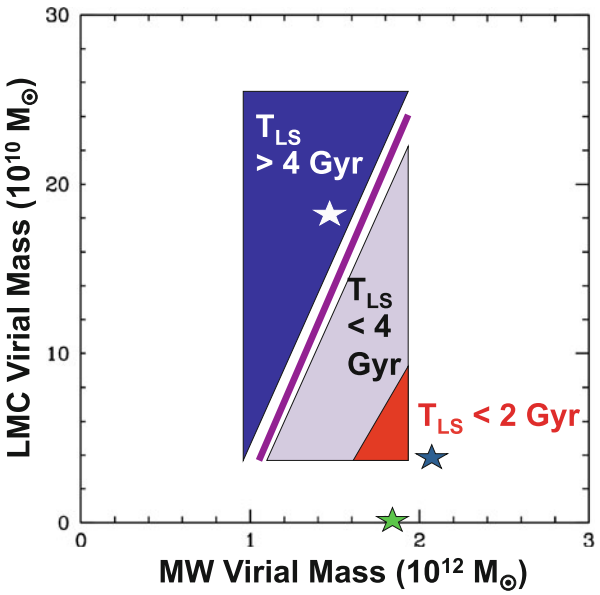

Fig. 2 Similar to Fig. 1, except now the SMC is also included in the orbital analysis; its 4σ proper motion error space is also searched in Monte Carlo fashion. Colored regions represent the same LMC orbital solutions as in Fig. 1, but here the longevity of the LMC-SMC binary is indicated. The SMC is assumed to be bound to the LMC if the relative velocity between the Clouds is less than the local escape speed of the LMC at any point in the past. Binary solutions are only viable in low/intermediate mass MW models + high LMC models; these are necessarily first infall orbits. Dynamical friction between the Clouds is not included in this analysis, but is expected to decrease the longevity of the binary orbit

6 Lessons From the Magellanic Clouds

The Magellanic Clouds are recent interlopers in our neighborhood. This statement is a consequence of the dramatically improved proper motions of the MCs made using the HST by K13 and our evolving understanding of the structure of dark matter halos. Specifically, these factors have forced us to reconsider the total dark matter masses of the MCs. The baryon fractions of the MCs and imply that their total masses must be at least a factor of 10 larger than traditionally modeled. Dynamical friction then requires their orbits to be highly eccentric, preventing short period orbits. Finally, the existence of a high relative velocity, LMC-SMC binary today strongly argues against their having completed a previous pericentric approach about our Galaxy, as MW tides can efficiently disrupt such tenuous configurations.

A first infall solution implies that the MCs have interacted as a binary pair prior to accretion; in B10 and B12 we argued that tidal interactions between the pair gave rise to the formation of the Magellanic Stream, Bridge and Leading Arm. As such, interactions between dwarfs galaxies are important drivers of their evolution and may explain the existence of Magellanic Irregular type galaxies (i.e. LMC analogs) in the field.

However, this scenario creates a large challenge for the theory that the satellite galaxies of the MW occupy a unique orbital plane and/or were formed in a common event (see the chapter in this volume by Pavel Kroupa). To be more concise, the biggest challenge posed to this plane of satellites and MOND orbital histories constructed for the MCs is the current gas fraction of the SMC and the consequent requirement that the **SMC must on a first infall**. Orbits for the SMC in MOND have small periods and apocenters (Zhao et al. 2013). Such orbital solutions cannot explain the absence of quenching in the star formation history of the SMC and the fact that there is currently just as much gas in the SMC as there is in its much larger companion the LMC.

References

Besla G., Kallivayalil N., Hernquist L., Robertson B., Cox T. J., van der Marel R. P., Alcock C., 2007, ArXiv Astrophysics e-prints
Besla G., Kallivayalil N., Hernquist L., van der Marel R. P., Cox T. J., Kereš D., 2010, ApJL, 721, L97
Besla G., Kallivayalil N., Hernquist L., van der Marel R. P., Cox T. J., Kereš D., 2012, MNRAS, 421, 2109
Bland-Hawthorn J., Sutherland R., Agertz O., Moore B., 2007, ApJL, 670, L109
Block D. L., Puerari I., Elmegreen B. G., Bournaud F., 2010, ApJL, 718, L1
Boylan-Kolchin M., Besla G., Hernquist L., 2011, MNRAS, 414, 1560
Boylan-Kolchin M., Bullock J. S., Sohn S. T., Besla G., van der Marel R. P., 2013, ApJ, 768, 140
Diaz J. D., Bekki K., 2012, ApJ, 750, 36
Diaz J., Bekki K., 2011, MNRAS, 413, 2015
Elmegreen B. G., Kim S., Staveley-Smith L., 2001, ApJ, 548, 749
Fakhouri O., Ma C.-P., Boylan-Kolchin M., 2010, MNRAS, 406, 2267
Fox A. J., Wakker B. P., Barger K. A., Hernandez A. K., Richter P., Lehner N., Bland-Hawthorn J., Charlton J. C., Westmeier T., Thom C., Tumlinson J., Misawa T., Howk J. C., Haffner L. M., Ely J., Rodriguez-Hidalgo P., Kumari N., 2014, ApJ, 787, 147
Gardiner L. T., Noguchi M., 1996, MNRAS, 278, 191
Harris J., Zaritsky D., 2006, AJ, 131, 2514
Kallivayalil N., van der Marel R. P., Alcock C., Axelrod T., Cook K. H., Drake A. J., Geha M., 2006a, ApJ, 638, 772
Kallivayalil N., van der Marel R. P., Alcock C., 2006b, ApJ, 652, 1213
Kallivayalil N., van der Marel R. P., Besla G., Anderson J., Alcock C., 2013, ApJ, 764, 161
Liu L., Gerke B. F., Wechsler R. H., Behroozi P. S., Busha M. T., 2011, ApJ, 733, 62
Moster B. P., Naab T., White S. D. M., 2013, MNRAS, 428, 3121
Murai T., Fujimoto M., 1980, PASJ, 32, 581
Nidever D. L., Majewski S. R., Burton W. B., 2008, ApJ, 679, 432
Nidever D. L., Majewski S. R., Butler Burton W., Nigra L., 2010, ApJ, 723, 1618
Piatek S., Pryor C., Olszewski E. W., 2008, AJ, 135, 1024
Růžička A., Theis C., Palouš J., 2010, ApJ, 725, 369
Saha A., Olszewski E. W., Brondel B., Olsen K., Knezek P., Harris J., Smith C., Subramaniam A., Claver J., Rest A., Seitzer P., Cook K. H., Minniti D., Suntzeff N. B., 2010, AJ, 140, 1719
Shattow G., Loeb A., 2009, MNRAS, 392, L21
Sohn S. T., Besla G., van der Marel R. P., Boylan-Kolchin M., Majewski S. R., Bullock J. S., 2013, ApJ, 768, 139
van den Bergh S., 2006, AJ, 132, 1571
van der Marel R. P., Kallivayalil N., 2014, ApJ, 781, 121
van der Marel R. P., Fardal M., Besla G., Beaton R. L., Sohn S. T., Anderson J., Brown T., Guhathakurta P., 2012, ApJ, 753, 8
Vieira K., Girard T. M., van Altena W. F., Zacharias N., Casetti-Dinescu D. I., Korchagin V. I., Platais I., Monet D. G., López C. E., Herrera D., Castillo D. J., 2010, AJ, 140, 1934
Weiner B. J., Williams T. B., 1996, AJ, 111, 1156
Weisz D. R., Dolphin A. E., Skillman E. D., Holtzman J., Dalcanton J. J., Cole A. A., Neary K., 2013, MNRAS, 431, 364
Zhang X., Lin D. N. C., Burkert A., Oser L., 2012, ApJ, 759, 99
Zhao H., Famaey B., Lüghausen F., Kroupa P., 2013, A&A, 557, L3

Structure and Evolution of Dwarf Galaxies

John Kormendy

Abstract Different structural parameter correlations show how classical bulge components and elliptical galaxies are different from spiral and S0 galaxy disks, irregular (Im) galaxies, and spheroidal (Sph) galaxies. In contrast, the latter, apparently diverse galaxies or galaxy components have almost identical parameter correlations. This shows that they are related. A review of galaxy transformation processes suggests that S0 and spheroidal galaxies are star-formation-quenched, "red and dead" versions of spiral and Im galaxies. In particular, Sph galaxies are bulgeless S0s. This motivates a parallel sequence galaxy classification in which an S0a–S0b–S0c–Sph sequence of decreasing bulge-to-total ratios is juxtaposed to an Sa–Sb–Sc–Im sequence of star-forming galaxies. All parameter sequences show a complete continuity from giant galaxies to the tiniest dwarfs. Dwarfs are not a new or different class of galaxies. Rather, they are the extreme products of transformation processes that get more important as gravitational potential wells get more shallow. Smaller Sph and S+Im galaxies have lower stellar densities because they retain fewer baryons. Comparison of the baryonic parameter correlations with those for dark matter halos allows us to estimate baryon loss as a function of galaxy mass. Extreme dwarfs are almost completely dominated by dark matter.

1 A Parallel Sequence Galaxy Classification

This paper combines visible-galaxy scaling relations from Kormendy and Bender (2012) with dark matter scaling relations from Kormendy and Freeman (2014). Results on visible galaxies are conveniently encoded in a parallel sequence galaxy classification scheme shown in Fig. 1.

J. Kormendy (✉)
Department of Astronomy, University of Texas at Austin,
2515 Speedway, Stop C1400, Austin, TX 78712-1205, USA
e-mail: kormendy@astro.as.utexas.edu

Max-Planck-Institut für Extraterrestrische Physik, Gießenbachstraße,
85748 Garching bei München, Germany

Universitäts-Sternwarte München, Ludwig-Maximilians-Universität,
Scheinerstraße 1, 81679 München, Germany

K. Freeman et al. (eds.), *Lessons from the Local Group,*
DOI 10.1007/978-3-319-10614-4_27

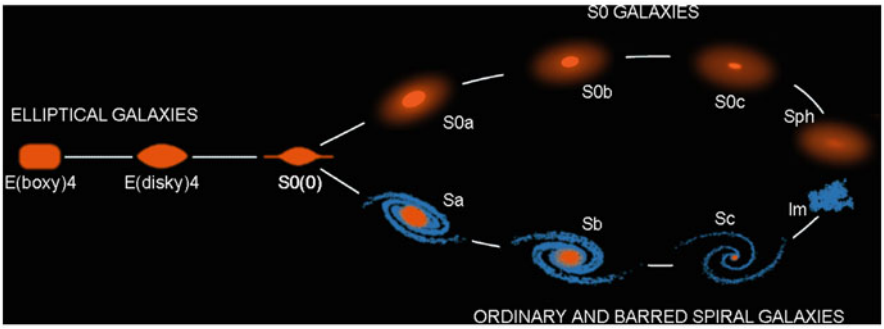

Fig. 1 Parallel sequence galaxy classification including spheroidal (*Sph*) galaxies as bulgeless *S0* galaxies juxtaposed with irregular (*Im*) galaxies. (From Kormendy and Bender 2012)

This updates a parallel sequence classification proposed by van den Bergh (1976). Kormendy and Bender add Sph galaxies as S0s that have no bulge component. This is motivated by the observation that S0 galaxies have bulge-to-total luminosity ratios that range from almost 1 to almost 0 (see also Laurikainen et al. 2010). Kormendy and Bender find a continuous transition in properties—including density profiles but also kinematic properties—between S0 disks and spheroidal galaxies. Figure 2 shows the parameter correlations that illustrate this continuity. S0-like galaxies are given a diffferent name when they have no bulges: They are called Sphs.

Cappellari et al. (2011) and Krajnović et al. (2011) propose a similar parallel sequence classification (without Sphs).

2 S0+Sph Galaxies as Transformed Spiral+Irregular Galaxies

The observational result that motivates the conclusions in this paper is illustrated in Fig. 3: Samples now of hundreds of galaxies show: *The continuous parameter sequence defined by Sphs and by the disks (but not bulges) of S0 galaxies is indistinguishable from the parameter sequence defined by Magellanic irregular (Im) galaxies and by the disks (but not bulges) of spiral galaxies.* This result was first found for dwarf galaxies by Kormendy (1985, 1987). Kormendy and Bender (2012) extend it to the highest-luminosity S and S0 disks.

The most robust conclusion is that Sph galaxies +S0 disks are related to Im galaxies + S galaxy disks. Both together are fundamentally different from classical bulges and ellipticals. This conclusion is also based on additional results that are not included in structural parameter correlations; one is that S+S0 disks are flat, whereas bulges+ellipticals are essentially three-dimensional. Understanding the above similarities and differences requires interpretation, but that interpretation now seems comfortably secure: (1) *Bulges+elliptical galaxies form via major mergers, whereas disks+Im+Sph galaxies form by cold gas accretion.* And more directly from Fig. 3: (2) *Sphs+S0 disks are transformed—i.e., star-formation-quenched—"red and dead" versions of Im galaxies + S galaxy disks.*

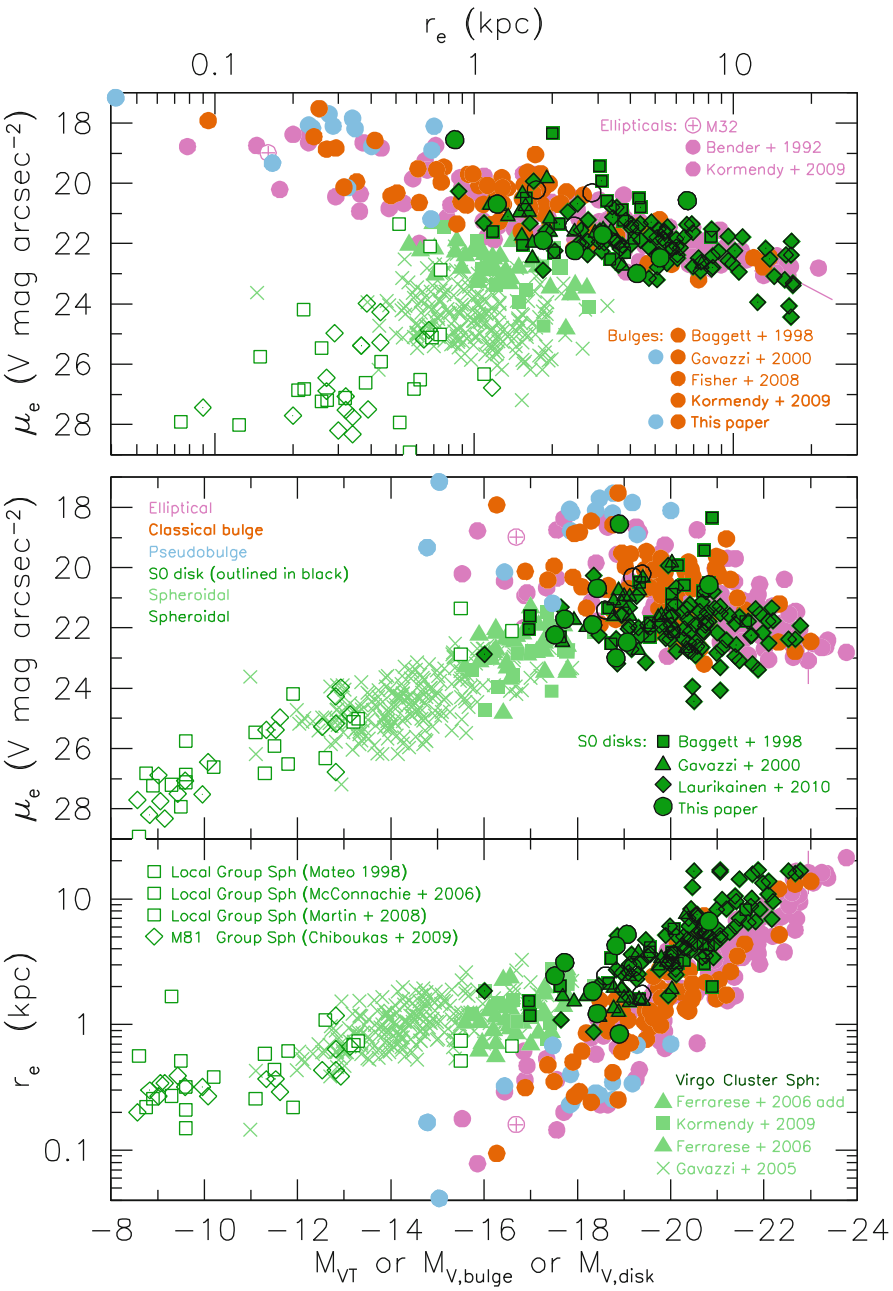

Fig. 2 Parameter correlations for ellipticals, bulges, Sph galaxies, and S0 disks. Bulges and disks of S0s are plotted separately. Plotted parameters are the major-axis effective radius r_e that encloses half of the light of the galaxy component, the effective brightness μ_e at r_e, and the total V-band absolute magnitude of the galaxy or galaxy component. The *middle panel* shows the Freeman (1970)

3 S+Im → S0+Sph Galaxy Transformation Processes

Kormendy and Bender (2012) provide an ARA&A-style review of physical processes that heat galaxy disks and that use up or remove gas and so quench star formation. They suggest that the following processes all are important in transforming Im + S disks into Sph + S0 disks:

1. *Internal process:* Dekel and Silk (1986; see also Larson 1974; Saito 1979) "suggest that *both the dIs and the [dSphs] have lost most of their mass* in winds after the first burst of star formation, and that this process determined their final structural relations. The dIs somehow managed to retain a small fraction of their original gas, while the [dSphs] either have lost all of their gas at the first burst of star formation or passed through a dI stage before they lost the rest of the gas and turned [dSph]." Kormendy and Bender conclude that "*the Sph + Im sequence of decreasing surface brightness with decreasing galaxy luminosity is a sequence of decreasing baryon retention*" (emphasis in both originals).
   Figure 2 shows that surface brightnesses in the Sph +S0 sequence start to decrease at $M_{V,\rm disk} \simeq -18$, just where bulges disappear and where we therefore change galaxy classifications from S0 to Sph (i.e., where plot symbols change from dark to light green). Figure 4 independently finds the S0→Sph transition from rotation curve decompositions. As dark matter $V_{\rm circ}$ decreases, bulges decrease in importance relative to disks until they disappear at $V_{\rm circ} \simeq 104 \pm 16$ km s^{-1}. The Tully–Fisher (1977) relation shows that this corresponds to $M_V \simeq -19$ for spirals (Courteau et al. 2007) and $M_V \simeq -18$ for S0s (Bedregal et al. 2006). It is probably not an accident that baryons start to be lost roughly where bulges stop to contribute to the gravitational potential.
   The transition in Figs. 2 and 3 to (I suggest) a baryon retention sequence in smaller dwarfs corresponds within errors to the transition in edge-on galaxies from giants that do to dwarfs that do not have well-defined dust lanes in their disk midplanes (Dalcanton et al. 2004). They argue that the transition is not caused by changes in gas density. Rather, they argue that it is caused by a transition in giant galaxies to a regime in which disk instability leads to lower gas turbulence, smaller gas scale heights, and enhanced star formation. It is plausible that star formation is less efficient in smaller dwarfs. However: *The observation that dwarf Im and Sph*

←

Fig. 2 (continued) result that disks of giant galaxies tend to have the same central surface brightness μ_0. Here, $\mu_e \simeq 22.0$ V mag arcsec^{-2} corresponds (for an exponential) to $\mu_0 = \mu_e - 1.82 \simeq 20.2$ V mag arcsec$^{-2} \simeq 21$ B mag arcsec^{-2}, brighter than Freeman's value 21.65 B mag arcsec^{-2} because μ_e is not corrected to face-on orientation. From Kormendy and Bender (2012), who conclude: (1) Sphs are continuous with the disks of S0 galaxies. (2) The kink in the $\mu_e - M_V$ relation at $M_V \sim -18$, where bulges disappear in Fig. 4, marks the transition to a baryon retention sequence: tinier dwarf galaxies retain fewer baryons (Fig. 6). Continuity between Sphs and S0 disks is one reason why Fig. 1 shows spheroidal galaxies as bulgeless S0s. Note that Sphs overlap in M_V with but are distinct from bulges and elliptical galaxies. They are not "dwarf ellipticals;" they are related to disks. (Kormendy 1985, 1987)

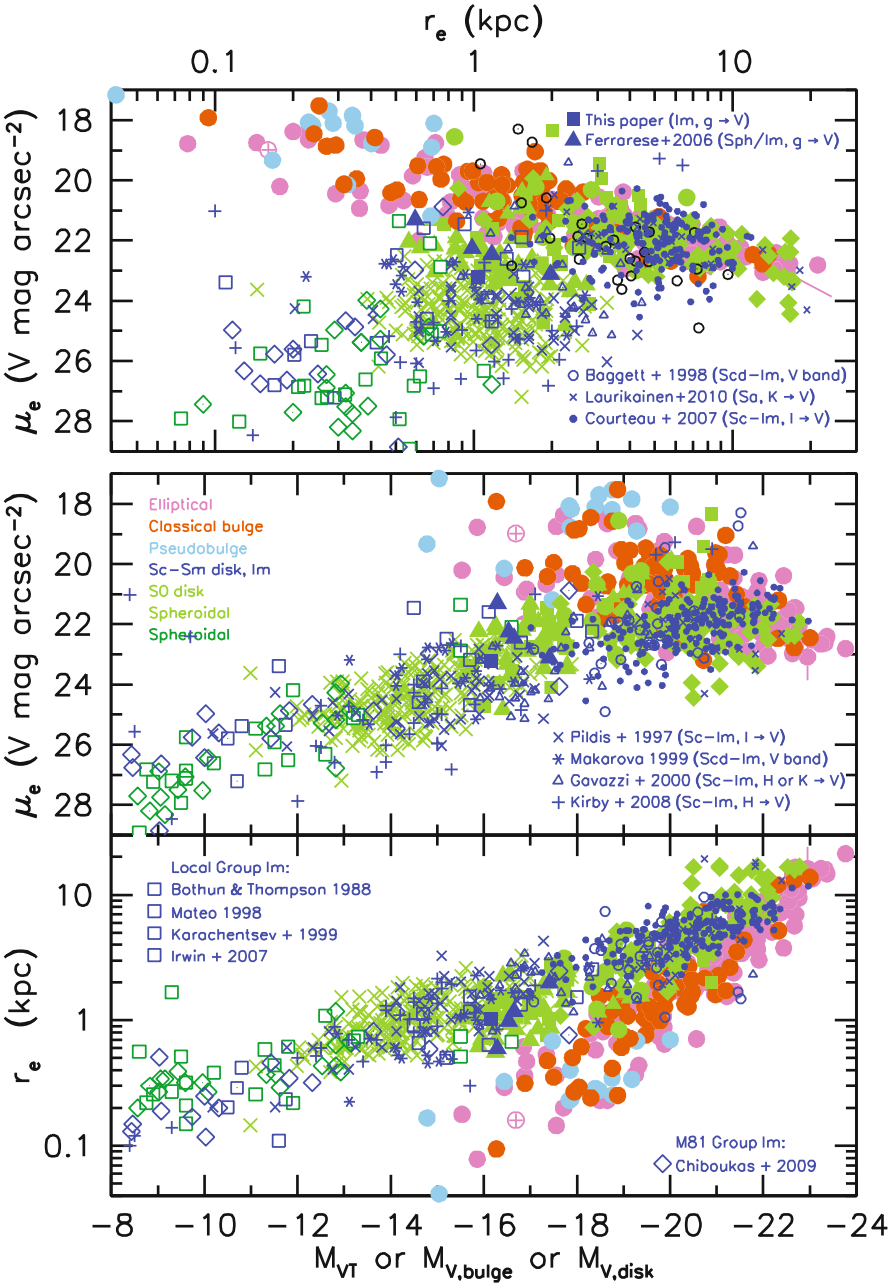

Fig. 3 Figure 2 parameter correlations with disks of Sa—Im galaxies added as *blue points*. When bulge-disk decomposition is necessary, the two components are plotted separately. Disks are not corrected to face-on orientation. The *blue points* represent 407 galaxies from 14 sources listed in the keys. From Kormendy and Bender (2012): They conclude that structural parameter correlations for Sa—Im galaxy "disks" are almost identical to those for S0—Sph "disks". This confirms conclusions in Kormendy (1985, 1987) using a large galaxy sample

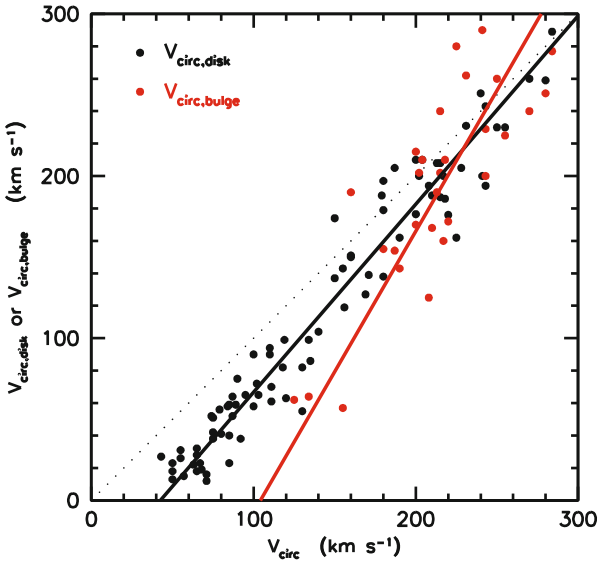

Fig. 4 Maximum rotation velocity of bulge ($V_{\rm circ,bulge}$: *red points*) and disk $V_{\rm circ,disk}$ (*black points*) components given in bulge-disk-halo decompositions of observed rotation curves $V(r)$ whose outer, dark matter rotation velocities are $V_{\rm circ}$ (Kormendy and Freeman 2014; references to the $V(r)$ decomposition papers are given there). The *dotted line* indicates that rotation velocities of the visible and dark matter are equal. Every *red point* has a corresponding *black point*, but many late-type galaxies are bulgeless, and then the plot shows only a *black point*. The *lines* are symmetric least-squares fits; the disk fit is $V_{\rm circ,disk} = (1.16\pm0.03)(V_{\rm circ}-200)+(183\pm3)$ km s^{-1}; $V_{\rm circ,bulge} = (1.73\pm0.29)(V_{\rm circ}-200)+(166\pm9)$ km s^{-1} is the bulge fit. The bulge correlation is steeper than the disk correlation. Bulges disappear at $V_{\rm circ} \simeq 104\pm16$ km s^{-1}

galaxies show the same decrease in surface brightness with decreasing luminosity shows that the dominant effect is not one that depends on the presence of gas. This favors the suggestion that the $\mu_e(M_V)$ relation in Figs. 2 and 3 is a baryon retention sequence at $M_V > -18$. See also Fig. 6. pt It may be surprising that Sph+S0 and Im+S galaxies have similar surface brightnesses, because the latter are star-forming and so presumably have smaller mass-to-light ratios. However, (1) at high luminosities, internal absorption partly compensates for smaller mass-to-light ratios, and (2) at low luminosities, star formation in Im galaxies is gentle. Nevertheless, it is fair to emphasize that more work is needed to understand the detailed engineering that results in Sph+S0 and Im+S correlations that look so nearly identical.

2. *Environmental processes I:* Ram-pressure stripping—long underestimated in importance—is now An Idea Whose Time Has Come. Gunn and Gott (1972) suggested, based on the detection of X-ray-emitting, hot gas in the Coma cluster (Meekins et al. 1971; Gursky et al. 1971) that "*a typical galaxy moving in it will be stripped of its interstellar material.* We expect *no normal spirals* in the

central regions of clusters like Coma. The lack of such systems is, of course, observed" (emphasis in the original). Calculations persuaded some people to neglect ram-pressure stripping even while many observations provided indirect evidence for its importance. Spirals near the center of the Virgo cluster are deficient in H I gas (Cayette et al. 1990, 1994; Chung et al. 2009). Also, Faber and Lin (1983); Lin and Faber (1983); Kormendy (1987), van den Bergh (1994b), and Kormendy et al. (2009, hereafter KFCB) suggested that Sph galaxies are ram-pressure-stripped dS+Im galaxies, based in part on observations (Einasto et al. 1974; van den Bergh 1994a, b; Mateo 1998) that—with a few (understandable) exceptions—close dwarf companions of Local Group giant galaxies are almost all spheroidals, that distant companions are irregulars, and that galaxies with intermediate (Sph/Im) morphologies live at intermediate distances. Ever since van den Bergh (1976), these ideas provided the interpretation of a parallel sequence classification (Fig. 1) that was constructed operationally to encode the full range of S0+Sph bulge-to-total luminosity ratios B/T from almost 1 to exactly 0.

Spectacular observations of ram-pressure stripping in action now clearly demonstrate the importance of this process (see Sun et al. 2010; Kormendy and Bender 2012 for reviews). Kenney et al. (2004, 2008), Oosterloo and van Gorkom 2005, and Chung et al. (2007, 2009) find that many spiral galaxies near the center of the Virgo cluster show long Hα or H I tails interpreted to be cold gas that is being stripped by the ambient X-ray-emitting gas (Böhringer et al. 1994). Kormendy and Bender emphasize that these galaxies and the H I - depleted galaxies are substantially brighter than almost all Sphs: "If even the deep gravitational potential wells of still-spiral galaxies suffer HI stripping, then the shallow potential wells of dS + Im galaxies are more likely to be stripped." The most impressive recent example of ram-pressure stripping is the multi-wavelength (CO gas+H II+X-ray) tail of the galaxy ESO 137-001 in Abell 3627 (Sun et al. 2006, 2007, 2010; Woudt et al. 2008; Sivanandam et al. 2010; Pavel et al. 2014; Fig. 5).

For a recent treatment of ram-pressure stripping in the Galactic halo, see Gatto et al. (2013).

3. *Environmental processes II:* Dynamical harassment results from many, high-speed encounters with other galaxies in a cluster and with the overall cluster potential. Simulations show that (1) it promotes gas flow toward galaxy centers, (2) it heats disks, especially vertically, and (3) it strips off the outer parts of galaxies (Moore et al. 1996, 1998, 1999; Lake et al. 1998). Even in poor environments like the Local Group, tidal stirring of dwarfs on elliptical orbits around the Galaxy or M 31 should have similar effects (Mayer et al. 2001a, b, 2006). One success of this picture is that inflowing gas can feed star formation and help to explain why spheroidals, in which star formation stopped long ago, do not have lower surface brightnesses than current versions of S+Im progenitors (Fig. 3). This process is clean and inescapable.

   Kormendy and Bender (2012) conclude that *dynamical harassment is much more important in the Virgo cluster than we thought.* Edge-on S0s with close companions show warps in their outer disks that will phase-wrap around the center into structures that resemble Sphs in their shapes and density profiles (NGC 4762 and

Fig. 5 Composite Hubble Space Telescope (HST) and Chandra X-Ray Observatory image of galaxy ESO 137-001 in Abell 3627. The HST image is a I-, g-, and U-band color composite. Added in *blue* is the X-ray image; it extends the *lighter blue optical streaks* of ongoing star formation toward the *lower-right*. This material is interpreted to be ram-pressure stripped. The image source is `http://www.spacetelescope.org/images/heic1404b/` and `http://apod.nasa.gov/apod/ap140328.html`. At a distance of $\sim$64 Mpc, the absolute magnitude of ESO 137-001 is $M_V \sim -20.8$. Conveniently, this field of view also shows a normal-looking Sph galaxy at *upper-right*; it is $\sim$3 mag fainter than ESO 137-001. Again, if we see a giant galaxy caught in the process of undergoing ram-pressure stripping, it is not surprising that a much smaller Sph galaxy is thoroughly "red and dead"

NGC 4452; their Figs. 4 and 8, respectively). They identify S0/Sph transition objects: (1) NGC 4638 is an edge-on S0 with a Gaussian (i.e., radially truncated) inner disk embedded in a boxy, E3 halo that has the properties of a large Sph (their Figs. 13, 14, 15, 16). (2) VCC 2048 is an E6 Sph with an embedded edge-on, S0 disk (their Fig. 10, 11, 12). Indeed, many Virgo S0s have Gaussian disk profiles. Most telling is the observation that several Virgo cluster S0s have bars embedded in steep-, often Gaussian-profile lenses with no sign of a disk outside the bar (NGC 4340, NGC 4442, and NGC 4483, their § A.12). We do not know how to form a bar that fills the whole disk, because an outer disk is generally required as an angular momentum sink to allow a bar to grow. Kormendy and Bender suggest that the outer disks in these galaxies have been heated or stripped off. Finally, they interpret the "new class of dwarfs that are of huge size and very low surface brightness" (Sandage and Binggeli 1984) as "spheroidals that have been harassed almost to death."

4. *Environmental processes III:* Starvation of late growth by cold-gas infall (Larson et al. 1980) seems inevitable in environments like the center of the Virgo cluster where the ambient gas is very hot. Even in environments like the Local Group, Sph galaxies that orbit around the Galaxy and M 31 at velocities $V \sim 200$ km s^{-1} are unlikely to encounter cold gas slowly enough to be able to accrete it. And much of the gas in the Local Group may in any case be in a warm-hot intergalactic medium (WHIM: Davé et al. 2001).

So Kormendy and Bender (2012) "suggest that the relevant question is not 'Which of these mechanisms is correct?' It is 'How can you stop any of them from happening?'

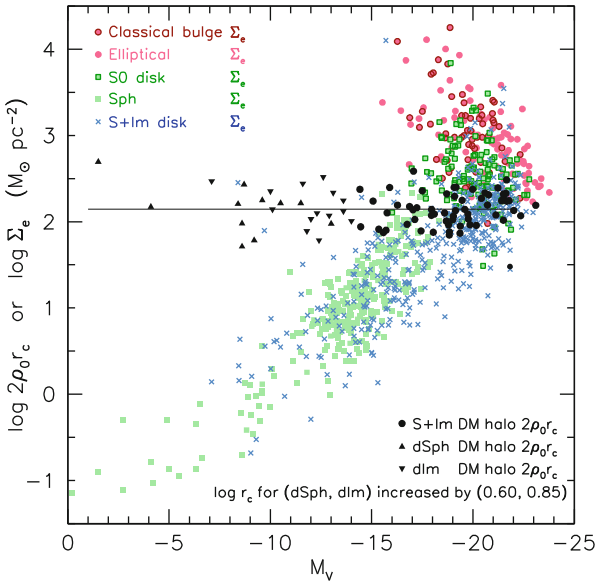

Fig. 6 Comparison of dark matter (DM) halo parameters from Kormendy and Freeman (2014) with visible matter parameters from Kormendy and Bender (2012). DM parameters are from maximum-disk rotation curve decompositions (*black circles*) or from cored isothermal halo models applied to the dispersion profiles of dSph galaxies (*black triangles*) or to the $V \propto r$ rotation curves and velocity dispersions of H I in dIm galaxies (*upside-down black triangles*) (see Kormendy and Freeman 2014, the source of this figure). Central projected densities are plotted for DM halos; effective surface densities $\Sigma_e = \Sigma(r_e)$ are shown for visible components. Here r_e is the radius that contains half of the light of the component. Surface brightnesses are converted to stellar surface densities using mass-to-light ratios $M/L_V = 8$ for ellipticals, 5 for classical bulges and S0 disks, and 2 for spiral galaxy disks, Im galaxies, and Sph galaxies

It seems likely that all of the above processes matter." Engineering details probably depend on environment.

4 Visible Matter and Dark Matter Parameter Correlations

Figure 6 illustrates our conclusion that, at $M_V \gtrsim -18$, the dwarf spiral, Im, and Sph galaxies in earlier figures form a sequence of decreasing baryon retention in smaller galaxies (KFCB; Kormendy and Bender 2012; Kormendy and Freeman 2014). In contrast, bulges and ellipticals together form a sequence of increasing dissipation during the formation of smaller galaxies. For $M_V < -18$ galaxies of all kinds, effective densities in stars are similar to DM densities at and interior to the same radius. For Sc–Im systems, this is by construction a consequence (1) of using maximum-disk decompositions and (2) of the "rotation curve conspiracy" (van Albada and Sancisi 1986), i. e., the observation that rotation curves of giant galaxies are roughly flat and

featureless, so the parts of galaxies that are controlled by dark matter are not easily distinguished from the parts that are controlled by visible matter or even the parts that are controlled by different components in the visible matter (Fig. 4). Caveat: for bulges and ellipticals, high baryon densities at $r \ll r_e$ may pull on DM halos enough to increase their central densities over the values for Sc—Im galaxies that are shown in Fig. 6. But bulges and ellipticals have *central* projected densities that are more than 3 dex higher than the effective densities shown in Fig. 6. So the central parts of early-type galaxies are *very* baryon-dominated. Even the central densities of disks are 0.7 dex (for an exponential) higher than the effective densities shown in Fig. 6. So even pure disks are moderately dominated by visible matter near their centers. Both results are qualitatively as expected: Visible matter needs to dissipate, sink inside the DM, and become self-gravitating enough to form stars and visible galaxies. And a great deal of dissipation happens in the wet mergers that make normal ellipticals (KFCB): their densities rise above DM densities by larger amounts at fainter M_V.

The important point here is this: At $M_V > -18$, tinier dwarfs are more DM dominated, until by $M_V \gtrsim -10$, they are essentially dark galaxies with just enough of a frosting of stars so that they can be detected. I emphasize two important points: (1) The differences between dIm and dSph galaxies in all parameter correlations shown in this paper are small. Whether or not a galaxy retains cold gas and can still form stars in today's Universe is a second-order effect. This argues—as Dekel and Silk (1986) already emphasizedandthat the primary effect that engineers the parameter correlations is supernova-driven baryon blowout or another process (such as a failure to capture baryons after cosmic reionization) that has the same effect. (2) Kormendy and Freeman (2014) suggest that there exists a large population of tiny halos that are essentially completely dark and that the discoverable galaxies at $M_V \gtrsim -13$ represent a smaller and smaller fraction of tinier DM halos. This has been suggested as the solution to the problem that the fluctuation spectrum of cold dark matter predicts more dwarfs than are observed in environments like the Local Group (e. g., Moore et al. 1999; Klypin et al. 1999).

5 Conclusions

Kormendy and Bender (2012) propose a parallel sequence galaxy classification (Fig. 1) in which Sph galaxies appear as bulgeless S0s juxtaposed with Im galaxies. In reality, their progenitors can include late-type spirals, but the Fig. 1 tuning fork is designed for simplicity. S0+Sph galaxies are suggested to be star-formation-quenched descendants of S+Im galaxies. It seems essentially guaranteed that all transformation processes discussed in §3 are important. Moreover, although there is good agreement between structural parameter correlations for (1) present-day Sphs+S0 disks and (2) present-day Im+S disks, it is of course not guaranteed that the progenitors of Sph and S0 galaxies were exactly like present-day late-type galaxies. The latter are, after all, survivors. The reasons can partly involve stochastic evolution, but they may also involve differences in internal structure and/or environment.

These ideas are slowly gaining acceptance. An observationally biased but still incomplete list of papers includes Grebel et al. (2003), van Zee et al. (2004), Mayer et al. (2006), Boselli et al. (2008a, b), Tolstoy et al. (2009), Ryś et al. (2013, 2014), and Janz et al. (2013). KFCB and Kormendy and Bender (2012) address remaining controversies.

From the perspective of this conference, the important—and robust!—conclusion is this:

Dwarf spiral, irregular, and spheroidal galaxies are not new and special kinds of galaxies, as has often been suggested. Rather: *There is a complete continuity in structural parameter scaling relations* (Figs. 2, 3, 4 and 6), *kinematics and dynamics, star formation properties, and metallicity distributions between the disks of giant galaxies and all three subsets of dwarf galaxies. Fainter than* $M_V \sim -18$*, the properties of galaxies change as their gravitational potential wells get more shallow; this is qualitatively consistent with the increased importance at lower masses of internal and environmental transformation processes. Also, many aspects of galaxy evolution get more stochastic in smaller galaxies. For example, star formation gets more bursty. Many quantitative details remain to be worked out. But this is engineering. A big-picture view of the evolution of dwarf galaxies seems comfortably in place:*

All forms of violence—including supernova energy feedback, dynamical harassment, and external ram-pressure stripping—get more important for smaller galaxies. The main result is that smaller galaxies lose more of their baryons or never acquire them. Smaller dwarfs are more dominated by dark matter. Whether or not they retain enough cold gas to feed some star formation is very much a second-order effect. Baryon loss at low halo masses may be so severe that we discover only a small fraction of the smallest, essentially dark halos. This can reconcile the observed scarcity of dwarf galaxies in field environments with our expectations of large numbers of dwarfs that are predicted by the cold dark matter fluctuation spectrum.

Acknowledgments It is a pleasure to thank Ralf Bender and Ken Freeman for their hospitality and support during my visits and for always enjoyable collaborations. My attendance at the Seychelles conference was supported by the Max-Planck-Institute for Extraterrestrial Physics and by the Observatory of the Ludwig-Maximilians-University, Munich. This paper was supported by the Curtis T. Vaughan, Jr. Centennial Chair in Astronomy at the University of Texas.

References

Bedregal, A. G., Aragón-Salamanca, A., & Merrifield, M. R. 2006, MNRAS, 373, 1125
Böhringer, H., et al. 1994, Nature, 368, 828
Boselli, A., Boissier, S., Cortese, L., & Gavazzi, G. 2008a, ApJ, 674, 742
Boselli, A., Boissier, S., Cortese, L., & Gavazzi, G. 2008b, A&A, 489, 1015
Cappellari, M., et al. 2011, MNRAS, 416, 1680
Cayette, V., van Gorkom, J. H., Balkowski, C., & Kotanyi, C. 1990, AJ, 100, 604
Cayette, V., Kotanyi, C., Balkowski, C., & van Gorkom, J. H. 1994, AJ, 107, 1003
Chung, A., van Gorkom, J. H., Kenney, J. D. P., & Vollmer, B. 2007, ApJ, 659, L115
Chung, A., van Gorkom, J. H., Kenney, J. D. P., Crowl, H., & Vollmer, B. 2009, AJ, 138, 1741
Courteau, S., et al. 2007, ApJ, 671, 203
Dalcanton, J. J., Yoachim, P., & Bernstein, R. A. 2004, ApJ, 608, 189
Davé, R., et al. 2001, ApJ, 552, 473
Dekel, A., & Silk, J. 1986, ApJ, 303, 39
Einasto, J., Saar, E., Kaasik, A., & Chernin, A. D. 1974, Nature, 252, 111
Faber, S. M., & Lin, D. N. C. 1983, ApJ, 266, L17
Freeman, K. C. 1970, ApJ, 160, 811
Gatto, A., et al. 2013, MNRAS, 433, 2749
Grebel, E. K., Gallagher, J. S., & Harbeck, D. 2003, AJ, 125, 1926
Gunn, J. E., & Gott, J. R. 1972, ApJ, 176, 1
Gursky, H., et al. 1971, ApJ, 167, L81
Janz, J., et al. 2013, arXiv:1308.6496
Kenney, J. D. P., van Gorkom, J. H., & Vollmer, B. 2004, AJ, 127, 3361
Kenney, J. D. P., Tal, T., Crowl, H. H., Feldmeier, J., & Jacoby, G. H. 2008, ApJ, 687, L69
Klypin, A., Kravtsov, A. V., Valenzuela, O., & Prada, F. 1999, ApJ, 522, 82
Kormendy, J. 1985, ApJ, 295, 73
Kormendy, J. 1987, in Nearly Normal Galaxies: From the Planck Time to the Present, ed. S. M. Faber (New York: Springer), 163

Kormendy, J., & Bender, R. 2012, ApJS, 198, 2 (They list references in the keys of Figures 2 and 3.)
Kormendy, J., & Freeman, K. C. 2014, ApJ, in preparation
Kormendy, J., Fisher, D. B., Cornell, M. E., & Bender, R. 2009, ApJS, 182, 216 (KFCB)
Krajnović, D., et al. 2011, MNRAS, 414, 2923
Lake, G., Katz, N., & Moore, B. 1998, ApJ, 495, 152
Larson, R. B. 1974, MNRAS, 169, 229
Larson, R. B., Tinsley, B. M., & Caldwell, C. N. 1980, ApJ, 237, 692
Laurikainen E., Salo H., Buta R., Knapen J. H., & Comerón S., 2010, MNRAS, 405, 1089
Lin, D. N. C., & Faber, S. M. 1983, ApJ, 266, L21
Mateo, M. 1998, ARA&A, 36, 435
Mayer, L., et al. 2001a, ApJ, 547, L123
Mayer, L., et al. 2001b, ApJ, 559, 754
Mayer, L., Mastropietro, C., Wadsley, J., Stadel, J., & Moore, B. 2006, MNRAS, 369, 1021
Meekins, J. F., Fritz, G., Chubb, T. A., Friedman, H., & Henry, R. C. 1971, Nature, 231, 107
Moore, B., Katz, N., Lake, G., Dressler, A., & Oemler, A. 1996, Nature, 379, 613
Moore, B., Lake, G., & Katz, N. 1998, ApJ, 495, 139
Moore, B., et al. 1999, ApJ, 524, L19
Oosterloo, T., & van Gorkom, J. 2005, A&A, 437, L19
Pavel, J., Combes, F., Cortese, L., Sun, M., & Kenney, J. D. P. 2014, arXiv:1403.2328
Ryś, A., Falcón-Barroso, J., & van de Ven, G. 2013, MNRAS, 428, 2980
Ryś, A., van de Ven, G., & Falcón-Barroso, J. 2014, MNRAS, 439, 284
Saito, M. 1979, PASJ, 31, 193
Sandage, A., & Binggeli, B. 1984, AJ, 89, 919
Sivanandam, S., Rieke, M. J., & Rieke, G. H. 2010, ApJ, 717, 147
Sun, M., et al. 2006, ApJ, 637, L81
Sun, M., Donahue, M., & Voit, G. M. 2007, ApJ, 671, 190
Sun, M., et al. 2010, ApJ, 708, 946
Tolstoy, E., Hill, V., & Tosi, M. 2009, ARA&A, 47, 371
Tully, R. B., & Fisher, J. R. 1977, A&A, 54, 661
van Albada, T. S. & Sancisi, R. 1986, Phil. Trans. R. Soc. London A, 320, 447
van den Bergh, S. 1976, ApJ, 206, 883
van den Bergh, S. 1994a, AJ, 107, 1328
van den Bergh, S. 1994b, ApJ, 428, 617
van Zee, L., Skillman, E. D., & Haynes, M. P. 2004, AJ, 128, 121
Woudt, P. A., Kraan-Korteweg, R. C., Lucey, J., Fairall, A. P., & Moore, S. A. W. 2008, MNRAS, 383, 445

Lessons from the Local Group (and Beyond) on Dark Matter

Pavel Kroupa

Abstract The existence of exotic dark matter particles outside the standard model of particle physics constitutes a central hypothesis of the current standard model of cosmology (SMoC). Using a wide range of observational data I outline why this hypothesis cannot be correct for the real Universe. Assuming the SMoC to hold, (i) the two types of dwarf galaxies, the primordial dwarfs with dark matter and the tidal dwarf galaxies without dark matter, ought to present clear observational differences. But in fact there is no observational evidence for two separate families of dwarfs, neither in terms of their location relative to the baryonic Tully–Fisher relation nor in terms of their radius–mass relation. This result is illuminated by the arrangements of the satellite galaxies around host galaxies for which we have data: the arrangements in rotating disk-of-satellites, in particular around the Milky Way and Andromeda, has been found to be only consistent with most if not all dwarf satellite galaxies being tidal dwarf galaxies. The predicted large numbers of independently or in-group accreted, dark-matter-dominated primordial dwarfs are most inconspicuously absent around the Milky Way in particular. The highly symmetric structure of the entire Local Group too is inconsistent with its galaxies stemming from a stochastic merger-driven hierarchical buildup over cosmic time. (ii) Dynamical friction on the expansive and massive dark matter halos is not evident in the data: the satellite galaxies of the Milky Way with proper motion measurements have no infall solutions as they would merge with the MW if they have dark matter halos, and galaxy groups such as the M81 group are found to not merge on the short time scales implied if each galaxy has a dark matter halo. *Taking the various lines of evidence together, the hypothesis that dynamically relevant exotic dark matter exists needs to be firmly rejected.*

P. Kroupa (✉)
Helmholtz-Institut für Kern und Strahlenphysik, University of Bonn,
Nussallee 14–16, 53115 Bonn, Germany
e-mail: pavel@astro.uni-bonn.de

K. Freeman et al. (eds.), *Lessons from the Local Group,*
DOI 10.1007/978-3-319-10614-4_28

1 Introduction

By applying Einstein's general relativistic field equation, i.e. Newtonian dynamics, to galaxies and to the Universe as a whole, disagreements with observational data had been found that require the additional assumptions of inflation, exotic dark matter particles and dark energy. These may constitute major new physics components, but none have supporting experimental evidence independently of the observational astronomical data that are used to make the three postulates. For example, dark matter particles are not contained in the standard model of particle physics and have not been found in any of the experiments designed to search for them. If they do not exist, then a major pillar of the modern standard model of cosmology (SMoC) collapses, such that the SMoC would be ruled out as a representation of the Universe and of the structures that develop within it over cosmic time. "*Does dark matter exist*?" is thus one of the most important questions of modern science. Direct searches for dark matter particles cannot falsify this question by design, since a non-detection may merely imply that the interaction cross section with baryons (e.g. via the weak force) is unmeasurably small. Direct detection experiments thus speculate on receiving the Nobel Prize, but they are not a well designed experimental procedure in which a prediction can be falsified.

Here I argue that the astronomical observational data *strongly*, if not unequivocally, show *dark matter to not be present*. I use three independent tests and many consistency checks. While this goes against the perceived majority opinion with corresponding sociological and possible career implications, the community does have to face a reality without dark matter, as bleak and dark as it may appear.

Weighty evidence for this conclusion comes from the best data at hand, namely what we learn from observing the galaxies and their star-formation processes in the Local Group. But extragalactic evidence has also been crucial in refining the conclusions.

With this text I provide a synopsis of the arguments presented in more depth in Kroupa (2012) and Kroupa (2014). Figure 1 outlines the structure of the argument.[1]

There are three main reasons why cold or warm dark matter (DM) particles, collectively referred to here as exotic DM particles, cannot be dynamically relevant on the scales of galaxies. These are discussed in Sect. 2. Sections 3 and 4 contain consistency checks, and Sect. 5 develops additional arguments to test the "no-DM" deduction based on galaxy populations over cosmic time. The conclusions are provided in Sect. 6

[1] Noteworthy is that the evidence provided in the year 2012 which are claimed to falsify the SMoC (Kroupa 2012) have, to this date, not been countered by the community but have instead been strengthened by recent progress (Ibata et al. 2014; Pawlowski et al. 2014; Kroupa 2014).

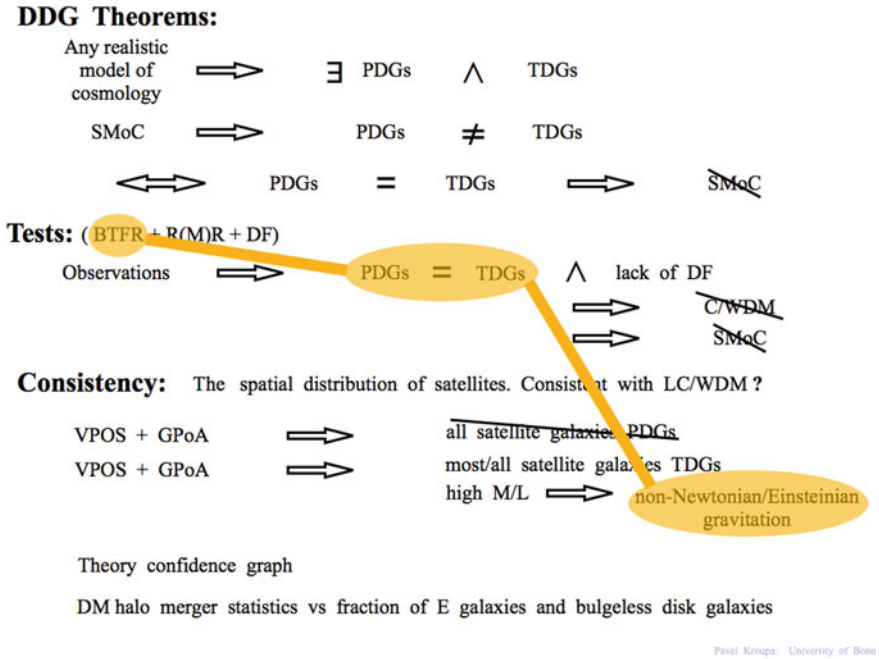

Fig. 1 Structure of the falsification of dynamically relevant cold or warm dark matter. The dual dwarf galaxy (*DDG*) theorems and the tests using the baryonic Tully Fisher relation (*BTFR*), the radius-mass relation (*R(M)R*) of pressure supported dwarf galaxies and using dynamical friction (*DF*) are discussed in Sect. 2. The consistency checks based on the vast polar structure (*VPOS*) of the Milky Way and on the great plane of Andromeda (*GPoA*) are in Sect. 3 (see also Fig. 2). A high degree of self-consistency of the argument emerges by the *VPOS* and *GPoA*, which are mutually correlated rotating structures, ruling out the satellite galaxies being primordial dwarf galaxies (*PDGs*) with dark matter halos. Thus their observationally deduced high dynamical M/L ratios needs to be accounted for by effective non-Newtonian gravitation, which is the same conclusion reached using the *BTFR* test. This consistency is emphasized by the connected orange regions. If this conclusion is true then the *SMoC* cannot be a good description of the observed Universe. The theory confidence graph for the *SMoC* is discussed in Sect. 4 and indeed confirms the *SMoC* to not be an acceptable model; neither CDM nor WDM thus exists. This is further ascertained by the evidence for a lack of mergers in the observed galaxy population as covered in Sect. 5, whereby DM halo merger statistics are discussed in Kroupa (2014) and Wu and Kroupa (2014). Other acronyms: *TDGs* tidal dwarf galaxies (Sect. 2), *C/WDM* cold or warm dark matter = exotic DM particles, i.e. particles outside the standard model of particle physics

2 Why Can There Be No Cold or Warm Dark Matter?

Assume the SMoC applies, and view the Universe through Newtonian eyes. By assuming the SMoC applies, we accept the cosmological merger tree to be a description of how the DM halos and the galaxies within them grow through many mergers due to dynamical friction on the DM halos. The first structures begin to form before recombination and many of them become primordial dwarf galaxies (PDGs). In the

SMoC these are contained in DM halos. Ignoring the well-known problem of downsizing, namely that dwarf galaxies are observed to be younger but ought to be older than more massive galaxies (Recchi et al. 2009; Vogelsberger et al. 2014a, b), the evolution of the galaxy population can be followed (Lu et al. 2012; Vogelsberger et al. 2014b). As the larger DM halos build up through coalescence, the galaxies within them merge. The gaseous and stellar matter that is expelled and which carries away the angular momentum and energy from the merger in the form of tidal arms often fragments and forms star clusters and new dwarf galaxies. These dwarf galaxies are called tidal dwarf galaxies (TDGs), and they may contain captured previously existing stars and they may form from pre-enriched gas, but this depends on the evolutionary stage of the pre-merger galaxies.

Differently to PDGs, TDGs do not contain significant amounts of DM, because TDGs have such small masses ($\lesssim 10^9\,M_\odot$) that DM particles from the much more massive DM halos of the pre-merger galaxies are rarely captured by them. Thus, in any realistic cosmological theory in which galaxies can interact, TDGs and PDGs must exist. This is the "*dual dwarf galaxy theorem*" (Kroupa 2012, 2014). In the SMoC, TDGs and PDGs differ in their DM content, and thus can be distinguished observationally.

Also, in the SMoC encounters between galaxies lead to them merging, and therefore to the emergence of the cosmological merger tree which drives galaxy evolution. Without dark matter halos, the merger rate decreases most significantly (Toomre 1977; Kroupa 2014), and there would be no cosmological merger tree which drives galaxy evolution. Our understanding of galaxy evolution is thus intimately connected to the existence of DM.

There are three tests which, independently of each other, rule out DM as a relevant physical aspect of galaxies, as long as the observational data remain undisputed. Two tests are based on the dual dwarf galaxy theorem, and one is based on the well-understood process of dynamical friction of the motions of galaxies through the DM halos of other galaxies.

1. Tidal dwarf galaxies cannot contain much DM and yet the three that have observed rotation curves show the same DM behavior as PDGs. Thus, the three TDGs lie on the observed baryonic Tully–Fisher relation (BTFR) but they should be displaced by a factor of 3–10 towards smaller velocities than the BTFR. Chance superposition of a TDG onto the DM-defined BTFR may occur if the velocity field of the gas in or around the TDG does not constitute a virialised (Keplerian) structure, but in such a case the TDG woud be more likely placed elsewhere in the BTF diagram. The rotational velocities of PDGs are assumed (but not understood) to be defined by the DM halos that are ten to hundred times more massive than the baryonic mass of the PDG (Lu et al. 2012; Vogelsberger et al. 2014b). That the baryonic masses do not correlate exactly one-to-one with the DM halos masses (Behroozi et al. 2013; Ferrero et al. 2012) comes from the stochastic and haphazard process of the mergers which build-up the DM halo, and the different modes of accretion (cold vs hot) in DM halos of different masses.

Since TDGs and PDGs lie on the same BTFR, which is supposed to be defined by primordial galaxies that are DM dominated, it follows that DM is ruled out to be the origin for the BTFR. This deduction is sound, as long as the data remain unchallenged, because TDGs cannot contain much DM, even if it exists, such that they cannot lie on the BTFR. But their rotation velocities can be obtained in a non-Newtonian gravitational framework (e.g. in Milgromian dynamics (Gentile et al. 2007)). PDGs can have DM, but their rotation curves can also be explained by non-Newtonian gravity. *Thus, non-Newtonian gravitation is the only unifying concept concerning TDGs and PDGs.*

2. Tidal dwarf galaxies must have different radii at the same mass than PDGs because they form without a DM halo, compared to pressure-supported PDGs which form within a substantial DM halo (Behroozi et al. 2013; Ferrero et al. 2012). But TDGs are found to have, at a given mass, the same radii as PDGs (Dabringhausen and Kroupa 2013). Since TDGs cannot contain DM this implies that the morphological appearance needs to be driven by a physical process common to both, the TDGs and PDGs. *Thus, only non-Newtonian gravitation can unify both types of dwarf galaxy.*
3. Dynamical friction is a necessary and required property of DM halos (Toomre 1977; Barnes 1998). Two similar galaxies that interact with relative velocities smaller than about the virial velocity dispersion of their DM halos and within a distance twice the virial radius of their DM halos will merge within an orbital time scale. A primordial satellite galaxy will merge with the main galaxy within a timescale given by Chandrasekhar's friction time scale.
   The dynamical simulations of the M81 group of galaxies has shown them to merge within a group-crossing time such that the matter bridges that are observed between the galaxies cannot be reproduced (Thomson et al. 1999; Yun 1999). Reproduction by models of the observed bridges and galaxy locations and line of sight velocities is only approximately successful in models without DM. Since galaxies do have flat rotation cuves, it follows that these need to be explained without dark matter, i.e. *with non-Newtonian dynamics*.
   And, the satellite galaxies of the Galaxy with proper motion measurements cannot be traced back to pre-infall dwarf galaxies if they have DM halos (Angus et al. 2011).

3 Consistency of the Deduction: The Arrangement of Galaxies in the Local Group and Elsewhere

If the deduction reached in Sect. 2 that DM does not exist is correct such that the cosmological merger tree would need to be discarded, then what is the origin of the satellite galaxies that are observed around the Milky Way (MW), Andromeda and other nearby galaxies, and where do the dwarf galaxies, e.g. in the Local Group, stem from? The lack of evidence for the cosmological merger tree being active is also discussed in Sect. 5.

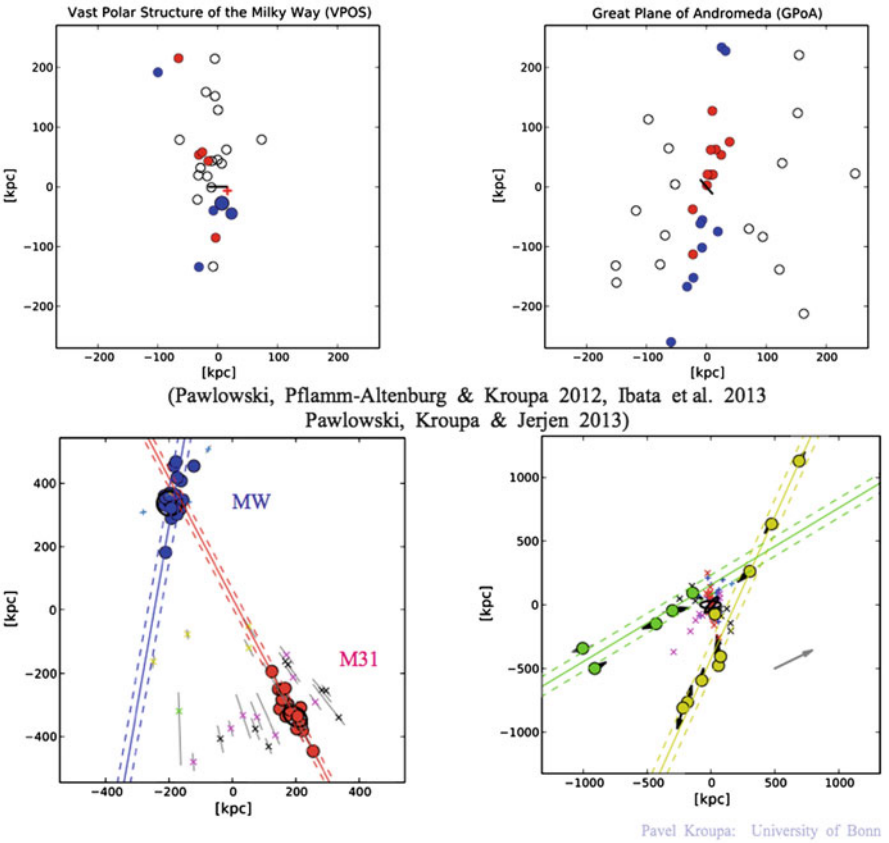

Fig. 2 The distribution of all galaxies known today in the Local Group which is defined by the zero velocity *sphere*. Galaxies outside this sphere of radius about 1.5 Mpc recede from the Local Group, while within the sphere the galaxies fall towards us. *The upper left* and *right panels* depict all satellite galaxies within about 250 kpc around the MW and Andromeda, respectively. The galactic disks of the MW and of Andromeda are seen nearly edge-on, the north Galactic pole direction being upwards, and both galaxies are viewed from the same direction from infinity. *MW* satellites with known proper motions and radial velocities (Pawlowski et al. 2012a; Pawlowski and Kroupa 2013), and Andromeda satellites that are in the *GPoA* (Ibata et al. 2013) are shown as *colored circles*. *Red* satellites are moving away from the observer, *blue* ones are approaching the observer. Thus the *VPOS* and *GPoA* are rotating in the same sense and the *GPoA* is seen edge-on from the *MW* as is evident in the *lower-left panel*. The *VPOS* and *GPoA* are statistically highly significant mutually correlated rotating structures inconsistent with being derived from accreted DM sub-halos which host PDGs (Ibata et al. 2014; Pawlowski et al. 2014). The *VPOS* and *GPoA* are inclined relative to each other by only about 38° whereby the *GPoA* is oriented edge-on to the *MW*. This is seen in the *lower left panel*, which is a view from near the north Galactic pole downwards such that the *VPOS* and *GPoA* are seen approximately edge-on. *Filled circles* are dwarf galaxies in the disks of satellites of both major galaxies, while the *crosses* near *M31* are satellite galaxies which are not in the *GPoA*. Viewing the Local Group along the line joining the *MW* and Andromeda it emerges that all non-satellite galaxies in the Local Group are arranged in two highly symmetrical equally thin planes (thickness about 50 kpc; diameters about 3 Mpc) equidistant from both, the *MW* and Andromeda, seen here edge on in the *lower right panel*. The *crosses* are as in the *lower left panel*; note the additional disk of satellite which lies in the equatorial plane of Andromeda and is here seen

3.1 Clues on Their Origin: Spatially Anisotropic Satellite Galaxy Populations

The spacial arrangement of satellite galaxies around the MW gives a strong clue to their possible origin. *All* known stellar systems beyond about 10 kpc distance from the Galactic centre (classical dSph satellite galaxies found on photographic plates, ultra faint dwarf galaxies found with robots scanning the sky, globular clusters) and half of all gas and stellar streams are arranged independently of each other in a vast polar structure (VPOS, Kroupa et al. 2005; Pawlowski et al. 2012a; Pawlowski et al. 2014; Pawlowski and Kroupa 2014). The proper motion measurements for the 11 brightest satellite galaxies show the VPOS to be rotating in one sense, the spin of the VPOS points into a direction which is close to the MW disk plane (lets call it direction **S**). Viewing along the direction Galactic-centre—Sun, the VPOS lies approximately face-on. The VPOS can be described as a polar disk with diameter of about 500 kpc and thickness of about 50 kpc.

Half of all satellite galaxies of Andromeda are in a vast thin disk of satellites (VTDS), i.e. in the great plane of Andromeda (GPoA, Ibata et al. 2013, 2014). This GPoA is rotating, and its spin is directed only about 38° away from **S**. That is, the GPoA and the VPOS are impressively aligned, with the GPoA also being nearly perpendicular to the MW disk as is the VPOS (Fig. 16 in Pawlowski et al. (2013)). Figure 2 shows the VPOS, the Andromeda satellite galaxy system and their relative orientation and location, and *the most remarkable and hitherto not noticed nor ever expected symmetric structure of the entire Local Group.*

3.2 Other Dwarf Satellite Galaxy Populations

Beyond the Local Group, Chiboucas et al. (2013) discuss the dwarf galaxy population in the M81 group of galaxies, which is a sparse group comparable to the Local Group, and they find evidence that the faint satellite galaxies are distributed anisotropically. They write "In review, in the few instances around nearby major galaxies where we have information, in every case there is evidence that gas poor companions lie in flattened distributions." Kroupa (2014) counts nine major galaxies with associated satellite systems which are anisotropic (see also Pawlowski and Kroupa 2014). *It thus seems to be more the rule than the exception that satellite galaxies appear to be highly correlated in phase-space such that they appear arranged highly anisotropically about their hosts.*

←

Fig. 2 (continued) as a string of dwarfs (*crosses*) between the two major planes of the Local Group. The *green* and *yellow filled circles* show all non-satellite dwarf galaxies comprising the Local Group. They are all situated in one of two major symmetric planes. The *short arrows* depict the galaxy motions as given by the line-of-sight velocities. The Local Group is moving along the *arrow* towards the CMB. *Evidently the Local Group is a highly structured symmetric distribution of galaxies which has never been predicted nor even hinted at as being a result of the structures forming through a SMoC merger tree.* The *upper two panels* are according to Kroupa (2014), while the *two lower panels* are according to Pawlowski et al. (2013)

3.3 Satellite Galaxies Are Tidal Dwarf Galaxies (TDGs)

How can the preponderance of such highly correlated satellite galaxies be explained? The occurrence of an anisotropic system of PDG satellites which is comparable to the VPOS or the GPoA is so unlikely that this possibility can be discarded safely, even if accretion of PDGs from cosmological filaments is considered (Pawlowski et al. 2012b; Ibata et al. 2014; Pawlowski et al. 2014). The only known viable physical process which can generate such correlated structures is if the satellite galaxies are TDGs which formed in tidal arms produced in a galaxy–galaxy encounter together with associated massive star clusters. Computer simulations of galaxy encounters show such structures to emerge readily (e.g. Barnes and Hernquist 1992; Wetzstein et al. 2007; Bournaud et al. 2008; Bournaud 2010; Pawlowski et al. 2011; Hammer et al. 2013; Yang et al. 2014), as shown by the pioneering work of Elmegreen et al. (1993).

The symmetric structure of the Local Group, and the mutually correlated disks of satellites around both, the MW and Andromeda, may have been created when the much younger Galaxy and Andromeda interacted closely (< 55 kpc) about 7–11 Gyr ago (Zhao et al. 2013). This encounter would have thrown out gas rich tidal arms in which the dwarf galaxies of the Local Group formed. It would have thickened the then existing disk of the MW and of Andromeda and it may have led to the rapid buildup of a MW pseudo bulge through an induced radial-orbit instability (Zhao et al. 2013; Kroupa 2014, see also the MSc thesis at Cambridge university: Banik (2014)).

Can TDGs, once formed, survive for a Hubble time? Yes they can. This has been shown by simulations that include star formation and feedback by Recchi et al. (2007) and Ploeckinger et al. (2014): self-consistent and thus self-regulated TDG formation implies that they do not blow themselves apart due to a star burst. TDGs may be destroyed on an orbital time scale if they are on highly plunging orbits. TDGs which have consumed their gas or have been partially stripped of it also do not dissolve easily. The simulations of gas free TDGs evolved dynamically over a Hubble time of tidal stressing have demonstrated them to survive (Kroupa 1997; Casas et al. 2012). Such satellite galaxies lose most of their stars but evolve into quasi-stable remnants which feign domination by DM although they do not contain any, as has been discovered by Kroupa (1997). In that paper (Kroupa 1997) a prediction of a satellite galaxy was made which was discovered ten years later and is today known as the Hercules satellite galaxy. The predicted model agrees with the radius, the velocity dispersion, the luminosity and dynamical M/L ratio nearly exactly with the real Hercules satellite galaxy (Fig. 6 in Kroupa et al. (2010)). And, observations have led to the discovery of a few Gyr old TDGs (Duc et al. 2014).

Thus, many and perhaps a majority of TDGs apear to survive over many Gyr such that the MW and Andromeda dSph and ultra-faint dwarf satellite galaxies may be ancient TDGs.

3.4 *If They Are TDGs, then There Is No Cold or Warm DM*

The above then implies the following for the existence of exotic dark matter, independently of the arguments made in Sect. 2. Since the satellite galaxies that are in the GPoA have the same morphological properties and the same high dynamical mass to light (M/L) ratios as the Andromeda satellite galaxies not in the GPoA, the former and latter must be described by the same dynamics. If the former are ancient TDGs then they cannot contain dark matter. Thus, the "dark matter effect", i.e. the elevated M/L ratios, *can only be due to non-Newtonian dynamics*. Also, since the MW satellites are all in the VPOS and because they have high M/L ratios, again non-Newtonian dynamics needs to be invoked. That Milgromian dynamics (Milgrom 1983; Famaey and McGaugh 2012) accounts well for the properties of the Andromeda and the MW satellites has been shown by McGaugh and Wolf (2010), McGaugh and Milgrom (2013) and Lüghausen et al. (2014a). Tidal modulation and shaping of TDGs as they evolve on eccentric orbits over many Gyr additionally changes the stellar phase space distribution function (Kroupa 1997; Casas et al. 2012) such that even in Milgromian dynamics elevated apparent (but not true) dynamical M/L ratios are expected to result which deviate from the pure-Milgromian values.[2]

Here the beautiful work by Block et al. (2006) becomes relevant as evidence: Block et al. have shown that the about 1 kpc sized dust ring near the centre of Andromeda may be explained by the compact and massive satellite M32 punching through the disk of Andromeda about 210 Myr ago. Given the present-day stellar mass of M32 ($\approx 3 \times 10^9\, M_\odot$), it would have had a pre-infall DM halo mass $> 10^{11}\, M_\odot$ (Behroozi et al. 2013; Ferrero et al. 2012), such that dynamical friction on the massive DM halo of Andromeda would have significantly altered the orbit of M32. This problem thus needs to be studied further.

4 Consistency of the Deduction: The Performance of the SMoC and the Theory Confidence Graph

If there is no dark matter, then the SMoC cannot be a realistic description of the Universe. How does the track-record of the SMoC in accounting for observational data fare? If it were to be good, i.e., if there is a long history of predictions which have been verified by observations performed after the prediction was published, then this would contradict the conclusion reached above that challenges the existence of exotic cold or warm dark matter. This has been studied using the *theory confidence graph* (Kroupa 2012). It turns out that the SMoC has a long history of failed predictions. If

[2] Although Kroupa (1997) suggested that the high M/L ratios of the dSph satellite galaxies may be due to repeated tidal shaping of the stellar phase-space velocity distribution function in a Newtonian universe, this process is unlikely to account for all dSph satellite galaxies because they are on very different orbits. Consequently, non-Newtonian dynamics is required to account for the observed dynamical masses of all dwarf satellites.

each failure or problem is associated with a reduction in confidence by 50 % in the fundamental theory (that Einstein's general relativity is valid everywhere, and that all matter emerged at the big bang), then the SMoC would currently retain a probability of being a valid representation of the Universe of less than 10^{-5} % (Kroupa 2014). This probability is further reduced taking into account the additionally failed predictions since 2012, such as the large-scale observational evidence against the cosmological principle (Clowes et al. 2013), and the observed significant under-density of matter within the local volume of about 400 Mpc (Fig. 7 in Kroupa (2014)). Thus, the present-day very low confidence in the SMoC is in agreement with the above no-DM conclusions. *Consequently the SMoC is not a physical representation of the real Universe.*

5 The Galaxy Population

If there is no dark matter, then the SMoC does not describe the Universe. The observed "dark matter effects" in galaxies then need to be explained by an effective non-Einsteinian/non-Newtonian theory of gravitation. In this case dynamical friction on DM would not occur and mergers would be much rarer despite galaxy–galaxy interactions. Can this be seen in the observed evolution of the galaxy population? A few important results:

- Lu et al. (2012) construct semi-analytically computed populations of galaxies based on a SMoC merger tree and star-formation recipes trimmed to agree with broad observed properties by discarding parameter ranges. The best final trimmed model leads to a curved BTFR in disagreement with the observed BTFR and to a much larger number of satellite galaxies than is observed, among other problems. The milestone Illustris project, which is the currently highest existing resolution calculation of structure formation of the Universe and includes gas dynamics and detailed star formation prescriptions (Vogelsberger et al. 2014b), yields a Tully-Fisher relation in disagreement with the one obtained by Lu et al. (2012). But this is not discussed nor is the disagreement clarified by Vogelsberger et al. (2014b). Both are steeper than the observed relation for galaxies with stellar masses larger than about $10^{10}\,M_{\odot}$. That is, the model galaxies have larger rotational speeds at a given mass than the observed ones. An unphysical aspect of such models is that they require stellar feedback to be a function of the hosting DM halo in order to have sufficient feedback energy to stop a sufficient amount of baryons making stars immediately such that they can be blown out and re-accreted slowly thereby helping to build-up galactic disks.[3]

[3] This would imply, essentially, that the table in my dining room would know it exists in the MW DM halo rather than in the DM halo of the Large Magellanic Cloud, in violation of the required fundamental property of DM particles which are supposed to not interact, apart maybe weakly, with the particles of the standard model of particle physics.

In contrast, scale-invariant or Milgromian dynamics yields the observed Tully-Fisher relation exactly (Famaey and McGaugh 2012; Kroupa 2014).

- Shankar et al. (2014) perform semi-analytical modelling of early-type galaxy formation. An interesting result from this work is that they need to suppress dynamical friction for improved agreement with the observational data. This is consistent with the independently deduced absence of evidence for dynamical friction noted in Sect. 2, Test 3.
- Weinzirl et al. (2009) and Kormendy et al. (2010) find the fraction of disk galaxies with classical bulges to be very small. The small fraction (6 %) of disk galaxies with classical bulges is supported by Fernández Lorenzo et al. (2014) for a sample of 189 isolated galaxies. Kormendy et al. (2010) point out that the small fraction of disk galaxies with classical bulges is incompatible with the merging history which would affect most galaxies if the SMoC were true. One deduction from this would be that mergers therefore cannot be a major aspect of galaxy evolution. The only way to suppress the occurrence of galactic mergers is to discard the massive DM halos made of particles.
- The population of galaxies is *vastly* dominated by late-type galaxies. According to Delgado-Serrano et al. (2010) only 3–4 % of all galaxies more massive in stars than about $10^{10}\,M_{\odot}$ are elliptical. This holds for the galaxy population about 6 Gyr ago and at the present epoch, and is in excellent agreement with the long-known result that disk galaxies are the by far dominant population in the field as well as in galaxy clusters (see Fig. 4.14 in Binney and Merrifield (1998)). It has never been successfully demonstrated that the merger-driven buildup of the galaxy population in the SMoC leads to the observed massive preponderance of rotationally supported, thin-disk star-forming late-type galaxies. Instead, galaxies that form in the SMoC are predominantly of early type, because angular momentum is ejected or cancelled-out during the many mergers. As emphasized by Disney et al. (2008), the vast majority of galaxies appear to be a one-parameter family of objects, much simpler than expected with little variation (see also Kroupa 2014). Consequently, dark-matter-driven mergers cannot be a physically relevant process in galaxy formation.
- That this dominating population of late-type disk star-forming galaxies lie on a main sequence, is discussed by Speagle et al. (2014). These authors show that the main sequence of galaxies which corresponds to an approximately constant specific star-formation efficiency (star-formation rate per unit stellar mass) has a small dispersion and persists to high redshift. Galaxies are thus much simpler than expected from the haphazard buildup through a DM-driven merger tree in the SMoC, a view already arrived at by Disney et al. (2008) in their principle-component analysis of a large sample of galaxies.

The overall implication of this discussion is thus consistent with the above conclusions that DM-driven processes do not appear to play a role in the astrophysics of galaxies.

6 Conclusions

With exotic DM particles being ruled out by observation as being an important aspect of galactic dynamics, there would be no reason to consider the existence of such particles at all. Therewith the central pillar of the SMoC collapses, and the SMoC becomes irrelevant as a theoretical framework for the Universe. Probably most aspects of current cosmological understanding then collapse as well: the standard redshift-age and redshift-distance relations would probably be wrong, the inferred cosmological evolution of the star-formation rate density and of galaxy masses and of their ages would probably be wrong as well.

The failures of the SMoC thus require a new paradigm which comes by without exotic DM particles (Kroupa et al. 2012). Important and successful hints have become available through the famous work of Milgrom (1983, 2009). The possible connections between the observed non-Newtonian but scale-invariant dynamics in the weak-field limit and cosmological parameters and the physics of the vacuum noted by Milgrom (1999) may indicate a deep interrelation of both. Based on

such ideas, a conservative cosmological model without exotic DM particles as described by Angus (2009), Angus and Diaferio (2011) and Angus et al. (2013) may be emerging (Kroupa 2014). As of very recently and thanks to special funding from the rectorate of the University of Bonn we have now, for the very first time, an adaptive mesh-refinement code, *Phantom of Ramses* (POR), which includes full treatment of baryonic processes (Lüghausen et al. 2014b). With POR cosmological structure formation simulations of a universe consisting only of the constituents of the standard model of particle physics and with Milgromian dynamics have become possible.

Irrespective of which cosmological model may be the next standard one, it will have to account for the time-dependent distribution and motion of matter on large-scales and on galaxy scales as well as for all properties of the microwave cosmic background.

Acknowledgements I thank Ken Freeman for organizing this conference on the Seychelles. It will remain memorable for decades to come. I also thank David Block and Bruce Elmegreen for being around so actively and for so many years such that we could have this splendidly luxurious meeting to honor both of them.

References

G. W. Angus. Is an 11eV sterile neutrino consistent with clusters, the cosmic microwave background and modified Newtonian dynamics? *MNRAS*, 394:527–532, March 2009.

G. W. Angus and A. Diaferio. The abundance of galaxy clusters in modified Newtonian dynamics: cosmological simulations with massive neutrinos. *MNRAS*, 417:941–949, October 2011.

G. W. Angus, A. Diaferio, and P. Kroupa. Using dwarf satellite proper motions to determine their origin. *MNRAS*, 416:1401–1409, September 2011.

G. W. Angus, A. Diaferio, B. Famaey, and K. J. van der Heyden. Cosmological simulations in MOND: the cluster scale halo mass function with light sterile neutrinos. *MNRAS*, 436:202–211, November 2013.

I. Banik. Galactic Archaeology with RAVE: Clues to the Formation of the Thick Disk. *MSc thesis, Cambridge University, ArXiv e-prints*, June 2014.

J. E. Barnes. Dynamics of Galaxy Interactions. In R. C. Kennicutt, Jr., F. Schweizer, J. E. Barnes, D. Friedli, L. Martinet, and D. Pfenniger, editors, *Saas-Fee Advanced Course 26: Galaxies: Interactions and Induced Star Formation*, page 275, 1998.

J. E. Barnes and L. Hernquist. Formation of dwarf galaxies in tidal tails. *Nature*, 360:715–717, December 1992.

P. S. Behroozi, R. H. Wechsler, and C. Conroy. The Average Star Formation Histories of Galaxies in Dark Matter Halos from z = 0-8. *ApJ*, 770:57, June 2013.

J. Binney and M. Merrifield. *Galactic Astronomy*. Princeton University Press, 1998.

D. L. Block, F. Bournaud, F. Combes, R. Groess, P. Barmby, M. L. N. Ashby, G. G. Fazio, M. A. Pahre, and S. P. Willner. An almost head-on collision as the origin of two off-centre rings in the Andromeda galaxy. *Nature*, 443:832–834, October 2006.

F. Bournaud. Tidal Dwarf Galaxies and Missing Baryons. *Advances in Astronomy*, 2010, 2010.

F. Bournaud, P.-A. Duc, and E. Emsellem. High-resolution simulations of galaxy mergers: resolving globular cluster formation. *MNRAS*, 389:L8–L12, September 2008.

R. A. Casas, V. Arias, K. Peña Ramírez, and P. Kroupa. Dwarf spheroidal satellites of the Milky Way from dark matter free tidal dwarf galaxy progenitors: maps of orbits. *MNRAS*, 424:1941–1951, August 2012.

K. Chiboucas, B. A. Jacobs, R. B. Tully, and I. D. Karachentsev. Confirmation of Faint Dwarf Galaxies in the M81 Group. *AJ*, 146:126, November 2013.

R. G. Clowes, K. A. Harris, S. Raghunathan, L. E. Campusano, I. K. Söchting, and M. J. Graham. A structure in the early Universe at $z\sim1.3$ that exceeds the homogeneity scale of the R-W concordance cosmology. *MNRAS*, 429:2910–2916, March 2013.

J. Dabringhausen and P. Kroupa. Dwarf elliptical galaxies as ancient tidal dwarf galaxies. *MNRAS*, 429:1858–1871, March 2013.

R. Delgado-Serrano, F. Hammer, Y. B. Yang, M. Puech, H. Flores, and M. Rodrigues. How was the Hubble sequence 6 Gyr ago? *A&A*, 509: A78, January 2010.

M. J. Disney, J. D. Romano, D. A. Garcia-Appadoo, A. A. West, J. J. Dalcanton, and L. Cortese. Galaxies appear simpler than expected. *Nature*, 455:1082–1084, October 2008.

P.-A. Duc, S. Paudel, R. M. McDermid, J.-C. Cuillandre, P. Serra, F. Bournaud, M. Cappellari, and E. Emsellem. Identification of old tidal dwarfs near early-type galaxies from deep imaging and H I observations. *MNRAS*, 440:1458–1469, March 2014.

B. G. Elmegreen, M. Kaufman, and M. Thomasson. An interaction model for the formation of dwarf galaxies and 10 exp 8 solar mass clouds in spiral disks. *ApJ*, 412:90–98, July 1993.

B. Famaey and S. S. McGaugh. Modified Newtonian Dynamics (MOND): Observational Phenomenology and Relativistic Extensions. *Living Reviews in Relativity*, 15:10, September 2012.

M. Fernández Lorenzo, J. Sulentic, L. Verdes-Montenegro, J. Blasco-Herrera, M. Argudo-Fernández, J. Garrido, P. Ramírez-Moreta, J. E. Ruiz, S. Sánchez-Expósito, and J. D. Santander-Vela. Are (pseudo)bulges in isolated galaxies actually primordial relics? *ArXiv e-prints*, May 2014.

I. Ferrero, M. G. Abadi, J. F. Navarro, L. V. Sales, and S. Gurovich. The dark matter haloes of dwarf galaxies: a challenge for the Λ cold dark matter paradigm? *MNRAS*, 425:2817–2823, October 2012.

G. Gentile, B. Famaey, F. Combes, P. Kroupa, H. S. Zhao, and O. Tiret. Tidal dwarf galaxies as a test of fundamental physics. *A&A*, 472:L25–L28, September 2007.

F. Hammer, Y. Yang, S. Fouquet, M. S. Pawlowski, P. Kroupa, M. Puech, H. Flores, and J. Wang. The vast thin plane of M31 corotating dwarfs: an additional fossil signature of the M31 merger and of its considerable impact in the whole Local Group. *MNRAS*, 431:3543–3549, June 2013.

R. A. Ibata, G. F. Lewis, A. R. Conn, M. J. Irwin, A. W. McConnachie, S. C. Chapman, M. L. Collins, M. Fardal, A. M. N. Ferguson, N. G. Ibata, A. D. Mackey, N. F. Martin, J. Navarro, R. M. Rich, D. Valls-Gabaud, and L. M. Widrow. A vast, thin plane of corotating dwarf galaxies orbiting the Andromeda galaxy. *Nature*, 493:62–65, January 2013.

R. A. Ibata, N. G. Ibata, G. F. Lewis, N. F. Martin, A. Conn, P. Elahi, V. Arias, and N. Fernando. A Thousand Shadows of Andromeda: Rotating Planes of Satellites in the Millennium-II Cosmological Simulation. *ApJL*, 784:L6, March 2014.

J. Kormendy, N. Drory, R. Bender, and M. E. Cornell. Bulgeless Giant Galaxies Challenge Our Picture of Galaxy Formation by Hierarchical Clustering. *ApJ*, 723:54–80, November 2010.

P. Kroupa. Dwarf spheroidal satellite galaxies without dark matter. *NA*, 2:139–164, July 1997.

P. Kroupa. The Dark Matter Crisis: Falsification of the Current Standard Model of Cosmology. *PASA*, 29:395–433, June 2012.

P. Kroupa. Galaxies as simple dynamical systems: observational data disfavor dark matter and stochastic star formation. *Canadian Journal of Physics, in press*, 2014.

P. Kroupa, C. Theis, and C. M. Boily. The great disk of Milky-Way satellites and cosmological sub-structures. *A&A*, 431:517–521, February 2005.

P. Kroupa, B. Famaey, K. S. de Boer, J. Dabringhausen, M. S. Pawlowski, C. M. Boily, H. Jerjen, D. Forbes, G. Hensler, and M. Metz. Local-Group tests of dark-matter concordance cosmology. Towards a new paradigm for structure formation. *A&A*, 523: A32, November 2010.

P. Kroupa, M. Pawlowski, and M. Milgrom. The Failures of the Standard Model of Cosmology Require a New Paradigm. *International Journal of Modern Physics D*, 21:30003, December 2012.

Y. Lu, H. J. Mo, N. Katz, and M. D. Weinberg. Bayesian inference of galaxy formation from the K-band luminosity function of galaxies: tensions between theory and observation. *MNRAS*, 421:1779–1796, April 2012.

F. Lüghausen, B. Famaey, and P. Kroupa. A census of the expected properties of classical Milky Way dwarfs in Milgromian dynamics. *ArXiv e-prints*, April 2014a.

F. Lüghausen, B. Famaey, and P. Kroupa. Phantom of RAMSES (POR): A new Milgromian dynamics N-body code. *ArXiv e-prints*, May 2014b.

S. McGaugh and M. Milgrom. Andromeda Dwarfs in Light of MOND. II. Testing Prior Predictions. *ApJ*, 775:139, October 2013.

S. S. McGaugh and J. Wolf. Local Group Dwarf Spheroidals: Correlated Deviations from the Baryonic Tully-Fisher Relation. *ApJ*, 722:248–261, October 2010.

M. Milgrom. A modification of the Newtonian dynamics as a possible alternative to the hidden mass hypothesis. *ApJ*, 270:365–370, July 1983.

M. Milgrom. The modified dynamics as a vacuum effect. *Physics Letters A*, 253:273–279, March 1999.

M. Milgrom. The Mond Limit from Spacetime Scale Invariance. *ApJ*, 698:1630–1638, June 2009.

M. S. Pawlowski and P. Kroupa. The rotationally stabilized VPOS and predicted proper motions of the Milky Way satellite galaxies. *MNRAS*, 435:2116–2131, November 2013.

M. S. Pawlowski and P. Kroupa. The VPOS of the Milky Way Attains New Members. *ApJ, in press*, 2014.

M. S. Pawlowski, P. Kroupa, and K. S. de Boer. Making counter-orbiting tidal debris. The origin of the Milky Way disc of satellites? *A&A*, 532: A118, August 2011.

M. S. Pawlowski, J. Pflamm-Altenburg, and P. Kroupa. The VPOS: a vast polar structure of satellite galaxies, globular clusters and streams around the Milky Way. *MNRAS*, 423:1109–1126, June 2012a.

M. S. Pawlowski, P. Kroupa, G. Angus, K. S. de Boer, B. Famaey, and G. Hensler. Filamentary accretion cannot explain the orbital poles of the Milky Way satellites. *MNRAS*, 424:80–92, July 2012b.

M. S. Pawlowski, P. Kroupa, and H. Jerjen. Dwarf galaxy planes: the discovery of symmetric structures in the Local Group. *MNRAS*, 435:1928–1957, November 2013.

M. S. Pawlowski, B. Famaey, H. Jerjen, D. Merritt, P. Kroupa, J. Dabringhausen, F. Lüghausen, D. A. Forbes, G. Hensler, F. Hammer, M. Puech, S. Fouquet, H. Flores, and Y. Yang. Co-orbiting satellite galaxy structures are still in conflict with the distribution of primordial dwarf galaxies. *MNRAS, in press*, June 2014.

S. Ploeckinger, G. Hensler, S. Recchi, N. Mitchell, and P. Kroupa. Chemo-dynamical evolution of tidal dwarf galaxies. I. Method and IMF dependence. *MNRAS*, 437:3980–3993, February 2014.

S. Recchi, C. Theis, P. Kroupa, and G. Hensler. The early evolution of tidal dwarf galaxies. *A&A*, 470:L5–L8, July 2007.

S. Recchi, F. Calura, and P. Kroupa. The chemical evolution of galaxies within the IGIMF theory: the [α/Fe] ratios and downsizing. *A&A*, 499:711–722, June 2009.

F. Shankar, S. Mei, M. Huertas-Company, J. Moreno, F. Fontanot, P. Monaco, M. Bernardi, A. Cattaneo, R. Sheth, R. Licitra, L. Delaye, and A. Raichoor. Environmental dependence of bulge-dominated galaxy sizes in hierarchical models of galaxy formation. Comparison with the local Universe. *MNRAS*, 439:3189–3212, February 2014.

J. S. Speagle, C. L. Steinhardt, P. L. Capak, and J. D. Silverman. A Highly Consistent Framework for the Evolution of the Star-Forming "Main Sequence" from z˜0-6. *ArXiv e-prints*, May 2014.

R. C. Thomson, S. Laine, and A. Turnbull. Towards an Interaction Model of M81, M82 and NGC 3077. In J. E. Barnes and D. B. Sanders, editors, *Galaxy Interactions at Low and High Redshift*, volume 186 of *IAU Symposium*, page 135, 1999.

A. Toomre. Mergers and Some Consequences. In B. M. Tinsley and R. B. G. Larson, D. Campbell, editors, *Evolution of Galaxies and Stellar Populations*, page 401, 1977.

M. Vogelsberger, S. Genel, V. Springel, P. Torrey, D. Sijacki, D. Xu, G. F. Snyder, S. Bird, D. Nelson, and L. Hernquist. Properties of galaxies reproduced by a hydrodynamic simulation. *ArXiv e-prints*, May 2014a.

M. Vogelsberger, S. Genel, V. Springel, P. Torrey, D. Sijacki, D. Xu, G. F. Snyder, D. Nelson, and L. Hernquist. Introducing the Illustris Project: Simulating the coevolution of dark and visible matter in the Universe. *ArXiv e-prints*, May 2014b.

T. Weinzirl, S. Jogee, S. Khochfar, A. Burkert, and J. Kormendy. Bulge n and B/T in High-Mass Galaxies: Constraints on the Origin of Bulges in Hierarchical Models. *ApJ*, 696:411–447, May 2009.

M. Wetzstein, T. Naab, and A. Burkert. Do dwarf galaxies form in tidal tails? *MNRAS*, 375:805–820, March 2007.

X. Wu and P. Kroupa. Galactic rotation curves, the baryon-to-dark-halo-mass relation and their space-time scale invariance. *MNRAS, submitted*, 2014.

Y. Yang, F. Hammer, S. Fouquet, H. Flores, M. Puech, M. S. Pawlowski, and P. Kroupa. Reproducing properties of MW dSphs as descendants of DM-free TDGs. *ArXiv e-prints*, May 2014.

M. S. Yun. Tidal Interactions in M81 Group. In J. E. Barnes and D. B. Sanders, editors, *Galaxy Interactions at Low and High Redshift*, volume 186 of *IAU Symposium*, page 81, 1999.

H. Zhao, B. Famaey, F. Lüghausen, and P. Kroupa. Local Group timing in Milgromian dynamics. A past Milky Way-Andromeda encounter at $z > 0.8$. *A&A*, 557:L3, September 2013.

The Planetary Nebulae Populations in the Local Group

Magda Arnaboldi

Abstract Planetary nebulae have been used as tracers of light and kinematics for the stellar populations in early-type galaxies for more than 20 years. Several empirical properties have surfaced: for example the invariant bright cut-off of the planetary nebulae luminosity function and correlations of the luminosity specific PN number with the integrated properties of the parent stellar populations. These observed properties are poorly understood in terms of a simple model of a ionized nebula expanding around a non-evolving central star. In order to make further steps, we need to study self-contained systems at known distances whose PN populations are sufficiently nearby to permit investigation into their physical properties. The galaxies in the Local Group represent valid proxies to study these late phases of evolved stellar populations with a spread of metallicities, α-element enhancements, and star forming histories.

1 Introduction

Galactic planetary nebulae (PNs) are roughly 0.3 pc in diameter. Hence when they are observed in external galaxies at distances larger than 50 kpc they are identifiable as unresolved emissions of monochromatic green light at 5007 Å, that is the strongest optical emission line of the [OIII] doublet. About 2000 PNs are known in the Milky Way (MW) out of 200 billion stars and are found mostly in the plane of the MW. In our own galaxy, 95 % of the stars end their lives as PNs, and the remaining 5 % as SNs. Single stars can be observed in their PNs phase because the ionized envelope of a PN is able to re-emit up to 15 % of the core star UV radiation in one single optical line, the [OIII] 5007 Å line, which can be detected in narrow band imaging surveys against the continuum light emitted by the rest of the stars. The total integrated flux in the [OIII] 5007 line emitted by a nebula can be expressed as

$$m_{5007} = -2.5 \log (F_{5007}) - 13.74 \quad (1)$$

M. Arnaboldi (✉)
European Southern Observatory, Garching, Germany
e-mail: marnabol@eso.org

K. Freeman et al. (eds.), *Lessons from the Local Group,*
DOI 10.1007/978-3-319-10614-4_29

When these magnitudes are measured for a PN population, they provide the planetary nebulae luminosity functions (PNLF). In external galaxies, the PNLFs show several empirical properties, for example the bright cut-off is observed to be empirically invariant and the overall shape seems to be reproduced by the Ciardullo's 1989 analytical formula

$$N(M) \propto exp(0.307M) \times (1 - exp(3(M* - M))); \; M* = -4.51 \qquad (2)$$

1.1 The PN.S Key Project on Early-Type Galaxies

PNs have been used as tracers of light and motions in the outer regions of early-type galaxies since more than 20 years, starting from the early models of the mass distribution in M32 by Nolthenius and Ford (1986) to the current Planetary Nebulae Spectrograph (PN.S)—Key Project—for the survey of PNs in early-type galaxies (ETGs). Such survey includes all ETGs within 20 Mpc, at airmass less than 1.5 which are observable from the William Herschel telescope on La Palma, Spain. This survey includes 20 ETGs, from E0 to E4, 11 S0s and it is now expanded to include spiral galaxies. Observational data are presented in Coccato et al. (2009) and Cortesi et al. (2013); data products can be downloaded at http://www.strw.leidenuniv.nl/pns/PNS_public_web/PN.S_data.html

The current results of these studies illustrate that the PN number density follows the surface brightness of the stars that dominate the light in these galaxies, and whenever PNs and absorption line kinematics overlap, they agree in all sample galaxies surveyed thus far. The results from the kinematical studies show that the specific angular momentum in the outer halo, out to 10 R_e, where R_e is the effective radius of the surface brightness distribution, correlates with the properties of the high surface brightness regions, but there are significant deviations (Coccato et al. 2009; Cortesi et al. 2013). Furthermore, the velocity *r.m.s.* dispersion profiles for the galaxies in this sample show a dichotomy between flat and quasi Keplerian dispersion profiles, see Fig. 1. The question whether there is a continuum or a separation between the two families is still open, and is going to be addressed by the new data release from the PN.S key project. Contrary to the initial claims of quasi Keplerian dispersion profile signaling lower dark matter content in these systems (e.g. Romanowsky et al. 2003), these galaxies can harbor a dark matter halo consistent with ΛCDM and their steep σ profiles at large radii are the results of the $R^{1/4}$ surface brightness profile and strong radial anisotropy in the outer parts (de Lorenzi et al. 2009; Morganti et al. 2013).

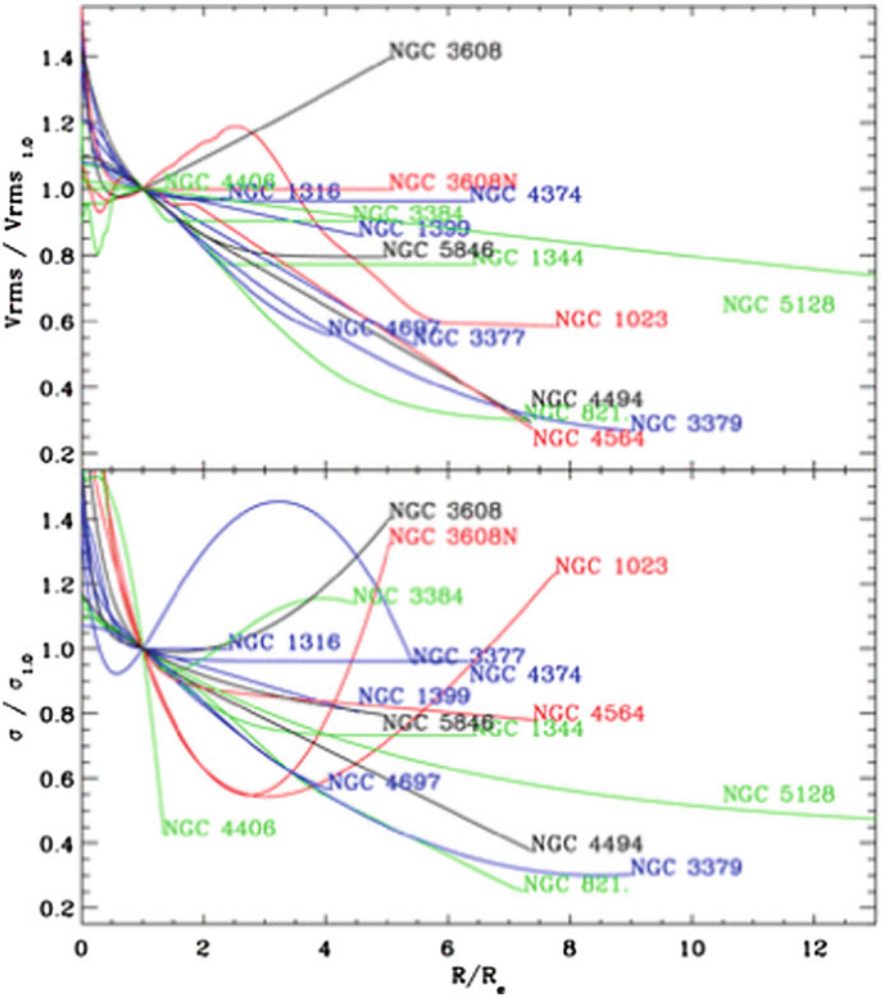

Fig. 1 Comparison between radial profiles of V_{rms} (*top panel*) and velocity dispersion (*bottom panel*) of the sample galaxies, obtained by combining the stellar and PNs kinematics along the major axis. Profiles have been scaled to the effective radius and normalized to their value at $1.0R_e$. Colors are chosen in order to highlight the contrast between lines and thus better distinguish different profiles. The velocity r.m.s. and σ/σ_0 profiles in ETGs as traced by PNs. From the PN.S Key Project, Coccato et al. (2009)

1.2 PNs in ETGs

The luminosity specific PN number, or α parameter for short is given by

$$\alpha = N_{PN}/L_{\odot,Bol} \tag{3}$$

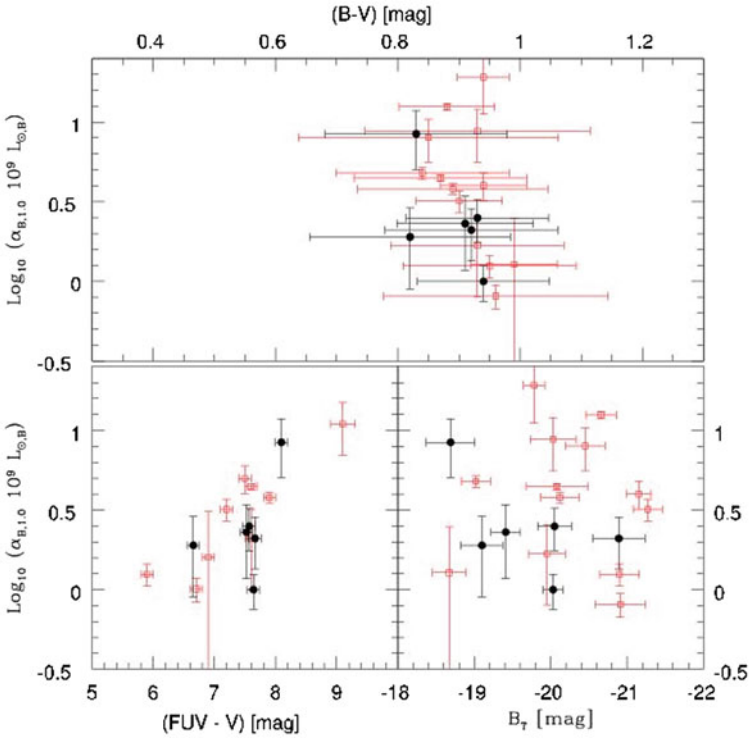

Fig. 2 The α parameter values measured in ETGs and correlations with $B - V$ color, total B magnitude and $FUV - V$ color. From Cortesi et al. (2013)

and it is a characteristic number that associates the PN population with its parent stellar population emitting the bulk of the light in an extragalactic system. In the simple stellar population theory, such number is also given by

$$\alpha = N_{PN}/L_{\odot,Bol} = B\tau_{PN} \tag{4}$$

whether B is the specific evolutionary flux and τ_{PN} is the PN visibility lifetime of a PN. In the simple model of a uniformly expanding nebula around a non-evolving core (Henize and Westerlund 1963), $\tau_{PN} = D/v_{exp}$, where D is the diameter of a PN when its m_{5007} has faded 8 mags below the bright cut-off, and v_{exp} is the nebula expansion velocity. For this simple model $\tau_{PN} = 30,000$ yrs. Empirically, the α parameter shows a constant value in stellar populations with integrated $B - V < 0.8$, and then the scatter increases for stellar populations with redder colors (Hui et al. 1993, Ciardullo et al. 2002, Buzzoni et al. 2006, Cortesi et al. 2013). Specific to ETGs, the α parameter correlates with $FUV - V$ colors, so that fewer PNs are observed in systems with an $FUV - V$ color excess, see Fig. 2.

From the relation between α and τ_{PN}, a lower value of α translates into a shorter visibility lifetime for the PN population of about 1000–5000 year in those systems where the low values of α are measured.

2 Surveys of PNs in the Local Group

In this section, a summary overview of the available surveys for PNs in the Local Group is provided, with emphasis on the surveys of the MW PNs, in the Large Magellanic Cloud (LMC) and the Andromeda galaxy (M31).

Survey of PNs in the MW The PN candidates in the MW are selected in Hα and confirmed spectroscopically. The most recent survey is the Macquarie/AAO/Strasbourg Hα Planetary Nebula Catalog (MASH I+ MASH II) with $\sim$ 1200 PNs detected (Frew et al. 2013; Parker et al. 2006 (MASH I), and Miszalski et al. 2008 (MASH II)). These latest results build on and expand the Strasbourg/ESO catalog of PN ($\sim$ 2000 PNs by Acker et al. 1992). The PN population that is specific to the Bulge includes 802 PNs, with 405 PNs from MASH I + II and 396 PNs from Acker et al. (1992). Independent surveys of the Bulge PNs (373 PNs) were carried out by Beaulieu et al. (1999). Weidmann et al. (2013) also identified PNs in the MW bulge from VVV survey data (about 381 PNs).

Survey of PNs in the Large Magellanic Cloud An extended survey in the LMC was carried out by Reid and Parker (2010) in the central 25°2 area. A total of 740 PNs were detected and spectroscopically confirmed with the AAT 2dF Spectrograph. The magnitude range covered by the sample spans 10 mags down the bright cut-off of the PNLF.

Survey of PNs in M31 The extensive survey of PNs in M31 was carried out with the Planetary Nebulae Spectrograph (PN.S) by Merrett et al. (2006), with the discovery of 2730 PN candidates. For this sample, the PNLF is complete 4 mag down the brightest cut-off (Merrett et al. 2006).

Survey of PNs in Local Group galaxies The PN populations in Local Group (LG) galaxies were surveyed and detected in 16 LG members (Reid 2012). There are no PN detected in LG galaxies with $M_V < -9.8 (\simeq 10^6 L_\odot)$. Empirically, it is consistent with a maximum specific PN luminosity number of $\alpha_{max} < 1 PN/10^7 L_{\odot,Bol}$.

3 Physical Properties of the PN Populations—Visibility Lifetimes and Planetary Nebulae Luminosity Functions

MW Bulge The distribution of angular diameter in arcsec for Bulge and Disk PNs is available from the MASH-I + II survey, with 90 % of the whole population within the maximum angular diameter of 35 arcsec. In the case of the PN sample restricted to

the MW Bulge, the plot log (SB) vs. log (D) shows that round PNs are the brightest and most compact objects, with average diameter of 0.3 pc: clearly these PNs are those preferentially detected when PN populations are observed in external galaxies.

There are 560 PNs in the Galactic Bulge with average diameter about 0.3 pc. The PN visibility lifetime τ_{PN} for this volume limited sample can be estimated using v_{exp} and D_{PN}, as D_{PN}/v_{exp}. Given that the average expansion velocity of Bulge PNs is 30 kms^{-1}, thus the observable lifetime of a Galactic Bulge PN is then only a few 10^3 years, which is consistent with visibility lifetime of PN samples in ETGs.

Kovacevic et al. (2011) carried out the [OIII] narrow band imaging of the PN population in the central $10° \times 10°$ region towards the MW Bulge. This sample accounts for 80 % of known PNs in this region. Fluxes and diameters are measured from narrow band imaging with the MOSAIC-II camera on the 4-m Blanco Telescope at the CTIO. They surveyed 60 deg^2 uniformly with a narrow band filter centered on the [O III] λ 5007 line; 104 objects were used for calibration of the m_{5007} magnitudes of 228 PNs. At 8 kpc, $m*$ is 10.00 ($M* = -4.51$), and one can ask whether the PN population associated with an old $\alpha-$element enhanced parent stellar population follows the PNLF analytical formula suggested by Ciardullo et al. (1989). The empirical PNLF for the MW Bulge is steeper than what is described by the Ciardullo's 1989 analytical formula, in a way similar to what is observed in the halo of M87 (Longobardi et al. 2013). For more detail, we refer to Arnaboldi, Longobardi, Gerhard in prep.

LMC Reid and Parker (2010) built the PNLF for the extended sample of PNs in the LMC. In order to use the PNLF for distance determination, they corrected the [OIII] fluxes from the confirmed spectra for line-of-sight reddening only. While the bright cut-off is consistent with M*=−4.51, once corrected for the metallicity dependence, the Ciardullo's 1989 formula is a poor fit to the empirical PNLF. The major departure from the analytical formula occurs 1.5 mag from the bright cut-off and lasts for 1.5 mag. The empirical PNLF is flatter in these magnitude ranges than what predicted by the double exponential formula (Eq. 2). This very sensitive survey illustrates another new feature of the PNLF: a peak in the PN number density which is caused by a rapid rise 4 mag below the brightest PN. This feature is characteristics of models where the [OIII] 5007 Å emission is driven by the rapid evolution of the central star. The peak and the steep descent represents the point at which the central star starts its trajectory down towards the white dwarf cooling track. Such a peak in the PNLF is predicted by the models of Meńdez et al. (1993)

The very deep survey of PNs in the LMC shows that Ciardullo's analytical formula fails to reproduce the faint end of the PNLF, with candidates being detected up to 2 mag fainter than the expected limit of 8 mag down the brightest PNs.

M31 The PN population in M31 illustrates the strength of PNs as tracers of light and motions of the stars that dominate the bulk of the light emitted in this galaxy. As shown by Merrett et al. (2006), the PN number density profile follows the surface brightness profile along the major and the minor axis out to 2 and 1 degree, respectively, from the galaxy center. The PNLF for the entire population is complete 4 magnitudes down the bright cut-off and it is well fitted by Eq. 2. Deviations from the Ciardullo's

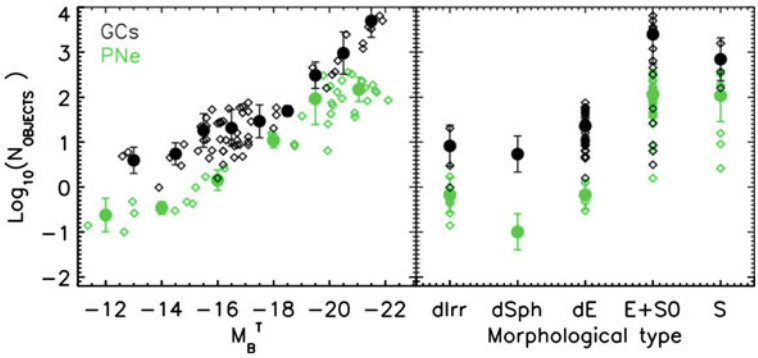

Fig. 3 Expected number of sources (GCs or PNs) as a function of galaxy absolute magnitude (*left*) and morphology (*right*). The expected number of GCs and PNs is computed from: (i) the specific frequencies of GCs and PNs and (ii) the total galaxies' luminosities in the V and B bands, for GCs and PNs, respectively. The observed number of PNs approaches the theoretical predictions from single-stellar-population models (Buzzoni et al. 2006) for LMC-like and L* systems. From Coccato et al. (2013)

analytical formula are measured for the PNLF in the very central bright region by Pastorello et al. (2013). The kinematics of the PN sample shows the presence of a substructure (Merrett et al. 2003), while the bulk of the PN follow the stellar disk, with a clear signature for the asymmetric drift and a flattening of σ_v at large radii in the disk, which is signaling an increase in the DM content.

Local Group galaxies The surveys of PN population in the LG galaxies can provide useful information on the frequency of PNs in different systems, and whether there are systems with higher specific frequencies as function of luminosities and morphological types. These analysis were carried out by Reid (2012) and Coccato et al. (2013); they show that galaxy systems with luminosities less than $10^8 L_{\odot,Bol}$ have fewer PNs that the number predicted from the theoretical maximum luminosity specific PN number of $1 PN/1.5 \times 10^6$ $L_\odot$ (Buzzoni et al. 2006). The observed number of PNs approaches the theoretical predictions for LMC-like and L* systems, see Fig. 3.

4 Physical Properties of the PN Populations in Old-Metal Rich vs. Poor-Star Forming Stellar Populations.

The oldest and most metal rich stellar populations are found in the bright, red, and passively evolving galaxies at the centers of massive clusters. The nearest such object is the galaxy M87, in the core of the Virgo cluster. Narrow band imaging surveys by Jacoby et al. (1990) provided the first PN candidates in M87, and the first PNs associated with the intracluster light (ICL) were discovered by Arnaboldi et al. (1996) and Feldmeier et al. (1998). The spectroscopic confirmation based on the detection

of the [OIII] 4959/5007 Å doublet in single objects was obtained by Arnaboldi et al. (2004) and Doherty et al. (2009). These 52 PNs turned out to be associated to the halo of M87 and ICL, as indicated by their line-of-sight velocities.

An important step forward in the study of PNs in M87 and the Virgo cluster comes with the availability of SuprimeCAM on the Subaru telescope, that allows the complete coverage of 0.25 deg^2 FoV, with the collecting power of an 8 m telescope. The results for the PN populations in M87 and ICL are reported in Longobardi et al. (2013) and Arnaboldi et al. (2003).

The deep narrow band imaging survey carried out by Longobardi et al. (2013) led to the identification of 688 PN candidates in the outer regions of M87, covering a radial range from 10 to 150 kpc. This sample is corrected for the contamination by Lyα emitters at redshift 3.14, [OII] emitters at redshift 0.34, faint continuum stars, and for color and spatial incompleteness. Longobardi et al. (2013) built the PN number density profile and compared it with the surface brightness profile of M87 in the V band. Deviations were clearly detected with the number density profile being flatter than the surface brightness profile at large radii. Such behavior was reproduced by a two component model where the PNs in the survey field come from the PN population associated with the M87 halo and the ICL. A two component model reproduces the observed profile when $\alpha_{2.5,ICL} = 3 \times \alpha_{2.5,M87}$. The values of α translate into PN visibility lifetimes that are $\tau_{PN} = 1.4 \times 10^4$ for PNs in the ICL and 4.5×10^3 for PNs in the M87 halo.

Longobardi et al. (2013) used their large PN sample in the outer regions of M87 to investigate the properties of the PNLF. They compared it with the PNLF predicted from Ciardullo's 1989 analytical formula and a distance modulus of 30.8. They reported strong deviations at 1.5 mag below the brightest cut-off with the observed gradient being steeper than what is predicted by the analytical formula in this magnitude range. Longobardi et al. (2013) compared the PNLFs extracted in three radial bins, and showed that the three PNLFs have high Kolmogorov-Smirnov (KS) probabilities of being drawn from the same distribution, while the KS test rejects the Ciardullo's formula, see Fig. 4.

The results are significant for old stellar populations because the steepening of the PNLF is thus shown to be present in all three radial bins, while it is known that the ICL contributes mostly at the largest radius. We can then compare the observed properties of the PNLF in M87 with the PNLF in the M31 bulge, which was used to calibrate the analytical formula from Ciardullo et al. (1989). The PN sample for M31 and the halo of M87 are normalized by the sampled luminosity and then corrected for the distance modulus. In Fig. 5, the results show that within one mag of the bright cutoff, the M87 population has fewer PNs than the PNLF of M31, i.e. the slope of the PNLF for the halo of M87 is steeper towards fainter magnitudes.

In old stellar populations, one expects the PN central stars to be mostly low mass cores, with $M_{core} \leq 0.55 M_{\odot}$. Thus, the slope of the PNLF may turned out steeper than the slope predicted by the fading of a uniformly expanding sphere ionized by a non-evolving star (Henize and Westerlund 1963). The comparison between the PNLFs of M87 and M31 may indicate that the M87 halo hosts a stellar population with a larger fraction of low mass cores, with respect to the M31 bulge. Comparison

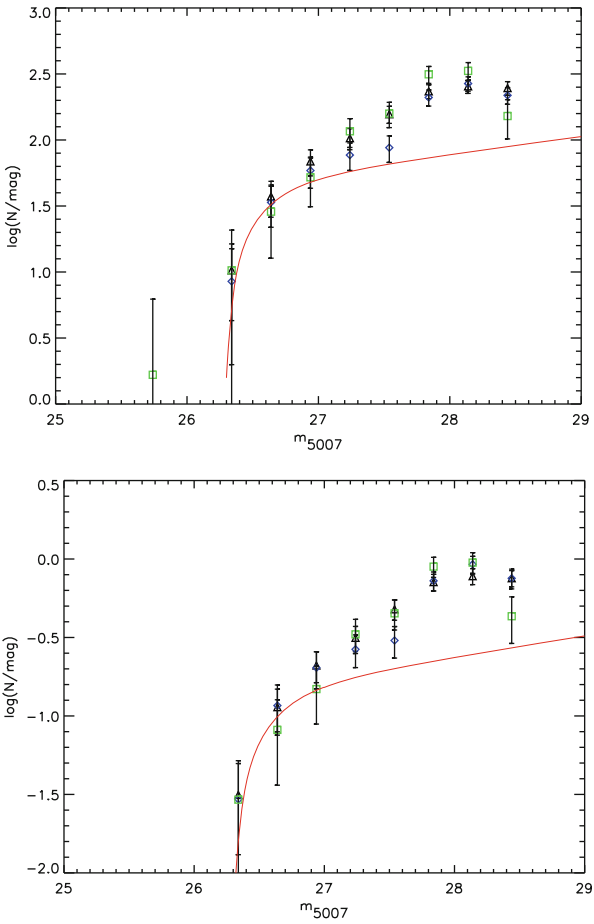

Fig. 4 *Top panel*: empirical PNLFs in three radial ranges corrected for color and detection incompleteness: PN candidates within 6.5′ from M87 center *triangles*, PN candidates between 6.5′ and 13.5′ from M87 center *diamonds*, PN candidates in the outermost region (distances greater than 13.5′) *squares*. The respective Lyα contribution expected in each radial bin was subtracted. Magnitudes are binned in 0.3 mag bins and the error bars represent the 1σ uncertainty from counting statistics combined with the uncertainty from cosmic variance in the Ly density. The *red solid line* is the convolved analytical formula of Ciardullo et al. (1989) for distance modulus 30.8. *Lower panel*: same as for the upper plot, but now the three PNLFs are normalized at the total number of objects in each radial bin. The three data sets are consistent with being drawn from the same underlying distribution. From Longobardi et al. (2013)

of the properties of PNLFs and their gradients 1.5 mag below the brightest PNs is further explored in Arnaboldi, Longobardi, Gerhard in prep.

5 Conclusions

The recent work on the PN populations in the halo of M87 and ICL shows that a second parameter is needed to generalize the Ciardullo's 1989 formula and account for population effects. In addition to the distance modulus and the normalization coefficient c_1, we need to vary the slope c_2, which is related to the gradient of the PNLF at magnitudes fainter then the PNLF cut-off.

Furthermore, one concludes (1) that PN populations are ubiquitous - deep photometry and kinematics from PNs show that they trace the bulk of star light in Local

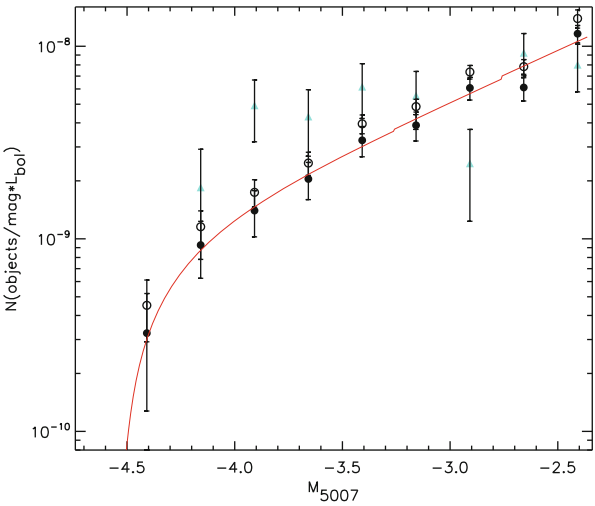

Fig. 5 Luminosity-normalized PNLFs for the bulge of M31 (*blue triangles*) and the halo of M87 (*black circles*). Data are binned into 0.25 mag intervals. The *red line* shows the improved fit with the second parameter c_2, in addition to the distance modulus and the normalization factor c_1. The M87 PNLF has a steeper slope towards faint magnitudes than M31. From Longobardi et al. (2013)

Group galaxies, early-type galaxies and in extended luminous halos, (2) that PN populations and their PNLFs show dependencies on stellar populations which are quantified by the gradient in the PNLF at magnitudes below the bright cut-off, and (3) that M* is empirically observed to be invariant in the systems studied thus far.

Acknowledgements MA would like to thank her collaborators for their enthusiasm and support, in particular Alessia Longobardi, Ortwin Gerhard and Lodo Coccato. She would like to thank the Scientific Organizing Committee for the invitation to give this review and the opportunity to take part in this very special and vibrant conference, and acknowledges ESO for financial support. All the best to Bruce and David!

References

Acker, A., Marcout, J., Ochenbein, F. et al. 1992, Strabourg-ESO Catalogue of Galactic Planetary Nebulae (Garching:ESO)
Arnaboldi, M., Freeman, K., Mendez, R., et al. 1996, ApJ, 472, 175
Arnaboldi, M., Freeman, K., Okamura, S., et al. 2003, AJ, 125, 514
Arnaboldi, M., Gerhard, O., Aguerri, J. , et al. 2004, ApJL, 614, 33
Beaulieu, S., Dopita, M., Freeman, K. 1999, ApJ, 515, 610
Buzzoni, A., Arnaboldi, M., Corradi, R. 2006, MNRAS, 368, 887
Ciardullo, R., Jacoby, G., Ford, H. et al. 1989, ApJ, 339, 53
Ciardullo, R., Feldmeier, J., Jacoby, G. 2002, ApJ, 577, 31
Coccato, L., Gerhard, O., Arnaboldi, M. et al. 2009, MNRAS, 394, 1249
Coccato, L., Arnaboldi, M., Gerhard, O. 2013, MNRAS, 436, 1322
Cortesi, A., Arnaboldi, M., Coccato, L. et al. 2013, A&A, 549, 115
Doherty, M., Arnaboldi, M., Das, P., et al. 2009, A&A, 502, 771
de Lorenzi, F. Gerhard, O., Coccato, L., et al. 2009, MNRAS, 395, 76
Feldmeier, J., Ciardullo, R., Jacoby, G. 1998, ApJ, 503, 109
Frew, D., Bojičić, I., Parker, Q. 2013, MNRAS, 431, 2

Henize, K. & Westerlund, B. 1963, ApJ, 1963, 137, 747
Hui, X. Ford, H., Ciardullo, R., et al. 1993, ApJ, 414, 463
Longobardi, A., Arnaboldi, M., Gerhard, O., et al. 2013, A&A, 558, 42
Jacoby, G., Ciardullo, R., Ford, H. 1990, ApJ, 356, 332
Kovacevic, A., Parker, Q., Jacoby, G., et al. 2011, MNRAS, 414, 860
Meńdez, R.H., Kudritzki, R.,Ciardullo, R., et al. 1993, A&A, 275, 534
Merrett, H., Kuijken, K., Merrifield, M., et al. 2003, MNRAS, 346, 62
Merrett, H., Merrifield, M., Douglas, N., et al. 2006, MNRAS, 369, 120
Miszalski, B., Parker, Q., Acker, A., et al. 2008, MNRAS, 384, 525 (MASH II)
Morganti, L., Gerhard, O., Coccato, L., et al. 2013, MNRAS, 431, 357
Nolthenius, R. & Ford, H. 1986, ApJ, 305, 600
Parker, Q., Acker, A., Frew, D., et al. 2006, MNRAS, 373, 79 (MASH I)
Pastorello, N., Sarzi, M., Cappellari, M., et al. 2013, MNRAS, 430, 121
Reid, W. 2012, IAU Symp., 283, 227
Reid, W & Parker, Q. 2010, MNRAS, 405, 1349
Romanowsky, A., Douglas, N. Arnaboldi, M., et al. 2003, Science, 301, 1696
Weidmann, W., Gamen, R., van Hoof, P., et al. 2013, A&A, 552, 74

Nearby Halo Streams

Carl J. Grillmair

Abstract The number of known halo streams has increased dramatically with the advent of deep, well-calibrated, wide-area sky surveys. Twenty nearby halo streams have been discovered to date, a number that is likely to at least double as surveys of the southern hemisphere progress. By themselves these streams tell us something about the accretion and disruption history of stellar aggregates in our Galaxy. More importantly, they will ultimately enable us to put much tighter constraints on the three dimensional shape of the Galactic potential. The morphologies of cold streams may also help us to constrain the occurrence and mass function of a predicted population of dark matter subhalos. We tabulate some basic properties of the known nearby streams, and discuss prospects for future discoveries.

1 Introduction

Nearby halo streams are a class of stellar debris streams that are close enough that we can measure all six phase space coordinates for at least some of their member stars, yet are far enough away that we can trace their trajectories over significant portions of their orbits around the Galaxy. This latter aspect distinguishes them from "local" streams or moving groups (e.g. Pleiades-Hyades, Hercules) which, though quite distinct in velocity space, are much more difficult to trace over large distances. By virtue of complete or well-defined sampling, local streams have given us interesting insights into the origins of halo stars in the solar neighborhood (Helmi et al. 1999; Starkenburg et al. 2009; Schlaufman et al. 2009), but owing to their very low surface densities, have been difficult to trace much beyond the solar neighborhood. By contrast, nearby halo streams have been traced over many tens of kpc (more than 100 kpc in the case of Sagittarius). This makes them far more useful for probing the shape of the Galactic potential. Moreover, their high surface densities are enabling detailed morphological studies that may shed light on both the tidal stripping process and on a presumed population of dark matter subhalos.

C. J. Grillmair (✉)
Spitzer Science Center, California Institute of Technology, Mail Stop 314-6,
1200 E. California Blvd., Pasadena, CA 91125, USA
e-mail: carl@ipac.caltech.edu

K. Freeman et al. (eds.), *Lessons from the Local Group,*
DOI 10.1007/978-3-319-10614-4_30

The known nearby streams are presumably only the tip of a very large iceberg. The nature of the data and the somewhat subjective methods used to find these streams have resulted in rather strong selection biases. Most streams detected to date appear to be nearly perpendicular or only slightly inclined ($\leq 15°$) to our line of sight. Highly inclined or nearly end-on streams will appear relatively short at any given distance, and are thus more likely to be missed or discounted as noise. This inevitably biases us against streams that are viewed end-on or at high inclinations to our line of sight. If we assume that stream orientations should be more or less isotropically distributed with respect to our line of sight, then we might reasonably expect there to be another six times as many streams out to 50 kpc, in just the SDSS footprint, than are currently known.

The streams we see presumably also represent only the upper end of a very extended mass function. We believe that all stars were born in associations or clusters of some size. All but the youngest or most tightly bound of such associations will have been torn apart by Galactic tidal forces. It follows that virtually all stars not still in associations, clusters or dwarf galaxies must be in streams. The aspect ratios of these streams will vary significantly, depending on the details of the stripping/disruption and subsequent heating processes. The vast majority of such streams will naturally be in the disk, where we may hope to identify a substantial number of them through large-scale chemical tagging (De Silva et al. 2009).

For streams in the halo, color-magnitude filtering of photometric datasets has thus far proven to be the most efficient way to find them. Matched-filtering in particular (Rockosi et al. 2002; Grillmair 2009) makes optimum use of all stars in a survey area, and takes maximum advantage of the somewhat bluer colors of the metal-poor halo stars compared with foreground disk stars. However, even with matched-filtering we appear to be reaching the limits of currently available survey data at a level of around ten stars per square degree. Pushing further down the mass function will require both deeper surveys and a concomitant improvement in our ability to distinguish stars from unresolved galaxies.

Despite deliberate and focused searches, only two of the many globular clusters in the SDSS footprint have been found to have convincing, lengthy tidal streams. This is in spite of the fact that many of these clusters have previously been shown to have significant extra-tidal, power-law extensions in their radial surface density profiles, indicative of ongoing tidal stripping (Grillmair et al. 1995; Leon et al. 2000). What made the progenitors of the known cold streams more susceptible to tidal disruption? The orbits of most of these streams do not appear to be particularly eccentric (and therefore subject to much stronger tidal forces). Are the extended tidal tails of globular clusters bunched up in some other part of the sky, near their apogalactica? Are the known cold streams indeed associated with known globular clusters and we have simply been unable to match them up using the data and models we have in hand? Or is it simply that, like Pal 5, the progenitors of the known cold streams were more loosely bound than most of the globular clusters we see today? These are just some of the questions we hope to answer as more and better data become available in the coming years.

One of the most exciting aspects of halo streams is that they provide us with sensitive probes of the Galactic potential in regions well away from the Galactic plane (Johnston et al. 1999). This is important both because we have few other comparable tracers in these regions, and because the shape of the halo may provide a strong test of the cold dark matter paradigm (Allgood et al. 2006). Cold streams are particularly interesting as the stars in such streams have relatively small random velocities and travel on nearly identical orbits. Simply measuring positions and velocities at several points along such streams can, in principle, yield the depth and shape of the potential (Koposov et al. 2010).

The discovery of these streams, and various attempts to use them to model the Galactic potential, has motivated several investigations of optimal methods for divining both the shape of the potential and the progenitor's orbit. Eyre and Binney (2011) have emphasized that the orbits of stars in even the coldest streams do not precisely correspond to the orbits of their progenitors, and that single-orbit fits are not generally appropriate. Various authors (Tremaine 1999; Helmi and White 1999; Eyre and Binney 2011) have shown that the dynamics of tidal streams are best described in terms of action-angle coordinates, and Bovy (2014) has developed a framework for straightforwardly modeling observed streams using actions, frequencies, and angles. Sanderson et al. (2014) have proposed an interesting method of constraining the potential that relies on action-space clustering of tidal streams. While the method requires full six-dimensional phase space information for a large sample of stars, it does *not* require that individual streams be identified in advance, relying rather on the principle that the correct form of the potential will always yield the most clustered distribution of actions.

The actual exercise of constraining the Galactic potential using tidal streams has had only limited applications to date. The most celebrated attempts include those of Law et al. (2009) and Koposov et al. (2010) using the Sagittarius and GD-1 streams, respectively. The results of Law et al. (2009) suggest a fairly triaxial halo, consistent with expectations of CDM, though the arrangement of axes is somewhat worrying, suggesting that orbits in the plane of the Galactic disk might be unstable. The GD-1 results of Koposov et al. (2010) have put very tight constraints on the circular velocity at the Sun's radius ($V_c = 224 \pm 13$ km s^{-1}), though constraints on the shape of the halo are comparatively weak owing to the relatively low orbital inclination and the strong influence of the Galactic disk.

Cold debris streams may also be useful for detecting dark matter concentrations in the halo. The collisional cross section for a many-kpc-long tidal stream is quite substantial, and if there are 100s or 1000s of dark matter subhalos orbiting in the halo, they should frequently leave their marks on tidal streams (Carlberg 2009; Yoon et al. 2011; Carlberg 2013). Recent work by Carlberg et al. (2012) and Carlberg and Grillmair (2013) suggest that the number of gaps in the Pal 5 and GD-1 streams are roughly consistent with the number of dark matter subhalos predicted by ΛCDM. There remains some controversy concerning the extent to which these gaps may be a product of epicyclic motions of stars within streams (Küpper et al. 2008, 2012). Both higher signal-to-noise ratios and a larger sample of cold streams will be needed to better address this issue.

2 Known Stellar Debris Streams in the Galactic halo

Twenty nearby halo streams have been discovered to date, with several more candidates currently under investigation. Most of the streams are many tens of degrees long, with some having multiple components, and others overlapping one another on the sky. Where once we ascribed every detected sub-population or velocity group to the Sagittarius stream, or subsequently to the Monoceros Ring, it now demands considerable poring through the literature to determine which stream, if any, a newly-discovered substructure might belong to.

Table 1 summarizes some basic properties of all known nearby halo debris streams in order of discovery. We do not include those clusters or dwarf galaxies with power-law tidal extensions (beyond the nominal King tidal radii). Grillmair et al. (1995) and Leon et al. (2000) found such extensions around most of the globular clusters in their respective studies. Given these results and theoretical expectations, it would probably be more surprising to find a globular cluster that, if examined sufficiently deeply, did *not* show evidence of tidal stripping. We therefore list only streams and structures with a projected extent of more than 10° on the sky.

2.1 Column Descriptions

Designation This column gives the common name by which the particular feature is known in the literature. There exists as yet no convention on how streams should be named and a delightful anarchy has ensued. In cases where the the progenitor is known, the feature is quite naturally named after the progenitor (e.g. Sagittarius stream, Pal 5, NGC 5466). Some researchers have named streams after the constellations or regions of the sky in which they were first found, or in which they currently appear strongest (e.g. Monoceros, Cetus Polar Stream, Anticenter Stream, Triangulum/Pisces). Still others are named for the surveys in which they were first detected (e.g. ATLAS stream, PAndAS MW stream), after some discovery characteristic (Orphan, EBS), or after rivers in Greek mythology (Acheron, Lethe, Cocytos, Styx, Alpheus, Hermus, & Hyllus).

Progenitor This column provides the name of the progenitor, if known or suspected. Where there is a question mark, readers are referred to the references for the source of the uncertainty. If the progenitor is listed as dG? (dwarf galaxy) or GC? (globular cluster), the actual progenitor is unknown, but its likely nature is conjectured based on the strength or morphology of the stream. Extensive, broad, or hot streams presumably arose from more massive systems such as dwarf galaxies, whereas narrower, less populous streams most likely arose from globular clusters. This latter conclusion is based primarily on the similarity in the cross-sectional widths of such streams ($\sim$100 pc) to known globular cluster streams (Pal 5, NGC 5466).

Table 1 Currently known nearby halo streams

Designation	Progenitor	Known extent	Distance kpc	V_{hel} km s^{-1}	[Fe/H]	Selected references
Sagittarius Stream	Sagittarius dSph	Circum-sky	7–25	x−x	−1.15−− 0.4	Ibata et al. (1994), Mateo et al. (1996), Alard (1996), Toten and Irwin (1998), Ibata et al. (2001), Majewski et al. (2003), Martinez-Delgado et al. (2004), Vivas et al. (2005), Belokurov et al. (2006b), Fellhauer et al. (2006), Bellazzini et al. (2006), Chou et al. (2007), Law et al. (2009), Law and Majewski (2010), Keller et al. (2010) Carlin et al. (2012), Koposov et al. (2012)
Virgo stellar Stream	NGC 2419?	$180° < \text{R.A.} < 195°$ $-4° < \delta < 0°$	19.6	128	−1.78	Vivas et al. (2001), Duffau et al. (2006), Newberg et al. (2007), Dufau et al. (2014)
Palomar 5	Palomar 5	$225° < \text{R.A.} < 250°$ $-3° < \delta < 8.5°$	23	− 55	−1.43	Odenkirchen et al. (2001, 2003, 2009), Rockosi et al. (2002), Grillmair and Dionatos (2006a), Carlberg et al. (2012)
Monoceros ring	dG?	$108° < \text{R.A.} < 125°$ $-3° < \delta < -41°$	≈ 10.5	≈ 100	−0.8	Newberg et al. (2002), Yanny et al. (2003), Ibata et al. (2003), Rocha-Pinto et al. (2003), Penarrubia et al. (2005), Li et al. (2012)
NGC 5466	NGC 5466	$182° < \text{R.A.} < 224°$	17	108	−2.2	Belokurov et al. (2006a),

Table 1 (continued)

Designation	Progenitor	Known extent	Distance kpc	V_{hel} km s^{-1}	[Fe/H]	Selected references
		$21° < \delta < 42°$				Grillmair and Johnson (2006), Fellhauer et al. (2007), Lux et al. (2012)
Orphan stream	dG?	$143° <$ R.A. $< 165°$ $-17° < \delta < +48°$	20–55		−2.1	Grillmair (2006a), Belokurov et al. (2007) Fellhauer et al. (2007), Sales et al. (2008), Newberg et al. (2010), Sesar et al. (2013) Casey et al. (2013)
GD-1	GC?	$134° <$ R.A. $< 218°$ $14° < \delta < 58°$	7–10	− 200–+ 100	−2.1	Grillmair and Dionatos (2006b), Willett et al. (2009), Koposov et al. (2010), Carlberg and Grillmair (2013)
AntiCenter stream	dG?	$121° <$ R.A. $< 130°$ $-3° < +63°$	≈ 8	50–90	−0.96	Grillmair (2006b), Grillmair et al. (2008), Li et al. (2012)
EBS	GC?	$132° <$ R.A. $< 137°$ $-3° < \delta < 16°$	10	71–85	−1.8	Grillmair (2006b), Grillmair (2011), Li et al. (2012)
Acheron	GC?	$232° <$ R.A. $< 258°$ $3° < \delta < 20°$	3.5–3.8		−1.7?	Grillmair (2009)
Cocytos	GC?	$197° <$ R.A. $< 257°$ $8° < \delta < 30°$	11		−1.7?	Grillmair (2009)

Table 1 (continued)

Designation	Progenitor	Known extent	Distance kpc	V_{hel} km s^{-1}	[Fe/H]	Selected references
Lethe	GC?	$176° < \text{R.A.} < 252°$ $22° < \delta < 37°$	13		−1.7?	Grillmair (2009)
Styx	Bootes III?	$201° < \text{R.A.} < 250°$	45		−2.2?	Grillmair (2009)
		$21° < \delta < 31°$				
Cetus Polar Stream	NGC 5824?	$19° < \text{R.A.} < 37°$ $-11° < \delta < +39°$	24–36	−200– − 160	−2.1	Newberg et al. (2009), Yam et al. (2013)
Pisces/ Triangulum	GC?	$21° < \text{R.A.} < 24°$ $23° < \delta < 40°$	35	120	−2.2	Bonaca et al. (2012), Martin et al. (2013, 2014)
Alpheus	NGC 288?	$22° < \text{R.A.} < 28°$ $-69° < \delta < 45°$	1.6–2.0		−1.0?	Grillmair (2013)
Hermus	GC?	$241° < \text{R.A.} < 254°$ $5° < \delta < 50°$	18.5		−2.3?	Grillmair (2014)
Hyllus	GC?	$245° < \text{R.A.} < 249°$ $11° < \delta < 34°$	20		−2.3?	Grillmair (2014)
ATLAS stream	Pyxis?	$18° < \text{R.A.} < 30°$ $-32° < \delta < -25°$	20		−1.4?	Koposov et al. (2014)
PAndAS MW Stream	dG?	$0° < \text{R.A.} < 22°$ $40° < \delta < 48°$	17	127	−1.5?	Martin et al. (2014)

Known Extent Here we provide the maximum extent of the streams on the celestial sphere, as determined either in the discovery paper or in subsequent investigations. While the positions and trajectories of some features are shown in Figs. 1 and 2, readers are referred to the discovery or follow-up papers for detailed maps of the streams.

Distance This column provides the range of heliocentric distances for different portions of streams. These distance estimates will undoubtedly be refined as deeper surveys are carried out, spectroscopic metallicities are obtained, proper motions and Galactic parallaxi are measured, or RR Lyrae can be physically associated with streams.

V$_{hel}$ If radial velocities have been measured for one or more portions of a stream, the range of velocities is given here. This range can be quite large (e.g. Sagittarius or GD-1), where the length of the stream, combined with the Sun's motion, can produce very substantial gradients over the length of the stream.

[Fe/H] Metallicity estimates can be based on the color-magnitude locus of stream stars, on the metallicity of the matched filter that yields the highest signal-to-noise ratio, or on spectroscopy of individual stars. Estimates based solely on photometry can have fairly large uncertainties and are consequently flagged with question marks.

Selected References For each stream we provide references to the discovery paper, along with any follow-up works that either provide additional field area or spectroscopy that can be unambiguously identified with the stream, or papers that attempt to model the stream in question.

3 Future Work

Given that currently available, large-area digital sky surveys do not cover the entire sky, we expect that a significant number of strong streams remain to be discovered within 50 kpc. The Pan-Starrs survey (Kaiser et al. 2002), which covers considerably more sky area than the SDSS, will presumably yield additional streams, and extend at least some of the streams whose known extent is currently limited by the SDSS footprint. In the southern hemisphere, the ATLAS (Shanks et al. 2013), Skymapper (Keller et al. 2007), and Dark Energy Surveys (Rossetto et al. 2011) remain to be completed. Covering regions of the sky that have been largely unexplored to date, they will almost certainly yield a number of new streams, in addition to extending some of the streams in Table 1. Note that extending known streams is at least as important as finding new ones, as longer streams both reduce the uncertainty in orbit shape and tighten the possible constraints on the potential.

Further progress in finding cold or tenuous streams in the SDSS and other surveys may result from simultaneously combining photometric filtering with velocity and proper motion measurements. Spectra are now available for $\sim 7 \times 10^5$ stars

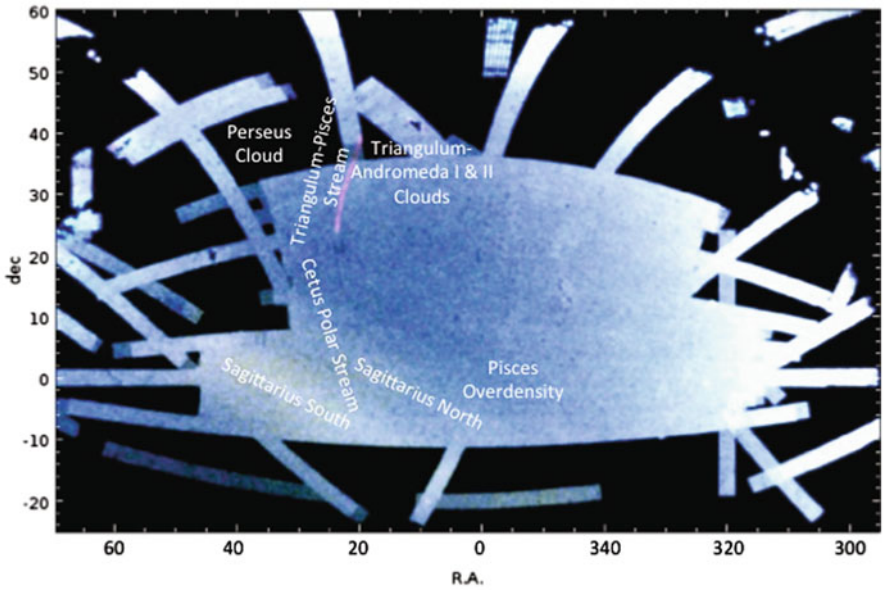

Fig. 1 A matched-filter surface density map of the northern part of the Sloan Digital Sky Survey. The filter used here is based on the color-magnitude distribution of the metal poor globular cluster M 13. The stretch is logarithmic and all but the Sagittarius streams have been enhanced using arbitrarily scaled Gaussians to make them visible at this stretch. *Bluer colors* correspond to more nearby stars ($\leq$ 15 kpc) while *redder colors* reflect the distribution of more distant stars

in the SDSS DR10. Newberg et al. (2009) combined photometric measurements with velocities and metallicities to detect the Cetus Polar Stream, a structure which had eluded prior discovery through photometric means alone. Several spectroscopic surveys either planned or in progress (e.g. LAMOST) will almost certainly make contributions in this area, particularly in detecting the streams more highly inclined to our line of sight (e.g. ECHOS, Schlaufman et al. 2009).

The Large Synoptic Survey, expected to begin early in the next decade, will greatly extend the reach of current photometric (e.g. matched filter) methods of stream detection. Even a single pass over the visible sky will be significantly deeper than the SDSS, and the end-of-survey photometric depth is expected to reach $r = 27.5$ (Grillmair and Sarajedini 2009). On the other hand, background galaxies will vastly outnumber stars at this depth, and significant improvements will need to made in the area of star-galaxy separation if we are to take full advantage of the data. If this can be achieved, then applying matched-filter techniques to upper main sequence stars should enable us to photometrically detect streams out to as much as 500 kpc. RR Lyrae will enable us to probe even more deeply into the halo (e.g. Sesar et al. 2013); even with fairly conservative single-pass detection limits, LSST should enable us to detect RR Lyrae out to more than 700 kpc.

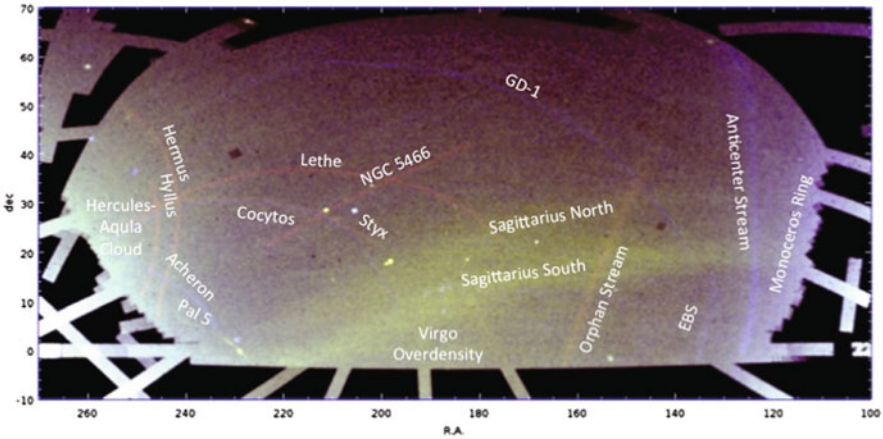

Fig. 2 As in Fig. 1, but for the southern footprint of the SDSS

Distance estimates are currently the largest source of uncertainty in the use of tidal streams as probes of the potential. The Gaia survey will clearly have an enormous impact here, providing *trigonometric* distances for giant branch stars out to tens of kpc. In addition, a number of synoptic surveys have detected many thousands of RR Lyrae, some of which have been associated with known streams (e.g. Sesar et al. 2013), and whose distances can now be measured to $\simeq 2\,\%$ using IR photometry. On the other hand, the coldest streams may have very few giant branch stars or RR Lyrae. Distances for these have often been estimated photometrically using filter matching or upper main sequence fitting, though the ages and metallicities of the stream stars are only poorly known and the distance uncertainties are correspondingly large. Eyre and Binney (2009) and Eyre (2010) have described and demonstrated an alternative method of finding distances by using proper motions to measure "Galactic parallax". This technique relies on the premise that any net proper motion component of stars perpendicular to a stream must be a consequence of the sun's reflex motion. The accuracy of the method is currently on par with photometric distances, limited primarily by the quality of the available proper motions. The Gaia survey should enable vast improvements in the application of this technique.

Proper motions could also be used to detect streams, and both Gaia and LSST are expected to make enormous contributions to the field. With expected end-of-mission proper motion accuracies of $\leq 200\mu$ as to 20th magnitude, the Gaia survey will enable us to push well down the stream mass function out to perhaps tens of kpc. Beyond that, the end-of-survey proper motion uncertainties for LSST will be on the order of 100 km s^{-1} at 100 kpc. With suitable averaging and/or Bayesian techniques, this should be sufficient to detect the remote and particularly high-value, extended tidal tails of many of the dwarf galaxies.

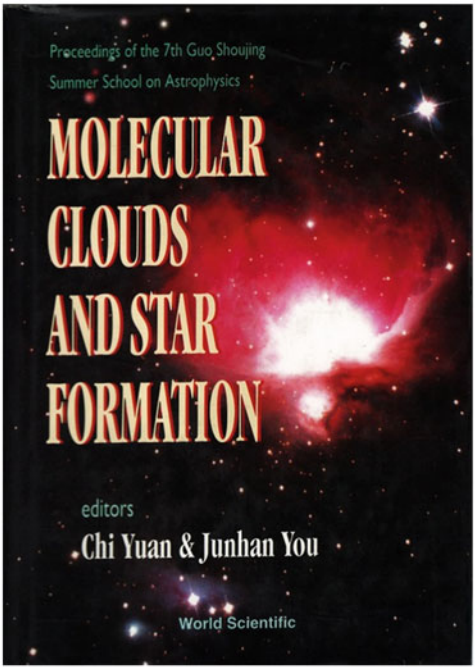

In Bruce/Debra's school
21 years ago

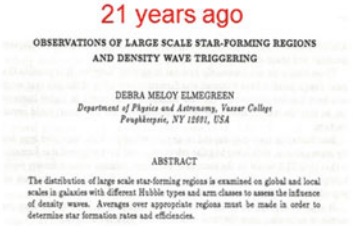

OBSERVATIONS OF LARGE SCALE STAR-FORMING REGIONS AND DENSITY WAVE TRIGGERING

DEBRA MELOY ELMEGREEN
Department of Physics and Astronomy, Vassar College
Poughkeepsie, NY 12601, USA

ABSTRACT

The distribution of large scale star-forming regions is examined on global and local scales in galaxies with different Hubble types and arm classes to assess the influence of density waves. Averages over appropriate regions must be made in order to determine star formation rates and efficiencies.

Wuxi, China

June 30 – July 5, 1993

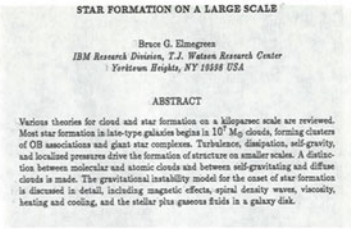

STAR FORMATION ON A LARGE SCALE

Bruce G. Elmegreen
IBM Research Division, T.J. Watson Research Center
Yorktown Heights, NY 10598 USA

ABSTRACT

Various theories for cloud and star formation on a kiloparsec scale are reviewed. Most star formation in late-type galaxies begins in 10^7 $M_\odot$ clouds, forming clusters of OB associations and giant star complexes. Turbulence, dissipation, self-gravity, and localized pressures drive the formation of structure on smaller scales. A distinction between molecular and atomic clouds and between self-gravitating and diffuse clouds is made. The gravitational instability model for the onset of star formation is discussed in detail, including magnetic effects, spiral density waves, viscosity, heating and cooling, and the stellar plus gaseous fluids in a galaxy disk.

Penetrating the Dust Masks …

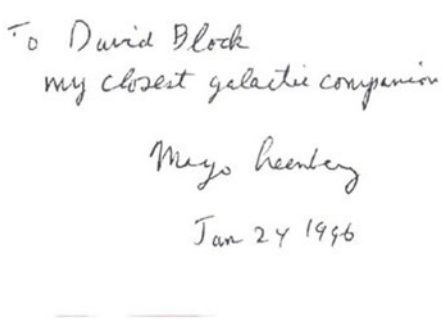

To David Block
my closest galactic companion
Mayo Greenberg
Jan 24 1996

眼中有尘心无尘，除却雾霾无尘埃！

Young stars are born out of dust ...

Congratulations on all the achievements, including in

Removing the dust masks …

Editorial Note. Figures on previous page kindly prepared by Aigen Li. The handwritten note selected by Aigen Li is from cosmic dust pioneer Mayo Greenberg, and reads "To David Block—My closest galactic companion".

References

Alard, C. 1996, ApJ, 458, L17
Allgood, B., Flores, R. A., Primack, J. R., Kravtsov, A. V., Wechsler, R. H., Faltenbacher, A., & Bullock, J. S. 2006, MNRAS, **367**, 1781
Bellazzini, M., Newberg, H. J., Correnti, M., Ferraro, F. R., Monaco, L. 2006, AA, 457, 21
Belokurov, V. et al. 2006a, ApJ, 637, L29
Belokurov, V. et al. 2006b, ApJ, 642, L137
Belokurov, V. et al. 2007, ApJ, 658, 337
Bonaca, A., Geha, M., & Kallivayalil, N. 2012, ApJ, **760**, 6
Bovy, J. 2014, arXiv:1401.2985v1
Carlin, J. L., Majewski, S. R., Casetti-Dinescu, D. I., Law, D. R., Girard, T. M., & Patterson, R. J. 2012, ApJ, **744**, 25
Carlberg, R. G. 2009, ApJ, **705**, 223
Carlberg, R. G. 2013, ApJ, **775**, 90
Carlberg, R. G., & Grillmair, C. J. 2013, ApJ, **768**, 171
Carlberg, R. G., Grillmair, C. J., & Hetherington, N. 2012, ApJ, **760**, 75
Casey, A. E., Da Costa, G., Keller, S. C., & Maunder, E. 2013, ApJ, **764**, 39
Chou, M.-Y., et al. 2007, ApJ, 670, 346
De Silva, G. M., Freeman, K. C., & Bland-Hawthorn, J. 2009, PASA, 26, 11
Duffau, S., Zinn, R., Vivas, A. K., Carraro, G, Mendez, R. A., Winnick, R., & Gallart, C. 2006, ApJ, **636**, L97
Duffau, S., Vivas, A. K., Zinn, R., Mendez, R. A., & Ruiz, 2014, arXiv:1403.2388
Eyre, A. 2010, MNRAS, **403**, 1999
Eyre, A., & Binney, J. 2009, MNRAS, **399**, 160
Eyre, A., & Binney, J. 2011, MNRAS, **413**, 1852
Fellhauer, M. et al. 2006, ApJ, 651, 167
Fellhauer, M. et al. 2007, MNRAS, **375**, 1171
Grillmair, C. J. 2006a, ApJ, **645**, L37
Grillmair, C. J. 2006b, ApJ, **651**, L29
Grillmair, C. J. 2009, ApJ, **693**, 1118
Grillmair, C. J. 2011, ApJ, **738**, 98
Grillmair, C. J. 2014, submitted
Grillmair, C. J., & Johnson, R. 2006, ApJ, **639**, L17
Grillmair, C. J., & Dionatos, O. 2006a, ApJ, **641**, L37
Grillmair, C. J., & Dionatos, O. 2006b, ApJ, **643**, L17
Grillmair, C. J., & Sarajedini, A. LSST Science Book, LSST Corporation, Tucson (2009)
Grillmair, C. J., Freeman, K. C., Irwin, M., & Quinn, P. J. 1995, AJ, **109**, 2553
Grillmair, C. J., Carlin, J. L., & Majewski, S. R. 2008, ApJ, **689**, L117
Grillmair, C. J., Cutri, R., Masci, F. J., Conrow, T., Sesar, B., Eisenhardt, P. R. M., & Wright, E. L. 2013, ApJ, **769**, 23
Helmi, A., & White, S.D.M. 1999, MNRAS, **307**, 495
Helmi, A., White, S.D.M, de Zeeuw, T., & Zhao, H. 1999, Nature, **402**, 53–55
Ibata, R. A., Gilmore, G., Irwin, M. J. 1994, Nature, **370**, 194
Ibata, R., Irwin, M., Lewis, G. F., Stolte, A. 2001, ApJ, 547, 133
Ibata, R. A., Irwin, M. J., Lewis, G. F., Ferguson, A. M. N., & Tanvir, N. 2003, MNRAS, 340, L21
Johnston, K. V., Sigurdsson, S., & Hernquest, L. 1999, MNRAS, **302**, 771

Kaiser, N. et al. 2002, SPIE, **4836**, 154
Keller, S. C. et al. 2007, PASA, **24**, 1
Keller, S. C., Yong, D., & Da Costa, G. S. 2010, ApJ, **720**, 940
Koposov, S., Rix, H-W, & Hogg, D. W. 2010, ApJ, **712**, 260
Koposov, S., et al. 2012, ApJ, 750, 80
Koposov, S., Irwin, M., Belokurov, V., Ganzalez-Solares, E., Kupcu Yoldas, A., Lewis, J., Metcalfe, N., & Shanks, T. 2014, MNRAS, in press.
Küpper, A. H. W., MacLeod, A., & Heggie, D. C. 2008, MNRAS, **387**, 1248
Küpper, A. H. W., Lane, R. R., & Heggie, D. C. 2012, MNRAS, **420**, 2700
Law, D. R., & Majewski, S. R., 2010, ApJ, 714, 229
Law, D. R., Majewski, S. R., & Johnston, K. V. 2009, ApJ, 703, L67
Leon, S., Meylan, G., & Combes, F. 2000, A&A, **359**, 907
Li, J., Newberg, H. J, Carlin, J. L, Deng, L., Newby, M., Willett, B. A., Xu, Y., & Luo, Z. 2012, ApJ, **757**, 151
Lux, H., Read, J. I., Lake, G., & Johnston, K. V. 2012, MNRAS, **424**, 16
Majewski, S. R., Skrutskie, M. F., Weinberg, M. D., & Ostheimer, J. C. 2003, ApJ 599, 1082
Martin, C., Carlin, J. L., Newberg, H. J., & Grillmair, C. J., 2013, ApJ **765**, 39
Martin, N. F. et al. 2014, ApJ, in press.
Martinez-Delgado, D., Gomez-Flechoso, M. A., Aparicio, A., & Carrera, R. 2004, ApJ, 601, 242
Mateo, M., Mirabal, N., Udalski, A., Szymanski, M., Kaluzny, J., Kubiak, M., Krezeminski, W, & Stanek, K. Z. 1996, ApJ, 458, L13
Newberg, H. J. et al. 2002, ApJ, 569, 245
Newberg, H. J., Yanny, B., Cole, N., Beers, T. C., Florentin, P. R., Schneider, D. P., & Wilhelm, R. 2007, ApJ, **668**, 221
Newberg, H. J., Yanny, B., & Willett, B. A. 2009, ApJ, **700**, L61
Newberg, H. J., Willett, B. A., Yanny, B., & Xu, Y. 2010, ApJ, **711**, 32
Odenkirchen, M. et al. 2001, ApJ, 548, L165
Odenkirchen, M., Grebel, E. K., Dehnen, W., Rix, H.-W., Yanny, B., Newberg, H. J., Rockosi, C. M., Martinez-Delgado, D., Brinkmann, J., Pier, J. R. 2003, AJ, 126, 2385
Odenkirchen, M., Grebel, E. K., Kayser, A., Rix, H.-W., & Dehnen, W. 2009, AJ, 137, 3378
Penarrubia, J., Martinez-Delgado, D., Rix, H. w., Gomez-Flechoso, M. A., Munn, J., Newberg, H., Bell, E. F., Yanny, B., Zucker, D. Grebel, E. K. 2005, ApJ, 626, 128
Rocha-Pinto, H. J., Majewski, S. R., Skrutskie, M. F., & Crane, J. D. 2003, 594, L115
Rockosi, C. M. et al. 2002, AJ, **124**, 349
Rossetto, B. M. et al. 2011, AJ, **141**, 185
Sales, L. V., Helmi, A., Starkenburg, E., Morrison, H. L., Engle, E., Harding, P., Mateo, M., Olszewski, E. W., & Sivarani, T. 2008, MNRAS, **389**, 1391
Sanderson, R. E., Helmi, A., & Hogg, D. W. 2014, arXive:1404.65341
Sesar, B. et al. 2013, ApJ, **776**, 26
Schlaufman, K. C. et al. 2009, ApJ, **703**, 2177
Shanks, D. J. et al. 2013, The Messenger, **154**, 38
Starkenburg et al. 2009, ApJ, **698**, 567–579
Toten, E. J., & Irwin, M. J. 1998, MNRAS, 294, 1
Tremaine, S. 1999, MNRAS, 307, 877
Vivas, A. K. et al. 2001, ApJ, **554**, L33
Vivas, A. K., Zinn, R., Gallart, C. 2005, AJ, 129, 189
Willett, B. A., Newberg, H. J., Zhang, H., Yanny, B., & Beers, T. C. 2009, ApJ, **697**, 207
Yam, W., Carlin, J. L., Newberg, H. J., Dumas, J., O'Malley, E., Newby, M., & Martin, C. 2013, ApJ, **776**, 133
Yanny, B. et al. 2003, ApJ, **588**, 824
Yoon, J. H., Johnston, K. V., & Hogg, D. W. 2011, ApJ, **731**, 58

Radial Migration in Spiral Galaxies

Rok Roškar and Victor P. Debattista

Abstract The redistribution of stars in galactic disks is an important aspect of disk galaxy evolution. Stars that efficiently migrate in such a way that does not also appreciably heat their orbits can drastically affect the stellar populations observed today and therefore influence constraints derived from such observations. Unfortunately, while the theoretical understanding of the migration process is becoming increasingly robust, there are currently few specific observable predictions. As a result, we do not yet have a clear handle on whether the process has been important for the Milky Way in the past or how to constrain it. I discuss some of the expected qualitative outcomes of migration as well as some current controversies.

1 Introduction

Galactic archaeology attempts to infer past history of our Milky Way disk from the rich datasets detailing stellar populations in terms of their chemistry, kinematics and ages. However, in order to ease interpretation, "population" is often loosely used to imply membership based on *current* cohabitation of a similar part of the Galaxy. This is borne out in the use of terminology like "the Solar Neighborhood" and the characterization of galactic disk properties in terms of the one-dimensional distance from the galactic center. For the most part, such groupings seem to make sense. After all, if the guiding radius R_g is defined by a star's angular momentum, i.e. $R_g \sim L_z/V_c$ where L_z is the z component of the angular momentum and V_c is the circular velocity, then the deviations from this radius during its orbit due to excess orbital energy are constrained to < 2 kpc *for the oldest stars* near the sun (Binney 2007). Furthermore assuming that the disk is mostly axisymmetric, then viewing the

R. Roškar (✉)
Institute for Computational Science, University of Zürich,
Winterthurerstrasse 190, CH-8057 Zürich, Switzerland
e-mail: roskar@physik.uzh.ch,

V. P. Debattista
Jeremiah Horrocks Institute, University of Central Lancashire,
PR1 2HE, Preston, UK

K. Freeman et al. (eds.), *Lessons from the Local Group,*
DOI 10.1007/978-3-319-10614-4_31

Solar Neighborhood as a representative random sample around $\sim R_{\odot}$ and using it to infer past history at this radius seems reasonable.

This simple assumption is remarkably powerful. By combining our knowledge of stellar evolution and metal production, just the metallicity distribution function (MDF) and the age-metallicity relation (AMR) are needed to infer the entire history of (this part of) the MW disk. Unfortunately, in its simplest incarnation, this type of modeling fails spectacularly in what is largely known as the 'G-dwarf problem', because it over-predicts the relative number of metal-poor stars (e.g. Searle and Sargent 1972; Tinsley 1975). One of the explanations for too many metal-poor stars is that the available gas is depleted too soon and therefore the simplest solution is to allow for an inflow of gas from the outside (Larson 1974; Lynden-Bell 1975). In this way, it is recognized that of course the Solar Neighborhood does not exist in isolation from other parts of the Galaxy, but that it is only a part of the whole.

Although gas is regarded free to stream in and out of the volume defining a local patch of the disk, stars are not usually assumed to do so due to small radial orbital excursions described above. While the authors themselves cautioned about observational bias resulting in the AMR, Edvardsson et al. (1993) data has frequently been used to support the idea that local stars of different ages represented generations of stars born out of the same recycled gas. This fits well with most one-dimensional chemical evolution models (e.g. Prantzos and Aubert 1995), which robustly predict a strong age-metallicity relation. However, more recent data (e.g. the Geneva-Copenhagen survey Holmberg et al. (2009) and its various re-interpretations, and the Gaia-ESO survey Bergemann et al. (2014)) show instead that the AMR is flat, that is, the AMR does not exist (Bergemann et al. (2014) do note, however, the lack of solar-metallicity stars older than 10 Gyr). The most striking feature of these observations is the large scatter in [Fe/H] at each age, which cannot easily be explained away by asymmetric drift arguments. These observations therefore expose a need to rethink disk evolution and let the stars jump out of the box.

2 Stellar Migration

If stars from very different parts of the disk can be found together today, and if there is a metallicity gradient in the star-forming gas, then a large spread in metallicity at each stellar age is expected. Consequently, much like gas flows were the answer to the G-dwarf problem, radial mixing of stars presents a convenient solution for the dispersed AMR problem described above. The idea that stars should be diffusing through the disk was first proposed by Wielen (1977), who suggested that determining the birth places of stars may be complicated due to orbital diffusion. However, because only diffusion due to random scattering off irregularities like GMCs was considered, the guiding radii R_g were shown to stay nearly constant (Grenon 1987). Nevertheless, Wielen et al. (1996) postulated that he Sun itself must have moved away from its birthplace in the inner disk, based on the fact that its metallicity is high compared to other stars of similar age in its vicinity. Using simplified arguments about the

evolution of the Milky Way metallicity gradient, they constrained the Sun's birthplace to be ~ 2 kpc closer to the Galactic center.

However, Sellwood and Binney (2002) showed that the treatment used in Wielen (1977), which considered only random scattering off GMCs, was insufficient as it did not take into account resonant interactions with spiral arms. In particular, Sellwoodand Binney (2002) showed that if a star's orbital speed matches the speed of a passing transient spiral wave, i.e. the star is at the corotation resonance of the spiral, the star's angular momentum L_z can be altered on a very short timescale. Due to the conservation of the Jacobi integral in such an interaction, the changes in energy and angular momentum are related simply by

$$\Delta E = \Delta L_z \Omega_p, \tag{1}$$

where Ω_p is the pattern speed of the passing spiral wave. Sellwoodand Binney (2002) showed also that the radial action, J_R of the migrating star changes as

$$\Delta J_R = \frac{\Omega_p - \Omega}{\omega_R} \Delta L_z, \tag{2}$$

where Ω and ω_R are the azimuthal and radial frequencies of the star. Therefore, at corotation, angular momentum and energy are exchanged without causing additional heating to the orbit, in stark contrast to changes in L_z at the Lindblad resonances where stars heat very efficiently. This remarkable result presents a serious hurdle for efforts trying to reconstruct Galactic history from present-day observations. Stellar kinematics are typically used to try and infer the dynamical histories of stars, i.e. postulate whether they had heated, were accreted, had interacted with the bar etc. If stars may change their guiding radii by *several* kpc without acquiring any kinematical trace of the process, it becomes very difficult to disentangle which stars are actually telling the story of this part of the Galaxy, and which are part of another history altogether.

There is an important caveat with regard to the corotation resonance. If the perturbing pattern is steady, the corotation resonance results simply in orbit trapping. In this case, a star on the inside of corotation gains angular momentum passing to the outside of corotation, where it is now leading the pattern slightly and being pulled back by the overdensity loses the previously gained angular momentum. This trapping results in a horseshoe orbit which in the steady-state remains at a constant L_z. Therefore, for the corotation resonance to impart secular changes to a star's angular momentum, the pattern must be transient but last just long enough to deposit the star on the other side of the resonance before it gets pulled back in the other direction.

3 Stellar Migration Mechanisms in Simulations

The expectation from Sellwood and Binney (2002) is therefore that if transient spirals are present, migration *must* take place. Figure 1 shows some examples of orbital histories from an idealized disk-formation simulation from Roškar et al. (2012). All

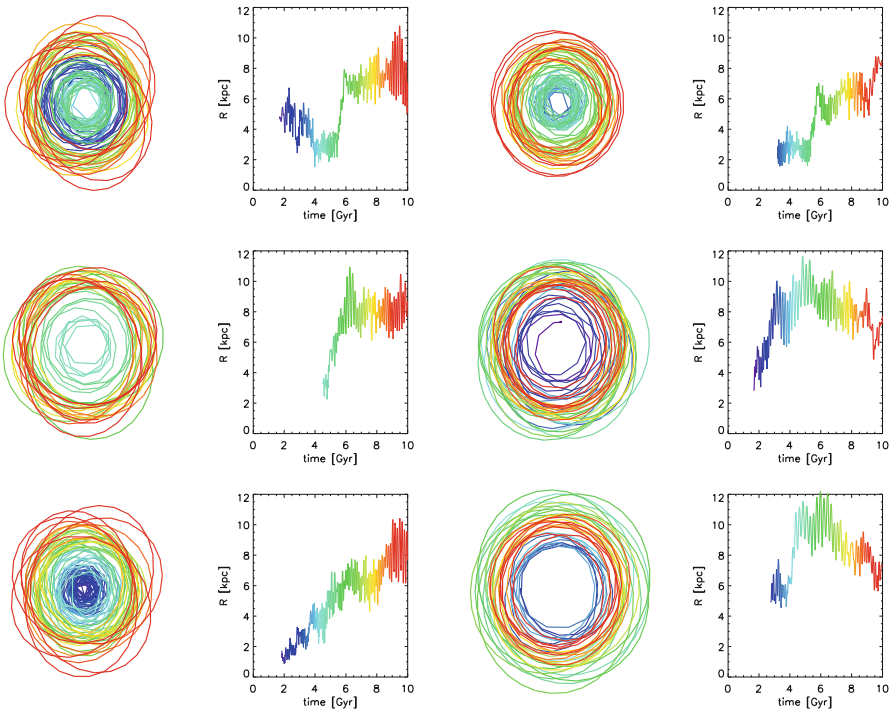

Fig. 1 Sample orbits from an idealized disk-formation simulation (Roškar et al. 2012). All particles are selected to be between 7–9 kpc at the end of the simulation

of the stars were selected to be between 7 and 9 kpc at the end of the simulation, but clearly they originated in very different places in the disk and had diverse orbital histories. Interactions with spirals lead some stars to migrate inwards, others migrate outwards, some orbits become more eccentric and others circularize.

Investigating the reasons for migration in their models further, Roškar et al. (2012) confirmed that the most likely mechanism for the large migrations occurring on short timescales was the corotation resonance mechanism of Sellwood and Binney (2002). Figure 2 shows one piece of evidence supporting this hypothesis: the top 5 % of migrators in the specified time interval straddle the peak of the spiral density wave at the distance corresponding to its corotation resonance. In addition, Roškar et al. (2012) showed that the particles cross corotation precisely at the time of peak spiral amplitude and that their Jacobi integrals are conserved during the migration phase, all of which are expected in the corotation resonance picture (Sellwood and Binney 2002).

In the models of Sellwood and Binney (2002) and Roškar et al. (2012), the spiral structure was shown, using Fourier methods (e.g. Sellwood and Athanassoula 1986), to host discrete pattern speeds with well-defined resonances. However, in some models the spiral structure pattern speed appears to match the rotation speed of the

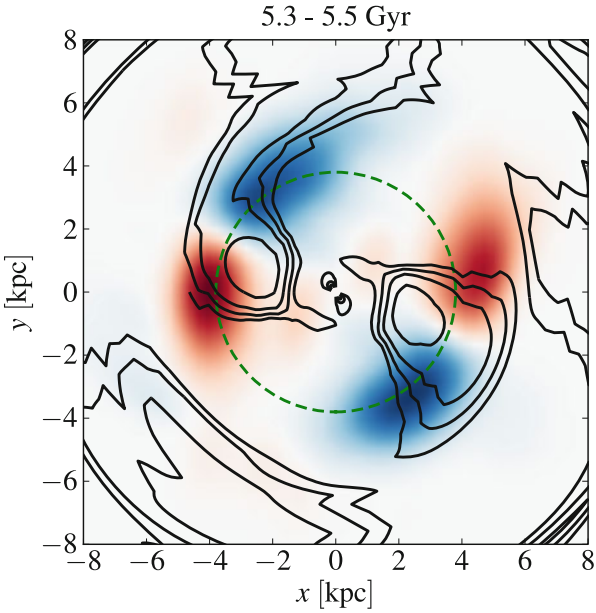

Fig. 2 Inward (*red*) and outward (*blue*) migrator density in the time interval from 5.3–5.5 Gyr. The particles are chosen only by virtue of being in the top 5 % of the ΔL_z distribution over this time interval. The *contours* show the stellar density reconstructed from the m = 2-4 Fourier components. The *dashed green line* shows the location of the corotation resonance for circular orbits

disk, essentially making the entire disk co-rotate with the spiral (e.g. Grand et al. 2012). Kawata et al. (2014) claim to have detected a signature of such spiral structure in the MW through a combination of measurements of gas and stellar motions. On the other hand, Meidt et al. (2009) used the modified Tremaine-Weinberg method to recover pattern speeds in several external galaxies and found that in general the pattern speeds were discrete, though the co-rotating spirals tend to be found in disks with lower surface-densities. The implications of co-rotating spirals is that mixing can be extremely efficient, though it is not clear whether it should lead to a unique chemo-dynamical signature.

Galactic disks are very prone to perturbations, so it is not surprising that other suggestions for redistributing material in the disks abound in the literature. For example, disks galaxies evolving in a cosmological environment are expected to undergo frequent encounters with substructure, which will not only disturb the disk (e.g. Kazantzidis et al. 2009) but also cause redistribution that can mimic migration due to the corotation resonance (Quillen et al. 2009).

Another important consideration is the influence of bars on the dynamical evolution of the disk. Bars are robust structures that once formed evolve slowly. During the initial bar growth phase, angular momentum is redistributed very efficiently but the process also results in a significant amount of heating (Debattista et al. 2006). When fully formed, bars mostly heat the disk through the inner and outer Lindblad resonances. Since bars are not transient, efficient exchange of angular momentum is not expected at the corotation resonance, because stars are mostly trapped on horseshoe orbits. However, Minchev and Famaey (2010) argued that in the presence of

overlapping resonances from other disk structure, the horseshoe orbits can be disrupted and stars may efficiently gain or lose angular momentum in a similar fashion to the transient spiral mechanism of Sellwood and Binney (2002). Such resonance overlap should result in non-linear evolution near the resonances whenever multiple patterns are present. Roškar et al. (2012) looked for signatures of this in their models where several spirals coexisted but found no clear evidence of this process. The orbits of stars undergoing rapid migration instead remained regular and clear signs of chaos were not found. Di Matteo et al. (2013) also argued that even steady bars can drive migration well after the instability epoch, but it is not clear whether the stellar dispersal in their model is due to heating and disk spreading or genuine radial migration. The diffusion of "hot stars" in barred galactic disks was shown already by Pfenniger and Friedli (1991), but those stars are distinctly chaotic and would result in non-circular orbits with large proper motions, which is very different from the Sellwood and Binney (2002) migrators described above.

In light of this discussion, it is crucial to point out that among the various mechanisms that can move material around the disk quickly and efficiently, migration due to the corotation resonance stands out because it causes very little radial heating. Satellite perturbations and bar formation, for example, affect the disk very differently and these diverse processes should not all be placed under the common label of "radial migration". They describe very different physical processes and should be treated as such. However, just as the corotation migration causes little heating, it also has the largest effect on cool stellar populations. Therefore, models whose velocity dispersions are too high may not show signatures of radial mixing that are representative of the Sellwood and Binney (2002) migration mechanism. Collisionless models with strong bars are strong candidates for this category, since the bar formation episode heats the disk very rapidly and can serve to prevent more subtle disk structure needed for radial migration from forming.

4 Influence of Migration on Disk Stellar Populations

4.1 Solar Neighborhood and Outer Disks

One of the clear results of radial mixing is that it increases the diversity of stellar populations everywhere in the disk, which is especially important for Solar Neighborhood diagnostics like the AMR relation (Roškar et al. 2008a, b; Schönrich and Binney 2009; Sellwood and Binney 2002). The left panel of Fig. 3 shows the distribution of formation radii for stars that end up between 7 and 9 kpc on mostly-circular orbits in the simulation of Roškar et al. (2008a, b), clearly indicating that stars born everywhere in the galaxy may find themselves in this part of the disk; 50 % of these stars originated at $R < 6$ kpc. Such redistribution has obvious consequences for the AMR (middle panel) and the MDF (right panel)—the AMR is flattened and the dispersion in metallicity at each age increases significantly, while the MDF is significantly broadened.

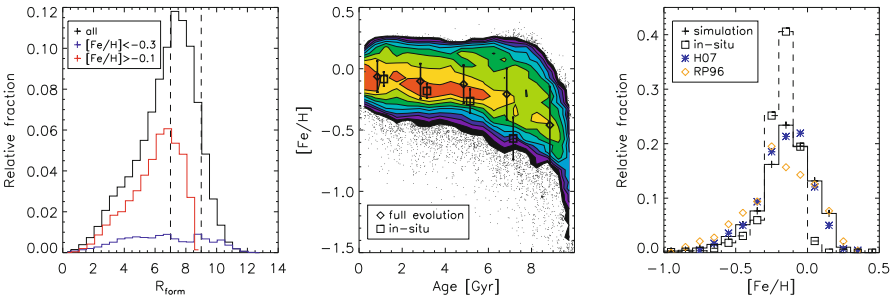

Fig. 3 *Left:* distribution of formation radii for particles found within the solar neighborhood (defined to be $7 < R < 9$ kpc) at the end of the simulation from Roškar et al. (2008a, b). *Center:* The age-metallicity relation (AMR) in the solar neighborhood. Migration adds significantly to the dispersion in metallicities at each age. *Right:* Metallicity distribution function (MDF) is significantly broadened by migration

A related and surprising early result of radial migration studies was that in a truncated disk (e.g. Pohlen and Trujillo 2006), the stellar age profile is expected to show an upturn beyond the break radius (Roškar et al. 2008a, b). This prediction has been confirmed by a number of observational studies, both indirectly in terms of color gradients (Bakos et al. 2008) and directly from stellar population modeling using IFU observations (Yoachim et al. 2010) as well as HST resolved-star data (Radburn-Smith et al. 2012). While this prediction is not unique to radial mixing, since it is possible that the outer disks are influenced also by cosmological gas accretion and subsequent star formation (e.g. Sánchez-Blázquez et al. 2009), radial migration nevertheless can deposit significant amounts of material in outer disks. The redistributed material can perhaps overshadow the stars formed from accreted gas (Roškar et al. 2010) so the age inversion remains one of the few robust predictions of the process that have been confirmed by observations.

4.2 Migrated Stars in the Thick Disk?

The thick disk is arguably one of the most coveted structures in the Milky Way, because of its potential to inform us about the early epoch of Milky Way's disk formation. The possibility that radial migration can influence and partially populate the thick disk has therefore received much attention in recent years. The concept is quite simple: as a star changes its radial distance from the galactic center, the change in the vertical restoring force felt at different parts of the orbit affects its vertical displacement due to action conservation (Binney and Tremaine 2008; Schönrich and Binney 2012). This depends on how much of the potential is due to the disk (the MW disk is believed to be close to maximal, Bovy and Rix 2013) and the effect is compounded when the star's guiding center is also changing.

In the model of Loebman et al. (2011) stars far away from the mid-plane at radii 7–9 kpc were found to be predominantly old and to originate in the inner disk, compared with stars closer to the mid-plane which were found to be younger and formed locally. They also showed that the V_ϕ - [Fe/H] were anti-correlated for young stars and only slightly correlated for old stars in the solar neighborhood. This is easy to understand in the context of migration because young stars have not had time to migrate significantly and were therefore populating the local volume by virtue of mild heating. The young stars coming from the outer disk therefore had lower metallicities and higher rotational velocities, while the opposite was true for those coming from the inner disk. The old stars, on the other hand, had time to migrate and mix and therefore showed only a weak trend between metallicity and rotational velocity. The models qualitatively agree with recent observations such as from Lee et al. (2011), which also show a strong negative correlation between metallicity and V_ϕ for young (α-deficient) stars and a slight positive correlation for old (α-enhanced) stars. Quantitatively, the models do not agree with the data, though they also are not designed to reproduce the MW. The flattening of the V_ϕ-[Fe/H] relation for old stars in the model is certainly due to the radial mixing but in this particular model it does not turn into an overwhelmingly positive correlation so it is not clear whether an external process is required. Note that this observation poses a problem for all scenarios where the disk grows from the inside out because it requires the metal poor and metal rich stars to swap places in the disk at some well-defined epoch, when the α-enhancement is still high.

The influence of radial migration on the thickness of stellar populations in the models from Loebman et al. (2011) was explored in detail by Roškar et al. (2013). They showed that vertical thickening is a function of both age (i.e. heating) and radial displacement in the disk. In other words, orbits of stars of the same age, which experienced a similar amount of heating, become vertically more extended if they migrate outwards and more compressed if they migrate inwards. At the same time, stars from the same part of the disk that migrate by a similar amount are thicker if they are older. These results also showed that as stars move radially in the disk, their vertical velocity dispersions decreased for inward migration and increased for outward migration, confirming the effect shown by Minchev et al. (2012).

It should be stressed that the increase of scale-height with outward migration is not incompatible with the idea that the vertical action is conserved and a consequent decrease in velocity dispersion. If the velocity dispersion decreases as $\sigma_z \propto e^{-R/2R_d}$ (Minchev et al. 2012), and we make an assumption that the disk is in hydrostatic equilibrium with a sech^2 vertical density profile, it is easy to show that the scale height $h_z \propto e^{R/R_d}$ and therefore

$$\frac{h_{z,f}}{h_{z,i}} \propto \exp\left(\frac{\Delta R}{2R_d}\right), \tag{3}$$

where $h_{z,i}$ and $h_{z,f}$ are the initial and final scale heights of the population and ΔR is the change in radius. Thus, the change in scale height with radial displacement follows naturally from action conservation (see also Schönrich and Binney 2012 for a better approximation).

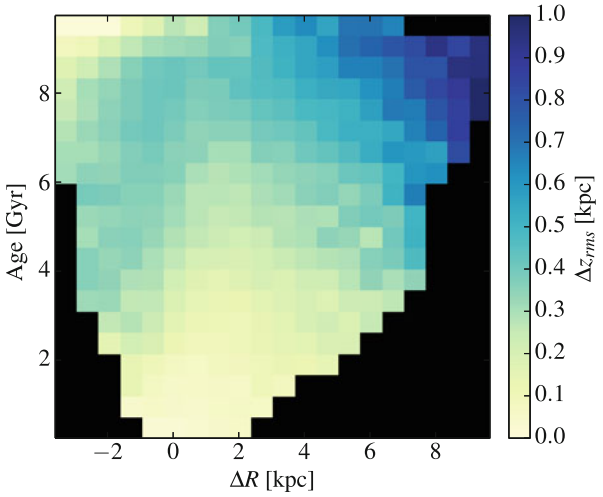

Fig. 4 Total change in z_{rms} (proxy for thickness) for stars forming between 2–4 kpc as a function of age and change in radius

4.3 Limitations of Simulations

The study of Roškar et al. (2013) showed unequivocally that a single population migrating outwards in their model will thicken, as expected based on the fact that the vertical actions are, on average, conserved (Solway et al. 2012). Does this mean that migration can form a thick disk? There are several caveats one must consider when interpreting simulated disks and their usefulness in generalizing disk thickening.

First, a disk must be resolved vertically in order for the simulation to say anything useful about the disk thickening process. In Roškar et al. (2013) the spatial resolution is 50 pc, but resolutions of > 100 pc are not uncommon in the literature dealing with vertical disk evolution. This means that within approximately one scale-height of the mid-plane, the forces on the particles are too low. The effect of this on migration studies has not been carefully scrutinized, but it is clear that it can affect how thick a migrated population looks compared to the stars already present at a given radius.

Second, when investigating the effect of migrators on the in-situ population, one must carefully consider the realism of the simulated star-forming layer, or in the case of collisionless simulations the assumptions about the initial disk structure. In Roškar et al. (2013), the gas disk out of which stars formed was significantly flared, meaning that although stars from the inner disk increased their thickness as they migrated outwards, they did not appear thicker than the in-situ population *because the in-situ population was thicker from the outset*. This is a general problem with hydrodynamic simulations using a temperature floor, since this means a fixed dispersion at all radii and consequently a radially increasing scale height h_z for the young stars because $h_z \propto \sigma_z/\Sigma$, where Σ is the disk surface density. However, while in that model the migrated stars therefore did not alone cause the thickening of the disk, they themselves still thickened as they migrated outwards. Therefore,

they would not have been in the thicker part of the disk in the first place was it not for the migration. These stars therefore certainly influenced the chemical abundance distributions at large distances from the plane even if their effect on thickening was not large. The question of migration and the thick disk is not necessarily whether migration can *create* a thick disk, but whether the chemical abundance patterns that characterize the thick disk can be influenced by migration.

Finally, numerical relaxation effects may have a disproportionate influence on the vertical structure of disks (Sellwood 2013). Therefore, numerical convergence tests must be performed to determine the robustness of simulated structures, since no obvious rule exists regarding sufficient particle numbers. This is further complicated by the fact that the evolution of disks is often highly stochastic, particularly when the disk supports multiple spiral modes (Roškar et al. 2012; Sellwood and Debattista 2009). Nevertheless, such tests can reveal strong divergences for certain parameter choices: for example, Roškar et al. (2012) showed that if they used 500 pc softening instead of 100 pc or less, the disk formed completely different non-axisymmetric structure. Determining whether numerical relaxation is affecting the disk may be considerably more difficult for most applications.

5 Conclusions and Challenges for the Future

By enriching the stellar diversity in any given part of the Galactic disk, radial migration of stars complicates our interpretations of the stellar population record left behind by the process of disk formation. Migration due to the corotation resonance is inherently a complicated process, due to its dependence on resonances with transient structure that is difficult to constrain. Such migration is special among the processes that redistribute material in galactic disks, because it introduces very little heating and therefore leaves behind no straightforward kinematic signatures. For this reason, N-body simulations have been instrumental in furthering our understanding of the underlying process.

At the same time, the simulations exploring the observational effects of migration have been very limited. On top of the dynamical complexity, simulations try to add in the processes of star formation and chemical enrichment in order to shed light on the expected effects in stellar population trends that migration leaves behind. While the purely dynamical modeling is potentially prone to numerical effects (as discussed above in relation to resolving disk scale heights), those are small compared to the uncertainties involved with sub-grid modeling required for capturing star formation and chemical enrichment within 3D N-body numerical simulations. We should therefore consider it a huge triumph that these simulations can agree with observations at all!

In the upcoming years, as data from Gaia, the GALAH survey (Freeman 2012), and other similar large-scale projects become available, simulations will be critical in aiding our interpretations of those results. Nevertheless, to fully utilize those datasets, the theoretical efforts need to strive for an understanding of the leverage that various numerical and physical parameters exert on the process of radial mixing.

On the other hand, one hopes that chemical tagging (Freeman and Bland-Hawthorn 2002; Mitschang et al. 2013) will directly constrain how much radial mixing has taken place in the MW disk. Combining such constraints with a clearer picture of the underlying physical drivers of the mixing process, we should be in a much better position to unravel the past history of our MW disk.

Acknowledgements RR is funded in part by a Marie Curie Career Integration Grant.

References

Bakos J., Trujillo I., Pohlen M., 2008, ApJL, 683, L103
Bergemann M., Ruchti G., Serenelli A., Feltzing S., Alvez-Brito A., Asplund M., Bensby T., Heiter U., Korn A., Lind K., et al., 2014, A&A, 565, A89
Binney J., 2007, Dynamics of Disks. p. 67
Binney J., Tremaine S., 2008, Galactic Dynamics: Second Edition. Princeton University Press
Bovy J., Rix H.-W., 2013, ApJ, 779, 115
Debattista V. P., Mayer L., Carollo C. M., Moore B., Wadsley J., Quinn T., 2006, ApJ, 645, 209
Di Matteo P., Haywood M., Combes F., Semelin B., Snaith O. N., 2013, A&A, 553, A102
Edvardsson B., Andersen J., Gustafsson B., Lambert D. L., Nissen P. E., Tomkin J., 1993, A&A, 275, 101
Freeman K. C., 2012, in Aoki W., Ishigaki M., Suda T., Tsujimoto T., Arimoto N., eds, Galactic Archaeology: Near-Field Cosmology and the Formation of the Milky Way Vol. 458 of Astronomical Society of the Pacific Conference Series, The HERMES Project: Reconstructing Galaxy Formation. p. 393
Freeman K., Bland-Hawthorn J., 2002, ARA&A, 40, 487
Grand R. J. J., Kawata D., Cropper M., 2012, MNRAS, 421, 1529
Grenon M., 1987, Journal of Astrophysics and Astronomy, 8, 123
Holmberg J., Nordström B., Andersen J., 2009, A&A, 501, 941
Kawata D., Hunt J. A. S., Grand R. J. J., Pasetto S., Cropper M., 2014, ArXiv e-prints
Kazantzidis S., Zentner A. R., Kravtsov A. V., Bullock J. S., Debattista V. P., 2009, ApJ, 700, 1896
Larson R. B., 1974, MNRAS, 169, 229
Lee Y. S., Beers T. C., An D., Ivezić Ž., Just A., Rockosi C. M., Morrison H. L., Johnson J. A., Schönrich R., Bird J., Yanny B., Harding P., Rocha-Pinto H. J., 2011, ApJ, 738, 187
Loebman S. R., Roškar R., Debattista V. P., Ivezić Ž., Quinn T. R., Wadsley J., 2011, ApJ, 737, 8
Lynden-Bell D., 1975, Vistas in Astronomy, 19, 299
Meidt S. E., Rand R. J., Merrifield M. R., 2009, ApJ, 702, 277
Minchev I., Famaey B., 2010, ApJ, 722, 112
Minchev I., Famaey B., Quillen A. C., Dehnen W., Martig M., Siebert A., 2012, A&A, 548, A127
Mitschang A. W., De Silva G., Sharma S., Zucker D. B., 2013, MNRAS, 428, 2321
Pfenniger D., Friedli D., 1991, A&A, 252, 75
Pohlen M., Trujillo I., 2006, A&A, 454, 759
Prantzos N., Aubert O., 1995, A&A, 302, 69
Quillen A. C., Minchev I., Bland-Hawthorn J., Haywood M., 2009, MNRAS, 397, 1599
Radburn-Smith D. J., Roškar R., Debattista V. P., Dalcanton J. J., Streich D., de Jong R. S., Vlajić M., Holwerda B. W., Purcell C. W., Dolphin A. E., Zucker D. B., 2012, ApJ, 753, 138
Roškar R., Debattista V. P., Quinn T. R., Stinson G. S., Wadsley J., 2008a, ApJL, 684, L79
Roškar R., Debattista V. P., Stinson G. S., Quinn T. R., Kaufmann T., Wadsley J., 2008b, ApJL, 675, L65

Roškar R., Debattista V. P., Brooks A. M., Quinn T. R., Brook C. B., Governato F., Dalcanton J. J., Wadsley J., 2010, MNRAS, 408, 783
Roškar R., Debattista V. P., Quinn T. R., Wadsley J., 2012, MNRAS, 426, 2089
Roškar R., Debattista V. P., Loebman S. R., 2013, MNRAS, 433, 976
Sánchez-Blázquez P., Courty S., Gibson B. K., Brook C. B., 2009, MNRAS, 398, 591
Schönrich R., Binney J., 2009, MNRAS, 396, 203
Schönrich R., Binney J., 2012, MNRAS, 419, 1546
Searle L., Sargent W. L. W., 1972, ApJ, 173, 25
Sellwood J. A., 2013, ApJL, 769, L24
Sellwood J. A., Athanassoula E., 1986, MNRAS, 221, 195
Sellwood J. A., Binney J. J., 2002, MNRAS, 336, 785
Sellwood J. A., Debattista V. P., 2009, MNRAS, 398, 1279
Solway M., Sellwood J. A., Schönrich R., 2012, MNRAS, 422, 1363
Tinsley B. M., 1975, ApJ, 197, 159
Wielen R., 1977, A&A, 60, 263
Wielen R., Fuchs B., Dettbarn C., 1996, A&A, 314, 438
Yoachim P., Roškar R., Debattista V. P., 2010, ApJL, 716, L4

Manifestations of the Galactic Center Magnetic Field

Mark R. Morris

Abstract Several independent lines of evidence reveal that a relatively strong and highly ordered magnetic field is present throughout the Galaxy's central molecular zone (CMZ). The field within dense clouds of the central molecular zone is predominantly parallel to the Galactic plane, probably as a result of the strong tidal shear in that region. A second magnetic field system is present outside of clouds, manifested primarily by a population of vertical, synchrotron-emitting filamentary features aligned with the field. Whether or not the strong vertical field is uniform throughout the CMZ remains undetermined, but is a key central issue for the overall energetics and the impact of the field on the Galactic center arena. The interactions between the two field systems are considered, as they are likely to drive some of the activity within the CMZ. As a proxy for other gas-rich galaxies in the local group and beyond, the Galactic center region reveals that magnetic fields are likely to be an important diagnostic, if not also a collimator, of the flow of winds and energetic particles out of the nucleus.

1 Introduction

The Central Molecular Zone (CMZ) of the Galaxy, which represents the strongest concentration of molecular gas in the Galaxy, is immersed in a magnetic field that is manifested in two rather distinct ways. First, the field within clouds appears to be predominantly toroidal, that is, oriented parallel to the Galactic plane, while the field external to clouds or in low-density gas is largely poloidal, or perpendicular to the Galactic plane. The following sections describe the evidence for each of these separately, and present the implications for the interactions of the two components. Previous reviews that emphasize other aspects of the magnetic field are given by Bicknell and Li (2001); Morris (2006) and Ferrière (2009, 2011). What has been learned from the Galactic center is probably generalizable to other barred galaxies having a substantial gas content in their central regions. However, it is only in our Galaxy that present techniques allow us to elucidate the essential details (Fig. 1).

M. R. Morris (✉)
Department of Physics and Astronomy, University of California, Los Angeles, USA
e-mail: morris@astro.ucla.edu

K. Freeman et al. (eds.), *Lessons from the Local Group,*
DOI 10.1007/978-3-319-10614-4_32

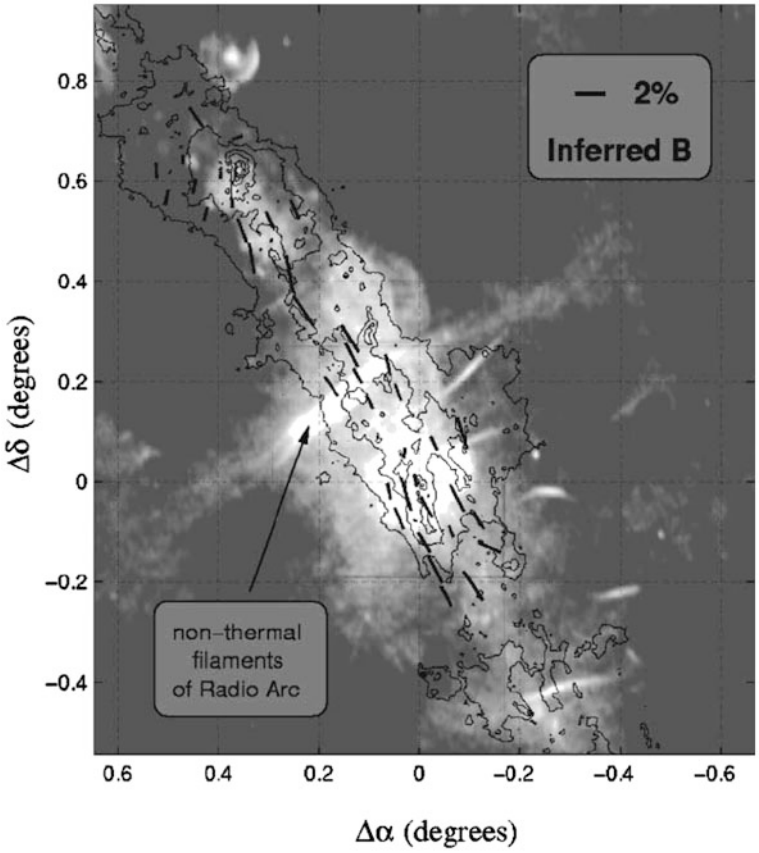

Fig. 1 Magnetic field vectors inferred from polarization measurements at 450 μm by Novak et al. (2003) superimposed upon a grayscale 90-cm radio continuum image from LaRosa et al. (2000) and contours of 850 μm continuum emission from Pierce-Price et al. (2000)

2 The Sheared Field in the Central Molecular Zone

The most successful way of probing the field within molecular clouds of the CMZ has been by measuring the polarization of the thermal emission from magnetically aligned dust grains (Hildebrand 2002). For a wide range of interpretations of the alignment mechanism, the field direction projected onto the plane of the sky is perpendicular to the measured polarization E-vector (Lazarian 2007). Measurements have been made at far-infrared (e.g., Chuss et al. 2003), submillimeter (e.g., Novak et al. 2003), and near-infrared (Nishiyama et al. 2010) wavelengths. On large scales near the Galactic plane, the field direction is generally found to be parallel to the Galactic plane, although in detail, the field direction tends to follow the long axis of the cloud being observed (Chuss et al. 2003). This has been attributed to tidal shear

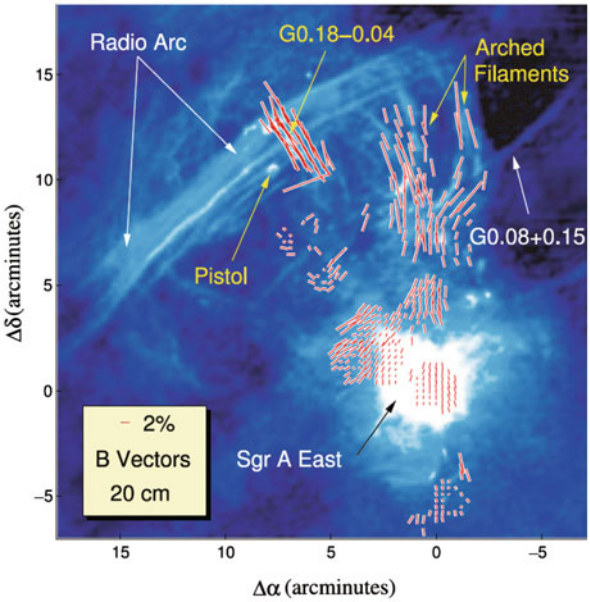

Fig. 2 Magnetic field vectors derived by Chuss et al. (2003) from polarization measurements, superimposed upon a 20-cm radio continuum image from Yusef-Zadeh et al. (1984). The Galactic plane is oriented in a position angle of about 30 degrees, so that the field vectors in G0.18-0.04 are well aligned along it. These vectors, plus the bundle of NTFs in the Radio Arc, best illustrate the orthogonality between the field inside and outside of clouds (see discussion in Morris and Serabyn 1996). Note also that the field in the arched radio filaments, which outline the surface of an underlying molecular cloud, follows the filament orientations quite closely. In addition, the indicated field directions in several low-density regions do not conform to the toroidal trend for field vectors in more massive clouds such as G0.18-0.04

of gas in the CMZ (Aitken et al. 1991, 1998; Chuss et al. 2003). The Galactic tidal force near the center is strong enough that clouds are not stable against tidal shear unless their density exceeds a fairly large value, 10^4 cm^{-3} [75 pc/R_{gc}]$^{1.8}$ (Güsten 1989), where R_{gc} is the galactocentric radius. Consequently, many of the "clouds" in the CMZ are in fact best described as tidal streams, some of which subtend a large wrapping angle around the Galactic center (e.g., Tsuboi et al. 1999). This continuous shearing, coupled with flux-freezing of the magnetic field to the partially ionized molecular medium, transforms any pre-existing magnetic field geometry within the clouds into one that is dominated by a large-scale toroidal (i.e., azimuthal) component in which the field lines follow the shear. Clouds that, for whatever local reason, are sheared in a direction at some angle to the Galactic plane, such as M0.10+0.02, the molecular cloud underlying the arched radio filaments (Morris et al. 1992; Chuss et al. 2003), are consistent with this picture, inasmuch as the field tends to follow the long axis of such clouds. These points are well illustrated by Fig. 2, from Chuss et al. (2003), which shows measured magnetic field vectors superimposed on a radio map.

The parsec-scale circumnuclear disk (CND) around the central black hole is an illustrative case that is consistent with the anticipated effects of shear. Field vectors implied by the 100-μm polarization measurements of Hildebrand et al. (1993) are consistent with a self-similar model by Wardle and Konigl (1990) in which an initially vertical field threading the differentially rotating disk is pulled into an axisymmetric configuration. The $\sim 20^\circ$ tilt of the CND with respect to the Galactic plane is reflected in the orientation of the inferred magnetic field vectors. The CND will be a key object for investigating the interplay between gas dynamics and the magnetic field as higher resolution polarization measurement capabilities are brought to bear on it in the future, such as with the HAWC+ instrument on SOFIA.

The above generalizations about shearing do not necessarily apply to the densest clouds of the CMZ—those which are presumed tidally stable. In such cases, the field geometry would reflect the peculiar dynamical history of the cloud, although shearing that took place in some of the pre-existing constituents of a dense cloud might still lead to its having a dominant toroidal field. The field vectors in the dense M-0.13-0.08 cloud are roughly parallel to the Galactic plane (Dotson et al. 2010), and might therefore provide an illustration of this last point. The dense clouds M-0.02-0.07 and Sgr B2, on the other hand, show field vectors that are complex and generally inconsistent with an overall toroidal geometry (Novak et al. 1997; Dotson et al. 2010). In the case of Sgr B2, the complexity is compounded by high optical depths in the dust emission; some of the polarization vectors in the central regions of Sgr B2 are determined by foreground absorption within the source (Novak et al. 1997).

Chuss et al. (2003) find a striking relationship between dust column density, as inferred from their measured 350m flux, and the mean angle between the measured polarization E-vector and that which would pertain to a purely poloidal magnetic field. They interpret this in terms of a pervasive poloidal field throughout the central few hundred parsecs of the Galactic center that becomes progressively more toroidal as the gas density increases, with the ratio of the gravitational energy density to the magnetic energy density therefore rising with density until the gravitational shear produces a toroidal magnetic field geometry in the relatively dense gas. Using their submillimeter fluxes to obtain column densities, Chuss et al. (2003) derive a strength for the poloidal magnetic field of a few milligauss[1]. A likely related trend was reported by Nishiyama et al. (2010). They find from their near-infrared observations that the mean magnetic field orientation evolves smoothly from a toroidal field near the Galactic plane to a poloidal field at Galactic latitudes above 0.4°. However, in contrast to Chuss et al. (2003), and in spite of their lower spatial resolution, Nishiyama et al. consider that the magnetic field near the Galactic plane remains toroidal even in the intercloud medium. Implications of the dual field geometry are discussed further below.

[1] If applicable, this and the considerations in the previous paragraph imply that there is both a lower and an upper limit to the density of clouds within which the field is likely to be toroidal.

3 Nonthermal Radio Filaments—the Poloidal Field

Over the past 30 years, the VLA has revealed a population of filamentary radio structures rising from within the CMZ. Their emission is polarized, indicative of synchrotron emission, and when the polarized E-vectors are corrected for foreground Faraday rotation, the implied magnetic field direction is found to be aligned with the nonthermal filaments (NTFs). Numerous ideas have been advanced to account for the NTFs (references in Morris 1996; Chevalier 1992; Rosner and Bodo 1996; Shore and LaRosa 1999; Bicknell and Li 2001; Yusef-Zadeh 2003; Boldyrev and Yusef-Zadeh 2006), but there is presently no consensus on the nature of the mechanism that has produced them. One important clue is that the predominant orientation of the NTFs—particularly the brighter and longer ones—is roughly perpendicular to the Galactic plane (Morris and Yusef-Zadeh 1985; Anantharamaiah et al. 1991; Nord et al. 2004; Yusef-Zadeh et al. 2004), as Fig. 1 illustrates. This has led some to the notion that there is a pervasive vertical field throughout the central ∼100 pc that is illuminated locally where relativistic electrons happen to be injected. Those electrons are constrained to diffuse primarily along the field lines, thereby producing the NTFs. The alternative is that the filaments are a local phenomenon, in which tubes of enhanced magnetic flux are produced by a phenomenon such as turbulence. In the model of (Boldyrev and Yusef-Zadeh 2006), for example, the enhanced-field filaments are confined by the effective pressure of large-scale turbulence. In their model, the turbulent cells expulse the field, and concentrate it in regions between the cells. A strong constraint of this model is that the helicity of the turbulence must be organized in such a way that the resulting NTFs are predominantly vertical. Another local model for NTF production is that of Shore and LaRosa (1999), in which the NTFs are interpreted as the plasma tails of molecular clouds in a Galactic wind. In the context of this scenario, it is not evident how local production of NTFs can lead to orientations of most of the NTF population on scales of a few hundred parsecs.

The other important clue to the nature of the NTFs is that all of them that have been adequately investigated appear to be undergoing an interaction with a molecular cloud somewhere along their length. Serabyn and Morris (1994) used this fact, and the orthogonality of the magnetic field in NTFs and that inside of clouds, to argue that the relativistic electrons responsible for the radio emission are produced by magnetic field line reconnection at cloud surfaces. The availability of free electrons is also an important element; the interaction sites of the clouds and the NTFs occur where the cloud surfaces have been ionized by a local stellar source of UV radiation. Not only do the surface HII regions supply the electrons, but the turbulent ionization fronts also mix the external and internal magnetic field systems, thereby enhancing the rate of reconnection. Examples of such interfaces include the G359.1-0.2 and G359.54+0.18 NTFs (Uchida et al. 1996; Staguhn et al. 1998, respectively), but there are numerous others.

A fraction of the NTFs does not conform to the uniform poloidal field picture. A few relatively long filaments (10's of pc) are tilted by relatively large angles relative to the vertical to the Galactic plane, and a population of short NTFs appears

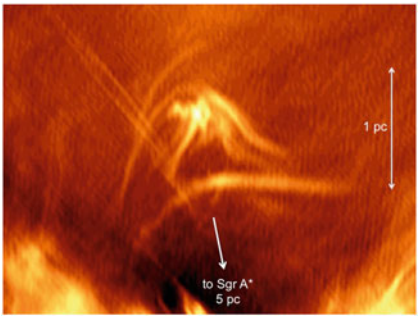

Fig. 3 The "Northern Curl" radio source, as observed with the JVLA at 6 cm (Morris et al. 2014, in preparation). All of the emission in this image is nonthermal. The direction to Sgr A* is indicated. A similar, but larger feature is observed on the opposite side of Sgr A*. The doubled filament that is superimposed on the strongly deformed magnetic structure is approximately parallel to the Galactic plane, and represents one of the small NTFs that does not conform to the presumed large-scale poloidal field

to have more or less random orientations (Lang et al. 1999; LaRosa et al. 2004; Yusef-Zadeh et al. 2004). The randomly oriented filaments may represent a separate population produced by local events such as jets or supernova shocks that can deform the magnetic field. Some of the non-conforming NTFs are clearly formed in this way. A few strongly curved NTFs in the Sgr A radio complex, for example, have their centers of curvature facing Sgr A*, suggesting that collimated outflows from the central black hole or the region around it have deformed what might otherwise have been a uniformly vertical magnetic field (Morris et al. 2014). Figure 3 shows the most highly distorted example from that work.

The rigidity of the magnetic field in the NTFs, as suggested by their smoothly varying and large-scale curvatures and the absence of significant deformations, led to an estimate of milligauss field strength within them (Yusef-Zadeh and Morris 1987a, b). The argument rests on the fact that certain NTFs are clearly interacting with molecular clouds in which the internal velocity dispersion, ΔV, is large—a few tens of km/sec. Yet despite the interaction, the NTFs are perturbed in only the most subtle ways, such as a bending by a few degrees or a slight, large-scale indentation at the site of an apparent cloud impact (e.g., Tsuboi et al. 1997). The magnetic field pressure thus must be at least comparable to the internal turbulent pressure, $\rho \Delta V^2$, of the clouds, where ρ is the cloud mass density, *unless* the Alfvén speed is large enough to radiate away the perturbations to the field lines on sufficiently short time scales that they remain unobservable. One potential concern about the milligauss field strength estimate is the implied short synchrotron lifetime of the electrons (see Ferrière 2009), but Morris (2006) offers reasons why this need not be a fatal concern. Another potential concern is that, if the milligauss field is pervasive throughout a region of radius $R_{gc} \sim 100$ pc, the total magnetic energy is quite large, amounting to $4 \times 10^{54}\ B_{mg}^2\ (R_{gc}/100\ \mathrm{pc})^3$ ergs (Morris 1994). However, this is not too much greater than the total energy content of the diffuse $\sim 10^8$ K gas that might occupy

the central few hundred parsecs of the Galaxy (Koyama et al. 2009; Koyama 2011, and references therein), and it is substantially less than the magnetic energy content of the overlying Fermi Bubbles (see below Carretti et al. 2013). Whether the X-ray evidence can be ascribed to such a hot gas reservoir or to an unresolved collection of point sources (Muno et al. 2004; Revnivtsev et al. 2009) remains one of the key questions in current Galactic center research.

On scales of a several hundred parsecs—substantially larger than the region occupied by the NTFs—there are constraints on the magnetic field strength provided by the diffuse radio synchrotron emission from cosmic rays, coupled with gamma ray emission up to TeV energies (Crocker et al. 2010). Crocker et al. (2011) find that the average field strength on such large scales lies within the range from 0.06 to 0.4 mG. This is not grossly inconsistent with the estimates from NTFs, given the likelihood that the field diverges, and its strength thereby declines with distance, but it does raise the question of whether the milligauss fields have been overestimated, or whether the milligauss estimates apply only locally to the NTFs.

4 Coexistence of the Two Field Systems

Soon after the NTFs were discovered (Yusef-Zadeh et al. 1984), Uchida et al. (1985) formulated a model in which gas in the differentially rotating Galactic disk interacts with a globally poloidal field by dragging it into a twisted, toroidal configuration. Inflow of gas toward the center along the field lines then leads to a contraction of the field, which, in turn, could be invoked to drive a helical galactic outflow toward the poles. This model has inspired considerable discussion, and in particular has been invoked to explain how the field within intermediate-density clouds of the CMZ can be largely toroidal while the field outside of clouds above the Galactic plane appears to be poloidal (e.g., Chuss et al. 2003). However, the shapes of the NTFs do not support this hypothesis. There is no evidence that the field lines are coupled strongly to the gas in the Galactic disk, or that the inertia of that gas has twisted the field lines away from a predominantly vertical orientation. The Radio Arc, for example, punches through the Galactic plane without significant distortions being introduced (Figs. 1 and 2). Another example, the isolated radio "thread", G0.08+0.15 (shown in Fig. 2), also passes through the gas layer without acquiring a component along the Galactic plane. All evidence points to the conclusion that the field systems inside and outside of clouds are quite independent. Clouds orbit through a poloidal field, perhaps suffering some magnetic reconnection activity at their surfaces which can, under the right circumstances lead to the illumination of the field lines (Serabyn and Morris 1994), and perhaps encountering some magnetic drag (Morris 1994), but not interacting strongly enough to affect the field geometry or the cloud dynamics, except on very long time scales. Any momentum transferred from CMZ clouds to the mass-loaded field is carried away from the plane by Alfvén waves having wavelengths much larger than the scale of the CMZ. It follows that clouds "slip through" the vertical field lines; there is less energy required to displace the intercloud field lines

around an orbiting cloud than in compressing the intercloud field along the direction of the cloud's motion.

For the field within CMZ clouds, we are left with the following scenario. Because of dynamical friction (Stark et al. 1991), plus magnetic drag, the residence time of CMZ material is limited to somewhat less than 10^9 years. The gas is brought in to the CMZ from the Galactic disk by the action of the bar potential, and migrates inexorably inwards until it most likely forms stars (only a tiny fraction apparently reaches the central parsec), or is ejected in a Galactic wind. Consequently, the magnetic field within CMZ clouds has been brought in with the gas, and is amplified by the differential rotation that quasi-continuously stretches it into tidal streams. Eventually, the predominantly toroidal field within clouds equilibrates as some magnetic flux is carried away by the wind and some is lost to reconnection.

The evidence for a Galactic wind is growing. If diffuse hot gas is truly present at the Galactic center at a temperature near 10^8 K, then it is unbound and should lead to a bipolar Galactic wind (Muno et al. 2004; Belmont et al. 2005). Indeed, Nishiyama et al. (2010) invoke such a wind to account for the evolution of their inferred magnetic field vectors with Galactic latitude. Even in the absence of an unbound, hot plasma, however, the fairly active star formation in the CMZ, accompanied by supernovae, can drive a Galactic fountain that carries magnetic flux out of the CMZ (Crocker 2012). According to Crocker, cosmic rays associated with star formation and supernovae in the CMZ are advected out of the CMZ by the wind at the rate needed to account for the gamma-ray flux from the very-large-scale Fermi Bubbles (Su et al. 2010). A recent discovery by Carretti et al. (2013) of polarized radio lobes apparently wrapping around the Fermi Bubbles has led them to interpret this in terms of magnetic flux that has been carried out from the CMZ by the wind. The helical "wrapping" is ascribed to Galactic rotation, carrying the most recent source of the wind—a site of major star formation—around the Galactic center.

The poloidal field could, in principle, be ascribed to shear in a Galactic wind rising out of the CMZ, but such a model would be unable to account for its strength. The vertical field at the Galactic center can instead be reasonably well modeled in terms of the concentration of the Galaxy's primordial field, driven by the inexorable inflow of gas toward the center over the lifetime of the Galaxy (Chandran et al. 2000). In that case, the poloidal and toroidal fields at the Galactic center are completely independent of each other. Many questions, remain, however, such as where and how the poloidal field transitions into the dominant toroidal field at some point in the disk, and how that might relate to the X1-X2 orbital transition near the inner Lindblad resonance (Morris and Serabyn 1996).

References

Aitken, D. K., Smith, C. H., Gezari, D., McCaughrean, M., & Roche, P. F. 1991, ApJ, 380, 419
Aitken, D. K., Smith, C. H., Moore, T. J. T., & Roche, P. F. 1998, MNRAS, 299, 743
Anantharamaiah, K. R., Pedlar, A., Ekers, R. D., & Goss, W. M. 1991, MNRAS, 249, 262
Belmont, R., Tagger, M., Muno, M., Morris, M., & Cowley, S. 2005, ApJL, 631, L53

Bicknell, G. V., & Li, J. 2001, Publ. Astron. Soc. Australia, 18, 431
Boldyrev, S., & Yusef-Zadeh, F. 2006, ApJL, 637, L101
Carretti, E., Crocker, R. M., Staveley-Smith, L., et al. 2013, Nature, 493, 66
Chandran, B. D. G., Cowley, S. C., & Morris, M. 2000, ApJ, 528, 723
Chevalier, R. A. 1992, ApJL, 397, L39
Chuss, D. T., Davidson, J. A., Dotson, J. L., et al. 2003, ApJ, 599, 1116
Crocker, R. M. 2012, MNRAS, 423, 3512
Crocker, R. M., Jones, D. I., Melia, F., Ott, J., & Protheroe, R. J. 2010, Nature, 463, 65
Crocker, R. M., Jones, D. I., Aharonian, F., et al. 2011, MNRAS, 313
Dotson, J. L., Vaillancourt, J. E., Kirby, L., et al. 2010, ApJS, 186, 406
Ferrière, K. 2009, A&A, 505, 1183
Ferrière, K. 2011, in IAU Symposium, Vol. 271, IAU Symposium, 170–178
Güsten, R. 1989, in IAU Symposium, Vol. 136, The Center of the Galaxy, ed. M. Morris, 89
Hildebrand, R. H. 2002, in Astrophysical Spectropolarimetry, ed. J. Trujillo-Bueno, F. Moreno-Insertis, & F. Sánchez, 265–302
Hildebrand, R. H., Davidson, J. A., Dotson, J., et al. 1993, ApJ, 417, 565
Koyama, K. 2011, in Astronomical Society of the Pacific Conference Series, Vol. 439, The Galactic Center: a Window to the Nuclear Environment of Disk Galaxies, ed. M. R. Morris, Q. D. Wang, & F. Yuan, 418
Koyama, K., Takikawa, Y., Hyodo, Y., et al. 2009, PASJ, 61, 255
Lang, C. C., Anantharamaiah, K. R., Kassim, N. E., & Lazio, T. J. W. 1999, ApJL, 521, L41
LaRosa, T. N., Kassim, N. E., Lazio, T. J. W., & Hyman, S. D. 2000, AJ, 119, 207
LaRosa, T. N., Nord, M. E., Lazio, T. J. W., & Kassim, N. E. 2004, ApJ, 607, 302
Lazarian, A. 2007, J.Quant.Spectrosc.Radiat.Trans., 106, 225
Morris, M. 1994, in NATO ASIC Proc. 445: The Nuclei of Normal Galaxies: Lessons from the Galactic Center, ed. R. Genzel & A. I. Harris, 185
Morris, M. 1996, in IAU Symposium, Vol. 169, Unsolved Problems of the Milky Way, ed. L. Blitz & P. J. Teuben, 247
Morris, M. 2006, Journal of Physics Conference Series, 54, 1
Morris, M., & Serabyn, E. 1996, Ann. Rev. Astron. Ap., 34, 645
Morris, M., & Yusef-Zadeh, F. 1985, AJ, 90, 2511
Morris, M., Davidson, J. A., Werner, M., et al. 1992, ApJL, 399, L63
Morris, M. R., Zhao, J.-H., & Goss, W. M. 2014, in IAU Symposium, Vol. 303, IAU Symposium, ed. L. O. Sjouwerman, C. C. Lang, & J. Ott, 369–373
Muno, M. P., Baganoff, F. K., Bautz, M. W., et al. 2004, ApJ, 613, 326
Nishiyama, S., Hatano, H., Tamura, M., et al. 2010, ApJL, 722, L23
Nord, M. E., Lazio, T. J. W., Kassim, N. E., et al. 2004, AJ, 128, 1646
Novak, G., Dotson, J. L., Dowell, C. D., et al. 1997, ApJ, 487, 320
Novak, G., Chuss, D. T., Renbarger, T., et al. 2003, ApJL, 583, L83
Pierce-Price, D., Richer, J. S., Greaves, J. S., et al. 2000, ApJL, 545, L121
Revnivtsev, M., Sazonov, S., Churazov, E., et al. 2009, Nature, 458, 1142
Rosner, R., & Bodo, G. 1996, ApJL, 470, L49
Serabyn, E., & Morris, M. 1994, ApJL, 424, L91
Shore, S. N., & LaRosa, T. N. 1999, ApJ, 521, 587
Staguhn, J., Stutzki, J., Uchida, K. I., & Yusef-Zadeh, F. 1998, A&A, 336, 290
Stark, A. A., Bally, J., Gerhard, O. E., & Binney, J. 1991, MNRAS, 248, 14P
Su, M., Slatyer, T. R., & Finkbeiner, D. P. 2010, ApJ, 724, 1044
Tsuboi, M., Ukita, N., & Handa, T. 1997, ApJ, 481, 263
Tsuboi, M., Handa, T., & Ukita, N. 1999, ApJS, 120, 1
Uchida, Y., Sofue, Y., & Shibata, K. 1985, Nature, 317, 699
Uchida, K. I., Morris, M., Serabyn, E., & Guesten, R. 1996, ApJ, 462, 768

Wardle, M., & Konigl, A. 1990, ApJ, 362, 120
Yusef-Zadeh, F. 2003, ApJ, 598, 325
Yusef-Zadeh, F., & Morris, M. 1987a, AJ, 94, 1178
Yusef-Zadeh, F., & Morris, M.. 1987b, ApJ, 322, 721
Yusef-Zadeh, F., Morris, M., & Chance, D. 1984, Nature, 310, 557
Yusef-Zadeh, F., Hewitt, J. W., & Cotton, W. 2004, ApJS, 155, 421

A One Galaxy Universe, the Discovery of Galaxies and the Shift to Modern Approaches to the Cosmos

Robert W. Smith

Abstract Astronomers in the late nineteenth century and at the very start of the twentieth century were very little interested in the broader universe, its history and what lay beyond our galactic system as well as what is sometimes termed the thermodynamic cosmos. Some were very concerned with the structure of our own stellar system, but astronomers played next to no part in debates at the end of the nineteenth century about the wider nature of the cosmos. The infinite universe beyond our stellar system was territory professional astronomers were more than were happy to leave to mathematicians, physicists, philosophers, and some popularizers. In this paper I will examine these attitudes and why and how they changed. I will then discuss the discovery of galaxies, which will be the focus of the final section of the paper.

1 Introduction

"The darkness grew apace; a cold wind began to blow in freshening gusts from the east, and the showering white flakes in the air increased in number. From the edge of the sea came a ripple and whisper. Beyond these lifeless sounds the world was silent. Silent? It would be hard to convey the stillness of it. All the sounds of man, the bleating of sheep, the cries of birds, the hum of insects, the stir that makes the background of our lives—all that was over." So we can read near the end of H. G. Well's *The Time Machine*, published in 1895, a portrayal of the heat death of the earth, a vision very much in line with a famous 1852 paper of William Thomson's. In the second half of the nineteenth century an extended version of this vision, initially developed by Hermann von Helmholtz in 1854, had very wide currency as the end of the universe in what was widely known as the heat death. But astronomers were little engaged in the debates around the heat death. They played even less part in debates around the possibility that space was non-Euclidean. Nor was what would later become generally known as Olbers' paradox a matter of much concern (Jaki 1969). Solutions were on hand, it was believed. As it was also generally agreed that the visible universe consists of our own stellar system alone, and the disputes

R. W. Smith (✉)
Department of History and Classics, University of Alberta, Alberta T6G 2H4, Canada
e-mail: rwsmith@ualberta.ca

K. Freeman et al. (eds.), *Lessons from the Local Group,*
DOI 10.1007/978-3-319-10614-4_33

around the nature of the nebulae were to do with objects within that stellar system, astronomers played little part at all in debates at the end of the nineteenth century about the broader nature of the cosmos. The infinite universe beyond our stellar system was territory professional astronomers were more than were happy to leave to mathematicians, physicists, philosophers, and some popularizers. As far as almost all astronomers were concerned the wider universe was the realm of metaphysics and their position can be termed 'anti-cosmological,' a term employed by Kragh (2008). Cosmology in the late nineteenth century, as Neswald has put it, occupies a "tenuous place between science and imagination. Aiming to describe the unknown universe, it inevitably reflects personal and cultural assumptions and concerns. Historically, it is intertwined with religion, philosophy and [world view]." Further, the interactions between these different elements were not necessarily ones of adversity, but often of selection, mutual accommodation and interpretation (Neswald 2014, p. 16).

2 Astronomers and the Limits of Legitimate Astronomy

Matters of course started to change radically around 1900 with the triumph of scientific naturalism, various institutional developments (most importantly the erection of major observatories and big telescopes in the west of the U.S.) and a series of novel observations, perhaps most notably the counts of spiral nebulae by James Keeler, Henrietta Leavitt's establishment of the period-luminosity relationship, the measurements of redshifts by V. M. Slipher, H. D. Curtis's observations of novae in spiral nebulae, together with a wide array of advances in astrophysics including new methods of determining distances, and a novel theory of gravitation in the form of Einstein's general relativity which he and Willem De Sitter applied to the large-scale properties of the universe in 1917 (on these developments see, among others, Smith 1982, 2006, 2008 and 2009). One result of this broad as well as deep transformation was to create a divide between what we can call the old and the new cosmologies, a divide that has made it hard to extend much sympathy or even interest to the older astronomy and cosmology. A great deal of effort has gone into researching the more recent side of this divide. In this paper, I will instead be on the far side of what we can think of as a 'Great Divide' looking forward toward the present, rather than take a present position and looking backwards. In particular, I will explore why in the late nineteenth century and early twentieth century astronomers were not interested in broad questions to do with the nature of the universe, an attitude which seems baffling by our contemporary standards. To bring to light what was truly modern about modern astronomy and cosmology, however, it's essential to explore elements of the older astronomy and cosmology. I'll do this in the following order: first, non-Euclidean geometries, second, the thermodynamic cosmos, third the one galaxy universe, and fourth the debates on the nebular hypothesis. We will then be in a better position to understand the importance of the discovery of galaxies, which will be the focus of the final section of the paper.

2.1 Astronomers and Non-Euclidean Geometry

Among the anti-cosmological positions adopted by astronomers in the late nineteenth and early twentieth century was their lack of engagement with non-Euclidean geometries. The first person to recognize the mathematical possibilities of non-Euclidean geometries was of course Karl Freidrich Gauss. By 1817, he had concluded that Euclidean geometry was not true by necessity. In that year Gauss wrote to Heinrich Wilhelm Olbers that "Maybe in another life we shall attain insights into the essence of space which are now beyond our reach. Until then we should class geometry not with arithmetic, which stands purely a priori, but, say, with mechanics" (quoted in Kragh 2012, p. 4).

But Gauss never published on non-Euclidean geometry, never sought to address the topic systematically, and likely did not perform the famous triangulation of three mountain peaks to test the non-Euclidean nature of space. It's more meaningful in historical terms therefore to regard the founders of non-Euclidean geometry as the Russian Nikolai Ivanovich Lobachevsky and the Hungarian mathematician János Bolyai, with Lobachevskys first work on the topic coming in 1829 and Bolyai's in 1831. With later and what turned out to be for readers clearer formulations by the Italian mathematician Eugenio Beltrami as well as the Göttingen mathematician Bernhard Riemann, the study of the subject began to take off. According to one count, there were a total of 28 published works on non-Euclidean geometry before 1865, but after that time the number increased rapidly so that from the 8 works in the 5 year period 1866–1970, there was there was a big jump to some 700 in the 5 year period 1896–1900 and a further 850 between 1901 and 1905. The result was that some 4000 entries were given in a bibliography of non-Euclidean geometry published in 1911.

Astronomers were very little engaged with this literature. In an important survey by Kragh, he has found very few professional astronomers after 1870 who expressed concern with non-Euclidean space. The number goes up by another half if we count Charles Sanders Pierce as part-astronomer though now he is far better known as a philosopher of science, his most prominent early studies were in astronomy and chemistry and while at the Harvard College Observatory he pursued researches in photometry and spectroscopy. He was also an enthusiast for curved space.

One of the few professionals to publish on non-Euclidean geometries was R.S. Ball, a distinguished Irish astronomer and an expert in stellar parallaxes who in 1892 became the Lowndean Professor of Astronomy and Geometry at Cambridge as well as director of the University Observatory. Six years earlier he had written a paper on measuring distances in elliptic space but in doing so he drew no connections to practical astronomy. Ball did however make remarks on the possibility of curved space in other works. In *The High Heavens* he discussed whether space is finite or infinite but he pegged this as a question that is "rather of a metaphysical complexion" and "depends more on the facts of consciousness than upon those of astronomical observation" (Ball 1893, p. 252). But in so doing he also noted that a positively curved space and a finite universe "provides the needed loophole for escape from the illogicalities and contradictions into which our attempted conceptions of [infinite] space otherwise land us." An important point here is that Ball was expressing

these opinions as a leading popularizer of astronomy rather than as a professional astronomer or geometer, indeed after the death of Richard Proctor in 1888 Ball was arguably the leading popularizer of astronomy in the English speaking world.

2.2 The Thermodynamic Cosmos

If non-Euclidean geometries drew little professional interest from astronomers, what about the thermodynamic cosmos? By the 1860s, the science of heat was centred on two fundamental laws, the law of energy conservation and the entropy law, what would later be called the first and second laws of thermodynamics, and what was still known in the early 1860s as the dissipation law was generally taken to show that energy transformations had a direction so that while the amount of energy in the world remained constant "the amount of transformable energy continuously diminished. According to the dissipation law, a world ruled by energy transformations would at some point come to an end" (Neswald 2014, p. 2. Also Neswald 2006 and Smith 1999). For many, the end clearly implied a beginning (Kragh 2008). The heat death was therefore widely reckoned to also point to the creation of the universe. We mentioned earlier Thomson's 1852 paper on "A Universal Tendency in Nature to the Dissipation of Mechanical Energy." Here he argued that "Within a finite period of time past, the earth must have been, and within a finite period of time to come the earth must again be, unfit for the habitation of man as at present constituted." This linear vision sat well with Thomson's broader view of history which was very deeply Christian and "thus inescapably linear: time, he believed, runs in one direction from the creation of the world to the incarnation of Christ and on to the final judgment" (Hunt 2010, p. 42). The main opposition to this linear view of history came from German materialists who advocated cyclical cosmologies and who regarded the dissipation hypothesis as an effort to reintroduce into science a Biblically inspired account of the history of the universe. They instead proposed, as Neswald has emphasized, "a living nature in an eternal process of becoming" (Neswald 2014, p. 16) and so were very interested in possible processes of renewal. As one of the cyclical cosmologists put it, "Either we must drop the consequences of [Lord Kelvin] and Clausius, or the infinity of the universe. We have not a moment's doubt, which side of the dilemma we must drop, since we are not inclined to let the mechanics of heat lead us back to the creation dogma" (quoted in Neswald 2014, p. 28).

In his 1854 essay on the heat death, Helmholtz had referred to the cold dead corpses of planets, but in one proposed scheme these could be revived through cosmic collisions and "were the substance of the universe cast in cold detached fragments into space, and there abandoned to the mutual gravitation of its own parts, the collision of the fragments would in the end produce the spangled heavens" (quoted in Neswald 2014, p. 22). Lest this seem odd, it's worth remembering for example that when in 1913 V. M. Slipher first announced the remarkable Doppler shift of the Andromeda Nebula, in the same paper he also suggested that the famous 1885 nova S Andromedae was the result of the Nebula smashing into a dark star and causing the dark star to flare-up (Slipher 1913; Smith 1982, pp. 17–21).

In the late nineteenth century, then, the thermodynamic cosmos was a matter of considerable religious and philosophical as well as scientific debate. Relatively few astronomers however were active participants in the debate and those that were tended to side with the cyclical cosmologists. The physicists and engineers who participated in the debates overwhelmingly supported the hypothesis of the heat death. The cyclical cosmologists were a diverse bunch and came from several fields, including astronomy, geology, meteorology, biology and philosophy (Neswald 2014, p. 29). For them, each "body, planet or system was subject to the second law, but the endless universe itself was not." What, in particular, they asked, did it mean to describe the infinite universe as a closed system?

2.3 The One Galaxy Universe

Let me turn then to the third part of the anti-cosmological position of the astronomers and the one galaxy universe. It's important to note here that some astronomers were deeply concerned with the structure of our own galactic system, witness the efforts in particular of J. C. Kapteyn and Hugo von Seeliger (see, among others, Paul 1993; van der Kruit and van Berkel 2001, and van der Kruit's paper in this volume), but here the issue is what lay beyond the galactic system. The notion of the one galaxy universe (Jaki 1972) is perhaps now most famously enshrined in a quotation by the science writer and historian of astronomy Agnes Clerke, in *The System of the Stars* first published in 1890. "The question whether nebulae are external galaxies hardly any longer needs discussion," she argued. "It has been answered by the progress of research. No competent thinker with the whole of the available evidence before him, can now, it is safe to say, maintain any single nebula to be a star system of coordinate rank with the Milky Way." She then went on: "A practical certainty has been attained that the entire contents, stellar and nebular, of the sphere belong to one mighty aggregation, and stand in ordered mutual relations within the limits of one all-embracing scheme. All embracing, that is to say, so far as our capacities of knowledge extend. With the infinite possibilities beyond, science has no concern (Clerke 1890, p. 368).

As Clerke drafted chapters for *The System of the Stars* she sent them for comments to David Gill, who of course was a leading professional. Gill objected to her firm statements on the finite nature of the stellar system. "I cannot bear metaphysical questions such as so many of my countrymen love but I confess to you that I do not like the airy way in which you make the assertion "since the stellar system is of finite dimensions" . . . If you say: "Provided that the stellar system is of finite dimensions" then so-and-so—you are then in a strictly logical satisfactory position." Gill went on: "It is useless to pursue an argument on such a subject you come at once to the unbreakable and insurmountable wall of the little hollow sphere which limits the mental conceptions of man, and which by death he alone can pass to the freedom of the space beyond to the wider knowledge of God and his creatures" (quoted in Brück 2002, p. 79).

The views of a single galaxy universe were of course far from original with Clerke. Simon Newcomb, for example, had presented a single galaxy universe in his *Popular Astronomy* that went through various editions in the late nineteenth century. Perhaps the key observational evidence used in support of this view was the distribution of the nebulae, the great majority of which of course shunned the plane of the Milky Way, a distribution mapped and discussed at length, for example, by Richard Proctor, a British popularizer (Proctor 1869). Indeed the one galaxy universe drew decidedly more attention from the popularizers than the professionals.

Another who did pay attention was the famous naturalist and co-discoverer of evolution by natural selection Alfred Russel Wallace. At the end of the nineteenth century Wallace was startled to discover that contemporary astronomers placed the Sun very close to the centre of our own stellar system, which he learnt nearly all of them reckoned to be the only such star system that could be sighted in the whole of the Universe. The Sun, it seemed, occupied a very special and privileged place. Wallace would use the Sun's central position as the starting point for a connected argument that led him to the conclusion that intelligent life on the earth is unique. This argument has been well examined by Steven Dick so there is no need to deal with it in any detail here here (Dick 2008). It's worth noting however that Wallace had a very long standing interest in astronomy, but he turned seriously to it for the expanded version of his 1898 book *The Wonderful Century*. The expanded edition contained four chapters on astronomy and described the astronomical progress of the second half of the nineteenth century. In preparing these chapters Wallace not only became aware that astronomers generally placed the Sun close to the centre of the entire stellar universe as well as to be surprised that the finite nature of the stellar system was little commented on.

Wallace then developed these ideas for his 1903 book *Man's Place in the Universe*. This began with five chapters of astronomical background. He explained that our Sun is very close to the centre of our own system of stars, the Galaxy, and further that all the observed phenomena in the heavens are part of this single system. There are no other visible star systems beyond our Galaxy; there are no distant galaxies to be sighted in even the largest telescopes. Agnes Clerke was Wallace's main correspondent and source in the preparation of the book and her influence is clear.

Wallace concluded that contemporary astronomy established that the stellar system is spherical and the cluster of stars to which the Sun belongs, the solar cluster, is part of the larger system. The larger system is itself some 3600 light years across while our local, solar cluster contains anywhere from several hundred to several thousand stars.

In making these points Wallace was broadly in line with the generally accepted astronomical thinking of the day. But Wallace had made the Sun *too* central for many astronomers and drew a barrage of criticism for this (Dick 2008). He had also been decidedly too metaphysical for their taste. Wallace discussed the infinite universe, remarking that in infinite space there may be infinite universes, but, as he put it, "I hardly think they would all be universes of matter. That would indeed be a low conception of infinite power!" Given the astonishing diversity of life on the earth and the amazing diversity of objects in the heavens with "no two stars, no two star

clusters, no two nebulae alike" then "Why should there be other universes of the same matter and subject to the same laws-as is implied by the conception that the stars are infinite in number, and extend through infinite space?" (Wallace 1903, p. 318). Wallace was therefore happy to engage with what we've seen Gill and Ball would have called, and indeed dismissed, as metaphysical questions. And looking back across what I earlier called the divide between the older and the newer cosmologies, Wallace and Clerke of course come off badly if we judge their efforts by present day standards. We also get a powerful reminder that what counts as a metaphysical question changes over time and who is posing the question, and that there was a very wide range of currents running through late nineteenth century and very early twentieth century cosmologies.

2.4 The Nebular Hypothesis

The fourth topic to consider in the examination of the anti-cosmological positions of astronomers is the debate around the nebular hypothesis. First, it's worth noting that there was not much of a debate at all in the nineteenth century on the existence of galaxies. It's much more accurate to say there was an often intense debate on the nebular hypothesis. And for much of the nineteenth century this debate involved the political, moral and theological meanings associated with the nebulae not just their scientific meaning. Here again we are very much looking to the far side of the divide I noted at the start of the paper. To make this point a bit more concrete, I will consider a couple of examples (and in doing so draw in part on Smith 2014).

In 1837 John Pringle Nichol, Regius Professor of Astronomy at the University of Glasgow, wrote the widely read *Views of the Architecture of the Heavens*. Through this and other works by Nichol, the term 'nebular hypothesis' came into widespread use. In his *Views*, which, as usual for Nichol's writings, delivered for his readers a deistic interpretation of the works of nature, he explained the forms of visible nebulae as the result of material contracting into groups of stars. In Nichol's cosmogonical scheme, even comets were composed of nebulous matter. The zodiacal light was evidence of a sort of celestial relic, the remnants of the nebula out of which the sun had been born. In a path-breaking study (Schaffer 1989), Schaffer argued that Nichol and his allies had seized on the nebular hypothesis as an object of both a natural and moral science. For them, the stellar progress evinced by the nebular hypothesis could be exploited as a general model of universal progress. This meant it could be forced into service to argue for political reform. Nichol, as the anonymous author of the infamous *Vestiges of the Natural History of Creation* was to do in 1844 (it was the Edinburgh journalist and publisher Robert Chambers), also wove together the nebular hypothesis, geological theorizing and speculations on the transformation of species.

The nebular hypothesis was very useful for political radicals. As I have argued elsewhere, "Chambers exploited it in 1844 as the starting point of the evolutionary epic in Vestiges. The nebulous matter had formed a "universal Fire Mist" and from this stars

and planets had been fashioned. The existence of nebulous matter was clearly essential for the nebular hypothesis to have any credibility. Starting in 1845, observations with the just built Leviathan of Parsonstown-a gigantic 72-in reflecting telescope that was one of the wonders of the age as well as the largest reflector of the nineteenth century-became key elements in the debate on nebulous material. The Reverend Thomas Romney Robinson and Sir James South, along with Lord Rosse, aimed the Leviathan at forty nebulae from John Herschel's catalogue. Robinson announced to the Royal Irish Academy in 1845 that no real nebulae seemed to exist among those selected as all of them appeared to be clusters of stars (Robinson 1845). Robinson, politically conservative and a robust critic of the nebular hypothesis had claimed even before the Leviathan was directed to the skies that it would undermine Laplace's hypothesis by resolving the nebulae intoclouds of stars" (Smith 2014, p. 117).

One of the leaders among the emerging group of astrophysicists in the 1860s was William Huggins. In 1866, he addressed the British Association for the Advancement of Science and showed himself an advocate of the plurality of worlds as well as the argument from design: "May we not believe that the individual peculiarities of each star are essentially connected with the special purpose which it subserves, and with the living beings, which may inhabit the planetary worlds by which it may possibly be surrounded." "Star differs from star in glory," he asserted at the end of this 1866 address, "each nebula and each cluster has its own special features, doubtless in wisdom and for high and important purposes the Creator has made them all" (Huggins 1866, p. 43). Here Huggins was almost repeating a quotation from I Corinthians 15:41 that he had written out on the first page of his first notebook of astronomical observations a decade earlier: "One star differs from another star in glory." Huggins published his collected scientific papers in 1909. Here, without comment, the explicit reference in his 1866 address to the individual peculiarities of stars being connected to their special purposes and to the living beings on the planets going around them was deleted. In so doing, he had obscured his 1866 position for his readers in 1909. But by 1909, Huggins had long made his personal journey to scientific naturalism across what we have called the Great Divide. Some of his key general assumptions from 1866 were no longer credible to him in 1909.

3 A Universe of Galaxies

By 1909, Huggins had embraced scientific naturalism as the correct approach to the pursuit of science and so had the overwhelming majority of his colleagues. But one of the crucial, if not the most crucial, steps to the discovery of galaxies in the early twentieth century came out of a continuation of the nineteenth century debate on nebulae when Percival Lowell told V. M. Slipher to turn his attention to spiral nebulae (as an astronomer at the Lowell Observatory Slipher was principally charged with pursuing those tasks Lowell posed for him). Lowell was extremely interested in the history of the solar system and the clues that could be offered on that history by the spirals as the spirals, almost everyone agreed in the 1900s, were proto-solar systems or perhaps sparse star clusters in formation.

The result was Slipher's remarkable series of observations of the radial velocities of spiral nebulae that were key for the discovery of the expanding universe around 1930, but they were also exceedingly important in sparking renewed debate on the question of whether or not the sprials are external galaxies. From being almost a non-question in 1910, it was very much alive by 1915, principally due to Slipher. H. D. Curtis was an astronomer who by 1915 had not planted himself fully on the modern side of the divide and so we find him making arguments from design for the island universe theory, but he also played a major role in providing evidence for the spirals as galaxies through observations of novae in spirals and the consequent distance calculations.

Indeed, by 1920 and the so-called 'Great Debate' between Curtis and Harlow Shapley, opinion had shifted very markedly. The majority of astronomers who cared about this question agreed with Curtis that the spirals are galaxies. The only serious evidence against this position came from Adriaan van Maanen's now infamous measurements of internal motions in spiral nebulae. The sizes of these motions pointed to distances of at most tens of thousands of light years rather than the many hundreds of thousands or millions of light years required for the spirals to be external galaxies (Smith 1982, pp. 97–136, 2008, pp. 3–4 and the references cited therein).

If this is the story of the discovery of galaxies, is this a story so far of Hamlet without the Prince? Where's Edwin Hubble? Didn't Hubble discover external galaxies? Hubble did play a very important role, but he did so by *clinching* the case for the spirals as galaxies and the discovery of galaxies needs to be seen as an extended process rather than a singular moment in time at a particular place (Smith 2008, p. 4)

Where did the clinching evidence come from? In October 1923, Hubble detected what he initially marked as a nova on a photographic plate of M31 (we need to remember that he had been hunting for novae in the Andromeda Nebula in an effort to better determine its distance). After he had reviewed a series of earlier plates of the Nebula, Hubble changed his mind. He was also he was so sure of his results by early 1924 he explained to Shapley-who had of course rejected the identification of spirals as visible galaxies in the Great Debate–that:

> You will be interested to hear that I have found a Cepheid variable in the Andromeda nebula (M31). I have followed the Nebula this season as closely as the weather permitted and in the last five months have netted nine novae and two variables . . . The two variables were found last week . . . Enclosed is a copy of the normal light curve, which, rough as it is, shows the Cepheid characteristics in an unmistakable fashion (Hubble 1924).

Hubble had determined the Cepheid's period. He had assumed, as Shapley had done in his earlier studies of the globular clusters that surround the Milky Way, that all the Cepheids in the universe of the same period have the same intrinsic luminosity (Smith 2006, pp. 317–24). Hubble then exploited the period-luminosity relationship for Cepheids to compute the Nebula's distance. His result was 900,000 light years. This placed the Nebula well outside the borders of even Shapley's model of the Galaxy (which, remember, Shapley calculated had a diameter of about 300,000 light years). His photographs also revealed, Hubble claimed, clouds of stars in the Nebula's outer regions. More discoveries of Cepheids in the Andromeda Nebula as well as a few other spirals followed quickly on the heels of the first in M31

(Smith 1982, pp. 112–26). For Hubble, the evidence of the Cepheids and other stars was unequivocal: the Andromeda Nebula and the other spirals are external galaxies.

Within a year or two of Hubble's chancing upon the first Cepheid, the public debate on external galaxies had all but ended. Even Shapley was converted after a short period of scepticism. After all, Hubble's results served to underline the reliability of the Cepheids as distance indicators. In so doing, they added credibility to Shapley's own results on the 'Big Galaxy,' always for him a bigger concern than the status of the spirals. For Hubble and others, the Cepheids were accurate distance indicators to the spirals, and their clear message was that the spirals are most assuredly external galaxies. All the other evidence pointed in the same direction except for Adriaan's van Maanen's measurements of internal motions, which he stuck to tenaciously.

News of Hubble's findings circulated among astronomers during 1924. In November of that year there was even a short report on them in the *New York Times* (Anon 1924). The "flat contradiction" between his results and van Maanen's measured internal motions, however, led Hubble to delay publishing his findings (Van Maanen, like Hubble, was a Mount Wilson astronomer and so their contradictory results formed a difficult management issue for Mount Wilson officials for a decade). While some astronomers were initially hesitant to discount the motions completely, by the late 1920s the internal motions had become so isolated that nearly everyone rejected them as hopeless exaggerations of any real motions. For practically all astronomers, the case for their accuracy had long since crumbled.

4 Conclusions

Astronomers in the late nineteenth century and at the very start of the twentieth century were little engaged with cosmological issues in general, including the nature of space or the thermodynamic cosmos. As George Darwin put it in 1905 in addressing the British Association for the Advancement of Science, was it not futile to imagine that man "can discover the origin and tendency of the universe as to expect a housefly to instruct us as to the theory of the planets?" (Darwin 1905, p. 405). Some astronomers *were* very concerned with the structure of our own stellar system, but astronomers were indifferent in their professional pursuits with what lay beyond the galactic system. In this paper I argued that there was a major divide between these older views and the positions that developed early in the twentieth century. The discovery of galaxies needs, then, to be seen as a key element in the emergence of a new outlook for astronomers, one which over time meant they displayed much more sympathy towards broader questions and topics to do with the structure, history and evolution of the universe as legitimate parts of astronomy. Questions and topics that had generally been rejected earlier by astronomers out of hand as metaphysics had begun to take on new meanings.

References

Anon 1924, "Finds spiral nebulae are stellar systems; Dr. Hubbell [sic] confirms view that they are 'island universes' similar to our own," New York Times, November 23, 1924, 6.
Ball, R.S. 1893, The High Heavens.
Brück, M. 2002, Agnes Mary Clerke and the Rise of Astrophysics.
Clerke, A. M. 1890, The System of the Stars.
Darwin, G.H. 1905. "Cosmical Evolution," The Observatory, 38, pp. 401–5.
Dick, S. 2008, "The Universe and Alfred Russel Wallace," pp. 320–340 in Smith, C.H. & Beccaloni, G. (eds.) Natural Selection and Beyond: The Intellectual Legacy of Alfred Russel Wallace.
Hubble, E. to Shapley, H., 19 February 1924, Harvard University Archives.
Huggins, W. 1866, On the Results of Spectrum Analysis.
Hunt, B.J. 2010, Pursuing Power and Light: Technology and Physics from James Watt to Albert Einstein.
Jaki, S.L. 1969. The Paradox of Olbers' Paradox: A Case History of Scientific Thought.
Jaki, S.L. 1972. The Milky Way: An Elusive Road for Science.
Kragh, H. 2008, Entropic Creation: Religious Contexts of Thermodynamics and Cosmology.
Kragh, H. 2012, "Geometry and Astronomy: Pre-Einstein Speculations of Non-Euclidean Space," http://arxiv.org/abs/1205.4909.
Neswald, E. 2006. Thermodynamik als kultureller Kampflatz. Zur Faszinationgeschichte der Entropie 1850–1915.
Neswald, E. 2014, "Saving the World in the Age of Entropy: John Tyndall and the Second Law of Thermodynamics," pp. 15-32, in Lightman, Bernard, and Reidy, Michael S., The Age of Scientific Naturalism: Tyndall and his Contemporaries.
Paul, E.R. 1993, The Milky Way Galaxy and Statistical Cosmology 1890–1914.
Proctor, R.A. 1869, "The distribution of nebulae," Monthly Notices of the Royal Astronomical Society, 29, pp. 337–44.
Robinson, T.R. 1845, 'On Lord Rosse's telescopes,' Proceedings of the Royal Irish Academy 3(1845–47), 114–33.
Schaffer, S. 1989, "The nebular hypothesis and the science of progress," pp. 131–64, in Moore, J.R. (ed.) History, Humanity and Evolution: Essays for John C. Greene.
Smith, C. 1999. The Science of Energy: A Cultural History of Energy Physics in Victorian Britain.
Slipher, V.M. 1913, "The Radial Velocity of the Andromeda Nebula," Lick Observatory Bulletin, 2, 56–7.
Smith, R.W. 1982, The Expanding Universe: Astronomy's 'Great Debate' 1900–1931.
Smith, R.W., 2006, Robert W. Smith, "Beyond the Big Galaxy: The structure of the stellar system 1900–1952," Journal for the history of astronomy, 37, pp. 307–42.
Smith, R.W. 2008, "Beyond the Galaxy: the development of extragalactic astronomy 1885 - 1965 Part 1," Journal for the history of astronomy, 39, pp. 91–119.
Smith, R.W., 2009, "Beyond the Galaxy: the development of extragalactic astronomy 1885 - 1965 Part 2," Journal for the history of astronomy, 40, pp. 71–107.
Smith, R.W. 2014, "The 'Great Plan of the Visible Universe:' William Huggins, Evolutionary Naturalism and the Nature of the Nebulae," pp. 113–136, in in Lightman, Bernard, and Reidy, Michael S., The Age of Scientific Naturalism: Tyndall and his Contemporaries.
Van der Kruit, P.C. & Van Berkel, K., 2001, The Legacy of J.C. Kapteyn: Studies on Kapteyn and the Development of Modern Astronomy.
Wallace, A.R. 1903, Man's Place in the Universe.

Cosmic Evolution of Gas Content and Accretion

Françoise Combes

Abstract In the present universe, the gas is a minor component of giant galaxies, and its dominant phase is atomic (HI). During galaxy evolution in cosmic times, models predict that gas fractions were much higher in galaxies, and gas phases could be more balanced between molecular (H_2) and atomic (HI). This gaseous evolution is certainly a key factor to explain the cosmic evolution of the star formation rate density. Star formation efficiency might also vary with redshift, and the relative importance of these factors is not yet well known. Our current knowledge of cosmic evolution of gas from molecular observations at high-z is reviewed and confronted with simulations.

1 Introduction

The abundance of gas observable in galaxies today can be expressed with dimensionless numbers, normalised with the critical density of the universe. While stars in galaxies account for $\Omega_* = 3\ 10^{-3}$ (e.g. Fukugita et al. 1998), the HI gas contributes by $\Omega_{HI} \sim 3.5\ 10^{-4}$ (Zwaan et al. 2005), and the molecular gas by $\Omega_{H_2} \sim 1.2\ 10^{-4}$ (Young et al. 1995; Sauty et al. 2003; Keres et al. 2003; Saintonge et al. 2011).

Theoretical considerations and semi-analytical models predict that the molecular-to-atomic gas ratio decreases regularly with cosmic time in galaxies (Obreschkow and Rawlings 2009; Obreschkow et al. 2009). The phase transition to molecular hydrogen can be formulated in terms of pressure (Blitz and Rosolowsky 2006), and the surface density and consequently the pressure is higher in high-z galaxies. The modelisation leads to a dependency of H_2/HI varying as $(1+z)^{1.6}$. This is essentially due to the expectation that the size of galaxies is growing as $(1+z)^{-1}$ with cosmic time.

The evolution with z of Ω_{HI} in galaxies is not yet known from emission, but can be derived from the damped Lyman-α absorption in front of quasars, since these systems are thought to correspond to galaxies. Albeit with large error bars, the abundance of HI appears about constant from $z=4$ to $z=0$ (Zwaan et al. 2005). It

F. Combes (✉)
Observatoire de Paris, LERMA, CNRS, 61 Av. de l'Observatoire, 75014, Paris, France
e-mail: francoise.combes@obspm.fr

K. Freeman et al. (eds.), *Lessons from the Local Group,*
DOI 10.1007/978-3-319-10614-4_34

is however expected to experience a strongly varying phase at higher z, when cold gas settles in galaxies, through accretion and cooling, mergers, etc. At these early epochs, molecules might have difficulties to form, since metals and dust are building up slowly, but the exact processes are not yet well known.

What is better known is the cosmic evolution of star formation rate density, from UV to far-infrared light, and its decrease by a factor 20 since $z = 2$ (e.g. Hopkins and Beacom 2006; Bouwens et al. 2011). How does this SFR evolution relate to the cosmic cold gas evolution? Is it linked to HI or H_2 density, or/and to the star formation efficiency (SFE)?

2 High-z Molecular Observations

For about 20 years now, molecular gas is observed in high redshift galaxies. Due to the lack of sensitivity, mostly lensed galaxies were first discovered (cf the review by Solomon and vanden Bout 2005). More and more "normal" objects, on the main sequence of star forming galaxies are observed now, and this will increase considerably with ALMA. The detection of CO lines at high redshift is made easier by the existence of the rotational ladder, where the flux of the higher transitions can be much higher than the fundamental line. This is not the sase of the HI gas and the only 21 cm line, which will have to wait SKA to be detectable at high redshift.

2.1 Starbursts and ULIRGs

Until very recently, only very luminous galaxies in the far-infrared (LIRGs and ULIRGs) were detected in the CO lines at high redshift, due to limited sensitivity. In the local universe, it is now well established that ULIRGs are starbursts triggered by galaxy interactions and mergers (e.g. Solomon et al. 1997). At high redshift, the global star formation rate is increasing rapidly, and even ULIRG are not all starbursts. It is thought now that the starburst mode is likely to represent only 10 % of the stars formed at $z = 2$, the cosmic peak of the star formation activity (Rodighiero et al. 2011).

Already Greve et al. (2005) showed that the SFE (defined by the ratio of FIR luminosity, taken as an indicator of SFR, to the CO luminosity, indicator of the gas mass) was increasing significantly with redshift, reaching maxima around $z = 2$ for submillimeter galaxies (SMG) with an SFE up to 2 orders of magnitude higher than for local LIRGs. The gas consumption time-scale, being the inverse of the SFE, could then fall to 20 Myrs, instead of the average 2 billion yrs locally.

The redshift range between $z = 0.2$ and $z = 1$ is very important for the cosmic gas evolution, since it is the period when the cosmic star formation density drops by a factor 10, and it corresponds to 40 % of the universe age. Unfortunately, this domain was not easily observed because of atmospheric lines, and the need of sensitive

2 mm instruments. A sample of 69 ULIRG was observed in different CO lines with the IRAM-30 m precisely in this redshift range (Combes et al. 2011, 2013). From the galaxies where the gas excitation is known, and from the dust masses derived from the continuum emission, the adoption of the ULIRG CO-to-H_2 conversion factor is justified (e.g. Solomon et al. 1997). This ratio is 5.7 times smaller than the standard ratio adopted for Milky Way-like galaxies. The average molecular mass is however 1.45 10^{10} $M_\odot$, an order of magnitude higher than in the Milky Way.

Compiling this sample with other LIRGs and ULIRGs, both the molecular gas to stellar mass ratio and the SFE significantly increase with redshift, by factors of ~ 3 from z = 0 to 1, as shown in Fig. 1, suggesting that both factors play an important role and complement each other in cosmic star formation evolution.

2.2 Main Sequence Galaxies

Not all star forming galaxies at $z = 1 - 2$ have a high SFE. Some galaxies, selected only from their optical colors, were detected in the CO lines with surprising high CO luminosities (Daddi et al. 2008). These galaxies, although still in the ULIRGs range, have a low gas excitation (Dannerbauer et al. 2009), and are relatively extended. They are interpreted as disk-like galaxies with steady star formation rate, while the most excited ULIRGs are nuclear starbursts. It is possible that the Milky Way-like conversion ratio applies for these objects, which will further lower their SFE. However, the adoption of a bimodal conversion ratio leads to an artificial bimodal star formation regime, separating the starbursts from the more quiescent disks with a gap of an order of magnitude in gas consumption time-scales. In reality, there must exist a continuous conversion ratio, according to gas density, temperature, and other factors like metallicity, and the SF regimes are certainly continuous too.

A continuity of galaxy properties between the two modes of star formation, main sequence and starburst, is developed further by Daddi et al. (2013) and Sargent et al. (2014). Although starbursts have larger SFE, it is not easy to know whether the cause is a lack of gas (may be the consequence of a short boost of star formation), or an excess of young stars. If the starburst is triggered by a merger, numerical simulations show that gas is driven inwards by gravity torques from the outer reservoir, and more gas is then observable (e.g. Di Matteo et al. 2007; Montuori et al. 2010). An excess of fresh gas in star forming galaxies is also supported by the fundamental mass-metallicity relation, which precisely depends on SFR (Mannucci et al. 2010). Starbursts have also a larger molecular gas to stellar mass ratio, so their elevated SFR is both due to a larger gas content and a larger SFE. The latter could be due to the larger central concentration of the gas, and this will be clarified through resolved SFR/gas density studies.

The PHIBSS large program on the IRAM interferometer (Tacconi et al. 2010; 2013, see also this conference) has targeted a sample of massive star forming galaxies, likely to be on the main sequence as defined in the stellar mass-SFR diagram (e.g. Wuyts et al. 2011). From the 52 CO-detected objects at $z = 1 - 3$, the gas mass

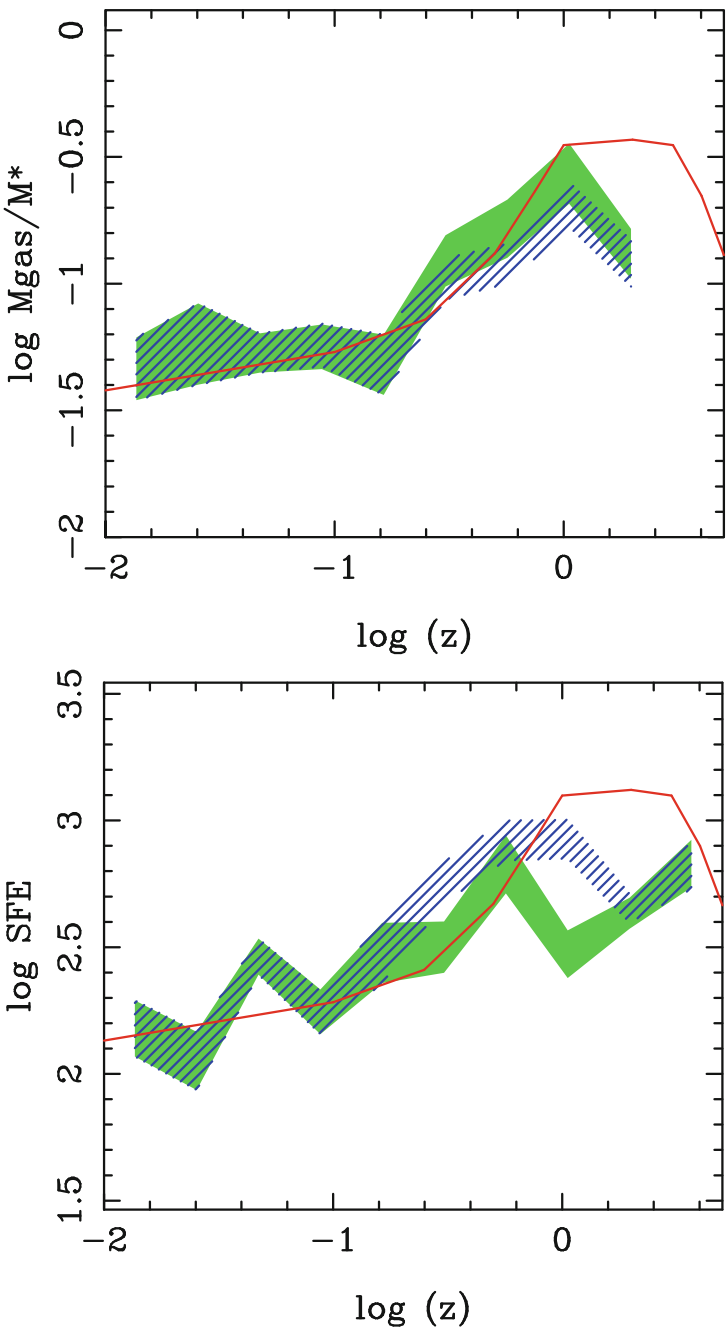

Fig. 1 *Left*: Evolution of the star formation efficiency (SFE) with redshift. *Right*: Cosmic evolution of the gas to stellar mass ratio, for the LIRG and ULIRG compilation of Combes et al. (2013). The green area corresponds to the CO-detected points, and the hatched area also includes the 3σ

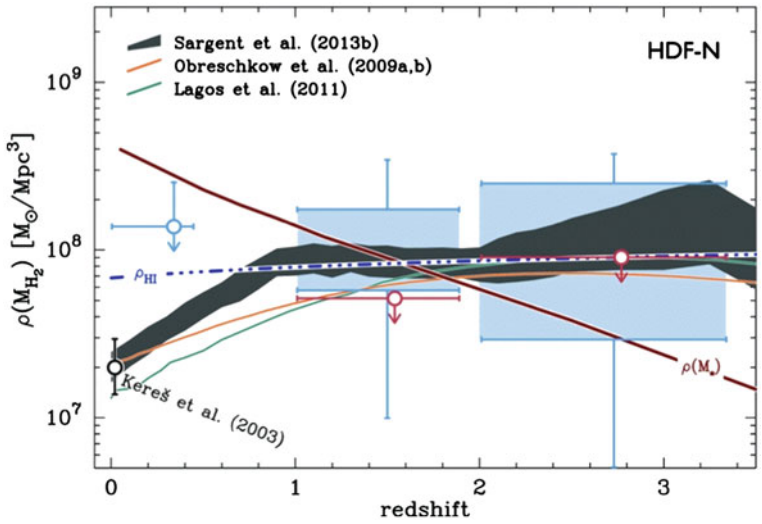

Fig. 2 Evolution of the cosmic H_2 mass density versus redshift, comparing observational limits obtained from blind detections in the Hubble Deep Field North by Decarli et al. (2014) shown in blue-shaded areas, to predictions from semi-analytical cosmological models (Obreschkow et al. 2009; Lagos et al. 2011) and empirical predictions by Sargent et al. 2014 (*grey-shaded areas*). The red upper limit corresponds only to galaxies selected via optical spectroscopic redshifts. The evolution of the atomic gas mass density (ρ_{HI}) and of the stellar mass density $\rho(M_*)$ are also plotted (from Walter et al. 2014)

fraction is found to increase with z, up to 50 %, and decrease with mass. Most of the objects look like disks with regular rotation, and are more steady star forming disks than starbursts, without any interaction or merger. Since the molecular gas depletion time-scale is typically 0.7 Gyr and varies as $(1+z)^{-1}$, the star formation must be fueled by gas accretion episodes, which are frequent at high and moderate redshift (e.g. Combes 2014). The resolved Kennicutt-Schmidt relation obtained in a few objects is compatible with a linear relation, and a depletion time-scale lower at high-z (Freundlich et al. 2013; Genzel et al. 2013).

In all these massive star forming galaxies, atomic gas cannot be dominating the cold gas, since the sum of the molecular and stellar masses are so close to the dynamical mass. Unless the CO-to-H_2 conversion factor is largely in error, the H_2/HI ratio has indeed increased with z, as predicted by models. Another recent study supports this conclusion: Decarli et al. (2014) have carried out a blind molecular line survey in the Hubble Deep Field North, scanning the whole 3 mm band with the IRAM interferometer. Their blind detection of 17 CO lines, together with the upper limit obtained by stacking the observations towards spectroscopically identified objects,

←

Fig. 1 (continued) upper limits. The width of the shaded regions correspond to the statistical scatter in $N^{-1/2}$. The red curve is indicative of the logarithmic variations of the cosmic star formation rate density (Hopkins and Beacom 2006)

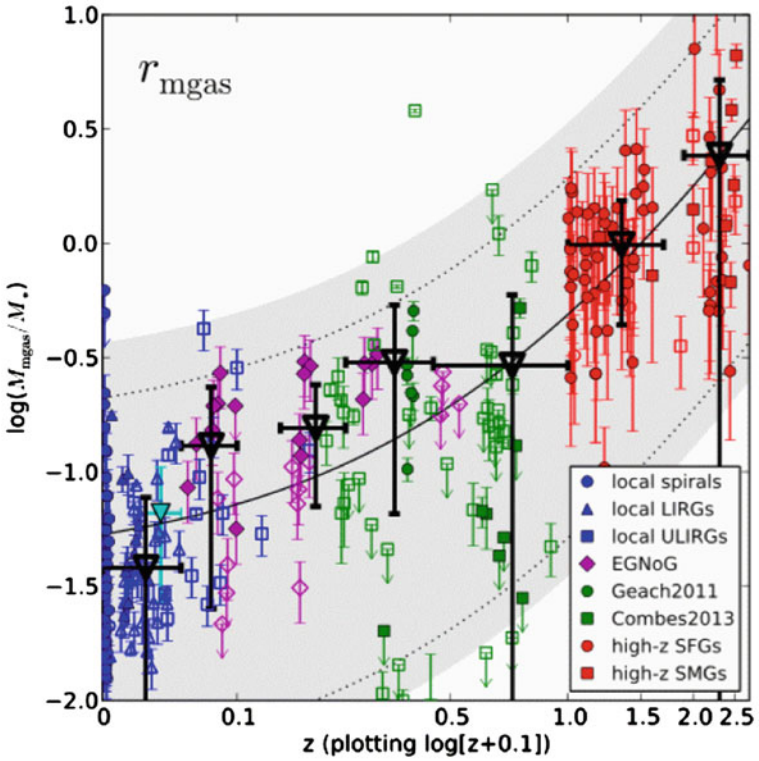

Fig. 3 Evolution of the molecular gas to stellar mass ratio (r_{mgas}) versus z, from the compilation of Bauermeister et al. (2013). Symbols are filled for main sequence galaxies, and empty for starbursts. The 7 bold black triangles are the average for the different redshift bins. The shaded grey zone indicates the expected region for normal galaxies, with the solid curve being the average

constrain the CO luminosity functions at the corresponding redshifts. They deduce that optical/MIR bright galaxies contribute less than 50 % to the star formation rate density at $1 < z < 3$. Their derived evolution of the H_2 mass density is compared to models in Fig. 2.

A recent 870 μm continuum survey with ALMA of SMG in the Extended Chandra Deep Field South (Swinbank et al. 2014) has discovered that the well detected sources ($S_{870} > 2$mJy) are in average ULIRGs with SFR=300 $M_\odot$/yr. The extrapolation of the counts down to $S_{870} > 1$mJy show that these sources contribute to 20 % of the cosmic star formation density over $z = 1-4$. Deriving H_2 masses from dust masses, the average SFE is found rather high, with depletion time-scale of 130 Myr. This is to be compared to the compilation by Bauermeister et al. (2013), who observed normal star forming galaxies in the redshift range $z = 0.05 - 0.5$. They find a depletion time-scale for normal galaxies of 760 Myr, and for starbursts 60 Myr. Their derived molecular gas to stellar mass ratio is plotted in Fig. 3, and is compatible with the model-expected behavior.

3 Models and Simulations

Semi-analytical models (SAM) have been run, within the standard ΛCDM model, to compute the cosmic evolution of the cold gas content in galaxies. Lagos et al. (2011) show that the best recipe to control the phase transition from atomic to molecular is the pressure model (Blitz and Rosolowsky 2006), rather than the theory-based model from Krumholz et al. (2009) taking into account UV-dissociation of molecules and their reformation on grains. In their best fit model, the H_2/HI ratio rises above one at high redshift, as in Obreschkow et al. (2009). Fu et al. (2010, 2012) claim that the Krumholz et al. (2009) recipe is better, but on a limited mass range. Their best fit requires that the depletion time-scale remains 1–2 Gyr at high redshift.

Using a simple phenomenological model, Feldmann (2013) claims that the relation between SFR and H_2 content is likely to be linear at all redshift. This assumption provides the best fit to the data, i.e. the cosmic star formation history, the evolution of the mass-metallicity relation, and the gas-to-stellar mass ratio in galaxies. This means that the variation of SFE with redshift might be too little to be sensitive. Models where the SFR relation is non-linear with gas density produce too much stars and metals early on to be compatible with the observations. To obtain the right star formation histories, gas accretion must be limited to a halo mass range between a critical minimum mass $M_c(z)$, below which photoionisation limits the baryon fraction, and an upper limit $M_{shock} \sim 2\ 10^{12}\ M_\odot$, above which the gas is heated by shocks in entering the galaxy (Birnboim and Dekel 2003). At early epochs, for redshifts higher than 2, the gas accretion time-scale is very short, and the SFR not enough to consume the accreted gas, which accumulates in galaxies. After $z = 2$, the SFR has increased to its maximum; within the halo mass range between M_c and M_{shock}, the depletion time-scale is comparable to the accretion time-scale, and the SFR is limited by gas accretion (Bouché et al. 2010). In this global model, an equilibrium settles between gas inflow and outflow, and star formation rate, equalling depletion time to accretion time. Stellar masses, metallicity, and cosmic gas evolution are moderated by this equilibrium.

The relation between SFR and stellar mass on the main sequence has been examined in detail from 25 studies in the literature, and the corresponding slope is a decreasing function of cosmic time (Speagle et al. 2014). The star formation histories derived from these are delayed-τ models, where the SFR is first increasing linearly with time in the first half of the universe age, and then decreasing exponentially.

With a SAM approach Popping et al. (2012, 2014) also tested several recipes for the molecular gas and star formation evolution; either pressure-based, or metallicity-based models represent rather well observations, with some variations for low mass galaxies. To compare with high-z observations, they deduce their gas content from their SFR, through inversion of the Kennicutt-Schmidt (KS) relation, but in this case the best fit is for a density-dependent SFE. Also, the CO-to-H_2 conversion factor should be continuous, as a function of the galaxy physical properties.

That the SFE should depend on gas surface density (non-linear KS relation) is certainly a solution to explain why SFE varies with redshift. Galaxies were more

compact at high z (Newman et al. 2012; Morishita et al. 2014), so not only their surface density was higher for a given gas content, but also their dynamical time was shorter, which favors the dynamical triggers. Another feature is the volumic density dependency, which could play a role, even for a linear KS relation. It has already been observed that SFE is declining with radius in galaxy disks at z = 0, possibly due to gas disk flaring (Bigiel et al. 2010; Dessauges-Zavadsky et al. 2014).

There are still large uncertainties on key factors to determine the cosmic evolution of cold gas content in galaxies: not only the SFR laws as a function of density, the phase transition between atomic and molecular gas, but also the star formation efficiency, regulated by feedback mechanisms due to supernovae or AGN, the quenching due to environment, slowing down the gas accretion. We are just at the beginning of the ALMA era, and our knowledge on these physical processes will progress exponentially.

Acknowledgements My great thanks to the organisers of this wonderful meeting with wide scientific interests. The European Research Council is gratefully acknowledged for the Advanced Grant Program Num 267399-Momentum.

References

Bauermeister A., Blitz L., Bolatto A., et al. 2013, ApJ, 768, 132
Bigiel, F., Leroy, A., Walter, F., et al. 2010, AJ, 140, 1194
Birnboim Y., Dekel A.: 2003 MNRAS 345, 349
Blitz L., Rosolowsky E.: 2006, ApJ 650, 933
Bouché N., Dekel A., Genzel R. et al. 2010, ApJ 718, 1001
Bouwens, R. J., Illingworth, G. D., Oesch, P. A. et al. : 2011 ApJ 737, 90
Combes F., 2014, Arkansas conf. , arXiv:1309.1603
Combes F., García-Burillo S., Braine J. et al. 2011, A&A, 528, A124
Combes F., García-Burillo S., Braine J. et al. 2013, A&A, 550, A41
Daddi E., Dannerbauer, H., Elbaz, D. et al. 2008, ApJ 673, L21
Daddi E., Sargent M. T., Béthermin M., Magdis G., 2013, IAUS, 295, 64
Dannerbauer, H., Daddi, E., Riechers, D. A. et al. 2009, ApJ 698, L178
Decarli, R., Walter, F., Carilli, C. et al. 2014 ApJ 782, 78
Dessauges-Zavadsky M., Verdugo C., Combes F., Pfenniger D.: 2014, A&A in press
Di Matteo, P., Combes, F., Melchior A-L., Semelin, B.: 2007, A&A 468, 61
Feldmann R. 2013, MNRAS 433, 1910
Freundlich J., Combes F., Tacconi L. et al. 2013, A&A 553, A130
Fu, J., Guo, Q., Kauffmann, G., Krumholz, M. R. 2010, MNRAS 409, 515
Fu, J., Kauffmann, G., Li, C., Guo, Q. 2012, MNRAS 424, 2701
Fukugita M., Hogan C. J., Peebles P. J. E., 1998, ApJ, 503, 518
Genzel, R., Tacconi, L. J., Kurk J. et al. 2013, ApJ 773, 68
Greve. T. R., Bertoldi, F., Smail, I. et al. 2005, MNRAS, 359, 1165
Hopkins A. M., Beacom J. F.: 2006, ApJ 651, 142
Keres, D., Yun, M. S., Young, J. S. 2003, ApJ, 582, 659
Krumholz M. R., McKee C. F., Tumlinson J.: 2009 ApJ 699, 850
Lagos C. d P., Baugh C. M., Lacey C. G. et al. 2011, MNRAS 418, 1649
Mannucci, F., Cresci, G., Maiolino, R. et al. 2010, MNRAS 408, 2115
Montuori M., Di Matteo, P., Lehnert, M. D., Combes, F., Semelin, B.: 2010, A&A 518, A56

Morishita T., Ichikawa, T., Kajisawa, M.: 2014, ApJ 785, 18
Newman A. B., Ellis, R. S., Bundy, K., Treu, T. : 2012, ApJ 746, 162
Obreschkow D., Rawlings S.: 2009, ApJ 696, L129
Obreschkow D., Croton D., de Lucia G. et al. 2009, ApJ 698, 1467
Popping G., Caputi K. I., Somerville R. S., Trager S. C., 2012, MNRAS, 425, 2386
Popping G., Somerville R. S., Trager S. C., 2014, arXiv:1308.6764
Rodighiero, G., Daddi, E., Baronchelli, I. et al. 2011, ApJ 739, L40
Saintonge, A., Kauffmann, G., Kramer, C. et al. 2011, MNRAS 415, 32
Sargent, M. T., Daddi, E., Bethermin, M et al. : 2014, ApJ in press, arXiv1303.4392
Sauty S., Casoli, F., Boselli, A. et al. 2003, A&A, 411, 381
Solomon P., Downes D., Radford S., Barrett J.: 1997, ApJ 478, 144
Solomon, P. M., Vanden Bout, P. A.: 2005, ARA&A 43, 677
Speagle J. S., Steinhardt C. L., Capak P. L., Silverman J. D: 2014, ApJ sub arXiv1405.2041
Swinbank A. M., Simpson J. M., Smail I., et al. 2014, MNRAS, 438, 1267
Tacconi L. J., Genzel R., Neri R. et al. 2010 Nature 463, 781
Tacconi L. J., Neri R., Genzel R. et al. 2013, ApJ 768, 74
Walter F., Decarli R., Sargent M. et al. 2014, ApJ, 782, 79
Wuyts, S., Förster Schreiber, N. M., van der Wel, A. et al. 2011, ApJ 742, 96
Young, J. S., Xie, S., Tacconi, L. et al. 1995, ApJS 98, 219
Zwaan, M. A., Meyer, M. J., Staveley-Smith, L., Webster, R. L.: 2005, MNRAS 359, L30

Rings in Spiral Galaxies in the Local Group: Lessons from René Magritte

David L. Block

Abstract In this review, I wish to focus on the veritable goldmine of lessons one can glean from The Local Group. By way of a prelude, I wish to highlight the treachery of photographic or digital images of galaxies, by introducing the work of the Belgian surreal artist René Magritte. We discuss his famous painting "The Treachery of Images" (La trahison des images, 1928), which portrays a pipe. Below it, Magritte painted these words, "Ceci n'est pas une pipe" ('This is not a pipe'). The painting is not a physical pipe, but rather a representation of a pipe. And so it is with galaxies in the Local Group and their masks: what we see is only a representation of what actually is. The definition of a galaxy given in the Hubble Atlas beautifully portrays the treachery of photographic images of galaxies, being then defined as closed dynamical systems, or island universes. We conclude with "perspective", not only in the world of astrophysics, but in our human condition as well.

1 Galaxy Morphology and René Magritte

The Treachery of Images ("La trahison des images") is a painting by the Belgian René Magritte. The picture shows a pipe. Below it, Magritte painted, "Ceci n'est pas une pipe" which, translated from the French, is "This is not a pipe." The painting is indeed not a pipe, but rather an image of a pipe, which was Magritte's point.

Magritte's work frequently displays a juxtaposition of ordinary objects in an unusual context, giving new meanings to familiar things. The representational use of objects as other than what they seem is typified in his painting *The Treachery of Images*, which shows a pipe that looks as though it is a model for a tobacco store advertisement (Fig. 1). Below the pipe appear these words "Ceci n'est pas une pipe" ("This is not a pipe"), which seems to be a contradiction, but it is actually true: the painting is not a pipe, it is an *image* of a pipe.

In 1968, Michel Foucault wrote a delightful book entitled *Ceci n'est pas une pipe* ("This Is Not a Pipe"), inspired by René Magritte's painting. What is so captivating

D. L. Block (✉)
School of Computational and Applied Mathematics,
University of the Witwatersrand, Johannesburg, South Africa
e-mail: david.block@wits.ac.za

K. Freeman et al. (eds.), *Lessons from the Local Group,*
DOI 10.1007/978-3-319-10614-4_35

Fig. 1 'La trahison des images'—The Treachery of Images, by René Magritte. "Ceci n'est pas une pipe" (*This is not a pipe*) provides the viewer with an apparent contradiction. An interpretation and discussion of this remarkable painting appears in Sect. 1. Photo credit: © 2014 C. Herscovici, London/Artists Rights Society (ARS), New York

about this work by Magritte is the highly realistic depiction of a pipe on the one hand and the legend that Magritte writes below it, which echoes these words loud and clear: "This is not a pipe."

Foucault (1982) eloquently argues that "[neither words nor the visible] can be reduced to the other's terms: it is in vain that we say what we see; what we see never resides in what we say. And it is in vain that we attempt to show, by the use of images, metaphors, or similes, what we are saying . . . " As we cast our eyes carefully upon Fig. 1, we are gripped by a sense of surprise—a surprise which "inaugurates a play of transferences that run, proliferate, propagate, and correspond within the layout of the painting, affirming and representing nothing."

In the beginning of his book, Foucault sets the stage for the treachery of images—the curtain doors figuratively unfold, and we behold "a carefully drawn pipe, and underneath it (handwritten in a steady, painstaking, artificial script, a script from the convent, like that found heading the notebooks of schoolboys . . .), this note: 'This is not a pipe.' "

It is, as Foucault notes: "as simple as a page borrowed from a botanical manual: a figure and the text that names it. Nothing is easier to recognize than a pipe, drawn thus—our language knows it well in our place—than the 'name of a pipe.' "

Magritte's work is a brilliant interplay between the all pervasive power of language and that of image. Do we not, especially as young children, conjure up images in our minds by means of linguistics and the act of naming?

"Magritte names his paintings in order to focus attention upon the very act of naming," Foucault writes. "And yet in this split and drifting space, strange bonds are knit, there occur intrusions, brusque and destructive invasions, avalanches of images into the milieu of words, and verbal lightning flashes that streak and shatter the drawings."

The neurophysiology of vision, limitation and representation—and subsequent conclusions about "what is seen"—has remained a great interest of mine, over many years. No matter how vividly the painting conjures the thought of a real pipe in one's mind, the viewer is aware of the fact that it isn't a real pipe, bur rather an analogue of a real pipe.

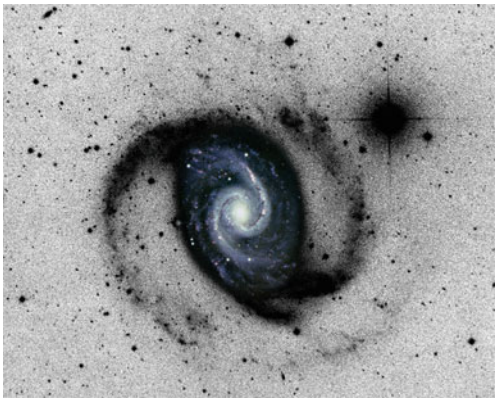

Fig. 2 A deep image of NGC 1566, reaching a surface brightness of $\sim$ 28 mag arcsec^{-2}, produced by David Malin in the stacking of photographic glass plates. An optical photograph of the galaxy is overlayed, for comparative purposes. Although the dust content in the outer disk must be low and almost devoid of bright young OB stars, the morphology seen here remains too faint to be recorded by conventional infrared detectors. Photograph courtesy David Malin

The pipe so depicted (Fig. 1) does not "satisfy emotionally". When Magritte once was asked about this image, he replied that of course it was not a pipe, just try to fill it with tobacco.

And so it is with galaxies and their masks, or shrouds. What *is* a galaxy? Do we, at best, merely see representations of a galaxy, such as the Andromeda Galaxy, or do we see the galaxy itself? Without a futuristic telescope dubbed by us a 'mass telescope' (Block and Freeman 2008), the failure of current arrays to capture dynamically active dark matter haloes poignantly highlights the treachery of images in an astronomical context.

The Oxford English Dictionary gives the established definition of a galaxy as follows:

"a luminous band or track, encircling the heavens ... ; the Milky Way", and states that the transferred and figurative use is "now chiefly applied to a brilliant assemblage or crowd of beautiful women or distinguished persons."

2 The Treachery of Conventional Images of Galaxies

Astronomers are well acquainted with optical morphologies from the *Hubble Atlas*. But that is only a minute representation of what there is. The deep images which follow in Figs. 2 to 4 were made by David Malin stacking several plates, invariably all from the UK Schmidt Telescope. The represented wavelengths are those in a slightly broadened B-band: Kodak's IIIa-J emulsion, behind a Schott GG395 filter.

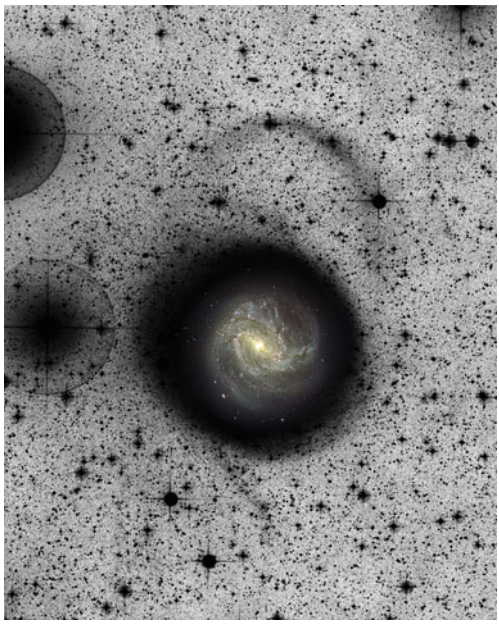

Fig. 3 A deep image of NGC 5236 (Messier 83) shows two remarkable outer 'handles'. A conventional, optical image of M83 is overlayed. Old stars in the faint outer disk must be responding to the dark matter halo in which the galaxy is embedded. Conversely, within the optical boundary, the dark matter distribution must be responding to the gravitational field of the stars. Photograph: David Malin

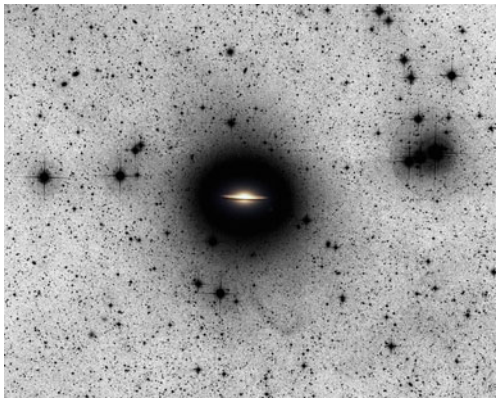

Fig. 4 A deep, photographically stacked image of the Sombrero Galaxy, shows extraordinary detail in its outer domains. Halos of dark matter and of stars are dynamically 'live' and interactions of stars in the outer disk and of dark matter must continuously be taking place. Photograph: David Malin

The passband is thus 3950 to 5500 Å, closely equivalent to the SDSS *g* band. (Occasionally, David Malin used a GG385 filter, yielding a slightly wider passband). The limiting surface brightness in these images is ~ 28 mag arcsec^{-2}.

Most of the light from stars in these deep Malin images comes from red giant branch (RGB) stars older than about 2 Gyr, with masses < 1.6 M$_\odot$. The stars near the tip of the RGB are K to M giants, depending on metallicity [Fe/H].

What is emphasized in astonishing detail is that none of these stellar haloes can be predicted from conventional images of these galaxies, shown as insets in Figs. 2–4. *La trahison des images* looms large.

3 The Dusty Universe

> We're now looking at a transition to a possible change in the way we look at galaxies. Sometimes ... we see disks that have a spiral structure that we couldn't have dreamt existed from looking at the optical picture ... we've got a possibility here of applying the morphology to a physical framework, perhaps in a way that none of us could have dreamt of before we had the capability of sweeping the dust away from the galaxy in a figurative sense.– R.J. Allen (1996).

In the early stages of my career, dust was regarded as a nuisance; something to be neglected. Cosmic dust pioneer J. Mayo Greenberg emphasized that to me, many times. From the pioneering photographic work of H.D. Curtis, E.E. Barnard, J. E. Keeler and others, to local cometary globules of dust in our Milky Way (e.g., the Rosette Nebula and its environs, Block 1990) ... what clues did these works hold regarding the prevalence of (cold) dust grains outside our Galaxy? Then, in 1994, we increased the dust/gas mass ratio in our Local Universe by one order of magnitude (Block et al. 1994a) and a pervasive population of cold (minus 250 C) dust grains was here to stay. Over the years, we have become painfully aware that optically thick dusty domains in galactic disks can completely camouflage or disguise underlying stellar structures. *Cosmic dust grains act as masks or shrouds* (Block and Freeman, 2008). The dust masks obscure whether or not the dust lies in an actual screen or is well intermixed with the stars. The presence of dust and the morphology of a galaxy are inextricably intertwined: indeed, the morphology of a galaxy can subtly change once the gaseous Population I disks of galaxies—the shrouds—are dust penetrated (e.g., Block and Wainscoat 1991; Block et al. 1994b). Such early papers of ours attracted the attraction of theoreticians such as F. Shu, G. Bertin and C.C. Lin (e.g., Bertin and Lin 1996)—and of course, Mayo Greenberg (see the volume edited by Block and Greenberg 1996).

The classification of galaxies has traditionally been inferred from photographs or CCD imaging shortward of the $1\mu m$ window, where *stellar* disks are not yet dust penetrated. Images through an I (0.83 μm) filter can still suffer from attenuations by dust at the 50 % level (e.g., Rix 1993). The NICMOS and other near-infrared camera arrays offer unparalleled opportunities for deconvolving gaseous and stellar morphologies, because the opacity at K (2.2 μm)—be it due to absorption or scattering—is always low. The extinction (absorption+scattering) optical depth at K is only 10 % of that in the V-band (Martin and Whittet 1990).

Many years before the advent of large format near-infrared camera arrays, it became increasingly obvious from rotation curve analyses that optical Hubble type is not correlated with the evolved stellar morphology. This was already evident in the pioneering work of Zwicky (1957) when he published his famous photographs showing the 'smooth red arms' in M51. In the *Hubble Atlas* and other atlases showing optical images of galaxies, we are looking at masks. At the gas. Not the stars, to which the properties of rotation curves are inextricably tied. Burstein and Rubin (1985) demarcate three principal types of mass distribution, with Hubble type a and b classes being found *among all three types* more or less equally. Clearly, one needs to probe what lies behind the dusty *Shrouds of the Night*.

The distribution of dust grains in the bulges and disks of galaxies may be very widespread as illustrated in the magnificent hand-drawn dust atlas of Beverly Lynds (1974). Seen there, through her masterful drawings, are interarm feathers and spurs. Furthermore, dust need not be confined to the disk itself. To cite but one striking example: the 2 kpc segment of bulge light scattered off the inner dust lane in NGC 2841, forms the largest reflection nebula yet identified, and lies ~ 0.5 kpc above the plane of the disk of NGC 2841 (see Block et al. 1999).

The tracing of dust grains in nature can be very elusive: high levels of dust extinction do *not* necessarily imply that the effects of dust attenuation (ie. observed reductions in surface brightness profiles) will also be large, because scattering by dust grains may fill in at least part of the lost surface brightness. The effective albedo of dust grains in the near-infrared can actually be higher than in the optical (for a determination of the near-infrared albedo of dust grains in M51, see Fig. 4 in Block 1996).

Furthermore, large amounts of dust do not necessarily imply red V−K colours. The dust column density on the far side of an inclined spiral with relatively *blue* V−K colours can be just as high as on the near side, where the V−K colour distribution can be much redder (Elmegreen and Block 1999).

It is important to stress that from a physical (dynamical) point of view, one requires *two* classification schemes—one for the gas, and a separate one for the stars. A near-infrared classification scheme can never *replace* an optical one, and vice-versa, because the *current* distribution of old stars strongly affects the *current* distribution of gas in the Population I disk.

The dynamic interplay between the two components—via a *self-regulation* mechanism—is crucial, and has been studied extensively (e.g., Bertin and Lin 1996), who term this mechanism a 'dynamical thermostat'; self-regulation may actually fail when the two components are not sufficiently well coupled. To quote Pfenniger et al. (1996), "The interesting aspect of [feedback] is that the systematic global properties of galaxies are then no longer necessarily determined by the initial conditions of collapse."

K band images are usually (but not always) dust penetrated, dependent upon $\tau(V)$, the optical depth. A few galaxies are so optically thick that even at K $(2.2\mu m)$ or K' $(2.1\mu m)$ one still sees long arms of dust: an example is NGC 2841 (Block et al. 1996).

Shu (2004) addressed this uncertainty in the coupling/decoupling of gaseous and stellar disks by drawing an analogy with the weather. To quote:

> Make all the measurements you can, still no one can predict the weather seven days from now. You can guess the weather tomorrow with some precision, but you really cannot guess well for a week later, no matter how fine are your observations because of the chaos in the system. We need to be prepared for this in our subject ...

Many galaxies show the presence of a significant m = 1 component in the near-infrared (lopsidedness of the spiral). The linear modal theory of Bertin et al. (1989a, b) predicts that m = 1 modes should generally be dominated by m = 2 modes when

available, since the latter are more efficient in transporting angular momentum outwards. However, modes with m>2 are generally suppressed in the stellar disk by the Inner Lindblad Resonance (ILR). Theoretical predictions were confirmed by observations (Block et al. 1989b; also Bertin and Lin 1996—a monograph containing many of our near-IR images). Infrared images show *a ubiquity of global one and two armed structures in the underlying stellar disk* and we believe that any classification of dust penetrated disks at K should take full account of this result (see Fig. 5). Theory and observations are in excellent agreement.

In contrast, the dynamics of the cold gaseous Population I disk, characterized by different scalelengths, velocity dispersion, thickness, and behaviour at the relevant Lindblad resonances, explains why spiral galaxies are optically so often overwhelmed by higher m modes and other more irregular fast evolving features, supported by the cold interstellar gas (Bertin 1991, 1993).

4 The Building of Galactic Disks: Active Evolution in the Triangulum Spiral M33

"That galaxies evolve is a trivial statement: galaxies are made of stars, stars evolve, and therefore galaxies evolve. But over and above such minimal evolution of the older stellar content of a galaxy, which is often called *passive* evolution, there exists the possibility of *active* galactic evolution . . . " Augustus Oemler, Jr.

A plethora of research papers in journals continue to focus on the formation of young galaxies, seen at high redshift. But what about learning of galaxy collisions and the formation of galaxies,from the Local Group? Do such studies concur that galaxies are built up by inflow from the environment as opposed to monolithic collapse (e.g. Block et al. 2002)? When using the terminology *active galactic evolution*, we include evolution of carbon stars in a galaxy—specifically in the outer domains. Carbon stars are important tracers of *intermediate age* stellar populations; they also make excellent test particles for investigating the kinematics of galaxies (Mould and Aaronson 1986). Carbon stars output such prodigious fluxes of light in the near-infrared that the K-band luminosity in galaxies containing a significant population of these intermediate age stars can be enhanced by up to a factor of 2 (Mouhcine and Lancon 2003).

Relative to the inner regions of spiral galaxies, the mean ages of the outer regions are known to be somewhat younger and more metal-poor (Bell and de Jong 2000). We thus expect the contribution from intermediate-age stars to be stronger in these outer regions, and the near-IR surface brightness of the outer disk of a galaxy will be preferentially enhanced by the presence of thermally pulsing—asymptotic giant branch (TP-AGB) stars. Astronomers routinely use near-IR observations to minimize the effects of dust extinction, but it is precisely in this band that TP-AGB stars are so bright; the actual contribution of carbon stars to the near-IR light of spiral galaxies beyond our Local Group is a field which remains to be exploited, especially with forthcoming extremely large telescopes such as the ELT. It was Aaronson (1986) and others who, many years ago, urged astronomers to remember the importance of the asymptotic giant branch for understanding the stellar content of nearer galaxies.

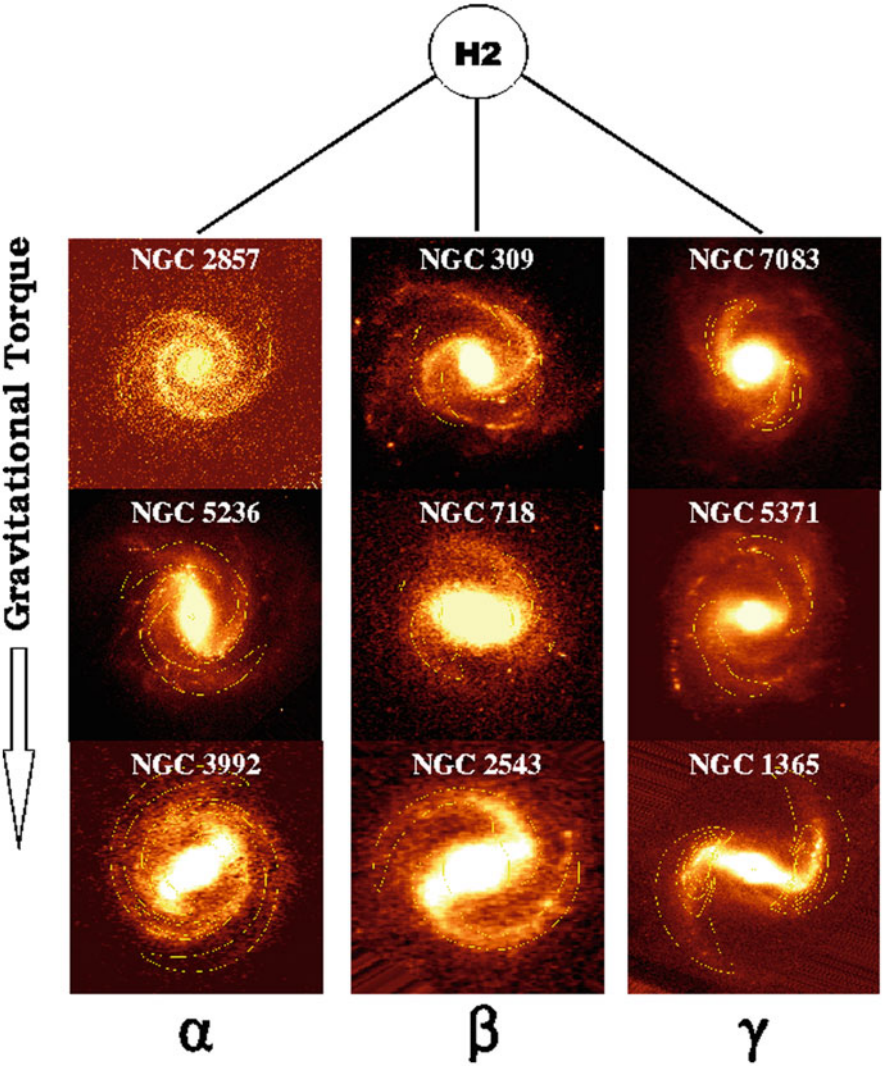

Fig. 5 Spiral galaxies in the dust penetrated regime are binned according to three quantitative criteria: firstly, Hm, where m is the dominant Fourier harmonic (illustrated here are the two-armed H2 family). As in Block and Puerari (1999), the dust penetrated pitch angle families α, β or γ are indicated. (For class α, the pitch angles range from $\sim$ 4–15°; for class β, the deprojected pitch angles range from $\sim$ 15–30°, while open-armed class γ spirals have pitch angles ranging between $\sim$ 35– 75°). Finally, we compute the gravitational torque, following Buta and Block (2001). Note that early type b spirals (NGC 3992, NGC 2543, NGC 7083, NGC 5371 and NGC 1365) are distributed within all three families (α, β and γ). Hubble type and dust penetrated class are uncorrelated

In the context of exploring the growth of a nearby disk, we present deep near-infrared images of the Triangulum Spiral Messier 33 in our Local Group (see Fig. 6 and the discussion in Block et al. 2004). M33 was probably first discovered by Giovanni Hodierna in 1654, before being independently discovered by Messier almost a century later, in 1764. The question beckons: Is Messier 33 an isolated, dynamically closed system of stars, as indeed suggested by early photographs, such as those secured using the Crossley reflector at the Lick Observatory? It was Heber D. Curtis who in 1918 described the Triangulum Galaxy as 'a close rival to the Nebula of Andromeda as the most beautiful spiral known'.

The galaxy presents somewhat of an optically flocculent (fleece-like) appearance, a fact already attested to by Lord Rosse in his early drawings ('the whole nebula in [is] flocculi'). In a range of 1–12, Elmegreen and Elmegreen (1987) place the Triangulum Galaxy in their class 5 bin. Sandage and Humphreys (1980) note that ten spiral arms may be identified in deep optical images, although the galaxy is most famous for its two bright inner set of spiral arms. At longer, near-infrared wavelengths, the galaxy appears much smoother as the older underlying population dominates the light (Regan and Vogel 1994). M33 extends over one degree along the major axis and it has a plethora of star clusters, emission regions and supernova remnants (see Hodgeet al. 2002 for a complete atlas of these). Its distance modulus is 24.64^m, corresponding to a linear distance of 840 kpc (Freedmanet al. 1991). Its linear diameter is $\sim$ 17 kpc, approximately one-half that of the Milky Way.

4.1 Lessons From the Triangulum Spiral M33: Farewell to Monolithic Collapse

Deep 2MASS images of M33 reveal remarkable arcs of red stars in the outer disk, spanning over 120° in azimuth and delineating a swath up to 5′ (see Fig. 6). These arcs are not revealed in the 2MASS survey itself. The integration time for these deeper images was increased by a factor of six, extending approximately 1 mag deeper than the standard survey. At $2.2\mu m$, the deep 2MASS images resolve larger-area features as faint as 22.5 magnitude arcsec^{-2}.

The northern arc in the outer domains of M33 is dominant, although a faint southern counterpart arc, forming a partial ring, can be seen in Fig. 6. In order to better see these plume features visually, we subtract off an axisymmetric disk model. The $J - K_s$ colours of stars in these arcs are so red (1.2 mag and cooler), that an M-giant population is excluded as the dominant light source. The arcs would be completely missed in conventional near-infrared surveys such as 2MASS.

To generate our Fourier spectra, we carefully determined the barycentre of the light (mass) distribution, and deprojected about that point. As in Deul & van der Hulst (1987) and Regan and Vogel (1994), we adopted the de Vaucouleurs values of log R = 0.23 (R is the ratio of the major-minor axis) and a position angle of 23 degrees.

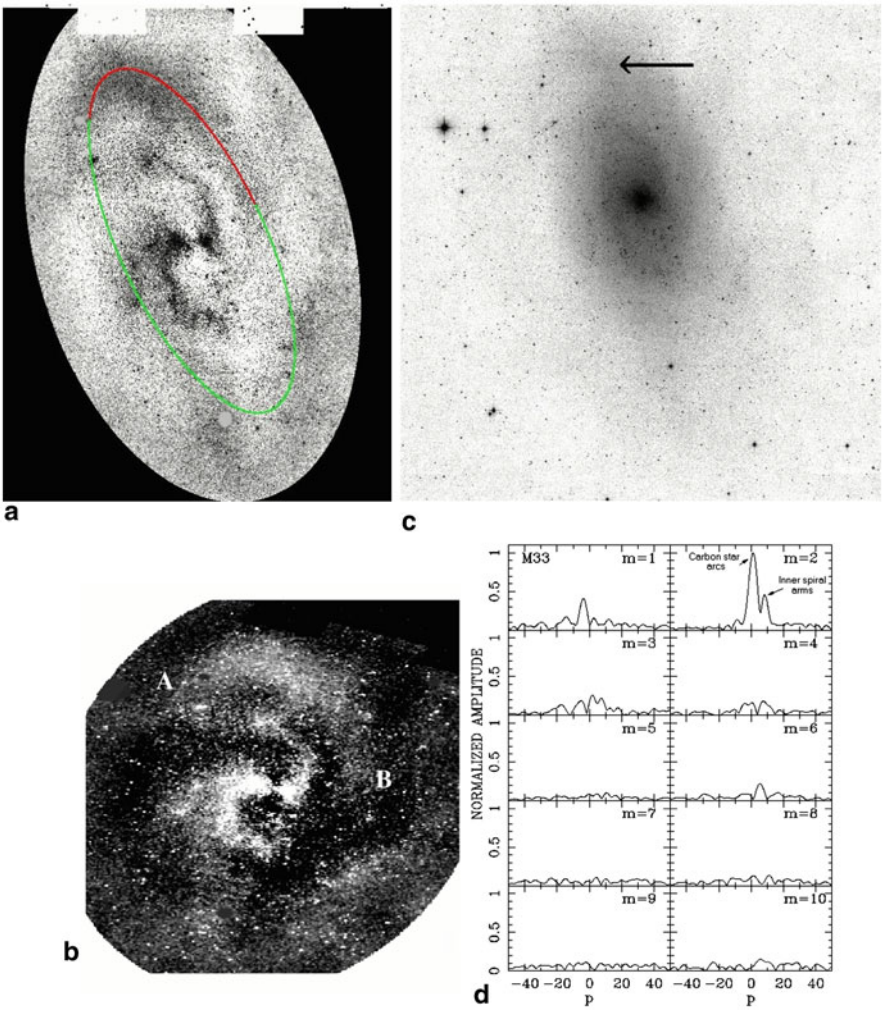

Fig. 6 **a** A deep JHK_s mosaic of M33. A gargantuan plume-like ring of red stars stretches in a swath (up to 5′ in width) for over 120 degrees, commencing at $\sim$ 14′ north of the centre of M33. In order to best reveal the plumes and inner arms, we have subtracted an axisymmetric model of the disk. **b** A deprojected JHK_s mosaic of M33, with an axisymmetric disk model subtracted. The northern plume is labelled A to B. **c** A deep 2MASS H band image of M33 (non-deprojected), reveals the northern arc (*arrowed*) and other red arcs in the outer disk of M33, **d** Fourier spectra generated from the deprojected near-infrared mosaic of M33. The dominant $m = 2$ mode in M33 arises from the giant outer ring or arcs of carbon stars

In M33, we comment that the only dominant modes are $m = 1$ and $m = 2$; the galaxy does not present ten arms in the near-infrared, as it does optically. The theme of the duality of spiral structure is ever recurrent. We immediately note that the two inner 'grand-design' trailing spiral arms seen optically show up rather strikingly in the near-infrared regime. The computed pitch angle is ~ 14 degrees. This inner set of near-infrared arms may also be seen in Regan and Vogel (1994) (see their Figs. 1 and 3).

Far more important, however, is the *dominant* and very high peak for m=2; the peak does not occur at zero (as expected for bars, for example, with pitch angles $\sim$ 90 degrees, corresponding to spectral m = 2 signatures with a peak at zero), as noted in Fig. 6. Rather, the dominant m = 2 peak corresponds to the set of giant arcs (very open two arm structures) on both the northern and southern sectors of the disk (Fig. 6, panel d). The pitch angle of the dominant m = 2 mode is ~ 58 degrees. *Surprisingly, it is these outer arcs (and not the inner grand design structure for which M33 is so famous) which dominates the m = 2 Fourier spectra.*

In Block et al. (2007), the Low Resolution Imaging Spectrograph (LRIS) attached to the Keck I telescope and the Echellette Spectrograph and Imager (ESI) on Keck II were used to secure spectra of stars in the arcs. To resolve individual stars in the arcs, the Hale 5-m reflector, equipped with the 2048 $\times$ 2048 near-IR camera WIRC, was employed to provide photometrically calibrated images at JHK. Keck spectra confirm that stars in the arcs are indeed carbon stars, being readily identified by the C_2 Swan and CN bands.

Where have these carbon stars in the outer disk formed? Where is accretion of gas in M33 most efficiently expected to take place? M33 has a huge warped envelope of neutral hydrogen gas, with a notable asymmetric extension toward the North-West (eg. Corbelli and Schneider 1997). These authors suggest that this NW extension may be a betrayal of tidal interaction between M33 and M31, which are only ~ 200 kpc apart.

In their modelling of the HI envelope, Corbelli and Schneider find that the phase changes at a radius of ~ 20 arcmin (2–3 disk scalengths), which is precisely the outer domain of the arcs reported in our study. It seems highly plausible therefore, that fresh, low-metallicity gas is being fed to the host galaxy M33, via external accretion. The outer disk from which mass is accreted is inclined to the inner disk of M33, and has a different angular momentum. We believe that it is the signature of gas flowing inward and accreting at ~ 20 arcmin, from which the very red, and relatively metal-poor stars, have been formed.

In summary, we propose that intermediate age (0.6–2 Gyr) carbon stars have formed as a result of accretion at the HI warp. If true, the disks of spiral galaxies in our Local Group (such as M33) have been built up by inflow from the environment, in contrast to monolithic collapse. Just as in the high redshift Universe.

Carbon star diagnostic for the evolution of outer disks hold enormous promise, due to prodigious output in K-band fluxes.

It is tempting to liken the ring in M33 to the one reported in the outer disk of our Milky Way (Ibata et al. 2003). For the Milky Way ring, the rotation period is ~ 600 Myr. For M33, the rotation time-scale at the radius of the ring would be ~ 240 Myr. Any carbon-bearing clusters of age 0.6 Gyr would have only undergone ~ 2 orbits.

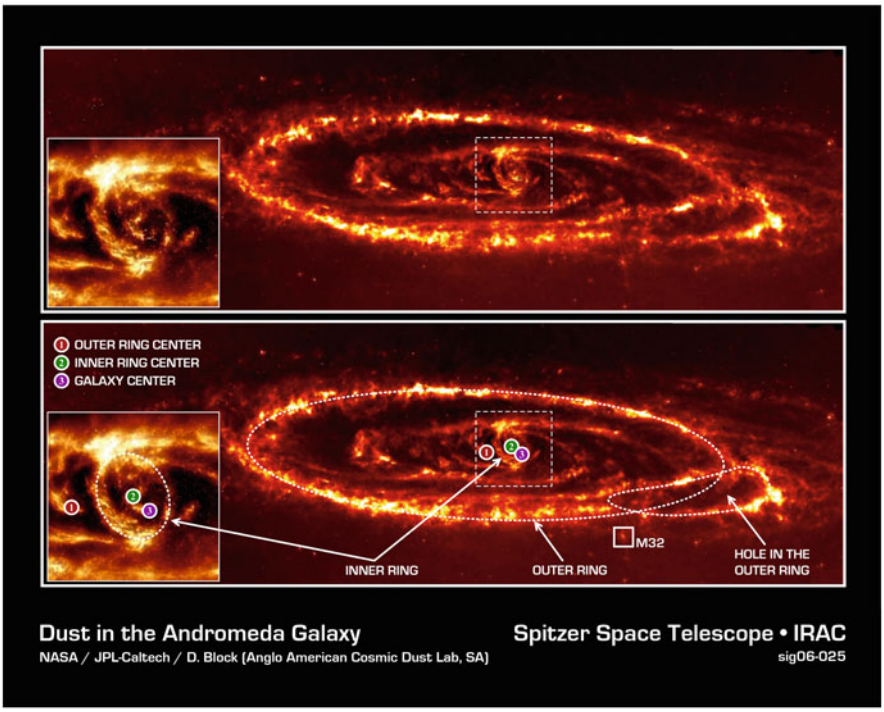

Fig. 7 A recently discovered inner dust ring in the Andromeda Spiral Galaxy, betraying crucial evidence of an almost head-on collision between M31 and M32. See Block et al. (2006) for further details. Courtesy: NASA and JPL-Caltech

5 Rings in the Andromeda Spiral: A Near Head-on Collision

Although regarded for decades as showing little evidence of a violent history, the Andromeda Spiral Messier 31 has a well known outer ring of star formation at a radius of 10 kpc whose centre is offset from the galaxy nucleus. Could there have been a relatively recent collision involving a massive spiral and one of its neighbours, in our Local Group? The sort of analog of a Cartwheel, but on our doorstep? Block et al. (2006, including F. Combes and G. Fazio at this meeting) report the presence of a second, inner dust ring with projected dimensions 1.5 by 1 kpc and offset by $\sim$ 0.5 kpc from the centre of the galaxy (Fig. 7). The two rings are interpreted to be density waves propagating in the disk of M31. We suggest that both rings result from a companion galaxy (presumably M32) plunging in a *near head-on collision* through the disk of M31. That an almost head-on collision has occurred only $\sim$ 210 million years ago suggests the treachery of optical images of the Andromeda Spiral, wherein one is tempted to believe that its morphology has existed quiescently for billions of years. And it underscores the point that to unravel the rich history of colliding galaxies and of rings, we need only take a peek upon our local cosmic

doorstep! An analogy: in terms of African game, do zoologists spend all their time trying to comprehend the behaviour of cheetahs *Acinonyx jubatus* by restricting their study to only those in the far distance—necessitating the use of especially powerful binoculars—or rather, selecting local specimens, seen moving swiftly at close spatial range, across the African savannah?

6 Conclusion—'La Condition Humaine'

"Lo, there, quod he, cast up thine eye. Se yonder, lo, the Galaxye, Which men clepeth the Milky Wey, For hitt is whytt, and some parfey, Callen hit Watlinge Strete."—Geoffrey Chaucer (The House of Fame)

" What are galaxies? No one knew before 1900. Very few people knew in 1920. All astronomers knew after 1924 . . . Each galaxy is a stellar system somewhat like our Milky Way, and isolated from its neighbors by nearly empty space."

The above definition (from the *Hubble Atlas*, 1961) is not true for the Andromeda Spiral, neither for the Triangulum Galaxy.

The morphological properties of galaxies are constrained by a wide range of processes, both internal and environmental (Freeman 2000). The pioneering research of Arnaboldi and collaborators (e.g., Arnaboldi et al. 2006) highlights the interaction of galaxies with their environment. They carefully trace diffuse intracluster light by means of the identification and radial velocity measurements of intracluster planetary nebulae, using their [OIII] 5007 Å emission.

Why bother about the definition of a galaxy?

Prior to the inference of dark matter haloes in spiral galaxies from rotation curve studies (Freeman 1970), dark matter was not regarded as a crucial component of a galaxy. Today we know otherwise, although we know that tidal dwarf galaxies show no evidence for dark matter. (Presumably these have formed from baryons stripped during an encounter).

In defining a galaxy, there are clearly different levels of complexity; here are a few:

Should magnetic fields be incorporated into the definition of a galaxy? We are reminded of a sobering thought by Shu (2004) in addressing this specific point at a Conference:

> We haven't yet heard a single talk that had Maxwell's equations in it. It [magnetic fields] is the only other long range force that we know about, right? When did magnetic fields become important in galaxy formation and evolution? The fact that we see synchrotron radiation in radio sources certainly says that in some parts of galaxies, magnetic fields were generated at early times. Magnetic fields are important because they are the dominant way, other than gravitational torques, by which you can transport angular momentum. So if angular momentum is a big problem in galaxy formation, maybe we should look at magnetic fields before we think of exotic forms of dark matter!

What about accretion of gas in the outer domains? What are the implications of the deep images of David Malin (Figs. 2–4), in defining the term 'galaxy'? New galaxy classification schemes are called for. Vera Rubin writes: "One look at the stunning

Fig. 8 Omega Centauri, captured by the Wide Field Imager at the European Southern Observatory, Chile. "Ceci n'est pas un amas globulaire" is translated "This is not a globular cluster". See Freeman (1993). Photograph: ESO

Fig. 9 Below the optical representation of Messier 104 appears these words: "Ceci n'est pas une galaxie" being translated "This is not a galaxy". Photograph: David Malin

images produced by astrophotographer David Malin is sufficient to convince any skeptic."

Without a clear understanding of what constitutes a galaxy, astronomers walk in a land of shadows and of masks. The same would be true for cosmological assumptions and presumptions, as the cosmic landscape there too, is filled with shadows and masks (Block 1974).

In the spirit of Magritte's "La trahison des images" seen in Fig. 1, we provide the reader with three astronomical equivalents, shown Figs. 8–10. The legend in Fig. 8 is translated "This is not a globular cluster", which might at first sight seem rather unusual for ω Centauri. It has been argued that what we see in Fig. 9 is rather a representation of an ancient galaxy (Freeman 1993 and subsequent papers).

The legend in Fig. 9 reads: "This is not a galaxy". Of course not. What we see is the optical mask only—a representation of the galaxy at optical wavelengths. How amazingly different is the morphology of the Sombrero in deep images (Fig. 4).

Fig. 10 NGC5084, the most massive disk system known, has a mass–to-light ratio of $\sim$ 200, and an inferred mass up to 1×10^{13} $M_{\odot}$. *This*—that which is represented in this optical photograph—is not *the galaxy NGC5084*—with its massive, undetected dark matter halo. Ceci n'est pas une galaxie. It remains a representation thereof, in the optical regime. Photograph: Anglo Australian Telescope

Likewise, Fig. 10 is an optical representation of the galaxy NGC 5084, with one of the highest mass-to-light ratios known (as studied by Freeman and collaborators. For a detailed discussion, see Carignan et al. 1997). Figure 10 fails to yield the minutest hint of its massive dark matter halo; *this photograph*—that which we see represented in Fig. 10—is *not* NGC 5084, with its massive dark matter halo.

In place of an astronomer who frames the Triangulum Galaxy or the Andromeda Spiral Galaxy or ω Centauri to picture it, Nature produces its own image without a necessary frame.

This is, after all, our human condition.

We tend to "frame reality" in our minds, as captured in a poignant and astute tone by René Magritte in his exquisite rendition of the human condition, entitled "La condition humaine" (1933). One of Magritte's most common artistic devices was the use of objects to hide what lies behind them. For example, in the human condition, the cover-up appears in the form a painting within a painting (Fig. 11).

Magritte had this to say of his 1933 work: "In front of a window seen from inside a room, I placed a painting representing exactly that portion of the landscape covered by the painting. Thus, the tree in the picture hid the tree behind it, outside the room. For the spectator, it was both inside the room within the painting and outside in the real landscape."

7 The Human Condition and Perspective

To any researcher, young or old, "La condition humaine" is a treasure, for the focus is on perspective. Along any career path, perspective is crucial. How well do I recall receiving a note on perspective from someone who had to face hostility—and overcome it. The note read thus:

"Please know that I am sorry about the hostile environment that you too have to live in. If you will forgive a bit of (accurate) hyperbole, you are a sturdy oak living in a field of scraggly bushes. The bushes don't much appreciate the shade, and I

Fig. 11 "La condition humaine" or "The Human Condition". Magritte pens this description: "In front of a window seen from inside a room, I placed a painting representing exactly that portion of the landscape covered by the painting. Thus, the tree in the picture hid the tree behind it, outside the room. For the spectator, it was both inside the room within the painting and outside in the real landscape." Photo credit: © 2014 C. Herscovici, London/Artists Rights Society (ARS), New York

doubt that they like being invisible from far away. The only tactics that they know are crowding and strangulation. Fortunately, being tall, you always get "first crack" at the sunlight. And having deep roots means that they can never deprive you of the most important nourishment. Besides which, crowned crane will always roost in your branches—they are safe there, and the view is good. And inevitably, they poop on the bushes."

To the person who once sent me that note some time ago, my most sincere thank you. Your perspective carried me through, as did a photograph, especially sourced by Ken Freeman. Perspective does bring peace and tranquillity. Figure 11 is, after all, "The Human Condition", so masterfully depicted by René Magritte.

Acknowledgements I remain most indebted to my collaborators and special friends, several of whom were with me in the Seychelles archipelago. Profound gratitude is expressed to our SOC Chair and my collaborator, Ken Freeman. We have both held a selection of Galileo's original manuscripts in our hands! Ken began spearheading this birthday Conference toward the beginning of 2013. A most blessed millionth (base 2) birthday year to Bruce: Amicus verus est rara avis—A true friend is a rare bird (see Fig. 12). An earlier version of the science-morphology-art interface was presented at the 70th birthday fest of Ken Freeman held in Namibia in 2010. Permission from Springer to reproduce, in large part, major sectors of the paper contained in the Block, Freeman and Puerari (2010) volume, is much appreciated. Deep gratitude is expressed to my long time friend David Malin in Sydney, Australia.

I remain indebted to the referee for most helpful and insightful comments.

Fig. 12 A ‘word cloud’, showing words from the titles of papers in which Bruce Elmegreen and I are both collaborators. The size of the words is indicative of the frequency in which they occur in the titles. Image courtesy: Bruce Elmegreen

References

Aaronson, M., 1986, *in Stellar Populations*, Cambridge University Press, 45

Allen, R.J. 1996, *in New Extragalactic Perspectives in the New South Africa*, Eds. D.L. Block & J.M. Greenberg, Kluwer, p. 585

Arnaboldi, M. et al. 2006, IAU Symposium 234, 337

Bell, E.F., & de Jong, R.S. 2000, MNRAS 312, 497

Bertin G., 1991, IAU 146, Dynamics of Galaxies and Their Molecular Cloud Distributions, Kluwer, 93

Bertin G., 1993, PASP 105, 604

Bertin G., & Lin C.C. 1996, Spiral Structure in Galaxies: A density wave theory, MIT Press, Cambridge, Massachusetts

Bertin G., Lin C.C., Lowe S.A., & Thurstans R.P., 1989a, ApJ 338, 78

Bertin G., Lin C.C., Lowe S.A., & Thurstans R.P., 1989b, ApJ 338, 104

Block, D.L. 1974, Q.J.R.A.S. 15, 264

Block, D.L. 1990, Nature 347, 452

Block, D.L. 1996, *in New Extragalactic Perspectives in the New South Africa*, Eds. D.L. Block & J.M. Greenberg, Kluwer, ASSL 209, p. 1

Block, D.L. & Greenberg, J.M. 1996, *New Extragalactic Perspectives in the New South Africa*, Eds. D.L. Block & J.M. Greenberg, Kluwer, ASSL 209. The entire volume

Block, D.L. & Freeman, K.C. 2008, *Shrouds of the Night*, Springer, New York

Block., D.L. & Puerari, I. 1999, A&A 342, 627

Block D.L. & Wainscoat R.J. 1991, Nature 353, 48

Block D.L., Witt A.N., Grosbøl P., & Stockton A. 1994a, A&A 288, 383

Block D.L., Bertin G., Stockton A., Grosbøl P., Moorwood A.F.M., & Peletier R.F. 1994b, A&A 288, 365

Block D.L., Elmegreen B.G., & Wainscoat R.J. 1996, Nature 381, 674

Block D.L., Stockton A., Elmegreen B.G., & Willis J. 1999, ApJ 522, L25

Block, D.L., Bournaud, F., Combes, F., Puerari, I., & Buta, R. 2002, A&A 394, L35

Block, D.L. et al. 2004, A&A 425, L37

Block, D.L., Bournaud, F., Combes, F. et al. 2006, Nature 443, 832

Block, D.L., Combes, F., Puerari, I., Freeman, K.C. et al. 2007, A&A 471, 467

Block, D.L., Freeman, K.C. & Puerari, I. 2010. Galaxies and their Masks: A conference in honour of K.C. Freeman, FRS. Eds. D.L. Block, K.C. Freeman & I. Puerari, Springer (New York), 23

Burstein D., & Rubin V. 1985, ApJ 297, 423

Buta, R.J., & Block, D.L. 2001, ApJ 550, 243
Carignan, C., Cotê, S., Freeman, K.C., & Quinn, P.J. 1997, AJ 113, 1585
Corbelli, E., & Schneider, S.E. 1997, ApJ 479, 244
Deul, E.R., & van der Hulst, J.M. 1987, A&AS 67, 509
Elmegreen B.G., & Block D.L. 1999, MNRAS 303, 133
Elmegreen, D.M., & Elmegreen, B.G. 1987, ApJ 314, 3
Foucault, M. 1982, *This Is Not a Pipe*, University of California Press
Freedman, W.L., Wilson, C.D., & Madore, B.F. 1991, ApJ 372, 455
Freeman, K.C. 1970, ApJ 160, 811
Freeman, K.C. 1993, ASP 48, 608
Freeman, K.C. 2000, in Towards a New Millenium in Galaxy Morphology, Eds. D.L. Block, I. Puerari, A. Stockton, & D. Ferreira, Kluwer, 119
Hodge, P.W., Skelton, B.P., & Ashizawa, J. 2002, *An Atlas of Local Group Galaxies*, Kluwer
Ibata, R.A., Irwin, M. J., Lewis, G.F., Ferguson, A.M.N., Tanvir, N. 2003, MNRAS, 340, L21
Lynds B.T. 1974, ApJS 28, 391
Martin P.G. & Whittet D.G.B. 1990, ApJ 357, 113
Mouhcine, M., Lancon, A. 2003, A&A 402, 425
Mould, J., & Aaronson, A. 1986, ApJ 303, 10
Pfenniger D., Martinet L., & Combes F. 1996, *in New Extragalactic Perspectives in the New South Africa*, Eds. D.L. Block & J.M. Greenberg, Kluwer, p. 291
Regan, M.W., & Vogel, S.N. 1994, ApJ 434, 536
Rix H.-W., 1993, PASP 105, 999
Sandage, A., & Humphreys, R.M. 1980, ApJ 236, L1
Shu, F.H. 2004, *in Penetrating Bars Through Masks of Cosmic Dust*, Eds. D.L. Block, I. Puerari, K.C. Freeman et al., Springer, p. 813
Zwicky F. 1957, Morphological Astronomy, Springer-Verlag, Berlin.

First Results from Project Dragonfly

Roberto G. Abraham, Pieter G. van Dokkum, Allison Merritt and Jielai Zhang

Abstract We describe first results from the Dragonfly Telephoto Array, a robotic imaging system optimized for the detection of extended ultra low surface brightness structures. The imaging system is comprised of multiple commercial 400 mm $f/2.8$ telephoto lenses which have high performance sub-wavelength nano-fabricated optical coatings designed to minimize scattered light and ghosting, resulting in wide-field low surface brightness imaging performance an order of magnitude better than that of the best reflectors optimized for wide-field imaging. The array is capable of directly imaging low surface brightness structures (such as streams and faint dwarf galaxies) that have hitherto only been detectable using star counts. Therefore a range of studies that have hitherto been restricted to the Local Group can now be undertaken using samples of hundreds of more distant galaxies. Harnessing this new capability, the Dragonfly Telephoto Array is now executing a fully-automated multi-year imaging survey of a sample of nearby galaxies in order to undertake the first census of ultra-faint substructures in galaxies in the nearby Universe. In this conference writeup, we report some early results from a single galaxy, M101, that we have used to help test the system. The radial surface brightness profile of this galaxy was measured down to $\mu_g \sim 34$ mag/arcsec^2, showing no significant upturn at large radius. The galaxy is well-approximated by a simple exponential disk model out to a radius of 70 kpc, corresponding to 18 disk scale lengths. The stellar halo mass fraction of this galaxy falls an order of magnitude below the expectations of theoretical predictions. Dragonfly data has also revealed the existence of seven large, low surface brightness objects in the field of M101, with effective radii of 10–30 arcsecond and central surface brightnesses of $\mu_g \sim 25.5 - 27.5$ mag/arcsec^2. Given their large apparent sizes and low surface brightnesses, these objects would likely be missed by standard galaxy searches in deep fields. Assuming these objects are companions to M101, the properties of these galaxies are similar to those of well-studied dwarf galaxies in the Local Group, such as Sextans I and Phoenix.

R. G. Abraham (✉)
Department of Astronomy & Astrophysics, University of Toronto, 50 St. George Street, ON L6M 2N5, Toronto, Canada
e-mail: abraham@astro.utoronto.ca

P. G. van Dokkum · A. Merritt · J. Zhang
Department of Astronomy, Yale University, 260 Whitney Avenue, CT 06511, New Haven, USA

K. Freeman et al. (eds.), *Lessons from the Local Group,*
DOI 10.1007/978-3-319-10614-4_36

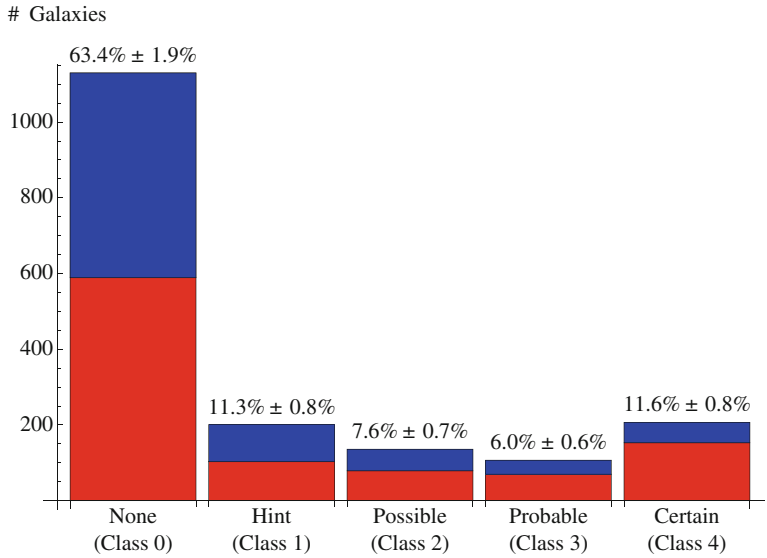

Fig. 1 Distribution of tidal feature detection classes in the CFHTLS-Wide dataset. Bins from *left to right* correspond to increasingly confident detections of tidal features. Each histogram bin is labeled by its fractional contribution to the total galaxy population, and each bin is subdivided into *red sequence* and *blue cloud* populations. The sample consists of 1781 luminous ($M_{r'} < -19.3$ mag) galaxies in the magnitude $15.5 < r' < 17$ mag and in the photometric redshift range $0.04 < z < 0.2$. Source: Atkinson et al. (2013)

1 Introduction

In a dark energy-dominated cold dark matter (ΛCDM) Universe with largely scale-invariant dark matter halos, $L \gtrsim L_*$ galaxies are thought to be very efficient in accreting smaller neighbours. This infall and accretion process leaves tell-tale features: streams left behind in the wake of the accreted satellites, and tidal distortions and tails. These features should have lifetimes of up to half the Hubble time, so every large galaxy in the Universe is expected to live in an extended, irregular tidal debris field (Dubinski et al. 1996; Moore et al. 1999; Naab et al. 2007; Cooper et al. 2010; 2013).

Although tidal features in galaxies have been identified and studied for many decades (e.g. Toomre and Toomre 1972), most galaxies appear stubbornly unperturbed. The situation is summarized in Fig. 1 (taken from Atkinsonet al. 2013) which shows that even on deep CFHT images, only around 12 % of luminous galaxies show absolutely clear evidence for tidal features at a high confidence level, rising to around 34 % if systems with hints of tidal features are included. On the whole, red galaxies are twice as likely to show tidal features than are blue galaxies down to a limiting surface brightness around $g \sim 28$ mag/arcsec^2.

A possible explanation for this 'missing substructure problem' is that that we are simply not yet probing the required surface brightness limits to detect the predicted structures. Detailed simulations of tidal debris around Milky Way-like galaxies based on 'painting' N-body data to mimic real observations (Johnston et al. 2008; Cooper et al. 2010) and elliptical galaxies (Naab et al. 2007) indicate that the majority of accreted stars live at surface brightness levels $\gtrsim$ 29 mag arcsec^{-2}. However, deep imaging surveys with standard reflecting telescopes typically reach surface brightness levels of 'only' $\sim$ 28 mag arcsec^{-2} (van Dokkum et al. 2005; Tal et al. 2009; Martinez-Delgado et al. 2010; Atkinson et al. 2013). Therefore it is natural to suspect that the 'missing substructure problem' finds its origin in the limitations of our telescopes for undertaking low surface brightness imaging. A related issue, the 'missing satellites problem' (in which the number of dwarf galaxies in the local group is lower than expected from numerical simulations) may have a similar solution, if the missing satellites have very low surface brightnesses.

2 A Low-Surface Brightness Optimized Imaging System

Imaging to surface brightnesses fainter than $\sim$ 28 mag arcsec^{-2} has proven very difficult. This is due to the fact that the limit is not defined by photon statistics, but rather by systematic errors. The most obvious of these is the error introduced by imperfect flat fielding. Flat fielding errors need to be smaller than 0.1 % to reach $\sim$ 30 mag arcsec^{-2}. This is challenging, but it is achievable if careful procedures are adopted. More difficult problems that must be overcome include ghosting and diffraction, which together result in a complex and spatially variable low-surface brightness point spread function (PSF) at large angles. This faint component of the PSF is ignorable in most applications, but it plays a central role at low surface brightness levels. For example, Slater et al. (2009) show that even with a telescope that is highly optimized for low surface brightness imaging, diffraction from the secondary mirror assembly, coupled with scattering and internal reflections in the optical train and micro-roughness in aluminized optical surfaces[1], produces a complex emission structure that fills the entire imaging frame below $\sim$ 29 mag arcsec^{-2}. The difficulties are compounded by the fact that a field of view of several degrees is desirable, because nearby galaxies are enormous at low surface brightness levels. For example, extrapolation of the profile of typical Virgo cluster elliptical suggests angular diameters of over a degree at surface brightness levels around 30 mag arcsec^{-2}. Ideally, such large areal coverage would be achieved without the need for mosaiced detectors, which can add significant challenges to low surface brightness imaging.

The Dragonfly Telephoto Array (Fig. 2) is an attempt to redefine the capabilities of ground-based telescopes for wide-field low surface brightness imaging. The array

[1] Interestingly, it appears that several of the basic design trades that make large telescopes possible (in particular, obstructed pupils and reflective surfaces) define the fundamental systematic errors that make pushing to very low surface brightnesses so difficult.

Fig. 2 The Dragonfly Telephoto Array installed at the New Mexico Skies telescope hosting facility. The array consists of eight Canon 400/f2.8 L IS II USM telephoto lenses attached to eight SBIG STF-8300M CCD cameras, all carried by a Paramount ME-II German equatorial mount. The system is controlled by the three computers shown in the foreground. (Source: Abraham and van Dokkum (2014))

consists of eight Canon EF 400 mm f/2.8 L IS II USM telephoto lenses on a common mount. Telephoto lenses have no central obstruction and are optimally baffled. Furthermore, the specific lenses used in the array are of superb optical quality, partially owing to nano-fabricated sub-wavelength corrugations on their anti-reflecting coatings. As we show in Abraham and van Dokkum (2014), the Dragonfly point spread function has an order of magnitude less scattered light than the best reflecting telescopes (Fig. 3). By combining eight lenses that image the same area of sky we built a "compound eye" that acts as a 0.4 m f/1.0 refractor. In its default configuration, four of the lenses are equipped with SDSS g-band filters and four with SDSS r filters. The pixel scale is 2.8 arc sec and the angular field covered by each camera is 2.6 x 1.9° . The potential of this system is best illustrated by example, and in this writeup we will use the nearby spiral galaxy M101 as a case study.

3 The Dragonfly View of M101

A 35 h integration of M101 obtained with Dragonfly is shown in Fig. 4. We refer the reader to van Dokkum et al. (2014) for the details of how the luminosity profile of M101 (extending down to $\mu_g \sim 34$ mag/arcsec^2) was obtained, but the corresponding

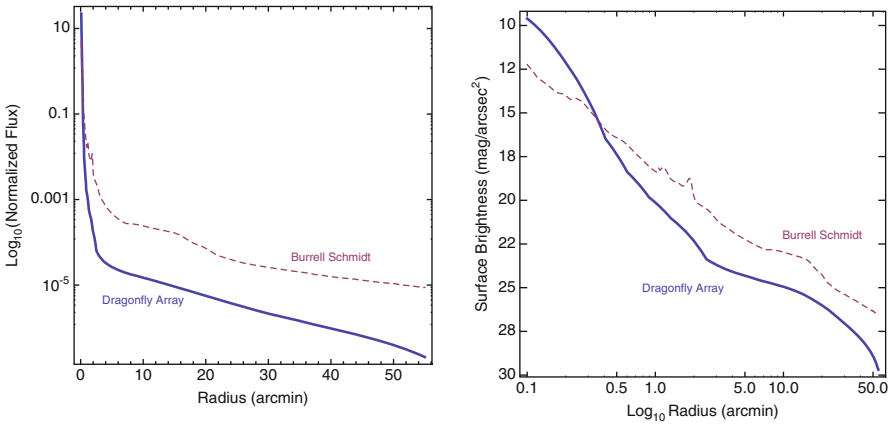

Fig. 3 Comparison of the wide-angle halo point-spread function of the Canon telephoto lenses used in the Dragonfly Telephoto Array with the corresponding point-spread function of the 0.9 Burrell Schmidt telescope on Kitt Peak (Slater et al. 2009). The Burrell Schmidt is optimized for low surface brightness imaging and has produced a well-known ultra-deep image of the Virgo cluster (Mihos et al. 2005). The minimum radius plotted is 0.1 arcmin, and in both cases $\gtrsim 90\%$ of the total stellar flux is interior to this, so only a small fraction of a star's total light is contained within the wide-angle halo (mainly due to scattering and internal reflections) shown in these plots. [*Left Panel*:] Flux as a function of linear radius, after normalizing both profiles to contain identical total fluxes. Note that in large part thanks to nano-fabricated anti-reflection coatings on some of its elements, the Canon lenses have a factor of $5 - 10$ less halo light at radii > 5 arcmin. [*Right Panel*:] The r-band AB mag/arcsec^2 surface brightness profile of Vega as a function of logarithmic radius for the Dragonfly Array and for the Burrell Schmidt telescope. (Source: Abraham and van Dokkum (2014))

mass density profile (extending out to 18 scale lengths) for the galaxy is shown in Fig. 5. The form is similar to the surface brightness profile, except for the central regions as those are more prominent in mass than in blue light. The data reach surface densities of $\lesssim 10^3\ M_\odot\ \mathrm{kpc}^{-2}$, and a non-parametric limit on the stellar halo of M101 is that it has a stellar mass density lower than this limit at $R \gtrsim 60$ kpc. The profile is well-described by an exponential disk and a Sersic (1968) bulge, taking the form

$$\rho(R) = \rho_{0,d} \exp\left(\frac{R}{R_d}\right) + \rho_{0,b} \exp\left[-4.85\left(\frac{R}{R_e}\right)^{1/n}\right], \qquad (1)$$

with $\rho_{0,d} = (4.40 \pm 0.11) \times 10^8\ M_\odot\ \mathrm{kpc}^{-2}$, $R_d = 3.98 \pm 0.06$ kpc, $\rho_{0,b} = (2.24 \pm 0.08) \times 10^{10}\ M_\odot\ \mathrm{kpc}^{-2}$, $R_e = 1.67 \pm 0.12$ kpc, and $n = 2.62 \pm 0.16$. This 'no halo' fit is shown by the red solid line in Fig. 5a. Of course the "bulge" may in fact be more appropriately called a pseudo-bulge or an inner disk; as is well known M101 has a very low central velocity dispersion and spiral arms that continue into the central few arcsec (Kormendy et al. 2010). A model with a small stellar halo contribution is shown in Fig. 5b, and while this gives a lower χ^2, the improvement in the fit is only marginally significant given the additional free parameters. The total mass implied by this model, integrated to $R = 200$ kpc (near the virial radius), is

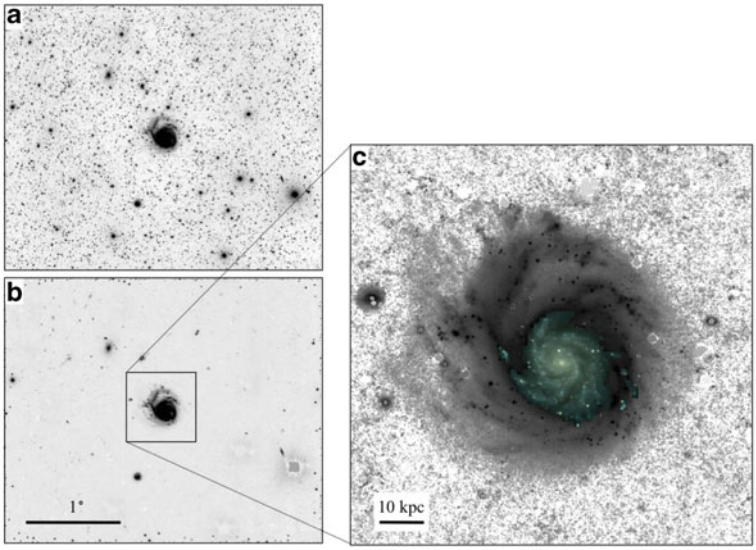

Fig. 4 **a** Dragonfly g-band image of the 3.33° × 2.78° area centered on the galaxy M101. North is up and East is to the left. **b** The same image, after subtraction of stars and a model for large scale ($\gtrsim$ 1°) background structure. Owing to the excellent PSF of Dragonfly, stars as bright as $\sim$ 6th magnitude affect only a relatively small number of pixels, and can be subtracted. **c** The 44′ × 44′ area around M101 at high contrast. The *faint spiral arms* on the *East side* of M101 (Mihos et al. 2013) have a surface brightness of $\mu_g \sim 29$ mag arcsec^{-2}. The *color image* in the *center* was created from the g and r exposures. (Source: van Dokkum et al., (2014))

$M_{\mathrm{tot},*} = 5.3^{+1.7}_{-1.3} \times 10^{10}\, M_\odot$. The halo mass is $M_{\mathrm{halo}} = 1.7^{+3.4}_{-1.7} \times 10^{8}\, M_\odot$, and we infer that the fraction of mass in the halo is $f_{\mathrm{halo}} = M_{\mathrm{halo}}/M_{\mathrm{tot},*} = 0.003^{+0.006}_{-0.003}$. This fraction is significantly lower than the halo fraction of M31, for which Courteau et al. (2011) find $f_{\mathrm{halo}} \sim 0.04$ using the same decomposition method. We illustrate this difference in Fig. 5c, where we show what M101's profile would look like if the galaxy had a 4 %, M31-like halo. Such halos are clearly inconsistent with the data.

The stellar halo fraction is lower than that of M31 ($f_{\mathrm{halo}} \sim 4$ %; Courteau et al. 2011) and also the Milky Way ($f_{\mathrm{halo}} \sim 2$ %; Carollo et al. 2010; Courteau et al. 2011). In Fig. 6 we show the relation between stellar halo fraction and galaxy stellar mass. The stellar masses of the Milky Way and M31 were taken from McMillan (2011) and Tamm et al. (2012) respectively. For comparison, we show the relation between the accreted fraction of stars and galaxy stellar mass as predicted by numerical models that trace the light of accreted satellites in dark matter halos. This relation was derived from the data in Fig. 12b of Cooper et al. (2013) for bulge-to-total ratios $B/T < 0.9$; the relation for other B/T limits is very similar.

Interestingly, the stellar halo masses of all three galaxies are below the predicted relation, with M101 a factor of $\sim$ 10 below the median expectation. Given the stochastic nature of accretion events and, as a consequence, the large scatter predicted in the $f_{\mathrm{halo}} - M_{\mathrm{tot},*}$ relation (Purcell et al. 2008; Cooper et al. 2013; Fig. 4), it

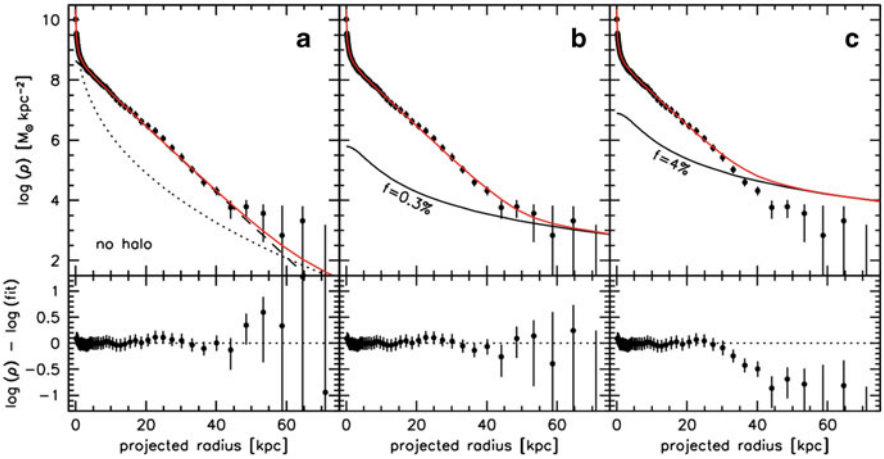

Fig. 5 **a** Mass density profile of M101. The *red line* is a bulge + disk fit to the profile, with the individual components indicated by *broken lines*. This fit provides an adequate description of the full profile, as shown by the residuals in the *bottom panel*. **b** Best-fitting bulge + disk + halo fit. The best fit is obtained for a stellar halo contributing $0.3^{+0.6}_{-0.3}$ % of the total mass. **c** Fit with a halo contributing 4 % of the mass, the same as the M31 halo. This is a poor fit: the halo of M101 is much less prominent than that of M31. (Source: van Dokkum et al. (2014))

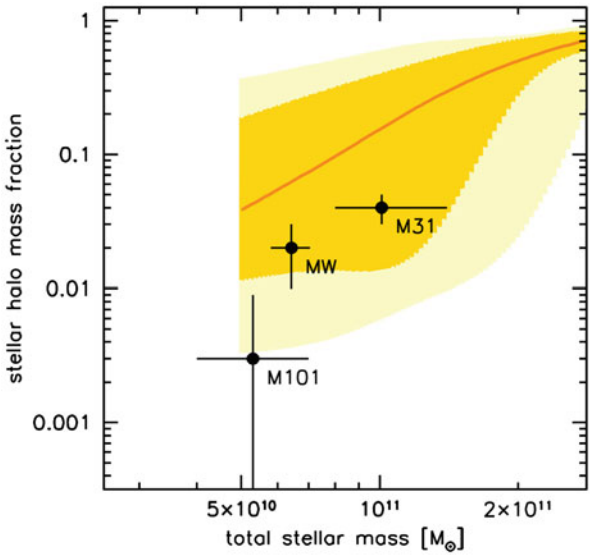

Fig. 6 The mass fraction in the stellar halo as a function of the total stellar mass. The stellar halo of M101 has significantly lower mass than those of the Milky Way and M31. The *orange line* is the predicted median relation between the accreted mass fraction and the total stellar mass from numerical simulations (Cooper et al. 2013; see text). The *yellow* and *bright yellow regions* indicate the 68 % and 95 % galaxy-to-galaxy variation in the simulations. (Source: van Dokkum et al. (2014))

is difficult to conclude very much from only three galaxies. Clearly it important to build up a sample of galaxies with radial profiles reaching surface densities of $\sim 10^4\ M_\odot\ \mathrm{kpc}^{-2}$. Perhaps the main lesson to draw from the figure shown is that such surveys are now quite feasible. Star count-based surveys with the Gemini telescope

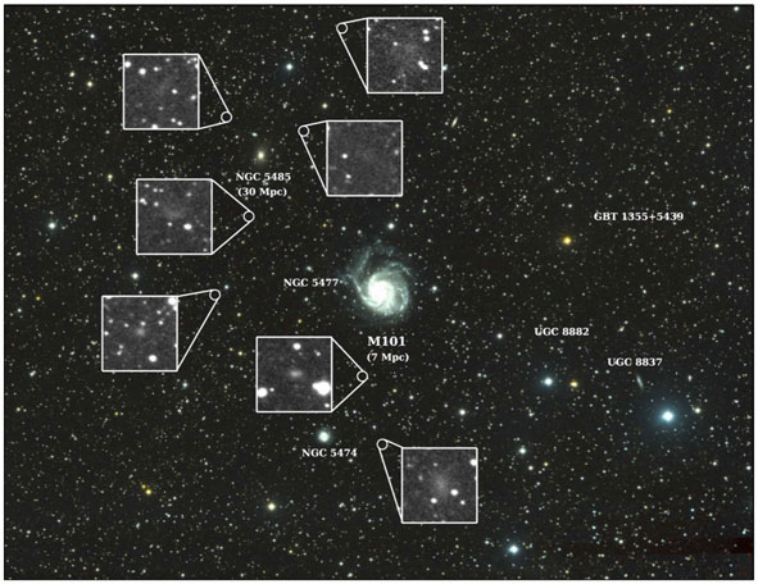

Fig. 7 The full 3.3° x 2.8° Dragonfly field of view, centered on M101. The *zoomed cutouts* highlight the position of each of the seven newly discovered LSB companions. North is *up*, and East is to the *left*. The five additional members of the M101 group that fall within our field of view (*NGC 5474*, *NGC 5477*, *UGC 8837*, *UGC 8882*) are labeled, as are the HI cloud GBT 1355 + 5439 and the background galaxy *NGC 5485*. (Source: Merritt et al. (2014))

(Bland-Hawthorn et al. 2005), the Subaru telescope (Tanaka et al. 2011) and the Hubble Space Telescope (Barker et al. 2009; Radburn-Smith et al. 2011; Monachesi et al. 2013) have reached depths of $\gtrsim 30$ mag arcsec^{-2} but only for very nearby, low mass galaxies. Reaching those limits at distances beyond ~ 5 Mpc is exceedingly difficult as the apparent brightness of stars decreases with the square of their distance. By contrast, the integrated-light surface brightness is independent of distance, and low surface brightness-optimized telescopes such as Dragonfly can map galaxy stellar mass profiles down to $\lesssim 10^3\ M_\odot$ kpc^{-2} in systems out to the Virgo cluster and beyond. Additionally, telescopes such as Dragonfly are now enabling us to detect the subtle relics of galaxy formation that should be present around every $\gtrsim L_*$ galaxy out to these same distances.

Another interesting perspective on M101 is provided by a Dragonfly investigation of its environment (Merritt et al. 2014). Figure 7, taken from the latter paper, shows seven previously unknown low surface brightness (LSB) galaxies within the projected viral radius of the galaxy. Given their location relative to M101, we consider it probable that these are seven new LSB dwarf satellite galaxies. The galaxies have central surface brightness in the range 25.5−27.5 mag/arcsec^2 and have Sérsic indices $n < 1$. The structural properties of the candidate dwarfs are compared to other local samples in Fig. 8. We conclude that the structural properties of the candidate dwarfs

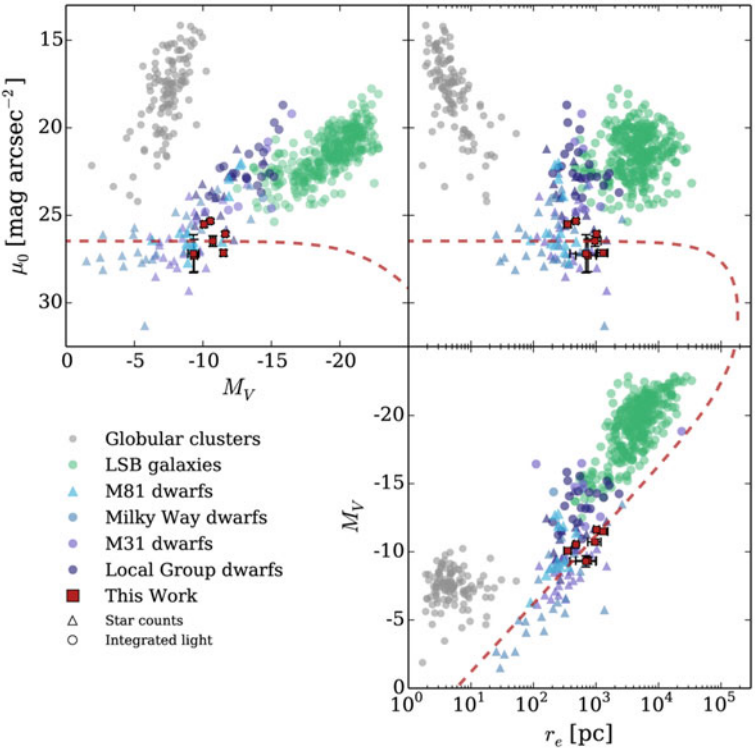

Fig. 8 Comparison of the range in surface brightness, absolute V magnitude and effective radius of our candidate M101 dwarf sample with that of the Local Group dwarfs (as compiled by McConnachie 2012, see also references therein), nearby field low surface brightness galaxies (Impey et al. 1996), M81 dwarfs (Chiboucas et al. 2013) and galactic globular clusters (Harris 1996). The V magnitudes of the M81 dwarfs were converted from r-band using the conversions of Fukugita et al. 1996 and the $< B-V >$ color of the Local Group dwarfs, and we assume $< B-V > \sim 0.43$ (Romanishin et al. 1983) for the field LSBs. We assume an M101 distance of 7 Mpc. The *red dashed line* indicates where the median properties of our sample would fall for distances from the edge of the Milky Way halo out to $z \sim 2$ (including the effects of cosmological dimming). (Source: Merritt et al. (2014))

are quite similar to those of dwarf satellites in the Local Group. However, without distance measurements other interpretations are possible (although Merritt et al. 2014 argues that these are unlikely). To date,the M101 group is known to consist of seven relatively bright companions ($-19 < M_V < -14$; Giuricin et al. 2000; Karachentsev et al. 2014), five of which fall within our field of view. Additionally, Mihos et al. (2012) discovered two HI clouds in the vicinity of M101 and one of these, GBT 1355 + 5439, lies in our field, but we do not detect any signal above the limiting surface brightness at that location. Note that in Fig. 8 systems first identified from star count analyses are shown using triangles, while those first identified from

direct imaging are shown as circles. Clearly the modest Dragonfly imager is quite competitive with the star count work being undertaken using much larger telescopes.

Another an example of the utility of these sorts of investigations for characterizing the distribution of sub-halos within virialized systems is given in Merritt et al. (2014), which presents the cumulative luminosity function (CLF) for the M101 group with the LSBs included, along with the observed CLFs of the Milky Way and M31 for comparison. For $M_V \lesssim -9$, the M101 group CLF is remarkably similar to that of M31, though the latter extends to significantly lower luminosities. Given the large pixels of the Dragonfly imager (the image scale is 2.85 arcsec/pixel) it is likely that fainter satellites of M101 exist, but were not detected, and it is too early to conclude very much from the single example shown. But it is certainly the case that considerable discovery space exists for Dragonfly for to extend searches for faint LSB dwarfs to well outside the Local Group, opening up the possibility of making measurements of dark matter halo masses for individual galaxies (e.g., Zaritsky and White 1994; Battaglia et al. 2005) as well as placing interesting constraints on cosmology and galaxy evolution on small scales.

A youthful Bruce Elmegreen photographed in 1974 by Debbie Elmegreen.

References

Abraham, R. G., & van Dokkum, P. G. 2014, PASP, 126, 55
Atkinson, A. M., Abraham, R. G., & Ferguson, A. M. N. 2013, ApJ, 765, 28
Barker, M. K., Ferguson, A. M. N., Irwin, M., Arimoto, N., & Jablonka, P. 2009, AJ, 138, 1469
Battaglia, G., Helmi, A., Morrison, H., et al. 2005, MNRAS, 364, 433
Bland-Hawthorn, J., Vlajić, M., Freeman, K. C., & Draine, B. T. 2005, ApJ, 629, 239
Carollo, D., Beers, T. C., Chiba, M., Norris, J. E., Freeman, K. C., Lee, Y. S., Ivezić, Ž., Rockosi, C. M., et al. 2010, ApJ, 712, 692
Chiboucas, K., Jacobs, B. A., Tully, R. B. & Karachentsev, I. D. 2013, ApJ, 146, 126
Cooper, A. P., Cole, S., Frenk, C. S., White, S. D. M., Helly, J., Benson, A. J., De Lucia, G., Helmi, A., et al. 2010, MNRAS, 406, 744

Cooper, A. P., D'Souza, R., Kauffmann, G., Wang, J., Boylan-Kolchin, M., Guo, Q., Frenk, C. S., & White, S. D. M. 2013, MNRAS, 434, 3348
Courteau, S., Widrow, L. M., McDonald, M., Guhathakurta, P., Gilbert, K. M., Zhu, Y., Beaton, R. L., & Majewski, S. R. 2011, ApJ, 739, 20
Dubinski, J., Mihos, J. C., & Hernquist, L. 1996, ApJ, 462, 576
Fukugita, M., Ichikawa, T., Gunn, J. E., Doi, M., Shimasaku, K., & Schneider, D. P. 1996, AJ, 111, 1748
Giuricin, G., Marinoni, C., Ceriani, L., & Pisani, A. 2000, ApJ, 543, 178
Harris, W. E. 1996, AJ, 112, 1487
Impey, C. D., Sprayberry, D., Irwin, M. J., & Bothun, G. D. 1996, ApJS, 105, 209
Johnston, K. V., Bullock, J. S., Sharma, S., Font, A., Robertson, B. E., & Leitner, S. N. 2008, ApJ, 689, 936
Karachentsev, I. D., Bautzmann, D., Neyer, F., et al. 2014, ArXiv e-print.
Kormendy, J., Drory, N., Bender, R., & Cornell, M. E. 2010, ApJ, 723, 54
Martínez-Delgado, D., Gabany, R. J., Crawford, K., Zibetti, S., Majewski, S. R., Rix, H.-W., Fliri, J., Carballo-Bello, J. A., et al. 2010, AJ, 140, 962
McConnachie, A. W. 2012, AJ, 144, 4
McConnachie, A. W., Irwin, M. J., Ibata, R. A., Dubinski, J., Widrow, L. M., Martin, N. F., Côté, P., Dotter, A. L., et al. 2009, Nature, 461, 66
McMillan, P. J. 2011, MNRAS, 414, 2446
Merritt, A., van Dokkum, P. & Abraham, R. G. 2014. ApJ (in press)
Mihos, J. C., Harding, P., Feldmeier, J., & Morrison, H. 2005, ApJ, 631, L41
Mihos, J. C., Keating, K. M., Holley-Bockelmann, K., Pisano, D. J., & Kassim, N. E. 2012, ApJ, 761, 186
Mihos, J. C., Harding, P., Spengler, C. E., Rudick, C. S., & Feldmeier, J. J. 2013, ApJ, 762, 82
Monachesi, A., Bell, E. F., Radburn-Smith, D. J., Vlajić, M., de Jong, R. S., Bailin, J., Dalcanton, J. J., Holwerda, B. W., et al. 2013, ApJ, 766, 106
Moore, B., Lake, G., Quinn, T., & Stadel, J. 1999, MNRAS, 304, 465
Naab, T., Johansson, P. H., Ostriker, J. P., & Efstathiou, G. 2007, ApJ, 658, 710
Purcell, C. W., Bullock, J. S., & Zentner, A. R. 2008, MNRAS, 391, 550
Radburn-Smith, D. J., de Jong, R. S., Seth, A. C., Bailin, J., Bell, E. F., Brown, T. M., Bullock, J. S., Courteau, S., et al. 2011, ApJS, 195, 18
Romanishin, W., Strom, K. M., & Strom, S. E. 1983, ApJS, 53, 105
Sersic, J. L. 1968, Atlas de galaxias australes (Cordoba, Argentina: Observatorio Astronomico, 1968)
Slater, C. T., Harding, P., & Mihos, J. C. 2009, PASP, 121, 1267
Tal, T. & van Dokkum, P. G. 2011, ApJ, 731, 89
Tal, T., van Dokkum, P. G., Nelan, J., & Bezanson, R. 2009, AJ, 138, 1417
Tamm, A., Tempel, E., Tenjes, P., Tihhonova, O., & Tuvikene, T. 2012, A&A, 546, A4
Tanaka, M., Chiba, M., Komiyama, Y., Guhathakurta, P., & Kalirai, J. S. 2011, ApJ, 738, 150
Toomre, A. & Toomre, J. 1972, ApJ, 178, 623
van Dokkum, P. G. 2005, AJ, 130, 2647
van Dokkum, P. G., Leja, J., Nelson, E. J., Patel, S., Skelton, R. E., Momcheva, I., Brammer, G., Whitaker, K. E., et al. 2013, ApJ, 771, L35
van Dokkum, P. G., Abraham, R., & Merritt, A. 2014, ApJ, 782, L24
Zaritsky, D., & White, S. D. M. 1994, ApJ, 435, 599

Galaxy Morphology at High Redshift

Debra Meloy Elmegreen

Abstract The morphology of galaxies at high redshift ranges from elliptical and spiral to clumpy, including chains, clump clusters, doubles and tadpoles. Clumpy galaxies observed in the Hubble Ultra Deep Field at redshifts $z = 1$–5 contain star-forming complexes that are hundreds of times more massive than those forming in local galaxies, reflecting the more turbulent and gas-rich conditions in the early Universe. Numerical simulations suggest that the clumpy phase lasts for about a Gyr, fueled by cold flow accretion; feedback from supernovae does not quench star formation. Bulges and disks build up through coalescence or dispersal of large clumps. Grand design spiral structure first appears in the Universe at about $z = 2$. Local analogs of high redshift tadpole and clumpy galaxies have high star formation rates but metallicities that are lower in star-forming regions, consistent with ongoing external gas accretion.

1 Introduction

The morphology of galaxies provides insight into their formation and evolution. Observations of galaxies at high redshift reveal morphologies dominated by a clumpy appearance (Cowie et al. 1995; van den Bergh et al. 1996; Williams et al. 1996; Abraham et al. 1996; Elmegreen et al. 2004a, b, 2005a). Conselice (2004) showed that peculiar galaxies dominate over spirals and ellipticals beyond redshift $z = 1.5$ in the Hubble Deep Fields, and Lotz et al. (2006) found that the fraction of late types and irregulars increases over ellipticals and early type spirals beyond $z = 0.7$ for galaxies with absolute B magnitudes brighter than $M_B = -21$. Among starburst galaxies in the Hubble Ultra Deep Field (UDF), the co-moving density of chains and clumpy galaxies exceeds that of spirals by a factor > 2 at $z > 1$, suggesting that all spirals could pass through a clumpy phase (Elmegreen et al. 2007). Based on Sérsic fits to over 1000 galaxies in the Sloan Digital Sky Survey, Buitrago et al. (2013) concluded that for galaxies more massive than 10^{11} $M_\odot$, disk-like galaxies

D. M. Elmegreen (✉)
Department of Physics & Astronomy, Vassar College,
Poughkeepsie, NY 12604, USA
e-mail: elmegreen@vassar.edu

K. Freeman et al. (eds.), *Lessons from the Local Group,*
DOI 10.1007/978-3-319-10614-4_37

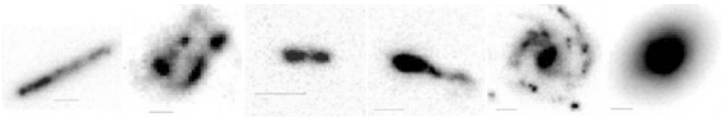

Fig. 1 Morphologies in the Hubble UDF include chains, clump clusters, doubles, tadpoles, spirals, and ellipticals, respectively. (Adapted from Elmegreen et al. 2007)

(those with Sérsic $n < 2.5$) dominated over spheroids until $z < 1$. Earlier than z = 2, irregular (= clumpy) galaxies were the most prominent types based on HUDF09 and Early Release GOODS-S data (Cameron et al. 2011), consistent with the earlier studies. Here we review properties of star-forming galaxies in the UDF and compare them to local analogs.

2 The UDF Zoo

Galaxies with radii larger than 10 pixels in the UDF out to $z = 5$ (corresponding to 1.5 kpc) have been classified into spiral, elliptical, and clumpy types, with the latter divided into chain, clump cluster, double, and tadpole galaxies (Elmegreen et al. 2005b; see Fig. 1). The clumpy types are distinctive because of their blue star-forming clumps.

About 30 % of ellipticals in the UDF between $z = 1$ and 5 are clumpy; the star-forming regions have ages of 10^7–10^9 year with corresponding masses of 10^6–$10^{7.5}$ $M_\odot$ (Elmegreen et al. 2005a). In contrast, among resolved GOODS ellipticals out to $z \sim 0.5$, about 10 % have central clump-like features, which have masses of 10^8–10^{10} $M_\odot$. These clumps tend to be older than a few Gyr (Elmegreen et al. 2014, in prep.). Thus, the GOODS clumps are not recent star formation; if they are the result of previous disk star formation rather than mergers, their ages are consistent with the aging of the Universe for clump formation earlier than $z \sim 1$.

UDF doubles are galaxies that are dominated by two big clumps (Elmegreen et al. 2005b), which could be mergers or star-forming clumps in disks. Photometry of nine UDF double galaxies from $z = 1$ to 5 based on nine bands, from F435W through F160W (IR), indicates masses of the two main components of the doubles ranging from $10^{7.5}$ to 10^9 $M_\odot$, corresponding to ages ranging from 10^8 to 5×10^9 year. The average age decreases with increasing redshift. The surface density of the clumps and the interclumps is roughly constant over this redshift range, and ranges from 30 to 200 $M_\odot$ pc^{-2} (Elmegreen and Elmegreen 2014, in prep.). This is typical of the surface densities in simulations of clumpy galaxies (Dekel et al. 2009).

Photometry of the star-forming clumps in chain and clump cluster galaxies was done using ACS optical and NICMOS infrared images. The regions are young, a few $\times 10^8$ year, and massive, ranging from a few $\times 10^6$ to 10^9 $M_\odot$ for restframe galaxy M_B ranging from −15 to −22 (Elmegreen and Elmegreen 2005; Elmegreen

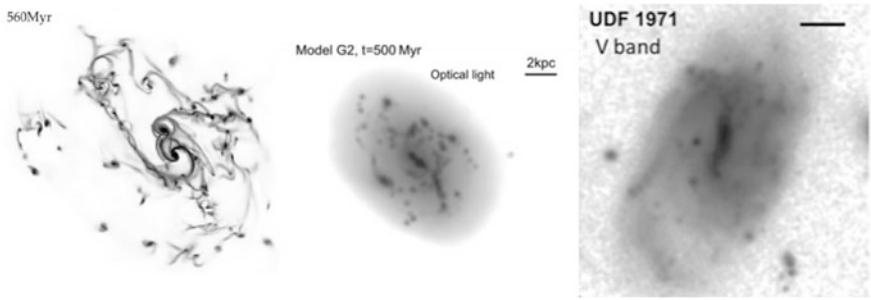

Fig. 2 Simulations of giant clumps in gas (*left*) and optical light (*middle*) after about 0.5 Gyr compared with a UDF galaxy (*right*). (Adapted from Bournaud et al. 2014)

et al. 2007, 2009a, 2013). These massive complexes reflect the more turbulent, gas-rich conditions in the early Universe (Tacconi et al. 2013; Bournaud et al. 2007). Kinematic studies of BzK and CANDELS galaxies in SINFONI surveys (Genzel et al. 2006, 2011, 2014; Guo et al. 2012; Newman et al. 2012; Wuyts et al. 2012) indicate hot rotating protodisks at $z \sim 2$; the clumps are young and massive, in agreement with our UDF results.

Cosmological simulations show cold gas streaming along cosmic web filaments onto young galaxies (Dekel and Birnboim 2008, Dekel et al. 2009; Ceverino et al. 2010; Keres et al. 2012), leading to gas surface densities > 100 $M_\odot$ pc^{-2} pc at $z = 2$–3. An initially flat clumpy disk evolves into an exponential disk with a bulge after about 1 Gyr, as clumps merge to the center or dissipate (Bournaud et al. 2007). Clumpy structure only appears if the gas and $> 80\,\%$ of the stars are in the disk, which requires smooth gas accretion rather than mergers to build up the galaxies (Bournaud and Elmegreen 2009). Massive winds from outflows are inferred from kinematic observations of a $z = 2$ galaxy (Newman et al. 2012). Simulations indicate that giant clumps survive for hundreds of Myr (Fig. 2) even in the presence of stellar feedback from strong winds (Bournaud et al. 2014).

These results lead to the question of when the first spiral structure appeared. Galaxies in the GOODS fields out to $z \sim 1.4$ include spirals with grand design structure, indicative of a density wave, and with flocculent structure (Elmegreen et al. 2009a). Among spirals in the UDF, five main spiral types are evident: grand design, multiple thin arm, woolly, irregular long arm, and flocculent (Elmegreen and Elmegreen 2014), as shown in Fig. 3. The woolly and irregular long arm spirals are not common in the local Universe; they resemble late stages in the evolution of clumpy galaxies such as in the simulations shown in Fig. 2.

While flocculent spirals are observed as early as $z \sim 3$, grand design spirals are not present until $z \leq 2$ in the UDF. At a given redshift over the range $z = 0.2$–1.4, flocculent spirals have restframe V-band brightnesses and surface brightnesses that are 1–2 mag fainter than grand design and multiple arm spirals. This result is consistent with local grand design and flocculent galaxies; grand design galaxies tend to be larger for a given Hubble type (Elmegreen and Elmegreen 1987). The

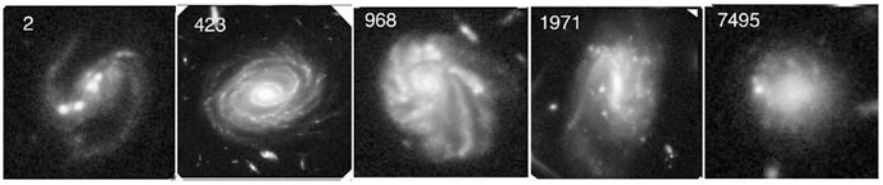

Fig. 3 Spiral galaxies in the UDF include grand design, multiple thin arm, woolly, irregular long arm, and flocculent morphologies, respectively. The woolly and irregular long arm types are not common in the local universe. (Adapted from Elmegreen and Elmegreen 2014)

onset of grand design spiral structure makes sense in the context of disk turbulence; Kassin et al. (2012) find in DEEP2 kinematic studies from redshifts 0.2–1.2 that the fraction of galaxies with settled disks, defined as those where $v_{rot}/\sigma > 3$ for rotational velocity v_{rot} and velocity dispersion σ, is greater for higher mass galaxies at each redshift interval. For the most massive galaxies ($>10^{10.3}$ $M_\odot$), the fraction with settled disks is about 40 % at $z = 1$ and 80 % at $z = 0.5$.

Spirals in the GOODS and UDF fields have young massive complexes, although they tend to be 10^7 $M_\odot$ or less (Elmegreen et al. 2009a). In contrast, local spirals have star-forming complexes 10–100x less massive (Elmegreen et al. 2013).

3 Local Counterparts to High z Galaxies

There are local counterparts to the high redshift clumpy galaxies. The local galaxies tend to be much smaller and less massive, corresponding to downsizing in the Universe. For examples, local dwarf Irregulars resemble UDF clumpy galaxies when displayed at the same resolution and restframe band, but the local galaxies and their clumps are about 100 times less massive than the UDF galaxies (Elmegreen et al. 2009b). Counterparts to high redshift tadpoles exist in the local Universe but are rare. Whereas 10 % of the 1000 galaxies in the Hubble UDF zoo are tadpoles (Elmegreen and Elmegreen 2010), only 0.2 % of the nearly 10,000 galaxies in the Kiso UV sample (Miyauchi-Isobe 2010) are tadpoles. In both cases, the galaxies are characterized by prominent star-forming heads and long tails; examples are shown in Fig. 4.

Comparison of photometric measurements of HST UDF images and SDSS images of local tadpoles with population synthesis models yields head ages of 0.1–0.2 Gyr in both samples. The UDF tadpole tails are younger than the local tadpole tails (0.1 Gyr and 1–3 Gyr, respectively). The head masses scale with galaxy restframe absolute magnitude and range from $\sim 10^7$–10^9 $M_\odot$ for the UDF and 10^5–10^7 $M_\odot$ for locals. For a given galaxy mass, the star formation rates are about an order of magnitude higher for UDF tadpoles compared to local tadpoles (Elmegreen et al. 2012).

Hα spectra show clear evidence for rotation in five of the seven observed Kiso tadpole galaxies (Sanchez et al. 2014). These local tadpoles are metal-poor for their mass, but match the metallicities of high z galaxies. There are metallicity gradients

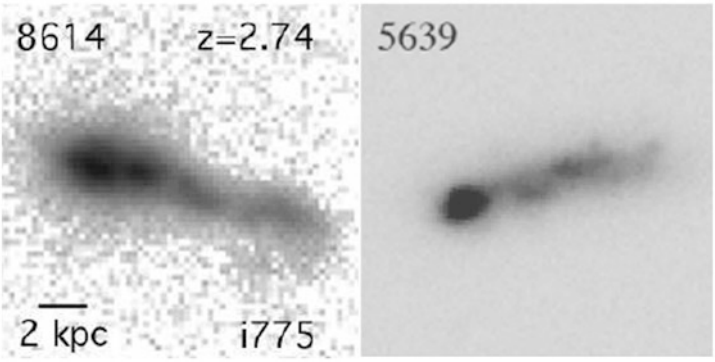

Fig. 4 Tadpole galaxies in the Ultra Deep Field (*left*) and local (*right*). (Adapted from Elmegreen and Elmegreen 2010; Elmegreen et al. 2012)

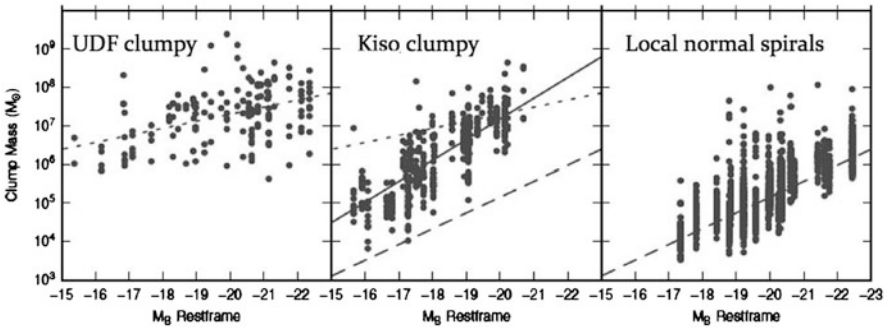

Fig. 5 Clumpy galaxies in the UDF have more massive clumps for a given restframe galaxy magnitude than local (Kiso) clumpy galaxies, which in turn are more massive than those in local spirals. (Adapted from Elmegreen et al. 2013)

across the tadpoles, with dips at the Hα peaks. These dips are unusual, suggesting that the star-forming regions are driven by cold gas accretion; the lower metallicity acquired gas could account for the metallicity drop.

Galaxies in the Kiso survey have a range of morphologies. Three dozen galaxies with massive clumps were measured from photometry and spectra to derive clump masses, ages, and star formation rates. Their star formation rates are higher than those of normal spiral galaxies in the SDSS, and match those of the UDF clumpy galaxies. Kiso clumpy galaxies have clumps that are 10x more massive than local spirals for a given restframe magnitude, as shown in Fig. 5 (Elmegreen et al. 2013). However, the Kiso clump masses are 1–2 orders of magnitude less than the masses of clumps in the UDF galaxies. This result is consistent with the observations of higher gas fractions and higher turbulence at higher z.

Extremely metal poor galaxies (XMPs) have tadpole or clumpy morphologies in 75 % of the Kiso local sample. HI observations indicate that they are gas-rich, with a

gas fraction typically 20–60 % of their dynamical mass (Filho et al. 2013). Their star formation rates are high, falling on the SFR-mass line for $0.5 < z < 1.5$ star-forming galaxies observed by Wuyts et al. (2012). However, the XMP galaxy metallicities are lower for their absolute magnitudes than metallicities for dwarf irregular and star-forming galaxies in the SDSS, which is consistent with accretion of metal-poor gas.

4 Conclusions

Galaxies at high redshift display a variety of morphologies, from several types of clumpy structures to spiral and elliptical. There are star-forming clumps in 30 % of UDF ellipticals out to $z \sim 1.5$ and in < 10 % of GOODS ellipticals out to $z \sim 0.5$; the clumps in the more nearby GOODS ellipticals are older than those in the UDF ellipticals. Clumpy disks dominate in the early Universe until about redshift $z = 2$, when spirals become more prominent, disks begin to settle, and grand design structure first appears. Star-forming galaxies in the early Universe are observed to have more massive star-forming complexes than those in local galaxies by about two orders of magnitude for a given galaxy restframe magnitude, consistent with observations of high gas content and high turbulence at higher redshift. Local tadpole and clumpy galaxies are downsized analogs of high redshift tadpole and clumpy galaxies. The low metallicities associated with star-forming regions in these local galaxies may be the result of cold flow gas accretion.

Acknowledgments It is a pleasure to thank and congratulate my closest collaborator, Bruce Elmegreen, as we celebrate his illustrious career. Most of the work described here was done with him. I also congratulate my dear friend David Block for his stellar achievements as he joins the ranks of sexagenarians, and thank him and Ken Freeman for orchestrating another incomparable conference.

References

Abraham, R. et al. 1996, ApJS, 107, 1
Bournaud, F. & Elmegreen. B. 2009, ApJL, 694, 158
Bournaud, F. Elmegreen, B., & Elmegreen, D. 2007, ApJ, 670, 237
Bournaud, F. et al. 2014, ApJ, 780, 57
Buitrago, F., Trujillo, I., Conselice, C., & Haussler, B. 2013, MNRAS, 428, 1460
Cameron, E. et al. 2011, ApJ, 743, 146
Ceverino, D., Dekel, A., & Bournaud, F. 2010, MNRAS, 404, 2151
Conselice, C. 2004, ASSL, 319, 489
Cowie, L., Hu, E. & Songaila, A. 1995, AJ, 110, 1576
Dekel, A. & Birnboim, Y. 2008, MNRAS, 383, 119
Dekel, A., Sari, R., & Ceverino, D. 2009, ApJ, 703, 785
Elmegreen, D., & Elmegreen, B. 1987, ApJ, 314, 3
Elmegreen, B. & Elmegreen, D. 2005, ApJ, 627, 632
Elmegreen, B. & Elmegreen, D. 2010, ApJ, 722, 1895
Elmegreen, D., & Elmegreen, B. 2014, ApJ, 781, 11
Elmegreen, D., Elmegreen, B., & Sheets, C. 2004a, ApJ, 603, 74
Elmegreen, D., Elmegreen, B., & Hirst, A. 2004b, ApJ, 604, L21
Elmegreen, D., Elmegreen, B., & Ferguson, T. 2005a, ApJL, 623, L71
Elmegreen, D., Elmegreen, B., Rubin, D., & Schaffer, M. 2005b, ApJ, 631, 85

Elmegreen, D., Elmegreen, B., Ravindranath, S. & Coe, D. 2007, ApJ, 658, 763
Elmegreen, B., Elmegreen, D., Fernandez, M., & Lemonias, J. 2009a, ApJ, 692, 12
Elmegreen, D., Elmegreen, B. et al. 2009b, ApJ, 701, 306
Elmegreen, D., Elmegreen, B. et al. 2012, ApJ, 750, 95
Elmegreen, B., Elmegreen, D. et al. 2013, ApJ, 774, 86
Filho, M. et al. 2013, A&A, 558, 18
Genzel, R. et al. 2006, Nature, 442, 786
Genzel, R. et al. 2011, ApJ, 733, 101
Genzel, R. et al. 2014, ApJ, 785, 75
Guo, Y., Giavalisco, M., Ferguson, H., Cassata, P., & Koekemoer, A. 2012, ApJ, 757, 120
Kassin, S. et al. 2012, ApJ, 758, 106
Keres, D., Vogelsberger, M., Sijacki, D., Springel, V., & Hernquist, L. 2012, MNRAS, 425, 2027
Lotz, J. et al. 2006, ApJ, 636, 592
Miyauchi-Isobe, N., Maehara, H., & Nakajima, K. 2010, Publ. Natl. Astron. Obs. Japan, 13, 9
Newman, S. F., Shapiro Griffin, K., Genzel, R., et al. 2012, ApJ, 752, 111
Sanchez Almeida, Munoz-Tunon, Elmegreen, Elmegreen, Mendez-Abreu 2014, ApJ, 783, 45
Tacconi, L. et al. 2013, ApJ, 768, 74
van den Bergh, S. et al. 1996, AJ, 112, 359
Williams, R. et al. 1996, AJ, 112, 1335
Wuyts, S. et al. 2012, ApJ, 753, 114

Lyman Alpha Emitting and Related Star-Forming Galaxies at High Redshift

Daniel Schaerer

Abstract I provide an overview about star-forming galaxies at high redshift and their physical properties. Starting from the populations of Lyα emitters and Lyman break galaxies, I summarize their common features and distinction. Then I summarize recent insight onto their physical properties gained from SED models including nebular emission, and various implications from these studies on the properties of star-formation at high redshift. Finally, I present new results and an overview on the dust content and UV attenuation of $z > 6$ galaxies obtained from IRAM and ALMA observations.

1 Introduction

The so-called Lyman alpha emitters (LAEs) and Lyman break galaxies (LBGs) make up the dominant population of the current known star-forming galaxies at high redshifts, both in terms of numbers and of contributors to the total star formation rate (SFR) density of the Universe. They constitute one of the main windows to study the early Universe and address a variety of questions concerning galaxy formation and evolution, star formation at high redshift, the connection between galaxies and the cosmic web, cosmic reionisation and others. We will briefly address some of these questions here, providing, however, a non-exhaustive, partial view on LAEs and LBGs, and presenting some recent results on dust emission and UV attenuation of high-z star-forming galaxies. Other types of high redshift galaxies, as found e.g. by selection at IR—millimeter wavelengths or GRB host galaxies, are not discussed here.

D. Schaerer (✉)
Observatoire de Genève, Université de Genève,
51 Ch. des Maillettes, 1290 Versoix, Switzerland
e-mail: daniel.schaerer@unige.ch

IRAP, CNRS, 14 Avenue E. Belin, 31400 Toulouse, France

K. Freeman et al. (eds.), *Lessons from the Local Group,*
DOI 10.1007/978-3-319-10614-4_38

2 LAEs and LBGs

When discussing the properties, nature, precursors, progenitors etc. of LAEs and LBGs it is important to remember the fundamental selection criteria defining these galaxy populations. The well-known Lyman break selection, or drop-out technique, targets the UV restframe emission of galaxies using the rapid flux decrease ("break") shortward of Lyα (1216 Å) or of the Lyman limit (912 Å) to chose a specific redshift domain. To avoid confusion with old stellar populations or very dusty galaxies, a color cut retaining only relatively blue objects in their rest UV is also adopted, implying a selection for star-forming galaxies which are not too strongly reddened. The LAE selection targets galaxies with Lyα in emission, which are selected through excess in a narrow-band filter with respect to the nearby continuum. Often this criterium is combined with "drop-out" criteria to select a specific redshift range and avoid "contamination" by other emission lines (cf. Ouchi et al. 2008). As for LBGs, follow-up spectroscopy is frequently carried out, largely confirming the redshift/nature of these galaxies (cf. Rhoads et al. 2003; Kashikawa et al. 2006).

The selection criteria are important, as they will to some extend determine distinctions and overlaps between the two galaxy populations. Here, since both LAEs and LBGs are targeting the same spectral range (i.e. rest-frame UV, generally dominated by emission from young/recent massive star formation) it is evident that they must overlap. Indeed, numerous findings/results show that this is the case, by how much they overlap, and what distinguishes them. We shall now summarize the most important arguments.

- A subset of LBGs shows strong enough Lyα emission (e.g. Lyα equivalent width $W_{Ly\alpha} > 20$ Å) to be selected by the traditional narrow-band excess surveys for LAEs. At $z \sim 3$ this corresponds to ~ 25 % of LBGs (Shapley et al. 2003), and LAEs restricted to the same continuum magnitude limit are statistically indistinguishable from these LBGs (Verhamme et al. 2008). Conversely, LAEs generally also fulfill LBG selection criteria, when data/depth permits.
- The number density of LAEs increases with redshift, converging towards the same density as LBGs at $z \sim 6$ (Ouchi et al. 2008). Also, the fraction of LBGs showing Lyα in emission increasing towards higher redshift (Stark et al. 2011; Schaerer et al. 2011; Curtis-Lake et al. 2012), further direct proof of the increasing overlap between the two populations at high z.
- Observable properties, such as $W_{\rm Ly\alpha}$ versus UV magnitude, of LAEs and LBGs show the same behavior, i.e. the absence of high $W_{\rm Ly\alpha}$ in UV bright galaxy, a trend often called the "Ando-plot" (see Fig. 1).
- The emergent Lyα flux (line profile) is strongly dependent on the dust content, and intrinsic Lyα emission related to the presence of massive stars (H II regions) in LBGs is readily transformed by radiation transfer effects into the observed variety of Lyα profiles including Lyα absorption (Verhamme et al. 2008; Schaerer and Verhamme 2008). This demonstrates how LAEs and LBGs can be transformed into each other, and suggests that dust is the main physical distinction between them (at least on average). Obviously, since the amount of dust attenuation generally

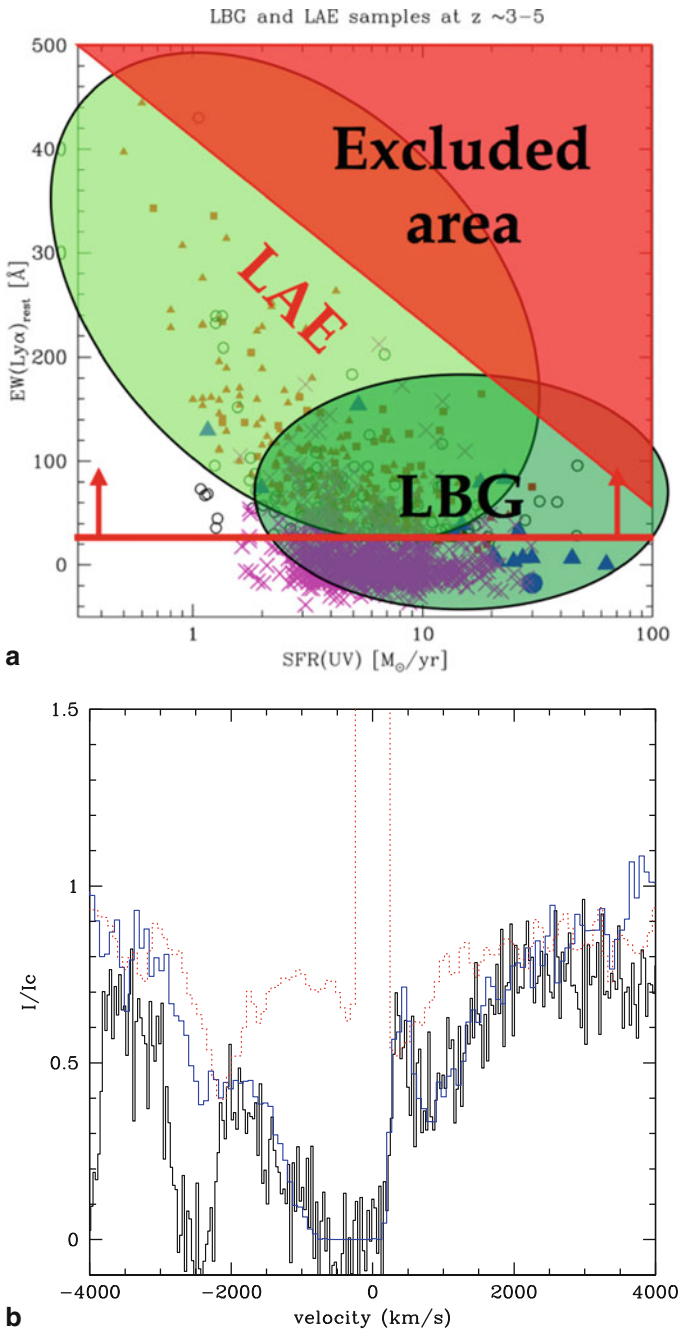

Fig. 1 *Left*: Lyα equivalent width as a function of UV SFR (from the UV magnitude) for *LAEs* and *LBGs* at $z \sim 3-4$ showing the overlap between the two galaxy populations. *Right*: Observed (*black solid line*) and modeled Lyα line profile (*blue*) of the $z = 2.7$ LBG cB58 using a radiation transfer

depends on stellar mass, the latter quantity may be a more fundamental, underlying driver. Indeed lower masses (on average) have been found by many studies for LAEs (e.g. Gawiser et al. 2007).

- Radiation transfer effects also naturally explain the observed changes of the Lyα properties and LAE/LBG populations with redshift, as long as the average dust extinction diminishes towards high-z (Verhamme et al. 2008; Hayes et al. 2011; Garel et al. 2012), which is in line with other observations (Burgarella et al. 2013).
- Correlation lengths of populations of LAEs and LBGs at $z \sim 3$ are comparable and indicate lower halo masses for LAE (cf. Adelberger et al. 2005; Gawiser et al. 2007; also Cooke et al. 2013). Cooke et al. (2013) also find an influence of environment (galaxy density) on the difference between LBGs with or without Lyα emission.

In short, the above arguments demonstrate a fundamental overlap between the UV-selected star-forming galaxy populations of LAEs and LBGs (growing with redshift), and that lower dust content related to lower mass makes the main distinction between them (at a given redshift). For most purposes we can therefore consider them as a "continuum" of star-forming galaxies in a unified manner. For other information on these galaxy populations see also the reviews of Shapley (2011) and Dunlop (2012).

2.1 Star Formation in UV Selected Galaxies at High Redshift

Numerous studies have recently discussed and revised the physical properties of LBGs and LAEs at high z, such as their stellar mass, SFR, specific SFR, age, dust attenuation, and related quantities. Indeed, thanks to great progress achieved primarily with HST (the new WFC3 camera in particular), deep ground-based imaging in complementary bands (e.g. U and K), and deep imaging with Spitzer's IRAC camera, we now have sizable samples of galaxies at $z \sim 3$–8 with a decent photometric coverage, allowing such studies. E.g. the recent work of Bouwens et al. (2014) has identified more than 10,000 LBGs at $z > 4$ with photometric coverage up to 1.6 μm at least.

Regarding the derivation of the physical properties of high-z LBGs, a significant advance has been the recognition that emission lines (nebular emission) significantly contribute to the broad-band photometry of theses galaxies, and that their effect must be taken into account (Schaerer and de Barros 2009; Schaerer and de Barros 2010a; Shim et al. 2011; de Barros et al. 2014; Smit et al. 2013; Labbé et al. 2013; Stark et al. 2013). While the importance of emission lines is now widely established, its precise effect on the physical parameters remains debated to some extent (cf. e.g. de Barros et al. 2014; Gonzalez et al. 2012; Oesch et al. 2013).

←

Fig. 1 (continued) model with outflows and dust. The observed amount of dust attenuation transforms the intrinsic Lyα emission (*dotted line*) into the observed broad absorption line profile. This demonstrates how Lyα emission from massive star formation inside this galaxy is changed into absorption after processing by the ISM; i.e. how the transition between *LAEs* and *LBGs* can be understood. (From Verhamme et al. 2008)

Overall implications from the inclusion of nebular emission are manyfold, as discussed in detail by Schaerer and de Barros (2010a), de Barros et al. (2014), Schaerer and de Barros (2014) and also by Castellano et al. (2014). Schematically one finds younger ages, lower stellar masses, higher dust attenuation, and a higher specific SFR (rising with increasing redshift), when nebular lines are included in SED fits. Furthermore the data seems to favor star-formation histories varying over relatively short timescales, which are not compatible with the often-made assumption of constant SFR over > 100 Myr. This latter result implies e.g. that standard calibrations, such as the SFR (UV) or SFR (IR) relations from Kennicutt (1998) are not valid, and that the simple relation between color excess and the UV slope β, which is commonly used to determine dust attenuation of high-z galaxies, breaks down (see discussions in Schaerer et al. (2013); Castellano et al. (2014)). The preference for variable star-formation histories comes (for $z \sim 3.8$ to 5 galaxies) from their broad range of (3.6–4.5) μm colors, a direct tracer of the Hα equivalent width, which is not compatible with constant SFR and ages > 50 Myr (de Barros et al. 2014). It seems unavoidable to introduce some variation of SFR (probably some stochastic events), although exponentially declining and rising SF histories do a reasonable job and are difficult to distinguish (de Barros et al. 2014). Again, measures of the Balmer break (cf. Oesch et al. 2013) and the Hα excess (3.6–4.5 color) cannot be reconciled with simple models assuming constant SFR (Fournier and Schaerer 2014). Other support for variable SF histories come from clustering analysis (Lee et al. 2009), galaxy models including feedback (Wyithe et al. 2013; Hopkins et al. 2013).

As already pointed out several years ago (Schaerer and de Barros 2010a; de Barros et al. 2011) SED models including nebular emission yield quite naturally significantly higher specific star formation rates, sSFR, than more simple models, and an average sSFR(z) rising with redshift, in better agreement with predictions from the popular gas accretion-driven galaxy models (e.g. Bouché et al. 2010; Weinmann et al. 2011; Lilly et al. 2013). A more recent plot showing sSFR as a function of redshift, determined from a large sample of LBGs analyzed in a homogeneous fashion including nebular emission and variable SF histories, is shown in Fig. 2.

If the star formation histories of distant galaxies vary on relatively short timescales, another logical implication is that of (significant) scatter in quantities related to the SFR, i.e. in the SFR—mass diagram, in the sSFR (at a given redshift) etc. (see e.g. Fig. 2 and discussions in de Barros et al. (2011); Schaerer et al. (2013); Castellano et al. (2014)). Note, however, that different observables, such as the UV or IR luminosity, or the Hα flux, which all trace the SFR, respond on different timescales, i.e. are expected to show various degrees of scatter (Schaerer et al. 2013). Establishing clearly the amount of scatter, hence variability/stochasticity of star formation in distant galaxies, and how this fits together with apparently more smooth star formation—i.e. a well-defined star formation main sequence observed at lower redshifts ($z < 1 - 2$, e.g. Noeske et al. (2007); Daddi et al. (2007); Elbaz et al. (2011a))—remains to be done. Physically, variations of star formation on timescales < 100 Myr inside high-z galaxies seem quite natural e.g. in view of decreasing timescales (e.g. the dynamical timescale) and strong feedback effects, which must occur in small galaxies with intense star formation. They are currently not accounted

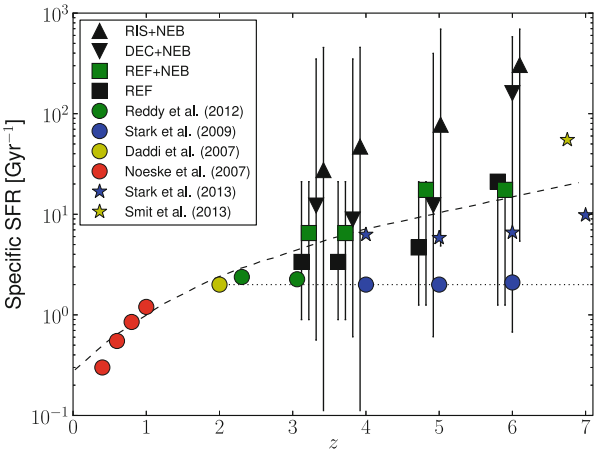

Fig. 2 Specific star formation rate sSFR as a function of redshift determined for a large sample of LBGs at $z > 3$ using models including nebular emission. Note the average increase of sSFR(z) and the large scatter. (From de Barros et al. 2014)

for in the various models describing the evolution of galaxies at equilibrium, such as the "bathtub" model.

Among the LBGs from $z \sim 3 - 6$ (Castellano et al. 2014) find indications for approximately 2/3 of galaxies showing more signs of current SF activity (nebular emission), and 1/3 showing weak or absent emission lines. This behavior seems present at all UV magnitudes, but both its significance and origin remain uncertain. Other authors, have suggested duty cycles for the star-forming galaxies at $z > 4$ (Jaacks et al. 2012; Wyithe et al. 2013), which, if correct, may imply the existence of currently undetected galaxy populations.

Clearly, further progress both observationally and our theoretical understanding of distant galaxies remains to be done. Even if current accretion-driven galaxy ("bathtub") models provide important insight into galaxy formation and its connection with the cosmic web, these models represent a simplified picture, which still lack significant ingredients. From observations, we need more direct and precise measures of their star formation rate, stellar masses, dust attenuation, star formation histories, "burstyness" and related quantities, which will rely both on new observations (e.g. with the JWST and with ALMA) and more realistic modeling to infer the galaxy properties.

In the next Section, I briefly present recent results from attempts to determine the dust content and UV attenuation in high-z galaxies.

3 Dust and UV Attenuation in $z > 6$ Galaxies and Comparisons to Low Redshifts

Using the GISMO 2 mm camera and Widex 1.2 mm observations with the Plateau de Bure interferometer we have recently targeted to $z \gtrsim 7$ galaxies, the strongly lensed LBGs A1703-zD1 with a well-defined photometric redshift $z \approx 7.0$ discovered by

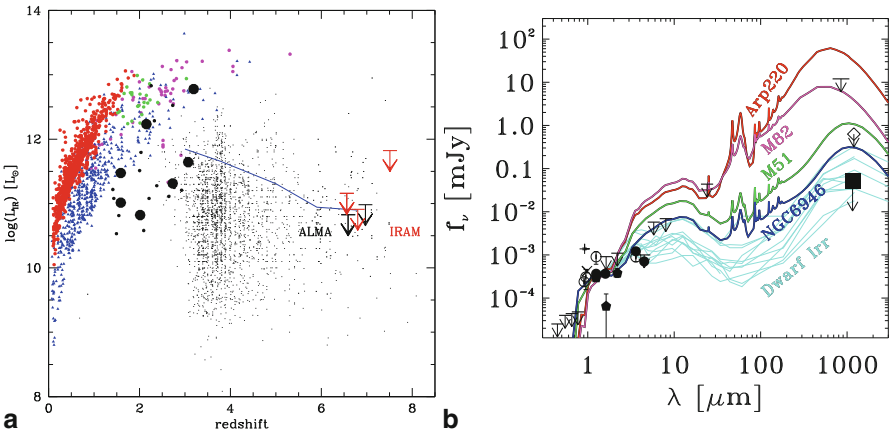

Fig. 3 *Left*: IR luminosity (derived for $T_d = 35$ K, taking the CMB into account) versus redshift for the objects discussed in this paper (*arrows* at $z > 6.5$) and for other samples. *Colored small circles* show galaxies detected with HERSCHEL in various blank fields (*red*: Symeonidis et al. (2013); *blue*: Elbaz et al. (2011b); *green*: Magdis et al. (2010)). *Large and small black circles* show the lensed galaxies studies by Sklias et al. (2014) and Saintonge et al. (2013) respectively. The *small dots* show the predicted IR luminosity of LBGs from the sample studied by de Barros et al. (2014) and Schaerer and de Barros (2014); the *blue line* shows the median $L_{\rm IR}$. *Right*: Observed SED of HIMIKO covering the optical, near-IR, to IR/mm domain and comparisons to the SEDs of local/nearby galaxies. (Taken from Ouchi et al. 2013)

Bradley et al. (2012) and the spectroscopically confirmed $z = 7.508$ LBG from Finkelstein et al. (2013). Both galaxies were non-detected with an rms of 0.12–0.17 mJy/beam in the continuum at 1.2 mm, and their [CII] emission was not also not detected. This new data, together with recent ALMA and IRAM observations of three other $z > 6$ galaxies (the LAEs named Himiko, IOK-1, and HCM6A), are analyzed in a homogenous way in Schaerer et al. (2014), from which we here show some preliminary results.

The upper limits on the IR luminosity determined from this data are shown in Fig. 3, where we also plot $L_{\rm IR}$ measurements with Herschel at lower redshift ($z \lesssim 3$), and the predicted IR luminosities of LBGs from the sample of de Barros et al. (2014). As expected, the IR luminosity limits of strongly lensed galaxies observed with IRAM (A1703-zD1, HCM6A) reach comparable effective depth as recent ALMA data for blank field (unlensed) galaxies. They are reaching luminosities $L_{\rm IR} \lesssim 10^{11}$ below the LIRG regime.

The SED of one of these galaxies, here HIMIKO, is show in the right of Fig. 3. Clearly, the SED of this object shows comparatively significantly less IR emission than that of ULIRGs, such as Arp220 and M82, and than spiral galaxies. It is more compatible with that of nearby dwarf galaxies, a results which also holds for the other four $z > 6$ galaxies included in our sample, as discussed previously by Boone et al. (2007), Walter et al. (2012), Kanekar et al. (2013), Ouchi et al. (2013), and Ota et al. (2014).

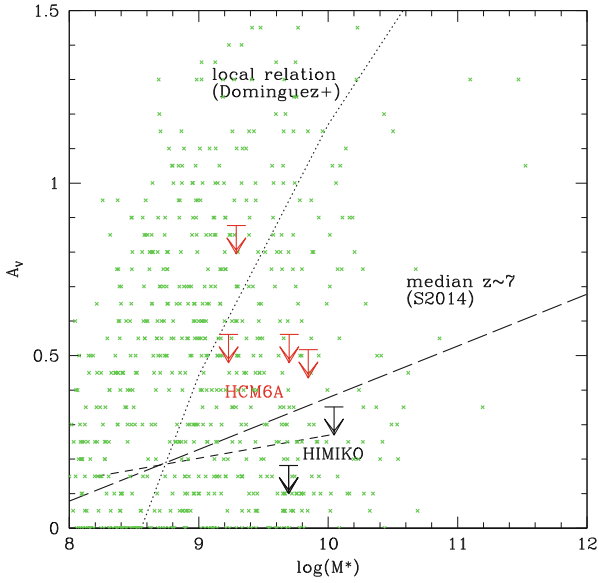

Fig. 4 Visual attenuation, $A_V \approx A_{\rm UV}/2.5$, for the objects of this study as a function of stellar mass. *Small green dots* show the values determined by de Barros et al. (2014) for a large sample of $z \sim 4$ LBGs. The *dotted line* shows the mean relation for local star-forming galaxies from Domínguez et al. (2013a). Two median relations for LBGs at $z \sim 7$ from Schaerer and de Barros (2014) are shown as *long-* and *short-dashed lines* respectively

From the ratio of the IR/UV luminosity it is straightforward to determine the upper limits on dust attenuation in these galaxies. From the nearby Universe out to $z \sim 2$ and possibly higher, various measurements (Balmer decrement, IR/UV, and others) yield a correlation between the dust attenuation and stellar mass, which apparently also shows little or no evolution with redshift (Dominguez et al. 2013b; Whitaker et al. 2012; Schaerer and de Barros 2010b). Even LBG samples at $z \sim 3$–7 show such a correlation (Schaerer and de Barros 2010b; de Barros et al. 2014; Schaerer and de Barros 2014) although these may obviously affected by selection effects and biases. It is therefore interesting to examine the constraints placed by the new UV attenuation data as a function of the galaxy mass. This is shown in Fig. 4, where we also plot the mean relation derived at low redshift, the values derived from SED fits for $z \sim 4$ LBGs, and the median relation for $z \sim 6.8$ LBGs using the same SED fitting procedure.

The upper limits for several of our galaxies fall below the local relation, indicating less dust attenuation than would be expected on average for $z \sim 0$ galaxies with the same stellar mass. On the other hand, the limits on dust attenuation are in good agreement or do not deviate strongly from the median relation found from our modeling of a sample of 70 LBGs with a median $z_{\rm phot} = 6.7$ (SdB14). Although the upper limit for HIMIKO deviates most from this relation, we do not consider this as discrepant with expectations. Indeed, from SED modeling one also finds relatively massive galaxies with low attenuation (cf. de Barros et al. 2014), as probably also corroborated by the empirical finding of an increasing scatter of the UV slope towards brighter magnitudes (cf. Bouwens et al. 2009).

Finally, the non-detections at 1.2 mm provide information on the dust mass of the $z > 6$ galaxies. In Fig. 5 we plot the limits on dust mass as a function of stellar

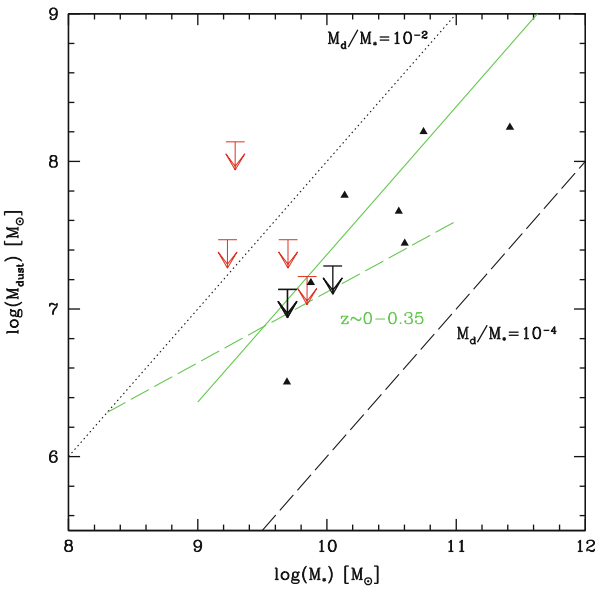

Fig. 5 Dust mass as a function of stellar mass for our objects (upper limits) and other related galaxies. The typical uncertainty on M_d due to the unknown dust temperature is $\sim \pm 0.4$ dex. Strongly lensed galaxies at $z \sim 1.5$–3 from Saintonge et al. (2013) and Sklias et al. (2014), probing a similar mass range, are shown as *black triangles* and *squares* respectively. *Solid, dashed lines*: $M_d/M_\star = 10^{-2}$, 10^{-4} ($M_\star$ here assumes Salpeter IMF). The *green dashed line* shows the location of the sequence observed by the H-ATLAS/GAMA survey at $z \sim 0$–0.35 (Bourne et al. 2012); the *green solid line* the median value of $M_d/M_\star = -2.63$ obtained by Smith et al. (2012) from the H-ATLAS survey after adjustment to the Salpeter IMF used here. The dust-to-stellar mass ratio of the high-z galaxies studied here is compatible with values observed at lower redshift, down to the nearby Universe

mass and compare this to average values found in the nearby Universe and at higher redshift. The present limits on dust mass are not incompatible with the standard dust-to-stellar mass ratios observed at low redshifts. They also agree with the recent observations of strongly lensed galaxies at $z\sim$ 1–3 detected with Herschel. In short, we conclude that the available data for high redshift star-forming galaxies shows no significant evolution from $z \sim 0$–3 and remains compatible with this out to the highest redshifts currently probed. The current data does not show evidence for a downturn of $M_d/M_\star$ at high redshift, in contrast e.g. to the claim by Tan et al. (2014). As already mentioned before, deeper observations and larger samples are needed to determine the evolution of dust with redshift, galaxy mass, and other important parameters.

Acknowledgements I wish to warmly thank the organizers, David Block, Ken Freeman, and Bruce Elmegreen for this very interesting and exceptional meeting. I thank my collaborators, in particular Anne Verhamme, Frederic Boone, Mirka Dessauges, Michel Zamojski, Stephane de Barros, and Panos Sklias for their contributions to some of the work presented here.

References

K.L. Adelberger, C.C. Steidel, M. Pettini, A.E. Shapley, N.A. Reddy, D.K. Erb, ApJ **619**, 697 (2005). DOI 10.1086/426580

F. Boone, D. Schaerer, R. Pelló, F. Combes, E. Egami, A&A **475**, 513 (2007). DOI 10.1051/0004-6361:20078253

N. Bouché, A. Dekel, R. Genzel, S. Genel, G. Cresci, N.M. Förster Schreiber, K.L. Shapiro, R.I. Davies, L. Tacconi, ApJ **718**, 1001 (2010). DOI 10.1088/0004-637X/718/2/1001

N. Bourne, S.J. Maddox, L. Dunne, R. Auld, M. Baes, I.K. Baldry, D.G. Bonfield, A. Cooray, S.M. Croom, A. Dariush, G. de Zotti, S.P. Driver, S. Dye, S. Eales, H.L. Gomez, J. González-Nuevo, A.M. Hopkins, E. Ibar, M.J. Jarvis, A. Lapi, B. Madore, M.J. Michałowski, M. Pohlen, C.C. Popescu, E.E. Rigby, M. Seibert, D.J.B. Smith, R.J. Tuffs, P.v.d. Werf, S. Brough, S. Buttiglione, A. Cava, D.L. Clements, C.J. Conselice, J. Fritz, R. Hopwood, R.J. Ivison, D.H. Jones, L.S. Kelvin, J. Liske, J. Loveday, P. Norberg, A.S.G. Robotham, G. Rodighiero, P. Temi, MNRAS **421**, 3027 (2012). DOI 10.1111/j.1365-2966.2012.20528.x

R.J. Bouwens, G.D. Illingworth, M. Franx, R. Chary, G.R. Meurer, C.J. Conselice, H. Ford, M. Giavalisco, P. van Dokkum, ApJ **705**, 936 (2009). DOI 10.1088/0004-637X/705/1/936

R.J. Bouwens, G.D. Illingworth, P.A. Oesch, M. Trenti, I. Labbe', L. Bradley, M. Carollo, P. van Dokkum, V. Gonzalez, B. Holwerda, M. Franx, L. Spitler, R. Smit, D. Magee, (2014). URL http://fr.arxiv.org/abs/1403.4295

L.D. Bradley, R.J. Bouwens, A. Zitrin, R. Smit, D. Coe, H.C. Ford, W. Zheng, G.D. Illingworth, N. Benítez, T.J. Broadhurst, ApJ **747**, 3 (2012). DOI 10.1088/0004-637X/747/1/3

D. Burgarella, V. Buat, C. Gruppioni, O. Cucciati, S. Heinis, S. Berta, M. Béthermin, J. Bock, A. Cooray, J.S. Dunlop, D. Farrah, A. Franceschini, E. Le Floc'h, D. Lutz, B. Magnelli, R. Nordon, S.J. Oliver, M.J. Page, P. Popesso, F. Pozzi, L. Riguccini, M. Vaccari, M. Viero, A&A **554**, A70 (2013). DOI 10.1051/0004-6361/201321651

M. Castellano, V. Sommariva, A. Fontana, L. Pentericci, P. Santini, A. Grazian, R. Amorin, J.L. Donley, J.S. Dunlop, H.C. Ferguson, F. Fiore, A. Galametz, E. Giallongo, Y. Guo, K.H. Huang, A. Koekemoer, R. Maiolino, R.J. McLure, D. Paris, D. Schaerer, P. Troncoso, E. Vanzella, A&A **566**, A19 (2014). DOI 10.1051/0004-6361/201322704

J. Cooke, Y. Omori, E.V. Ryan-Weber, MNRAS **433**, 2122 (2013). DOI 10.1093/mnras/stt875

E. Curtis-Lake, R.J. McLure, H.J. Pearce, J.S. Dunlop, M. Cirasuolo, D.P. Stark, O. Almaini, E.J. Bradshaw, R. Chuter, S. Foucaud, W.G. Hartley, MNRAS **422**, 1425 (2012). DOI 10.1111/j.1365-2966.2012.20720.x

E. Daddi, M. Dickinson, G. Morrison, R. Chary, A. Cimatti, D. elbaz, D. Frayer, A. Renzini, A. Pope, D.M. Alexander, F.E. Bauer, M. Giavalisco, M. Huynh, J. Kurk, M. Mignoli, ApJ **670**, 156 (2007). DOI 10.1086/521818

S. de Barros, D. Schaerer, D.P. Stark, in *SF2A-2011: Proceedings of the Annual meeting of the French Society of Astronomy and Astrophysics*, ed. by G. Alecian, K. Belkacem, R. Samadi, D. Valls-Gabaud (2011), pp. 95–99

S. de Barros, D. Schaerer, D.P. Stark, A&A **563**, A81 (2014). DOI 10.1051/0004-6361/201220026

A. Domínguez, B. Siana, A.L. Henry, C. Scarlata, A.G. Bedregal, M. Malkan, H. Atek, N.R. Ross, J.W. Colbert, H.I. Teplitz, M. Rafelski, P. McCarthy, A. Bunker, N.P. Hathi, A. Dressler, C.L. Martin, D. Masters, ApJ **763**, 145 (2013a). DOI 10.1088/0004-637X/763/2/145

A. Dominguez, B. Siana, A.L. Henry, C. Scarlata, A.G. Bedregal, M. Malkan, H. Atek, N.R. Ross, J.W. Colbert, H.I. Teplitz, M. Rafelski, P. McCarthy, A. Bunker, N.P. Hathi, A. Dressler, C.L. Martin, D. Masters, ApJ **763**, 145 (2013b). DOI 10.1088/0004-637X/763/2/145

J.S. Dunlop, (2012). URL http://fr.arxiv.org/abs/1205.1543

D. Elbaz, M. Dickinson, H.S. Hwang, T. Díaz-Santos, G. Magdis, B. Magnelli, D. Le Borgne, F. Galliano, M. Pannella, P. Chanial, L. Armus, V. Charmandaris, E. Daddi, H. Aussel, P. Popesso, J. Kartaltepe, B. Altieri, I. Valtchanov, D. Coia, H. Dannerbauer, K. Dasyra, R. Leiton, J. Mazzarella, D.M. Alexander, V. Buat, D. Burgarella, R.R. Chary, R. Gilli, R.J. Ivison, S. Juneau, E. Le Floc'h, D. Lutz, G.E. Morrison, J.R. Mullaney, E. Murphy, A. Pope, D. Scott, M. Brodwin,

D. Calzetti, C. Cesarsky, S. Charlot, H. Dole, P. Eisenhardt, H.C. Ferguson, N. Förster Schreiber, D. Frayer, M. Giavalisco, M. Huynh, A.M. Koekemoer, C. Papovich, N. Reddy, C. Surace, H. Teplitz, M.S. Yun, G. Wilson, A&A **533**, A119 (2011a). DOI 10.1051/0004-6361/201117239

D. Elbaz, M. Dickinson, H.S. Hwang, T. Díaz-Santos, G. Magdis, B. Magnelli, D. Le Borgne, F. Galliano, M. Pannella, P. Chanial, L. Armus, V. Charmandaris, E. Daddi, H. Aussel, P. Popesso, J. Kartaltepe, B. Altieri, I. Valtchanov, D. Coia, H. Dannerbauer, K. Dasyra, R. Leiton, J. Mazzarella, D.M. Alexander, V. Buat, D. Burgarella, R.R. Chary, R. Gilli, R.J. Ivison, S. Juneau, E. Le Floc'h, D. Lutz, G.E. Morrison, J.R. Mullaney, E. Murphy, A. Pope, D. Scott, M. Brodwin, D. Calzetti, C. Cesarsky, S. Charlot, H. Dole, P. Eisenhardt, H.C. Ferguson, N. Förster Schreiber, D. Frayer, M. Giavalisco, M. Huynh, A.M. Koekemoer, C. Papovich, N. Reddy, C. Surace, H. Teplitz, M.S. Yun, G. Wilson, A&A **533**, A119 (2011b). DOI 10.1051/0004-6361/201117239

S.L. Finkelstein, C. Papovich, M. Dickinson, M. Song, V. Tilvi, A.M. Koekemoer, K.D. Finkelstein, B. Mobasher, H.C. Ferguson, M. Giavalisco, N. Reddy, M.L.N. Ashby, A. Dekel, G.G. Fazio, A. Fontana, N.A. Grogin, J.S. Huang, D. Kocevski, M. Rafelski, B.J. Weiner, S.P. Willner, Nature **502**, 524 (2013). DOI 10.1038/nature12657

B. Fournier, D. Schaerer, A&A **in preparation** (2014)

T. Garel, J. Blaizot, B. Guiderdoni, D. Schaerer, A. Verhamme, M. Hayes, MNRAS **422**, 310 (2012). DOI 10.1111/j.1365-2966.2012.20607.x

E. Gawiser, H. Francke, K. Lai, K. Schawinski, C. Gronwall, R. Ciardullo, R. Quadri, A. Orsi, L.F. Barrientos, G.A. Blanc, G. Fazio, J.J. Feldmeier, J.s. Huang, L. Infante, P. Lira, N. Padilla, E.N. Taylor, E. Treister, C.M. Urry, P.G. van Dokkum, S.N. Virani, ApJ **671**, 278 (2007). DOI 10.1086/522955

V. Gonzalez, R. Bouwens, G. llingworth, I. Labbe, P. Oesch, M. Franx, D. Magee, ArXiv e-prints (2012). URL http://fr.arxiv.org/abs/1208.4362

M. Hayes, D. Schaerer, G. Östlin, J.M. Mas-Hesse, H. Atek, D. Kunth, ApJ **730**, 8 (2011). DOI 10.1088/0004-637X/730/1/8

P.F. Hopkins, D. Keres, J. Onorbe, C.A. Faucher-Giguere, E. Quataert, N. Murray, J.S. Bullock, (2013). URL http://fr.arxiv.org/abs/1311.2073

J. Jaacks, K. Nagamine, J.H. Choi, MNRAS **427**, 403 (2012). DOI 10.1111/j.1365-2966.2012.21989.x

N. Kanekar, J. Wagg, R. Ram Chary, C.L. Carilli, ApJL **771**, L20 (2013). DOI 10.1088/2041-8205/771/2/L20

N. Kashikawa, K. Shimasaku, M.A. Malkan, M. Doi, Y. Matsuda, M. Ouchi, Y. Taniguchi, C. Ly, T. Nagao, M. Iye, K. Motohara, T. Murayama, K. Murozono, K. Nariai, K. Ohta, S. Okamura, T. Sasaki, Y. Shioya, M. Umemura, ApJ **648**, 7 (2006). DOI 10.1086/504966

R.C. Kennicutt, Jr., ARAA **36**, 189 (1998). DOI 10.1146/annurev.astro.36.1.189

I. Labbé, P.A. Oesch, R.J. Bouwens, G.D. Illingworth, D. Magee, V. González, C.M. Carollo, M. Franx, M. Trenti, P.G. van Dokkum, M. Stiavelli, ApJL **777**, L19 (2013). DOI 10.1088/2041-8205/777/2/L19

K.S. Lee, M. Giavalisco, C. Conroy, R.H. Wechsler, H.C. Ferguson, R.S. Somerville, M.E. Dickinson, C.M. Urry, ApJ **695**, 368 (2009). DOI 10.1088/0004-637X/695/1/368

S.J. Lilly, C.M. Carollo, A. Pipino, A. Renzini, Y. Peng, ApJ **772**, 119 (2013). DOI 10.1088/0004-637X/772/2/119

G.E. Magdis, D. Elbaz, H.S. Hwang, A. Amblard, V. Arumugam, H. Aussel, A. Blain, J. Bock, A. Boselli, V. Buat, N. Castro-Rodríguez, A. Cava, P. Chanial, D.L. Clements, A. Conley, L. Conversi, A. Cooray, C.D. Dowell, E. Dwek, S. Eales, D. Farrah, A. Franceschini, J. Glenn, M. Griffin, M. Halpern, E. Hatziminaoglou, J. Huang, E. Ibar, K. Isaak, E. Le Floc'h, G. Lagache, L. Levenson, C.J. Lonsdale, N. Lu, S. Madden, B. Maffei, G. Mainetti, L. Marchetti, G.E. Morrison, H.T. Nguyen, B. O'Halloran, S.J. Oliver, A. Omont, F.N. Owen, M.J. Page, M. Pannella, P. Panuzzo, A. Papageorgiou, C.P. Pearson, I. Pérez-Fournon, M. Pohlen, D. Rigopoulou, D. Rizzo, I.G. Roseboom, M. Rowan-Robinson, B. Schulz, D. Scott, N. Seymour, D.L. Shupe, A.J. Smith, J.A. Stevens, V. Strazzullo, M. Symeonidis, M. Trichas, K.E. Tugwell,

M. Vaccari, I. Valtchanov, L. Vigroux, L. Wang, G. Wright, C.K. Xu, M. Zemcov, MNRAS **409**, 22 (2010). DOI 10.1111/j.1365-2966.2010.17551.x
K.G. Noeske, B.J. Weiner, S.M. Faber, C. Papovich, D.C. Koo, R.S. Somerville, K. Bundy, C.J. Conselice, J.A. Newman, D. Schiminovich, E. Le Floc'h, A.L. Coil, G.H. Rieke, J.M. Lotz, J.R. Primack, P. Barmby, M.C. Cooper, M. Davis, R.S. Ellis, G.G. Fazio, P. Guhathakurta, J. Huang, S.A. Kassin, D.C. Martin, A.C. Phillips, R.M. Rich, T.A. Small, C.N.A. Willmer, G. Wilson, ApJL **660**, L43 (2007). DOI 10.1086/517926
P.A. Oesch, I. Labbé, R.J. Bouwens, G.D. Illingworth, V. Gonzalez, M. Franx, M. Trenti, B.P. Holden, P.G. van Dokkum, D. Magee, ApJ **772**, 136 (2013). DOI 10.1088/0004-637X/772/2/136
K. Ota, F. Walter, K. Ohta, B. Hatsukade, C.L. Carilli, E. da Cunha, J. González-López, R. Decarli, J.A. Hodge, H. Nagai, E. Egami, L. Jiang, M. Iye, N. Kashikawa, D.A. Riechers, F. Bertoldi, P. Cox, R. Neri, A. Weiss, (2014). URL http://fr.arxiv.org/abs/1405.5387
M. Ouchi, K. Shimasaku, M. Akiyama, C. Simpson, T. Saito, Y. Ueda, H. Furusawa, K. Sekiguchi, T. Yamada, T. Kodama, N. Kashikawa, S. Okamura, M. Iye, T. Takata, M. Yoshida, M. Yoshida, ApJS **176**, 301 (2008). DOI 10.1086/527673
M. Ouchi, R. Ellis, Y. Ono, K. Nakanishi, K. Kohno, R. Momose, Y. Kurono, M.L.N. Ashby, K. Shimasaku, S.P. Willner, G.G. Fazio, Y. Tamura, D. Iono, ApJ **778**, 102 (2013). DOI 10.1088/0004-637X/778/2/102
J.E. Rhoads, A. Dey, S. Malhotra, D. Stern, H. Spinrad, B.T. Jannuzi, S. Dawson, M.J.I. Brown, E. Landes, AJ **125**, 1006 (2003). DOI 10.1086/346272
A. Saintonge, D. Lutz, R. Genzel, B. Magnelli, R. Nordon, L.J. Tacconi, A.J. Baker, K. Bandara, S. Berta, N.M. Förster Schreiber, A. Poglitsch, E. Sturm, E. Wuyts, S. Wuyts, ApJ **778**, 2 (2013). DOI 10.1088/0004-637X/778/1/2
D. Schaerer, S. de Barros, A&A **502**, 423 (2009). DOI 10.1051/0004-6361/200911781
D. Schaerer, S. de Barros, A&A **515**, A73+ (2010a). DOI 10.1051/0004-6361/200913946
D. Schaerer, S. de Barros, A&A **515**, A73 (2010b). DOI 10.1051/0004-6361/200913946
D. Schaerer, S. de Barros, A&A **in preparation** (2014)
D. Schaerer, A. Verhamme, A&A **480**, 369 (2008). DOI 10.1051/0004-6361:20078913
D. Schaerer, S. de Barros, D.P. Stark, A&A **536**, A72 (2011). DOI 10.1051/0004-6361/201117685
D. Schaerer, S. de Barros, P. Sklias, A&A **549**, A4 (2013). DOI 10.1051/0004-6361/201220002
D. Schaerer, F. Boone, et al., A&A **in preparation** (2014)
A.E. Shapley, ARAA **49**, 525 (2011). DOI 10.1146/annurev-astro-081710-102542
A.E. Shapley, C.C. Steidel, M. Pettini, K.L. Adelberger, ApJ **588**, 65 (2003). DOI 10.1086/373922
H. Shim, R.R. Chary, M. Dickinson, L. Lin, H. Spinrad, D. Stern, C.H. Yan, ApJ **738**, 69 (2011). DOI 10.1088/0004-637X/738/1/69
P. Sklias, M. Zamojski, D. Schaerer, M. Dessauges-Zavadsky, E. Egami, M. Rex, T. Rawle, J. Richard, F. Boone, J.M. Simpson, I. Smail, P. van der Werf, B. Altieri, J.P. Kneib, A&A **561**, A149 (2014). DOI 10.1051/0004-6361/201322424
R. Smit, R.J. Bouwens, I. Labbe, W. Zheng, L. Bradley, M. Donahue, D. Lemze, J. Moustakas, K. Umetsu, A. Zitrin, D. Coe, M. Postman, V. Gonzalez, M. Bartelmann, N. Benitez, T. Broadhurst, H. Ford, C. Grillo, L. Infante, Y. Jimenez-Teja, S. Jouvel, D. Kelson, O. Lahav, D. Maoz, E. Medezinski, P. Melchior, M. Meneghetti, J. Merten, A. Molino, L. Moustakas, M. Nonino, P. Rosati, S. Seitz, (2013). URL http://fr.arxiv.org/abs/1307.5847
D.J.B. Smith, L. Dunne, E. da Cunha, K. Rowlands, S.J. Maddox, H.L. Gomez, D.G. Bonfield, S. Charlot, S.P. Driver, C.C. Popescu, R.J. Tuffs, J.S. Dunlop, M.J. Jarvis, N. Seymour, M. Symeonidis, M. Baes, N. Bourne, D.L. Clements, A. Cooray, G. De Zotti, S. Dye, S. Eales, D. Scott, A. Verma, P. van der Werf, E. Andrae, R. Auld, S. Buttiglione, A. Cava, A. Dariush, J. Fritz, R. Hopwood, E. Ibar, R.J. Ivison, L. Kelvin, B.F. Madore, M. Pohlen, E.E. Rigby, A. Robotham, M. Seibert, P. Temi, MNRAS **427**, 703 (2012). DOI 10.1111/j.1365-2966.2012.21930.x
D.P. Stark, R.S. Ellis, M. Ouchi, ApJL **728**, L2+ (2011). DOI 10.1088/2041-8205/728/1/L2
D.P. Stark, M.A. Schenker, R. Ellis, B. Robertson, R. McLure, J. Dunlop, ApJ **763**, 129 (2013). DOI 10.1088/0004-637X/763/2/129

M. Symeonidis, M. Vaccari, S. Berta, M.J. Page, D. Lutz, V. Arumugam, H. Aussel, J. Bock, A. Boselli, V. Buat, P.L. Capak, D.L. Clements, A. Conley, L. Conversi, A. Cooray, C.D. Dowell, D. Farrah, A. Franceschini, E. Giovannoli, J. Glenn, M. Griffin, E. Hatziminaoglou, H.S. Hwang, E. Ibar, O. Ilbert, R.J. Ivison, E.L. Floc'h, S. Lilly, J.S. Kartaltepe, B. Magnelli, G. Magdis, L. Marchetti, H.T. Nguyen, R. Nordon, B. O'Halloran, S.J. Oliver, A. Omont, A. Papageorgiou, H. Patel, C.P. Pearson, I. Pérez-Fournon, M. Pohlen, P. Popesso, F. Pozzi, D. Rigopoulou, L. Riguccini, D. Rosario, I.G. Roseboom, M. Rowan-Robinson, M. Salvato, B. Schulz, D. Scott, N. Seymour, D.L. Shupe, A.J. Smith, I. Valtchanov, L. Wang, C.K. Xu, M. Zemcov, S. Wuyts, MNRAS **431**, 2317 (2013). DOI 10.1093/mnras/stt330

Q. Tan, E. Daddi, G. Magdis, M. Pannella, M. Sargent, D. Riechers, M. Béthermin, F. Bournaud, C. Carilli, E. da Cunha, H. Dannerbauer, M. Dickinson, D. Elbaz, Y. Gao, J. Hodge, F. Owen, F. Walter, (2014). URL http://fr.arxiv.org/abs/1403.7992

A. Verhamme, D. Schaerer, H. Atek, C. Tapken, A&A **491**, 89 (2008). DOI 10.1051/0004-6361:200809648

F. Walter, R. Decarli, C. Carilli, D. Riechers, F. Bertoldi, A. Weiß, P. Cox, R. Neri, R. Maiolino, M. Ouchi, E. Egami, K. Nakanishi, ApJ **752**, 93 (2012). DOI 10.1088/0004-637X/752/2/93

S.M. Weinmann, E. Neistein, A. Dekel, MNRAS **417**, 2737 (2011). DOI 10.1111/j.1365-2966.2011.19440.x

K.E. Whitaker, P.G. van Dokkum, G. Brammer, M. Franx, ApJL **754**, L29 (2012). DOI 10.1088/2041-8205/754/2/L29

S. Wyithe, A. Loeb, P. Oesch, ArXiv e-prints (2013)

Formation of Stars and Clusters over Cosmological Time

Bruce G. Elmegreen

Abstract The concept that stars are currently forming began some 60 years ago with the key observation of expanding OB associations. Now we see that these associations are an intermediate scale in a cascade of hierarchical structures that begins on the ambient Jeans length close to a kiloparsec in size and continues down to the interiors of clusters, perhaps even to binary and multiple stellar systems. The origin of this structure lies with the dynamical nature of cloud and star formation, driven by supersonic turbulence and interstellar gravity. Dynamical star formation is also relatively fast compared to the timescale for cosmic accretion, and in this limit of rapid gas consumption, the star formation rate essentially keeps up with the accretion rate, whatever that rate is, leading to a sequence of near-equilibrium states during galaxy formation and evolution. In these states, most of the large-scale and statistical properties of galaxies and of star formation inside them depend on the rate of cosmic accretion, which is a function of galaxy mass and epoch. This simplification of star formation on a cosmic scale allows successful simulations and modeling even when the details of star formation on the scale of molecular clouds is unclear. Dynamical star formation also helps to explain the formation of bound clusters, which require a local efficiency that exceeds the average by more than an order of magnitude. Efficiency increases with density in a hierarchically structured gas. Cluster formation should vary with environment as the relative degree of cloud self-binding varies, and this depends mostly on the ratio of the interstellar velocity dispersion to the galaxy rotation speed. As this ratio increases, galaxies become more clumpy, thicker, and have more tightly bound star-forming regions. The formation of old globular clusters is understood in this context, with the metal-rich and metal-poor globulars forming in high-mass and low-mass galaxies, respectively, because of the galactic mass-metallicity relation. This relation is a result of the accretion equilibrium. Metal-rich globulars remain in the disks and bulge regions where they formed, while metal-poor globulars get captured as parts of satellite galaxies and end up in today's spiral galaxy halos. Blue globulars in the disk could have formed very early when the whole Milky Way had a low mass.

B. G. Elmegreen (✉)
IBM Research Division, T. J. Watson Research Center,
1101 Kitchawan Road, Yorktown Heights, NY 10598, USA
e-mail: bge@us.ibm.com

K. Freeman et al. (eds.), *Lessons from the Local Group,*
DOI 10.1007/978-3-319-10614-4_39

1 Celebrating the Beginnings: 60 and 64 Years Ago

A good place to begin this story is with the publications by Viktor Ambartsumian in 1949 and 1950, and then again in the Western literature in 1954, of his discovery that luminous stars are in loose associations that expand over time. This was the beginning of the modern era of star-formation research. The only explanation for the systematic motion was that the associations are young, with expansion ages of several million years, and therefore that the stars themselves are young. Before this, astronomers could not really tell if star formation was still going on in the present-day universe. The age of the solar system, galactic stars, and the Hubble time were all thought to be about 3 Gyr (see 1935 *Science* Volume 82). Blaauw (1952) quickly confirmed Ambartsumian's discovery. Prior speculation about the mechanisms and locations of star formation (Bok 1936; Edgeworth 1946; Whipple 1946; Spitzer 1949), whether it took place in the early universe or more recently (as suggested to Spitzer by the high luminosities of supergiant stars), suddenly fell into place.

A flurry of activity followed. In 1952 Herbig speculated that the variable stars he had been studying in nebulae could actually be young and not just interacting with nearby gas. Öpik (1953) proposed that stellar associations expanded because of supernova-induced star formation, and Zwicky (1953) proposed that the expansion came from cluster unbinding as the gas left. Morgan et al. (1953) discovered spiral arms in the Milky Way from the positions of OB associations. Hoyle (1953) proposed that collapsing clouds would fragment, making clusters. Soon after, Salpeter (1955) determined the distribution function of stellar masses at intermediate mass in the solar neighborhood. Also at about this time, Ewen and Purcell (1951) and Muller and Oort (1951) discovered the 21 cm emission line of hydrogen, after which Lilley (1955) determined the gas-to-dust ratio, and Bok (1955) found that dark clouds had too little HI for their dust, suggesting that the gas is molecular.

It is interesting to note that a possible impediment to early recognition that the interstellar medium is gravitationally unstable to collapse into clouds and stars was the wrong gas-to-dust ratio; the interstellar gas mass was thought to be too low by a factor of $\sim$ 10 (see Spitzer 1941, p. 243). This was before interstellar HI was detected, and, although heavy elements like sodium and calcium were observed in interstellar absorption lines, it was also before the extent of their depletion onto grains was known. Oort (1932) showed from vertical gravity that the non-stellar mass amounted to an average density of about 1 atom cm^{-3}, but the form of this matter was not known (he included meteorites in his possible list of mass contributors). Thus Spitzer (1941) and Whipple (1946) tried to make stars by the convergence of radiation pressure on mutually shielding dust particles, which had a 1/2 Gyr timescale in the ambient medium. The idea that a medium with an average density of $\sim$ 1 atom cm^{-3} could be gravitationally unstable on an enormous scale, forming kiloparsec-size cloud complexes with a cascade to smaller scales forced by supersonic turbulence, had to wait for a more general understanding of spiral structure and large-scale disk dynamics, and for extensive observations of correlated gas structures and motions.

(For a review of the contributions by Lyman Spitzer Jr. to the early developments of star formation theory, see Elmegreen 2009).

A personal milestone was the IAU Symposium 76 on "Star Formation," held in Geneva Switzerland in 1976. This marked the year of my first publication on this topic. It was also a good place for a honeymoon. In the context of the present talk, the conference summary by Donald Lynden-Bell (1977) was noteworthy. There he said: "There are three great areas of astronomy to which a theory of star formation is vital," and the first area listed was "The formation and evolution of galaxies." For this he described a complicated hypothetical star formation rate $\mathcal{R}$ that is a function of many environmental variables but then said "However, if we knew the true functional form of $\mathcal{R}$ and offered it to a galaxy builder he would probably tell us 'Oh, go jump in the lake, that's far too complicated'. Thus galaxy builders need oversimplified average laws like Schmidt's suggestion $\mathcal{R} = C\rho^2$." After much research since then by a large community on star formation triggering in pillars, shells, spiral arms, and supersonically compressed turbulent clouds, we have come back to Lynden-Bell's suggestion.

2 The Oversimplified Average Law

"Oversimplified average laws" like the Schmidt law, or, in today's terms, the Kennicutt–Schmidt law, have indeed become the preferred form for galaxy builders. In fact, the star formation law can be even simpler, i.e., linearly proportional to total galactic gas mass, and even then most of the statistical properties of galaxies can be derived without regard to detailed processes on stellar scales. These properties include the distribution functions of stellar, gaseous, and metal masses over cosmic time, along with the star formation rates. The reason for this simplification is that the star formation timescale in terms of the time to use up the available gas is generally shorter than the timescale for cosmic evolution. Then star formation keeps up with the accretion rate and all of these large-scale distribution functions depend primarily on the properties of cosmic accretion (Larson 1972; Edmunds 1990; Davé et al. 2012; Lilly et al. 2013; Dekel et al. 2013; Peng and Maiolino 2014).

Following Dekel et al. (2013), the baryonic accretion rate through the galaxy virial radius at redshift z is

$$\frac{dM_{\rm acc}}{dt} = 30 f_b M_{\rm halo,0,12} e^{-0.79z}(1+z)^{2.5}\ M_\odot\ {\rm yr}^{-1}, \tag{1}$$

where $M_{\rm halo,0,12}$ is the halo mass today in units of $10^{12}\ M_\odot$ (equal to about 2 for the Milky Way), and the baryonic fraction is $f_b = 0.16$. The accretion rate to the disk could be about the same as the rate through the virial radius when the halo mass is equal to or less than $10^{12}\ M_\odot$, because then accretion mostly penetrates the halo in a cold flow (Kereš et al. 2005; Dekel and Birnboim 2006). For a review of accretion and star formation, see Sánchez Almeida et al. (2014).

The star formation rate in these simple models is

$$\mathrm{SFR} = M_{\mathrm{gas}}/\tau \tag{2}$$

for gas consumption time τ that may depend on stellar or halo mass and redshift. Gas is also lost to the halo in a wind at the rate

$$\frac{dM_{\mathrm{gas}}}{dt} = -w \times \mathrm{SFR} \tag{3}$$

where w is the mass loading factor for winds ($w \sim 1$ in Peng and Maiolino 2014); w may also depend on galaxy mass and redshift (Zahid etal. 2014). If stars return a fraction R (~ 0.4; Peng and Maiolino 2014) of their mass to the interstellar medium, then the interstellar mass varies with time as

$$\frac{dM_{\mathrm{gas}}}{dt} = \frac{dM_{\mathrm{acc}}}{dt} - (1 - R + w)M_{\mathrm{gas}}/\tau. \tag{4}$$

If τ is small compared to timescales for changes in the accretion rate, then there is a steady state where $dM_{\mathrm{gas}}/dt \sim 0$ and

$$\mathrm{SFR} \sim \left(\frac{1}{1 - R + w}\right)\frac{dM_{\mathrm{acc}}}{dt}. \tag{5}$$

Dekel et al. (2013) show that these equations compare well to numerical simulations. They also derive the consumption time τ to be about $0.17t_{\mathrm{H}}$ for instantaneous Hubble time t_{H}. This time relation comes from the ratio of the virial radius to the virial speed, which depends on t_{H}, combined with the ratio of the disk radius to the virial radius, which comes from the halo spin parameter, plus the similarity between the free fall time at the average gas density and the disk dynamical time, and the efficiency of star formation per unit free fall time. The point is that τ is smaller at earlier times and always small enough to keep the galaxy in a quasi-equilibrium state, even when the galaxy is young.

Equation (2) comes from a more fundamental relation

$$\mathrm{SFR/Volume} = \epsilon_{\mathrm{ff}}\rho/\tau_{\mathrm{ff}} \tag{6}$$

where τ_{ff} is the free fall time and ϵ_{ff} is the fraction of the gas mass that turns into stars in a free fall time. Generally ϵ_{ff} is small, several per cent, for densities close to the average interstellar density (Krumholz and Tan 2007). Krumholz et al. (2012) show that all regions of star formation, ranging from individual molecular clouds to normal galaxies to starburst galaxies to high-redshift galaxies, satisfy this relation if the free fall time is taken to be the minimum of two values, the value for giant molecular clouds, which have much higher densities than the average ISM in normal disks, and the value for the ambient medium, with the additional conditions that the gas pressure is determined by the weight of the mass column density and the Toomre instability parameter is constant and of order unity.

3 Why Is $\epsilon \sim 0.01$?

The low value of $\epsilon_{\rm ff} \sim 0.01$ suggests a broad spectrum of possibilities, ranging from molecular clouds and other interstellar gas that is prevented from collapsing for several tens of free fall times, to the presence of only a small fraction of the gas in a form that can collapse into a star, with a rapid collapse rate for this small fraction. The observation of bound star clusters that form locally in only several free fall times (Getman et al. 2014) suggests that $\epsilon_{\rm ff}$ is actually high in dense regions, because a high total efficiency is necessary to keep the stars bound to the cluster after the gas leaves (Parmentier and Fritze 2009). In this case $\epsilon_{\rm ff}$ should be an increasing function of density. However, such an increase is inconsistent with the expected speed-up of collapse at high density: $\epsilon_{\rm ff} M/\tau_{\rm ff}$ in a region of total mass M should give the same star formation rate whether it is measured at high density or low density. Because $\tau_{\rm ff} \propto \rho^{1/2}$, $\epsilon_{\rm ff}$ should scale as $\rho^{-1/2}$ to keep $\epsilon_{\rm ff} M/\tau_{\rm ff}$ constant if M is constant.

A solution to this problem (Elmegreen 2002) is that only a low fraction of the total mass M can be at a high density, collapsing rapidly on its local dynamical time, while a much larger fraction of M is at a low density, collapsing slowly or unable to collapse at all on its own dynamical time. The collapsing fraction has to decrease with increasing average density. Thus $\epsilon_{\rm ff}$ should be viewed as including a term equal to the fraction of the gas at a density greater than ρ (Elmegreen 2008). Then the star formation rate is independent of the scale of measurement because

$$\epsilon_{\rm ff}(\rho)\rho^{1/2} f_{\rm M}(\rho) = \epsilon_{\rm ff}(\rho_0)\rho_0^{1/2} f_{\rm M}(\rho_0) \tag{7}$$

for either some normalization at an average density ρ_0, or, what is more physically motivated, a normalization at a some high density ρ_0 where the local efficiency has its maximum possible value close to unity. Here $f_{\rm M}(\rho)$ is the mass fraction at density larger than ρ. Depending on the details of collapse and cloud structure, we could alternatively write the above equation as

$$\epsilon_{\rm ff}(\rho) \int_\rho \rho^{1/2} f'_{\rm M}(\rho) d\rho = \epsilon_{\rm ff}(\rho_0)\rho_0^{1/2} f_{\rm M}(\rho_0) \tag{8}$$

where f' is the differential form of f, namely the fraction of the gas between density ρ and $\rho + d\rho$. As a result of these considerations, the local efficiency increases with ρ as

$$\epsilon_{\rm ff}(\rho) = \epsilon_{\rm ff}(\rho_0) \left(\frac{\rho_0}{\rho}\right)^{1/2} \frac{f_{\rm M}(\rho_0)}{f_{\rm M}(\rho)}. \tag{9}$$

The mass fraction $f_M(\rho)$ is most likely determined by turbulent fragmentation (Elmegreen 2002, 2008), which makes this function a log-normal in weakly self-gravitating regions or a log-normal with a power-law tail in strongly self-gravitating regions (Klessen 2000; Vázquez-Semadeni et al 2008; Kritsuk et al. 2011; Elmegreen 2011). Turbulent fragmentation partitions a cloud hierarchically so that dense regions are inside and to the side of lower-density regions (Burkhart et al. 2013). With

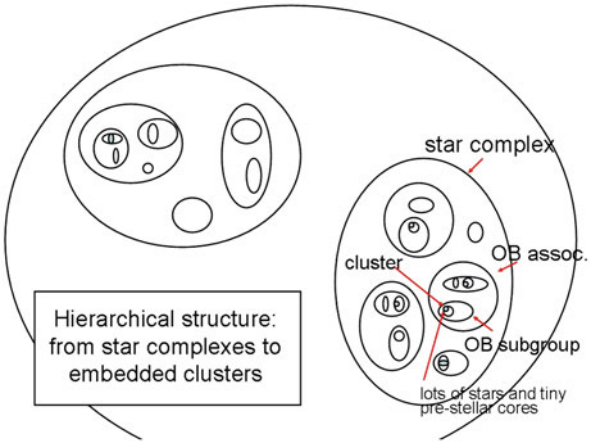

Fig. 1 Schematic showing hierarchical structure with smaller and younger star formation regions nested inside larger and older star forming regions. As we zero in on the densest regions, the low-density inter-region gas gets left behind and the average density increases. Also increasing at the same time is the fraction of the gas at this high density that is at even higher density. If the efficiency of star formation in some region is the mass fraction of the densest sub-clumps (where stars form), then this mass fraction increases with average density simply because of the hierarchical structure. The efficiency therefore increases with average density

hierarchical structure, the fraction of the mass in the highest density regions increases as the average density increases (Fig. 1). If we consider that the formation of a bound cluster requires a certain minimum local efficiency, like ∼10–20 %, depending on the timescale for gas clearing (it has to be 50 % in the immediate neighborhood of the stars for rapid clearing), then this minimum local efficiency corresponds to a minimum average local density in comparison to the fiducial density ρ_0 (Elmegreen, 2008, 2011). Thus star formation at low average density, as in star complexes (Efremov 1995) or OB associations, has a low efficiency, several percent, and leaves the stars expanding, as found by Ambartsumian 64 years ago. Star formation at high average density, inside molecular cloud cores, for example, has a high efficiency, 10 % or more, often leaving a bound cluster. At even higher density, where individual or multiple stellar systems form, the efficiency can approach 50 % or more. There is no characteristic length or mass scale for star formation (aside from the lower mass limit to the power law in the initial stellar mass function). Stellar groupings form with a wide range of densities, following the log-normal distribution (Bressert et al. 2010).

This simplified view of bound cluster formation glosses over many details, of course, but it has predictive value and it coincides qualitatively with the current picture of star formation in a turbulent medium. One prediction of it is that the density at which star formation becomes highly efficient, perhaps viewed as a critical density for star formation or a density at which self-gravity becomes stronger than other forces, should increase in regions with higher Mach number and/or higher average

density. The critical density should be viewed as relative to the average rather than as absolute. This prediction comes from the efficiency function $\epsilon(\rho)$, which, for a log-normal density pdf and mass function $f_{\rm M}(\rho)$, reaches a certain high value when the density exceeds a certain multiple of the average. There is no absolute scale in this argument. Moreover, the ratio of the density at high efficiency to the average density increases with both Mach number (Elmegreen 2008) and central concentration of the cloud (Elmegreen 2011). Higher pressures should therefore correspond to higher threshold densities, a higher fraction of star formation in bound clusters, and denser clusters. Applications of this scaling to the central molecular zone of galaxies were made by Kruijssen et al. (2014), who explained the modest star formation rate there (considering the $\times 100$ density compared to the disk) as a result of a higher threshold density.

Another application is to clumpy galaxies, such as high redshift clumpy galaxies and local dwarf irregulars. As discussed more in Sects. 6 and 7 below, clumpy galaxies have high ratios of velocity dispersion to rotation speed. In this case the relative binding energy of the star-forming regions is high too. Such high binding energy corresponds to more strongly concentrated clouds and a higher mass fraction forming stars at high efficiency, according to the discussion above. Thus we predict a higher fraction of star formation in bound clusters, and possibly denser clusters, in clumpy galaxies than in smooth-disk galaxies.

Also important in the determination of ϵ is the geometry of the star-forming gas at high density, which tends to be filamentary (e.g. Hacar et al. 2013; Palmeirim et al. 2013). Filamentary gas drains down to cores on a timescale equal to about the dynamical time, $(G\rho)^{-1/2}$, for local filament density ρ, multiplied the ratio of the length to width of the filament. This extra multiplicative factor is the result of gravity being an isotropic central force with a dynamical time proportional to the inverse square root of the average density inside an enclosing sphere, rather than the inverse square root of the local density inside sub-regions of that sphere. Thus there is a slowness to filamentary star formation compared to spherical star formation at the same local (peak) density. This means that the accreting core can sustain prestellar growth for many local dynamical times as the attached filament or filaments drain into it. Still the process is dynamical, that is, without equilibrium from feedback or delays from magnetic diffusion. It is just that the timing has a contribution from the geometry in addition to the local peak density.

4 Starbursts Are Thick

Krumholz et al. (2012) model Eq. (6) in a way that allows them to convert from a volume density ρ to a surface density Σ, for comparison with observations. To do this they make two reasonable assumptions, that the value of Toomre $Q = \kappa\sigma/(\pi G\Sigma)$ is about constant, as determined by gravitational instability feedback regulating the velocity dispersion σ (κ is the epicyclic frequency), and the gas pressure is determined by hydrostatic equilibrium, $\rho\sigma^2 \sim 0.5\pi G\Sigma^2$. The first relation says that $\sigma \propto \Sigma$ for

a given κ and then the second says that $\rho =$ constant at that κ. This means that the midplane density is about the same in all galaxy disks of the same size and rotation rate, regardless of whether the galaxy has low or high surface brightness from star formation.

The projected star formation rate in this interpretation is $\epsilon_{\rm ff}\Sigma/\tau_{\rm ff}$, and so it varies only as Σ varies for a given midplane density (i.e., fixed $\tau_{\rm ff}$), and $\Sigma \propto \sigma$, the velocity dispersion. Thus higher star formation rate densities correspond to higher velocity dispersions. Considering also that the galaxy thickness varies as $H \sim \sigma^2/(\pi G\Sigma)$ for a one-component disk, it follows that $H \propto \sigma \propto \Sigma$. Thus galaxies with a high surface brightness of star formation are thicker on the line of sight, and have a higher gas velocity dispersion, than galaxies with a low surface brightness from star formation, all else being equal. Starburst galaxies have more layers of fixed density on the line-of-sight than low-surface brightness galaxies of the same size and rotation rate. A starburst merger of a given size, like the Antennae galaxies, is thicker than an isolated galaxy (and has a larger velocity dispersion). Large HI velocity dispersions in interacting galaxies were measured long ago (Elmegreen et al. 1993) and have been modeled by computer simulations (Powell et al. 2013).

5 LEGUS

A recent HST survey of nearby galaxies in the ultraviolet, LEGUS (Calzetti et al. 2014) has been analyzed to determine the characteristics of hierarchical structure in star-forming regions (Elmegreen et al. 2014). There were 12 galaxies in the analysis covering a range of late Hubble types and star formation rates, including NGC 1705 and NGC 5253, which contain super star clusters. The analysis consisted of blurring the images in successively increasing sizes and counting the number of regions in each blurred image. A log-log plot of this number versus the blur scale typically gives a power law, and the slope of this power law is the projected fractal dimension.

The study indicated that the fractal dimension of a whole galaxy is higher, more like 2 than 1, in the most actively star-forming galaxies (including NGC 1705, NGC 5253, and UGC 695) and that individual regions in all of the galaxies also have high dimensions (~ 2). Inactive galaxies have low overall dimensions ($\sim$1–1.5) although their individual regions have high dimensions. This means that the basic building block for star formation is a bright patch with a high dimension, and that the most active galaxies are composed of only one or two of these patches, which essentially cover a high fraction of the disk. The less active galaxies, including some with spiral arms, typically have their star-forming regions spread out, and this gives them a lower overall fractal dimension. A high fractal dimension, ~ 2, corresponds to a region that is filled with emission in projection; there are relatively few empty lines of sight.

6 Clumpy Galaxies and Super Star Clusters

The number of giant star-forming regions, or star complexes, in a galaxy is an important discriminant of star formation activity. Each region typically has a size and mass comparable to the Jean length and mass at the average turbulent speed and average density of the interstellar medium. The Jeans length is essentially $\sigma/(G\rho)^{1/2}$. The galaxy size, on the other hand, scales with the rotation speed $V_{\rm circ}$ instead of the velocity dispersion, and may be written approximately as $V_{\rm circ}/(G\rho)^{1/2}$. The number of Jeans lengths in a galaxy of a given average density is therefore $(V_{\rm circ}/\sigma)^2$. This number is small when the gaseous velocity dispersion is a high fraction of the rotation speed. This is the case for local dwarf Irregulars and BCDs, which have about the same σ as local spirals but lower $V_{\rm circ}$, and also for high redshift clumpy galaxies, which have about the same $V_{\rm circ}$ as local spirals but much higher σ (Förster Schreiber et al. 2009).

The disk thickness and turbulent Jeans length are nearly the same, $\sigma^2/(\pi G\Sigma)$, so galaxies with high $\sigma/V_{\rm circ}$ have relatively thick disks (relative to their diameters). This is the case for local dwarf irregulars and clumpy high-redshift disks. In the case of the clumpy high-z disks, the relative thickness is presumably what produced the old thick disks in today's galaxies (Bournaud et al. 2009). Considering the results of the previous paragraph, the relative disk thickness scales inversely with the number of giant star complexes.

7 Super Star Clusters

Now we come to the formation of super star clusters. How can some small galaxies like NGC 1705 produce a $10^6\ M_\odot$ bound cluster when large galaxies like the Milky Way only produce clusters up to $\sim 10^5\ M_\odot$? (Some local spiral galaxies have more massive clusters, Larsen and Richtler 1999, but the Milky Way apparently does not.). The answer again seems to come down to the number of star complexes. The ratio of the gravitational binding energy in a Jeans mass cloud complex to the background energy density from the galaxy (in the form of tidal forces, shear, rotation, etc.) also involves only the ratio of σ^2 to $V_{\rm circ}^2$ (in the present approximation where background stars are ignored). This ratio of binding energy scales inversely with the number of star complexes.

It follows that morphologically clumpy galaxies produce thicker disks and have more strongly bound star-forming regions than smooth galaxies. The thicker disks (for the same galaxy size) correspond to higher star formation rates (see previous section), and the tighter self-binding reasonably transforms to a higher fraction of star formation in the form of bound clusters (Elmegreen 2011). Greater self-binding should also correspond to a more massive cluster at the upper end of the cluster mass range, and possibly denser clusters of all mass. This shift toward a more massive largest cluster corresponds to the formation of a super star cluster at the upper end of a power law distribution of cluster masses. The power law need not change as

$\sigma / V_{\rm circ}$ increases, because that is determined by turbulent and gravitational fragmentation, with some contribution from sub-cluster coalescence, which are all scale-free processes.

We can now see where the old globular clusters might have come from. The metal-rich globular clusters, which tend to coincide with the disks and bulges of today's galaxies, were presumably made in the giant clumps of high-redshift clumpy galaxies (Kravtsov and Gnedin 2005; Shapiro et al. 2010), which were also massive enough to hold on to their winds and metals, and thereby achieve a high metallicity. These clumpy galaxies are the predecessors of today's giant spirals. The metal-poor globular clusters, which tend to coincide with the halos of today's galaxies, presumably came from high redshift dwarf galaxies (Elmegreen et al. 2012), which should also have been clumpy, like today's dwarfs, but because of their inability to contain their star-formation winds, lost the metal-enriched material that stellar evolution generated. Here we are using the galaxy mass dependence of the wind mass loading factor, w, discussed in Sect. 2, to explain the mass-metallicity relationship in galaxies (Mannucci et al. 2009; Lilly et al. 2013). Metal-poor globulars associated with disk populations could have originated *in-situ* (Brodie et al. 2014) when the disk had a much lower mass and metallicity than today.

8 Summary

Lynden-Bell's wish of an "oversimplified average law like Schmidt's suggestion" came true. The law is essentially SFR$\sim \epsilon\rho/\tau_{\rm ff}$ or SFR$\sim M_{\rm gas}/\tau$ for $\tau \sim 0.17 t_{\rm H}$ with instantaneous Hubble time $t_{\rm H}$. Because the gas depletion time τ is relatively short compared to the accretion time, whole galaxies can be in approximate equilibrium with the star formation rate equal to the cosmic accretion rate and the metallicity approximately constant, increasing only as the galaxy mass increases.

Locally, star formation is more dynamic than this, acting on a timescale of several crossing times for each region and with an efficiency that is low at the average density but increases with density, considering the hierarchical distribution of mass and density during turbulent fragmentation. This increasing efficiency explains how bound clusters can form at high density when the average efficiency is low at low density. The dependence of the efficiency on the shape of the density distribution function may also explain how the clustering fraction in star formation varies with environment, including an expected increase with $\sigma / V_{\rm rot}$ from more tightly bound clouds.

Galaxies go through a sequence of equilibrium states while star-forming regions inside galaxies change, move, and disrupt on dynamical times. The difference is that galaxies have inert dark matter halos which hold the star formation in place, while star-forming regions have nothing to hold them down but disrupt by internal processes soon after they form. Both systems accrete gas on dynamical timescales and return a high fraction of this gas to the surrounding medium, but for galaxies, the returned gas falls back into the dark matter potential, while for star formation, it moves to the side and falls into another potential well when the next cloud forms.

References

Ambartsumian, V.A. 1949, AJ, USSR, 26, 3
Ambartsumian, V.A. 1950, Izv. Ak. Nauk, USSR Phys. Ser. XIV, 15
Ambartsumian, V. A. 1954, Les Processus Nucléaires dans les Astres, Communications présentées au cinquième Colloque International d'Astrophysique tenu à Liège, p. 293
Blaauw, A. 1952, BAN, 11, 405
Bok, B.J. 1936, Obs, 59, 76
Bok, B.J. 1955, AJ, 60, 146
Bournaud, F., Elmegreen, B. G., & Martig, M. 2009, ApJ, 707, L1
Bressert, E., Bastian, N., Gutermuth, R., et al. 2010, MNRAS, 409, L54
Brodie, J.P., Romanowsky, A.J., Strader, J. et al. 2014, arXiv.1405.2079
Burkhart, B., Lazarian, A., Goodman, A., Rosolowsky, E. 2013, ApJ, 770, 141
Calzetti, D., Lee, J.C., Sabbi, E. et al. 2014, submitted to AJ
Davé, R., Finlator, K., & Oppenheimer, B. D. 2012, MNRAS, 421, 98
Dekel, A. & Birnboim, Y. 2006, MNRAS, 368, 2
Dekel, A., Zolotov, A., Tweed, D., et al. 2013, MNRAS, 435, 999
Edgeworth, K. E. 1946, MNRAS, 106, 470
Edmunds, M. G. 1990, MNRAS, 246, 678
Efremov, Y.N. 1995, AJ, 110, 2757
Elmegreen, B.G. 2002, ApJ, 577, 206
Elmegreen, B.G. 2008, ApJ, 672, 1006
Elmegreen, B.G. 2009 in Reviews in Modern Astronomy, Formation and Evolution of Cosmic Structures, Vol. 21, Wiley-VCH, p. 157-181
Elmegreen, B.G. 2011, ApJ, 731, 61
Elmegreen, B.G., Kaufman, M. & Thomasson, M. 1993, ApJ, 412, 90
Elmegreen, B.G., Malhotra, S., & Rhoads, J. 2012, ApJ, 757, 9
Elmegreen, D.M., Elmegreen, B.G., Adamo, A. et al. 2014, ApJ, 787, L15
Ewen, H. I., & Purcell, E. M. 1951, Nature, 168, 356
Förster Schreiber, N. M., Genzel, R., Bouché, N. et al. 2009, ApJ, 706, 1364
Getman, K.V., Feigelson, E.D., Kuhn, M. A. et al. 2014, arXiv1403.2741
Hacar, A., Tafalla, M., Kauffmann, J., Kovács, A. 2013, A&A, 554A, 55
Herbig, G.H. 1952, JRASC, 46, 222
Hoyle, F. 1953, ApJ, 118, 513
Kereš, D., Katz, N., Weinberg, D. H., & Dav'e, R. 2005, MNRAS, 363, 2
Klessen, R. S. 2000, ApJ, 535, 869
Kravtsov, A. V., & Gnedin, O. Y. 2005, ApJ, 623, 650
Kritsuk, A. G., Norman, M. L., & Wagner, R. 2011, ApJ, 727, L20
Kruijssen, J.M.D., Longmore, S.N., Elmegreen, B.G., et al. 2014, MNRAS, 440, 3370
Krumholz, M.R., Tan, J.C. 2007, ApJ, 654, 304
Krumholz, M.R., Dekel, A., & McKee, C.F. 2012, ApJ, 745, 69
Larsen, S.S. & Richtler, T. 1999, A&A, 345, 59
Larson, R. B. 1972, Nature Physical Science, 236, 7
Lilley, A. E. 1955, ApJ, 121, 559
Lilly, S. J., Carollo, C. M., Pipino, A., Renzini, A., & Peng, Y. 2013, ApJ, 772, 119
Lynden-Bell, D. 1977, IAUS 75, 75, 291
Mannucci F. et al., 2009, MNRAS, 398, 1915
Morgan, W. W., Whitford, A. E., & Code, A. D. 1953, ApJ, 118, 318
Muller, C. A., & Oort, J. H. 1951, Nature, 168, 357
Oort, J.H. 1932, BAN, 6, 249
Öpik, E. J., 1953, IrAJ, 2, 219
Palmeirim, P., André, Ph., Kirk, J., et al. 2013, A&A, 550A, 38
Parmentier, G., & Fritze, U. 2009, ApJ, 690, 1112

Peng, Y.-J. & Maiolino, R. 2014, MNRAS, 438, 262
Powell, L.C., Bournaud, F., Chapon, D., Teyssier, R. 2013, MNRAS, 434, 1028
Salpeter, E.E. 1955, ApJ, 121, 161
Sánchez Almeida, J., Elmegreen, B.G., Muñoz-Tuñón, C. & Elmegreen, D.M. 2014, A&AR, in press
Shapiro, K.L., Genzel, R., & Förster Schreiber, N.M. 2010, MNRAS, 403, L36
Spitzer, L., Jr. 1941, ApJ, 94, 232
Spitzer, L. Jr. 1949, Astronomical Society of the Pacific Leaflets, 5, 336
Vázquez-Semadeni E., González, R.F., Ballesteros-Paredes, J., Gazol, A., & Kim, J. 2008, MNRAS, 390, 769
Whipple, F. 1946, ApJ, 104, 1
Zahid, H.J., Torrey, P., Vogelsberger, M., Hernquist, L., Kewley, L., Davé, R. 2014, Ap&SS, 349, 873
Zwicky, F. 1953, PASP, 65, 205

Conference Summary: Postcards from Seychelles

Michael L. Norman

Abstract Forty-eight speakers attending *Lessons from the Local Group* gave talks on a wide variety of topics over a period of 5 days to celebrate the careers of David Block and Bruce Elmegreen. In this short summary I highlight some of the lessons I learned when I wasn't being distracted by the awesome beauty of our surroundings.

1 Introduction

I have been given the unenviable task of summarizing 48 × 30 min. = 24 h = 1 solid day's worth of talks in roughly a half an hour. That breaks down to 37 s per talk—a challenge indeed. So as not to leave anyone out, I decided on the following approach: First, ask what was the single lesson I learned from each talk and state that in 30 s or less; and second, ask what are the overall lessons I learned. Because the talks were across such a broad range of topics, the majority of which were unfamiliar to me, I really had no alternative to taking a personal approach. I can say that for me personally, the talks were of very high quality and very interesting. I learned alot about new things and old things that were new to me. I offer this meager summary as a reminder of what an outstanding conference this was.

2 Postcards from Seychelles

The format of my conference summary was a day-by-day recapitulation of the talks we heard, in the order that we heard them. While the logical structure of the program was not manifest since it contained no topical headings whatsoever, just a list of talks, the hidden structure became evident to me as I grouped talks and assigned cute titles to each group. A group consisted of 3–4 talks, which I could summarize on a single Power Point slide. Each slide was adorned with one graphic and one lesson

M. L. Norman (✉)
Center for Astrophysics and Space Sciences, University of California,
CASS/UCSD 0424, 9500 Gilman Dr., La Jolla, CA 92093, San Diego, USA
e-mail: mlnorman@ucsd.edu

K. Freeman et al. (eds.), *Lessons from the Local Group,*
DOI 10.1007/978-3-319-10614-4_40

per talk; in other words, 3–4 graphics and lessons per slide. All together, I present 16 such slides covering all the talks with the exception of the last two immediately preceeding my summary. I think of these slides as a collection of "postcards from the Seychelles Islands" that evoke the memory of the conference. A PDF file containing these postcards is available from me per a simple email request.

The list below shows the talks as I grouped them along with a suggestive title and speaker list.

DAY 1

- *What's old is new* (Van der Kruit, Asplund, Freeman)
- *Evolving anatomy of the Milky Way* (Gilmore, Gerhard, Benjamin, Palous)
- *That messy stuff: gas, B-fields, and star formation* (Andre, Burkert, Lazarian)
- *Chemical forensics* (Li, Haywood, d'Orazi)

DAY 2

- *The Local Group like you've never seen it* (Fazio)
- *Simulations tackle the big questions* (Klessen, Dobbs)
- *M31 and M33: testbeds of our understanding* (Matteucci, Braun, Lewis, Corbelli)
- *Globular clusters: confounding clues of galaxy formation* (Charbonnel, Brodie, Mackey)
- *Bring in the dwarfs* (Majewski, Hunter, Carraro)

DAY 3

- *LMC: an ideal star formation laboratory* (Gallart, Fukui, Gouliermis)
- *More lessons from dwarfs* (Rubio, Besla, Kormendy, Kroupa)
- *Bits and pieces and green stars* (Putnam, Arnoldi, Grillmair)
- *Back to the Galaxy* (Roskar, Genzel, Morris)

DAY 4 (before lunch)

- *Evolution of cosmology, and cosmological evolution* (Smith, Steinmetz, Combes)
- *Galaxies as they really are (and were)* (Block, Abraham, D. Elmegreen, Tacconi)

2.1 What's Old Is New

The conference was opened by **Ken Freeman** who presented **Piet van der Kruit's** excellent historical review "Kapteyn's Universe" (van der Kruit unfortunately missed the conference due to a family emergency.) The famous Dutch astronomer used extensive star counts to deduce the structure of the Milky Way. He arrived at an incorrect size and centroid because he assumed interstellar space was transparent since interstellar dust was not yet discovered. *Lesson:* a model is only as good as its assumptions; perfectly "reasonable" assumptions can be dead wrong (Fig.1).

Martin Asplund reported on an ambitious survey to find the first stars (i.e., stars of extremely low metallicity—EMPs) in the Milky Way's bulge and halo. Inspired by cosmological simulations which suggest that the Galactic bulge is the best place

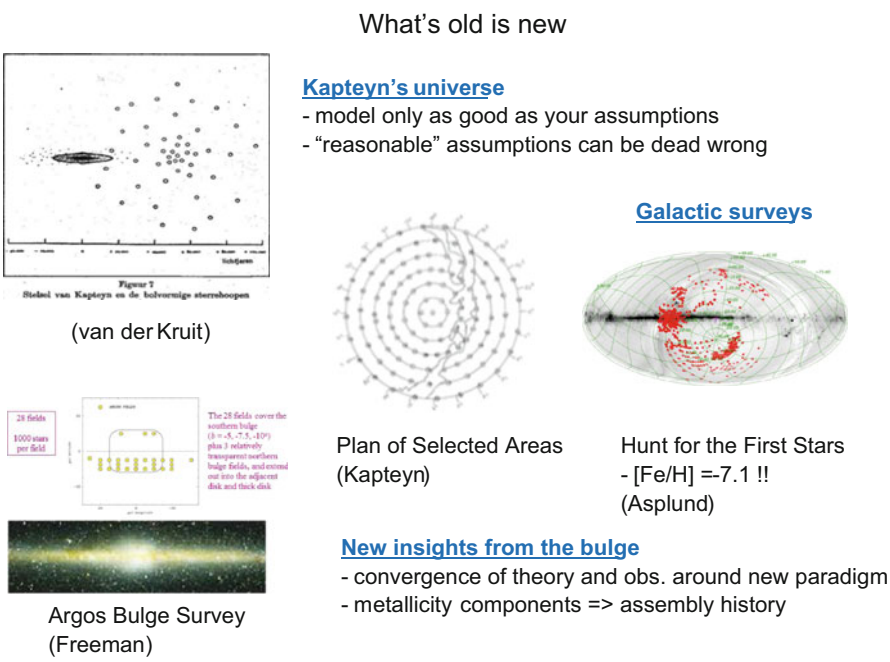

Fig. 1 Example postcard from Seychelles (see text for explanation)

to look for them, the ANU team is doing just that. Using a wide area survey strategy reminiscent of Kapteyn's "Plan of Selected Areas", as well as efficient color selection, a survey of the bulge+halo has yielded a large sample of EMPs, including one with undetectable iron lines, implying [Fe/H] < -7.1. Known as Keller's star, (Keller et al. 2014), the *Nature* discovery paper went through 58 title iterations. *Lesson:* What's old is new.

Ken Freeman concluded this session with a progress report of the Argos Bulge Survey. The goal of this spectroscopic survey is to characterize the stellar populations in the bulge. The emerging view of the origin of the MW's peanut-shaped bulge is that it is the result of a bar-buckling instability. This predicts that the bulge structure in younger than its oldest stars, which were originally part of the inner disk. Argos is looking for, and seeing evidence of this. *Lesson:* the convergence of theory and observation support a new paradigm in understanding the assembly history of the Galaxy.

2.2 Evolving Anatomy of the Milky Way

The talks in this session focused on the latest data on specific parts of the Milky Way's anatomy. **Gerry Gilmore** spoke about the MW's stellar *thick disk* and the growing recognition that it is key to undertstanding the Galaxy's early star formation

history. In particular, the ubiquity of thick disks in other galaxies, and the striking elemental correlations measured in our own Galaxy have made thick disks an active area of study.

Ortwin Gerhard discussed the structure and dynamics of the MW's *bar* from both an observational and theoretical perspective. Numerical simulations of increasing fidelity show that the bar and boxy bulge in the MW's center are a natural consequence of disk instabilities. Infrared surveys by 2MASS allow us to map the bar-bulge structure in 2D and 3D. A new map was presented.

Bob Benjamin presented the latest results about the MW's *thin disk* and its spiral structure. A variety of new observations, including the GLIMPSE survey and follow-ons from Spitzer Legacy have ushered in the era of "high precision Galactic cartography". Benjamin argued that GLIMPSE data show a break or warp of the thin disk at a Galactocentric radius of $\approx 13 - 14$ kpc.

Jan Palous concluded this quartet of talks with a discussion of *Gould's Belt*, one of the MW's more studied piece of anatomy. New kinematic data for the young OB stars reveal complex motions that argue against expansions from a single source, such as the collision of a high velocity cloud with the gas disk. The ubiquity of HI shells in the Galaxy suggest that Gould's Belt may be nothing special.

Lesson: The basic anatomy of the Milky Way continues to be revised as we get new data. Depictions in old astronomy textbooks are inaccurate!

2.3 That Messy Stuff: Gas, B-fields, Star Formation

A trio of talks were presented on aspects of a new, emerging picture of star formation on large and small scales, both Galactic and cosmic. **Philippe André** reviewed observations from the Herschel Space Telescope which reveal that the interstellar medium is filamentary in its structure. He pointed out that this is true of star-forming and non star-forming molecular clouds, as well as the ISM in general. Protostellar cores are observed to be aligned with the filaments. André suggested a 'universal' scenario for low-mass star formation in which (1) large-scale MHD supersonic turbulence generates filaments, and (2) gravity fragments the densest filaments into prestellar cores. Within this scenario, the low observed efficiency of star formation is a direct consequence of the small fraction of the mass in dense filaments and the timescale for fragmentation.

Andy Burkert gave an entertaining and enlightening talk on galaxy-scale star formation, applicable to any galaxy including the MW. He presented a so-called bathtub model of star formation which is derived from applying the mass conservation equation to a galaxy as a whole. A prediction of the model is that the global star formation rate is set by the net mass accretion rate onto the galaxy. How gas ultimately is converted into stars is an unimportant detail from a global perspective.

Alex Lazarian discussed the theory of interstellar turbulence, focusing mostly on incompressible MHD turbulence which well-describes the warm interstellar medium. He showed from theory and numerical simulations that such turbulence obeys Kolmogorov's $E(k) \propto k^{-5/3}$, which offers an explanation as to why the observed ISM electron density spectrum obeys Kolmogorov scaling over a vast range of scales.

Lesson: Observations, simulations, and theory are converging on a new understanding of star formation on molecular cloud and galaxy scales. Turbulence phenomenology is fundamental.

2.4 Chemical Forensics

The first day concluded with three talks that illustrated the power of detailed chemical analysis. **Aigen Li** schooled us on dust in the Local Group. He showed that dust properties are different wherever you look. To illustrate this he showed dust extinction curves for the MW, LMC, and SMC that have different shape. *Lesson:* Be careful simply scaling the Galactic extinction curve to different metallicities when analyzing high redshift galaxies.

Misha Haywood took up where Freeman and Gilmore left off exploring in more detail MW stellar metallicities and fossil cosmology. He presented data showing that the bulge metallicity distribution function (MDF) is the most unbiased estimate of the disk MDF, not the local MDF. He showed how the abundance ratios and ages of thick and thin disk stars can be used to infer their star formation and chemical evolution histories. *Lesson:* the thick disk is a massive population (as massive as the thin disk.)

Valentina d'Orazi closed the first day's presentations with high resolution element abundance studies of globular clusters using the VLT. Supported by exquisite data she highlighted the Na–O anticorrelation seen in GC's and argued that this requires at least 2 generations of star formation. She discussed several models of GC formation in light of this and other data sets. *Lesson:* GC formation models face difficult challenges when confronted with such high quality data.

2.5 The Local Group Like You've Never Seen It

Giovanni Fazio opened the second day with a stunning photo gallery of the MW and Local Group as see through the eyes of the Spitzer Space Telescope. The instrument, launched in 2003 is still producing science. Spitzer's imagers and spectroscopes were cleverly designed to dissect a galaxy over the wavelength range 3–160 μm and 5–40 μm, respectively. A host of Legacy and Exploration Programs have given us the most complete view of star forming regions in the MW and nearby galaxies ever accomplished. *Lesson:* Infrared astronomy rules! \$670M very well spent.

2.6 Simulations Tackle the Big Questions

Ralf Klessen and **Clare Dobbs** showed results from the latest numerical simulations that in visual appeal and complexity rivaled that of the previous speaker. That is a consequence of the fact that modern supercomputers permit simulations with hundreds of millions of particles and cells–commensurate with the resolution of CCD array cameras. *Lesson:* with such visual "realisim" it becomes more essential than ever to ask what the assumptions and limitations of the simulation are, and what we are looking at.

Klessen presented high resolution simulations of primoridal star formation investigating the primordial initial mass function. The simulations show fragmentation of the massive disk into a small number of accreting cores. If any of these cores are ejected out of the disk by 3-body encounters, as seems to be indicated by the simulations, then these could remain low mass and survive to the present day. A key question is would we recognize one if we saw it?

Dobbs presented a moderately high resolution SPH simulation investigating the formation of molecular clouds in a differentially rotating thin gaseous disk. The simulations feature most of the relevant physics with the exception of magnetic fields, with and without self-gravity. Molecular cloud formation is triggered by an imposed spiral potential, and the clouds are distributed along the spiral arms and "feathers" extending into the interarm region. They form in the absence of self-gravity, suggesting that they are the result of thermal instability. *Lesson:* Given the observational difficulties of defining what is a molecular cloud, how should they be defined simulationally for comparison with data?

2.7 M31 and M33: Testbeds of Our Understanding

M31 and M33 serve as testbeds for our theories of galaxy formation and chemical evolution. **Francesca Matteucci** described successful chemical evolution models for M31 incorporating gas accretion and radial redistribution of metals by galactic fountains and radial migration. *Lesson:* closed-box models are dead.

Robert Braun presented exquisite HI maps of M31 corrected for self-absorption. This correction increases HI mass estimates by $\sim$ 10 %. *Lesson:* don't forget the basics of radiative transfer.

Geraint Lewis presented the latest results on the outer disk and halo of M31. Using the CFHT MegaCam the PAndAS survey has assembled a mosaic image comprising $\sim$ 350 fields. They found a smooth stellar halo, streams, clumps and tidal debris reminiscent of results from ΛCDM simulations. They found evidence that globular clusters may accrete along streams, and discovered a new population of dwarf galaxies arranged in a rotating sheet. The later finding stimulated much discussion. *Lesson:* there is a healthy tension between theory and observation.

Edvige Corbelli enlightened us before lunch with a tour of the many portraits of M33 and van Gogh. She highlighted how science evolves in bursts using her collaborations with Bruce Elmegreen (BE) as an example. In a clever juxtaposition of subjects, she connected BE's recurrent interests in the IMF, turbulence, and spiral waves & disk dynamics to van Gogh's paintings and M33. *Lesson:* M33 is a science laboratory and a work of art.

2.8 Globular Clusters: Confounding Clues of Galaxy Formation

The afternoon began with a session on the confounding and fascinating topic of globular cluster (GC) formation. **Corrine Charbonnel** presented a 2-phase GC formation scenario involving a first generation of massive chemical polluters (long gone), followed by a second generation of low mass pollutees (still present). The second generation stars are thought to form in the "decretion disk" of the rapidly rotating first generation stars. This model offers a possible explanation for the elemental abundance correlations and anti-correlations seen in the data presented by d'Orazi. *Lesson:* Theorists have to be creative to explain the data. How to validate such theories?

Jean Brodie returned us to the realm of observations, and said that the well-known bimodality in the GC metallicity distribution function implies a 2-phase galaxy formation process. This is supported by the fact that the blue GC's trace halos, and red GC's track bulges. Inspired by "cold-stream" numerical simulations of galaxy assembly, she speculated that the "wild disks" seen at high z in such simulations could be red GC factories.

Alasdair Mackey concluded the session with a census of Local Group GCs. M31 and MW have a disproportionate share of them, however every galaxy has a few and even dwarf galaxies have them. *Lesson:* It is clear from observations that a subset of GC's are of external origin; see evidence of accretion now, but no convincing GC streams.

2.9 Bring in the Dwarfs

The last three talks of the day focused on the lessons dwarf galaxies teach us. **Steve Majewski** discussed the multiple uses of observations of the Sagittarius dwarf galaxy tidal stream: (1) to constrain the Galactic dark matter halo, (2) to measure the MW local standard of rest; and (3) to assess its contribution to the Galactic halo. Most impressive was the first application, where detailed modeling concludes that the MW's dark halo is triaxial and strongly oblate. *Lesson:* This approach may provide a critical test of CDM and MOND.

Diedre Hunter impressed upon us the tremendous variety of properties that exist among the dwarf irregulars in the Local Group, in particular their star formation which she characterized as *in extremis*. She presented a Kennicutt diagram which showed that star formation in dIrrs follows the locus of star formation in the outer disks of massive galaxies. She noted evidence for *positive stellar feedback* on star formation. *Lesson:* A complete theory of star formation should explain these "edge cases."

Giovanni Carraro discussed the morphological evolution of DGs of all type in the LG. He presented evidence for harassment and tidal interactions. He argued that supernova expulsion of gas from DGs is not viable, favoring photoevaporation during reionization and ram-pressure stripping. *Lesson:* The Local Group is an active environment.

2.10 LMC: An Ideal Star Formation Laboratory

The LMC is in many ways superior to the MW for studying star formation phenomenology in detail. It is close enough that we can study the properties of large samples of stars while far enough away that we can see the big picture. The 3 talks in this session showed how the LMC is like looking into a Petri dish to see how cultures of bacteria develop. **Carme Gallart** showed how the detailed star formation history and metallicity evolution of the LMC can simply be read out from high sensitivity color-magnitude diagrams. Results were presented for individual regions as well as the intermediate disk of the LMC as a whole. *Lesson:* Star formation is quite variable on gigayear timescales. Why?

Yasuo Fukui used radio CO observations to dig into the process by which GMCs transform into massive stars. By combining radio and optical observations of a large sample of GMCs ($\sim$ 100) he classified the three evolutionary stages and characteristic timescales. He also presented compelling evidence that the rapid massive star formation in NGC3603 is the result of GMC-GMC collision. *Lesson:* Look and you shall see.

Dimitrious Gouliermis used the LMC to test a basic prediction of the turbulent star formation picture. He used a correlation function analysis drawn from statistical mechanics to see if young stars exhibit hierarchical stucture like turbulence. *Lesson:* The answer is YES! He is extending this analysis to an analysis across space and time, which will tell us about where stars born in clusters migrate.

2.11 More Lessons from Dwarfs

LG dwarfs were not done teaching us lessons. We heard 4 more talks on the subject, each with their own lessons. **Monica Rubio** discussed dark molecular gas in the

SMC. CO is hard to detect (and hence dark) because of the SMC's low metallicity. One resorts to submm dust emission mass estimates, in particular 870 μm LABOCA measurements. Rubio reported molecular cloud mass estimates obtained in this way are $3\times$ the virial mass estimate using the standard (i.e., MW) approach. *Lesson:* Now well-understood turbulence phenomenology provides an alternate framework for understanding MC properties (Kritsuk et al. 2013).

Gurtina Besla used the LMC/SMC galaxies and stream to constrain formation scenarios. The introduction of the recently measured proper motion of the galaxies into the analysis finds a good fit with a first infall solution. *Lesson:* The LG is dynamically young.

John Kormendy introduced a new tuning fork diagram for galaxies that is substantially different from Hubble's (John Henry Reynold's). It places SO's of various bulge dominance along a parallel sequence to the spirals. Within this scheme dSph's and dIrr's are at the ends of opposite tines. Supporting this proposal is a convincing fundamental plane analysis. *Lesson:* don't be fooled by morphology. (Cows and dolphins are both mammals!)

Pavel Kroupa worked up our appetites for lunch by drawing our attention to the vast polar structure of MW dwarfs which lie largely within a plane. That a second plane of dwarfs has recently been discovered around M31 (Lewis talk) suggests that these structures are fundamental to galaxy formation and not incidental. Kroupa built a logical edifice to try to demonstrate that the standard model of cosmology (i.e., CDM) is invalidated by not only these observations, but by other kinds of observations as well. His contrarian view generated lively debate and perhaps some heartburn. *Lesson:* all voices and opinions need to be considered, especially in light of new "inconvenient" data.

2.12 Bits and Pieces and Green Stars

Mary Putnam resolved the mystery of High Velocity Clouds (HVC). HVC's have now been mapped in 3D and shown to be largely within 10 kpc of the MW. Their properties are broadly consistent with hydro-cosmology simulations she has carried out with the Enzo code with colleagues at Columbia. *Lesson:* If star formation is to be fed by cold gas accretion at all epochs, it would be embarrasing if HVC's turned out to be something else.

Magda Arnaboldi reviewed the large amount of information being gathered about planetary nebulae (PNe) in the Local Group from the ESO PN.S key project. PNe are bright and green, and fade after about 1000 yr. These properties make them visible throughout the LG. *Lesson:* PNe are good tracers of light and kinematics in Early-type galaxies, and provide a new tool to study different stellar populations.

Carl Grillmair presented the latest data on nearby halo streams. Many new streams have been discovered in SDSS data—more than 20—collectively referred to as the "field of streams." An unanswered question is whether the MW's halo is just a network of streams? *Lesson:* yet another reason to suspect old astronomy textbook depictions of the MW.

2.13 Back to the Galaxy

Day 3 concluded with 3 talks that provide new and radically different views of the MW. The session was led of by **Rok Roskar** who presented numerical evidence for the radial migration of stellar orbits due to transient spiral waves. The migration is found to be a non-negligible fraction of the local radius, which couples different radii in chemical evolution models. If operative in the MW, it affects how we interpret solar neighborhood stellar populations. *Lesson:* This result, discovered in numerical simulations, is a paradigm shift, but much work remains to be done to explore its consequences in different circumstances.

Reinhard Genzel and **Mark Morris** took us on a journey to the Galactic Center (GC) where things are very odd indeed. Genzel views the GC as a laboratory for testing the massive black hole (MBH) paradigm. He showed the impressive combined MPE VLT and UCLA Keck data on the stellar orbit S2/SO2. This orbit yields a precise mass for the ultracompact central object in Sgr A* to two significant figures. He also discussed origin scenarios for the cluster of massive young stars ($>$ 100 O stars!) in the central parsec, and the tidal disruption of a gas cloud nearing the hole. *Lesson:* The gift that keeps on giving. Keep observing.

Morris reviewed the many bizarre and beautiful magnetic features in the GC on multiple scales. The radio observations look superficially like SOHO observations of the solar photosphere, with magnetic arches and filaments everywhere. Is there a causal relationship between these structures and the bar-driven gas flows? the MBH? *Lesson:* this is a MHD theorist's playground, but it does not seem it has drawn much attention so far.

2.14 Evolution of Cosmology, and Cosmological Evolution

In a great juxtaposition of talks, science historian **Robert Smith** and numerical cosmologist **Matthias Steinmetz** told us about cosmological thinking separated by roughly a century. Smith helped us understand the limited mindset of working astronomers in the late nineteenth/early twentieth centuries. Astronomers worked on what they could see; science had no concern beyond that. What could not be seen was metaphysics, or worse, depending on whose sage opinion you consulted. Walking us through the discovery of the galaxies, Smith illustrated how data revises what we consider "real". *Lesson:* dark matter and dark energy are a good case in point.

Steinmetz reviewed the current state-of-the-art in cosmological simulations and our current conceptual framework ΛCDM. The field has moved from simulating structure formation in random Gaussian density fields to ones that are constrained to reproduce the main features of the Local Group. He showed impressive results from the CLUES simulations with sufficient resolution and physics to model the formation of the LG including dwarf galaxies. *Lesson:* dwarf galaxy evolution is very dependent on environment.

Francoise Combes reviewed available data and theories on the cosmic evolution of gas and star formation. Observations of 800,000 galaxies over the redshift interval $0.02 \leq z \leq 2.5$ reveal a *main sequence* of star-forming galaxies. Some 90 % of star formation occurs within this main sequence. She discussed the proposal by Feldmann (2013) that the shape of the Madau diagram (cosmic star formation rate density vs. redshift) is driven by evolution of a single key parameter: (star formation rate)/(accretion rate) of individual galaxies. *Lesson:* this subject is becoming data rich; key insights are starting to emerge.

2.15 Galaxies Are They Really Are (and Were)

The last group of talks I was able to summarize were given by celebree **David Block** as well as **Roberto Abraham**, **Debra Elmegreen** and **Linda Tacconi**. Block took us on a passionate personal journey of the seen and unseen parts of well-known galaxies. The unseen parts are revealed by deep infrared imaging. *Lesson:* the bright optical galaxy images are no more the galaxy than Magritte's famous painting of a pipe is a real pipe.

Abraham took us on a passionate personal journey for a better telescope to see the unseen extremeties of galaxies. It was a rollicking good story about basic telescope design and the construction of a refractor array built from telephoto lenses (with Peter van Dokkum) that achieves unprecendented low surface brightness limits. Interesting results about M101 are published in van Dokkum et al. (2014). **Lesson:** it pays to think out of the box if you know what you are doing.

D. Elmegreen presented the high-z galaxy zoo in fascinating detail. She reviewed the classification of all 1003 galaxy morphologies in the Hubble Ultra-deep Field larger than 10 pixels to $z \approx 5$. Most striking are the chain, clump cluster, double, and tadpole morphologies commonly seen at high redshift.

Tacconi complemented Elmegreen's morphological view with integral field spectroscopy results on high-z star forming galaxies. She and the MPE team find that these galaxies are gas rich, turbulent, clumpy, globally unstable disks with strong feedback signatures. She argued that star-forming clumps may be the largest fragmentation scale in gas rich disks.

Lesson: these talks illustrate the importance of powerful new instruments and careful, systematic observations to revealing new facts about the universe.

3 Overall Lessons

To conclude, I list my overall takeaways from what I found to be a most fascinating and informative conference.

- Without data, anything goes. Data guides science in productive directions.
- New data, new tools are driving progress across a broad range of topics within the Local Group. Some really inventive approaches are being used. Simulations are providing key insights in some areas.
- What's old is new again: the research presented here is revising *basic facts* about the MW and LG that I thought were solid and well-established.
- The Local Group is full of fascination and mysteries still to be discovered. Remember the admonishment of the famous Caltech astronomer Jesse Greenstein: don't get carried away by grand theories; appreciate "the thing itself".

References

Feldman, R. *MNRAS*, 433, pp 1910–1929, (2013)
Keller, S., Bessell, M., Frebel, A., Casey, A., Asplund, M., Jacobson, H., Lind, K., Norris, J., Yong, D., Heger, A., Magic, Z., da Costa, G., Schmidt, B. & Tisserand, P. *Nature*, 506, pp 463–466, (2014).
Kritsuk, A., Lee, C. & Norman, M. *MNRAS*, 436, pp 3247–3261, (2013)
van Dokkum, P., Abraham, R. & Merritt, A. *ApJL*, 782, L24–L28, (2014)

Concluding Thoughts: G. K. Chesterton

David L. Block

In the Conference summary, Michael Norman alluded to an admonishment by the Caltech astronomer Jesse Greenstein—not to get carried away by grand theories, but rather, to appreciate "the thing itself".

And Ken Freeman reminded me of an appalling quotation: "It is also a good rule not to put overmuch confidence in observational results until they are confirmed by theory" (attributed to Sir Arthur Eddington, 1882–1944). Exceedingly hard to believe, that *observations*, in the mind of Eddington, should only be selectively adopted.

In his masterful book entitled "Tremendous Trifles", G. K. Chesterton focused on appreciating "the thing itself":

> To appreciate anything we must always isolate it, even if the thing itself symbolise something other than isolation. If we wish to see what a house is it must be a house in some uninhabited landscape. If we wish to depict what a man really is we must depict a man alone in a desert or on a dark sea sand. So long as he is a single figure he means all that humanity means; so long as he is solitary he means human society; so long as he is solitary he means sociability and comradeship. Add another figure and the picture is less human—not more so. One is company, two is none. If you wish to symbolise human building draw one dark tower on the horizon; if you wish to symbolise light let there be no star in the sky. Indeed, all through that strangely lit season which we call our day there is but one star in the sky—a large, fierce star which we call the sun. One sun is splendid; six suns would be only vulgar. One Tower of Giotto is sublime; a row of Towers of Giotto would be only like a row of white posts. The poetry of art is in beholding the single tower; the poetry of nature in seeing the single tree . . .

A parallel in the microcosm: in portraiture, one does exactly that: the photographer isolates the person in his-her environment and the story of their life is etched in their faces (Figs. 1 and 2). In the poetry of art, Figure 3 masterfully depicts and individual

D. L. Block (✉)
School of Computational and Applied Mathematics, University of the Witwatersrand, Johannesburg, South Africa
e-mail: igalaxy@iafrica.com; david.block@wits.ac.za

K. Freeman et al. (eds.), *Lessons from the Local Group,*
DOI 10.1007/978-3-319-10614-4_41

Fig. 1 Etched in the face of Phillipos Kleovoulou (a carpenter and the owner of a small store in Randfontein, South Africa) are years of courage, toil, determination and of wisdom. As Chesterton would say: "One is company, two is none." (Photograph: Fidos Kleovoulou)

on a journey. Chesterton is correct: "So long as he is a single figure he means all that humanity means; so long as he is solitary he means human society; so long as he is solitary he means sociability and comradeship."

Chesterton also penned these words, in his book "Charles Dickens": "It is when we pass our own private gate, and open our own secret door, that we step into the land of the giants."

One individual in his environment, the owner of a small store in Randfontein, South Africa (Fig. 1). The other individual, a lady in rural China (Fig. 2). Two giants, indeed. Perhaps photographic portraiture too, resonates with the same message as that so aptly described by the legendary G. K. Chesterton:

> One is company, two is none ... if you wish to symbolise light let there be no star in the sky.

Fig. 2 It was a brief encounter. A lady in rural China, with her hat. Her face speaks volumes of unspoken words. To paraphrase Chesterton: "If we wish to depict what a person really is we must depict that person alone." (Photograph: David Block)

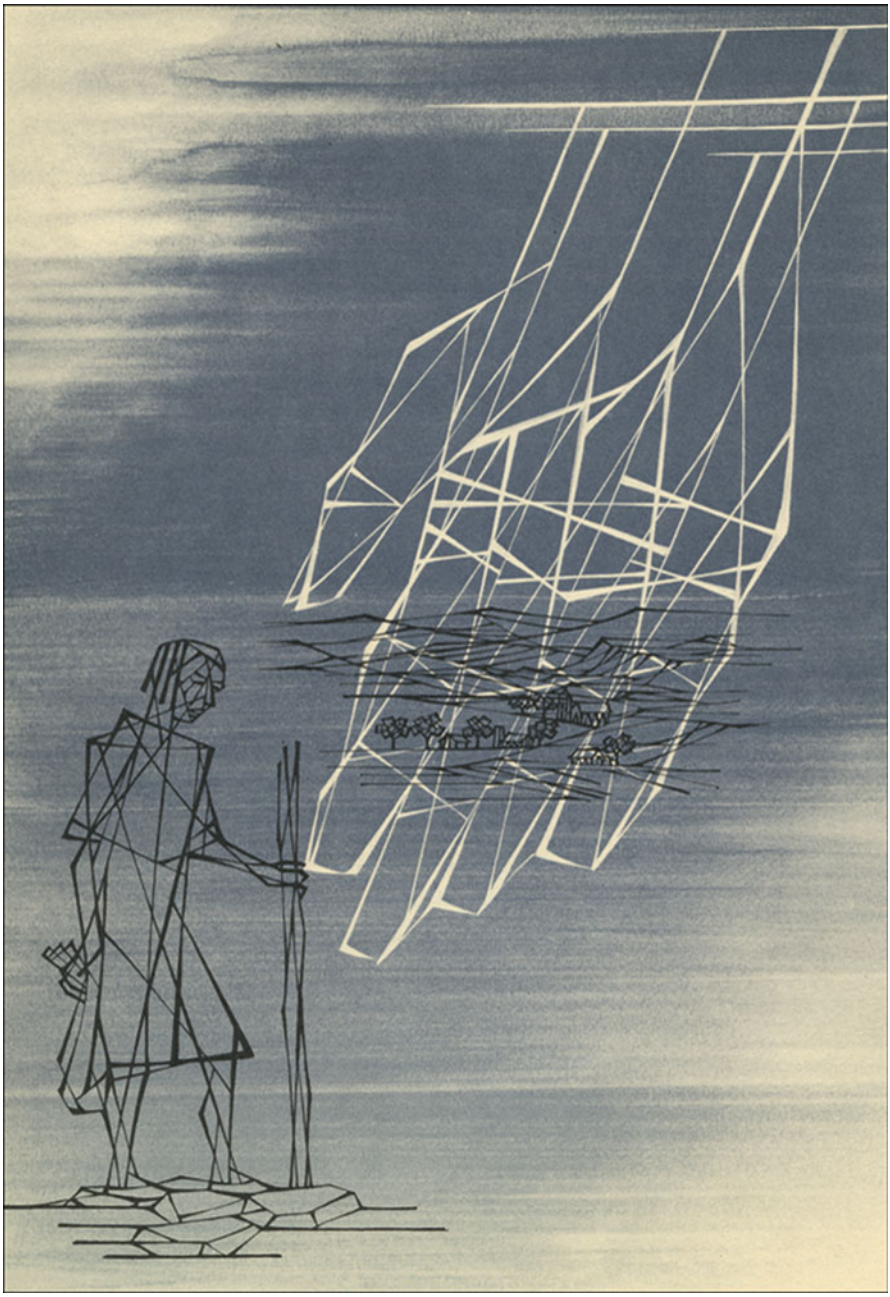

Fig. 3 The legendary artist Ismar David depicts one individual on a journey. Guiding that person, step by step, is the Hand of God. A gripping read is *Pensées* by the brilliant scientist Blaise Pascal. "To appreciate anything we must always isolate it" pens G. K. Chesterton. (Image courtesy: Ismar David Collection, RIT Cary Graphic Arts Collection)

Group Photographs: From 1927 to 2014

Giovanni Fazio eloquently contrasts two Group Photographs: one secured in 1927; the other in 2014.

"It has long been the custom at important scientific conferences to record the event with a group picture of the participants. Comparison of the group picture of the Fifth Solvay Conference in Brussels, in 1927 (Fig. 1), with our *Lessons from the Local Group* conference picture (Fig. 2), provides some very interesting observations. The Solvay scene is very impressive, with Max Planck, Albert Einstein, and Hendrik Lorentz sitting in the front row on this cold, dreary day, dressed in their formal attire. However, even more impressive is our *Local Group* conference picture with Ken Freeman, Bruce Elmegreen, and David Block in the front row, in a more relaxed mood and dress, with a beautiful sandy beach in the foreground and the warm, blue water of the Seychelles Islands in the background. It is also interesting to note that the only woman in the Solvay picture is Madame Marie Curie, whereas in the *Local Group* picture about one-third of the participants are women. Indeed, times have changed for the better!"

Editorial Note It is always a challenge to have every delegate present in a single group photograph, especially if the number of delegates exceeds a few dozen in size. For this reason, the photographers at Hotel Ephelia captured one other photograph of our group. That photograph (Fig. 3) was secured on the lawns adjacent to the Conference Venue.

K. Freeman et al. (eds.), *Lessons from the Local Group,*
DOI 10.1007/978-3-319-10614-4

Fig. 1 The Solvay Conference in Belgium, 1927. Only one woman was present. Delegates included Paul Ehrenfest, Erwin Schrödinger, Wolfgang Pauli, Werner Heisenberg, William Lawrence Bragg, Hendrik Anthony Kramers, Paul Dirac, Arthur Compton, Louis de Broglie, Max Born, Niels Bohr, Irving Langmuir, Max Planck, Marie Skłodowska-Curie, Hendrik Lorentz and Albert Einstein. (Photographer: Benjamin S. Couprie)

Fig. 2 Delegates at the Block-Elmegreen Conference gather on the beach, on the island of Mahe in the Seychelles, for a group photograph. Giovanni Fazio (see text) compares Figs. 1 and 2

Fig. 3 Delegates gather on the lawns outside the conference venue, for another group photograph amidst the lush vegetation in the Seychelles Archipelago

Fig. 4 "What you are you do not see, what you see is your shadow" penned Nobel laureate Rabindranath Tagore. The elongated shadow of a delegate on an early morning beach walk, in the Seychelles

List of Participants

Roberto G. Abraham Department of Astronomy and Astrophysics, University of Toronto, ON L6M 2N5, Canada, abraham@astro.utoronto.ca

Philippe André Laboratoire d'Astrophysique (AIM) de Paris-Saclay, CEA Saclay, 91191 Gif-sur-Yvette, France, pandre@cea.fr

Magda Arnaboldi European Southern Observatory, Garching, Germany, marnabol@eso.org

Martin Asplund Research School of Astronomy and Astrophysics, Australian National University, Canberra, ACT 2611, Australia, martin@mso.anu.edu.au

Gurtina Besla Steward Observatory, University of Arizona, 933 North Cherry Avenue, Tucson, AZ 85721, USA, gbesla@email.arizona.edu

Robert A. Benjamin Dept of Physics, University of Wisconsin-Whitewater, USA, benjamir@uww.edu

David L. Block School of Computational and Applied Mathematics, University of the Witwatersrand, Johannesburg, South Africa, igalaxy@iafrica.com; david.block@wits.ac.za

Robert Braun CSIRO Astronomy and Space Science, P.O. Box 76, Epping, NSW 1710, Australia, Robert.Braun@csiro.au

Jean P. Brodie University of California Observatories, 1156 High Street, Santa Cruz, CA 95064, USA, brodie@ucolick.org

Andreas Burkert Universitäts-Sternwarte München, Scheinerstraße 1, D-81679 München, Germany; Max-Planck-Fellow, Max-Planck-Institut für extraterrestrische Physik, Postfach 1312, Giessenbachstraße, D-85741 Garching, Germany, burkert@usm.uni-muenchen.de

Giovanni Carraro European Southern Observatory, Alonso de Cordova 3107, 19001, Santiago de Chile, Chile, gcarraro@eso.org

K. Freeman et al. (eds.), *Lessons from the Local Group,*
DOI 10.1007/978-3-319-10614-4

Corinne Charbonnel Department of Astronomy, University of Geneva, CH 1290 Versoix, Switzerland & CNRS UMR 5277 IRAP, University of Toulouse, F 31400 Toulouse, France, Corinne.Charbonnel@unige.ch

Françoise Combes Observatoire de Paris, LERMA, CNRS, 61 Av. de l'Observatoire, F-75014, Paris, France, francoise.combes@obspm.fr

Edvige Corbelli INAF-Osservatorio di Arcetri, L. E. Fermi,5 - 50125 Firenze, Italy, edvige@arcetri.astro.it

Clare Dobbs School of Physics & Astronomy, University of Exeter, EX4 4QL, UK, dobbs@astro.ex.ac.uk

Valentina d'Orazi Dept. of Physics and Astronomy, Macquarie University, NSW, 2109, Sydney, Australia; Monash Centre for Astrophysics, Monash University, School of Mathematical Sciences, Building 28, VIC 3800 Clayton, Melbourne, Australia, valentina.dorazi@mq.edu.au

Bruce G. Elmegreen IBM Research Division, T. J. Watson Research Center, 1101 Kitchawan Road, Yorktown Heights, NY 10598, USA, bge@us.ibm.com

Debra M. Elmegreen Department of Physics & Astronomy, Vassar College, Poughkeepsie, NY 12604 USA, elmegreen@vassar.edu

Giovanni G. Fazio Harvard Smithsonian Center for Astrophysics, 60 Garden St., Cambridge, MA 02138, USA, gfazio@cfa.harvard.edu

Ken C. Freeman Research School of Astronomy and Astrophysics, Mount Stromlo Observatory, ANU, Canberra, Australia, kcf@mso.anu.edu.au

Yasuo Fukui Department of Physics, Nagoya University, Chikusa-ku, Nagoya, Aichi, 464-8601, Japan, fukui@a.phys.nagoya-u.ac.jp

Carme Gallart Instituto de Astrofísica de Canarias, E-38200 La Laguna, and Universidad de La Laguna, Dpto. Astrofísica, E-38206 La Laguna, Tenerife, Spain, carme@iac.es

Ortwin Gerhard Max Planck Institute for extraterrestrial Physics, PO Box 1312, Giessenbachstr., 85741 Garching, Germany, gerhard@mpe.mpg.de

Reinhard Genzel Max-Planck-Institut für extraterrestrische Physik, Giessenbach-strasse, D-85748 Garching, Germany, genzel@mpe.mpg.de

Gerry Gilmore Institute of Astronomy, University of Cambridge, Madingley Road, Cambridge, CB3 0HA, UK, gil@ast.cam.ac.uk

Dimitrios A. Gouliermis University of Heidelberg, Centre for Astronomy, Institute for Theoretical Astrophysics, Albert-Ueberle-Str. 2, 69120 Heidelberg, Germany; Max Planck Institute for Astronomy, Königstuhl 17, 69117 Heidelberg, Germany, dgoulierm@googlemail.com; dgoulier@mpia.de

Carl J. Grillmair Spitzer Science Center, California Institute of Technology, Mail Stop 314-6, 1200 E. California Blvd., Pasadena, CA 91125, USA, carl@ipac.caltech.edu

Misha Haywood GEPI - Observatoire de Paris, UMR 8111, 5 Place Jules Janssen F-92195 Meudon Cedex France, Misha.Haywood@obspm.fr

Deidre A. Hunter Lowell Observatory, 1400 West Mars Hill Road, Flagstaff, AZ 86001 USA, dah@lowell.edu

Ralf S. Klessen Universität Heidelberg, Zentrum für Astronomie, Institut für Theoretische Astrophysik, Albert-Ueberle-Straße 2, 69120 Heidelberg, Germany, klessen@uni-heidelberg.de

John Kormendy Department of Astronomy, University of Texas at Austin, 2515 Speedway, Stop C1400, Austin, TX 78712-1205, USA; kormendy@astro.as.utexas.edu;
Max-Planck-Institut für Extraterrestrische Physik, Gieenbachstraße, 85748 Garching bei München, Germany; Universitäts-Sternwarte München, Ludwig-Maximilians-Universität, Scheinerstraße 1, 81679 München, Germany

Pavel Kroupa Helmholtz-Institut für Kern und Strahlenphysik, University of Bonn, Nussallee 14-16, 53115 Bonn, Germany; pavel@astro.uni-bonn.de

Alex Lazarian Department of Astronomy, University of Wisconsin-Madison, Madison, WI 53706, USA, lazarian@astro.wisc.edu

Geraint F. Lewis Sydney Institute for Astronomy, School of Physics,
The University of Sydney, NSW 2006, Australia, Geraint.lewis@sydney.edu.au

Aigen Li Department of Physics and Astronomy, University of Missouri, Columbia, MO 65211, USA, lia@missouri.edu

Dougal Mackey Research School of Astronomy & Astrophysics, Australian National University, Mount Stromlo Observatory, Cotter Road, Weston Creek, ACT 2611, Australia, dougal.mackey@anu.edu.au

Steven R. Majewski Department of Astronomy, University of Virginia, Charlottesville, VA 22904, USA, srm4n@virginia.edu

Fancesca Matteucci Department of Physics, Astronomy Section, Trieste University, Via G. B. Tiepolo, 11, 34131 Trieste, Italy, matteucci@oats.inaf.it

Mark R. Morris Department of Physics and Astronomy, University of California, Los Angeles, USA, morris@astro.ucla.edu

Michael L. Norman CASS/UCSD 0424, 9500 Gilman Dr., La Jolla, CA 92093
Center for Astrophysics and Space Sciences, University of California, San Diego, USA, mlnorman@ucsd.edu

Mary Putman Department of Astronomy, Columbia University, New York, NY 10027, USA, mputman@astro.columbia.edu

Jan Palouš Astronomical Institute, Academy of Sciences of the Czech Republic, Boční II, 141 00 Prague 4, Czech Republic,palous@ig.cas.cz

Rok Roškar Institute for Computational Science, University of Zürich, Winterthurerstrasse 190, CH-8057 Zürich, Switzerland, roskar@physik.uzh.ch

Mónica Rubio Departamento de Astronomía, Universidad de Chile, Chile, mrubio@das.uchile.cl

Daniel Schaerer Observatoire de Genève, Universitè de Genève, 51 Ch. des Maillettes, 1290 Versoix, Switzerland; CNRS, IRAP, 14 Avenue E. Belin, 31400 Toulouse, France, daniel.schaerer@unige.ch

Robert W. Smith Department of History and Classics, University of, Alberta, Edmonton, Alberta T6G 2H4, Canada, rwsmith@ualberta.ca

Matthias Steinmetz Leibniz-Institut für Astrophysik Potsdam (AIP), An der Sternwarte 16, 14482, Potsdam, Germany, msteinmetz@aip.de

Linda Tacconi Max-Planck-Institut für Extraterrestrische Physik, Giessenbachstrasse, D-85748 Garching, Germany, linda@mpe.mpg.de

Piet C. van der Kruit Kapteyn Astronomical Institute, University of Groningen, P.O.Box 800, 9700AV Groningen, The Netherlands, vdkruit@astro.rug.nl

Marie-Lou Simaan of *Mars Travel* in Johannesburg. (Photo: David Block)

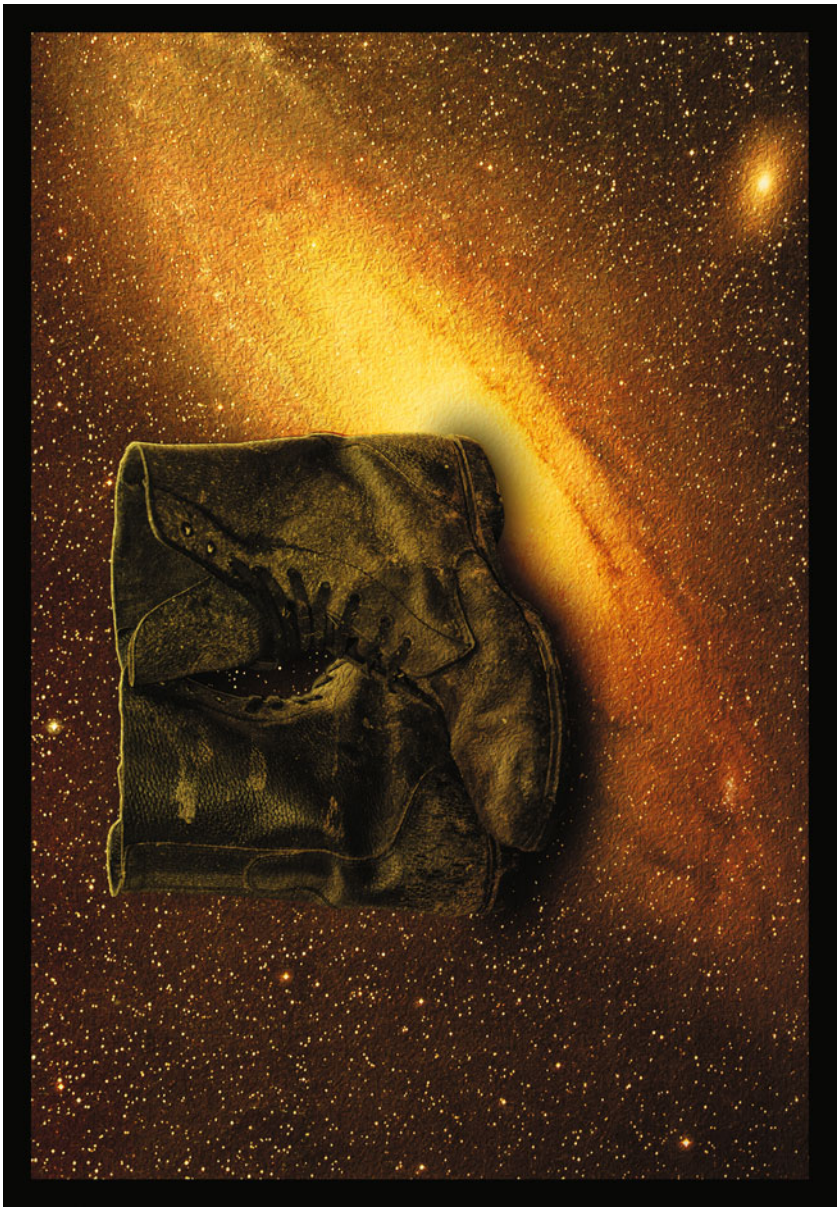

"Mining Galaxies"—An old pair of boots juxtaposed against M31. This specific photograph of M31 ranks as one of the first-ever (oldest) astronomical colour images—and certainly the first colour rendition of M31. The 120 min exposure was made in 1958, August 11, by William C. Miller using the Palomar 48-in. Schmidt Telescope and was later subject to digital manipulation by the legendary Australian astrophotographer, David Malin. Miller used the then revolutionary Super Ansco reversal film which had a nominal speed of 100 ASA. (Image of M31: Courtesy David Malin. Image of boots and montage: David Block)

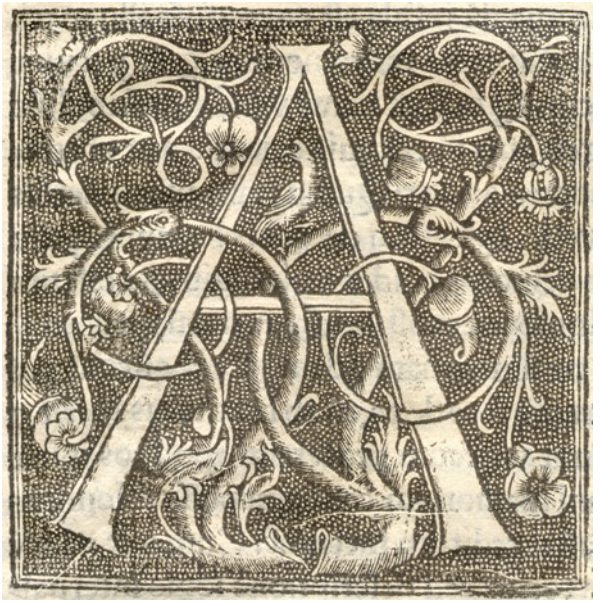

dedication in a volume by Edmund Spenser (c. 1552–1599), one of the greatest and most influential poets of the Elizabethan Age.

In his treatise “The Shepheardes Calender”, Spenser sends his book forth into the world, thus:

Go, little Book; thy self present,
As Child whose Parent is unkent,
To him that is the President
Of Nobleness and Chivalrie:
And if that Envy bark at thee,
As sure it will, for Succour flee
Under the shadow of his Wing.
And, asked who thee forth did bring,
A Shepherd’s Swain say did thee sing,
All as his straying Flock he fed:
And when his Honour hath thee read,
Crave pardon for thy Hardy-head.
But if that any ask thy Name,
Say, thou wert base begot with blame:
Forthy thereof thou takest shame.
And when thou art past Jeopardy,
Come tell me what was said of me,
And I will send more after thee.

IMMERITO